

2000

# Management of acid sulfate soils by groundwater manipulation

Bruce Geoffrey Blunden  
*University of Wollongong*

---

## Recommended Citation

Blunden, Bruce Geoffrey, Management of acid sulfate soils by groundwater manipulation, Doctor of Philosophy thesis, Faculty of Engineering, University of Wollongong, 2000. <http://ro.uow.edu.au/theses/1834>

Research Online is the open access institutional repository for the University of Wollongong. For further information contact the UOW Library: [research-pubs@uow.edu.au](mailto:research-pubs@uow.edu.au)

## **NOTE**

This online version of the thesis may have different page formatting and pagination from the paper copy held in the University of Wollongong Library.

## **UNIVERSITY OF WOLLONGONG**

### **COPYRIGHT WARNING**

You may print or download ONE copy of this document for the purpose of your own research or study. The University does not authorise you to copy, communicate or otherwise make available electronically to any other person any copyright material contained on this site. You are reminded of the following:

Copyright owners are entitled to take legal action against persons who infringe their copyright. A reproduction of material that is protected by copyright may be a copyright infringement. A court may impose penalties and award damages in relation to offences and infringements relating to copyright material. Higher penalties may apply, and higher damages may be awarded, for offences and infringements involving the conversion of material into digital or electronic form.

# **MANAGEMENT OF ACID SULFATE SOILS BY GROUNDWATER MANIPULATION**

A thesis submitted in fulfilment of the requirements of the degree of

**DOCTOR OF PHILOSOPHY**

from

**UNIVERSITY OF WOLLONGONG**

by

**BRUCE GEOFFREY BLUNDEN**

B.Nat Res. (Hons), M.Eng.

Faculty of Engineering

October 2000

## **AFFIRMATION**

I, Bruce Blunden, declare that this thesis, submitted in fulfilment of the requirements for the award of Doctor of Philosophy, in the Faculty of Engineering, University of Wollongong, is wholly my own work unless otherwise referenced or acknowledged. This document has not been submitted for qualifications at any other academic institution.

Bruce Blunden.



## PUBLICATIONS RELATED TO THIS RESEARCH

Blunden, B. and Indraratna, B. (2000). Evaluation of Surface and Groundwater Management Strategies for Drained Sulfidic Soil using Numerical Models. *Australian Journal of Soil Research* **38**, 569-590

Blunden, B. and Indraratna, B. (2000). Pyrite Oxidation Model for Assessing Groundwater management Strategies in Acid Sulphate Soils. *Journal of Geotechnical and Geoenvironmental Engineering*, (in press).

Indraratna, B. and Blunden, B. (1999). Nature and Properties of Acid Sulphate Soils in Drained Coastal lowland in NSW, *Australian Geomechanics Journal*, **34**(1), 61-78.

Blunden, B., Indraratna, B. and Morrison, J. (2000) Change in groundwater chemistry due to water table fluctuations in pyritic sediments. *Quarterly Journal of Engineering Geology and Hydrogeology*, (in prep)

Blunden, B., Indraratna, B. and Morrison, J. (2000) Management of acid generation in sulfidic soils by drain manipulation: a case study. Proceedings of ASSMAC Conference on the management of acid sulfate soils. ASSMAC, Wollongbar.

Indraratna, B. and Blunden, B. (2000). Modeling of Acid Generation and Distribution in Pyritic Estuarine Soils. International Conference on Geotechnical and Geological Engineering, Melbourne, November 2000.

Blunden, B. and Indraratna, B. (1999). Estuarine Acidification caused by Drainage of Pyritic Sediments in Coastal Lowlands. ASCE-CSCE Environmental Engineering Conference, Norfolk, Virginia, USA, July, pp. 131-140.

Blunden, B. and Indraratna, B. (1999). Management of Acid Sulfate Soils in Drained Coastal Lowlands in Australia. 27th Annual CSCE Conference, Regina, Saskatchewan, Canada, June, Vol. 2, pp. 317-326.

Blunden, B., Indraratna, B. and Morrison, J. (1998). Problems of Acid Sulphate Soils and their Remediation by Watertable Management. 2nd International Conference on Environmental Management, University of Wollongong, pp. 583-590.

Indraratna, B. and Blunden, B. (1997). Remediation of Acid Sulphate Soils by Management of Groundwater Table. Contaminated and Derelict Land, 2nd International Symposium on Geotechnics & the Environment, Krakow, Poland, Thomas Telford, London, pp. 324-333.

Blunden, B., Indraratna, B. and Nethery A. (1997). Effect of Groundwater Table on Acid Sulphate Soil Remediation, First ANZ Conference on Environmental Geotechnics, Melbourne (November), Balkema, pp. 549-554.

## **DEDICATION**

My friend, colleague and supervisor Dr Andrew Nethery (NSW Environment Protection Authority, South Coast Region) was instrumental in the development, implementation and the success of this research project in collaboration with University of Wollongong researchers. His enthusiasm and support for this research and other projects related to improving the management of acid sulfate soils was the catalyst for much of the current work being carried out in the Shoalhaven River floodplain.

During 1999 Andrew was stricken by a debilitating brain injury. The nature, severity and suddenness of his conditions has saddened everyone who enjoyed his friendly encouragement and professional support. He is keenly missed.

This research and the ongoing improvements to the management of coastal floodplains emanating from this work are dedicated to Andrew.

## ACKNOWLEDGEMENTS

The success of this research is in no small part attributed to the excellent collaboration and professionalism of all the team involved in this project. I would like to express my gratitude to my supervisors Professor Buddhima Indraratna and Professor John Morrison who have cheerfully guided me through the highs and lows of this PhD. Post-graduate study was made to be a pleasure through their invaluable technical advice, diligent editorial assistance and consistent positive encouragement throughout my term at University. Mr John Downey (Shoalhaven City Council) has also provided excellent technical and practical supervision of this project, in addition to creating awareness of acid sulfate soils issues in the south coast community.

This research would not have been possible without the generous support of the Morris, Stuart, Carolin and the Miller families. Having a research study performed on their working farms has been a trial in more ways than one. I thank you all for your good humour, persistence and observations throughout this work.

Numerous people have provided technical assistance during field sampling and laboratory testing. Life in the field had always been educating and enjoyable with Roy Lawrie and Narwash Haddad (NSW Agriculture) who have contributed beyond the call of duty in drilling piezometers and taking so many soil samples. Similarly, Ian Laird (UOW) provided excellent technical assistance in the field and laboratory. Joanne George, Norm Gall and Matthew Clark (UOW) have given generous assistance in the chemistry laboratories. Thankyou to the staff led by Graham Lancaster of the laboratories at Southern Cross University for assistance with soil chemical testing. A fantastic effort by the maintenance staff at Shoalhaven City Council greatly assisted in repairing the weirs after the August 1998 floods. Roy Foley, Narayan Pradhan and others at the EPA Analytical Chemistry Laboratories performed much of the routine water quality testing.

Special thanks goes to my father and unpaid technical sidekick Graham Blunden who has made all sorts of novel gadgets and walked hundreds of kilometres with me making routine field monitoring much more efficient and enjoyable. My mother, Gwen, has also encouraged and supported me through this project.

Ongoing technical discussions with Dr Ric Morris, Mr Richard Bush (Southern Cross University) and fellow members of the ASSMAC Technical Coordinating Committee have provided valuable insight and information towards this research.

I gratefully acknowledge the financial support provided through the Australian Postgraduate Award (Industry) scholarship administered by the DEETYA, the ASSPRO funding provided by the NSW Government through NSW Agriculture and the monitory contribution of Shoalhaven City Council.

My loving and long suffering partner Jennifer Bean can now look forward to getting a life as we both move to the next stage in our lives together. Thankyou for your endless support, advice and encouragement through these years of study.

## ABSTRACT

The effectiveness of manipulating drain water levels using weirs in flood mitigation drains to improve the groundwater and drain water quality was investigated for agricultural land affected by previously oxidised acid sulfate soil near Berry on the South Coast of New South Wales. Groundwater elevation data measured prior to the installation of the weirs showed that significant groundwater drawdown was caused by the low water level in the drains. Drawdown from the drains, in conjunction with high rates of evapotranspiration, caused the groundwater elevation to fall into the pyritic soil causing the oxidation of pyrite and the generation of acidic oxidation products. The high hydraulic gradient caused by the low water level in the drains facilitated the rapid transport of these acidic oxidation products into the drains for discharge into a nearby waterway.

Installation of the weirs promoted higher groundwater elevations by reducing the influence of groundwater drawdown from the drain. The lower hydraulic gradients established under the influence of the higher drain water level maintained by the weir reduced the rate of discharge of acidic oxidation products from the groundwater to the drain. In addition to the assessment of installing weirs in drains to manipulate the groundwater table, numerical simulations combining groundwater flow and pyrite oxidation models were used to predict the magnitude and distribution of pyrite oxidation for various boundary conditions that simulate potential groundwater management strategies. Application of these simulation models shows that substantial reductions in the volume of pyritic soil exposed to oxidising conditions can be achieved by maintaining a higher water level in the drains and/or applying regular irrigation. The rate of acid generation was also investigated in the laboratory by maintaining samples at a constant suction for a specific length of time. Simple multiple regression equations can predict the magnitude and rate of acid generation accurately using these easy to measure independent variables.

Higher groundwater levels did not substantially improve the groundwater quality. High concentrations of stored acidity in the form of acidic cations on the cation exchange sites of the soil as well as the presence of aluminium and iron sulfate minerals formed under acidic conditions ensures that the groundwater has low pH (3.5-4) and high concentrations of dissolved aluminium (30-100 mg/L). The hydrolysis of jarosite and the oxidation of pyrite by  $\text{Fe}^{3+}$  under acidic, reducing conditions may also give rise to low pH in the groundwater. The maintenance of poor groundwater quality was further investigated by using geochemical models to simulate the effect of the dissolution of acidic minerals and the importance of acidic cation exchange sites. Similarly, acid management strategies including controlled saline intrusion into drains and the injection of dilute lime slurry into the soil were investigated.

Implementation of weirs in flood mitigation drains was shown to be beneficial in terms of reducing the generation of 'new' acid from the oxidation of pyrite in the sulfidic soil as well as facilitation the slow leakage of acid products into waterways rather than the discharge of low pH/high aluminium slugs. However, the management of groundwater elevation alone will not substantially improve groundwater quality without due attention to the 'stored' acid in the soil profile.

**TABLE OF CONTENTS**

**AFFIRMATION ..... ii**

**PUBLICATIONS RELATED TO THIS RESEARCH..... iii**

**DEDICATION ..... v**

**ACKNOWLEDGEMENTS ..... vi**

**ABSTRACT..... viii**

**TABLE OF CONTENTS ..... x**

**LIST OF FIGURES ..... xix**

**LIST OF TABLES..... xxvii**

**LIST OF PLATES ..... xxix**

**Chapter 1: Introduction ..... 1**

1.1 General background..... 1

1.2 Objectives of the study ..... 2

1.3 Thesis organisation..... 3

1.3.1 Part I: Literature review ..... 3

1.3.2 Part II: Field trial of groundwater table management using weirs ..... 4

1.3.3 Part III: Development and application of geo-hydraulic models..... 6

1.3.4 Part IV: Modeling of acid generation and geochemistry..... 7

1.3.5 Part V: Conclusions and recommendations ..... 8



<b>Chapter 2: Introduction to acid sulfate soils .....</b>	<b>9</b>
2.1 Acid sulfate soil.....	9
2.2 Formation of acid sulfate soils.....	10
2.3 Distribution of acid sulfate soils.....	14
2.4 Properties of acid sulfate soils.....	16
2.4.1. Oxidation processes .....	17
2.4.2 Soil physical properties .....	21
2.4.2.1 Oxygen transport.....	23
2.4.2.2 Water flow in soils.....	25
2.4.2.3 Water retention and unsaturated hydraulic conductivity curve.....	26
2.4.3 Hydrological interactions .....	30
2.4.3.1 Effect of prolonged wet periods.....	32
2.4.3.2 Effect of prolonged dry periods .....	35
2.4.3.3 Artificial drainage .....	37
2.5 Implications for this research.....	40
 <b>Chapter 3: Review of pyrite oxidation studies and management strategies.....</b>	 <b>42</b>
3.1 Field investigation of acid generation from acid sulfate soils .....	42
3.2 Laboratory column studies of pyrite oxidation.....	46
3.3 Pyrite oxidation models.....	52
3.3.1 Theory and approximate analytical solution: Davis and Ritchie (1986).....	52
3.3.2 Numerical models for pyrite oxidation .....	53
3.3.2.1 Reactive Tailings Assessment Program (RATAP).....	54
3.3.2.2 Model developed by Elberling et al. (1994) .....	59
3.3.2.3 POLS.....	63
3.3.2.4. PYROX-MINTRAN-MINTOX.....	67

3.3.2.5 Simulation Model for Acid Sulfate Soils (SMASS)..... 71

3.4 Pyrite oxidation management strategies at the sub-catchment scale ..... 79

3.5 Conclusions ..... 81

3.5.1 Relationship of previous research to the current study ..... 81

**Chapter 4: Field study site and monitoring equipment ..... 83**

4.1 Introduction ..... 83

4.2 Study site location ..... 84

4.2.1 Geology and Geomorphology ..... 86

4.2.2 Shoalhaven drainage system ..... 89

4.3 Design and construction of weirs ..... 93

4.4 Field equipment and monitoring..... 98

4.4.1 Site topographic survey ..... 98

4.4.2 Installation of piezometers ..... 99

4.4.3 Measurement of routine groundwater parameters..... 101

4.4.4 Weather station..... 105

3.4.5 Drain water level ..... 105

**Chapter 5: Site climatic conditions ..... 106**

5.1 Introduction ..... 106

5.2 Site weather ..... 107

5.2.1 Rainfall..... 108

5.2.2 Evapotranspiration ..... 113

5.2.3 Southern Oscillation Index..... 116

5.3 Implications for acid sulfate soil ..... 118

<b>Chapter 6: Soil chemical, physical and morphological properties.....</b>	<b>120</b>
6.1 Introduction .....	120
6.2 Soil sampling and testing methods .....	121
6.2.1 Study site topography, soil profile description and stratigraphy .....	121
6.2.2 Pyrite micromorphology.....	123
6.2.3 Soil chemistry.....	123
6.2.4 Soil physics .....	125
6.3 Results and discussion.....	126
6.3.1 Stratigraphy and soil profile description .....	126
6.3.2 Pyrite morphology .....	132
6.3.3 Soil chemical properties.....	133
6.3.3.1 Soil pH .....	134
6.3.3.2 Titratable acidity .....	135
6.3.3.3 Dissolved sulfate and chloride .....	137
6.3.3.4 Oxidisable sulfur.....	140
6.3.3.5 Electrical conductivity .....	142
6.3.3.6 Effective cation exchange capacity .....	145
6.3.3.7 Soil carbon .....	149
6.3.4 Soil physical properties .....	151
6.3.4.1 Particle size distribution.....	152
6.3.4.2 Bulk density and porosity .....	153
6.3.4.3 Saturated hydraulic conductivity.....	154
6.3.4.3 Moisture characteristic curves .....	156
6.4 Conclusions .....	160

<b>Chapter 7: Groundwater dynamics .....</b>	<b>162</b>
7.1 Introduction .....	163
7.2 Pre-weir groundwater dynamics .....	164
7.2.1 Observed groundwater profile during pre-weir period.....	171
7.3 Groundwater dynamics - falling groundwater table .....	184
7.3.1 Evapotranspiration .....	184
7.3.2 Drainage .....	191
7.4 Groundwater dynamics - rising groundwater table.....	195
7.5 Oxidation of pyritic soil during the pre-weir period.....	199
7.6 Post-weir groundwater dynamics .....	213
7.6.1 Observed groundwater profile during post-weir period .....	213
7.7 Comparison between pre and post weir groundwater profiles .....	221
7.8 Oxidation of pyritic soil during the post-weir period .....	225
7.9 Drain water level .....	227
7.10 Conclusions .....	230
 <b>Chapter 8: Soil and water quality with respect to groundwater dynamics.....</b>	 <b>231</b>
8.1 Introduction .....	231
8.2 Change in soil chemistry .....	231
8.3 Change in water quality parameters associated with pyrite oxidation.....	234
8.3.1 Generation of pyrite oxidation products in groundwater .....	235
8.3.2 Evolution of the groundwater chemistry .....	242
8.3.3 Assessment of pyrite oxidation by anion concentration.....	250
8.3.4 Evaluation of the status of groundwater chemistry after pyrite oxidation ...	251
8.3.5 Change in pyrite oxidation product concentration in the drain water .....	256
8.3.6 Discharge of acidic cations to the drain water .....	261

8.3.7 Ingress of saline water into the drains .....	264
8.4 Conclusions .....	266
<b>Chapter 9: Evaluation of surface and groundwater management strategies for drained acid sulfate soil using existing numerical models .....</b>	<b>268</b>
9.1 Introduction .....	268
9.2 Methods and materials.....	268
9.2.1 FEMWATER .....	269
9.2.2 Element properties and numerical solution.....	272
9.2.3 Material properties for FEMWATER .....	273
9.2.4 FEMWATER mesh and boundary conditions .....	274
9.2.5 Bottom flux boundary calibration .....	279
9.2.6 Simulation Model for Acid Sulfate Soils (SMASS) .....	280
9.2.7 SMASS material and boundary conditions .....	281
9.3 Results and discussion.....	284
9.3.1 Observed groundwater profiles for existing drained situation .....	284
9.3.2 Simulated groundwater profiles for water management options.....	287
9.3.3 Measured and simulated pyrite concentration for the existing drained situation .....	289
9.3.4 Simulated sulfate production and pyrite consumption for water management options.....	291
9.3.5 Simulated moisture content profiles for water management options.....	294
9.3.6 Assessment of water management options.....	297
9.3.7 Other acid sulfate soil management strategies .....	300
9.4 Conclusions .....	301

<b>Chapter 10: A pyrite oxidation model for assessing groundwater management in acid sulfate soils.....</b>	<b>303</b>
10.1 Introduction .....	303
10.2 Theoretical formulations for the pyrite oxidation model.....	304
10.2.1 Oxygen transport down macropores.....	304
10.2.2 pyrite oxidation in the aerobic soil matrix .....	308
10.2.3 Oxygen transport in the soil matrix.....	312
10.2.4 Oxygen diffusion and consumption in the macropores.....	316
10.3 Numerical model .....	317
10.5 Comparisons between analytical and numerical solutions .....	319
10.6 Conclusions .....	323
<b>Chapter 11: Validation and application of ASS3D.....</b>	<b>324</b>
11.1 Introduction .....	324
11.2 Validation of ASS3D.....	324
11.2.1 FEMWATER simulation of the existing drained state .....	325
11.2.2 ASS3D input data.....	326
11.2.3 Simulated pyrite oxidation for the existing drained state.....	327
11.2.4 Validation of ASS3D against measured field data.....	330
11.3 Application of ASS3D to assess drain management options .....	334
11.3.1 Drain boundary conditions for FEMWATER simulation .....	334
11.3.2 FEMWATER simulations - groundwater elevation.....	339
11.3.3 ASS3D simulations - sulfate production.....	344
11.3.4 Assessment of simulated drain management options.....	347
11.4 Limitations of the ASS3D model .....	349
11.5 Advantages of the 3D pyrite oxidation model approach .....	350

11.6 Recommendations .....	351
11.7 Conclusions .....	352
<b>Chapter 12: Laboratory modelling of acid generation.....</b>	<b>353</b>
12.1 Introduction .....	353
12.2 Experimental methods .....	354
12.2.1 Soil sampling and preparation.....	355
12.2.2 Application of variable depth to groundwater table.....	356
12.2.3 Measurement of soil acidity .....	358
12.3 Results and discussion.....	358
12.3.1 Soil moisture characteristics .....	358
12.3.2 Acid generation in field structured soil.....	361
12.3.3 Acid generation in laboratory structured soil.....	363
12.4 Implications for better understanding of acid sulfate soil .....	370
12.4.1 Assessment of acid generation in the field.....	370
12.4.2 Numerical modelling.....	371
12.5 Conclusions .....	372
<b>Chapter 13: Application of geochemical concepts to the management of pyritic soil.....</b>	<b>374</b>
13.1 Introduction .....	374
13.2 Controlled saline intrusion into flood mitigation drains with weirs.....	375
13.2.1 Worked example: change in pH due to controlled saline intrusion .....	375
13.3 Geochemical modelling of groundwater in actual acid sulfate soil.....	377
13.3.1 Application of chemical equilibrium concepts .....	377
13.3.2 Iron geochemistry.....	378
13.3.3 Saturation indices .....	380
13.4 Conclusions .....	385

**Chapter 14: Summary and recommendations ..... 387**

14.1 Summary..... 387

14.2 Recommendations for further research..... 391

14.2.1 Field investigations ..... 391

14.2.2 Laboratory investigations ..... 393

14.2.3 Numerical modelling..... 394

**References ..... 396**

**Appendix A: Climatic variables ..... 410**

A.1 Temperature..... 410

A.2 Wind speed ..... 412

A.3 Solar radiation..... 414

**Appendix B: Groundwater quality data from all piezometer locations ..... 416**

**Appendix C: Source code for the ASS3D program. .... 425**

**Appendix D: Derivation of the solution for  $\phi_T$ ..... 469**

**Appendix E: PHREEQC simulations ..... 470**

E.1 Influence of acid saturated cation exchange complex on soil solution water quality ..... 471

E.2 Influence of acid saturated cation exchange complex and acidic minerals on soil solution water quality ..... 474

E.3. Controlling soil solution acidity by injecting calcium carbonate solution..... 477



**LIST OF FIGURES**

**Figure 2.1** Environmental conditions required for pyrite formation..... 12

**Figure 2.2:** Distribution of acid sulfate soils in NSW. .... 15

**Figure 2.3:** Relationship between pH and the concentration of  $Al^{3+}$  and  $Fe^{3+}$  ..... 19

**Figure 2.4:** Soil water retention and hydraulic conductivity for a clay soil..... 28

**Figure 2.5:** Artificial drainage system for a coastal floodplain ..... 38

**Figure 3.1** Relationship between drain level and pH..... 43

**Figure 3.2** Pyrite oxidation rate vs average groundwater level..... 45

**Figure 3.3** Water quality parameters for a drained, carbonate deficient acid sulfate soil. .... 48

**Figure 3.4** Exchangeable cations at the beginning (A) and end (B) of the drainage experiment. .... 49

**Figure 3.5** Observed and simulated pH in tailings ..... 57

**Figure 3.6** Observed and predicted pyrite concentration ..... 58

**Figure 3.7** Pyrite oxidation rate as a function of time ..... 61

**Figure 3.8** Pyrite oxidation rate as a function of depth shown for different effective diffusion coefficients ..... 62

**Figure 3.9** The acid mine drainage model POLS..... 64

**Figure 3.10** MINTOX simulation in comparison to field results from Elliot Lake, Ontario..... 70

**Figure 3.11** Schematic of a SMASS soil profile. Arrows indicate water and solute fluxes. .... 72

**Figure 3.12.** Structure of SMASS..... 73

**Figure 3.13.** Comparison between measured and computed pyrite distribution..... 75

<b>Figure 3.14</b> Measured and computed oxygen concentrations in soil macropores at 5, 25, 45, 65 cm depth. ....	76
<b>Figure 3.15</b> Measured and computed sulfate concentration. ....	77
<b>Figure 4.1:</b> Location of the study site. ....	84
<b>Figure 4.2</b> Evolution of the lower Shoalhaven River catchment.....	87
<b>Figure 4.3</b> Geomorphology of the Shoalhaven River catchment.....	88
<b>Figure 4.4</b> Broughton Creek floodplain and drainage system infrastructure.....	92
<b>Figure 4.5.</b> Expected effect of weir installation on adjacent groundwater elevation. ....	94
<b>Figure 4.6</b> Schematic diagram of the weir design. ....	97
<b>Figure 4.7.</b> Location of the piezometers and weirs.....	100
<b>Figure 5.1a</b> Daily rainfall for the pre-weir period. ....	108
<b>Figure 5.1b</b> Daily rainfall for the post-weir period.....	109
<b>Figure 5.2</b> Monthly rainfall measured at the site compared to the long term monthly average.....	111
<b>Figure 5.3a</b> Distribution of daily rainfall intensities for the pre-weir period. ....	112
<b>Figure 5.3b</b> Distribution of daily rainfall intensities for the post-weir period. ....	112
<b>Figure 5.4a</b> Calculated evapotranspiration during the pre-weir period. ....	114
<b>Figure 5.4b</b> Calculated evapotranspiration during the post-weir period. ....	114
<b>Figure 5.5</b> Long term evaporation relative to site ET data. ....	115
<b>Figure 5.6</b> SOI for the study period. ....	117
<b>Figure 5.7.</b> Relative contribution of rainfall and evapotranspiration to the site water balance.....	119
<b>Figure 6.1</b> Study site showing surface topography, soil sampling locations and transect AB. ....	122
<b>Figure 6.3</b> pyrite crystal size distribution for potential acid sulfate soil.....	132
<b>Figure 6.4</b> Soil pH at 10 m and 90 m from the drains.....	134

<b>Figure 6.5</b>	Titratable acidity at 10 m and 90 m from the drains .....	136
<b>Figure 6.6</b>	Dissolved sulfate at C90.....	138
<b>Figure 6.7</b>	Dissolved chloride at C90 .....	139
<b>Figure 6.8</b>	Peroxide oxidisable sulfur concentration, with depth. ....	140
<b>Figure 6.9</b>	Electrical conductivity.....	143
<b>Figure 6.10</b>	Effective cation exchange capacity .....	145
<b>Figure 6.11</b>	Aluminium saturation on the ECEC .....	147
<b>Figure 6.12</b>	Calcium saturation on the ECEC .....	147
<b>Figure 6.13</b>	Base saturation of the ECEC .....	149
<b>Figure 6.14</b>	Average organic carbon.....	150
<b>Figure 6.15</b>	Particle size distribution curves.....	152
<b>Figure 6.16</b>	Saturated hydraulic conductivity in the vertical and horizontal orientation.....	155
<b>Figure 6.17</b>	Moisture characteristic curves.....	157
<b>Figure 6.18</b>	RETC calculated unsaturated hydraulic conductivity curves.....	159
<b>Figure 7.1a</b>	Pre-weir groundwater elevations at piezometer transects C,D and F...	165
<b>Figure 7.1b</b>	Pre-weir groundwater elevations at piezometer transects H, I and K. .	166
<b>Figure 7.2</b>	Positive (a) and negative (b) groundwater gradients towards drains.....	172
<b>Figure 7.3</b>	Groundwater elevation at Transect I showing positive and negative gradients.....	173
<b>Figure 7.4</b>	Groundwater elevation profile - day 90.....	176
<b>Figure 7.5</b>	Groundwater elevation profile - day 180.....	178
<b>Figure 7.6</b>	Groundwater elevation profile - day 235.....	180
<b>Figure 7.7</b>	Groundwater elevation profile - day 302.....	181
<b>Figure 7.8</b>	Groundwater elevation profile - day 362.....	183
<b>Figure 7.9</b>	Hourly groundwater elevation and calculated evapotranspiration .....	185

<b>Figure 7.10</b> Daily fall in groundwater elevation at C10, F10, K10. ....	187
<b>Figure 7.11</b> Average daily change in groundwater elevations during negative groundwater flow gradients (ie, flow away from the drain). ....	190
<b>Figure 7.12</b> Fall of the groundwater level after a flood event .....	192
<b>Figure 7.13</b> Daily rate of groundwater fall at 10 m from the drain.....	193
<b>Figure 7.14</b> Rainfall events that caused no increase in the groundwater elevation. ....	196
<b>Figure 7.15</b> Rise in groundwater elevation due to rainfall. ....	197
<b>Figure 7.16</b> Cumulative rise in groundwater elevation caused by rainfall (Transect I).....	199
<b>Figure 7.17</b> Groundwater elevation for Transect I. Contour line is elevation of potential acid sulfate soil. ....	203
<b>Figure 7.18</b> Period where the groundwater is below the upper boundary of the potential acid sulfate soil for Transects I, J and K.....	204
<b>Figure 7.19</b> Number of days where the groundwater is below the elevation of the upper surface of the potential acid sulfate soil layer .....	207
<b>Figure 7.20</b> Relationship between the elevation of the groundwater table and the potential acid sulfate soil. Transect I through F90, E90, D90 and C90. Hatched area is where the GWL is below the PASS, thereby creating oxidising conditions.....	208
<b>Figure 7.21</b> Relationship between the elevation of the groundwater table and the potential acid sulfate soil. Transect C. Hatched area is where the GWL is below the PASS, thereby creating oxidising conditions. ....	209
<b>Figure 7.22</b> Volume of potential acid sulfate soil exposed to oxidising conditions in the area bounded by Transects C-K.....	211
<b>Figure 7.23(a)</b> Post-weir groundwater elevations at piezometer transects C, D and F.	214
<b>Figure 7.23(b)</b> Post-weir groundwater elevations at piezometer transects H, I and K.	215
<b>Figure 7.24</b> Groundwater elevation profile at day 539 .....	218
<b>Figure 7.25</b> Groundwater elevation profile at day 768 .....	219

<b>Figure 7.26(a)</b> Comparison of the average groundwater elevation at transects C and F, also showing the maximum and minimum groundwater elevation and standard error bars. ....	221
<b>Figure 7.26(b)</b> Comparison of the average groundwater elevation at transects I and K, also showing the maximum and minimum groundwater elevation and standard error bars. ....	222
<b>Figure 7.27</b> Period where the groundwater is below the upper boundary of the pyritic soil for Transect K. ....	225
<b>Figure 7.28</b> Volume of pyritic soil exposed to oxidising conditions adjacent to Transect K during the post-weir period. ....	226
<b>Figure 7.29</b> Drain water level measured at the weir locations.....	228
<b>Figure 8.1</b> Change in soil pH.....	232
<b>Figure 8.2</b> Change in soil electrical conductivity .....	233
<b>Figure 8.3</b> Concentration of pyrite oxidation products at C90. ....	236
<b>Figure 8.4</b> Fe:SO <sub>4</sub> ratio in groundwater.....	241
<b>Figure 8.5</b> Groundwater Al <sup>3+</sup> and total acidity concentration.....	243
<b>Figure 8.6</b> Evolution of groundwater toxicity at C90.....	245
<b>Figure 8.7</b> The Al <sup>3+</sup> :Fe <sup>2+</sup> molar ratio in groundwater at C90. ....	247
<b>Figure 8.8</b> Concentration of basic cations measured at C90.....	248
<b>Figure 8.9</b> Chloride concentration and Cl:SO <sub>4</sub> ratio at C90. ....	250
<b>Figure 8.10</b> Assessment techniques for evolutionary change in groundwater chemistry .....	253
<b>Figure 8.11</b> Relationship between electrical conductivity, total dissolved solids, and the sum of the toxic pyrite oxidation products. ....	255
<b>Figure 8.12</b> Concentration of pyrite oxidation products in the drains. ....	257
<b>Figure 8.13</b> Concentration of environmentally toxic drain water constituents.....	262
<b>Figure 8.14</b> Saline intrusion characterised by chloride and cation concentration ...	265

<b>Figure 9.1</b>	Triangular prismatic element used by FEMWATER.....	273
<b>Figure 9.2</b>	Schematic of FEMWATER mesh. a) side view showing boundary conditions and the initial groundwater level; b) plan view showing element geometry and nodes.....	276
<b>Figure 9.3</b>	Cross section of the drain and weir simulations, and dimension of the flood mitigation drain.....	278
<b>Figure 9.4.</b>	Observed and simulated groundwater elevations.....	280
<b>Figure 9.5.</b>	Initial soil chemical properties for SMASS. ....	284
<b>Figure 9.6.</b>	Groundwater profiles from deep drains.....	286
<b>Figure 9.7</b>	Groundwater elevation at 10 and 90m from drain with rainfall - evapotranspiration. ....	286
<b>Figure 9.8.</b>	Observed and simulated groundwater elevations for water management options. ....	288
<b>Figure 9.9</b>	Measured and simulated pyrite concentrations with depth. ....	290
<b>Figure 9.10.</b>	Cumulative sulfate production and pyrite consumption from water management options.....	292
<b>Figure 9.11.</b>	Amount of pyrite oxidised during simulation period. ....	293
<b>Figure 9.12.</b>	Volumetric moisture content distribution at day 250.....	296
<b>Figure 9.13.</b>	Relative sulfate production for water management options.....	298
<b>Figure 10.1</b>	Schematic of the soil structure and oxygen transport in the pyrite oxidation model. $R$ is the radius of the soil aggregates, $r$ is the radius of the anaerobic zone.....	307
<b>Figure 10.2</b>	Flow chart of FEMWATER and ASS3D models .....	318
<b>Figure 10.3</b>	Solution of Equations (10.11) and (10.13) for oxygen consumption in dependence of the local dissolved oxygen concentration.....	321
<b>Figure 10.4</b>	Dissolved oxygen concentration profiles into the saturated soil matrix.....	322
<b>Figure 11.1</b>	Drain water elevation boundary condition for the existing drain simulation .....	325

<b>Figure 11.2</b> Simulated groundwater elevation.....	327
<b>Figure 11.4</b> Simulated cumulative sulfate production from pyrite oxidation for the existing drain .....	331
<b>Figure 11.5</b> Cumulative sulfate measured in groundwater at 10 m and 90 m from the drain.....	333
<b>Figure 11.6</b> FEMWATER head boundary conditions used to simulate the drain water level for the various drain management options.....	335
<b>Figure 11.7</b> Drain water level under tidal influence.....	336
<b>Figure 11.8</b> Groundwater elevation for drain water levels simulated by variable tidal range on an hourly time step, constant drain level on an hourly time step and constant drain level on an daily time step.....	337
<b>Figure 11.9</b> Simulated groundwater elevations for various drain management options.....	339
<b>Figure 11.10(a)</b> Groundwater elevation at Days 230, 250 and 270 for the Weir -0.3 m AHD drain management option.....	340
<b>Figure 11.10(b)</b> Groundwater elevation at Days 230, 250 and 270 for the Weir -0.5 m AHD drain management option.....	341
<b>Figure 11.10(c)</b> Groundwater elevation at Days 230, 250 and 270 for the tidal ingress drain management option.....	342
<b>Figure 11.11</b> Cumulative sulfate production for the ASS3D simulation of drain management options.....	346
<b>Figure 11.12</b> Relative effectiveness of drain management strategies.....	347
<b>Figure 12.1</b> Moisture characteristic curves for field and laboratory structures soils.....	359
<b>Figure 12.2</b> Acid generation with respect to suction and time for field structured pyritic soil .....	361
<b>Figure 12.3</b> Acid generation with respect to suction and time for laboratory structured pyritic soil with; a) no pores, b) 5 pores and c) 10 pores.....	365

<b>Figure 12.4</b> Amount of acid generated (mol H <sup>+</sup> /tonne) for: (a) field structure and laboratory structure with (b) no pores, (c) 5 pores, (d) 10 pores. ....	367
<b>Figure 12.5</b> Implicit model linking macropore oxygen diffusion and pyrite crystal distribution.....	371
<b>Figure 13.1</b> Neutralising pond strategy for controlled salt water intrusion into drain.	376
<b>Figure 13.2</b> Plot of pe - pH for Fe speciation in groundwater during post-weir period.	379
<b>Figure 13.3</b> Saturation Indices (SI) for Fe and Al minerals at measured pH-pe for Fe, Al, SO <sub>4</sub> and K activities of 5 x 10 <sup>-3</sup> , 1 x 10 <sup>-3</sup> , 5 x 10 <sup>-2</sup> and 5 x 10 <sup>-4</sup> , respectively. ....	381
<b>Figure 13.4</b> Al <sup>3+</sup> activity versus pH with lines of equilibrium with respect to aluminium solid phases gibbsite and jurbanite.....	383
<b>Figure E.1</b> Equilibrium pH for 100 pore volume flushing for CEC simulation.....	472
<b>Figure E.2</b> Cation concentration for 100 pore volume flushing for CEC simulation	473
<b>Figure E.3</b> Equilibrium pH for 100 pore volume flushing for soil with measured CEC/phase composition .....	475
<b>Figure E.4</b> Aqueous species equilibrium for 100 pore volume flushing for soil with measured CEC/phase composition .....	475
<b>Figure E.5</b> Equilibrium pH for 100 pore volume flushing for soil with measured CEC/phase composition with injection of 0.01 M CaCO <sub>3</sub> .....	478
<b>Figure E.6</b> Equilibrium ion concentration for 100 pore volume flushing for soil with measured CEC/phase composition with injection of 0.01 M CaCO <sub>3</sub> .....	479



## LIST OF TABLES

<b>Table 2.1:</b> World wide distribution of acid sulfate soils.....	14
<b>Table 2.2:</b> Soil physical data for an acid sulfate soil profile.....	23
<b>Table 2.3:</b> Components of the water balance for Tuckean Swamp - March 1994 flood .....	34
<b>Table 3.1:</b> Summary of oxidation rates using different methods, cover materials and water levels from Elberling <i>et al.</i> (1994).....	51
<b>Table 5.1</b> Rainfall design criteria for major rainfall events .....	109
<b>Table 6.1:</b> Average dry bulk density for sites P1-5.....	153
<b>Table 6.2.</b> Soil physical properties.....	160
<b>Table 7.1</b> Relations between groundwater elevations and soil topography .....	167
<b>Table 7.2</b> Hydraulic gradients and flow directions for Transect I .....	174
<b>Table 7.3</b> Regression equations: rate of groundwater fall .....	194
<b>Table 7.4</b> Hydraulic gradients and flow directions for Transect C and I.....	216
<b>Table 7.5</b> Difference in average groundwater elevation after installation of the weirs. ....	223
<b>Table 7.6</b> Total discharge across weirs.....	229
<b>Table 9.1.</b> Soil physical properties.....	274
<b>Table 9.2:</b> FEMWATER boundary conditions .....	277
<b>Table 9.3:</b> SMASS input data .....	283
<b>Table 10.1</b> Variables required for of the analytical and numerical solutions .....	
for two pyrite concentrations. ....	320
<b>Table 10.2</b> Analytical and numerical values for $\phi_T$ .....	322

<b>Table 11.1</b>	Measured and simulated pyrite concentrations.....	330
<b>Table 12.1</b>	Regression equations for soil acidity against suction .....	362
<b>Table 12.2</b>	Regression equations for soil acidity against time.....	362
<b>Table 12.3</b>	Change in the pyrite concentration of field structured sample .....	363
<b>Table 12.4</b>	Change in the pyrite concentration of laboratory structured samples.....	366
<b>Table 12.5</b>	Multiple regression coefficients for Equation 12.1 .....	369
<b>Table E.1</b>	Initial and influent water quality for PHREEQC simulations.....	470
<b>Table E.2.</b>	CEC composition used in PHREEQC simulations.....	471

LIST OF PLATES

Plate 4.1 Aerial photo of the study site. .... 85

Plate 4.2 Flood mitigation drain at the study site..... 90

Plate 4.3 Floodgate at the study site..... 91

Plate 4.4. Construction of the weirs..... 96

Plate 4.5 Operation of the high weir. .... 97

Plate 4.6. Installation of a PS300 water level recorder in to a piezometer ..... 102

Plate 6.1 Soil profile features showing the organic rich topsoil, an estuarine clay with jarosite, and the dark grey sulfidic sediments at depth. .... 128

Plate 7.1 Flood event caused by 87 mm rainfall at day 87..... 170

Plate 7.2 Discharge of flood water through floodgate at day 87..... 170

Plate 10.1 Structural features of the potential acid sulfate soil at 1.5 m depth. .... 306

# Chapter 1: Introduction

## 1.1 General background

Acid sulfate soils pose significant constraints with respect to the implementation of environmentally sustainable development within coastal lowland areas in Eastern Australia. Where inappropriate land management strategies have been practiced on land affected by acid sulfate soils, severe environmental, social and economic problems have become apparent as a result of the discharge of large volumes of sulfuric acid and other pyrite oxidation products into estuarine waterways. Strategies that minimise acid generation and/or its discharge to waterways require development, validation and implementation in order to address some of the problems induced by the inappropriate management of acid sulfate soils.

The processes that lead to the generation of acidic pyrite oxidation products and their transport to estuarine waterways in Eastern Australia are now well understood and have been linked to the installation and operation of coastal lowland drainage schemes (Sammut *et al.*, 1996; Pease *et al.*, 1997; White *et al.*, 1997; Wilson *et al.*, 1999). In short, groundwater drawdown from the operation of deep, floodgated drains and evapotranspiration from crops or pastures can cause the groundwater table to fall into or below the elevation of the pyritic soil layer thereby creating the necessary conditions for pyrite oxidation. Pyrite oxidation, particularly in the absence of soil neutralising capacity, generates sulfuric acid and dissolved  $\text{Fe}^{2+}$ . After rainfall causes the groundwater table to rise through the oxidised zone, the acidic pyrite oxidation products are entrained into the groundwater. The groundwater in areas of drained, oxidised pyritic soils is often about pH 3 and has concentrations of dissolved aluminium and iron many orders of magnitude greater than Australian New Zealand Environment Conservation Council (1992) water quality guidelines. The acidic groundwater can be transported to drains via groundwater flow in accordance with the hydraulic gradients caused by the low water level in the drains or by overland flow during flood events.

Very large volumes of acidic drain water have been measured discharging into estuarine waterways from drainage schemes that may result in significant environmental degradation, damage to engineering infrastructure and loss of agricultural/fisheries productivity.

Although the processes that contribute to the generation of acidic pyrite oxidation products from coastal lowlands and their transport to estuarine waterways are understood, this information has not been applied to the development and validation of acid sulfate soil management strategies that are applicable at the sub-catchment scale. Dent (1986), Indraratna *et al.* (1995) and Pease *et al.* (1997) recommended that the generation and transport of pyrite oxidation products could be reduced through the installation of weirs in flood mitigation drains. This research focuses on the validation of improved drain management techniques with respect to the management of pyritic soils.

## **1.2 Objectives of the study**

The specific objectives of this research were:

- The implementation of a comprehensive field trial to verify that groundwater table management using adjustable weirs in flood mitigation drains can achieve significant improvement of the groundwater and drain water quality in areas where acid sulfate soil occur;
- Evaluate the impact of drain management and climatic factors on the groundwater and drain water elevation, soil and water chemistry and drainage of floodwater from a field study site using manual and automatic monitoring techniques;

- The development and application of computer aided geo-hydraulic models to predict the changes in the groundwater regime from the installation of improved drain management techniques and associated changes in acid generation;
- The experimental determination of the rate of acid generation from pyritic soil with field and artificially made macropore structures to develop empirical equations that enable the magnitude of acid generation to be estimated using easy to measure independent variables such as time and depth to the groundwater table;
- Application of geo-chemical equilibrium models to investigate the long term water quality from acid sulfate soils that have acid saturated cation exchange complexes and acidic minerals such as jarosite and alunite that forms under highly acidic conditions caused by pyrite oxidation.

### **1.3 Thesis organisation**

This thesis is divided into five major parts. A brief outline of each part and its component Chapters is described below.

#### *1.3.1 Part I: Literature review*

The nature and properties of acid sulfate soil are described in Chapter 2. This includes a review of the formation and distribution of acid sulfate soils in Australia. In addition, the chemical processes that are involved in pyrite oxidation, the soil physical properties that determine the rate of acid generation and the hydrological interactions between the climate, vegetation, the groundwater regime and acid generation are discussed.

In Chapter 3, a review of pyrite oxidation studies and management strategies is presented. This Chapter discusses field and laboratory studies of acid generation and management of in pyritic soils, simulation models that attempt to predict the magnitude, rate and distribution of acid from pyrite oxidation in both acid sulfate soils and pyritic rock dumps, and the development of acid sulfate soil management strategies at the sub-catchment scale.

### *1.3.2 Part II: Field trial of groundwater table management using weirs*

A major component of this research was the investigation and validation of manipulating groundwater table elevation by the installation of adjustable weirs in flood mitigation drains. Part II of the thesis is divided into five Chapters.

Chapter 4 describes the location and geomorphology of the study site and the equipment used to monitor both physical and chemical attributes of the groundwater and drain water. The design, installation and operation of the three weirs that were placed in the flood mitigation drains at different elevations relative to the pyritic soil layer is also described in Chapter 4.

In Chapter 5, the climatic variables relating to the addition or removal of water from the groundwater aquifer at the study site are presented. The rainfall and evapotranspiration data are presented in two parts, namely, the pre-weir and post-weir periods. The importance of the Southern Oscillation Index for the study period with respect to understanding the climatic conditions that may have caused acid generation and discharge in the past is discussed. Temperature, wind speed and solar radiation data measured during the study period are also shown and briefly discussed in Appendix A.

The chemical, physical and morphological properties of the soils found at the beginning of the monitoring period are described in Chapter 6. A comprehensive soil investigation process was carried out to provide a detailed baseline description of the site conditions at the start of the field trial and to provide site specific input data for initialisation of geo-hydraulic models used in Part III.

The groundwater elevation data measured at the study site are presented in Chapter 7. The groundwater data, and its interpretation, are divided in two parts, namely the pre- and post-weir periods. For the pre-weir period, the dynamic nature of the groundwater table is explained by exploring the processes that contribute to falling and rising groundwater tables. The contributions of evapotranspiration, drawdown from the flood mitigation drains and rainfall to the rise and fall of the groundwater table are presented and discussed. The elevation of the groundwater table is assessed relative to the height of the acid sulfate soil layer at the study site. The distribution and magnitude of acid sulfate soil exposed to oxidising conditions across the study site were determined. The implications of the magnitude and distribution of exposed acid sulfate soil for water and soil quality at the study site is discussed. The influence of installing the weirs at different levels relative to the pyritic soil layer on the groundwater regime is discussed in the post-weir section of Chapter 7. A comparison between the pre and post weir groundwater table dynamics is presented and potential improvements with respect to the adoption of adjustable weirs is also discussed. The change in the drain water level as a result of the installation of the weirs is presented and shown to have negligible influence on the removal of excess floodwater after heavy rainfall.

The changes in soil chemistry, groundwater and drain water quality parameters that occurred with respect to the groundwater dynamics are described in Chapter 8. The temporal changes in soil pH and electrical conductivity are presented and discussed. These data showed that the generation of acid is determined by the groundwater elevation, and that maintenance of high groundwater levels after pyrite oxidation does not substantially improve the chemical properties of the soil. The second part of this Chapter describes changes in the groundwater and drain water chemical properties. The groundwater and drain water chemical properties that were measured at the site are



described and related to the groundwater hydrology that influences the generation and transport of pyrite oxidation products. The evolution of groundwater toxicity from pyrite oxidation is explored, and an assessment technique for interpreting the general toxicity of groundwater after pyrite oxidation events is presented.

### *1.3.3 Part III: Development and application of geo-hydraulic models*

In order to predict the consequences of groundwater management strategies prior to the installation of expensive engineering structures, geo-hydraulic models can be applied to simulate the groundwater regime and the generation and transport of acidic pyrite oxidation products. Three Chapters are presented in Part III of this thesis which use, extend and develop numerical models to investigate the influence of a variety of groundwater management strategies.

Chapter 9 evaluates water management options that may be applicable for the management of acid sulfate soils at the Berry study site using two numerical models. In addition, the utility of the numerical models used for this purpose is also assessed. Groundwater regimes were simulated using FEMWATER, a 3D finite element flow and transport model for variably saturated media (Lin *et al.* 1997), and the oxidation of pyrite was simulated using the Simulation Model for Acid Sulfate Soils (SMASS) developed by Bronswijk and Groenenberg (1992). The modelling period includes a wet period with groundwater being close to the surface as well as a prolonged dry period that resulted in the groundwater falling below the acid sulfate soil layer.

In Chapter 10, a model that simulates the magnitude and distribution of pyrite oxidation in pyritic soil in a three dimensional landscape is described. In the first part of the Chapter, the relevant equations which describe the transport of oxygen through soil macropores and then laterally into the soil matrix where aerobic conditions exist, are derived using a similar approach to that used by Bronswijk *et al.* (1993). The second

part of this Chapter shows how these equations are solved numerically. A description of how the 1D pyrite oxidation numerical scheme is linked to the 3D soil moisture content distribution produced from the simulation of saturated/unsaturated conditions using FEMWATER is also given. A comparison of the analytical and numerical solutions for the oxygen consumption terms derived in the pyrite oxidation model gives very good agreement, indicating that the numerical approach adopted in the ASS3D Fortran code accurately simulates that amount of pyrite oxidised in the soil matrix.

The accuracy and application of the ASS3D model described in Chapter 10 is investigated in Chapter 11. In the first part of this Chapter, ASS3D is validated by comparing the model output to measured field data. ASS3D output compares favourably with the change in pyrite concentration measured at the end of the period simulated. The second part of this Chapter demonstrates the application of the ASS3D model. Four drain management alternatives were simulated, namely the existing drained state, maintenance of elevated drain water levels at -0.5 and -0.3 m AHD through the installation of weirs at these elevations, and the effect of removing the floodgates to allow tidal ingress into the drains.

#### *1.3.4 Part IV: Modeling of acid generation and geochemistry*

The magnitude and rate of acid generation from the oxidation of pyrite and the maintenance of acidic groundwater after the cessation of pyrite oxidation was investigated and the outputs reported in Part IV of the thesis.

In Chapter 12, the rate of acid generation from the oxidation of pyrite was determined for field and laboratory structured pyritic soil. The magnitude of the change in acid production is linked to the height of the pyritic soil above the groundwater table and the time that the pyritic soil remains in that state. Empirical equations that describe the acid generation rate for homogenous and macropore structured soil are presented.

Application of these equations enable land managers to determine the amount of acid produced during periods, where the groundwater table is below the pyritic soil in a semi-quantifiable fashion.

The management of the existing acid that was present in the soil, groundwater and drains is addressed by the application of geochemical concepts in Chapter 13. Two potential acid management strategies were investigated. Firstly, the potential benefits associated with allowing a controlled volume of saline water to intrude into the flood mitigation drains during high tide is investigated. A worked example is used to illustrate the potential improvement in water quality discharged from the drains to Broughton Creek. The second area of investigation is associated with the iron and aluminium geochemistry of acidic minerals in the actual acid sulfate soil. Two geochemical equilibrium models are used to demonstrate that: the groundwater quality will remain poor for a substantial period of time due to the dissolution of acidic iron and aluminium minerals, and the injection of a calcium carbonate slurry into the soil will improve the groundwater quality and facilitate the rapid dissolution of these acidic minerals.

#### *1.3.5 Part V: Conclusions and recommendations*

Conclusions are given in Chapter 14 which summarises the findings of this research in relation to the effectiveness of manipulating groundwater tables by the installation of weirs in flood mitigation drains to control the generation and discharge of pyrite oxidation products. For the benefit of future studies related to the management of pyritic soils, a number of recommendations and issues that require further research are discussed.

## **Chapter 2: Introduction to acid sulfate soils**

This Chapter presents a discussion of the nature and properties of acid sulfate soil. The development and implementation of rehabilitation strategies aimed at mitigating the impact of acid discharge from areas of poorly managed acid sulfate soils requires a thorough understanding of their chemical, physical and hydrological properties and how these properties are interrelated. The behaviour of acid sulfate soils in response to wet and dry climatic conditions and artificial drainage is also described in order to highlight the challenges involved in the development of sustainable management practices land affected by for acid sulfate soils. Identification and understanding of the mechanisms that lead to acid generation from either climatic or management factors provides information that may be employed to rehabilitate degraded actual acid soil areas or at least mitigate against extreme acid discharge events. The first part of this Chapter briefly describes what constitutes acid sulfate soils, how these soils form and how they are distributed, both world wide and in Australia. The behaviour of acid sulfate soil is described in the second part of this Chapter.

### **2.1 Acid sulfate soil**

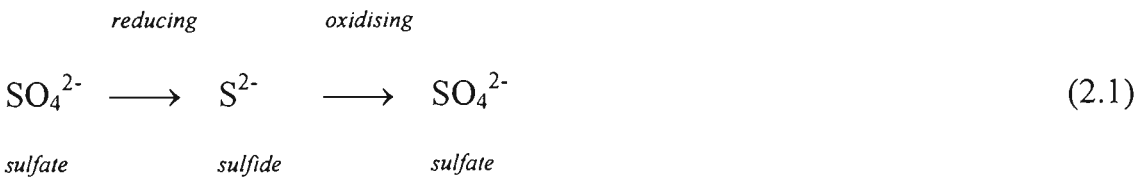
Acid sulfate soil is the common name given to coastal floodplain soil and sediment containing oxidisable, or partly oxidised, sulfide minerals. The usual form of these sulfides is cubic iron pyrite ( $\text{FeS}_2$ ). Other sulfide compounds, such as iron monosulfide ( $\text{FeS}$ ), greigite ( $\text{Fe}_3\text{S}_4$ ) and various organic sulfides, may also exist in small concentrations (Bush and Sullivan, 1996).

Where acid sulfate soils remain under reducing conditions, the sulfides remain chemically stable. These soils are called ‘potential acid sulfate soils’. Sulfide oxidation

can occur where the pyritic soils are exposed to oxygen or other oxidising agents. Oxidising conditions usually occur when potential acid sulfate soils are drained thereby enabling oxygen to enter the pyritic layers. The oxidation reaction generates acidic products which acidifies both the soil and soil water. These acidic soils are called ‘actual acid sulfate soils’. In many instances, oxidising conditions overlie reducing conditions in a soil profile so that actual and potential acid sulfate soils exist in the same soil profile. The term acid sulfate soils refers to the whole soil profile regardless of its oxidation/reduction status. White *et al.* (1996) suggest that the term acid sulfate soil should be used to convey the notion that these soils can pose a significant threat to the integrity of the environment and should be handled with caution.

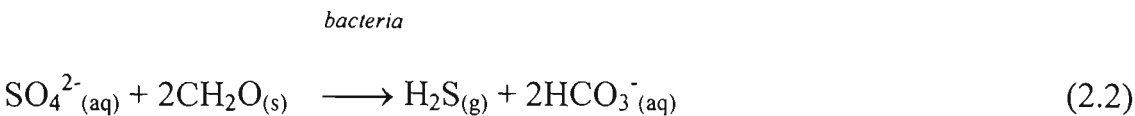
## 2.2 Formation of acid sulfate soils

Acid sulfate soils form part of the global sulfur cycle. In short, dissolved sulfates are reduced to sulfides which precipitate in sediments. When these sediments are exposed to oxygen in the air, the sulfides are oxidised to either soluble sulfates or gases, such as sulfur dioxide. The generalised component of the sulfur cycle, relevant to the formation and oxidation of acid sulfate soils, is described by Equation (2.1).



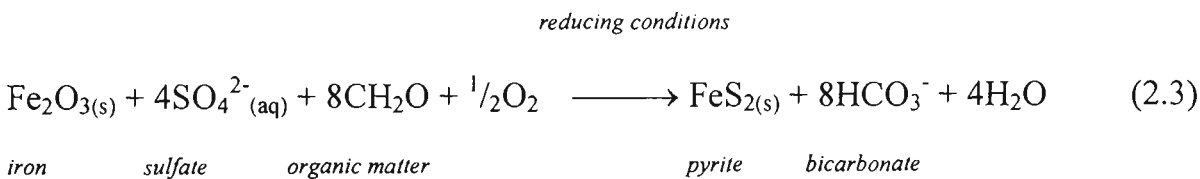
Pyrite is formed in low energy estuarine systems by a bacterial catalysed reaction requiring a reducing environment, a source of sulfate, presence of labile organic matter and a source of iron (Dent, 1986). A reducing environment can be maintained in coastal floodplains where excess rainfall, regular tidal inundation and long water retention times create waterlogged conditions that are essential for the existence of sulfate reducing

bacteria. Dissolved sulfate is abundant in seawater with a concentration of approximately 2700 mg/L. Inundation of low lying land by brackish or sea water provides an ample source of dissolved sulfate for the formation of pyrite. Sulfate reducing bacteria require a source of organic matter for energy as described by Equation (2.2)



Mangroves and coastal wetlands exist in brackish, reducing environments and produce large amounts of organic matter. Iron is abundant in low-lying clay soil and alluvial sediments. Under anoxic conditions,  $\text{Fe}^{3+}$  is reduced to  $\text{Fe}^{2+}$  and made available for pyrite formation.

The formation of pyrite and other associated sulfidic compounds is complex and poorly understood. However, a generalised reaction has been described by Dent (1986) as:



A schematic cross section of a mangrove tidal swamp showing the necessary conditions for pyrite formation is given in Figure 2.1.

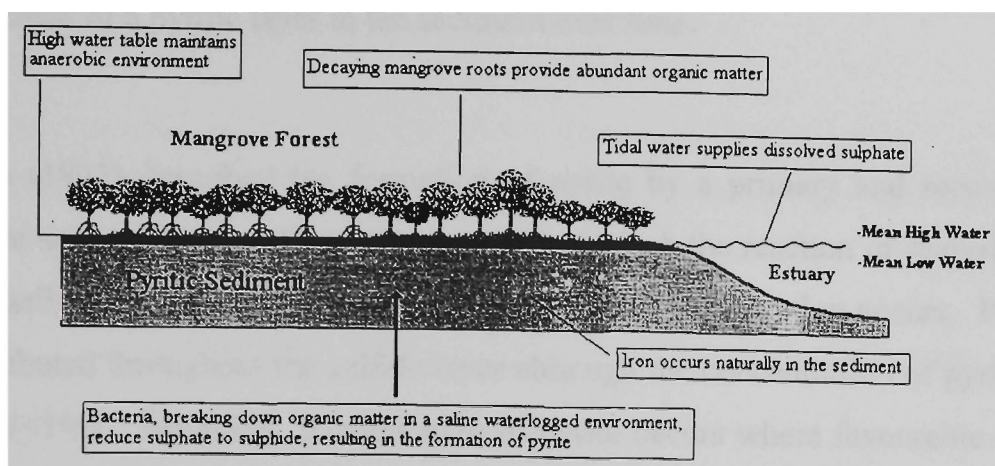


**Figure 2.1** Environmental conditions required for pyrite formation

[from Naylor *et al.* 1995].

Pons (1973) showed that the formation of pyrite in acid sulfate soils is proportional to the organic content of the sediment. Pyrite concentrations have been reported as high as 15% (by mass) in acid sulfate soils from South East Asia, though Australian climatic conditions generally limit the formation of pyrite to concentrations less than 5%.

Even under favourable conditions, the rate of formation of pyrite is very slow. Dent (1986) suggested that it may take in the order of 100 years to form 1% pyrite (by mass) in reduced sediments. The conversion of iron monosulfide ( $\text{FeS}$ ) to pyrite ( $\text{FeS}_2$ ) is a typically slow solid-solid reaction. However, the precipitation of pyrite from dissolved  $\text{Fe}^{2+}$  reacting with dissolved  $\text{SO}_4^{2-}$  is significantly quicker. Warmer temperatures and slightly acidic conditions enhance the kinetics for the pyrite formation pathways.

Wada and Seisuwan (1988) propose that pyrite is formed at the interface of oxidising and reducing conditions in the sediment profile. Sediments closer to the surface have a higher oxidation status than deeper sediments that will enable  $\text{Fe}^{2+}$  to be oxidised to  $\text{Fe}^{3+}$ .  $\text{H}_2\text{S}$ , produced by the microbial reduction of sulfate at depth (see Equation 2.2), diffuses towards the surface. Where upwardly diffusing  $\text{H}_2\text{S}$  meets with dissolved  $\text{Fe}^{2+}$ , pyrite will form. Where sediment accumulation occurs at a slow rate, the zone of pyrite

formation rises with the height of the deposited sediment leading to the increasing thickness of a pyritic layer in the sediment over time.

Pons (1973) described the formation of pyrite by a primary and secondary reaction. Pyrite accumulates by the primary reaction through the reaction of seawater ( $\text{SO}_4^{2-}$ ) and the sediment ( $\text{Fe}^{3+}$ ) at the soil-water interface when inundation occurs. Pyrite is evenly distributed throughout the sulfide layer although the concentration of pyrite is generally low (<1%). Secondary accumulation of pyrite occurs where favourable conditions are present in micro-environments, usually associated with root channels or decaying organic matter covered by sediment. The distribution of pyrite in the sediment formed by the secondary reaction is extremely heterogenous.

Bush and Sullivan (1996) confirmed the secondary accumulation process and reported that the distribution of pyrite is strongly correlated to structural features in the sediment. In non-root soil material, Bush and Sullivan (1996) found that framboidal, irregular massive clusters and unordered loose microcrystalline clusters were found in planar fissures, other structural pores, and within the clay matrix. Partly decomposed root remnants were frequently filled and coated with botryoidal clusters of pyrite framboids and loose clusters of unordered micro-crystals. A large variation was also reported in the size distribution of pyrite in the sediment, ranging from 0.5  $\mu\text{m}$  for individual pyrite crystals to 20  $\mu\text{m}$  for framboids.

Alkalinity in the form of bicarbonate ions is a reaction product of pyrite formation reaction (Equations 2 and 3). In waterlogged environments, bicarbonate ions cannot be precipitated from the soil solution and are subsequently lost from the soil by leaching. Loss of stored alkalinity from the soil has significant implications with respect to the rate and concentration of acid generated during oxidation of pyrite. Where the concentration of pyrite is in excess of the acid buffering capacity of the sediment, there is potential for the system to be a net generator of acid.



2.3 Distribution of acid sulfate soils

The area of acid sulfate soils deposited during the Holocene epoch occupies between  $10^7$ - $10^8$  ha throughout the world (Brinkman, 1982) as shown in Table 2.1.

**Table 2.1:** World wide distribution of acid sulfate soils  
(after Brinkman, 1982)

Region	Area of ASS (x 10 <sup>6</sup> ha)
Africa	3.7
Asia	6.7
Latin America	2.1
Australia	1.0

The conditions suitable for the formation of pyrite in sediments lend useful clues to the location of acid sulfate soils in the coastal zone (Naylor *et al.*, 1995). Acid sulfate soils occur in wave protected mangroves and marches, outer barrier tidal lakes, and backswamp areas where the accumulation of organic matter and reduced sediments can occur (Naylor *et al.* 1995). Roy (1984) shows that these geomorphological features extend the length of the NSW coastline. Since tectonic activity in eastuer Australia has been limited it is important to recognise that acid sulfate soils also exist in relics of these environments. The distribution of acid sulfate soils mapped by Naylor *et al.* (1995) is shown in Figure 2.2.

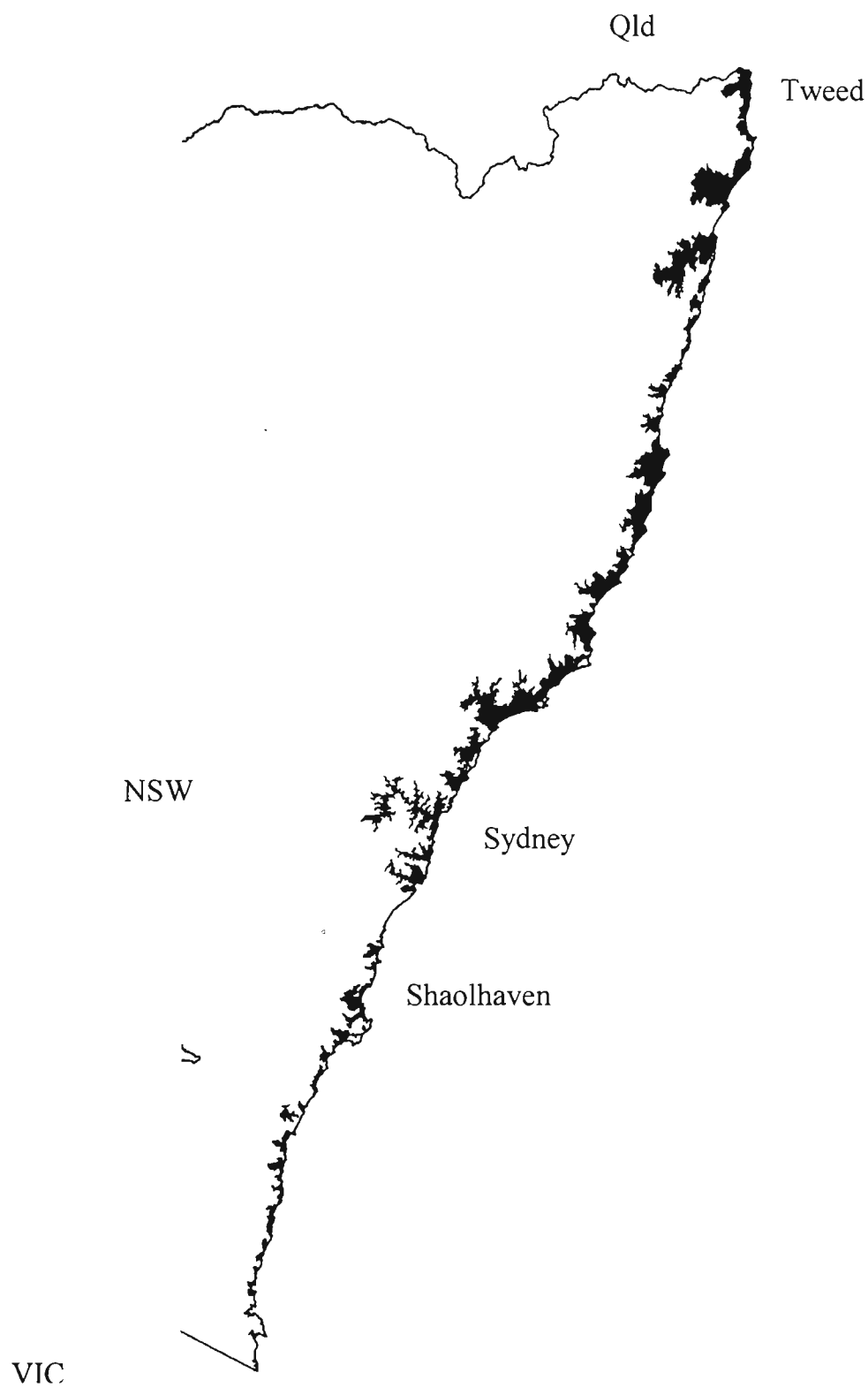


**Figure 2.2:** Distribution of acid sulfate soils in coastal NSW.

[after Naylor *et al.*, 1995]

The surface of the sulfidic horizon should be close to the elevation of mean sea level when the acid sulfate soil was being formed. In eastern Australia, this is about 1 m above the current mean sea level or 1 m Australian Height Datum [AHD]. The acid sulfate soil has been buried by a variable thickness of alluvial or peat soil, usually to a depth of less than 10 m. It is, therefore, a reasonable assumption to preclude the presence of acid sulfate soils from coastal land at elevations in excess of 10 m AHD.

The extent of acid sulfate soils in Australia estimated by Brinkman (1982) in Table 2.1 appears to be understated. Naylor *et al.* (1995) have mapped landform elements likely to contain acid sulfate soils for the coast of New South Wales (approximately 1500 km in length). These maps show that New South Wales has  $0.4\text{--}0.6 \times 10^6$  ha of acid sulfate soils. White *et al.* (1997) suggest that acid sulfate soils are likely to occur through extensive areas of Queensland, the Northern Territory and Western Australia. If the extent of acid sulfate soils throughout Northern Australia is similar to that in New South Wales, then more than  $3 \times 10^6$  ha of acid sulfate soils may exist in Australia (White *et al.*, 1997). The potential for acid generation from acid sulfate soils was reported during the period of aggressive implementation of flood mitigation works in NSW by Walker (1972), however, his recommendations with respect to the drainage these soils were not adopted.

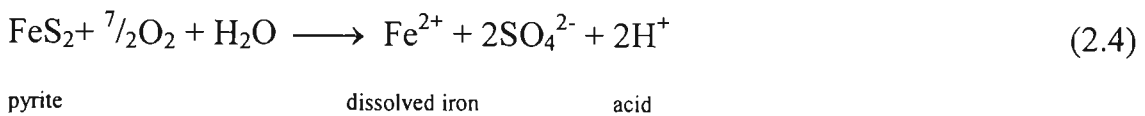
## **2.4 Properties of acid sulfate soils**

The chemical, physical and biological reactions, and the interactions between these processes, that occur during the oxidation of pyrite in acid sulfate soils, are complex and not well understood (Dent, 1986). In general terms, three principal processes combine to generate and transport toxic acidic products from acid sulfate soils to the broader environment. These processes include the chemistry of pyrite oxidation and the generation of acidic toxicants, soil physical processes that enable oxidation to occur, and

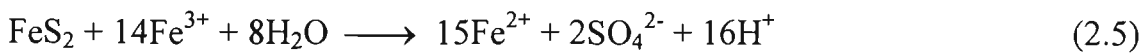
the landscape hydrology that controls the water balance across the site. A summary of how these processes influence acid sulfate soils is described below.

#### 2.4.1. Oxidation processes

Pyrite in moist acid sulfate soils will oxidise when its is exposed to oxygen. As the soil pH falls below 4, oxidation occurs rapidly through a temperature dependant, bacteria catalysed reaction. The oxidation reaction involves the conversion of solid pyrite to dissolved iron and sulfate through a series of complex oxidation steps (Willett *et al.*, 1992). This reaction can be summarised as:

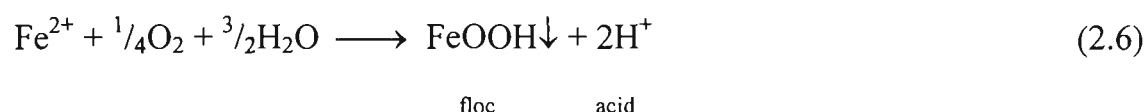


Dissolved  $\text{Fe}^{2+}$  produced in Equation (2.4) may be oxidised to  $\text{Fe}^{3+}$ , a reaction which generates more acid. If the  $\text{pH} > 4$ , a precipitate of ferric hydroxide will form. If the  $\text{pH} < 4$ ,  $\text{Fe}^{2+}$  can remain in solution.  $\text{Fe}^{3+}$  can directly oxidise pyrite whilst it undergoes a reduction reaction, thereby promoting an  $\text{Fe}^{2+} \leftrightarrow \text{Fe}^{3+}$  cycle, which accelerates the pyrite oxidation process. This reaction, catalysed by the influence of *Thiobacillus ferrooxidans*, can be described by:



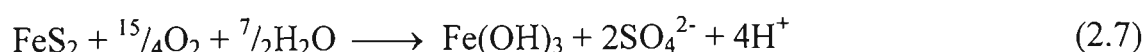
Where inundation of oxidised acid sulfate soils occurs, thereby limiting the source of oxygen, oxidation of pyrite by the reduction of  $\text{Fe}^{3+}$  can still occur as described in Equation (2.5), provided the soil remains at  $\text{pH} < 4$ . This reaction may continue until such a time as sufficient  $\text{Fe}^{3+}$  is leached from the soil to stop the oxidation of pyrite.

Under acidic conditions,  $\text{Fe}^{2+}$  liberated as shown in Equations (2.4) and (2.5) is soluble and can be transported into streams at a considerable distance from the source of pyrite (Nguyen and Wilander, 1995). In the stream,  $\text{Fe}^{2+}$  oxidises to produce ferrihydrite ( $\text{FeOOH}$ ), the characteristic red-brown floc, and a further 2 moles of acid. This reaction can be described by:

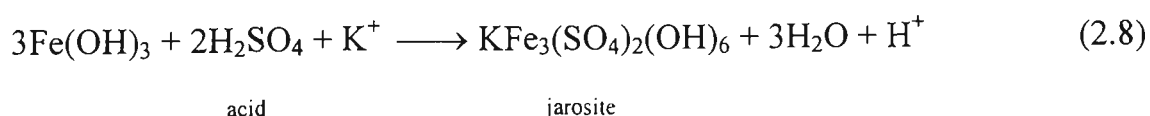


Iron flocs contribute to environmental and infrastructure damage by smothering benthos (Sammut *et al.*, 1996) and clogging bores and filters. The  $\text{Fe}^{2+}$  oxidation reaction consumes oxygen from the water column and can give rise to low dissolved oxygen concentrations in streams.

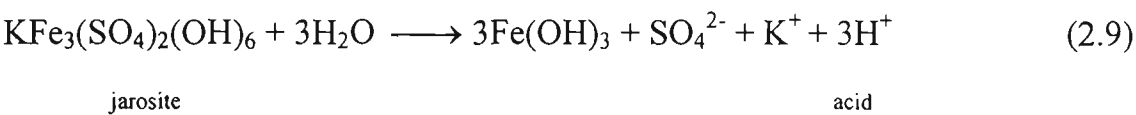
The overall reaction for the complete oxidation of pyrite in moist sediments has been described by Dent (1986) as:



For each mole of pyrite that is oxidised, four moles of acid are produced. Partial oxidation products such as jarosite, the pale yellow coloured mineral,  $\text{KFe}_3(\text{SO}_4)_2(\text{OH})_6$ , are commonly formed under strongly acidic conditions during the reaction process and can be used as an indicator of previous pyrite oxidation. The formation of jarosite is described by:



Jarosite hydrolyses slowly and represents a substantial store of acidity in the oxidised soil profile as shown in Equation (2.9).



Clay minerals can dissolve under strong acidic conditions to release silica and metal ions. Nriagu (1978) showed that the hydrolysis of the common estuarine clay, illite, under acidic conditions liberates soluble aluminium, iron, potassium, sodium and magnesium. Willett *et al.* (1992) and van Breeman (1973) showed that manganese and trace heavy metals can also be released. Blunden *et al.* (1997), Sammut *et al.* (1996) and many others report that the concentration of dissolved metals, particularly aluminium and iron, is logarithmically proportional to the soil solution and/or groundwater pH. This is illustrated in Figure 2.3 using data from Blunden *et al.* (1997),

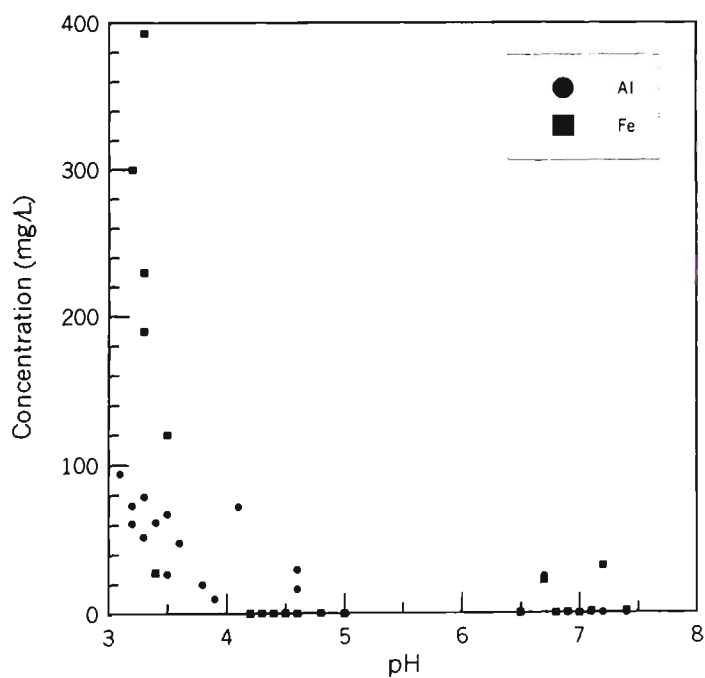


**Figure 2.3:** Relationship between pH and the concentration of Al<sup>3+</sup> and Fe<sup>3+</sup>

Metal toxicity is dependent on the nature and concentration of the specific metal ions, the nature and concentration of suspended particulate matter, pH, redox potential,

salinity, alkalinity, temperature, competing cations and a host of other physio-chemical factors (Ferguson and Eyre, 1996). However, the solubility of monomeric forms of common metal ions (for example, Al, Fe) increases as pH falls below pH~5.5. Sammut *et al.* (1995) reported that dissolved species of monomeric aluminium and iron contribute to the injury and death of fish and crustaceans. ANZECC (1992) recommended that aluminium concentrations in coastal waterways should be less than  $5\mu\text{g L}^{-1}$  when the  $\text{pH} < 6.5$  to ensure ecosystem protection. Sammut *et al.* (1996), Indraratna and Blunden (1997) and many others have reported dissolved aluminium concentrations up to three orders of magnitude in excess of these guideline recommendations in surface and groundwater discharged from oxidising acid sulfate soils.

Various metals, such as nickel and cobalt, may substitute for iron during pyrite formation. Similarly, copper, zinc, lead and arsenic sulfides are related to pyrite and may exist in small concentrations in acid sulfate soil environments. During sulfide oxidation, these metals may be released in soluble forms (van Breeman, 1992).

The pH decrease caused by pyrite oxidation is mitigated by the neutralising capacity of the soil (van Breeman, 1992). Calcium carbonate, clay dissolution and exchangeable bases are important for instantaneous in situ acid neutralisation. Where acid neutralising materials are abundant and of sufficiently small particle size to react instantaneously with acid, the rate of pyrite oxidation is retarded by reducing the catalytic effect of the  $\text{Fe}^{3+}$  reduction-pyrite oxidation reaction. Caution must be exercised when assessing the buffering capacity of acid sulfate soil so that non-reactive calcium carbonate (such as coarse shells) is excluded from any calculation of in situ neutralising capacity (Blunden and Naylor, 1995). Also of concern is the change in composition of cations on the cation exchange complex of soil under severely acidic conditions. Where low soil pH occurs, agriculturally beneficial cations such as calcium, magnesium and potassium are replaced on the exchange complex by acidic cations such as hydrogen and aluminium, both of which are toxic to plants in elevated concentrations.

The chemistry and kinetics of pyrite oxidation are more complex than suggested by Equations 2.4-2.7. Different sulfur species of intermediate oxidation states ( $S^0$  to  $S^{4+}$ ) may be formed, and various autotrophic iron and sulfur bacteria are involved in different oxidation steps (van Breeman, 1992). However, for practical purposes relating to the management and rehabilitation of acid sulfate soils, the descriptions of the reactions described above are adequate.

#### *2.4.2 Soil physical properties*

The physical properties of acid sulfate soils determine the rate of acid generation and discharge to the surrounding environment. Potential acid sulfate soils are generally saturated estuarine clays. In many instances, the potential acid sulfate soils have volumetric moisture contents between 80-120% giving rise to a soil texture approaching that of a gel (White and Melville, 1993). These soils are texturally uniform with a fine, tortuous, heterogenous pore space. The absence of large and/or continuous pore space ensures that the hydraulic conductivity and oxygen diffusivity of these soils is extremely low. Chapman (1994) reported saturated hydraulic conductivities between 0.83-1.21  $\text{mm h}^{-1}$  for potential acid sulfate located near Berry, NSW. Low hydraulic conductivity impedes drainage of these soils and the influx of oxygen into the profile, thereby limiting any potential for the oxidation of pyrite.

After burial of acid sulfate soils by younger alluvial sediments and less frequent tidal inundation, sodium is leached from the cation exchange sites on the clays by fresh water and is replaced by higher valance cations, such as calcium and magnesium. Similarly, hydrogen and aluminium ions are liberated from the cation exchange sites. When higher valance basic cations occupy the cation exchange sites, the clays flocculate, forming aggregates. Such aggregation causes significant change in the pore size distribution (i.e., tending towards larger pores) thereby allowing greater drainage and



diffusion of oxygen into the soil profile. Oxygenation of the soil also gives rise to exploration by plant roots and soil fauna in search of soil moisture. Roots and burrows increase the macroporosity, permeability and diffusivity of the soil. The establishment of vegetation above potential acid sulfate soils also gives rise to dewatering of the profile by evapotranspiration. Entry of oxygen into the potential acid sulfate soil layer causes oxidation of pyrite in accordance with Equation (2.7). Inherent in the pyrite oxidation process are irreversible changes to the colloidal structure of the clay fraction of the soil. This process is called 'ripening' by van Breeman (1973) and Dent (1986). In the ripening process, potential acid sulfate soils undergo irreversible shrinkage due to the removal of water from the profile and are transformed over geological time scales into dryland, non-acid sulfate soils.

Water is lost through consolidation of the saturated potential acid sulfate sediment by the overlying alluvial material deposited on top of it, evaporation from the surface and through extraction of water by plant roots. Oxidation of pyrite is promoted down preferred pathways created by old roots. Severe acidification caused by oxidation of pyrite strips clay colloids of some cations. The soluble oxidation products help flocculate the unconsolidated clays. The flocculated clays form an aggregated soil structure which is more permeable to oxygen and therefore enhances the oxidation of pyrite in the ripening acid sulfate soil. Oxidation products are transported more rapidly through the more porous flocculated soil matrix and macropores caused by roots. Flocculation of the clay by oxidation products leads to the irreversible shrinkage of the deposited clays. White and Melville (1993) reported that a potential sulfate soil with 80% volumetric moisture content had a shrinkage of 50% upon complete drying. The flocculated clays do not disperse on rewetting that occurs during rainfall or flooding. Thus, the ripening process gives rise to accelerated rates of pyrite oxidation in the acid sulfate soil layers as the generation of acid leads to greater ripening. Arresting the self promoting ripening-oxidation cycle is extremely difficult but necessary to prevent the generation and discharge of acid.

Ripening of potential acid sulfate soils to actual acid sulfate soils occurs above the water table in unsaturated soil horizons where sufficient oxygen can react with pyrite. A

typical acid sulfate soil profile may include a surface layer of non-pyritic alluvium, a horizon of actual acid sulfate soil grading down into unconsolidated potential acid sulfate clay gels below the water table. White and Melville (1993) reported substantial changes in soil physical indices for an acid sulfate soil profile near Tweed Heads (NSW). These data are shown in Table 2.2.

**Table 2.2:** Soil physical data for an acid sulfate soil profile.

(from White and Melville, 1993)

Soil horizon	$K_{sat}$ (mm h <sup>-1</sup> )	Bulk density (t m <sup>-3</sup> )	Air filled porosity (vol vol <sup>-1</sup> )
Jarosite layer	33.0	0.98	0.35
Transition zone	28.6	0.89	0.13
Blue estuarine clay	1.1	0.57	0.0

As the permeability of the soil increases, the conditions for pyrite oxidation become more favourable. The ripening process becomes self-fulfilling where changes to the soil structure induced by severe acidification promote further oxidation of pyrite which generates even more acid.

2.4.2.1 *Oxygen transport*

The concentration of oxygen in acid sulfate soil is the main determinant of the rate of pyrite oxidation. Diffusion is the main transport mechanism for the entry of oxygen into the soil (Refsgaard *et al.*, 1991), when disregarding advective transport through very large cracks in the soil and/or air pressure differences within the soil profile. The diffusion process is described by Fick’s second law:

$$\frac{\partial C_a}{\partial t} = D \frac{\partial^2 C_a}{\partial z^2} \quad (2.10)$$

where  $D$  is the diffusion coefficient of oxygen in the soil,  $C_a$  is the concentration of oxygen in soil air,  $z$  is depth and  $t$  is time.

Several empirically derived relationships between the diffusion coefficient and air-filled porosity have been reported (e.g., Troeh *et al.*, 1982; Hodgson and MacLeod, 1989). These relationships show that the diffusion coefficient is dependant upon the air-filled porosity, and by difference, the volumetric moisture content of the soil.

Once the oxygen diffusion coefficient for a soil is known, the concentration of oxygen in the soil pore space can be determined using equations like that developed by Refsgaard *et al.* (1991):

$$\frac{\partial \epsilon_g C_a(x)}{\partial t} = \frac{\partial}{\partial x} \left( D_s(\epsilon_g) \frac{\partial C_a(x)}{\partial x} \right) - \alpha_v \quad (2.11)$$

where,  $C_a(x)$  is the concentration of oxygen in air-filled pores ( $\text{m}^3 \text{ m}^{-3}$ ),  $D_s$  is the diffusion coefficient of oxygen in air-filled pores ( $\text{m}^2 \text{ d}^{-1}$ ),  $t$  is time (d),  $x$  is distance (m),  $\alpha_v$  is the volumetric oxygen consumption rate ( $\text{m}^3 \text{ m}^{-3} \text{ d}^{-1}$ ) and  $\epsilon_g$  is air-filled porosity ( $\text{m}^3 \text{ m}^{-3}$ ).

As noted earlier, the oxidation of pyrite is directly related to the concentration of oxygen within the acid sulfate soil. Once the concentration of oxygen in a potential acid sulfate soil is determined, it is relatively simple to calculate the rate of pyrite oxidation and the generation of oxidation products according to Equation (2.7).

#### 2.4.2.2 Water flow in soils

The flow and moisture status of water in soil is caused by differences in hydraulic head within the soil profile. In unsaturated soil, the hydraulic conductivity is dependant on the moisture content ( $\theta$ ) of the soil. Hence, an unsaturated hydraulic conductivity function,  $K(\theta)$ , can be determined. The flux of water through unsaturated soil at a specific soil volumetric moisture content can be determined by the solution of Darcy's Law. Darcy's Law in one dimension can be expressed as:

$$q_x = -K(\theta) \frac{\partial H}{\partial x} \quad (2.12)$$

where,  $q_x$  is the component of the soil-water flux in the x direction and  $H$  is the total pressure potential (unsaturated flow).

By substituting Darcy's Law into the continuity equation, a general unsaturated flow equation can be described for three dimensional water flow in isotropic media. This equation is defined as:

$$\frac{\partial \theta}{\partial t} = \frac{\partial}{\partial x} \left( K(\theta) \frac{\partial H}{\partial x} \right) + \frac{\partial}{\partial y} \left( K(\theta) \frac{\partial H}{\partial y} \right) + \frac{\partial}{\partial z} \left( K(\theta) \frac{\partial H}{\partial z} \right) \quad (2.13)$$

Substituting  $H = z + h$  yields:

$$\frac{\partial \theta}{\partial t} = \frac{\partial}{\partial x} \left( K(\theta) \frac{\partial h}{\partial x} \right) + \frac{\partial}{\partial y} \left( K(\theta) \frac{\partial h}{\partial y} \right) + \frac{\partial}{\partial z} \left( K(\theta) \frac{\partial h}{\partial z} \right) + \frac{\partial K(h)}{\partial z} \quad (2.14)$$

where,  $z$  is depth relative to an arbitrary datum and  $h$  is the matric potential in the soil.

Since  $\theta$  is related to  $h$  via the soil water retention curve,  $K(\theta)$  can also be expressed as  $K(h)$ . Through the introduction of the specific water capacity  $C(h)$ :

$$\frac{\partial \theta}{\partial t} = \frac{d\theta}{dh} \frac{\partial h}{\partial t} = C(h) \frac{\partial h}{\partial t} \quad (2.15)$$

where,  $C(h)$  is the slope of the water retention curve. Equation (2.14) can be converted into an equation with one dependant variable. Replacing  $K(\theta)$  with  $K(h)$  and substituting into (2.14) yields the well known Richard's Equation (2.16), describing the flow of water in a 3 dimensional porous media:

$$\frac{\partial \theta}{\partial t} = C(h) \frac{\partial h}{\partial t} = \frac{\partial}{\partial x} \left( K(h) \frac{\partial h}{\partial x} \right) + \frac{\partial}{\partial y} \left( K(h) \frac{\partial h}{\partial y} \right) + \frac{\partial}{\partial z} \left( K(h) \frac{\partial h}{\partial z} \right) + \frac{\partial K(h)}{\partial z} \quad (2.16)$$

Solution of Richard's Equation for defined boundary and initial conditions enables the volumetric moisture content and water flux to be determined for a three dimensional soil profile. This data can be employed in the calculation of oxygen diffusivities for the subsequent determination of the concentration of oxygen in the soil pore space and oxidation of pyrite.

#### 2.4.2.3 *Water retention and unsaturated hydraulic conductivity curve*

Where unsaturated soil conditions exist, the soil water matrix potential is negative. Soil macropores drain according to their diameter, with large pores offering least resistance to the suction applied by drainage or evapotranspiration. As drying increases and the applied matrix suction ( $h$ ) becomes more negative, progressively smaller macropores are drained of water and are subsequently filled with air. The amount of water remaining in

the soil at equilibrium is a function of the size and volume of the water-filled pores and hence is a function of the matrix suction.

The soil structure affects the shape of the soil moisture characteristic curve, particularly in determining the air-entry value (often in the range  $-1 < h < -10$  kPa), which corresponds to the suction at which the largest pores will start to drain. Where soils have continuous, large macropores created by roots or soil fauna, these pores readily drain at relatively low matrix potential thereby increasing the air-filled porosity of the soil and enabling diffusion of oxygen into the soil profile. In fine textured soil with few macropores (or where pores have been reduced in size by compaction), the capillary forces holding water in the pores are greater, resulting in loss of water from the pores only at a relatively high applied suction. The general form of the relationship between soil moisture content, hydraulic conductivity and suction are shown in Figure 2.4 for a sand and a clay.

van Genuchten (1980) empirically derived an “S” shaped curve for the water retention function and formulated a closed-form analytical expression for the unsaturated hydraulic curve using the Mualem (1976) statistical pore size conductivity model. It is important to note that the van Genuchten (1980) expression is valid only for non-swelling soils, which include most acid sulfate soils. The van Genuchten equation is:

$$\theta = \theta_r + \frac{\theta_s - \theta_r}{(1 + |\alpha h|^n)^m} \quad (2.17)$$

where  $\theta_s$  is the saturated volumetric moisture content,  $\theta_r$  is the residual moisture content,  $\alpha$  is a shape parameter approximately the inverse of the air entry value ( $\text{m}^{-1}$ ),  $n$  is a dimensionless shape parameter and  $m=1-1/n$ .

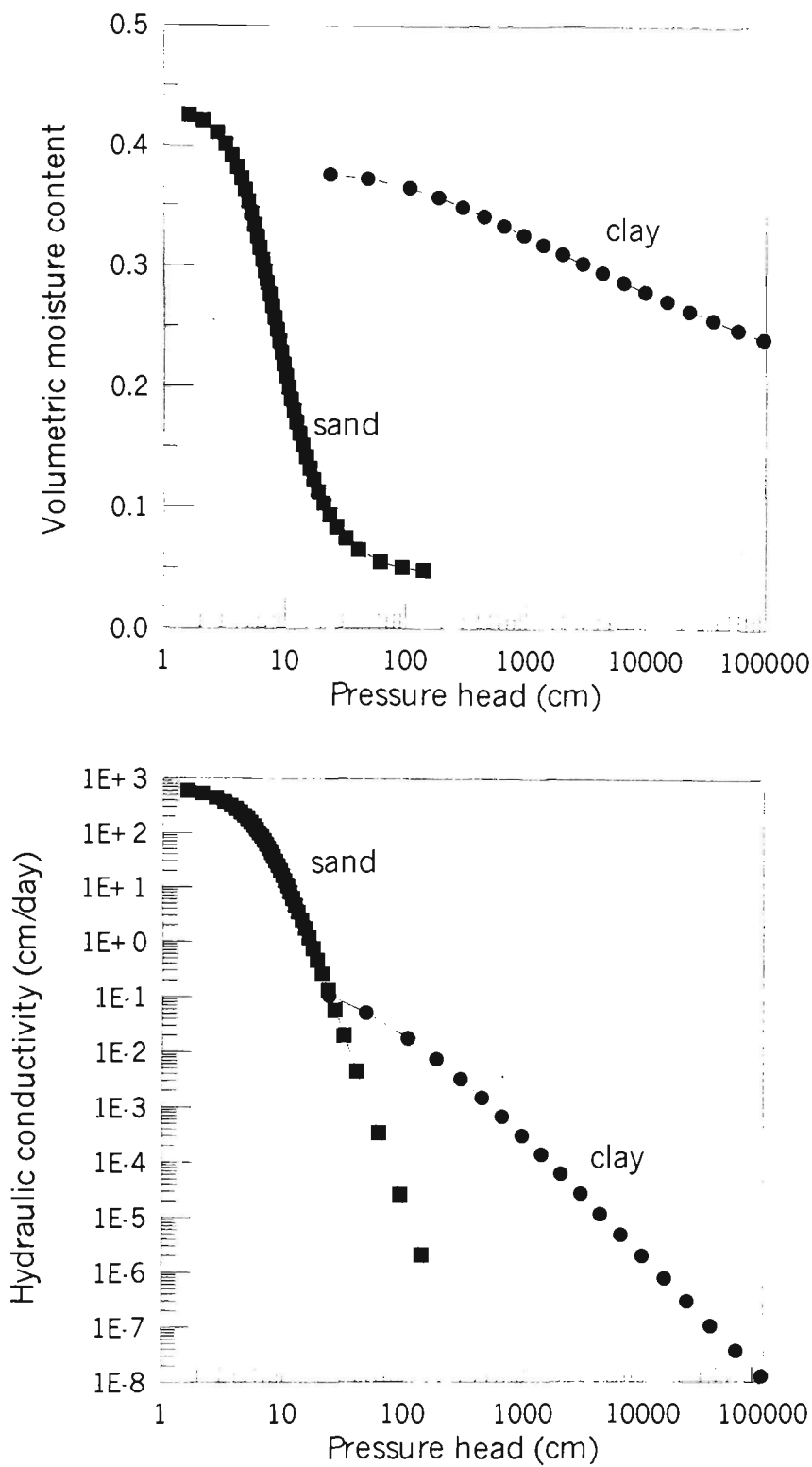


**Figure 2.4:** Soil water retention and hydraulic conductivity for a clay soil.

Combining (2.17) with the Mualem hydraulic conductivity model describes unsaturated hydraulic conductivity as a function of the soil-water matrix potential. This closed-form analytical expression is:

$$K(h) = K_s \frac{\left[1 - |\alpha h|^{n-1} (1 + |\alpha h|^n)^{-m}\right]^2}{\left[1 + |\alpha h|^n\right]^{m\lambda}} \quad (2.18)$$

where,  $K_s$  is the saturated hydraulic conductivity and  $\lambda$  is a shape parameter depending on  $dK/dh$ .

Other researchers, including Fredlund *et al.* (1994) and Leong and Rahardjo (1997), have developed closed-form equations to derive unsaturated hydraulic conductivity expressions from moisture retention curves. In the main, these newer expressions are more complex than the van Genuchten equation and offer only marginal improvement in the accuracy of determining  $K(h)$ . All the closed-form equations appear to derive very similar outcomes for  $K(h)$ , where  $h$  is close to zero (i.e., near saturation). Given that acid sulfate soils are likely to remain relatively wet even under ‘normal’ climatic conditions, calculation of the  $K(h)$  function by any of the closed form equations described above should give a reasonably accurate approximation for the physical parameters of the soil likely to be encountered in the field. In fact, many numerical simulation models derive soil material properties by using van Genuchten input parameters (e.g. FEMWATER, HYDRUS-2D, SWMS-3D).

Once the volumetric moisture content ( $\theta$ ) of the soil can be established, the air-filled porosity ( $\theta_a$  or  $\varepsilon$ ) of the soil can be calculated by  $\theta_a = \theta_s - \theta$ . The diffusivity of oxygen in a soil profile increases as the air-filled porosity increases. Equation (2.19) describes an empirically derived relationship between the oxygen diffusion coefficient and air-filled porosity down a vertical section of the macropore space (Bronswijk *et al.*, 1993).

$$D_s(\varepsilon_g) = F \times \left[1 - (1 - \varepsilon_g)^{\frac{2}{3}}\right] \times D_o \quad (2.19)$$

where,  $D_o$  is the oxygen diffusivity in the air ( $\text{m}^2 \text{d}^{-1}$ ) and  $F$  is a tortuosity factor.



The distribution of water in the soil profile determined by the solution of Richard's equation can be readily converted to give the air-filled porosity of a soil at a particular depth within a profile.

### 2.4.3 Hydrological interactions

The generation and transport of acid produced from the oxidation of pyrite in sulfidic sediments is largely determined by the shallow groundwater hydrology of the catchment. Various studies, summarised by White *et al.* (1997), show that it is essential to know:

- a) the depth of the acid sulfate soil layer from the surface;
- b) the dynamics of the groundwater table relative to the acid sulfate soil layer;
- c) the impact of climate, drain and land management on the floodplain water balance and its control of water table dynamics and export of oxidation products.

in order to develop appropriate acid sulfate soil management strategies or to better manage existing drains in areas affected by acidification.

A simplified representation of the water balance of a coastal floodplain (White *et al.* 1997) may be described by:

$$\begin{array}{ccccccc}
 P + I + L_i & = & E_t + R + L_o & + & D & + & \Delta S \\
 \text{inputs} & & \text{outputs} & & \text{storage} & & 
 \end{array} \tag{2.20}$$

where, P is precipitation, I is irrigation,  $L_i$  is the lateral inflow of water,  $E_t$  is evapotranspiration, R is surface runoff, D is drainage to the water table,  $\Delta S$  is change in soil moisture content above the water table, and  $L_o$  is the lateral outflow.

Using Equation (2.20), a simple assessment of the implications of land and water management in areas of acid sulfate soils can be undertaken. Acid sulfate soils occur in coastal floodplains where  $P > E_t$ .  $R$  and  $L_o$  can be large components of the water balance, resulting in the inundation of low lying backswamps for considerable periods of time. In order to use such low lying areas for agricultural purposes, extensive drainage networks have been constructed to efficiently remove excess surface water. One-way floodgates have been installed where drainage systems discharge into tidal systems at low tide to protect against inundation and to drain the land as quickly as possible.

Channelised, high density drainage systems have greatly increased the rate of  $L_o$ . Where backswamps may have been inundated for say 100 days under natural hydraulic conditions, the installation of floodgated drainage systems has resulted in excess water being removed from backswamps in less than one week. Since drainage does not alter  $P$  or  $E_t$  (assuming that crop vigour approximates native vegetation water use) but greatly increases  $L_o$ , a net increase in the water discharged from the system occurs. This results in a lowering of the watertable below its natural position. When the watertable is lowered below the level of sulfidic sediments, pyrite is oxidised, thereby acidifying the unsaturated soil column above the watertable. Acid is subsequently discharged via the efficient drainage system by removing shallow groundwater directly to the drains and by the removal of excess surface water on filling of the acidified storage component of the soil profile during subsequent flooding.

According to White *et al.* (1997), the change in height of the shallow water table ( $\Delta H$ ) at any given time period is a function of the vertical drainage ( $D$ ), lateral groundwater inflow ( $L_{gi}$ ) and outflow ( $L_{go}$ ), evaporation from the water table ( $E_g$ ) and the available porosity of the soils expressed as the specific yield ( $Y_s$ ), which is the volume of groundwater per unit area per unit change in water table height. The shallow groundwater dynamics in the vertical plane can be calculated by:

$$Y_s \cdot \Delta H = D + L_{gi} - E_g - L_{go} \quad (2.21)$$

Groundwater recharge,  $E_g \leq E_t$  and  $D - E_g$ , can be calculated by comparing Equations (2.20) and (2.21).

As described in Section 2.4.2, highly permeable actual acid sulfate soils often overly unoxidised impermeable potential acid sulfate soils. Rain which falls on the oxidised acid sulfate soils (or the permeable veneer of alluvium which may overlie the acid sulfate soil) rapidly flows to the water table with little surface runoff. The unoxidised potential acid sulfate soils form an impermeable base and the oxidised actual acid sulfate soils rapidly fill up during rainfall. Shallow acidic groundwater is transported laterally to drainage lines through the highly transmissive shallow soil horizons. If sufficient rainfall occurs, the soil storage may fill giving rise to significant volumes of acidic surface runoff. In dry or drought periods,  $D$ ,  $L_{gi}$  and  $L_{go}$  in Equation (2.21) are zero. The water table height ( $H$ ) falls due to evaporative losses. If  $H$  falls below the depth of the potential acid sulfate soil layer, pyrite may be exposed to oxygen and the acid forming reactions described in Equations 2.4-2.7 may proceed.

White *et al.* (1997) suggested that it is useful to analyse the hydrology of coastal floodplains for wet and dry periods separately. In addition, artificial drainage has had substantial impact on the hydrology of coastal floodplains.

#### 2.4.3.1 *Effect of prolonged wet periods*

In wet periods, or over a longer term, changes in the storage components described in Equation (2.20) are insignificant in comparison to rainfall, upland inflow, outflow and evapotranspiration. Inflow ( $L_i$ ) is dependant on the area of the upland catchment ( $A_u$ ), the upland precipitation ( $P_u$ ) and the partitioning of upland rainfall ( $r_u$ ) that becomes inflow to the floodplain area ( $A_f$ ). White *et al.* (1997) show that:

$$L_i = \frac{r_u P_u A_u}{A_f} \quad (2.22)$$

In very wet periods,  $P_u \approx P$ ,  $r_u \approx 1$  and the water table is at or above the soil surface. Consequently, vertical drainage in Equation (2.20) is close to zero and the only store is ponded water on the surface ( $\Delta S_p$ ). Under these very wet conditions the water balance for the floodplain becomes (White *et al.*, 1997):

$$P \frac{A_f + A_u}{A_f} \approx E_t + L_o + DS_p \quad (2.23)$$

White *et al.* (1997) suggest that the ratio,  $A_f:A_u$ , for coastal eastern Australian rivers is small and typically of order 10. Given this relatively small ratio, Equation (2.23) shows that upstream inflow can be a major contributor to the water balance of the floodplain during wet periods.

Data collected by Sammut *et al.* (1996) and White *et al.* (1997) show the components of the monthly water balance during a flood in the Tuckean Swamp, a tributary of the Richmond River in Northern New South Wales. These data are shown in Table 2.3. The water balance example shown in the table demonstrates that upland inflows and outflows dominate the floodplain water balance during wet periods. The excess water fills floodplain depressions and backswamps by overtopping natural levees and overland flow onto already saturated or ponded lowland landscapes.

**Table 2.3:** Components of the water balance for Tuckean Swamp - March 1994 flood  
(from Sammut *et al.* 1996; White *et al.* 1997).

Water balance component	Amount (mm)	Volume ( $\times 10^6 \text{ m}^3$ )	Mean pH (SE)	Quantity of acid (t $\text{H}_2\text{SO}_4$ )
Floodplain rainfall, P	590	2306	5.8	-
Upland inflow, $L_i$	1980	79.2	6.9 (0.1)	-
Evapotranspiration, $E_t$	150	6.0	-	-
Surface water, $\Delta S_p$	200	8.0	3.1 (0.1)	320
Drainage network	20	0.8	3.0 (0.04)	39
Outflow, $L_o$	2200	88.0	3.7 (0.5)	860
Groundwater store	380	15	3.0 (0.06)	750

In natural landscapes, floodplain outflow is conducted by tortuous drainage channels with appreciable hydraulic roughness and by swamps existing behind natural levees. Under these conditions, ponded surface water persists for long periods because of the slow rate of surface drainage. Once the water level in the backswamps falls below the minimum height of the levees and drainage channels, the reduction in the surface water level in the backswamps is by evapotranspiration only. Water depths in backswamp areas are typically 0.5 m with evapotranspiration rates of about  $5 \text{ mm d}^{-1}$ . Ponded water may persist for periods of about 100 days given no further rainfall. The volume of acidic water ponded in the backswamp area is reduced by evapotranspiration and the underlying layer of oxidising acid sulfate soils is flushed of  $\text{Fe}^{3+}$  and re-saturated

thereby minimising further oxidation of pyrite until oxidising conditions in the soil profile can be re-established.

#### 2.4.3.2 *Effect of prolonged dry periods*

In dry periods when inflows, drainage and outflows are zero, Equation (2.20) becomes (White *et al.*, 1997):

$$Y_g \cdot \Delta H = -E_g \quad (2.24)$$

The rate of evapotranspiration from the water table is determined by the surface vegetation, its leaf area and rooting depth, solar radiation, humidity, wind speed, air temperature and pressure, water availability, the position of the water table and soil hydraulic properties.

White *et al.* (1997) used Brutsaert's (1982) equation to calculate the potential evapotranspiration ( $E_p$ ) at a well watered site with short grass.

$$E_p = E_q + E_a \quad (2.25)$$

where,  $E_q$  is the equilibrium evapotranspiration determined by net solar radiation and air temperature, and  $E_a$  is the drying power of the air dependant on wind speed, vapour pressure deficit, air temperature and pressure.

When soil water is not limiting, actual evapotranspiration ( $E_t$ ) is often estimated by:

$$E_t = C_t \cdot E_p \quad (2.26)$$

where,  $C_t$  is a time dependant crop factor ranging between 0.5 for bare soil and 1 for a fully developed crop.

In coastal areas where air humidity is high so that  $E_a$  is a relatively small component of  $E_p$ , actual evapotranspiration simply becomes:

$$E_t = E_q \quad (2.27)$$

Brutsaert (1982) describes  $E_q$  as:

$$E_q = \frac{\Delta(R_n - G)}{(\Delta + \gamma)\lambda} \quad (2.28)$$

where  $R_n$  is net radiation,  $G$  is the daytime heat flux into the ground (about 5% of  $R_n$ ),  $\Delta$  is the slope of the saturation vapour pressure versus temperature curve at the air temperature of interest,  $\gamma$  is the psychrometric constant and  $\lambda$  is the latent heat of vaporisation.

Blunden *et al.* (1998), White and Melville (1993) and Wilson (1995) have shown that substantial reduction in the height of the water table from evapotranspiration occurs on coastal, acid sulfate soil floodplains during periods of prolonged drought or vigorous crop water use. Water tables sloping down away from drains into adjacent fields indicate that the drains are supplying water to the field. It is important to note that during dry periods the depth of the water table may not be controlled by the depth of water in shallow drains but by the evapotranspiration of rigorous, deep rooting crops such as sugar cane or by evaporation from large, deep cracks that form during desiccation of the soil in dry periods. In more temperate regions where drainage may be

shallower and crops less vigorous, the water table depth may be influenced through manipulation of the hydraulic gradient caused by altering the height of water in drains (Pease, 1995).

Mean annual evapotranspiration varies about 20% along the New South Wales coast however, mean annual rainfall varies by a factor of about 2. White *et al.* (1997) hypothesised that the water table at lower rainfall sites should fall further than at higher rainfall sites and that the oxidation front in acid sulfate soils should be at shallower depths in drier areas. However, cyclic climatic patterns associated with the El Niño/Southern Oscillation are more likely to determine the depth of oxidation fronts. Willett *et al.* (1992) and Lin and Melville (1993) describe oxidised zones buried beneath river levees that are several thousand years old. This suggests that periodic oxidation of acid sulfate soils occurred during severe droughts independent of artificial drainage. Ferguson and Eyre (1995) contended that long term periodic climatic variations may control hydrological processes such as water table heights and freshwater discharges. This may result in oxidation of pyrite in drought conditions and severe impacts during drought breaking rains due to the discharge of substantial volumes of acid stored in the soil profile and the low buffering capacity of the fresh water rainfall leaching the acid from the soil.

#### 2.4.3.3 Artificial drainage

Artificial drainage has substantially altered the hydrology of coastal floodplains. In order to increase the agricultural productivity, governments in eastern Australia have carried out extensive drainage of coastal floodplains through the implementation of flood mitigation and drainage policies. Flood mitigation systems and drains have been constructed to protect towns and farmland from inundation by diverting upland flows from the floodplain, routing them through the floodplain or draining floodwater from the floodplain within a period of about five days (White *et al.*, 1997). Natural drainage features have been straightened, widened and deepened, side drainage channels have



been constructed, levee banks raised and floodgates installed where drainage channels enter tidal rivers and streams. A schematic representation of a typical artificial drainage system is shown in Figure 2.5

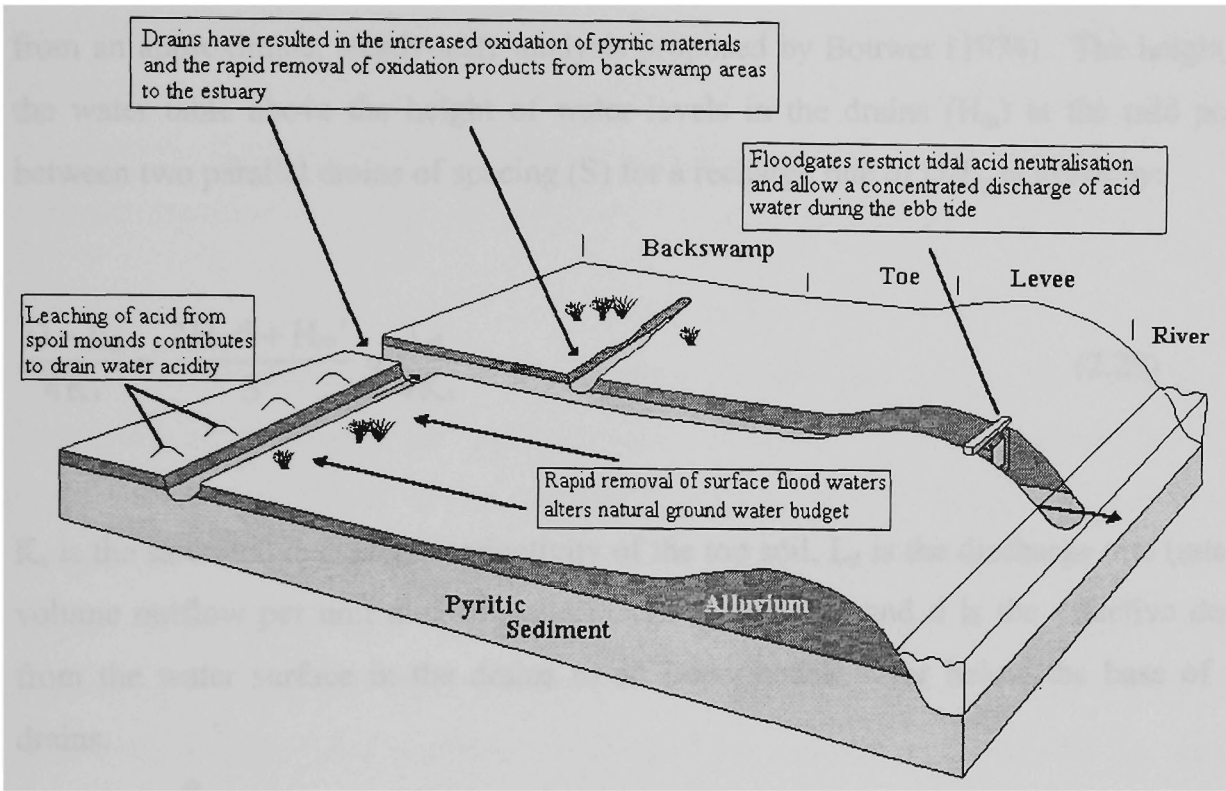


**Figure 2.5:** Artificial drainage system for a coastal floodplain

[after Naylor *et al.* 1995].

In almost all instances, the presence of acid sulfate soil was not taken into account during the implementation of these flood mitigation/drainage systems. Indeed, it has been argued that little consideration of hydraulic engineering (Robertson and Creighton, 1996), cost/benefit analysis for expenditure of public monies (Read, 1996) or assessment of the negative impacts of acid discharge, wetland destruction and habitat loss (Leadbeater, 1993) has been given to the implementation and operation of such flood management schemes. White *et al.* (1997) stated that:

Drainage design has been the least understood and used aspect of coastal floodplain management in eastern Australia, despite the large areas which have been drained. The principle objective for drainage appears to have been the

control of water table height, despite the fact that the source of water used by most coastal crops in dry seasons is predominantly groundwater.

There are numerous methods for determining the groundwater elevation in drained landscapes. The water table height between parallel drains can be readily determined from an approximate, steady-state analysis proposed by Bouwer (1974). The height of the water table above the height of water levels in the drains ( $H_m$ ) at the mid point between two parallel drains of spacing ( $S$ ) for a recharge rate of  $D-E_g$  is given by:

$$\frac{D - E_g}{4K_s} \approx \frac{2H_m d + H_m^2}{S^2} \approx \frac{L_d}{4K_s} \quad (2.29)$$

$K_s$  is the saturated hydraulic conductivity of the top soil,  $L_d$  is the discharge rate (rate of volume outflow per unit area of drain discharge surface) and  $d$  is the effective depth from the water surface in the drains to an impermeable layer below the base of the drains.

Chapman (1994) used a steady state, two dimensional finite element model, PC-SEEP (Geoslope International), to determine the height of the water table by altering the pressure head ( $H$ ) or water levels in drains. PC-SEEP uses the governing differential equation:

$$\frac{\partial}{\partial x} \left( k_x \frac{\partial H}{\partial x} \right) + \frac{\partial}{\partial y} \left( k_y \frac{\partial H}{\partial y} \right) + Q = \frac{\partial \theta}{\partial t} \quad (2.30)$$

where,  $k$  is hydraulic conductivity in the  $x$  and  $y$  plane,  $Q$  is the applied boundary flux,  $\theta$  is the volumetric moisture content and  $t$  is time.

Blunden *et al.* (1997) numerically solved the steady state height of the water table by setting maximum and minimum drain water levels, steady state water table boundary conditions as measured in the field under existing drained conditions and solving Equation (2.30) for  $d\theta/dt = 0$ , that is, where the flux entering and leaving an elemental volume is the same at all times for steady state conditions. By solving this differential equation across a two dimensional finite element mesh, Blunden *et al.* (1997) were able to establish optimal water level management criteria for flood mitigation drains to minimise the discharge of acid sulfate soil oxidation products. No account of rainfall, evapotranspiration or storage was given in the solution of Equation (2.30).

Steady state analysis described by Equations (2.29) and (2.30) has fundamental limitations for Australian east coast climatic conditions. A steady water table state could only be achieved where catchment inputs (rainfall, irrigation) and losses (evapotranspiration, runoff) are uniform throughout the year. Coastal eastern Australia is characterised by strongly seasonal rainfall, particularly in the tropical and sub-tropical regions, and the cyclic influence of the El Nino - Southern Oscillation causing prolonged drought-flood regimes. The marked seasonality of rainfall in eastern Australia means that drainage systems designed to remove water at a steady state recharge rate are unable to meet the drainage requirements during the wet season and extract too much water from the soil profile during the dry season. Numerical simulation to understand the hydrology of coastal floodplains and to optimise water table management strategies must consider the temporal variation of catchment inputs, outputs and storages to be successful in the Australian climatic context.

## **2.5 Implications for this research**

A thorough understanding of the processes that determine the magnitude and rate of pyrite oxidation, as well as the mechanisms by which acidic pyrite oxidation products are transported to nearby waterways, is required for the development of acid sulfate soil

management strategies for drained floodplains. As outlined above, a complex inter-relationship exists between the oxidation of pyrite in acid soils, the physical properties of the soil that determine the transport of both air and water through the soil, and the hydrology of coastal floodplains. Floodplain management practices, particularly the construction of drainage systems and establishment of vigorous crops, have significantly altered the catchment hydrology, which has in turn resulted in pyrite oxidation.

The hypothesis for this research is that the elevation of the groundwater table relative to the height of the acid sulfate soil layer controls the oxidation of pyrite and the subsequent generation of acid. Given the extent and geometry of the drainage scheme at the study site, it follows that inappropriate drainage of this landscape has resulted in the generation of acid from oxidising acid sulfate soils in the past. The objective of this research is to assess the effectiveness of a groundwater management strategy involving the construction of weirs in the drains to increase the elevation of the drain water level with a view raising surrounding groundwater elevations, which in turn should minimise acid generation and its discharge into the drains.

To assess the effectiveness of the drain-groundwater management strategy, the interrelationship between the soil chemistry and physics, hydrology, groundwater and drain water quality and climatic influences were studied at a comprehensively instrumented and monitored field site. This research examines if groundwater manipulation is sufficient to improve groundwater and drain water quality, and thereby minimise further pyrite oxidation.

## **Chapter 3: Review of pyrite oxidation studies and management strategies**

This Chapter reviews the literature relevant to the prediction of pyrite oxidation and its management in acid sulfate soils or pyritic mine spoils at the field scale. Fundamental studies that investigate the geochemical attributes of pyrite oxidation in the laboratory have been excluded. Four major topics associated with the prediction and management of acidity from pyrite oxidation in the field have been reviewed. These include; field investigations of acid generation from acid sulfate soils, laboratory studies of pyrite oxidation in both acid sulfate soils and pyritic mine spoils collected from the field, computer simulations used to predict pyrite oxidation for various management regimes, and pyrite oxidation management strategies that may be appropriate for the application in areas of acid sulfate soil at the sub-catchment scale.

### **3.1 Field investigation of acid generation from acid sulfate soils**

Empirical site-specific relationships have been developed for acid discharge rates in eastern Australia. Wilson (1995), Sammut *et al.* (1996) and Indraratna and Blunden (1999) have made general approximations of the rate of acid formation in catchments, where substantial drainage and/or vigorous evapotranspiration has lowered water tables below the level of acid sulfate soil horizons. Analysis of water quality parameters, coupled with an approximation of the catchment discharge, enabled Wilson (1995) and Sammut *et al.* (1996) to estimate acid generation rates of 100 and 300 kg ha<sup>-1</sup> year<sup>-1</sup> for sub-catchments within the Tweed and Richmond Rivers (NSW) respectively.

Indraratna *et al.* (1995) showed that there is a correlation between the height of the water in the drains and the pH of the surrounding groundwater at their study site in the

Shoalhaven River (NSW) catchment. Figure 3.1 shows that where the water level in the drain is high, then groundwater pH in the surrounding land is relatively high.

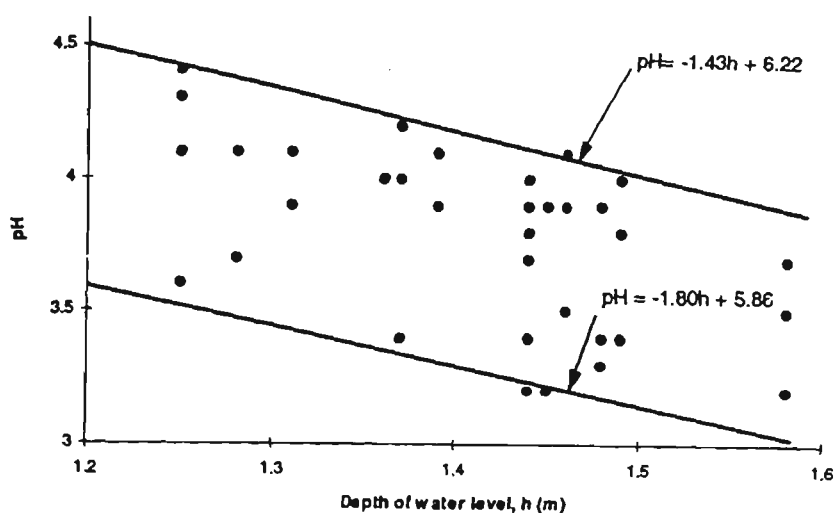


**Figure 3.1** Relationship between drain level and pH

[after Indraratna *et al.*, 1995]

Regression of groundwater pH against the difference between the crest of the drain and drain water height (h) gave:

$$\text{pH} = -1.4h + 6.22 \quad (\text{upper bound})$$

$$\text{pH} = -1.8h + 5.86 \quad (\text{lower bound}) \quad (3.1)$$

Equation (3.1) suggests that raising the drain water height will improve the pH of the surrounding groundwater. High drain levels are transient in floodgated drainage systems and are usually associated with periods of excessive rainfall than may lead to flooding. Where flooding occurs, acid can be flushed from the groundwater and diluted thereby giving relatively high pH. The steady state drain water level is low tide level.

As this drain water level is achieved, groundwater drawdown occurs and the surrounding groundwater table falls. As the groundwater table falls, the groundwater chemistry equilibrates with the surrounding soil which is often pH 3-4. As such, interpretations made by Indraratna *et al.* (1995) may not reflect the more usual status of the groundwater - drain hydrology, and its impact on groundwater chemistry.

Pease *et al.* (1997) and Wilson (1995) monitored groundwater fluctuations and water quality parameters for study sites located on the Shoalhaven and Tweed Rivers, respectively. Both studies found that groundwater drawdown caused by nearby deep drains was a major factor in lowering the groundwater level below the acid sulfate soil horizon. Wilson (1995) also found that evapotranspiration from sugar cane has a significant influence on groundwater elevation.

Pease *et al.* (1997) found that watertable fluctuation in response to rainfall was rapidly followed by changes in groundwater pH. Increases in the groundwater elevation caused the pH to rise to 6, particularly when flooding occurred on the site. When the watertable fell slightly below the ground surface, pH fell as the groundwater chemistry came into equilibrium with the previously oxidised acid sulfate soils. When the groundwater fell to -0.2 m AHD (about 0.5 m below the surface), groundwater pH was 2.8-3.3. The concentration of sulfate and dissolved iron increased by about one order of magnitude as the groundwater fell below the elevation of the acid sulfate soil layer, indicating that pyrite oxidation was occurring. Groundwater remained highly acidic (pH 3) upon subsequent rainfall and elevation of the groundwater table above the acid sulfate soil layer.

Wilson (1995) described a similar trend between groundwater elevation and acidity. When the watertable was above the acid sulfate soil layer, the groundwater was pH 3.6, indicating that previous pyrite oxidation had occurred in the acid sulfate soil layer at deeper depths. Interestingly, when the groundwater fell into unoxidised acid sulfate soils, the groundwater was pH 7.5. At greater depths, the unoxidised potential acid sulfate soil has remnant calcium carbonate deposits and a high component of basic

cations on the cation exchange complex. These factors buffer any acidity in the soil water, giving rise to neutral or slightly alkaline conditions. However, when the groundwater table rose through the more elevated acid sulfate soil layers, the groundwater become very acidic once again.

Both Pease *et al.* (1997) and Wilson (1995) have confirmed the link between groundwater elevation relative to the acid sulfate soil layer and acid generation. These authors come to the logical conclusion that if the groundwater elevation can be maintained above the acid sulfate soil layer then the subsequent generation of acid should be minimised. These conclusions led to the implementation of the drain management strategy being trialed in the research presented in this thesis.

Bronswijk *et al.* (1995) used both field investigations and numerical modelling to develop a relationship between the average groundwater level in the acid sulfate soil layer and the annual pyrite oxidation rate. This relationship is shown in Figure 3.2.

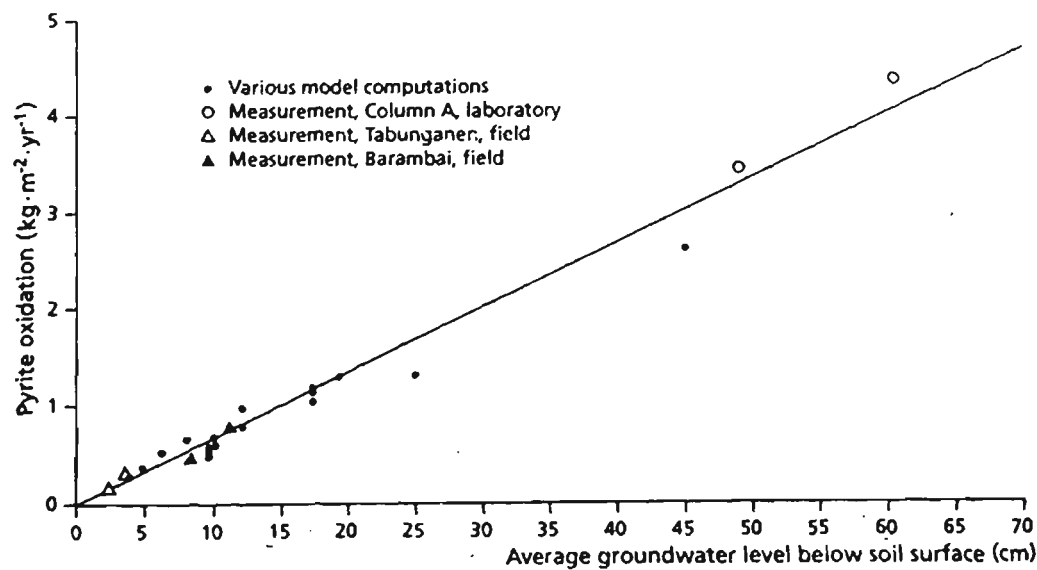


**Figure 3.2** Pyrite oxidation rate vs average groundwater level.

(from Bronswijk *et al.*, 1995)



The relationship derived by Bronswijk *et al.* (1995) shows that the amount of pyrite oxidised on an annual basis increases in a linear fashion as the average depth of groundwater falls in the acid sulfate soil. In effect, these data suggest that the elevation of groundwater, which in turn controls the transport of oxygen into the soil profile, is the key process that controls pyrite oxidation and the generation of sulfuric acid.

The predictions made by Wilson (1995), Sammut *et al.* (1996), Indraratna *et al.* (1995) and Bronswijk *et al.* (1995) reveal little for other sites affected by oxidation of pyrite in acid sulfate soils with different soil, hydrological, topographic or climatic influences. Predictive tools need to simulate the numerous physical and chemical processes, their interactions and the temporal variations associated with site specific climatic regimes are required to predict the practical, long term consequences of land management strategies and rehabilitation techniques.

However, valuable management rules can be derived from these studies. In short, these researchers confirm that lowering groundwater levels below the elevation of the acid sulfate soil layer promotes pyrite oxidation and the subsequent generation of acid. Effective management of acid sulfate soils therefore requires the implementation of systems that manipulate groundwater regimes so that the elevation of the groundwater is maintained above the acid sulfate soil layer. A comprehensive trial of manipulating groundwater level by the installation of weirs in the flood mitigation drains at the Berry (NSW) field site is reported in this thesis.

### **3.2 Laboratory column studies of pyrite oxidation**

Laboratory column studies have been used to investigate the rate of pyrite oxidation and generation of oxidation products from oxidising sulfidic materials. In many instances, the carefully controlled column studies have been used to calibrate and/or validate

numerical models that simulate the oxidation of pyrite in acid sulfate soils or waste rock dumps.

Ritsema *et al.* (1992) studied the transformation of potential acid sulfate soils into actual acid sulfate soils in two column experiments conducted over a 450 day period to determine the rate and extent of pyrite oxidation and the accompanying buffering processes. Both columns were subjected to intensive drainage for 450 days then were submerged for 300 days to investigate the effect of leaching. Drainage of the potential acid sulfate soils caused an increase in the rate of pyrite oxidation. Iron released during the oxidation process was instantly immobilised due to the precipitation of jarosite and/or iron hydroxides. In one of the columns, the presence of carbonates prevented the acidification of the soil solution, whereas the absence of carbonate in the other column gave rise to strongly acidic pore water (pH 3.5). Pore water quality data for the carbonate deficient column (note that acid sulfate soils at the study site for this research are also carbonate deficient) are shown in Figure 3.3.

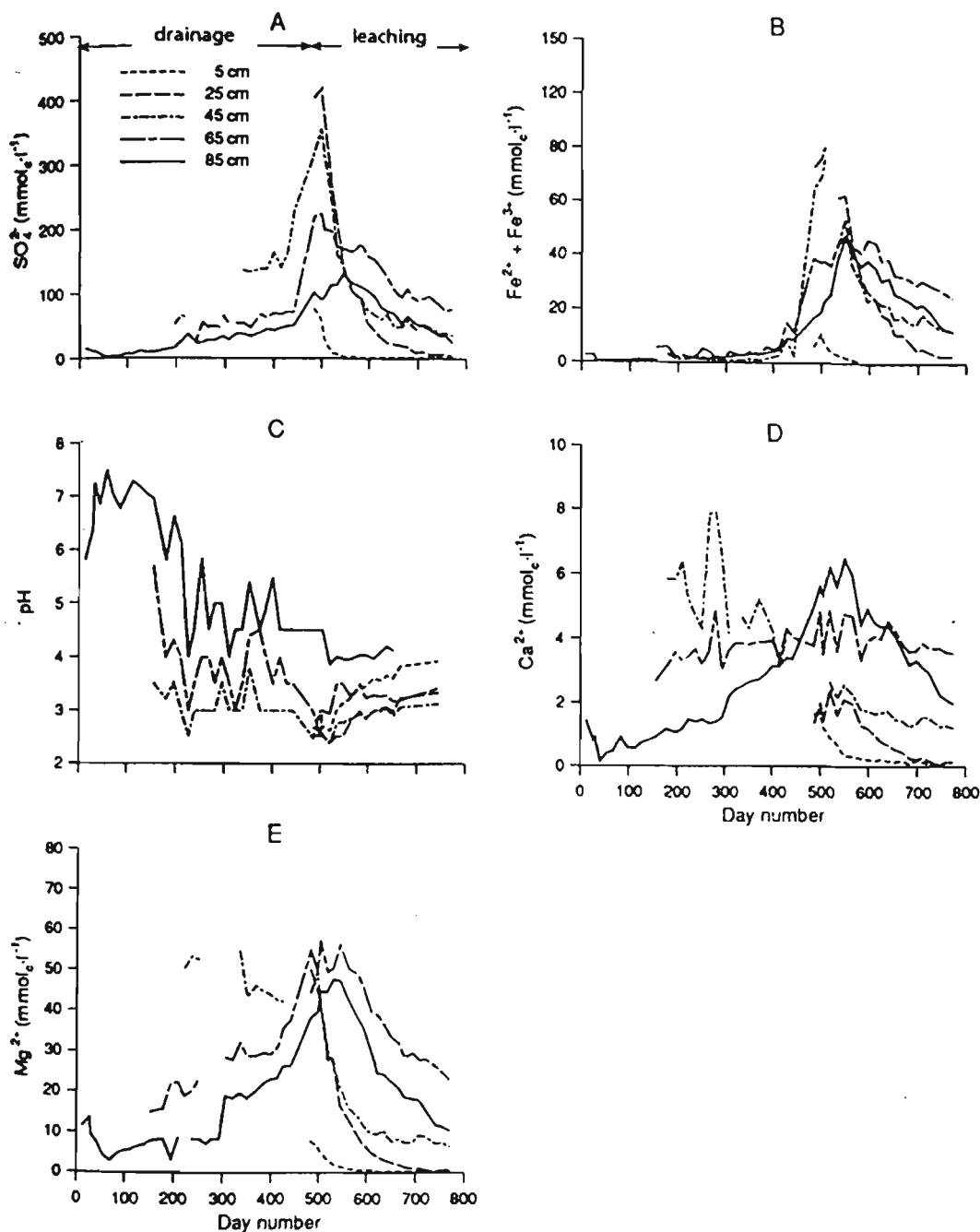


**Figure 3.3** Water quality parameters for a drained, carbonate deficient acid sulfate soil.  
(from Ritsema *et al.*, 1992)

In the carbonate deficient soil, pH in the acid sulfate soil layers fell from 6-7 to 3-4 as a result of drainage induced pyrite oxidation. However, subsequent submergence of the acid sulfate soil layer and ongoing leaching did not have a corresponding rise in pH. This indicates that acidic soil conditions will remain even after submergence has reduced the pyrite oxidation rate. Leaching was demonstrated to remove much of the

Mg, Ca and Fe ions from the pore water. The concentrations of Ca and Mg were shown to increase in the pore water as the pH of the pore water fell, suggesting that dissolution of clays occurred. This is confirmed by measured changes in the composition of the cation exchange complex in layers where pyrite oxidation had occurred. The exchangeable cations of the carbonate-deficient acid sulfate soil before and after drainage are shown in Figure 3.4.

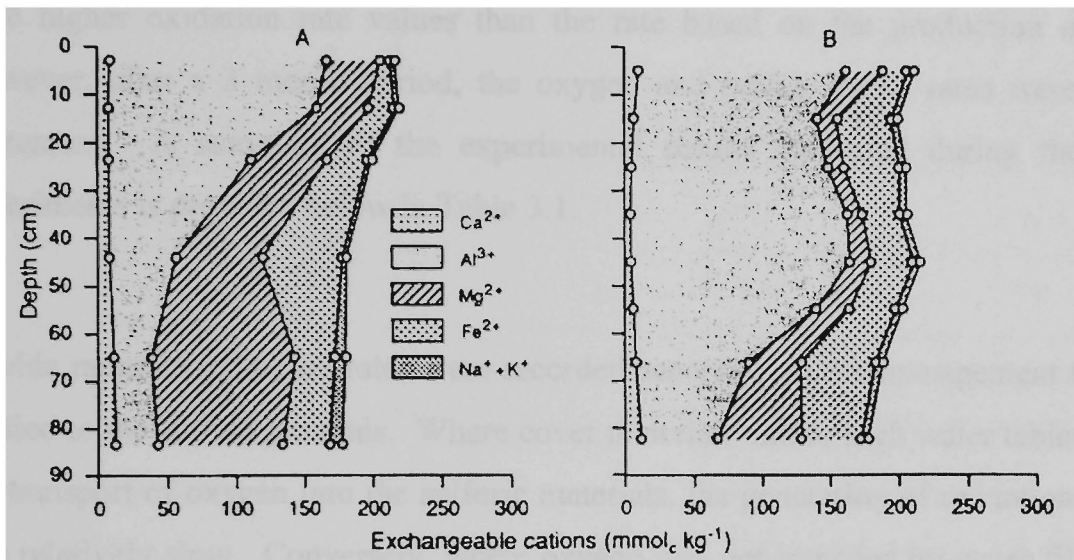


**Figure 3.4** Exchangeable cations at the beginning (A) and end (B) of the drainage experiment.

(from Ritsema *et al.*, 1992)

Figure 3.4 shows that in the areas where pyrite was oxidised,  $\text{Ca}^{2+}$  and  $\text{Mg}^{2+}$  were exchanged for  $\text{Al}^{3+}$ . High levels of exchangeable  $\text{Al}^{3+}$  are toxic to plants and this has implication for pasture/crop productivity. Clearly the column experiments demonstrate that drainage of acid sulfate soil leads to the oxidation of pyrite and generation of acidic products. The generation of acid gives rise to undesirable soil conditions for plant productivity as well as providing a large store of acid to be transported to nearby waterways.

Elberling *et al.* (1994) measured the oxygen flux across the surface of mine tailings, the oxygen consumption rates at the tailings surface and the total sulfate produced in pore

water over time in columns of quartz sand and pyrrhotite. Fourteen experiments were conducted to assess the effectiveness of varying thicknesses of a non reactive layer made of either fine or coarse material. The two oxygen methods provided instantaneous rate measurements (daily) whereas the measured sulfate production gave an oxidation rate based over a longer experiment time (weekly). The instantaneous rate methods showed that the oxidation rate initially increased over the first two days of the experiments but then remained constant over the next five days. At early times, the oxygen methods gave higher oxidation rate values than the rate based on the production of sulfate. However, after a 3 month period, the oxygen and sulfate based rates were in close agreement. A summary of the experimental results measured during the column experiments is provided below in Table 3.1.

A wide range in oxidation rates were recorded according to the management technique applied to the sulfide minerals. Where cover materials and/or high water tables reduced the transport of oxygen into the sulfuric materials, the generation of oxidation products was relatively slow. Conversely, where oxygen was not impeded by water filled pores in the cover layers or sulfidic spoil, a rapid oxidation rate was measured.

**Table 3.1:** Summary of oxidation rates using different methods, cover materials and water levels from Elberling *et al.* (1994).

Run No.	Thickness of fine layer (m)	Thickness of course layer (m)	Depth to water table (m)	Sulfate release	Oxygen gradient (mol Fe <sub>1-x</sub> S <sub>x</sub> /m <sup>2</sup> /y)	Oxygen consumption (mol Fe <sub>1-x</sub> S <sub>x</sub> /m <sup>2</sup> /y)
1	0.08	0.0	2	58	328	436
2	0.00	0.0	2	116	933	655
3	0.08	0.0	2	53	163	98
4	0.00	0.0	2	117	1025	519
5	0.08	0.0	1	55	197	62
6	0.00	0.0	1	156	972	499
7	0.00	0.1	2	122	892	373
8	0.00	0.3	2	42	196	142
9	0.00	0.1	2	122	874	187
10	0.00	0.3	1	28	-	77
11	0.00	0.1	0.7	64	884	184
12	0.00	0.3	0.7	20	112	53
13	0.00	0.1	0.7	54	841	121
14	0.00	0.3	0.7	22	115	53

Both the studies by Ritsema *et al.* (1992) and Elberling *et al.* (1994) confirm the importance of water management in minimising the amount of oxidation in pyritic materials. However, Ritsema *et al.* (1992) also showed that submergence of the acid sulfate soil layer after pyrite oxidation had previously occurred did not give rise to

improved water quality as a result of physio-chemical changes in CEC of the soil. This suggests that although the generation of acid in the future may be able to be minimised by elevated groundwater levels, the groundwater quality may not substantially improve until basic cations replace the acidic cations, such as aluminium and hydrogen, on the cation exchange complex.

The effectiveness of maintaining high groundwater tables by better drain management for a 120 ha study site is investigated in Chapter 7. Other water management options are also investigated using numerical simulations in Chapters 9 and 11.

### **3.3 Pyrite oxidation models**

Considerable effort has been placed into the development of analytical and numerical solutions for modelling the oxidation of pyrite or other similar sulfidic minerals. In the main, development of these models has been focused on better understanding the generation of acidic leachate from waste rock dumps and tailings lagoons associated with discard from sulfidic mineral mining activities, and as such, are only partly applicable to the study of acid sulfate soils. Only one pyrite oxidation model (Bronswijk *et al.* 1993) has been designed specifically for the simulation of acid generation and transport in acid sulfate soils.

#### *3.3.1 Theory and approximate analytical solution: Davis and Ritchie (1986)*

The basis for most of the pyrite oxidation models discussed in Section 3.3.2 are derived from the development of a mathematical model and an approximate analytical solution by Davis and Ritchie (1986) for the diffusion of oxygen through a porous media, and the subsequent pyrite oxidation reaction within the media. Davis *et al.* (1986) developed a

numerical approach that showed good agreement with their approximate analytical solution.

The waste material was assumed to be a porous slab with the surface open to the atmosphere and the base impermeable to gas transport. The horizontal extent of the waste is assumed to be significantly greater than the height of the waste dump so that the transport of oxygen through the pore space of the dump is considered to be one dimensional. The model equations consist of a coupled system of three partial differential equations linking the oxygen concentration within the pore space of the waste, the oxygen concentration within the particles comprising the waste and the position of the oxidation front within the particles. An analytical expression for the concentration of oxygen within a particle was derived based on the assumption of pseudo-steady state diffusion within the particles. Expressions for the sulfate production rate and the spatial heat source distribution, which is an estimation of the rate of oxidation as a function of depth, were also derived.

The mathematical derivation of the approximate analytical solution and its conversion into numerical code is complex and not required for understanding of the development of subsequent numerical approaches to the solution of pyrite oxidation. For a comprehensive study of the derivation of the approximate solution, the reader is referred to Davis and Ritchie (1986) and Davis *et al.* (1986).

### 3.3.2 Numerical models for pyrite oxidation

A number of numerical models which simulate the oxidation of pyritic minerals have been reported in the literature. These models range in sophistication from reasonably simple coupling of oxygen diffusion through an unsaturated medium to the ‘shrinking core’ pyrite oxidation approach to complex oxygen diffusion-pyrite oxidation-reactive solute transport models.



The following discussion is restricted to the development of the pyrite oxidation sub-models only. In most instances, the complete numerical models discussed below are not immediately applicable to the simulation of acid sulfate soils problems due to the way in which the water and air content profiles and solute fluxes are calculated. In short, the flow of water through coarse rock and tailings empoundments is usually non-Darcian, and is therefore not applicable for simulation of water flow through naturally deposited soils. The development of a numerical model that couples an appropriate unsaturated soil flow model with a subroutine that calculates the amount of pyrite oxidised during periods where the groundwater table is lower than the pyritic layer is an objective of this research. The development of this model is discussed in Chapter 9. A discussion of recent pyrite oxidation models is given below.

### 3.3.2.1 Reactive Tailings Assessment Program (RATAP)

A numerical model called Reactive Tailings Assessment Program (RATAP) was developed by Scharer *et al.* (1992) to predict acid generation and geochemical events caused by the oxidation of sulfide minerals in mining discard. The moisture profile through the unsaturated and capillary fringe layers of the spoil profile is determined using an empirically derived expression based on the 10 percentile particle size, residual water retention and distance to the water table. This approach for determining the water and air content distribution for a multi-horizon soil profile is not adequate. From this calculation, the effective oxygen diffusion coefficient is determined by Equation (3.2):

$$D_e = 0.203 \left( \frac{n_a - 0.05}{0.95} \right)^{1.7} + D_w \quad (3.2)$$

where,  $n_a$  is the air filled porosity,  $D_e$  is the effective diffusion coefficient of oxygen and  $D_w$  is the diffusion coefficient of oxygen in water.  $D_e$  was then used to solve the oxygen

transport diffusion equation that determined oxygen concentration in the unsaturated pore space through the spoil profile.

The kinetics of sulfide oxidation has been divided between abiotic and biological oxidation. The abiotic rate constant for sulfide oxidation is determined by:

$$r_c = Ae^{-E_a/RT} [O_2] 10^{-x\text{pH}} \quad (3.3)$$

where,  $r_c$  is the abiotic rate constant,  $[O_2]$  is the concentration of dissolved oxygen and  $E_a$  is the Arrhenius activation energy. The biological rate constant is expressed as:

$$r_b = b \frac{\mu_m \sigma}{Y_{x/s}} e^{-E_a/RT} \frac{[O_2]}{K_o + [O_2]} \frac{1}{1 + 10^{2.5-\text{pH}} + 10^{\text{pH}-4}} \quad (3.4)$$

where,  $r_b$  is the biological oxidation rate constant,  $b$  is a biological scaling factor,  $\mu_m$  is the specific growth rate,  $\sigma$  is the specific surface coverage,  $Y_{x/s}$  is the growth yield and  $K_o$  is the half saturation constant for oxygen.

The oxidation of the mineral sulfides is modelled on the concept of a shrinking core of distinct, homogenous particles of pure sulfides. The rate of shrinkage of a spherical particle is calculated by:

$$k_i(t) = \frac{r_{c,i} + r_{b,i}}{\rho_i} \quad (3.5)$$

where,  $k_i(t)$  is the rate of radial particle shrinkage and  $\rho_i$  is the molar density of the  $i^{\text{th}}$  sulfide.

The fraction of unreacted sulfide mineral concentration in any layer was determined by combining (3.5) with the particle size density function for the mineral sulfide tailings. The unreacted mineral sulfide concentration at any time  $t$  is given by:

$$M_i(t) = M_{i,0} \int_x^R \left( \frac{r - X_i}{r} \right)^3 \left[ Y \alpha \left( \frac{r}{R} \right)^{\alpha-1} - (Y - 1) \beta \left( \frac{r}{R} \right)^{\beta-1} \right] \frac{dr}{R} \quad (3.6)$$

where,  $M_i(t)$  is the unreacted sulfide mineral concentration and  $M_{i,0}$  is the initial sulfide mineral concentration.

The concentrations of oxidation products are calculated in the solute transport module of the model. Transport calculations include, kinetically controlled reactions (for example, sulfate formation by sulfide oxidation) and equilibrium controlled reaction, (for example, sulfate formation from gypsum dissolution). Aqueous speciation and the pH of pore water are also calculated. Figures 3.5 and 3.6 show that the predicted values from the simulation of pyrite oxidation in fine and course tailings correspond reasonably well to measured field data.

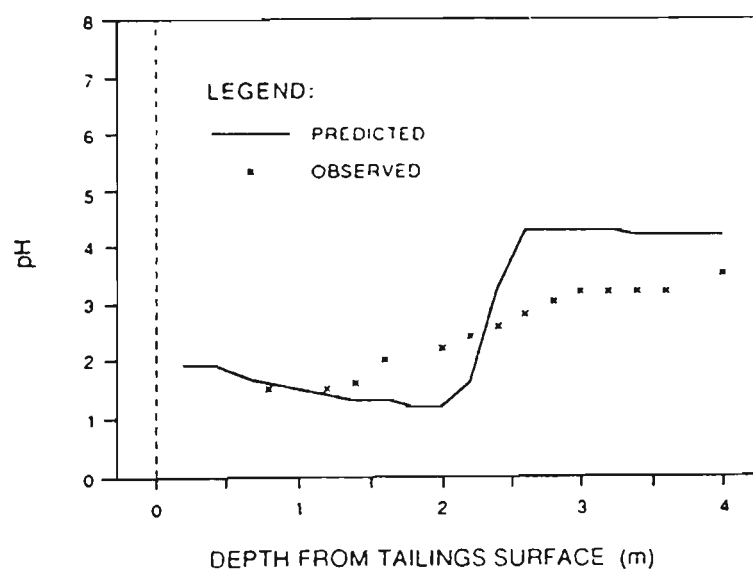
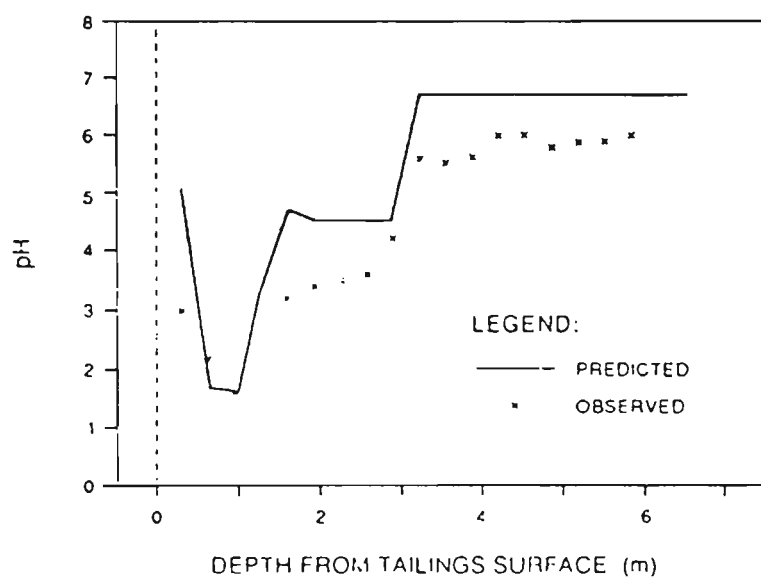


**Figure 3.5** Observed and simulated pH in tailings

(from Scharer *et al.*, 1992)

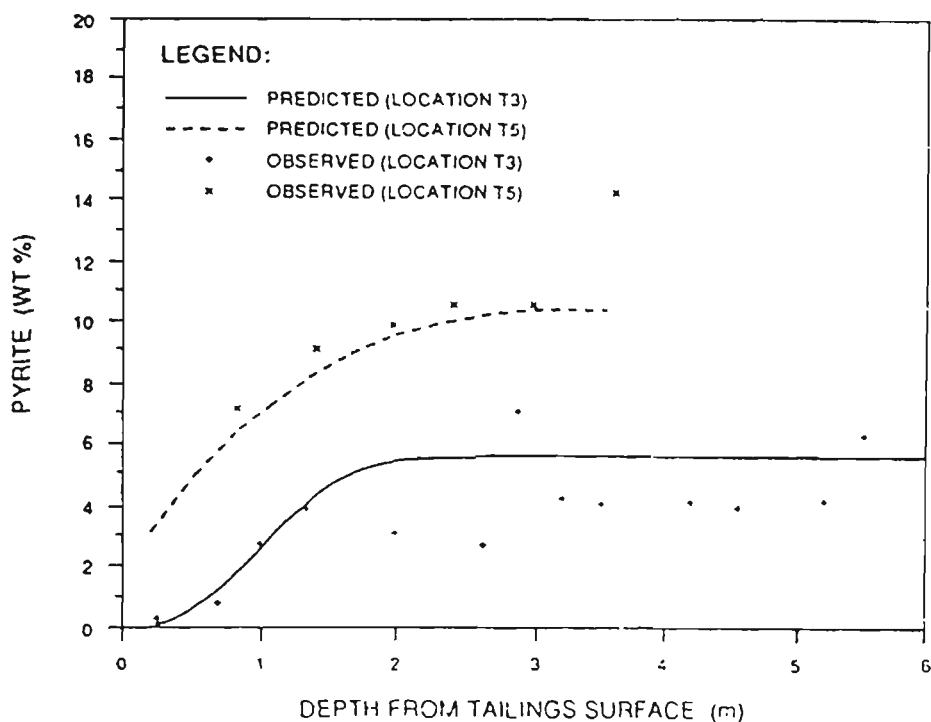


**Figure 3.6** Observed and predicted pyrite concentration

(from Scharer *et al.*, 1992)

RATAP can be run either as a deterministic or probabilistic model. In the probabilistic assessment mode, several input parameters are specified as distributions as opposed to definite inputs as is the case for deterministic simulations. The distributed parameters are sampled by a statistical sampling procedure and then used as input data for the simulation run. This procedure is repeated numerous times to determine a probabilistic assessment of the output. Whilst this process is expensive in terms of time and computer processing capacity, it offers a sophisticated method of evaluating the model outputs for the known variability that exists within the materials being simulated.

RATAP has limited application for acid sulfate soils as a result of the way the tailings water and air profiles are determined. Similarly, RATAP has a focus on the biologically controlled kinetics associated with pyrite oxidation and precipitate mineralisation associated with sulfate and cation reaction that occur with pore water which are not as well understood in acid sulfate soil as for pyritic mine tailings.

### 3.3.2.2 Model developed by Elberling *et al.* (1994)

Elberling *et al.* (1994) developed a numerical approach for the simulation of acid generation by the oxidation of sulfidic mining wastes. The rate of sulfide oxidation in the model is based on the continuity relationship for oxygen for both the transport of oxygen through the tailings and the consumption of oxygen at the surface of the sulfide minerals. The transport of oxygen is assumed to be via diffusion and has been modelled in accordance with Fick's law. One-dimensional diffusion of oxygen into the tailings was calculated by:

$$\frac{dC}{dt} = \frac{D_e d^2 C}{dz^2} - G \quad (3.7)$$

where,  $C$  is the concentration of gaseous oxygen,  $D_e$  is the effective diffusion coefficient,  $z$  is depth and  $G$  is the volumetric consumption of oxygen. The model assumes that pyrite particles are of equal diameter. As the pyrite particles oxidise they shrink in size resulting in smaller surface areas values for each particle. As a result, consumption of oxygen from the pyrite oxidation reaction decreases with time. Although the stoichiometry of the pyrite oxidation reaction is not explicitly modelled, the reaction kinetics for the pyrite reaction are described by:

$$\frac{-d[\text{FeS}_2]}{dt} = \frac{-4dt}{15d[\text{O}_2]} = KSC^n \quad (3.8)$$

where,  $K$  is the chemical rate constant and  $S$  is the surface area per unit volume.

Based on the assumption that the oxidation reaction can be approximated by first order kinetics ( $n=1$ ) at low oxygen concentrations, and using empirically derived data for  $K$ , the consumption of oxygen by pyrite oxidation was described by:

$$\frac{-dC}{dt} = 22.1 \times 10^{-10} C_z / C_0 \quad (3.9)$$

where,  $C_z$  is the concentration of oxygen at the depth within which the oxidation of tailings takes place, and  $C_0$  is the concentration of oxygen at the surface. The final equation used to describe oxygen transport with the first order rate reaction at a steady state was:

$$\frac{D \cdot d^2 C}{dz^2} - KC = 0 \quad (3.10)$$

where, the  $K$  value is recalculated for each time step a result of changes in pyrite surface area. The reduction in surface area  $S$  is approximated to a radial shrinkage rate to the oxidation rate  $dFeS_2/dt$  for one time step over the molar density of pyrite  $D_{py}$  using the equation:

$$S_t = S_{t-1} - \frac{K \cdot dt}{D_{py}} \quad (3.11)$$

Elberling *et al.* (1994) evaluated the sensitivity of the model against physical parameters associated with the tailings, such as grain size, pyrite content and the effective diffusion coefficient using a series of seven simulation runs, assuming that the tailings had not previously been oxidised. They found that, at early times, the depth of the oxidation front is determined by the effective diffusion coefficient for a specific rate constant value  $K$ . With time, the oxidation front moves downward resulting in lower oxygen concentrations being available for pyrite oxidation and a greater diffusion distance. As such, the rates of diffusion and oxidation decrease with time. The model output showed that the overall oxidation rate was largely independent of particle size and the pyrite content after long periods (100 months). This is demonstrated in Figure 3.7.

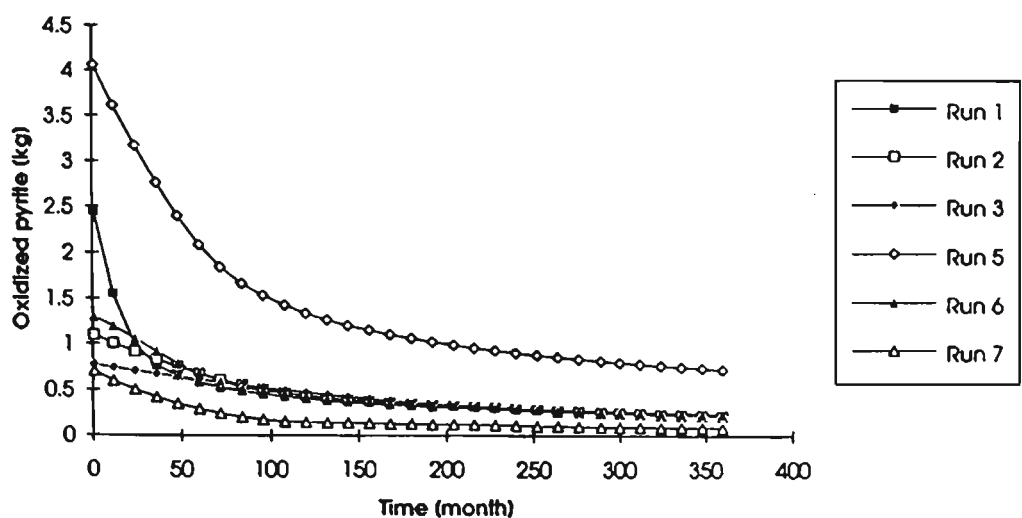


**Figure 3.7** Pyrite oxidation rate as a function of time

(from Elberling *et al.*, 1994)

However, the oxidation rate was highly sensitive to the effective diffusion coefficient (highest oxidation rates corresponding to high diffusion coefficients) as shown by Figure 3.8, yet the effect of the diffusion coefficient reduced with the passage of time.



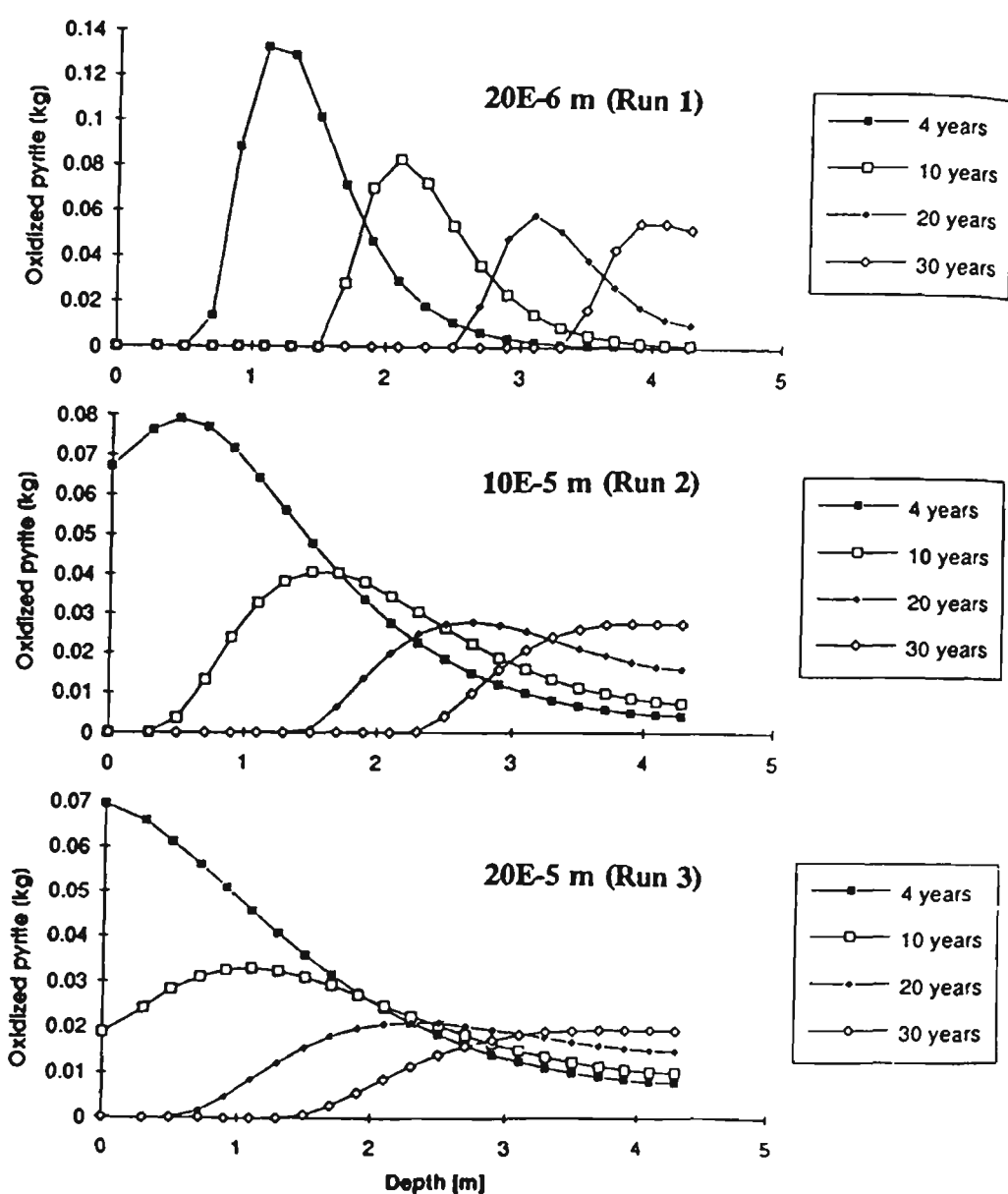


**Figure 3.8** Pyrite oxidation rate as a function of depth shown for different effective diffusion coefficients

(from Elberling *et al.*, 1994)

For sulfidic mine tailings, Elberling *et al.* (1994) concluded that the overall pyrite oxidation rate is largely determined by the effective diffusion coefficient of the tailings. In turn, the diffusion coefficient is determined by the saturation and grain size of the tailings. Where the effective diffusion coefficient of the tailings can be lowered by maintaining high levels of saturation within the tailings pore space, then Elberling *et al.* (1994) suggested that the contaminant generation rate (that is, generation of acidic oxidation products) is substantially reduced.

A problem associated with this pyrite oxidation model is its reliance on an empirically derived value for K, rather than an explicit function relating the stoichiometry of pyrite oxidation with oxygen. Values for K vary considerably depending on the chemical and physical properties of the pyritic material. Determination of a K value for individual material is expensive. Similarly, uniform effective diffusivity was assumed for the pyritic material. For variably saturated soil, the diffusivity of oxygen in the soil matrix is dependant on the soil saturation. As such, reliance on a uniform effective diffusivity for the whole pyritic material is unrealistic for application to acid sulfate soils where highly variable soil saturations are likely to occur.

#### 3.3.2.3 POLS

Jaynes *et al.* (1984) describe a model for the long term oxidation of pyrite and the removal of reaction products from reclaimed coal strip mines. Direct molecular oxygen oxidation and ferric iron oxidation are considered in the model. Pyrite oxidation is assumed to be controlled by first order kinetics and the rate of diffusion of oxidant into the reactive material. A schematic diagram of the model is shown in Figure 3.9

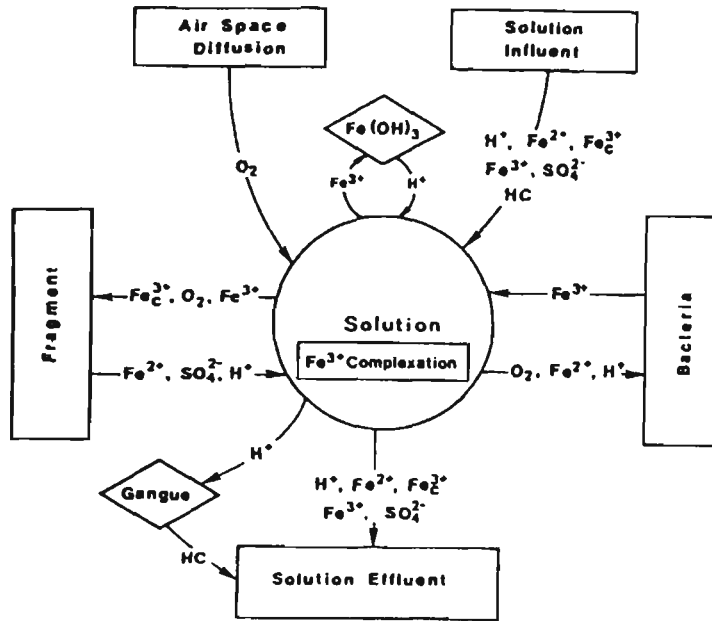


**Figure 3.9** The acid mine drainage model POLS.

(from Jaynes *et al.*, 1984)

A shrinking core model was used to determine the rate of oxidation of pyrite within the material. The oxidation rate per unit area of pyrite within a fragment was given by:

$$\frac{dX}{dt} = \frac{-1}{2t_D(1-X) + t_c} \quad (3.12)$$

where,  $X$  is the fraction of pyrite remaining in a fragment,  $t$  is time,  $t_D$  is the total time required for complete pyrite oxidation. If diffusion processes are the rate limiting step, then  $t_D$  is calculated by:

$$t_D = \frac{\sigma l^2}{2bD.C_0} \quad (3.13)$$

where,  $\sigma_f$  is the molar density of pyrite within a fragment,  $l$  is one half the thickness of a fragment,  $b$  is the stoichiometric ratio between pyrite and oxygen consumption,  $D_c$  is the effective diffusion coefficient for coupled oxidant-product counter diffusion, and  $C_0$  is the oxidant concentration at the fragment surface.

Where chemical reactions are the rate controlling process, the time ( $t_c$ ) required for complete pyrite oxidation is given by:

$$t_c = \frac{\sigma_f l}{b K_s C_0 \beta \alpha} \quad (3.14)$$

where  $K_s$  is the first order surface reaction rate constant for pyrite oxidation per unit surface area of pyrite,  $\beta$  is the effective thickness of the fragment within which pyrite is oxidised, and  $\alpha$  is the surface area of pyrite per unit volume of fragment.

When both oxygen and ferric iron are present, the rate of pyrite oxidation is the sum of the rates of each oxidant acting alone:

$$\frac{dX}{dt} = \frac{-1}{t_b(O_2)(1-X) + t_c(O_2)} + \frac{-1}{t_c(Fe^{3+})(1-X) + t_c(Fe^{3+})} \quad (3.15)$$

In the model, oxygen was considered to diffuse from the surface of the spoil into the pore space of the spoil profile at a constant rate. The vertical oxygen concentration within the spoil profile was described by:

$$\phi \cdot \frac{d}{dt}(\sigma_f Y_o) = \frac{P}{R} \frac{d}{dz} \left[ \frac{D_o \phi \cdot dY_o}{T \tau dz} \right] + Q_o \quad (3.16)$$

where,  $\phi_a$  is air-filled porosity,  $\sigma_a$  is molar density of air,  $Y_0$  is the mole fraction of oxygen in gas,  $P$  is atmospheric pressure,  $R$  is the gas constant,  $T$  is temperature,  $\tau$  is tortuosity,  $Q_0$  is oxygen uptake and  $z$  is depth. The  $Q_0$  term is partitioned into three components ( $Q_0 = Q_P + Q_A + Q_C$ ) where  $Q_P$  is the rate of oxygen consumption by the oxygen-pyrite oxidation reaction;  $Q_C$  is the oxygen consumed by the chemical oxidation of ferrous iron and  $Q_A$  is the rate at which bacteria consume oxygen while oxidising iron.

The model also considers the complexation reactions of ferric iron and assumes that the ferric iron concentration is limited by the solubility of amorphous ferric hydroxide. Acidity is produced by pyrite oxidation reactions (involving oxidation by oxygen or  $Fe^{3+}$ ) and is consumed or transformed into reserve forms of acidity by reactions with the spoil matrix. The effect of the hydrogen ion spoil reactions on acidity concentration is expressed by a simple empirically derived equation where all  $H^+$  produced ( $\Delta H_P$ ) is partitioned between the active solution hydrogen ion concentration and a lumped term (HC) which represents  $H^+$  lost by neutralisation and soluble stored acidity on exchange sites such as  $Al^{3+}$ . The expression used to partition the  $H^+$  produced by pyrite oxidation into solution  $H^+$  ( $\Delta H_A$ ) and neutralised or transformed  $H^+$  ( $\Delta H_P - \Delta H_A$ ) is:

$$\Delta H_A^+ = \Delta H_P^+ [1.0 - \exp(G_A - pH)] \quad (3.17)$$

where,  $G_A$  is an empirical constant.

The solution of the series of equations described above is very unstable due to the interdependence of the variables and the non-linearity of some of the equations. A numerical model POLS was developed to solve these equations. Jaynes *et al.* (1984b) assessed the sensitivity of POLS by running a series of eight simulations for two levels of pore space tortuosity, air-filled porosity, presence of chemoautotrophic bacteria and  $H^+$  interactions in the spoil. They concluded that for systems without iron-oxidising bacteria, oxygen is the only important oxidising agent for pyrite. Chemical oxidation of

ferrous to ferric iron was not rapid enough to affect the overall pyrite oxidation reaction. The pyrite oxidation reaction rate decreased by a reducing the air-filled pore space and an increase in pore space tortuosity or by burying the pyritic spoil at deeper depths within the spoil mound. Whether or not bacteria are important in those zones was found to be dependant on the solution pH. If the solution pH was maintained in the range between reduced bacterial efficiency ( $2.0 < \text{pH} < 3.0$ ), the oxidation rate of pyrite will be increased by bacterially produced ferric iron. Validation results for POLS were not presented.

POLS is a sophisticated model that simulates pyrite oxidation via direct oxygen oxidation, iron reduction and bacterially catalysed reactions. The issue of bacterially catalysed  $\text{Fe}^{3+}$  reduction being involved in pyrite oxidation at low pH is certainly worthy of investigation in acid sulfate soil, though this is not in the scope of the research presented in this thesis. The oxidation of pyrite as a result of the reduction of  $\text{Fe}^{3+}$  to  $\text{Fe}^{2+}$ , coupled with the change in the composition of the CEC as a result of acidity generated by previous pyrite oxidation (Ritsema *et al.*, 1992), suggests that minimising pyrite oxidation by removing oxygen from the pyritic material by saturating with water may not stop subsequent acid generation or result in improved water quality. On the other hand, direct chemical oxidation of pyrite with oxygen has been found to be the major contributor to acidification by other researchers (e.g., Elberling *et al.*, 1994; Nicholson *et al.*, 1989).

#### 3.3.2.4. PYROX-MINTRAN-MINTOX

Wunderly *et al.* (1996) developed the simulation model PYROX that couples one dimensional oxygen diffusion and sulfide mineral oxidation to simulate the oxidation of pyrite in the unsaturated zone within mine tailings. The PYROX model has then been coupled with a two dimensional reactive transport model, MINTRAN, which uses a finite element scheme for the transport of contaminants and MINTEQA2 to solve the

equilibrium geochemistry in the mine tailings solution. The coupled model has been called MINTOX.

The mass balance equation for oxygen diffusion into the pore space for PYROX is:

$$a_{por}(x) \frac{\partial U_A(x, t)}{\partial t} = D1(x) \frac{\partial^2 U_A(x, t)}{\partial x^2} - q(x, t) \quad (3.18)$$

where,  $a_{por}(x)$  is the air-filled porosity of the tailings,  $D1(x)$  is the diffusion coefficient of the tailings,  $U_A$  is the oxygen concentration in the pore space, temp is in kelvins and  $q(x, t)$  is the sink term due to oxygen consumption in the tailings particles. The diffusion coefficient is calculated using an empirically derived expression:

$$D1(x) = 3.98 \times 10^{-9} \left[ \frac{a_{por}(i) - 0.05}{0.95} \right]^{1.7} \times (temp)^{1.5} \quad (3.19)$$

PYROX is based on the assumption that all particles are spherical, uniform in size and surrounded by an immobile film of water. The model uses a shrinking core approach and assumes that pyrite is homogenously distributed within the solid space of the tailings. The oxygen diffuses from the particle-pore space surface through the porous oxidised outer layer of the particle towards the unoxidised zone towards the centre of the particle where oxidation takes place. As the reaction between the oxygen and the sulfide mineral within the particle progresses, the radius of the unreacted core shrinks, whilst the thickness of the oxidised zone increases. Given that the rate of shrinkage of the unoxidised core is approximately 1000 times slower than the flow rate of oxygen within the particle, then the reaction front within the particle is assumed to be stationary with respect to the oxygen concentration gradient between the outside of the particle and the reaction front.

Given the assumption described above, the sink term representing oxygen consumption by oxidation of pyrite within a unit volume of tailings,  $q(x,t)$ , was calculated by:

$$q(x,t) = \frac{3[1 - \text{por}(x)]D_2}{R^{*3}} \left( \frac{R^* r_c^*(x)}{R^* - r_c^*(x)} \right) U_w^*(x,t) \quad (3.20)$$

where,  $r_c^*(x)$  is the radius of the reaction front,  $R^*$  is the unreacted radius of a particle,  $\text{por}$  is the porosity of the tailings,  $D_2$  is the diffusivity of the oxidised rim of the particle and  $U_w^*$  is the oxygen concentration of the water film around the particle.

By combining (3.18) and (3.20), Wunderly *et al.* (1996) derived an expression for oxygen diffusion into tailings with the sink term represented as shrinking core particles. This expression can be written as:

$$\text{apor}(x) \frac{\partial U_A^*(x,t)}{\partial t} = D_1(x) \frac{\partial^2 U_A^*(x,t)}{\partial x^2} - \frac{3[1 - \text{por}(x)]D_2}{R^{*3}} \left( \frac{R^* r_c^*(x)}{R^* - r_c^*(x)} \right) U_w^*(x,t) \quad (3.21)$$

Equation (3.21) expresses the mass balance for oxygen diffusing into the pore space of the tailings including the loss of oxygen to the particles. To gain a unique solution for (w4), another equation relating  $U_A^*(x,t)$  and  $r_c^*(x,t)$  was required. To define a system of two equations with two unknowns that is able to be solved to gain a unique solution, an expression for determining the radius of the reaction front within the tailings particles was rewritten as:

$$\frac{dr_c^*}{dt} = \frac{D_2(1 - \text{por})}{\epsilon \rho r_c^{*2}} \left( \frac{R^* r_c^*(x)}{R^* - r_c^*(x)} \right) U_w^*(x,t) \quad (3.22)$$

The PYROX model was coupled with the finite element reactive transport model MINTRAN. The two models were coupled in such a manner that MINTOX was



capable of running as a 1-D or 2-D simulation, where oxygen diffusion was assumed to occur only in the vertical direction. As MINTOX marches through time, the degree of pyrite oxidation occurring within the current time step is calculated. The concentrations of the oxidation products (namely  $\text{H}^+$ ,  $\text{SO}_4^{2-}$ ,  $\text{Fe}^{2+}$  and  $\text{Fe}^{3+}$ ) are calculated at each node within the finite element mesh in the unsaturated zone and then added to the corresponding spatial node in the reactive transport part of the code. The aqueous components are transported individually and a new equilibrium is calculated at each node before continuing on to the next time step. Once all the pyrite is consumed at a particular depth, the program calculates a zero concentration increase at that node for all the reaction products.

MINTOX has been extensively validated by the Wunderly *et al.* (1996). Results of 1-D simulations reported in this paper corresponded closely to field data from which the initial conditions for MINTOX were taken. These data are shown in Figure 3.10.

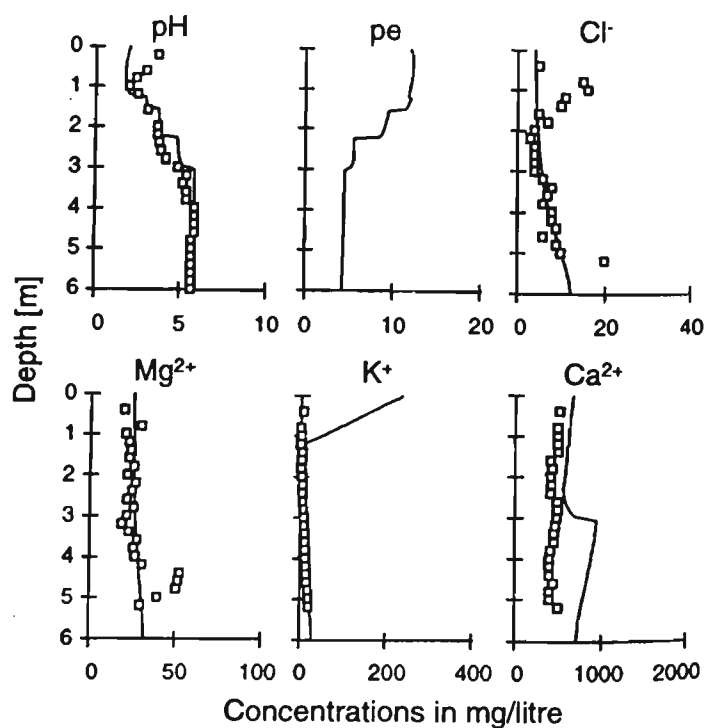


**Figure 3.10** MINTOX simulation in comparison to field results from Elliot Lake, Ontario.  
(from Wunderly *et al.*, 1996).

Calculations of aqueous chemistry made during the numerical simulations match general trends observed in water chemistry to the field study site after 12 years of pyrite oxidation had taken place.

The approach adopted by Wunderly *et al.* (1996) of calculating the air-filled porosity using a 2D unsaturated flow model and coupling this to a pyrite oxidation routine represents a major advance in being able to simulate the influence of the geometry of tailings lagoons (or drains for acid sulfate soil). A similar approach was adopted in the development of the model described in Chapter 10. However, Wunderly *et al.* (1996) simulated the diffusion of oxygen through the mine tailings as a front moving parallel with the surface. This assumption may be valid for relatively uniform tailings; however, it is not appropriate for acid sulfate soils where large macropores readily transport oxygen in the soil as the groundwater falls. The influence of macroporosity in determining oxygen transport onto the soil is taken into consideration in the development of pyrite oxidation model for acid sulfate soils described in Chapter 10.

The sophistication of MINTOX is arguably unnecessary for the assessment of appropriate pyrite management options available for tailings or acid sulfate soils, although it is valuable as a research tool. Many of the parameters required for PYROX and MINTRAN are expensive and difficult to measure, thereby making accurate parameterisation of the model hard to achieve.

#### 3.3.2.5 *Simulation Model for Acid Sulfate Soils (SMASS)*

To date, the most sophisticated process based model that has been developed to predict the effects of water management strategies on the acidification and de-acidification, release and movement of oxidation products from acid sulfate soils is the Simulation Model for Acid Sulfate Soils (SMASS) developed by Bronswijk and Groenberg (1992). SMASS consists of a number of sub-models in which the various physical and chemical

processes occurring in acid sulfate soils are simulated using mathematical equations. SMASS is a one-dimensional compartmentalised numerical simulation model requiring initial conditions for the physical and chemical state of each compartment. The physical and chemical conditions within each compartment, as well as the water and solute fluxes at the boundary of the soil system, are computed at selected time intervals. A description of the analytical and numerical techniques used in SMASS is given in Chapter 9 where SMASS is used to assess various surface and groundwater management options for the management of acid sulfate soil at the Berry study site. Figure 3.11 describes the compartmentalised structure of SMASS.

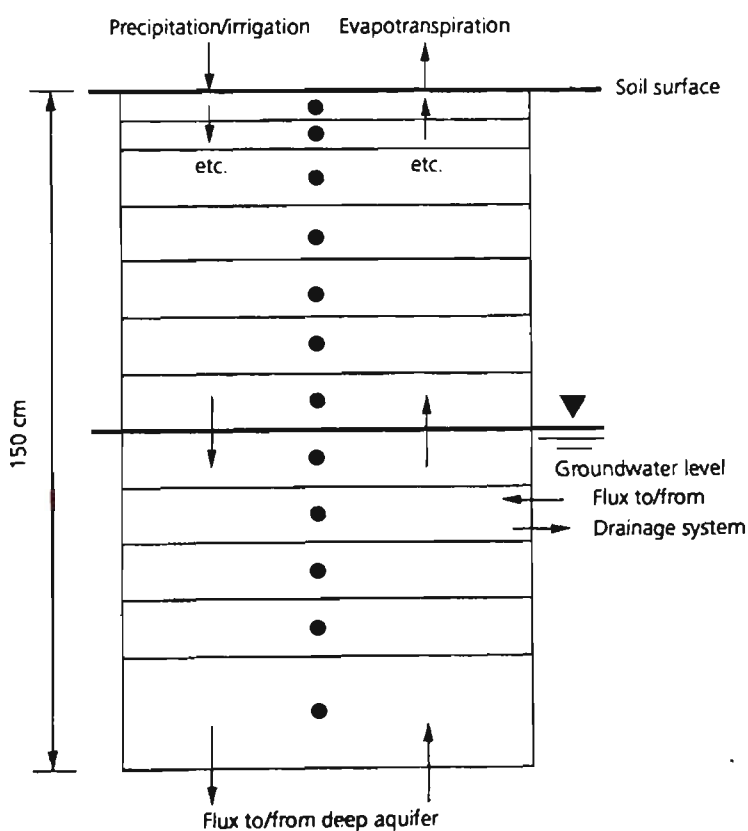


**Figure 3.11** Schematic of a SMASS soil profile. Arrows indicate water and solute fluxes.  
(from Bronswijk and Groenberg, 1992).

The model structure in which the various model sub-routines are computed within each time step is shown in Figure 3.12

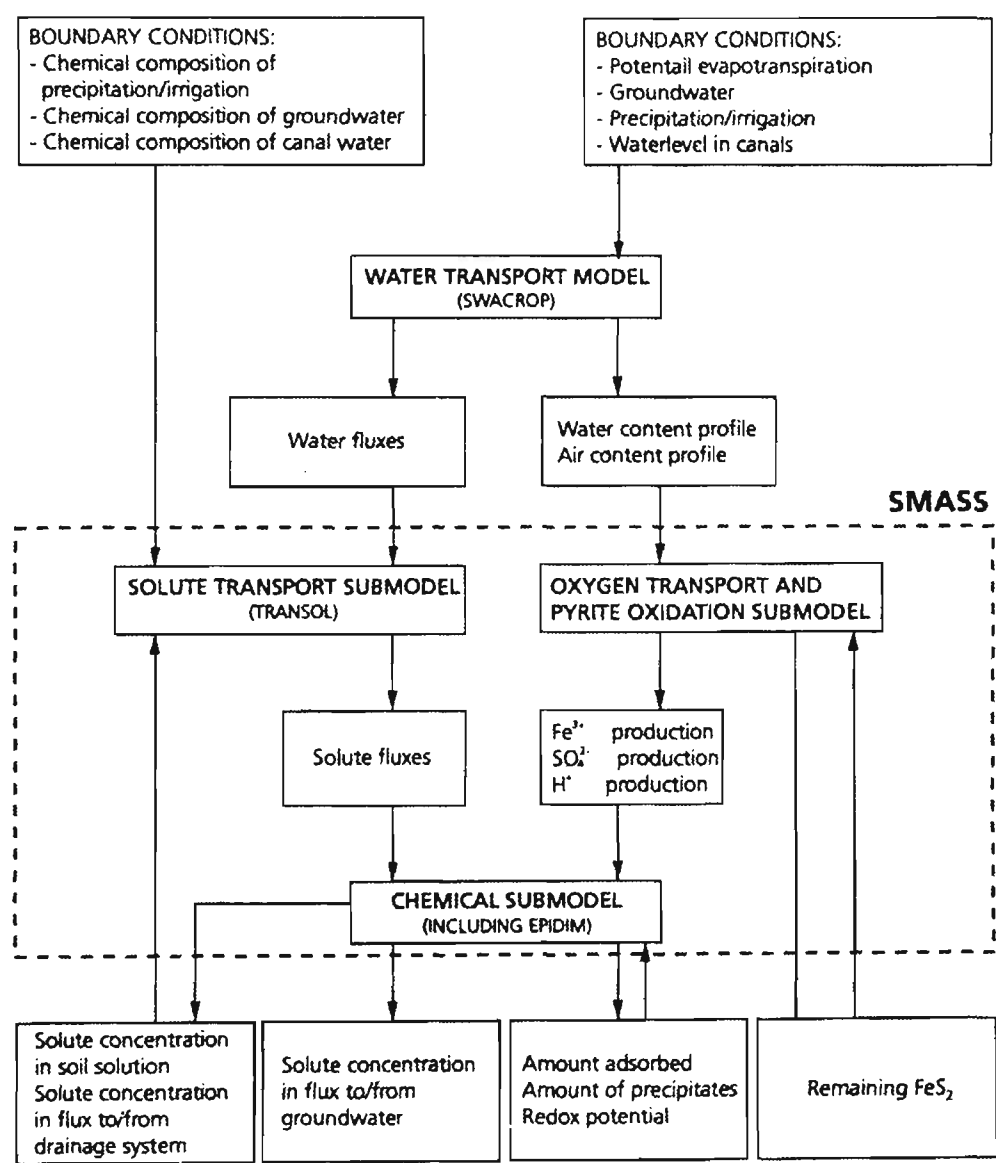


**Figure 3.12.** Structure of SMASS  
(from Bronswijk and Groenberg, 1992).

The function of each sub-component of SMASS is briefly described below.

- a) The *water transport sub-model* calculates the vertical water transport to give a water content profile and air-filled porosity.
- b) The *oxygen transport and pyrite oxidation model* is based on Bronswijk *et al.* (1993). Air contents are used to calculate oxygen diffusion coefficients in the air-filled macropore space, and oxygen consumption for pyrite and organic matter is calculated. The oxygen content profile in the soil macropores is then calculated.
- c) Depending on the oxygen concentration in a given compartment, the rate of pyrite oxidation in that compartment is calculated in the *oxygen transport and pyrite oxidation sub-model*. The amount of pyrite is converted into amounts of  $\text{H}^+$ ,  $\text{Fe}^{3+}$  and  $\text{SO}_4^{2-}$  produced in each compartment. The remaining pyrite remaining is calculated for the next iteration.
- d) The *solute transport sub-model* computes the solute fluxes between compartments depending on the water fluxes from step (1).
- e) In the *chemical sub-model*, the equilibrium concentrations in the soil solution, the composition of the exchange complex and the amount of minerals and precipitates are calculated.

Bronswijk *et al.* (1993) proposed a pyrite oxidation model based on the assumptions that the consumption of oxygen by organic matter in the soil matrix is constant where oxygen is available in the soil matrix and that the dissolution of pyrite by oxidation takes place according to an 'equal diameter reduction' model. Both these assumptions are validated by Bronswijk *et al.* (1993) by extensive testing of their model against experimental data and comparison with analytical solutions. In addition, the contribution of oxygen consumption by organic matter was shown to be small in comparison to the consumption of oxygen by pyrite.

The amount of oxygen consumed by pyrite in the aerobic part of the soil profile is calculated by the difference between the total mass of oxygen consumption and the consumption of oxygen by organic matter. The amount of pyrite oxidation product ( $H^+$ ,  $SO_4^{2-}$  and  $Fe^{2+}$ ) is calculated using stoichiometric conversion from the consumption of oxygen by pyrite in a soil layer.

Bronswijk *et al.* (1993) validated SMASS by comparing model output with measured data from a column experiment. Figure 3.13 shows that the computed pyrite content in the soil profile after 440 days of oxidation corresponded well with the measured pyrite concentration. The large difference between measured and computed values at 65 cm depth is attributed to experimental error in the measurement of pyrite concentration.

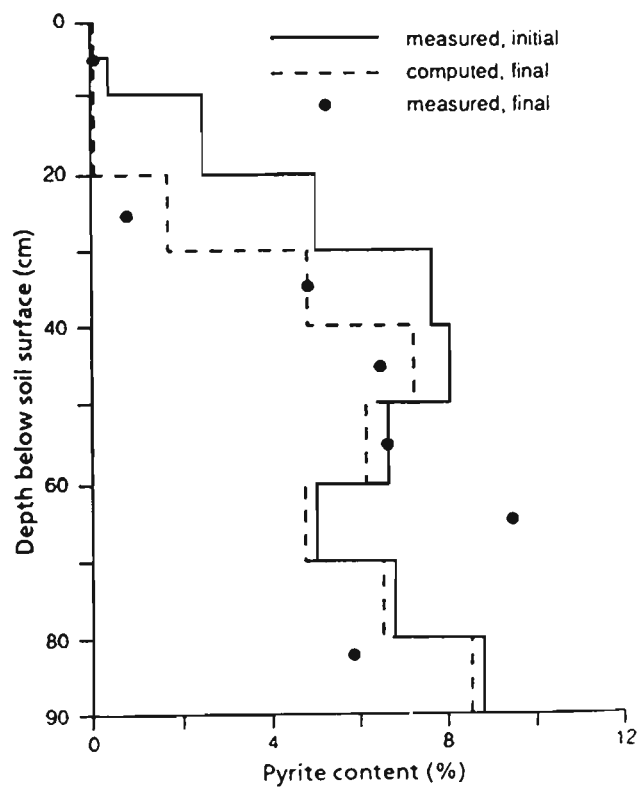


**Figure 3.13.** Comparison between measured and computed pyrite distribution.  
(from Bronswijk and Groenberg, 1992).

The computed oxygen concentration in the macropore air also matched measured concentrations (Figure 3.13). Bronswijk *et al.* (1993) suggested that the slightly higher oxygen concentration in the measured soil profiles may be attributed to higher oxygen consumption by easily decomposable organic matter in the saturated soil. Oxygen consumption by organic matter is assumed to be constant in SMASS, which may lead to an under-estimation of oxygen consumption for short periods of time during profile drainage.

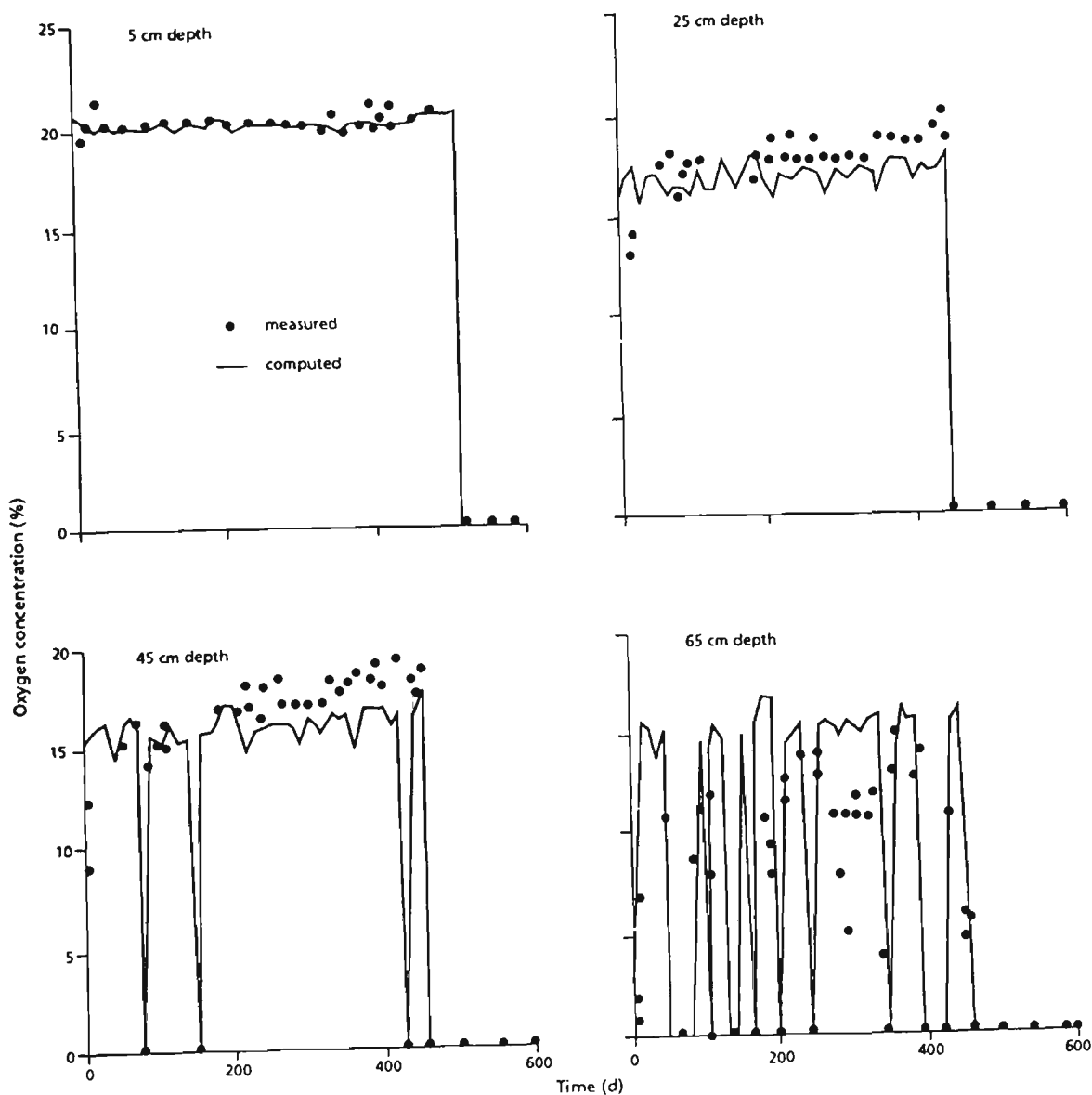


**Figure 3.14** Measured and computed oxygen concentrations in soil macropores at 5, 25, 45, 65 cm depth.

(from Bronswijk and Groenberg, 1992).

The measured and computed sulfate concentrations of the soil solution at various depths in the soil profile are shown in Figure 3.14.

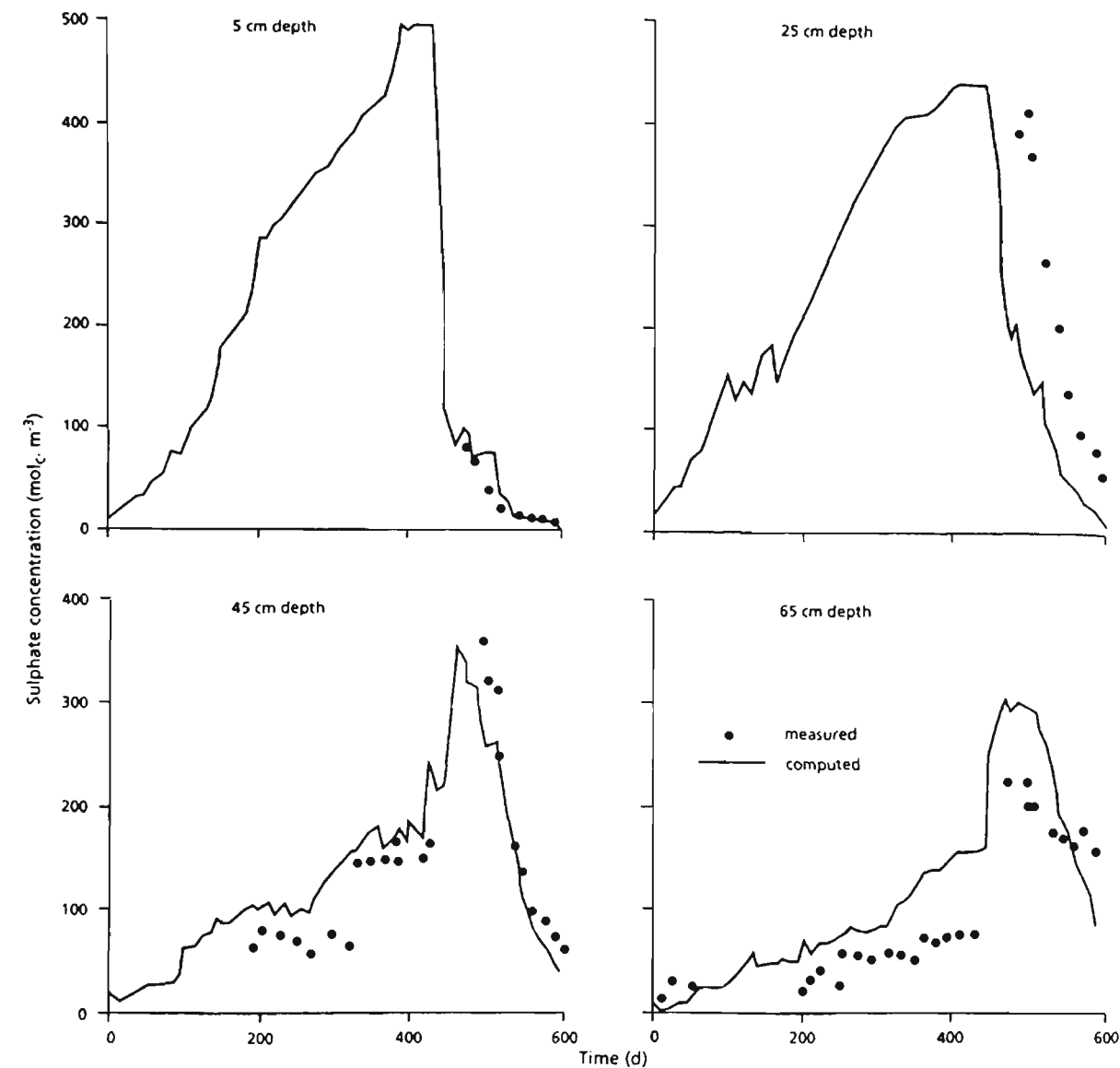


**Figure 3.15** Measured and computed sulfate concentration.

(from Bronswijk and Groenberg, 1992).

The comparison of measured and computed sulfate concentrations at various depths in the soil profile is not as good as for other relevant soil properties. The general trends in sulfate production between the measured and computed sulfate concentrations appear to



correspond well, although Bronswijk *et al.* (1993) suggested that accurate determination of the sulfate concentration in the pore water by numerical means is extremely difficult due to the large number of chemical reactions that involve sulfate and problems associated with modelling sulfate leaching in soil with large macropores.

Although calculation of the concentration of the pyrite oxidation products in the soil solution is difficult, the numerical scheme devised by Bronswijk *et al.* (1993) adequately simulated oxygen transport and the consumption. This is extremely useful for comparing the adequacy of acid sulfate soil management strategies, particularly where alternative surface or groundwater management strategies aim to minimise the generation of more acid by the maintenance of reducing conditions within the soil profile. In this sense, the concentration of pyrite oxidation products is of secondary importance in comparison to the effectiveness of the acid sulfate soil water management strategy's ability to reduce pyrite oxidation.

However, the application of the one-dimensional SMASS to the real world management of acid sulfate soils in a three dimensional landscape is difficult. SMASS does not enable an assessment of the effectiveness of various water management practices to be simulated, for example, the operation of flood mitigation drains at the sub-catchment scale. Drainage and evapotranspiration affects the elevation of groundwater in different ways across a site, giving rise to areas where pyrite oxidation is promoted due to the influence of drainage structures or cropping practices.

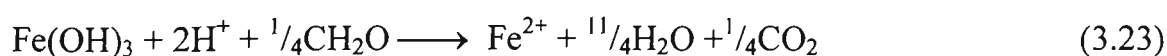
This deficiency in SMASS is shown in Chapter 9, and in Blunden and Indraratna (2000), where the groundwater profile across the study site varied considerably from a position close to the drain to a location further away. In Blunden and Indraratna (2000), the groundwater profile at the study site had to be simulated using FEMWATER (Lin, *et al.* 1997) and the groundwater elevation data calculated by FEMWATER was then transcribed to SMASS for simulation of pyrite oxidation two locations, one close to and the other further away from the drain. The processes that are simulated by SMASS must be integrated into a broader two, or better three, dimensional model that describes the

hydrological state and fluxes of the catchment at appropriate time intervals that are caused by the interaction of climatic influences and land management actions prior to any assessment of long term acid sulfate soil management practices. The development of a coupled 3D water flow - pyrite oxidation numerical model is an objective of this research and is comprehensively discussed in Chapters 10 and 11.

### 3.4 Pyrite oxidation management strategies at the sub-catchment scale

Management of acid sulfate soils at the sub-catchment scale is determined by the water balance of the site. The effectiveness of acid sulfate soil rehabilitation projects at the sub-catchments scale has not been reported in the literature for Australian conditions. A few rehabilitation techniques such as surface ponding of water (Smith and Yerbury, 1996) and drain reshaping (Neal, 1996) have been initiated but not monitored in a scientifically justifiable manner. Additional acid sulfate soil management trials are currently underway in eastern Australia, but the outcomes of these trials are yet to be published.

It has been suggested (Dent, 1986) that pyrite oxidation could be minimised, or even reversed, by the establishment of reducing conditions in acid sulfate soils by reflooding. In a flooded environment, a microbial catalysed reaction in the presence of organic matter may reduce dissolved sulfate to hydrogen sulfide (H<sub>2</sub>S) and precipitated Fe<sup>3+</sup> to dissolved Fe<sup>2+</sup> as described below.



Nicholson *et al.* (1989) showed that reducing the transport of oxygen into tailings by employing a fine grained moisture retention barrier can effectively decrease acid

generation rates. Indraratna *et al.* (1995), Blunden *et al.* (1997) and Blunden and Indraratna (2000) have shown that manipulation of drain water levels can influence surrounding groundwater levels. It has been suggested by these authors that raised groundwater levels will reduce the diffusivity of oxygen into the profile and thereby reduce acid generation rates. Pease *et al.* (1997) promoted groundwater elevation as an acid sulfate soil management technique.

White *et al.* (1997) urge caution for proponents of freshwater reflooding by surface inundation. They suggested that the organic matter content in oxidised acid sulfate soil in eastern Australia may be inadequate to fuel the microbial catalysed reduction reaction, that the frequency of acidic discharges may increase until the store of acid present in the soil is leached from the profile and that water levels may be difficult to maintain over the longer term due to the unreliable nature of Australian rainfall.

White *et al.*'s. (1997) assessment of re-flooding may not be wholly warranted if their suggestions are extended to raising groundwater above the acid sulfate soil layer. Given that substantial discharges of acid are occurring during the falling stage of flood events after dry periods in areas of oxidised acid sulfate soils, better water management techniques that have potential for long term improvement in water quality should be trialed and their effectiveness assessed. It is inevitable that a long, largely unquantifiable, time will be required for  $\text{Fe}^{3+}$  and other oxidation products to be leached from the soil, after which a substantially reduced volume of acid may be generated in the saturated pyritic sediments. A common complaint is that opposing industry groups expect that acid sulfate soil remedial works will give immediate benefits in water quality. More realistic timeframes and better information on the effectiveness of acid sulfate soil remediation strategies must be communicated to land managers and other interested community groups if the adoption of remedial strategies is to be successful.

### 3.5 Conclusions

Field, laboratory and numerical modelling studies all conclude that where groundwater falls below or into pyritic materials, oxidation of the pyrite occurs. Given this conclusion, it is reasonable to assert that groundwater management is the key to minimising future oxidation of pyrite and the generation of acid. Some authors (e.g., Jaynes *et al.*, 1994) caution that pyrite oxidation by the reduction of  $\text{Fe}^{3+}$  at low pH may still continue to oxidise pyrite under reducing conditions, whilst others (e.g., Ritsema *et al.*, 1992) suggest that groundwater quality will remain poor until the status of the soil CEC can be improved. The dissolution of acidic iron and aluminium minerals will also maintain acidic groundwater conditions. Irrespective of these authors' cautionary notes, there is no disputation that oxidation by molecular oxygen is the primary pyrite oxidation agent responsible for the generation of acid in acid sulfate soil or pyritic mine wastes.

#### 3.5.1 Relationship of previous research to the current study

Two major inadequacies of previous research have been identified and are addressed in this research. Firstly, the application of large scale field trials involving the manipulation of groundwater elevation to maintain acid sulfate soil in a reducing environment has not been attempted in Australia, although many authors (e.g., Pease *et al.*, 1997; Indraratna *et al.*, 1995) have recommend that such a field experiment should be implemented. The research reported in this thesis examines the effectiveness of installing weirs in major flood mitigation drains at three different elevations relative to the surrounding acid sulfate soil layer for a site located on the south coast of New South Wales. Two broad measures of the effectiveness of the trial are described, namely the groundwater hydrology of the study area before and after the installation of the weirs, and changes in the quality of the groundwater and water in the drains with respect to the

elevation of the groundwater relative to the acid sulfate soil layer. These results are reported and discussed in Chapters 7 and 8.

Secondly, the pyrite oxidation models presented in this Chapter are not readily applicable to the assessment of groundwater manipulation techniques at the sub-catchment scale. A new approach is adapted from the work of Bronswijk *et al.* (1993) for pyrite oxidation which considers oxygen transport through structural features in the soil, namely macropores, and the lateral diffusion and consumption of oxygen by pyrite oxidation in the surrounding soil matrix. This theoretical approach has been used to develop the pyrite oxidation model ASS3D, which uses the output from a commercially available 3D water flow model, to simulate pyrite oxidation and acid generation for 3D landscapes. Application of ASS3D enables various water management strategies to be simulated and assessed for their effectiveness in controlling pyrite oxidation at the sub-catchment scale. The development and application of the 3D pyrite oxidation model is described in Chapters 10 and 11 of this thesis.

## **Chapter 4: Field study site and monitoring equipment**

### **4.1 Introduction**

The study site and the equipment used to monitor both physical and chemical attributes of the groundwater and drain water are described in this Chapter. The study site was selected so that the installation of weirs in flood mitigation drains to raise groundwater levels above the acid sulfate soil layer in the surrounding sub-catchment could be monitored and assessed. The study site is suitable for this purpose because of two major attributes, namely;

- a) the site is underlain by acid sulfate soil, and
- b) the site is intersected by deep flood mitigation drains that have, in the past, lowered groundwater tables below the elevation of the acid sulfate soil layer giving rise to acidic soil and groundwater conditions.

The geomorphology of the catchment and the nature of the drainage works undertaken within the catchment area are described in this Chapter. The exact location of the study site within the Shoalhaven Catchment and the nature of the drainage scheme at the site are also presented. The design and construction of the three weirs installed in the flood mitigation drains, together with an explanation of why weirs were thought to be a potential acid sulfate soil management strategy are provided.

The equipment installed at the site or used on a routine basis for monitoring groundwater and drain water elevation and quality is described. This includes the installation, location and operation of piezometers, routine pH testing of groundwater and drain water, the location and operation of automatic water level recorders in both piezometers and drains, and the collection of water quality samples for laboratory testing. The location and the instruments on the weatherstation installed at the site to record climatic variables are also presented.

## 4.2 Study site location

The study site is a small sub-catchment of approximately 120 ha that has been drained for agricultural and flood mitigation purposes. The site is adjacent to the township of Berry (34°S, 150°E) on the South Coast of New South Wales, Australia. A network of deep drains was constructed across the site in the late 1960s. The drains discharge into Broughton Creek, a left bank tributary of the Shoalhaven River through one-way floodgates that discharge during the low tide. The site is located approximately 14 km from the junction of Broughton Creek and the Shoalhaven River. The study site is bounded by Broughton Creek to the east and extends into elevated land above the floodplain on the western and northern perimeters. The area of the Broughton Creek catchment is 184 km<sup>2</sup>. A location map of the study site is shown in Figure 4.1 and an aerial photograph of the site is shown in Plate 4.1

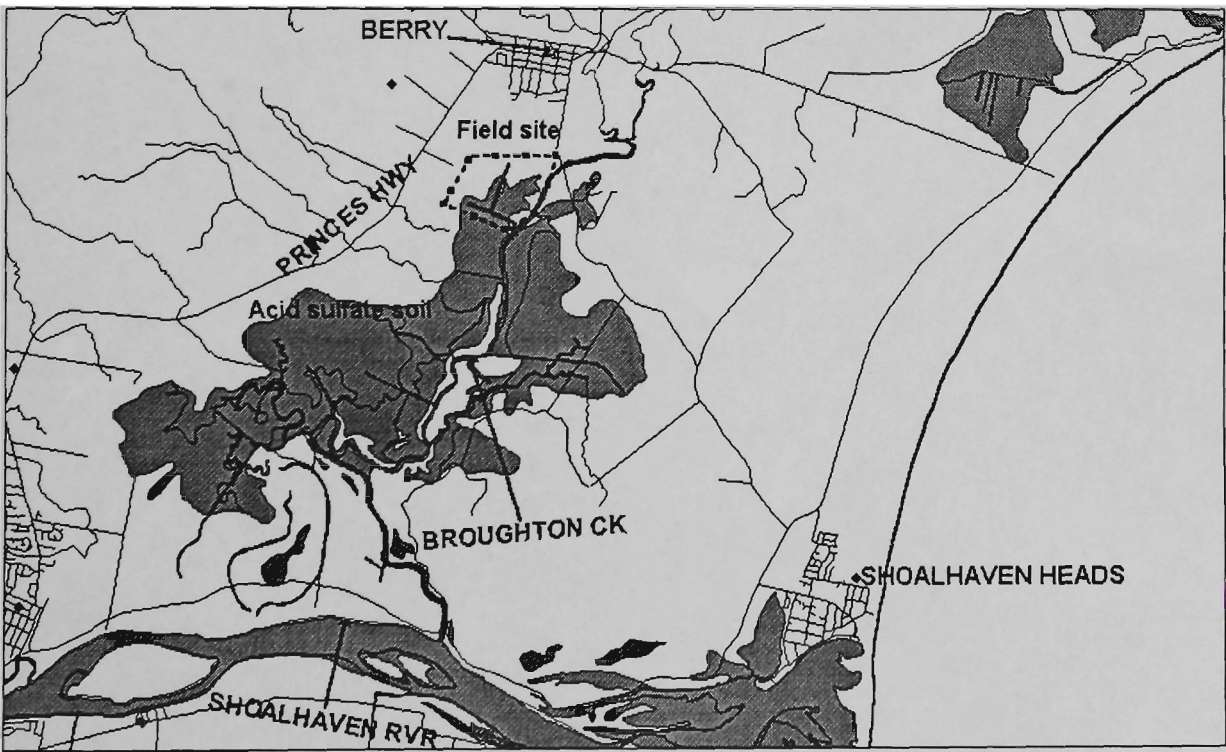


**Figure 4.1:** Location of the study site.





**Plate 4.1** Aerial photo of the study site.



#### *4.2.1 Geology and Geomorphology*

The lower Shoalhaven River catchment is comprised of low hillslopes, a coastal sand barrier and coastal floodplains (Wright, 1970). Low hillslopes form the undulating terrain surrounding the river floodplain to the north, west and south which rise further to a steep escarpment defining the western extent of the coastal strip. The hillslopes cut through strata of Permian age which consist of siltstones, shales and sandstones of the Berry Formation (Wollongong 1:250000 Geological Sheet, 1966, SI 56-9). To the east, a late Quaternary sand barrier separates the floodplain from the Pacific Ocean. An extensive floodplain extends on both the northern and southern sides of the Shoalhaven River. The unconsolidated sediments of the floodplain are underlain by Berry Siltstone and Nowra Sandstone.

The evolution of the lower Shoalhaven River belongs to the “barrier estuary” system as described by Roy (1984). Other estuaries with problems associated with acid sulfate soils such as the Tweed, Richmond and Macleay have also evolved as “barrier estuary” systems. Barrier estuaries experience significant changes in shoreline morphology during infilling. According to Roy (1984), in early stages of development, the shorelines of barrier estuaries are often rocky and highly irregular (Fig. 4.2a). The deposition of a coastal sand barrier (e.g. behind Seven Mile Beach) gives rise to an extensive area of well protected, shallow depositional basins. As the estuary infills and shallows, smoother sedimentary shorelines develop (Fig 4.2b). These shorelines develop into lobate deltas with bifurcating distributary channels, shoal grounds and embayments (Fig 4.2c). Final stages of infilling are characterised by sinuous channels with smooth levee banks (Fig 4.2d). These final stages of deposition are typical in the lower Shoalhaven floodplain.

The infilling of the Shoalhaven River valley commenced about 12000 years ago with the Post Glacial Marine Transition (PGMT), when sea levels were about -30-40 m AHD. During the PGMT, there was rapid landward movement of marine sediments with the

rising sea level, resulting in the drowning of prior river valleys by about 7000 years ago (Roy *et al.*, 1980). The estuary floodplains started to develop as sedimentation and infilling began when the sea level stabilised (Dent, 1986). It is widely believed that sea levels stabilised about 6000-6500 years ago when the PGMT ceased, but Young *et al.* (1993) have suggested that sea levels were higher than current levels during the Holocene along the central and southern coasts of New South Wales. Radiocarbon dated materials collected in the Shoalhaven floodplain by Willett and Walker (1982) showed that the age of unoxidised estuarine sediments and shell collected in these sediments was  $4280 \pm 110$  and  $3800 \pm 110$  years BP, respectively. This suggests that elevated sea levels, which provide the necessary conditions for the formation of pyrite in acid sulfate soils, may have been present up to about 4000 years BP.

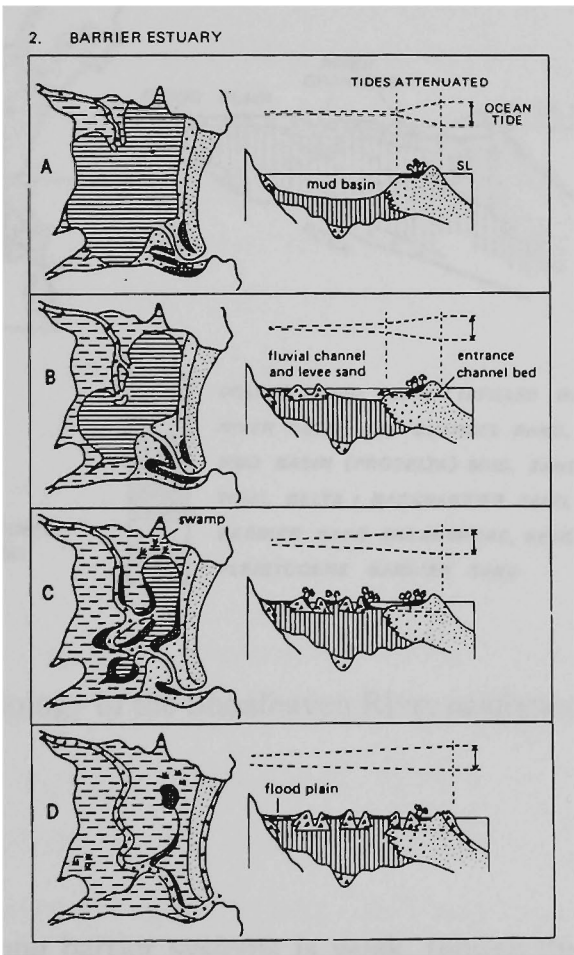


**Figure 4.2** Evolution of the lower Shoalhaven River catchment  
(after Roy 1984)

Roy (1984) suggested that sedimentation in the Shoalhaven proto-estuary occurred at about  $5 \text{ mm year}^{-1}$  to form an extensive sub-aqueous “mud basin” up to 30 m thick. In the landward direction, these muds interlayer with fluvial silts and sands, and in the seawards direction with tidal deltaic sand deposits within the river mouth. The stratigraphy of the study site is discussed in Chapter 6. The Shoalhaven barrier estuary system is at a mature stage of development as infilling has all but ceased, and river sand is being exported from the estuarine system and accreting on the beach. A schematic diagram of the stratigraphy of the Shoalhaven River catchment is shown in Figure 4.3.

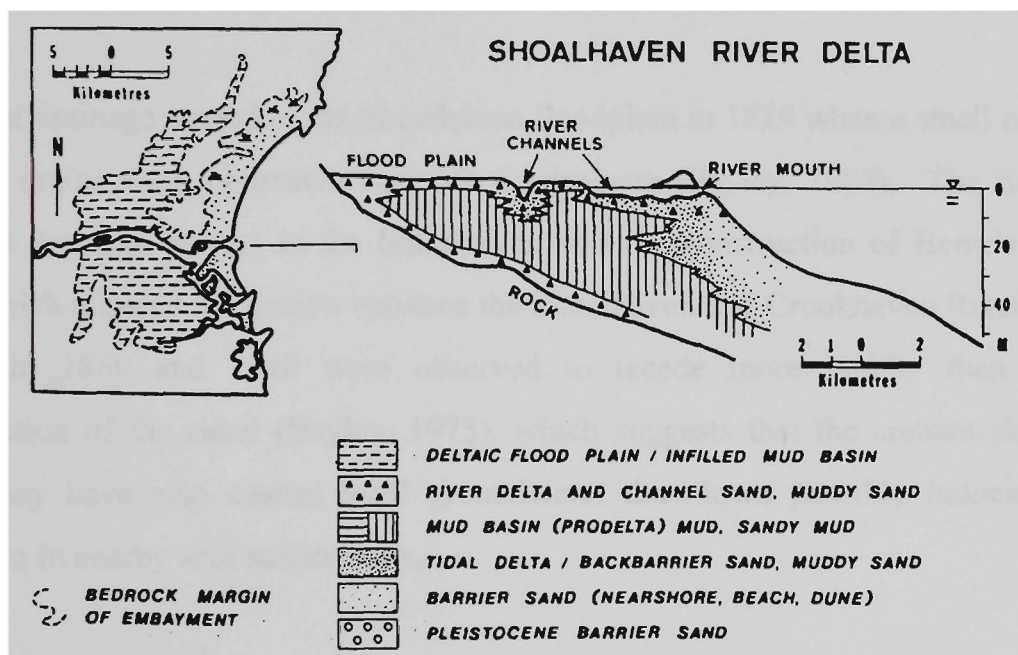


**Figure 4.3** Geomorphology of the Shoalhaven River catchment

(after Roy, 1984)

The tidal range of young barrier systems is weak, though this increases until a strong tidal regime is established in mature systems. Pease (1994) observed a significant tidal range up to 0.75 m at a location 11.5 km up Broughton Creek from the junction with the Shoalhaven River.

The geomorphic evolution of the Shoalhaven estuary lends itself to the formation of acid sulfate soils (see Chapter 2). The NSW Department of Land and Water Conservation has produced Acid Sulfate Soil Risk Maps according to the methodology described by Naylor *et al.* (1995). Approximately 2500 ha of land with a high risk of occurrence of acid sulfate soil is found in the Broughton Creek floodplain (Naylor *et al.*, 1995). The distribution of acid sulfate soil in the Shoalhaven floodplain is shown in Figures 4.1 and 4.4 (see swamp soils).

#### 4.2.2 Shoalhaven drainage system

Artificial drainage started in the Shoalhaven floodplain in 1829 when a small number of shallow drains were excavated near Mt Coolangatta (Bayley, 1975). The first major artificial drainage project in the Shoalhaven was the construction of Berry's canal in 1840 which allowed navigation between the Shoalhaven and Crookhaven Rivers. Flood waters in 1860 and 1870 were observed to recede more rapidly than prior to construction of the canal (Bayley, 1975), which suggests that the construction of the canal may have also caused local groundwater drawdown possibly inducing pyrite oxidation in nearby acid sulfate soils.

Artificial drainage was originally constructed to increase the amount of prime dairy land in the Shoalhaven area. During the 1890s, the introduction of improved *Paspalum* pasture for cattle feed significantly increased milk and cream production. Additional flat land which was suitable for the introduction of *Paspalum* was sought. By 1901, 32 km<sup>2</sup> of floodplain surrounding Broughton Creek was drained with 210 km of drains fitted with floodgates and walls.

The present drainage network on the Broughton Creek floodplain was in place by 1949 (Downey, Shoalhaven City Council, 1997). During 1965-72 all of the existing drains were deepened and widened by dragline in accordance with government flood

mitigation policies and funding arrangements of the day. In addition, all floodgate structures were upgraded during 1965-72. The geometry of the flood mitigation drains and the operation of the floodgates at the study site are shown in Plate 4.2 and 4.3.



**Plate 4.2** Flood mitigation drain at the study site.





**Plate 4.3** Floodgate at the study site.

All floodgates installed on Broughton Creek consist of a battery of 1-4 concrete culverts with vertically suspended steel plates operating to control the ingress of salt water from the Creek into the drains. Each culvert has the dimensions 2 m high x 2 m wide x 10 m long. The gates are lined with rubber sheet to seal between the steel and concrete to minimise leakage. However, floodgates often leak due to either objects being stuck between the gate and the culvert wall holding the gate open, or poor sealing of the gate due to the rubber sheet perishing or the steel gate warping.

No further major drain excavation or floodgate construction has been carried out since 1972. Regular floodgate maintenance and mechanical weed control within the drains ensures that rapid removal of surface floodwater, as well as rapid drawdown of

groundwater. The present drainage network on the Broughton Creek floodplain is shown in Figure 4.4.

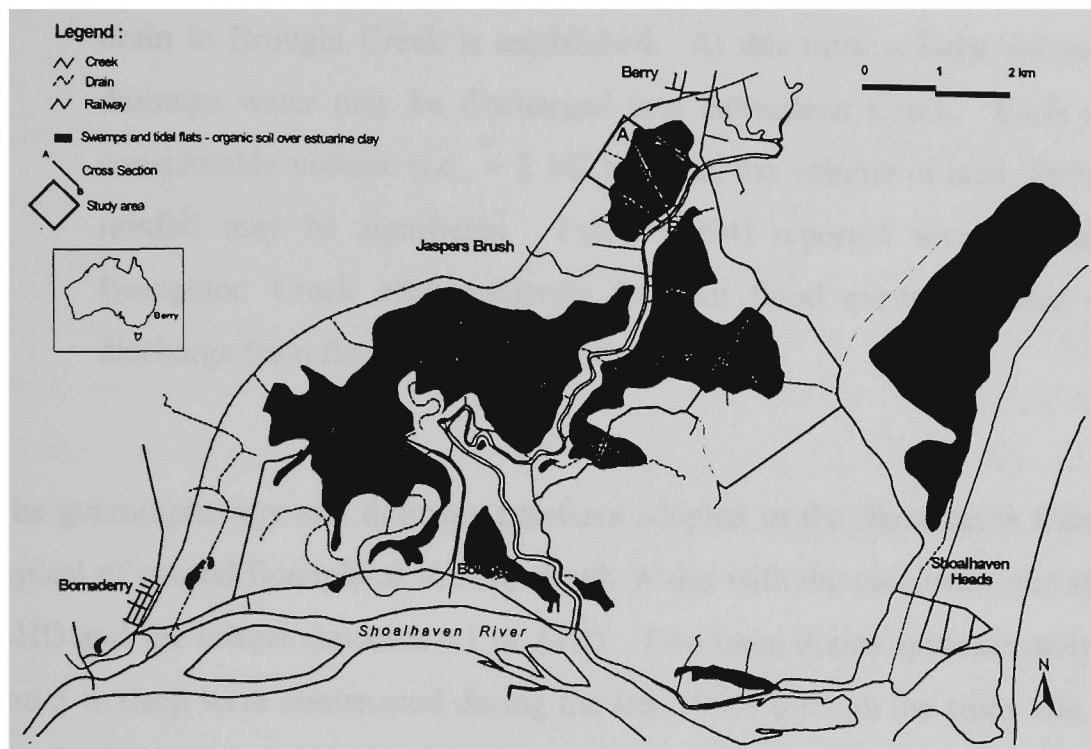


**Figure 4.4** Broughton Creek floodplain and drainage system infrastructure

Analysis of the drainage system and infrastructure has three major points of interest with respect to the implementation of drainage on the Broughton Creek floodplain.

1. Artificial drainage has been implemented across most of the floodplain. Approximately 230 km of drains are found on 40 km<sup>2</sup> of land prone to inundation, giving a drainage density of 5.75 km km<sup>-2</sup> (Pease, 1994). Given the geometry of the drains and the operation of the floodgates, it would be expected that the high drainage density would lead to significant and extensive groundwater drawdown.
2. Given the expected (usually shallow) depth to the acid sulfate soil layers described in Figure 4.1, it would be expected that groundwater drawdown would cause the acid sulfate soil to become periodically unsaturated, thereby giving rise to pyrite oxidation and subsequent generation of acidic oxidation products.

3. Floodgates are present on all but one of the drainage channels as they discharge to Broughton Creek. As groundwater drawdown occurs, acidic water discharges into the drains and remains there until a sufficient hydraulic gradient from the drain to Broughton Creek is established. At this time, a large volume of acidic drainage water may be discharged into Broughton Creek. Each drain has a considerable volume (i.e., > 2 ML), hence, the volume of acid discharged after rainfall may be significant. Pease (1994) reported severe acidification of Broughton Creek after relatively frequent flood events initiated acid water discharge from flood mitigation drains.

The geomorphology and drainage practices adopted in the Shoalhaven Catchment are typical of coastal floodplains in New South Wales with the maximum elevation of 4 m AHD and the lowest elevation <1 m AHD. Two large drains approximately 8 m wide and 3 m deep were constructed during the late 1960s through the study site. From the floodgated junction with Broughton Creek, one drain extends 600 m in a westerly direction perpendicular from the Creek. A second drain 1200 m long joins the first drain at 500 m from Broughton Creek and is orientated in a north-south direction. As the second drain extends northwards, it becomes shallower and narrower. Numerous secondary drains transport water from upland catchments to the main drains and/or remove surface water from fields used for pasture production. Plate 4.1 shows the distribution of major and secondary drains on the study site, as well as prior stream channels that no longer play a significant role in the transport of surface water.

#### **4.3 Design and construction of weirs**

The installation of weirs in the flood mitigation drains to elevate the water levels in the drains has been proposed as one method of elevating groundwater levels at the sub-catchment scale (e.g., Indraratna *et al.*, 1995; Pease *et al.*, 1997). In order to minimise the amount of acid generated in acid sulfate soils in a drained subcatchment, it is



necessary to limit the exposure of pyrite in the soil to oxygen. Raising the groundwater table above the pyritic layer reduces the diffusion of oxygen to the pyritic sediments, thereby limiting the generation of acid.

The current operation of floodgated drainage systems ensures that the elevation of water in the drains is at about the low tide level (approximately  $-1.0$  m AHD). At the study site, low tide level is well below the elevation of the acid sulfate soil layer in the surrounding catchment. Such a low drain water level gives rise to a hydraulic gradient where the shallow groundwater flows into the drain, thereby lowering the surrounding groundwater table. As groundwater drainage occurs, the acid sulfate soils become unsaturated giving rise to the entry of oxygen and subsequent generation of acid.

Setting the elevation of weirs above the acid sulfate soil layer reduces the groundwater drawdown caused by the drain. Under ‘normal’ climatic conditions, it is envisaged that elevated drain water levels will maintain groundwater levels above the acid sulfate soil horizon. In addition, as the hydraulic gradient from the groundwater to the drain will be reduced, the rate of discharge of the existing acidity in the soil to the drain will be slowed. The slower acid discharge rate may enable the natural buffering capacity of the receiving waters to neutralise the slow leakage of acidity. A schematic of the expected influence of the weirs is shown in Figure 4.5.

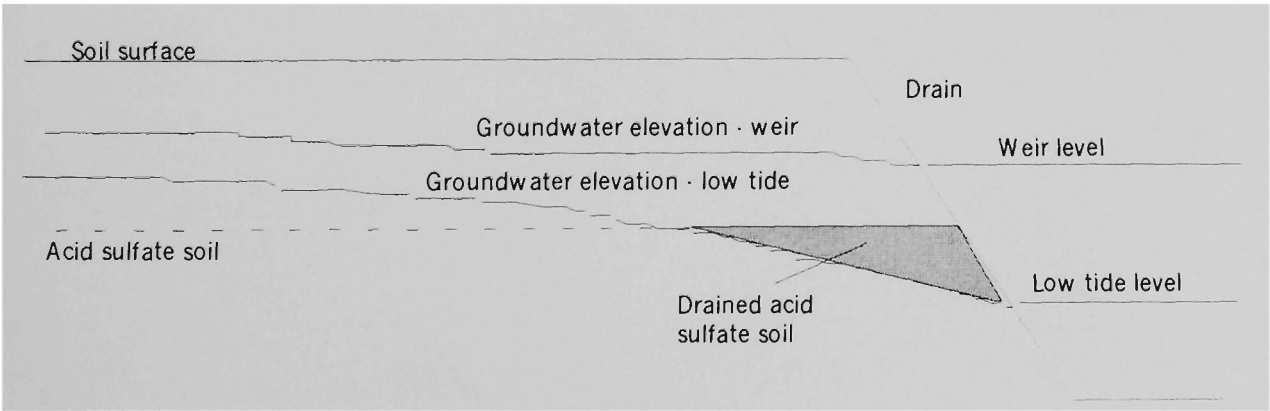


**Figure 4.5.** Expected effect of weir installation on adjacent groundwater elevation

Three weirs were installed in the flood mitigation drains at the Berry site at 0.1 (low), 0.4 (medium) and 0.6 (high) m above the acid sulfate soil layer in December 1997. The weirs were constructed by driving wooden poles approximately 3 m into the invert of the drain, then fixing marine plyboards to the poles to form the weir. The weirs were concreted into the sides of the drains then covered with rock to prevent erosion of the drain edge. Fill was placed on either side of the boards to ensure stability of the structure during flood events and to minimise leakage through the weir. A 'V' notch was incorporated into the weir so that the flow rate in the drain could be calculated during low flows. The sequence of construction of the weirs is shown in Plate 4.4.

Drought conditions between December 1997 and April 1998 precluded the filling of the weirs. As a result, drain water levels remained at low tide elevations during this period. Severe rainfall events during April-May 1998 and August 1998 resulted in erosion around the sites of the weir rendering them ineffective. The period of wet weather during mid-1998 prevented vehicle access to the site, thereby delaying prompt repairs to the damaged weirs. Permanent repairs were implemented in September 1998, and the weirs were successfully commissioned on 1 October 1998 (Day 440). A cross sectional diagram of the weir is given in Figure 4.6. A photograph of the high weir in operation is shown in Plate 4.5.



**Plate 4.4.** Construction of the weirs.



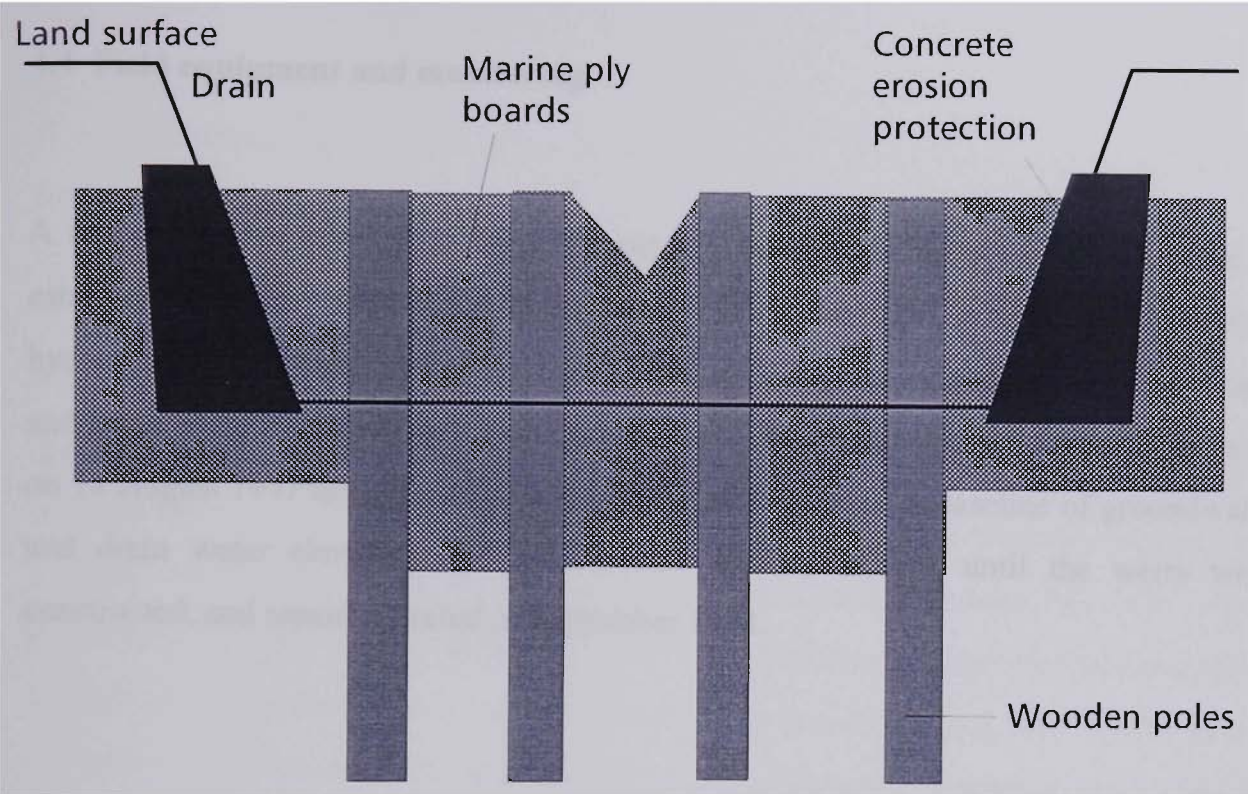


**Figure 4.6** Schematic diagram of the weir design.



**Plate 4.5** Operation of the high weir.

## 4.4 Field equipment and monitoring

A comprehensive monitoring program was implemented at the study site in order to establish the relationships between the water level in the drain, groundwater elevation, hydraulic gradients and groundwater flow direction. Regular monitoring of groundwater and drain water chemistry was also carried out. The monitoring program commenced on 18 August 1997 after the installation of the piezometers. A baseline of groundwater and drain water elevation and quality data was established until the weirs were constructed, and repairs effected in September 1998.

### 4.4.1 *Site topographic survey*

Coastal floodplains, including this study site, are very flat. As such, it is very important to ensure that all elevation data are accurately determined so that the position of the groundwater table relative to the acid sulfate soil layer can be assessed and groundwater flow properties calculated. A high resolution (0.1 m) topographic survey at 1:2000 scale of the site was prepared by the NSW Department of Land and Water Conservation in 1997 prior to the start of the study. An automatic laser level was used for all surveying. Site features such as: major and minor drains, property boundaries, Broughton Creek and farm infrastructure were included on the site map. The topographical elevation data were related to the Australian Height Datum (AHD). Two temporary bench marks at two bridges crossing the major drains were established for subsequent survey work.

#### *4.4.2 Installation of piezometers*

A comprehensive array of 59 piezometers arranged in 11 transects was established to monitor the groundwater elevation and quality. Each transect was located perpendicular to the direction of the adjacent flood mitigation drain, so that the groundwater drawdown could be measured. As drawdown was expected to be greatest adjacent to the drains, the piezometers were spaced close together near the drains (i.e., near the expected greatest hydraulic gradient) and were spaced further apart away from the drains (i.e., in the area of lowest expected hydraulic gradient). Piezometers within each transect were located at 1, 10, 20, 50, 90 and 150 m distance from the drain. Each piezometer transect was identified by a letter (A-K) with individual piezometers within a transect being identified by their distance from the drain (e.g., A10, E50, I150). Groundwater elevation data collected from the piezometer transects were used to determine hydraulic gradients, flow directions and flow velocities for the study site. The location of the piezometer transects at the study site is shown in Figure 4.7.

The piezometers were constructed using 3 m lengths of PVC pipe with an internal diameter of 50 mm. The bottom 2 m of the pipes were slotted using a bench mounted circular saw, and then wrapped in a protective geotextile to minimise the flow of sediment into the piezometer. The bottom of the piezometer was stoped with a PVC cap.

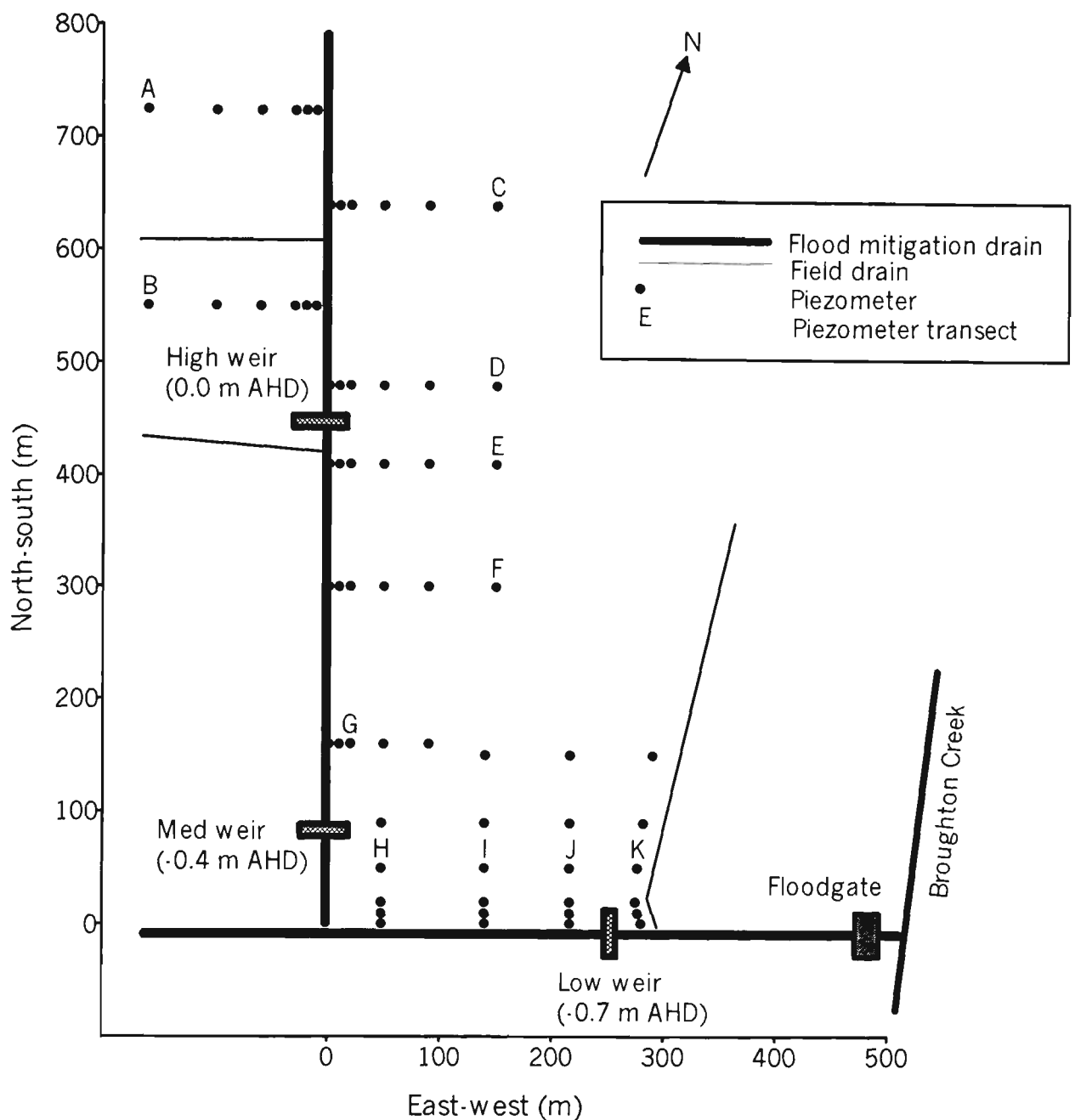


**Figure 4.7.** Location of the piezometers and weirs.

Each piezometer site was located in the field using the 1:2000 site topographic map and by measuring distances from the drain with a 100 m tape. At each piezometer location, a well approximately 2.5 m deep was drilled with the NSW Agriculture Proline drill rig fitted with a 100 mm spiral auger. After withdrawing the auger, a small quantity of sandy gravel was placed on the bottom of the well, and then the PVC piezometer was forcefully placed into the well, so that approximately 0.5 m PVC pipe extended above the ground surface. The volume between the PVC piezometer and the well was

backfilled with a sandy gravel mix to a depth about 0.5 m below the ground surface. A layer of bentonite was added to minimise any seepage down the piezometer, and then the remainder of the well was filled with top soil collected during the drilling process. The elevation of the top of each piezometer was surveyed from the known benchmarks using an automatic dumpy level.

Four piezometers with a 100 mm internal diameter were installed at C10, F10, I10 and K10 for installation of automatic water level recorders. These piezometers were constructed and installed in the same manner as described above.

#### *4.4.3 Measurement of routine groundwater parameters*

The elevation and pH of the groundwater at each piezometer was measured manually during the study period. Piezometers were monitored every 7-14 days or after an unusual event (e.g., flooding). The elevation of the groundwater table was measured using a rigid “plopper” device made from a 2.5 m length of 10 mm rod. Approximately 100 mm from the end of the rod, a PVC cone was fixed so that when it comes into contact with the groundwater as it is lowered into the piezometer, it makes a “plopping” sound. A steel tape measure was fixed to the rod from the PVC cone up to the other end of the rod. Once the rod was lowered into the piezometer and the groundwater level detected, the distance from the top of the piezometer to the groundwater table was recorded. This distance was later converted to a elevation in m AHD.

Automatic groundwater level recorders were installed at locations C10, F10, I10 and K10. The water level recorders were Greenspan PS300 pressure transducers with internal battery and data logger. The water level recorders were suspended in the 100 mm diameter piezometers to a depth of 2.7 m from the top of the piezometer. The data output cable was fixed to an adjacent star post approximately 1.5 m high. The data cable - computer connection was protected with a weather proof box and sealed with a



silica gel desiccant pack to prevent moisture entry into the probe. A PS300 being installed into a piezometer is shown in Plate 4.6. Unfortunately, the initial batch of PS300s had faulty o-ring seals that resulted in their failure. Some groundwater elevation data was lost during their replacement. Similarly, the water level recorder at K10 failed during the post-weir period.



**Plate 4.6.** Installation of a PS300 water level recorder in to a piezometer

pH was measured in groundwater extracted from each piezometer. A bailer was constructed using a 1.5 m length of 40 mm PVC pipe and by fixing a fitting with a 20 mm diameter hole in the end to be lowered into the piezometer. A 25 mm stainless steel ball bearing was placed inside the PVC pipe. As the bailer was lowered into the

groundwater in the piezometer, the water pressure would lift the ball bearing allowing groundwater to enter the bailer. Once the downwards motion ceased, the water pressure fell and the ball bearing fell onto the 20 mm diameter hole and acted as a plug. The bailer could be then raised from the piezometer with the groundwater sample. The sample was released into an acid washed plastic container for measurement of pH.

pH was measured in the field using a Horiba D-24 hand held probe. The pH probe has a silver/silver chloride reference electrode with a measurement range of 0 - 14 pH units. pH was automatically corrected for temperature by the probe. The pH probe was regularly calibrated using standards in the acid spectrum, typically pH 4 and pH 7 buffers.

The bailer was also used for the collection of groundwater samples analysed for a comprehensive suite of water quality parameters. These groundwater samples were collected on a monthly basis. The groundwater samples were stored in acid washed plastic containers supplied by the NSW Environment Protection Authority. The groundwater samples were stored at 4°C immediately after collection until they were delivered to the NSW Environment Protection Authority laboratories for analysis on a quarterly basis. The water quality parameters measured include: basic cations ( $\text{Ca}^{2+}$ ,  $\text{Mg}^{2+}$ ,  $\text{Na}^+$ ,  $\text{K}^+$ ), acidic cations ( $\text{Al}^{3+}$  and  $\text{Fe}^{\text{total}}$ ), anions ( $\text{Cl}^-$  and  $\text{SO}_4^{2-}$ ), pH and electrical conductivity.

Water quality analyses were performed at the NSW Environment Protection Authority laboratories using standard methods that are described by Easton *et al.* (1995). The only departure from the standard methods defined by Easton *et al.* (1995) was in relation to the determination of sulfate concentration. A brief description of the sample preparation and testing methodology is given below.

Acidic and basic cations were measured using the preparation method MA3030E and testing method MA3120\_B defined by Easton *et al.* (1995). Samples were initially digested with concentrated nitric acid in order to dissolve any metal cations that have

formed complex ions or chemicals with organic matter and/or precipitated during storage. The samples were then filtered through a 0.40-0.45  $\mu\text{m}$  polycarbonate or cellulose acetate membrane to remove any particles. Metal concentration was then measured using the Inductively Coupled Plasma Atomic Emission Spectrometry (ICP-AES) method. The results were reported in mg/L, then converted to mmol/L using appropriate stoichiometric conversions. Anions were determined on samples that had firstly been filtered through a 0.2  $\mu\text{m}$  membrane that removed any particulate matter. Chloride concentration was determined by ion chromatography with chemical suppression of eluent conductivity. The chloride testing method IIC\_A01 is fully described by Easton *et al.* (1995).

The determination of sulfate concentration in filtered samples using ion chromatography was found to be unsatisfactory due to the very high sulfate concentration in some samples. High sulfate concentration samples had to be diluted by up to 1000 times so that the concentration of sulfate in the samples was within the 0.2-20 mg/L range applicable to ion chromatography, giving rise to unacceptable errors associated with large dilutions. Pradhan (1999) developed an alternative routine sulfate testing method using ICP-AES. Using this testing procedure, a sample is introduced to the instrument as a stream of liquid. The liquid is converted to an aerosol, then transported to a high temperature argon plasma (about 6000°K) to produce an atomic emission. The intensity of the emission at specific wavelengths is measured and used to determine the concentration of the anolyte. The ICP-AES sulfate method is based on the direct measurement of the sulfur atomic emission line at 180.67 nm. The measured concentration of soluble sulfur is assumed to be present as sulfate. ICP-AES has linearity for samples with a sulfate concentration between 2-10000 mg/L.

#### *4.4.4 Weather station*

A Campbell Weatherwatch 2000 weather station was installed on elevated land approximately 500 m to the west of the study site in a flood free location. The weather station was mounted on a 3 m aluminium tower in excess of 100 m from the closest tall structure. The tower was lightning protected. The parameters measured by the station included: temperature and humidity, wind speed, wind direction, rainfall, and solar radiation. Data from the weather instruments was stored on a CX10 data logger fixed onto the tower. Data was removed from the logger by down loading to a laptop PC. The data were manipulated using Weatherwatch 2000 PC120 and PC208e software. These programs provide various reports of the meteorological data, including the calculated Penman-Monteith evapotranspiration. The weather station was located approximately 400 m to the West of the study site on an elevated area that is not flood prone.

#### *3.4.5 Drain water level*

The elevation of water in the flood mitigation drains was measured using three Greenspan PS300 water level recorders that were attached to galvanised steel poles upstream of the three weirs. The elevation of the sensor was surveyed and the water height data from the sensors corrected to elevation m AHD.

## **Chapter 5: Site climatic conditions**

### **5.1 Introduction**

In this Chapter, the climatic variables relating to the addition or removal of water from the groundwater aquifer at the study site are presented and discussed. The rainfall and evapotranspiration data are presented in two parts, the pre-weir (Day 1-440) and post-weir (Day 440-813) periods. The Southern Oscillation Index for the study period is also presented, and its importance with respect to understanding the climatic conditions that may have caused acid generation and discharge in the past is discussed. Temperature, wind speed and solar radiation data measured during the study period are shown and briefly discussed in Appendix A.

Management of the groundwater level relative to the elevation of the acid sulfate soil layer is the key for minimising acid generation and transport in drained sub-catchments. In most low-lying coastal environments where acid sulfate soils pose management challenges, two factors largely control the lowering of the groundwater table, namely drawdown from drains and evapotranspiration from crop transpiration and direct groundwater evaporation. Transpiration from vigorous crops, such as sugar cane, may be of the order  $1000-1500 \text{ mm yr}^{-1}$ , and has been shown to lower groundwater tables significantly in acid sulfate soil affected areas (Wilson, 1995). Less vigorous crops such as pasture may also have considerable influence on the extraction of moisture from the soil profile and groundwater aquifer. The position of a rising groundwater table is dependant on the magnitude of rainfall. Given the importance of rainfall and evapotranspiration in determining the position of the groundwater table, a comprehensive monitoring program of various climatic variables was carried out.

The relationship between climatic factors and the dynamics of the groundwater table for coastal floodplains can be presented as a simple water balance equation (White *et al.*, 1997) and was been described in Chapter 2. In summary,

$$\begin{array}{ccccccc} P + I + L_i & = & E_t + R + L_o & + & D + \Delta S & & (5.1) \\ \text{inputs} & & \text{outputs} & & \text{storage} & & \end{array}$$

where, P is precipitation, I is irrigation,  $L_i$  is the lateral inflow of water,  $E_t$  is evapotranspiration, R is surface runoff, D is drainage to the water table,  $\Delta S$  is change in soil moisture content above the water table, and  $L_o$  is the lateral outflow.

Given the characteristics of shallow aquifers in drained coastal lowlands, the change in groundwater elevation ( $\Delta W$ ) can be expressed as:

$$\delta \cdot \Delta W = \Delta (P - E_t - RO - Q_d - \Delta S) \quad (5.2)$$

where RO is runoff,  $Q_d$  is subsurface discharge to drains and  $\delta$  is specific yield of the soil (number of mm rainfall input per mm of groundwater table rise).

Clearly, two climatic variables, namely P and ET, contribute to the rise and fall of the groundwater table. Understanding the influence that P and ET has on the magnitude of change in groundwater elevation enables better management systems to be developed.

## 5.2 Site weather

The weather experienced during the study period, particularly during the pre-weir period, was characterised by periods of drought and intensive rainfall that led to flood

events. Weather experienced during the post-weir period was close to the long term average climatic condition reported for the Broughton Creek catchment (Pease, 1994).

The weather data for the pre-weir period is incomplete as a result of the weatherstation becoming operational on Day 208. However, a reliable daily rainfall record was obtained from the University of Wollongong (Berry Campus), located approximately 1 km from the study site between Days 1-207.

5.2.1 Rainfall

Daily rainfall collected at the University of Wollongong (Berry Campus) between Days 1-207 and weather station data between Days 208-440 collected at the study site are shown in Figure 5.1a. The daily rainfall record for the post-weir period is shown in Figure 5.1b

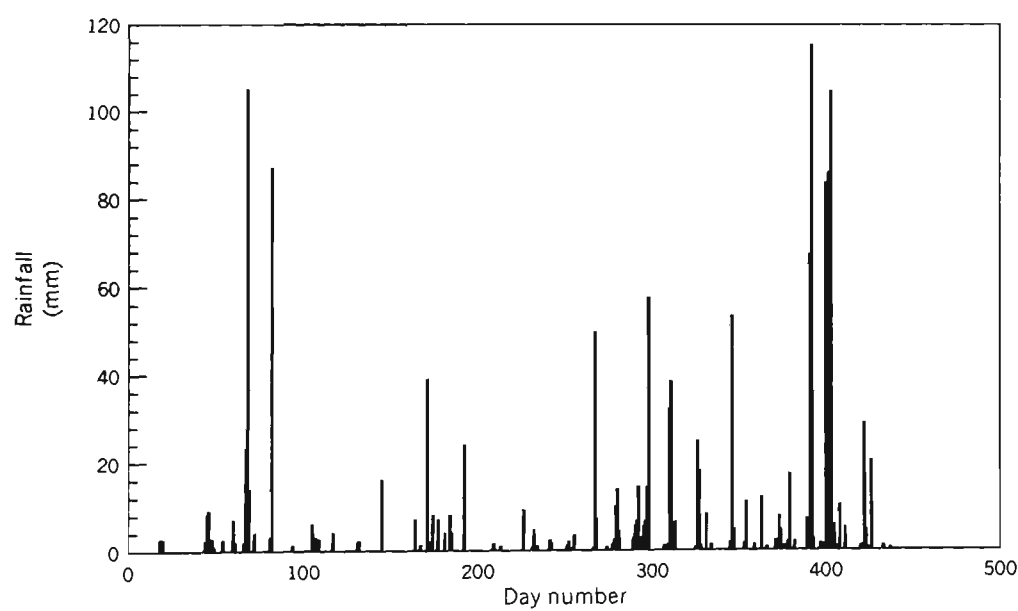


**Figure 5.1a** Daily rainfall for the pre-weir period.

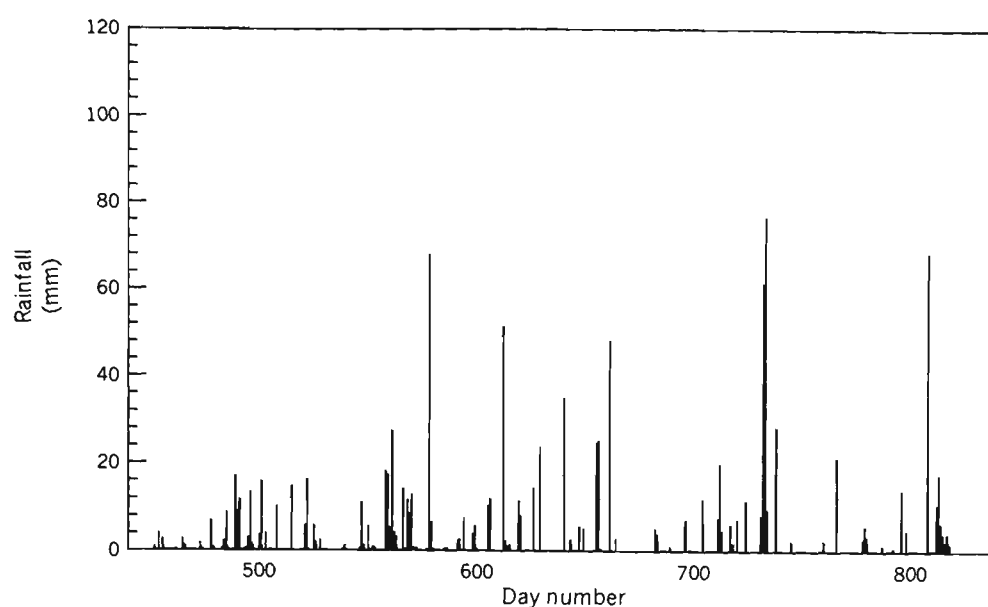


**Figure 5.1b** Daily rainfall for the post-weir period.

The rainfall distribution during the pre-weir study period was very variable. Three unusual rainfall trends occurred during this period, namely two very wet periods that resulted in short duration flood events on site, and a prolonged dry spell that caused draught conditions. The intensity-frequency-duration design criteria (Australian Rainfall and Runoff, 1998) for the high intensity rainfall events that caused flooding on site are shown in Table 5.1.

**Table 5.1** Rainfall design criteria for major rainfall events

Day	Intensity (mm)	Duration (hours)	Frequency (years)
69	105	24	2
83	87	24	1
385-386	176	48	2
404-406	242	72	3

The return interval (frequency) calculated from the daily rainfall record shows that rainfall events of the intensity measured at the site are not uncommon, with a maximum



frequency of three years for the Day 404-406 rainfall event. Shorter duration rainfall events of higher intensities than the daily results collected at the weather station would have occurred during these heavy rainfall days and probably would have resulted in runoff causing flooding events associated with longer return intervals. However these could not be calculated due to the measurement of rainfall intensity on a daily basis. Nevertheless, within the 440 days comprising the pre-weir period, four separate rainfall event greater than 1 year frequency occurred, indicating that the site was subject to greater than usual rainfall of high intensity and subsequent flooding. Another contributing factor towards flooding is the position of the field site in the Broughton Creek catchment. As shown in Chapter 4, the field site is located at the base of a very steep sub-catchment. Where high intensity rainfall events occur over this sub-catchment a substantial volume of run-off can be generated and rapidly transported onto the field site causing flooding. Clearly, the volume of rainfall that fell during these events was not sufficient to generate surface water up to 1 m deep on the field site without significant run-on inputs for the upstream catchment.

In contrast, the rainfall record for the post-weir period was evenly distributed. Four rainfall events in excess of 60 mm/day occurred during the post-weir period, although two of these events occurred on consecutive days (Day 732 - 62 mm, Day 733-77 mm). The 139 mm rainfall that fell between Days 732-733 caused minor surface flooding on the site that persisted for less than one day (R. Stuart, pers com).

The monthly average rainfall measured at the site is compared to the long term average calculated for the rain gauge at the University of Wollongong (Berry Campus) in Figure 5.2.

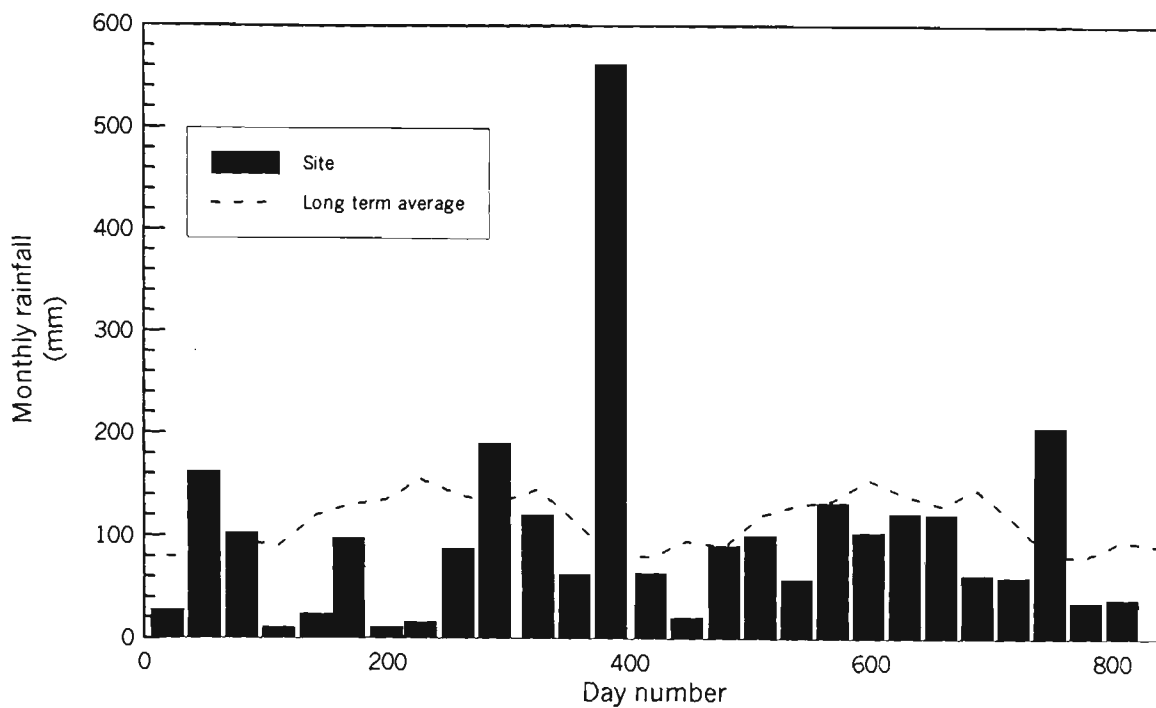


**Figure 5.2** Monthly rainfall measured at the site compared to the long term monthly average.

The long term record shows that rainfall is relatively uniformly distributed throughout the year, with only a slight summer dominance. The first part of the study period up to Day 260 experienced below average rainfall, with the exception of August and September 1997 which both had 24 hour duration, 1 year storm events. Rainfall close to the long term average returned from Day 260 onwards, although an extra-ordinary volume of rain fell in August 1998 causing two separate flooding events on the study site.

The monthly rainfall recorded during the post-weir period was close to the long term average. Figure 5.2 shows that rainfall from the commissioning of the weirs through to the end of the 1999 summer (Day 660) correspond to the long term average. Below average monthly rainfall was recorded for the final part of the post-weir period, with the exception of August 1999 where twice the average monthly rainfall was recorded, largely as a result of the 139 mm rain that was recorded during Days 732-733.

A total of 233 rainfall events were recorded during the monitoring period, with 101 events during the pre-weir period and 132 events during the post-weir period. Rainfall events were determined as recorded rainfall greater than 0.2 mm that occurred on a daily basis. Consecutive days where rainfall was recorded were not defined as a single event. The distribution of daily rainfall intensities is shown in Figure 5.3(a,b).

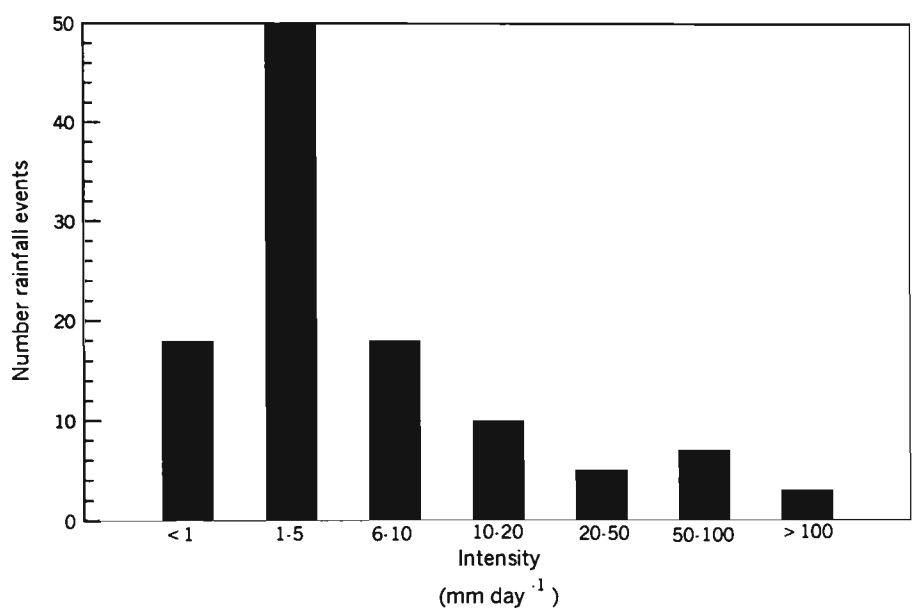


**Figure 5.3a** Distribution of daily rainfall intensities for the pre-weir period.

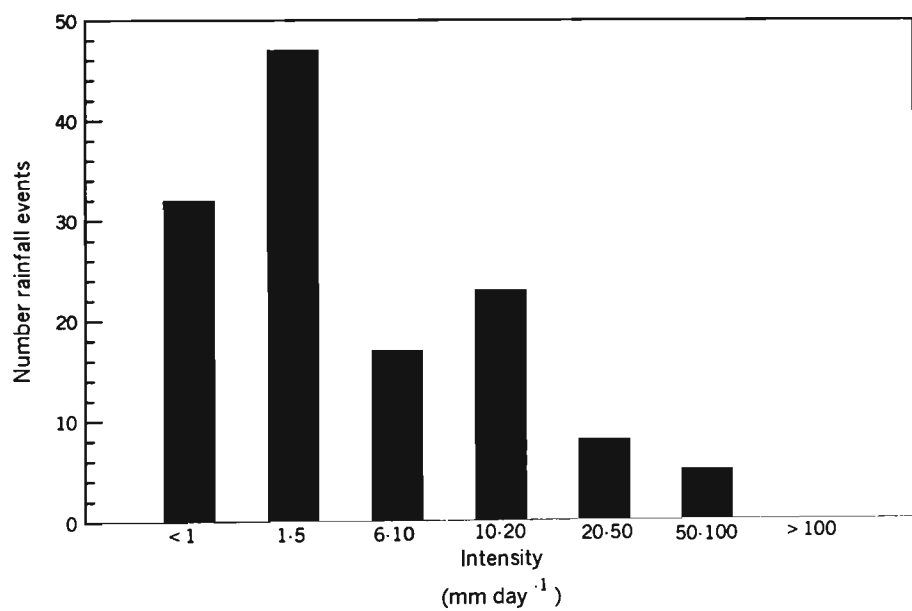


**Figure 5.3b** Distribution of daily rainfall intensities for the post-weir period.

The majority (68% pre-weir, 60% post-weir) of daily rainfall events were less than 6 mm day<sup>-1</sup>. However, the unusual variability of the rainfall measured during the pre-weir

period is evident where high rainfall intensities greater than 20 mm day<sup>-1</sup> comprised 15% of the number of rainfall events at the site. Only 10% of rainfall events greater than 20 mm day<sup>-1</sup> were recorded during the post-weir period.

### 5.2.2 Evapotranspiration

For evapotranspiration to occur, three physical requirements in the soil-plant-atmosphere continuum must be met (Ritzema, 1994), namely:

- a continuous supply of water
- energy available to change liquid water to vapour
- a vapour gradient to maintain a flux from the evaporating surface to the atmosphere.

Numerous methods for determining evapotranspiration have been developed based on one or more of these necessary physical principles. The Penman-Monteith approach has been widely adopted (Ritzema, 1994) for predicting potential evapotranspiration losses from the soil and has been used in this study.

The Penman-Monteith equation of potential evapotranspiration is:

$$ET = \frac{\frac{\Delta(R_n - G)}{\lambda} + \frac{c_p \rho_a}{\lambda} \cdot \frac{e_a - e_d}{r_a}}{\Delta + \gamma^*} \quad (5.3)$$

where; ET is evapotranspiration;  $\gamma^*$  is the modified psychrometric constant;  $\lambda$  is the latent heat of vaporisation;  $\Delta$  is a proportionality constant;  $R_n$  is the energy flux density of net incoming radiation;  $G$  is the heat flux density into the water body;  $e_a$  is the

saturated vapour pressure at the leaf surface at air temperature;  $e_d$  is the vapour pressure in the atmosphere ;  $\rho_a$  is the density of moist air;  $c_p$  is the specific heat of dry air at a constant pressure;  $e_a - e_d$  is the vapour pressure deficit.

The meteorological parameters are recorded by the WeatherWatch 2000 weatherstation and crop constants for pasture are used to calculate ET. ET was calculated by the ETPro software that is used to download the meteorological data from the weatherstation.

The potential evapotranspiration data calculated for the site are shown in Figure 5.4(a,b).

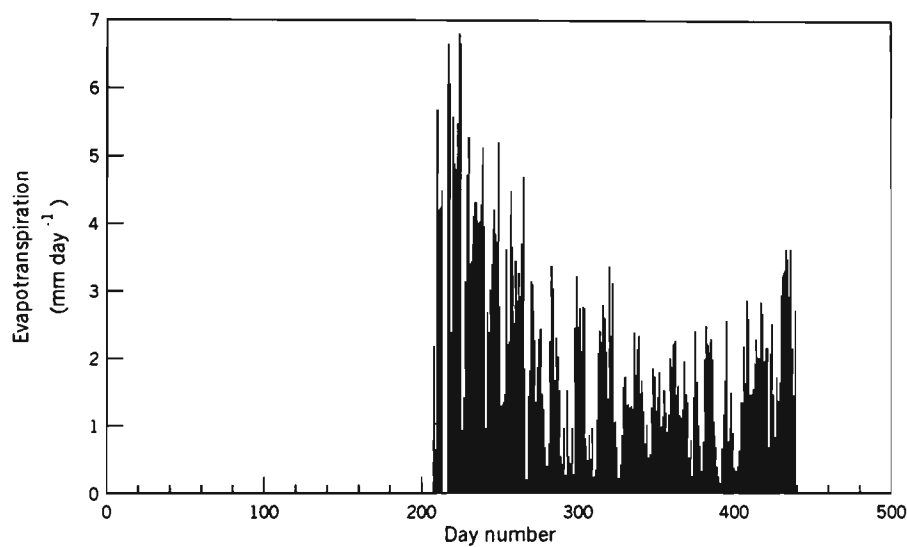


**Figure 5.4a** Calculated evapotranspiration during the pre-weir period.

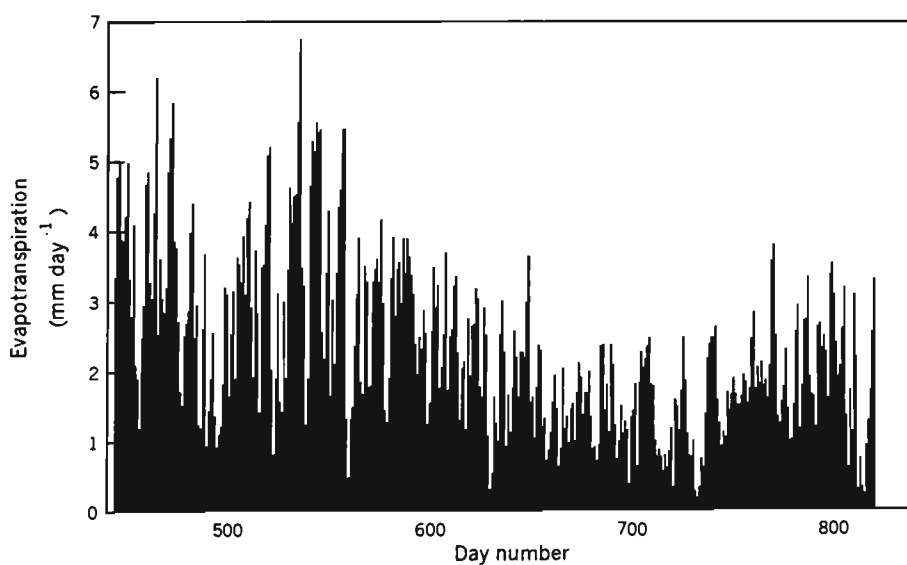


**Figure 5.4b** Calculated evapotranspiration during the post-weir period.

Figure 5.4 shows that evapotranspiration has the expected seasonal variation with high evapotranspiration rates occurring during summer when solar radiation and temperatures are highest. The highest evapotranspiration rate approaches 7 mm/day in summer and 2 mm/day in winter. Daily variability is attributed to factors such as cloudiness and rainfall which affects solar radiation, temperature and humidity.

Figure 5.5 shows that evapotranspiration has been considerably greater than the long term monthly pan evaporation rate measured at the Berry Sewerage Treatment Plant for both the summer of 1997/98 and the autumn of 1998. This is consistent with the drought conditions experienced at this time. The lower than average evapotranspiration calculated for the winter of 1998 is consistent with the above average rainfall recorded, low temperatures and a high proportion of cloudy days that reduced solar radiation.

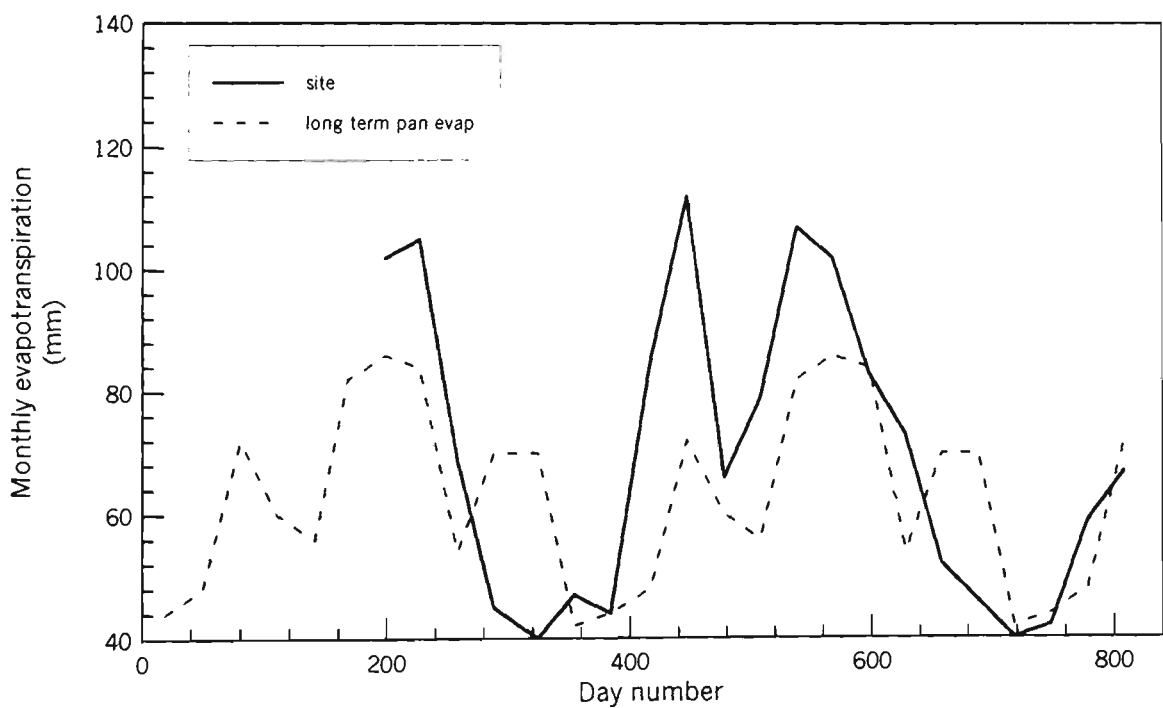


**Figure 5.5** Long term monthly evaporation relative to site ET data.

The higher than average evapotranspiration calculated in September 1998 (Day 420) can be attributed to a 2 week period of unseasonably high temperatures (30°C). Evapotranspiration returned to average values for the remainder of the post-weir period,

with the exception of January 1999 where high daily maximum temperatures and solar radiation give high evapotranspiration values.

### 5.2.3 *Southern Oscillation Index*

The Southern Oscillation Index (SOI) is calculated from the monthly fluctuations in the air pressure difference between Tahiti and Darwin. Sustained negative values of the SOI often indicate El Niño episodes. These negative values are usually accompanied by sustained warming of the central and eastern tropical Pacific Ocean, a decrease in the strength of the Pacific Trade Winds, and a reduction in rainfall over eastern and northern Australia. The most recent strong El Niño event was in 1997/98.

Positive values of the SOI are associated with stronger Pacific trade winds and warmer sea temperatures to the north of Australia, known as a La Niña episode. Waters in the central and eastern tropical Pacific Ocean become cooler during this time. Together these give an increased probability that eastern and northern Australia will be wetter than normal. The most recent strong La Niña was in 1988/89; a fairly weak event occurred in late 1995 and early 1996.

The SOI method used by the Australian Bureau of Meteorology is the Troup SOI, which is the standardised anomaly of the Mean Sea Level Pressure difference between Tahiti and Darwin. The SOI calculated as:

$$SOI = 10 \frac{(P_{diff} - P_{diffav})}{SD(P_{diff})} \quad (5.4)$$

where;  $P_{diff}$  = (average Tahiti MSL Pressure for the month) - (average Darwin MSLP for the month),  $P_{diffav}$  = long term average of  $P_{diff}$  for the month in question, and  $SD(P_{diff})$  = standard deviation of  $P_{diff}$  for the month in question.

Where the SOI is greater than 10 or less than -10, this indicates that either above average or below average rainfall, respectively, can be expected. SOI values between -10 and +10 indicate that average rainfall conditions are expected. The SOI for the study period is shown in Figure 5.6.

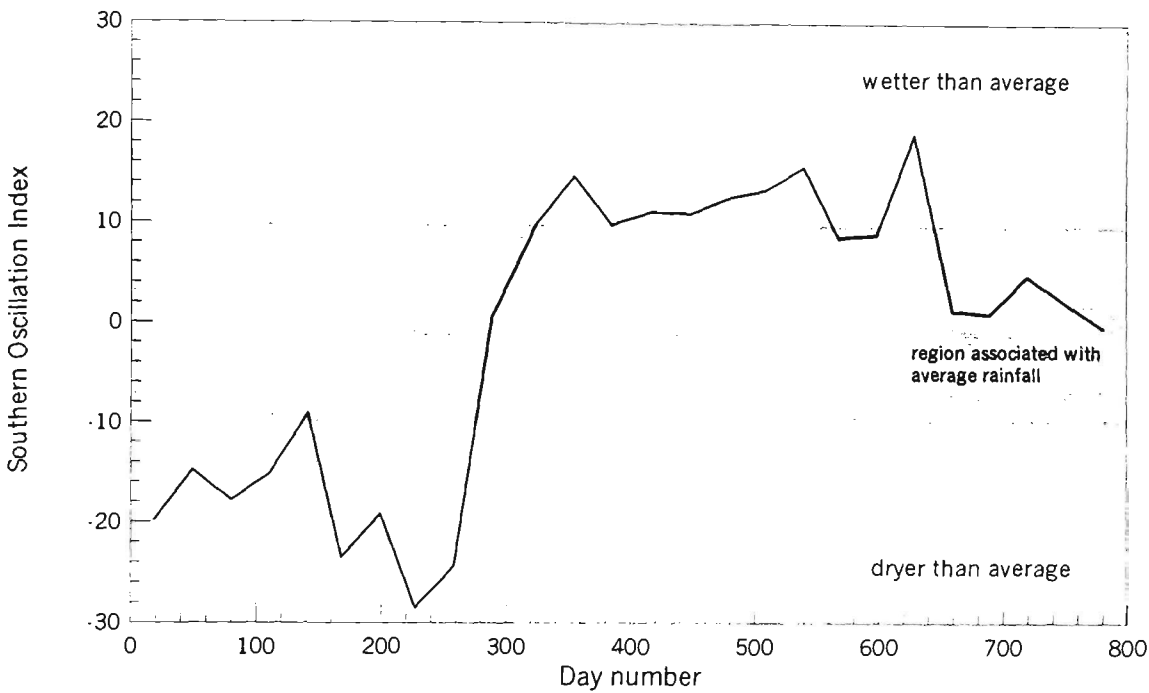


**Figure 5.6** SOI for the study period.

The SOI up to approximately Day 260 is very negative and associated with below average rainfall. Indeed Figure 5.5 for average monthly rainfall shows that the rainfall recorded during this period at the site is substantially lower than the long term average. Where the SOI becomes positive and is in the range associated with above average rainfall, the average monthly rainfall recorded at the site is close to the long term average for most months, although three months show that substantially above average monthly rainfall was experienced at the site during this period.

The SOI has a strong association with climatic conditions that create the necessary conditions for lowering of the groundwater table and the subsequent generation of acid from the oxidation of pyrite ( $\text{SOI} < -10$ ), and the export of acidic oxidation products



during heavy rainfall events that cause flooding ( $\text{SOI} > 10$ ), particularly when there is a sharp increase in the SOI from strongly negative to positive values. Given this association, the SOI may be used to predict the time of previous acidification-discharge events. If groundwater elevation change in drained and undrained catchments can be linked to the SOI then an estimation of the frequency and distribution of acid generation and discharge from acid sulfate soils in eastern Australia may be determined.

### **5.3 Implications for acid sulfate soil**

The direct water inputs (rainfall) and losses (evapotranspiration, lateral outflow) are the major factors that influence the dynamics of the groundwater in coastal lowlands. The relative contribution of rainfall and potential evapotranspiration from the site is shown in Figure 5.7.

Three periods of extreme weather were identified during the pre-weir period, namely two wet periods that resulted in surface flooding where  $\text{rain} \gg \text{ET}$  and a prolonged drought period where  $\text{rain} \ll \text{ET}$ . Calculated evapotranspiration was shown to be higher than long term pan evapotranspiration, indicating that removal of water from the soil profile occurred rapidly during the drought period. In contrast, rainfall inputs and losses via evapotranspiration were in close agreement during the post-weir period, with a small rainfall excess occurring through most of the post-weir period. The post-weir weather is close to the long term average for the site, and as such, provided an excellent opportunity to study the performance of the weirs in “average” conditions.

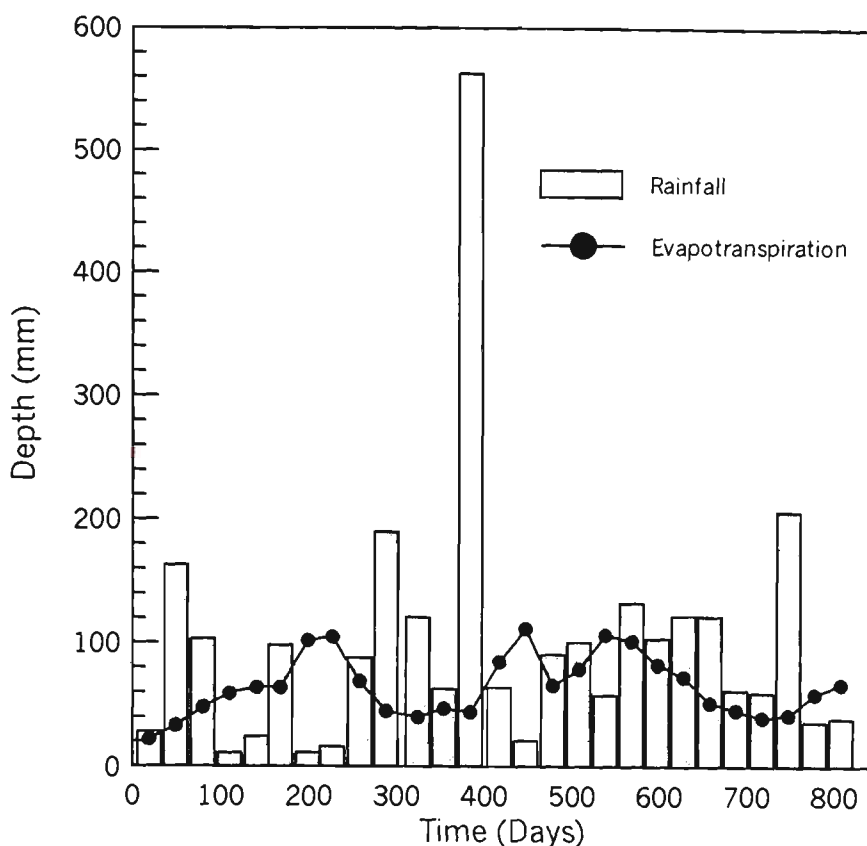


**Figure 5.7.** Relative contribution of rainfall and potential evapotranspiration to the site water balance.

The weather conditions experienced during the pre-weir period gave rise to the necessary conditions for the generation and export of pyrite oxidation products. These circumstances led to ideal conditions for testing the effectiveness of the weirs with respect to: minimising the subsequent generation of acid pyrite oxidation products by maintaining elevated groundwater tables above the pyritic layer, and manipulating the hydraulic gradient of the groundwater in order to slow the discharge of pyrite oxidation products entrained in the groundwater to the drains. The climate interactions with the groundwater dynamics, groundwater and drain water chemistry, and soil properties for the study site are discussed in Chapters 6, 7 and 8.

## **Chapter 6: Soil chemical, physical and morphological properties**

### **6.1 Introduction**

The chemical, physical and morphological properties of the soil found at the beginning of the monitoring period are described in this Chapter. A comprehensive soil investigation process was carried out for two specific purposes. Firstly, a well constructed base point was required so that any change in the soil properties that came from the maintenance of higher groundwater tables through the installation of the weirs could be established. This was specifically targeted at soil chemical attributes that were likely to exhibit some change (e.g., soil pH, electrical conductivity, dissolved sulfate, titratable acidity). Other chemical attributes (e.g., oxidisable sulfur concentration, organic carbon and effective cation exchange capacity) are not likely to exhibit substantial change during the course of a relatively short monitoring period. However, these measurements demonstrate many important features of acid sulfate soil behaviour, and they also offer some insights to the effectiveness of various acid sulfate soil management strategies.

A second reason for the development of this comprehensive soil attribute data set was for the initialisation of numerical models that are used in Chapters 8, 9 and 10 for the simulation of groundwater dynamics and pyrite oxidation. These models require a comprehensive array of soil chemical, physical and pyrite morphology data. In addition, quantification and understanding of the soil physical properties enable a better understanding of the groundwater dynamics and the pathways that influence oxygen transport from the surface to the pyritic soil.

## 6.2 Soil sampling and testing methods

A high density soil sampling program, both spatially and vertically down the soil profile, was carried out to characterise the nature of the soil at the study site. The soil testing methods were generally taken from well established procedures, although the methods currently described in the NSW Acid Sulfate Soils Manual (Ahern *et al.*, 1998) to quantify actual and potential acid sulfate soil remain under scientific review. However, in the absence of internationally recognised procedures for testing acid sulfate soil, these standardised methods developed for Australian conditions were deemed adequate.

### 6.2.1 *Study site topography, soil profile description and stratigraphy*

The ground surface at the site, while generally flat, is wavy with irregular meandering linear depressions and broader hollows 0.2-0.4 m deep. Adjacent to Broughton Creek is a natural levee approximately 100-200 m across and 0.5-1 m higher than the former backswamp behind it. There is no regular, connected, natural drainage network apart from a small area at the northern end of the site where a former stream channel joins Broughton Creek through a break in the levee. Surface water enters the site during back-up flooding through this break or via several ephemeral streams draining hilly terrain to the west. Two of these streams are flanked by small levees and are building up small alluvial fans where they debouch onto the floodplain. The channels of these streams have been artificially enlarged and connected to the flood mitigation network.

A transect was established across the site for soil mapping, profile description and stratigraphy. Transect AB (Fig. 6.1) crosses the study site from the base of the rising ground (A) to the levee of Broughton Creek south of the floodgate (B). Soil cores were collected adjacent to piezometer transects B, C, E, F, H, I and K at 10 m and 90 m from the drains by mechanical push tube sampling of the soil profiles to a depth of 1.5 m. At

both ends of the transect (i.e., A and B), and adjacent to F90, three larger diameter (100 mm) cores were also collected to a depth of 3 m. The topography of the site as well as the sampling locations are shown in Figure 6.1. The intact cores were described by field texturing, the presence and depth of major horizons, and the presence of features such as jarosite, iron mottles, iron coated macropores, shell and organic rich layers. Soil and mineral colour was matched against a Munsel chart.

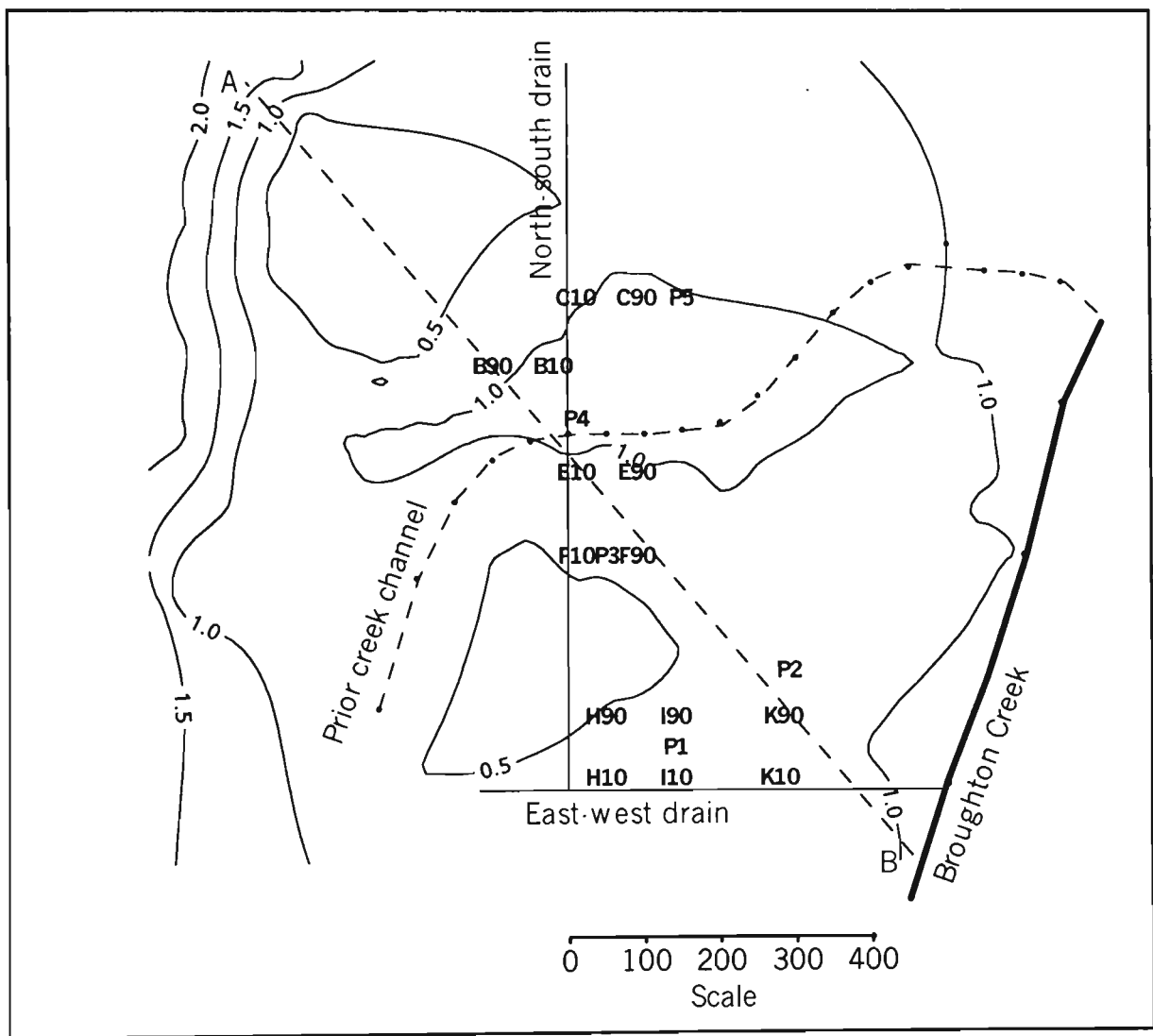


**Figure 6.1** Study site showing surface topography, soil sampling locations and transect AB.

### 6.2.2 Pyrite micromorphology

Samples of pyritic soil collected at I90 were frozen in liquid nitrogen, then dried using a freeze drier. The morphology and size of sulfide crystals was determined in fractures across undisturbed freeze-dried samples using a scanning electron microscope (SEM) equipped with an ISIS energy dispersive X-ray (EDX) system. These samples were affixed to 12 mm diameter aluminium pin type stubs with epoxy resin and coated with carbon. A quantitative EDX microanalysis procedure for rough surfaced specimens was used to characterise the sulfide minerals on these stubs (Bush and Sullivan, 1996).

### 6.2.3 Soil chemistry

At each sampling location, soil was collected to a depth of 1.5 m below the surface. The samples were collected by pushing a 60 mm diameter steel tube into the soil to a depth of 1.0 m using the NSW Agriculture Proline drill rig. Five cores were collected from within a 10 m x 10 m area and the main morphological features of the soil were described and recorded. Each core was then sectioned at 0.1 m intervals. Soil from the same 0.1 m depth interval was collected from each core and combined to make a 5 part composite sample. The additional 0.5 m was then sampled using a gouge auger inserted down the same 5 core holes, and composite samples prepared the same manner, after description. Soil samples were wrapped in plastic bags and were stored below 4°C for a few days until they could be oven dried at 85°C (Stone *et al.*, 1998). After drying the soil was ground and passed through a 2 mm sieve.

For chemical analysis, four sets of tests were carried out. These included:

1. Soil pH (1:5 in 0.01 M CaCl<sub>2</sub> solution) and electrical conductivity (1:5 soil/water).

2. The Peroxide Oxidation - Combined Acidity and Sulfate (POCAS) method described by Ahern *et al.* (1998) was used to determine the actual and potential acidity of the samples. Five grams of ground soil was made into a 1:5 suspension with 1 M KCl and shaken overnight. An aliquot was filtered then titrated against 0.25 M NaOH until pH 5.5. 2 ml of 30% hydrogen peroxide was added to the aliquot to oxidise any dissolved iron, then the sample was adjusted to pH 5.5 by the further addition of 0.25 M NaOH. The total actual acidity of the soil was determined from the total volume of NaOH used.

Potential acid sulfate soil was oxidised by applying additions of 5 ml 30% H<sub>2</sub>O<sub>2</sub> to 10 g soil samples suspended in 2 M KCl. The suspension was placed over a water bath at 85°C and further additions of H<sub>2</sub>O<sub>2</sub> were applied until effervescence ceased, indicating that all pyrite in the potential acid sulfate soil had been oxidised. Aliquots were filtered then titrated to pH 5.5 with 0.25 M NaOH (including the addition of 2 ml H<sub>2</sub>O<sub>2</sub> for iron oxidation) for determination of total potential acidity. An aliquot was also diluted for determination of peroxide extractable sulfate. Peroxide Oxidisable Sulfur (S<sub>pos</sub> %) and Total Sulfuric Acidity (TSA) were calculated by subtracting the KCl extract measurements from the H<sub>2</sub>O<sub>2</sub> extracts for acidity and sulfate, respectively.

3. Organic carbon was determined using a Leco furnace. Ground samples weighing 1-2 g were placed in disposable ceramic crucibles and placed into the resistance furnace. The carbon gases released during heating were monitored by an infra-red detector. Organic carbon concentration was determined by removing carbonate from the soil by pre-treatment with 4M HCl. Organic carbon was then calculated by subtracting the carbonate removed carbon concentration from the total carbon concentration (i.e. total C - carbonate C).
4. The Effective Cation Exchange Capacity (ECEC) was determined using prewashed, unbuffered compulsive exchange (Rayment and Higginson, 1992). Exchangeable cations including aluminium, calcium, potassium, magnesium and

sodium were measured using atomic absorption spectrophotometry. The percentage base, aluminium and calcium saturations were also calculated.

5. Dissolved sulfate and chloride concentrations were determined by extracting sulfate and chloride in a 1:100 soil/water solution. The extract was filtered, then the concentrations of sulfate and chloride were determined using ion chromatography.

#### *6.2.4 Soil physics*

Cores of intact soil were collected at 5 locations (P1-5) across the study site (Fig. 6.1). Sampling locations were selectively chosen across the site in order to establish soil physical characteristics both close to and further away from drains. Samples were collected at depths of 0.3, 0.6, 0.9, 1.2 and 1.5 m from the ground surface. A backhoe pit was carefully excavated at each sampling location until the correct depth was obtained for collection of undisturbed samples inside the pit. A thin walled brass core 100 mm diameter and 70 mm height was rapidly hit by guided drop hammer into the prepared bench of undisturbed soil at each of the five depths. Cores were used for determination of saturated hydraulic conductivity, dry bulk density and porosity. At each location and depth, 4 cores were collected in the vertical plane and 2 cores in the horizontal plane. Undisturbed cores, 50 mm diameter and 40 mm length, were also collected in the vertical plane for determination of the moisture characteristic curve. All cores were carefully excavated from the bench by hand and immediately wrapped in cling wrap and plastic bags to minimise moisture loss. Samples were stored at 4°C until laboratory testing was carried out.

Saturated hydraulic conductivity was determined using the falling head method (ACLEP, 1995) for 150 samples collected from 5 locations across the site, 5 depths within the soil profile and 2 orientations (horizontal and vertical). After the test, the soil



was removed from the core, weighed and dried at 105°C for 24 hours for calculation of saturated moisture content, dry bulk density and porosity.

Soil moisture characteristic curves were determined using a high pressure extractor vessel and 15 bar porous ceramic plate. Small intact cores were initially weighed and measured for height, then placed on the saturated ceramic plate and allowed to wet up by capillary rise from excess water left on the plate. A 7 point moisture retention curve was constructed by progressively applying vessel pressures of 10, 30, 60, 100, 330, 600 and 1000 kPa to the soil. After equilibrium was achieved at each pressure, the samples were carefully removed from the ceramic plate and weighed. Samples were then placed back onto the ceramic plate for application of the next pressure. After equilibrium was achieved at 1000 kPa, samples were weighed and oven dried at 105°C for 24 hours for the determination of volumetric moisture content at each pressure.

After drying and removal of large shell or root material, soil samples collected at 0-0.1, 0.6-0.7, 0.9-1.0 and 1.4-1.5 m depths at C10, F90 and I90 were hand ground and passed through a 1 mm sieve. A Malvern Mastersizer, which uses a collimated laser and a scattered light detector, was used to determine the particle size distribution of the samples.

## **6.3 Results and discussion**

### ***6.3.1 Stratigraphy and soil profile description***

The soils were originally described by Read (1974) as “organic soils over estuarine clay”. In the centre of the site, the surface soil of a typical profile is a crumbly grey brown loam 0.2 m thick which is well aggregated and containing abundant plant roots. It covers a very dark grey to black (Munsell colour code 2.5Y2/0) horizon with a friable

peaty consistency, representative of former backswamp conditions now buried by more recent alluvial deposition. Below there is a generally clear boundary to a dark greyish brown (10YR4/2) silty clay with prominent rusty mottles. This well aggregated clay sets hard when dry, and becomes sandy and poorly aggregated with increasing depth. Mottling increases with depth, with prominent rusty halos developed around pores and tubular iron encrustations which may be up to 12 mm in diameter. At greater depths (0.9-1.0 m) the profile becomes increasingly grey in colour, and more silty. Streaks of jarosite appear, sometimes filling the tubular encrustations. There is a clear horizon change at a depth of about 1.3 m below the surface to a dark grey (10YR4/1) massive sandy or silty clay, which effervesces vigorously with peroxide. This horizon is indicative of the sulfidic soils found across the study site, as well as found at other locations within the Shoalhaven catchment (Willetts and Walker, 1982; Pease, 1994). Below this sulfidic or potential acid sulfate layer, the soil is a massive, dense grey clay with prominent red-brown and yellow-brown mottles. Roy (1985) suggested that this is a Pleistocene clay which forms the base for the deposition for more recent Holocene pyritic and alluvial soils. Although profile features vary across the site, three distinct zones can be recognised to a depth of 1.5 m below the surface. Firstly, a dark surface zone rich in organic matter, secondly a heavily mottled zone of estuarine sediments with a band of jarosite mottles up to 0.4 m thick, and thirdly a neutral grey sulfidic zone containing partly decomposed plant material. These soil profile features are shown in Plate 6.1.



**Plate 6.1** Soil profile features showing the organic rich topsoil, an estuarine clay with jarosite, and the dark grey sulfidic sediments at depth.

The variation in profile morphology along the cross-section AB is shown in Figure 6.2. The cross-section runs from the base of the hillslopes across the backswamp and up onto the levee adjacent to Broughton Creek. The upper boundary of the pyritic soil layer falls from an elevation of 0.0 m AHD at the bottom of the hillslope (A) to approximately -0.6 m AHD in the backswamp (F10), and drops further to about -1.1 m AHD beneath the levee (B). A number of processes may have contributed to the sloping upper surface of the pyritic layer. Young *et al.* (1993) reasoned that the mean sea level was higher than its present elevation during the Holocene. Given the necessary conditions for the

formation of pyritic sediments (see Chapter 2), the deposition of pyritic sediments at the study site may have been associated with the gradual recession of the estuarine water level and the allied distribution of estuarine vegetation. It would be expected that the deposition of pyritic sediments would correspond with the presence of estuarine vegetation, and as the elevation of water in the estuary fell from its maximum level to its current position, the distribution of estuarine vegetation would follow the recession of the shallow water required for estuarine vegetation growth. If estuarine vegetation did migrate with the receding estuarine water elevation, then the upper elevation of the pyritic soil layer would also follow this receding elevation trend. The uniformity of the slope of the pyritic soil layer from the base of the hill at sampling location (A) to the levee at (B) suggests that this hypothesis of the pyritic soil deposition being related to the necessary condition for the formation of pyritic soils and the recession of sea levels during the Holocene appears reasonable. However, other factors may also contribute to the slope of the pyritic soil layer.

White *et al.* (1993) reported that irreversible shrinkage of pyritic sediments occurs as a result of dewatering. The site has been intensively drained which promotes ripening of the pyritic soils and their transformation from super-saturated gels to more solid terrestrial soils, may have been promoted by drains that lower the groundwater table below its natural state. Given the greater thickness of the pyritic sediments close to Broughton Creek in comparison to the western part of the site, dewatering of the pyritic sediments by drainage may have caused these sediments to shrink more (and therefore have a lower elevation) at the Creek than at sampling location (A). Shrinkage and dewatering of the pyritic sediment is also facilitated by the greater depth of alluvial overburden that has been deposited over the pyritic sediments closer to the levee. Below the levee (location B), approximately 2.4 m of overburden overlies the pyritic sediment whereas at sampling location (A) the depth of overburden is only 1.5 m. Increasing depths of overburden assists the consolidation of the pyritic soils. As such, greater consolidation of the pyritic sediment would be expected beneath the levee, which may cause the upper surface of the pyritic layer to be a lower elevation.

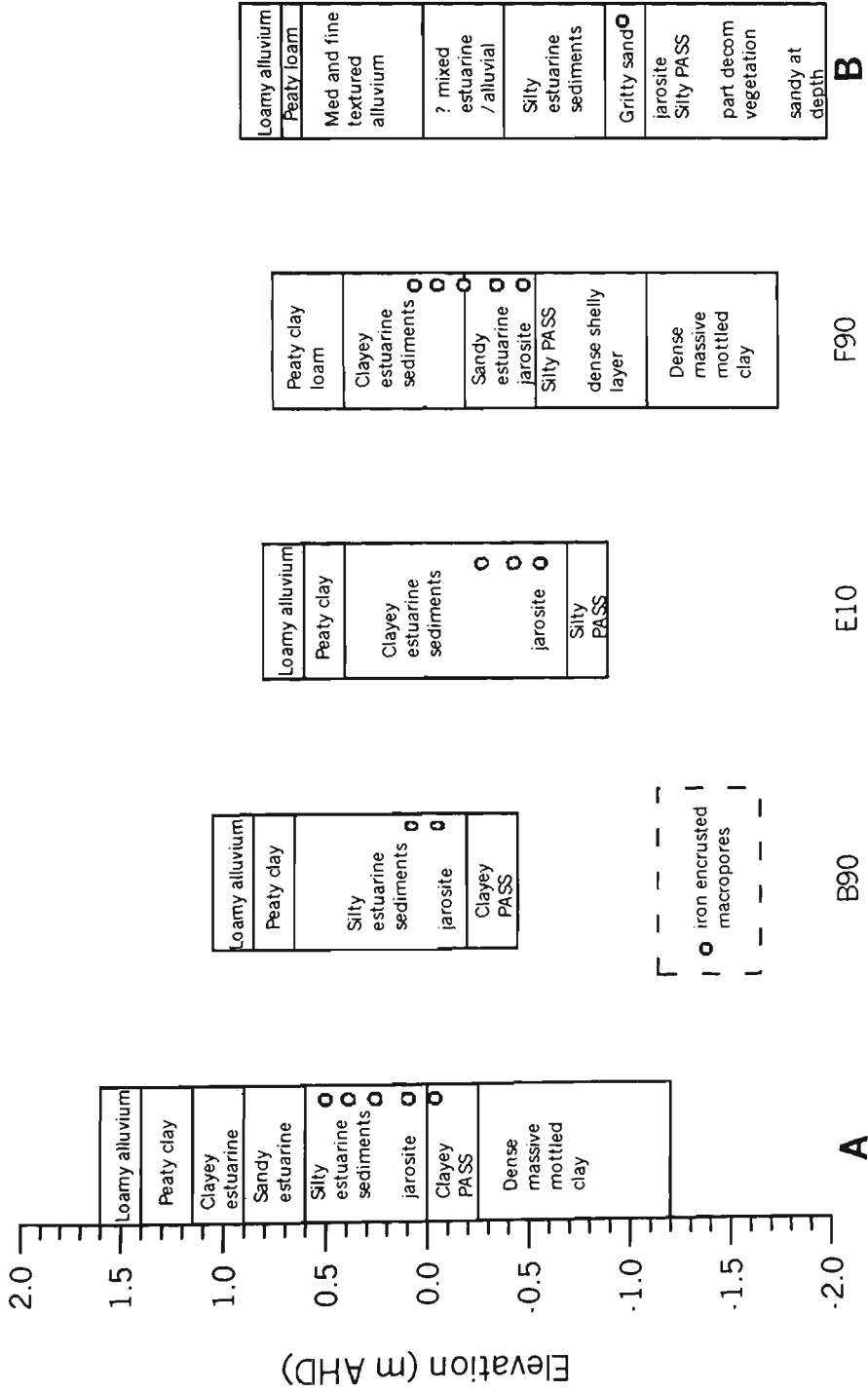


Figure 6.2 The variation in profile morphology along the cross-section AB

The upper boundary of the pyritic soil layer is not smooth and planar, but has a small depression in the vicinity of the former stream channel adjacent to the E10 and E90 sampling location. Jarosite mottles occur at a greater depth at E10 and E90 than at nearby sampling locations. These features suggest that the former stream channel provided better drainage and subsequent pyrite oxidation than in other areas of the backswamp. Where preferential drainage and dewatering has occurred, it may be expected that the elevation of the pyritic layer is lower due to greater soil ripening and shrinkage.

The thickness of the pyritic soil layer varies across the site. Against the hillslope, it is only 0.3 m thick, rising to over 0.8 m thick at the levee. The overlying jarositic zone at the base of the hillslope, however, is 0.4 m thick compared to only 0.1 m at the levee. The estuarine origin of the sediments in the sulfidic zone is confirmed by the heavy accumulation of shells in the F90 core, and the shelly grit observed in the sand at the levee core at a depth of -1.1 m AHD. In the F90 core at a depth of 1.6-2.0 m below the surface, intact shells comprising *Notospirula trigonella*, *Tellina deltoidalis* and *Trichomya hirsuta* (Buman, 1995) were observed. These shells made up 84% (by mass) of the solid material in this depth band within the pyritic sediment. The extract pH of the shelly sulfidic soil after oxidation with  $H_2O_2$  was 7.5, indicating that sufficient carbonate was present at this depth to buffer all the acidity generated by complete pyrite oxidation. The presence of this shelly material is an important source of acid buffering carbonate. The influence of this acid buffering material is demonstrated in Chapter 7, where high groundwater pH was measured during a period of low groundwater elevation when the necessary conditions for pyrite oxidation were present.

The distinctly silty nature of the estuarine sediments is noticeable from their field texture, although the content of sand and clay is variable. The upper boundary of the estuarine sediments is clear, except at the levee bank profile. Here, the alluvial material is initially earthy, with rough ped fabric below it as the colour becomes redder (to 5YR4/6). At greater depth, there is a diffuse wavy boundary to a grey-brown clay, with



reddish-brown mottles, which may represent a transition zone to the estuarine material below. Effervescence with peroxide was neither observed in this material nor in the deeper silty estuarine material until a depth of 2.0 m from the surface. The profile features at Berry have some similarities to those on the southern side of the Shoalhaven floodplain at a site previously described by Willett and Walker (1982). The backswamp profile at Berry has well developed acid sulfate soil horizons resembling the toe of levee profile of Willett and Walker (1982). The depth trend of pH of these two profiles is very similar. Particularly noticeable is the occurrence of the peak jarosite concentration at the point of lowest pH in the toe of levee profile. This feature is also seen at Berry, where jarosite mottling reaches its greatest intensity just above the sulfidic zone.

6.3.2 *Pyrite morphology*

Scanning electron microscopy was used to determine the pyrite crystal size distribution in the sulfidic soil. The pyrite crystal size distribution is shown in Figure 6.3

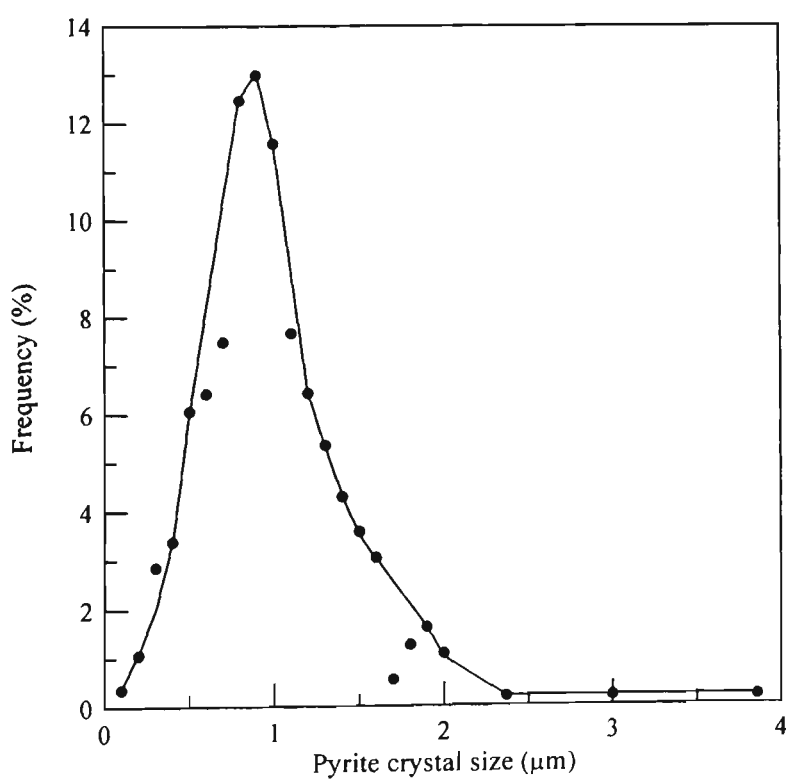


**Figure 6.3** pyrite crystal size distribution for potential acid sulfate soil

The pyrite crystal size distribution (Fig. 6.3) shows that the median pyrite crystal size is about 1  $\mu\text{m}$ , which is typical of the pyrite crystal size in pyritic soils found in New South Wales. Bush and Sullivan (1996) report that pyrite crystals have a diameter range between 0.5-2  $\mu\text{m}$  for potential acid sulfate soil collected on the North Coast of NSW, with framboidal pyrite clusters having a diameter of up to 20  $\mu\text{m}$ . Bronswijk *et al.* (1995) reported pyrite crystal diameters of 50  $\mu\text{m}$  for potential acid sulfate soil collected in South East Asia.

The rate of pyrite oxidation by oxygen in acid solutions is inversely proportional to the diameter of the pyrite crystals (Sasaki, 1994). Numerous pyrite oxidation models (e.g., Bronswijk and Groenenberg, 1992; Wunderly *et al.* 1996) use an 'equal diameter reduction' strategy to determine the dissolution of pyrite from oxidation. This indicates that as the pyrite crystal oxidises and becomes smaller, the surface to volume ratio of the crystal increases leading to a faster pyrite oxidation.

### 6.3.3 Soil chemical properties

A wide array of soil chemical properties can be used to describe pyritic soils and the influence that pyrite oxidation products have on the chemical properties of a soil profile. A number of routine soil chemical properties such as soil pH and electrical conductivity, titratable acidity and sulfate concentration both before and after pyrite oxidation have been suggested by Stone *et al.* (1998), as necessary for the evaluation of acid sulfate soil profiles. However, other soil chemical properties such as the composition of the cation exchange complex, soil carbon content and the presence/concentration of acidic pyrite oxidation minerals were not routinely tested, although these soil chemical processes can provide large volumes of stored acid.



6.3.3.1 Soil pH

The soil pH data (Fig 6.4) verify that the upper 1.5 m of the profiles are highly acidic. All profiles gave similar trends where pH decreases from a maximum of 4-4.5 at the surface to a minimum 2.5-3 at the actual-potential acid sulfate soil transition. Where sampling extended deep enough, the pH increases as depth increased beyond the transition zone, indicating that oxidation of pyrite decreased with increasing depth down the profile, or that internal acid buffering occurred in the clayey pyritic soil that had not undergone intensive oxidation. For instance, at 1.8 m below the surface at F90, the soil pH was 7.6. Samples deeper than 1.5 m below the surface were rarely taken due to limitation with sampling equipment. Stone *et al.* (1998) indicated that soil pH < 4 is only likely to occur as a result of the oxidation of pyrite. Acid conditions also exist at the surface, although with pH approximately 4.5 it is likely that this acidity is as a result of the decomposition of organic matter, as well as from the transport of pyrite oxidation products to the surface from depth.

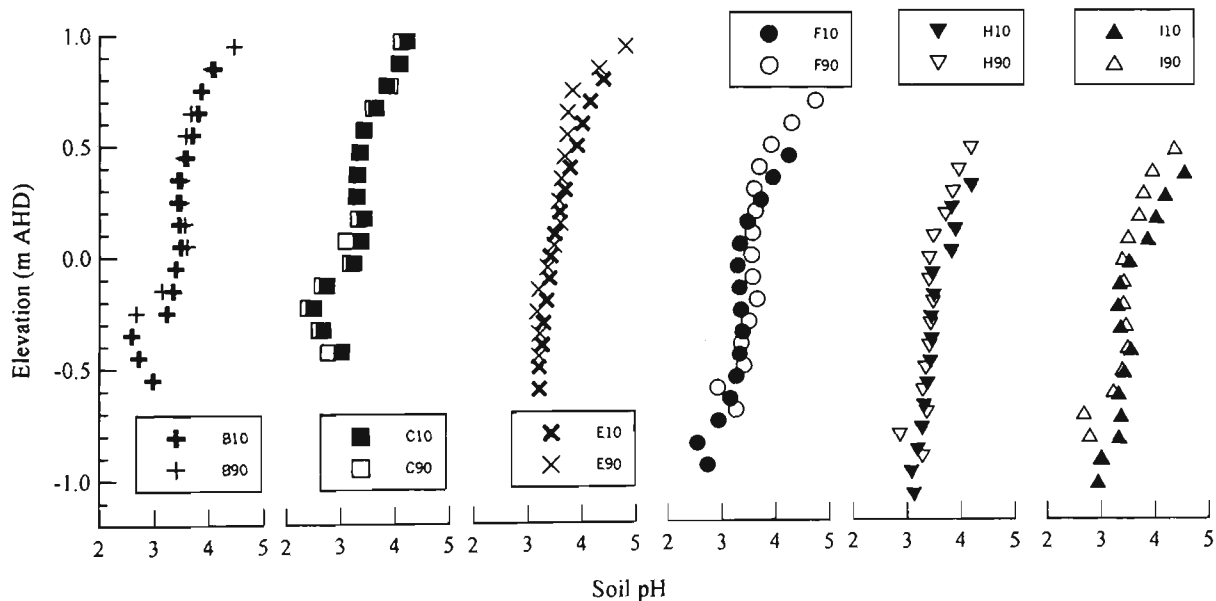
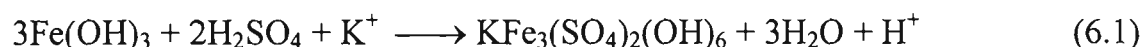


Figure 6.4 Soil pH at 10 m and 90 m from the drains

The zone 0.3-0.5 m immediately above the pyritic layer has a uniform pH of approximately 3.2 across all soil profiles tested. The acid stored within this part of the profile may have numerous sources, although they all emanate from the previous oxidation of pyrite. An obvious source of acidity is soluble sulfuric acid that has been transported from the pyrite oxidation zone to the higher elevation estuarine clay by rising groundwater.

The acidic estuarine clay also corresponds with the position of jarosite observed in the soil profile. The formation and dissolution of jarosite takes place according to Equations (6.1) and (6.2) respectively, where;



Both the formation and dissolution of jarosite contribute to acidity of the soil, ensuring low pH conditions. van Breeman (1985) showed that jarosite exists only between pH 2-4. A third source of acidity available in this soil layer is aluminium and hydrogen ions stored on cation exchange sites. The liberation of acidity from cations stored on the cation exchange sites is discussed in greater detail below.

#### 6.3.3.2 Titratable acidity

Titratable acidity or total actual acidity (Dent and Bowman, 1996) provides a measure of the amount of acidity stored within the soil, excluding potential sources of acidity such as unoxidised pyrite. The titratable acidity measured across the study site at the beginning of the monitoring period is shown in Figure 6.5.

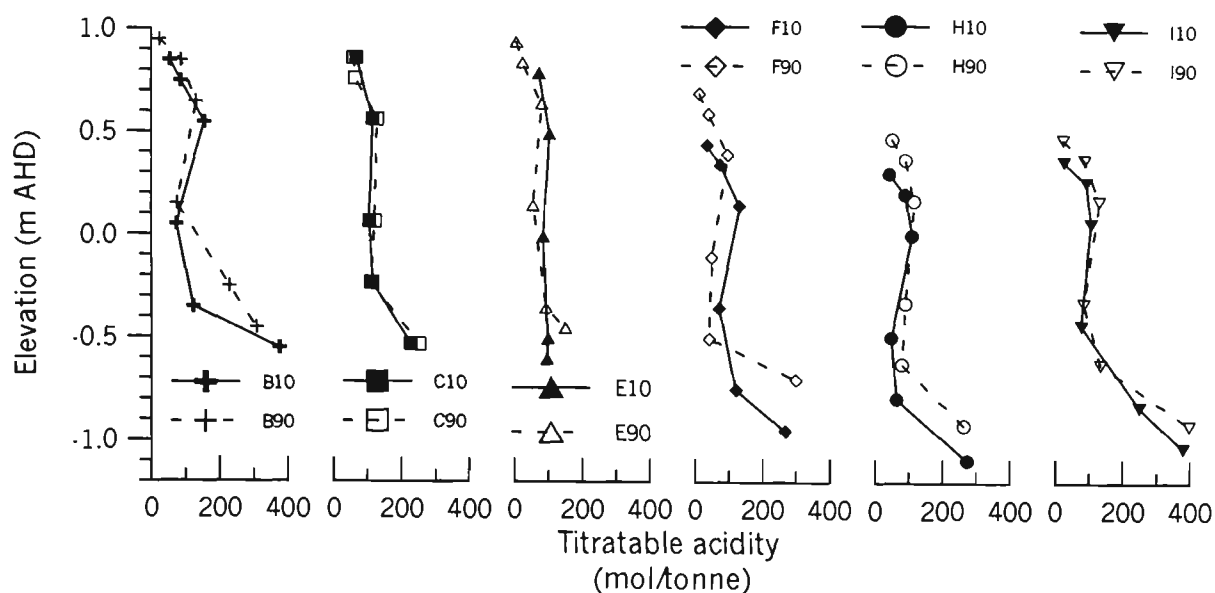


**Figure 6.5** Titratable acidity at 10 m and 90 m from the drains

Figure 6.5 shows that the soil profiles are extremely acid. All profiles gave similar trends where titratable acidity is relatively low at the surface ( $< 50 \text{ mol H}^+/\text{tonne}$ ), and increase to very high acidity concentrations at the actual-potential acid sulfate soil transition (200-400  $\text{mol H}^+/\text{tonne}$ ). A twofold increase in titratable acidity was measured between 0 - 0.4 m below the surface. This increase may be attributed to the presence of organic matter within the topsoil. The decomposition of organic matter previously buried/incorporated into the soil generates acid according to Equation (6.3):



A dark band of organic rich soil, sometimes containing ash, was observed during profile description. This may be the remnants of backswamp wetland vegetation that existed prior to the deposition of the most recent alluvial topsoil. However, organic acids are relatively weak and pose few management problems.

In contrast, titratable acidity concentrations in excess of 100  $\text{mol H}^+/\text{tonne}$  were measured between 1-1.5 m below the soil surface, with the highest concentration of acid being within the upper 0.1 m of the pyritic soil. This indicates that pyrite oxidation has

occurred in the past, generating acidic pyrite oxidation products that have been re-distributed through the soil profile by rising groundwater. A notable exception to the general trend of extremely acidic subsoils occurs at Transect E. At both 10 m and 90 m from the drain along Transect E, the concentration of titratable acidity (also reflected in soil pH data shown in Fig. 6.4) remains relatively low throughout the whole soil profile. This may be a function of the prior stream channel located through this transect. The elevation of the pyritic layer is at a lower elevation at both E10 and E90 (see Fig. 6.2), possibly as a result of scour from the prior stream channel. This depression in the pyritic layer may give rise to less pyrite oxidation in the immediate vicinity of the prior stream channel (as the groundwater has to fall further at E relative to adjacent sites), as well as providing a preferred drainage pathway for the transport of acidic oxidation products away from their source.

Conversion of the titratable acidity data to a volumetric basis averaged over the site shows that approximately 40 tonnes  $\text{H}_2\text{SO}_4/\text{ha}$  is present in the upper 1.5 m of the soil profile. This is comparable with other acid sulfate soil affected sites in Australia (e.g., Pease, 1994; Wilson, 1995). Managing the existing acidity poses numerous challenges. Neutralising the existing acidity using traditional liming techniques is prohibitively expensive as well as physically demanding on equipment. Neutralisation of the existing acidity would require in excess of 60 tonnes/ha of agricultural lime to be thoroughly incorporated into the profile to a depth greater than 1.5 m. Rapid profile flushing by maintenance of very high watertables or surface ponding can result in the export of large volumes of acid following relatively minor rainfall events. Dilution of the acid may not be sufficient to mitigate against severe acid impacts in the receiving waters.

#### 6.3.3.3 *Dissolved sulfate and chloride*

The concentration of dissolved sulfate and chloride down the soil profile at C10 and C90 is shown in Figures 6.6 and 6.7, respectively.

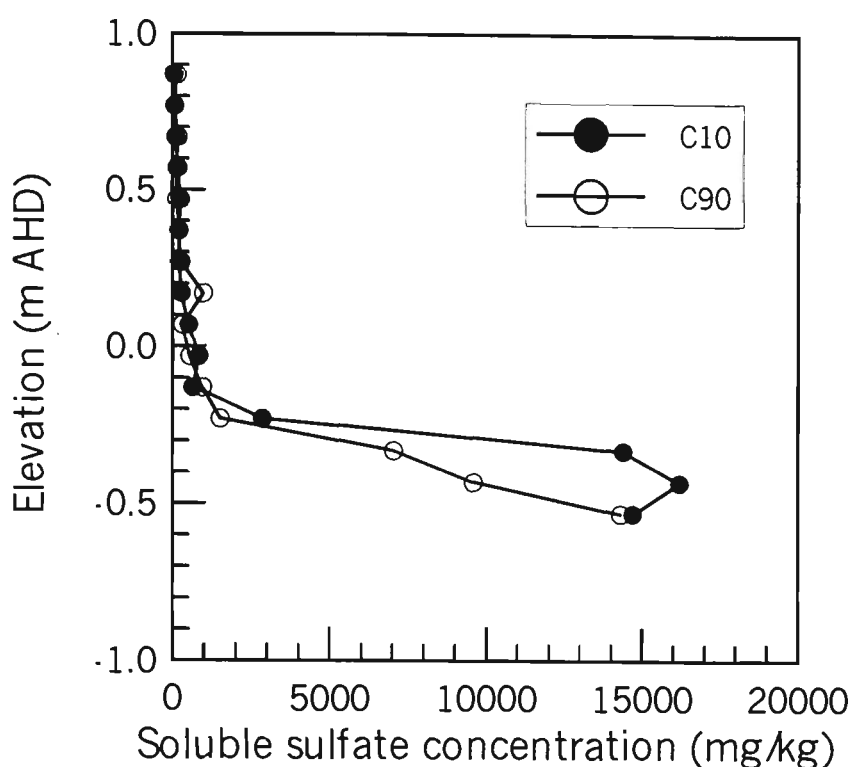


**Figure 6.6** Dissolved sulfate at C90

The concentration and distribution of dissolved sulfate is typical of soil profiles where the pyritic soil has undergone oxidation. The concentration of dissolved sulfate is greatest at an elevation of -0.3 to -0.4 m AHD, which corresponds to the upper surface of the pyritic soil layer. The high concentration of sulfate is expected at this elevation due to the previous generation of sulfate by pyrite oxidation. High concentrations of sulfate are also present in the 0.4 m immediately above the pyritic layer. This is indicative of the upwards migration of dissolved sulfate in the rising groundwater after pyrite oxidation events. High concentrations of dissolved sulfate in the non-pyritic soil may also be indicative of the dissolution of sulfate based minerals such as jarosite that were formed under low pH conditions. The concentration of dissolved sulfate in the soil decreases as the distance away from the source of sulfate production increases. As expected, regular flushing with fresh rainwater coupled with higher concentrations of organic matter which can complex sulfate, gives rise to substantially lower concentrations of dissolved sulfate in the top soil layers.

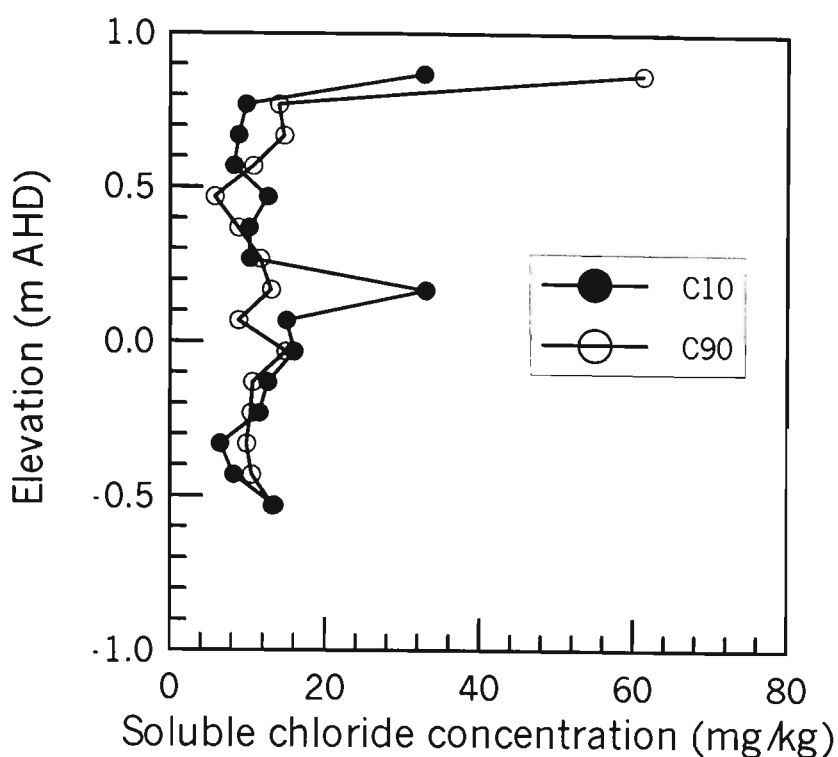


**Figure 6.7** Dissolved chloride at C90

In contrast to dissolved sulfate, the concentration of chloride is low and it is reasonably uniformly distributed through the soil profile. This is somewhat unexpected given the depositional characteristics necessary for the formation of pyritic soil. Pyritic soil can only be formed in estuarine environments where a source of sea water is present. Sea water has high concentrations of chloride. As such, pyritic soils may have elevated concentrations of chloride relative to non-estuarine deposited soils. However, as shown in Figure 6.7, the concentration of dissolved chloride down the profile is uniform. This may indicate that chloride originally stored in the pyritic soil has been leached away during ongoing freshwater flushing since the transformation of the site from an estuarine wetland to an elevated terrestrial landform. The higher concentration of chloride at the surface is likely to be attributed to the deposition of atmospheric seaspray or soil evaporation.

Mulvey (1993) suggested that the sulfate: chloride ratio could be used to indicate the presence of previously oxidised pyritic sediments. Previous pyrite oxidation is indicated where the ratio (by mass) falls below 2-4 and low pH conditions also exist. As shown in

Figures 6.6 and 6.7, the concentration of sulfate is higher than two orders of magnitude greater than for chloride. According to Mulvey (1993), this is indicative of previous pyrite oxidation.

### 6.3.3.4 Oxidisable sulfur

The concentration of pyrite in sulfidic sediments can be assessed by determining the peroxide oxidisable sulfur concentration (% S<sub>pos</sub>). The % S<sub>pos</sub> for various sampling locations across the study site is shown in Figure 6.8.

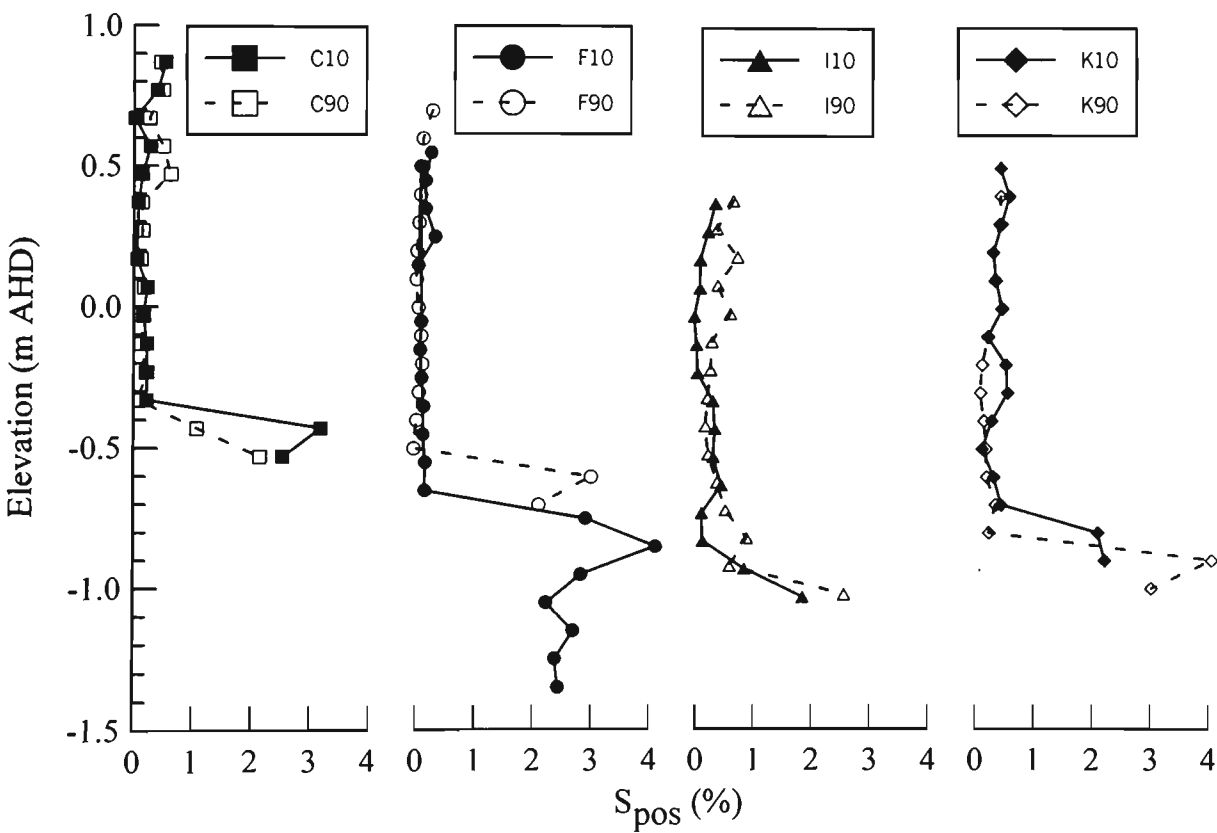


**Figure 6.8** Peroxide oxidisable sulfur concentration, with depth.

At the northern end of the study site (Transect C), the upper boundary of the pyritic layer occurs at approximately -0.3m AHD. It gradually falls to an elevation of -0.7m AHD at the southern end of the site (Transects I, K). This is consistent with the depth of

the lowest soil pH (Fig. 6.4) and highest titratable acidity (Fig. 6.5) measurements previously used to identify the actual-potential acid sulfate soil transition. Peroxide oxidisable sulfur has a maximum range of 2.5-4% in the pyritic soil and is, in general, uniformly distributed across the site. Stone *et al.* (1998) recommended that acid sulfate soil management strategies should be used when disturbing medium-heavy textured acid sulfate soils with  $S_{\text{pos}}$  greater than 0.06-0.1%. Given that the action criteria proposed by Stone *et al.* (1998) are conservative and are developed primarily for environmental protection goals, it is clear that pyritic soils at the study site pose significant risks to the environment, agricultural productivity and engineering infrastructure, if they are not managed appropriately.

Figure 6.8 shows an interesting trend with the upper most 0.1 m of the pyritic soil, where the highest peroxide oxidisable sulfur concentration exists. This may reflect the depositional sequencing of the formation of the pyritic soil. As discussed earlier, sea level regression may have caused a migration of estuarine vegetation across the site. Pons (1973) showed that the formation of pyrite in acid sulfate soils is dependant on the organic matter content of the sediment. As such, conditions for the formation of pyrite in the estuarine sediment may have been most favourable during the last stages of the sea level stabilisation, where both a source of dissolved sulfate in the estuarine water and a large concentration of organic matter was available. This is particularly evident at F10 where deeper sampling enabled  $S_{\text{pos}}$  testing to an elevation of -1.4 m AHD. Between -0.8 and -1.4 m AHD, the  $S_{\text{pos}}$  is approximately 2.5%, which is 0.5-1% lower than the peroxide oxidisable sulfur concentration for the upper most 0.1 m of the pyritic soil layer across the study site.

Although profile morphology and soil description enable a clear distinction to be made between the non-pyritic estuarine clay and the pyritic soil horizons, the boundary delineated by measuring % $S_{\text{pos}}$  at 0.1 m intervals is surprisingly sharp. The soil pH and titratable acidity measurements indicate that severe acidification of the soil profile has previously occurred. Presumably, this acidification caused by pyrite oxidation has been accelerated by the installation of the flood mitigation drainage scheme some 30 years ago which has resulted in generally lower groundwater tables than otherwise may have



existed. However, little evidence of lower concentrations of oxidisable sulfur in the upper part of the pyritic soil layer at the locations closer to the drain.

The even pyrite concentration across the site suggests that spatially uniform oxygen transport through the soil profile may have occurred. This may be a feature of the macropore dominated structure of the pyritic soil where oxidation of pyrite occurs radially from vertically orientated pores that pass down the soil profile. As such, there may be no preferential reduction in the oxidisable sulfur concentration in the pyritic soil that might be expected if the main mechanism of oxygen transport to the pyritic soil was by a horizontal diffusion front. Rather, preferential reduction in pyrite concentration may exist radially from macropores or other structural features in the soil. This conforms with the observation of jarosite filled macropores within the pyritic sediment, with little or no jarosite observed within the clayey matrix. However, it is unlikely that this phenomena would be detected in the  $S_{pos}$  data, given the nature of the sample collection or soil testing procedures adopted in this study.

#### *6.3.3.5 Electrical conductivity*

A regular pattern of increasing electrical conductivity with depth was found for all profiles investigated across the site. The electrical conductivity of the soil at various sampling location is shown in Figure 6.9.

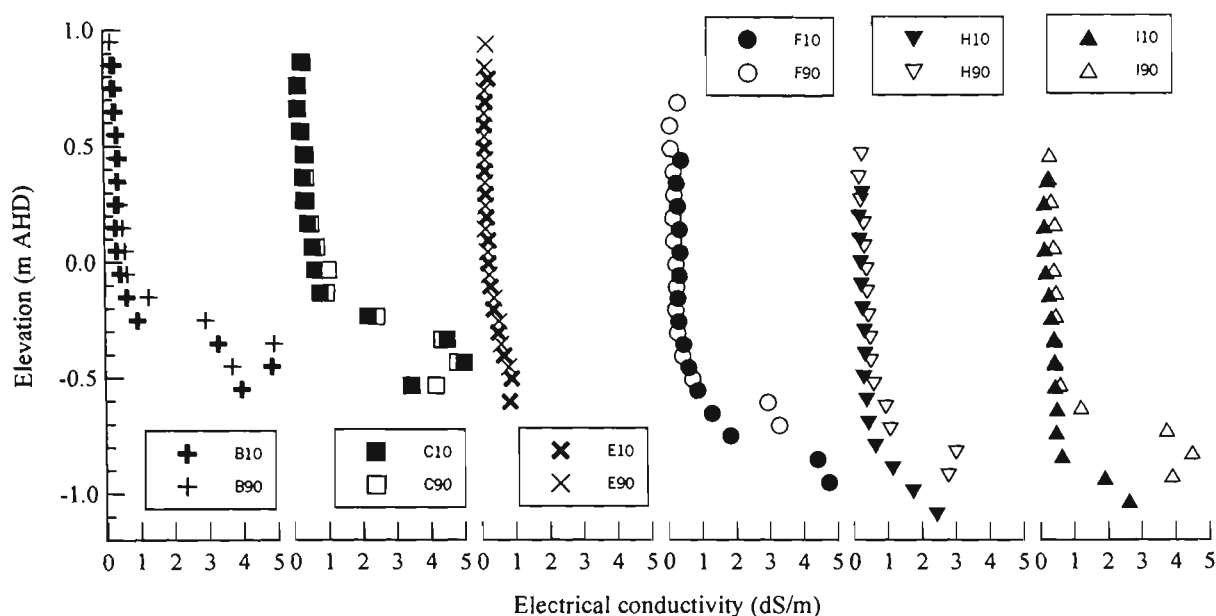
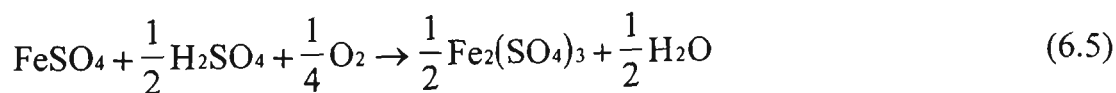
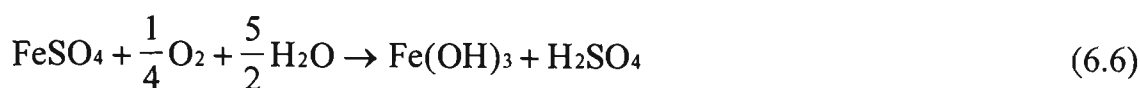


**Figure 6.9** Electrical conductivity.

Electrical conductivity is low (i.e., < 1 dS/m) in the upper metre of the soil profile. At greater depths, electrical conductivity increased to a maximum of about 3-5 dS/m. The onset of elevated salinity corresponds with the occurrence of elevated concentration of dissolved sulfate in the soil profile from the prior oxidation of pyrite. Elevated electrical conductivity values are an interesting aspect of the generation of dissolved pyrite oxidation products. Clearly, the dominant dissolved anion in the soil solution is sulfate. Fanning (1993) showed that a variety of ferrous sulfate minerals may precipitate in acid sulfate soils. Under dry, oxidising conditions, the iron of ferrous sulfate may oxidise to form soluble ferric sulfate minerals such as copiapite. This reaction is described in Equation (6.5)



Fanning (1993) also showed that some iron sulfate minerals are also significant sources of stored acidity. The direct oxidation and hydrolysis of ferrous sulfate to form iron oxides, as described in Equation (6.6), yields 1 mole of sulfuric acid for every mole of ferrous sulfate that is oxidised.



From the ecological point of view, Fanning (1993) suggested that the precipitation of ferrous sulfate salts are as important as the generation of acidity from the oxidation of pyrite. As such, he indicates that when developing management strategies for acid sulfate affected areas, salinity as well as acidity must be considered.

The measurement of electrical conductivity is usually understood to reflect the concentration of chloride salts in the soil. References which suggest acceptable soil solution electrical conductivities (e.g. Brady, 1984) base these values on the detrimental influence that chloride salts have on plant/crop growth. As such, any inferences based on electrical conductivity of soil that have been affected by pyrite oxidation products must be interpreted cautiously.

Electrical conductivity was greater at 90 m distance from the drains than at 10 m from the drain in Transects H and I. This may be due to two factors. Firstly, the water level in the drain adjacent to Transects H and I is often maintained between low and mean tide level through partial tidal ingress through leaky floodgates that bound the drain and Broughton Creek. This drain water level minimises the fall in groundwater elevation close to the drain as seepage from the drain can re-supply water to the groundwater table during dry periods (see Chapters 7, 8 and 10 for further explanation). As such, the magnitude of pyrite oxidation that occurs during drought periods is likely to be more severe further away from the drains than close to the drains. This gives rise to elevated concentrations of sulfate at 90 m from the drain, and by association, higher electrical conductivity. Maintenance of groundwater above the pyritic soil from seepage from the drain is less pronounced in Transects A-F, as the elevation of the pyritic soil increases relative to the water level that can be maintained during dry periods.

The second factor is dilution of the ionic strength of the soil solution by the ingress of lower ionic strength water by seepage from the drain. If, during tidal cycling in the

drain caused by leaking floodgates, drain water can flush the soil adjacent to the drain, then this can remove or dilute some of the dissolved ions from the soil solution. Lower ionic strength soil solutions would be apparent in lower electrical conductivity data.

A significant divergence from the electrical conductivity trend with depth is apparent at Transect E. The concentration of dissolved sulfate at Transect E is lower than at other locations, suggesting that less pyrite oxidation has occurred in this area. This is supported by higher pH and lower titratable acidity data. In addition, groundwater elevation data described in Chapter 7 shows that the former stream channel adjacent to Transect E acts as a sub-surface drainage feature. This drainage feature may remove dissolved pyrite oxidation products away from their point of origin, thereby increasing electrical conductivity values.

### 6.3.3.6 Effective cation exchange capacity

The effective cation exchange capacity (ECEC) measured for samples collected across the site is shown in Figure 6.10.

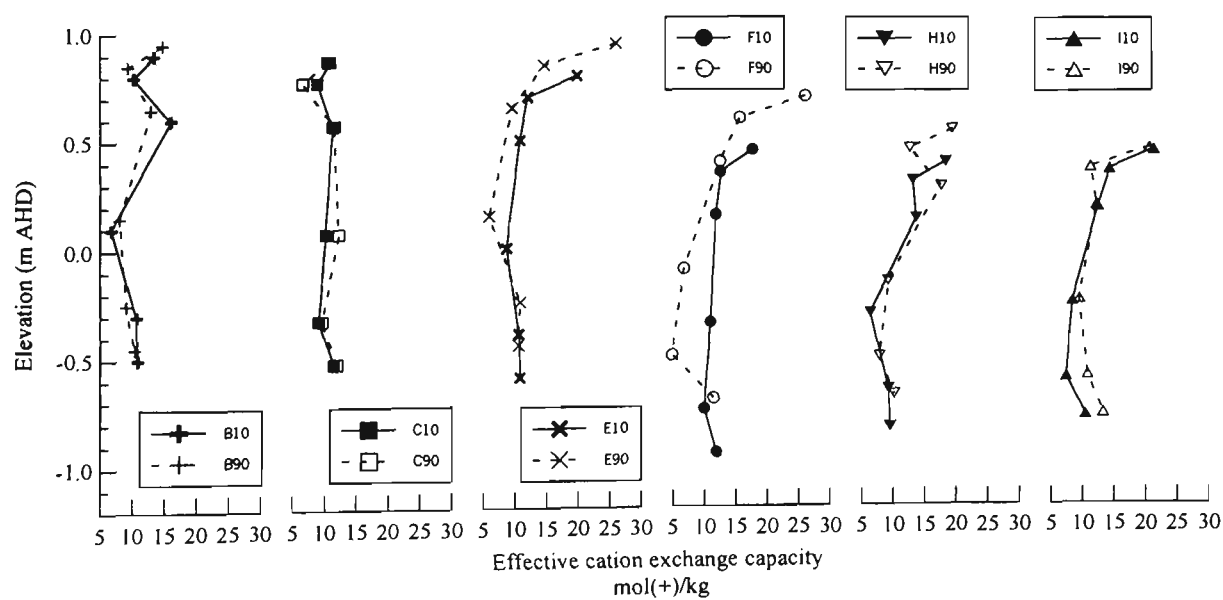


**Figure 6.10** Effective cation exchange capacity

The ECEC values reflect the variation in organic matter and the texture down the profile. High concentrations of organic carbon at the surface and in the sub-surface peaty layer (especially at Transects E, F and H) have boosted ECEC in the top 0.4 m of the soil profile. Deeper in the subsoil, sandy layers and highly acidic estuarine silty clays exhibit relatively low ECEC in the range of 7-12 mol/kg. This is typical of the ECEC range for kaolinite/illite clays that are often associated with estuarine deposition (Brady, 1984). The low ECEC values are further lowered by the low pH of the soil. At low pH, aluminium hydroxy ions (e.g.  $\text{Al}(\text{OH})_2^+$ ) block negatively charged sites in silicate clays and make them unavailable for cation exchange. At the low pH present in the sub-soil, variable or pH dependent charges on soil colloids become  $\text{OH}^+$  saturated, thereby reducing the ECEC even further. ECEC increases in the pyritic soils due to their higher clay content. Elevated ECEC values may also indicate the presence of relatively insoluble oxidation products such as gypsum, although the low pH of the pyritic soil also indicates that the ECEC may have been considerably higher in the absence of pyrite oxidation where variable charged colloids may have contributed to the ECEC. The generally low ECECs through the soil profile limits the amount of buffering between the soil colloids and the soil solution.

The composition of the cation exchange complex is important when considering the nature of the exchange of cations from the soil solution to the cation exchange sites (i.e., soil solution buffering), and the resultant composition and concentration of the soil solution. Figures 6.11 and 6.12 show the percentage saturation of aluminium and calcium on the ECEC, respectively.

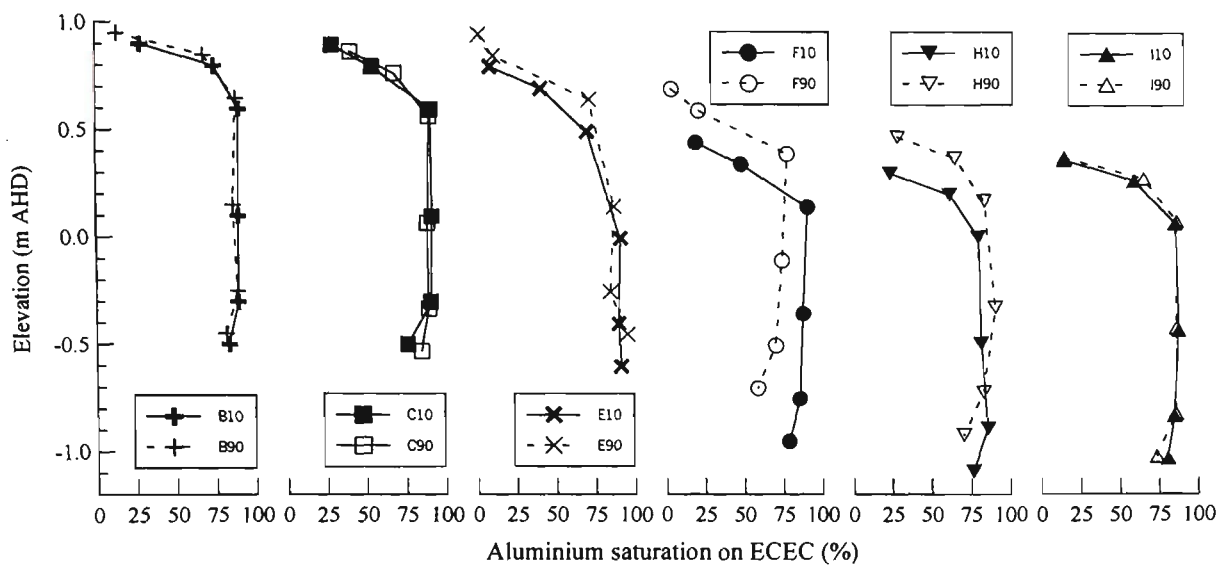


**Figure 6.11** Aluminium saturation on the ECEC

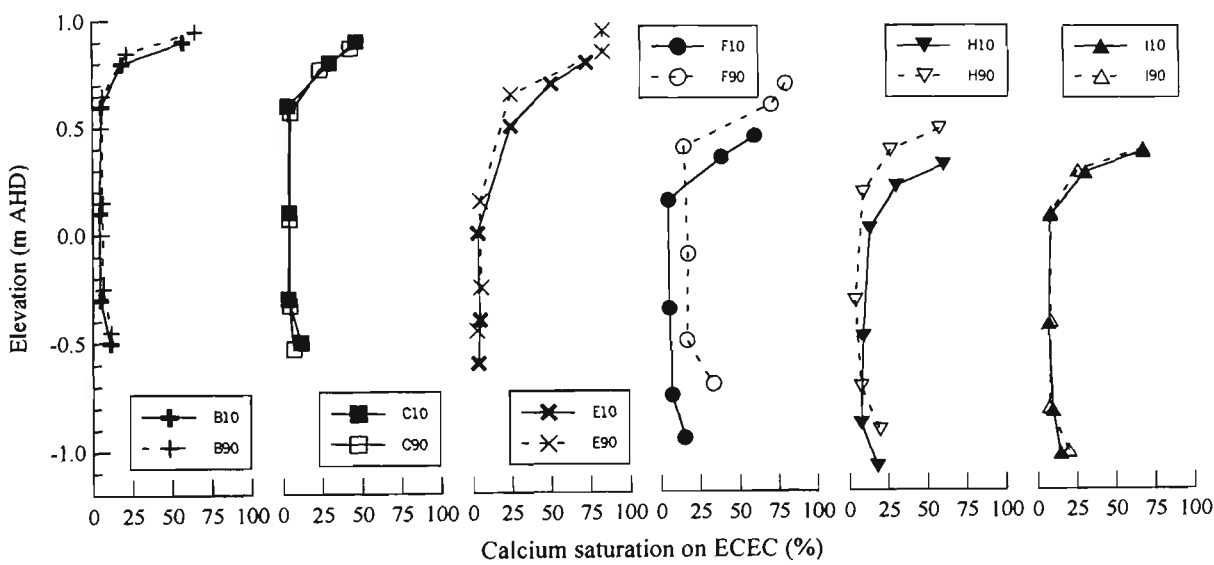


**Figure 6.12** Calcium saturation on the ECEC

Expressed as a percentage of ECEC, exchangeable aluminium saturation generally reaches a maximum of about of 90% in the highly acidic jarositic zone. The aluminium saturation of the ECEC is greater than 75%, except within 0.2 m of the soil surface. In contrast, the calcium saturation of the soils at depth is extremely low. The calcium saturation appears to increase slightly in the pyritic soil layer. This rise may be due to partial dissolution of gypsum during the extraction procedure. Ritsema *et al.* (1992)

showed that during the oxidation of pyrite in acid sulfate soils, calcium from the soil reacts with dissolved sulfate from the pyrite oxidation reaction to form gypsum. Higher calcium saturation at the surface is indicative of calcium uptake by plants and lime applied by farmers. The high aluminium saturation of the surface soils poses challenges for pasture production. Pasture productivity is related to the ability of the plants to exchange hydrogen ions from the roots for beneficial cations from the soil as well as the uptake of available phosphorus from fertilisers. The elevated aluminium saturation depresses the uptake of beneficial cations and the availability of applied phosphorus.

The high percentage of aluminium on the cation exchange sites also contributes to the soil solution acidity. As shown in Equations (6.6-6.8), as aluminium is replaced from the cation exchange sites by other cations, it hydrolyses through a series of reaction steps.



For every mole of  $\text{Al}^{3+}$  that is lost from the cation exchange site, an additional 3 moles of acidity is added to the soil solution. Ritsema *et al.* (1992) found that the main acid buffering processes in drained pyritic soils with no carbonate minerals present was the weathering of aluminium silicate minerals. The weathering of these aluminium minerals increases the concentration of aluminium in the soil solution, which then promotes the replacement of basic cations such as  $\text{Ca}^{2+}$  and  $\text{Mg}^{2+}$  from the cation exchange complex with acidic  $\text{Al}^{3+}$ .

The highly acidic nature of the composition of the ECEC is further demonstrated in Figure 6.13.

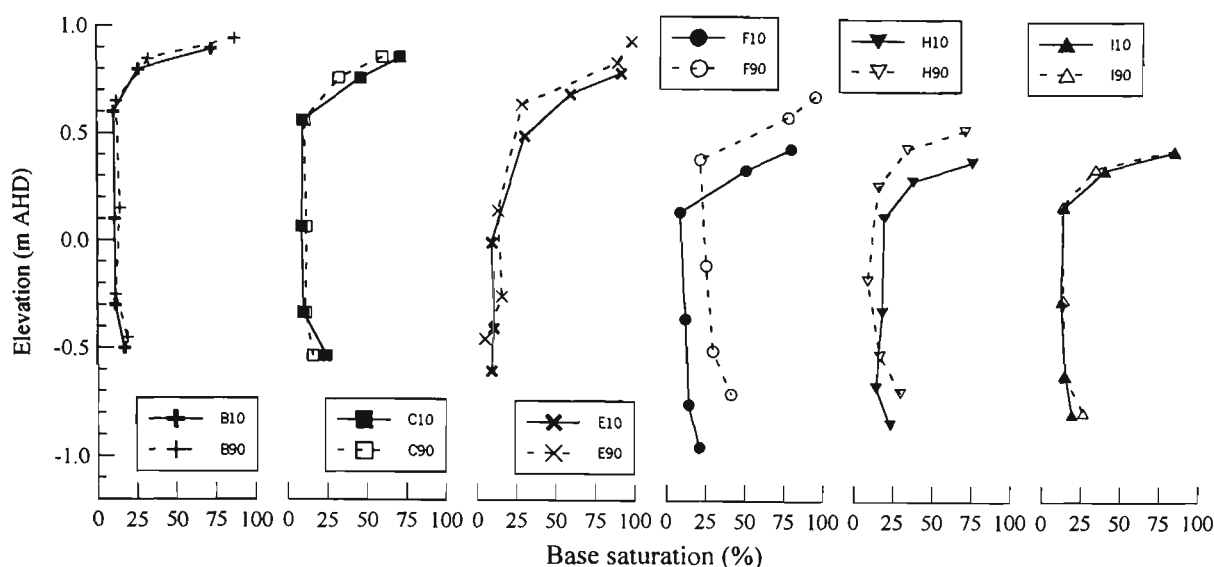


**Figure 6.13** Base saturation of the ECEC

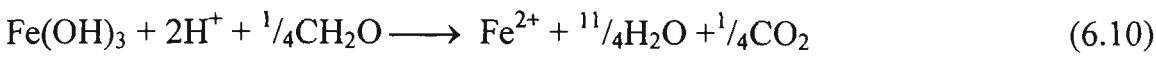
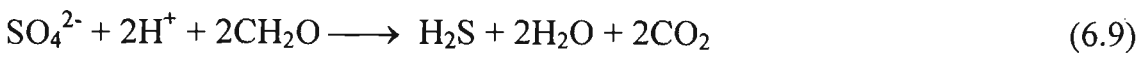
Calculation of base saturation gives a consistent trend across the site, with the highest base saturation ranging between 80-95% at the surface and a minimum at the actual-potential acid sulfate soil transition zone of only 5-10%. The base saturation of the pyritic soil increases slightly to 10-15%. The low base saturation between the pyritic soil and the bottom of the top soil layer is of concern for the establishment of improved water quality. The low base saturation represents a store of exchangeable acidity that must come into equilibrium with the soil water. If no further acidity is supplied to the system by oxidising pyrite, the addition of low ionic strength rain water will lower the steady state equilibrium concentration of  $Al^{3+}$  in the soil water, promoting the liberation of  $Al^{3+}$  stored on the cation exchange sites into the soil water.

### 6.3.3.7 Soil carbon

Dent (1986) suggested that reclamation of actual acid sulfate soils may be possible where sufficient organic matter is available to prevent the oxidation of  $Fe^{2+}$  to  $Fe^{3+}$ , or preventing the oxidation of pyrite by  $Fe^{3+}$  reduction. Dent (1986) also suggested that pyrite oxidation could be minimised, or even reversed, by the establishment of reducing



conditions in acid sulfate soils by water table management or reflooding. In a reduced environment, a microbial catalysed reaction in the presence of organic matter may reduce dissolved sulfate to hydrogen sulfide (H<sub>2</sub>S) and precipitated Fe<sup>3+</sup> to dissolved Fe<sup>2+</sup> as described in Equations (6.9-6.10).



To establish such conditions for the reduction of sulfate and Fe<sup>3+</sup>, a considerable amount of bio-available organic matter is required. The average concentration of organic carbon present down the soil profile at the study site is shown in Figure 6.14.

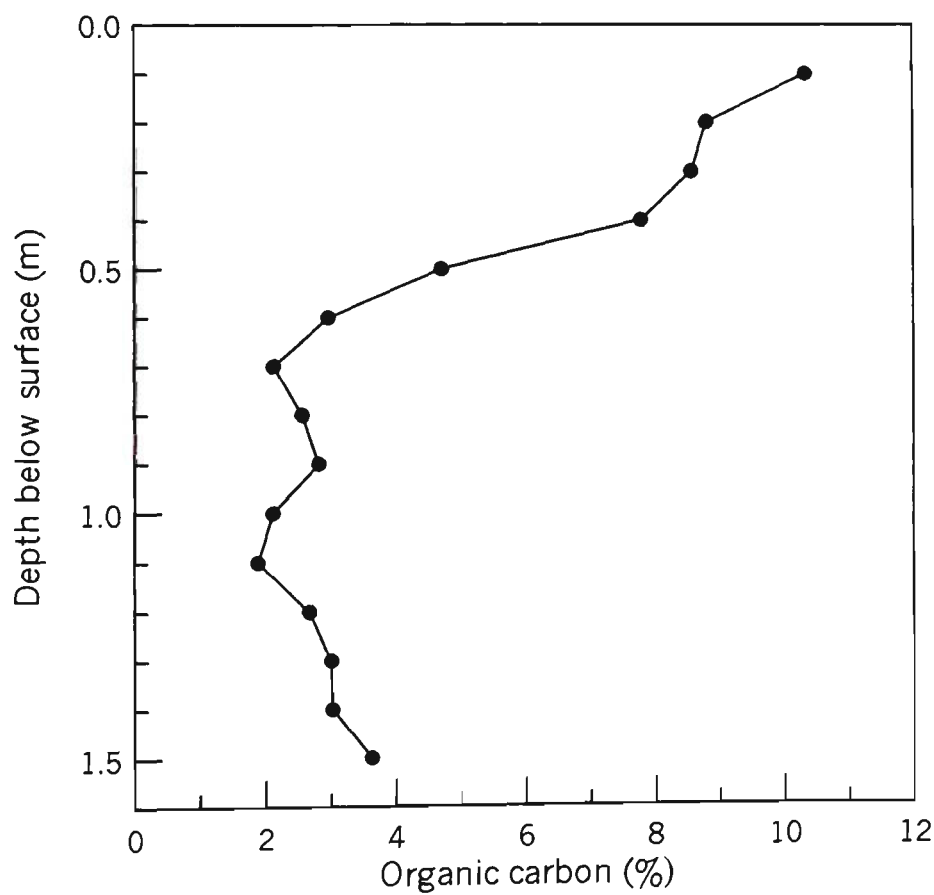


**Figure 6.14** Average organic carbon

Organic carbon is high at the soil surface (7-12%), which is consistent with the presence of growing vegetation at the surface. Carbon concentration decreases in the underlying layers to 2-5%. A small increase in organic carbon concentration (5-6%) is observed in the upper layers of the pyritic soil. This rise may be related to the maintenance of reducing conditions in the pyritic layer which has minimised organic matter decomposition. Since 2-4% carbon is generally present in the acidic transition zone, and of this only a fraction will be in a bio-available form, there is probably insufficient carbon present for the bio-chemical reduction reaction described in Equations (6.7-6.8). White *et al.* (1997) have suggested that this situation may be widespread throughout eastern Australia.

An interesting greenhouse gas emission phenomena identified by Hicks *et al.* (1999) has been linked to the acidification of the soil profile by the oxidation of pyritic sediments. Carbon dioxide is emitted when carbonate minerals react with acid and when organic matter oxidises. Both these reactions are facilitated by the generation of strong acid by the oxidation of pyrite. Hicks *et al.* (1999) suggested that as well as the environmental degradation caused by the generation and transport of acidity from the oxidation of pyrite, the emission of carbon from these soils may also be a significant contributor of greenhouse gasses. Further study and quantification of the transfer of carbon stored in acid sulfate soils to the atmosphere is required.

#### 6.3.4 Soil physical properties

Soil physical properties determine the rate of water and air transport through the soil. As such, understanding the physical properties of the soil facilitates the prediction of groundwater fluctuations that cause oxidising conditions in the pyritic soil, as well as the diffusivity of oxygen through the soil. Many authors (e.g., Elberling and Nicholson, 1996; McKibben and Barnes, 1986) have shown that the rate limiting step for the oxidation of pyrite is the supply (or concentration) of oxygen in the pyritic zone.

6.3.4.1 Particle size distribution

Particle size distribution curves for sampling locations C10, F90 and I90 at depths 0-0.1, 0.6-0.7, 0.9-1.0 and 1.4-1.5 m are described in Figure 6.15.

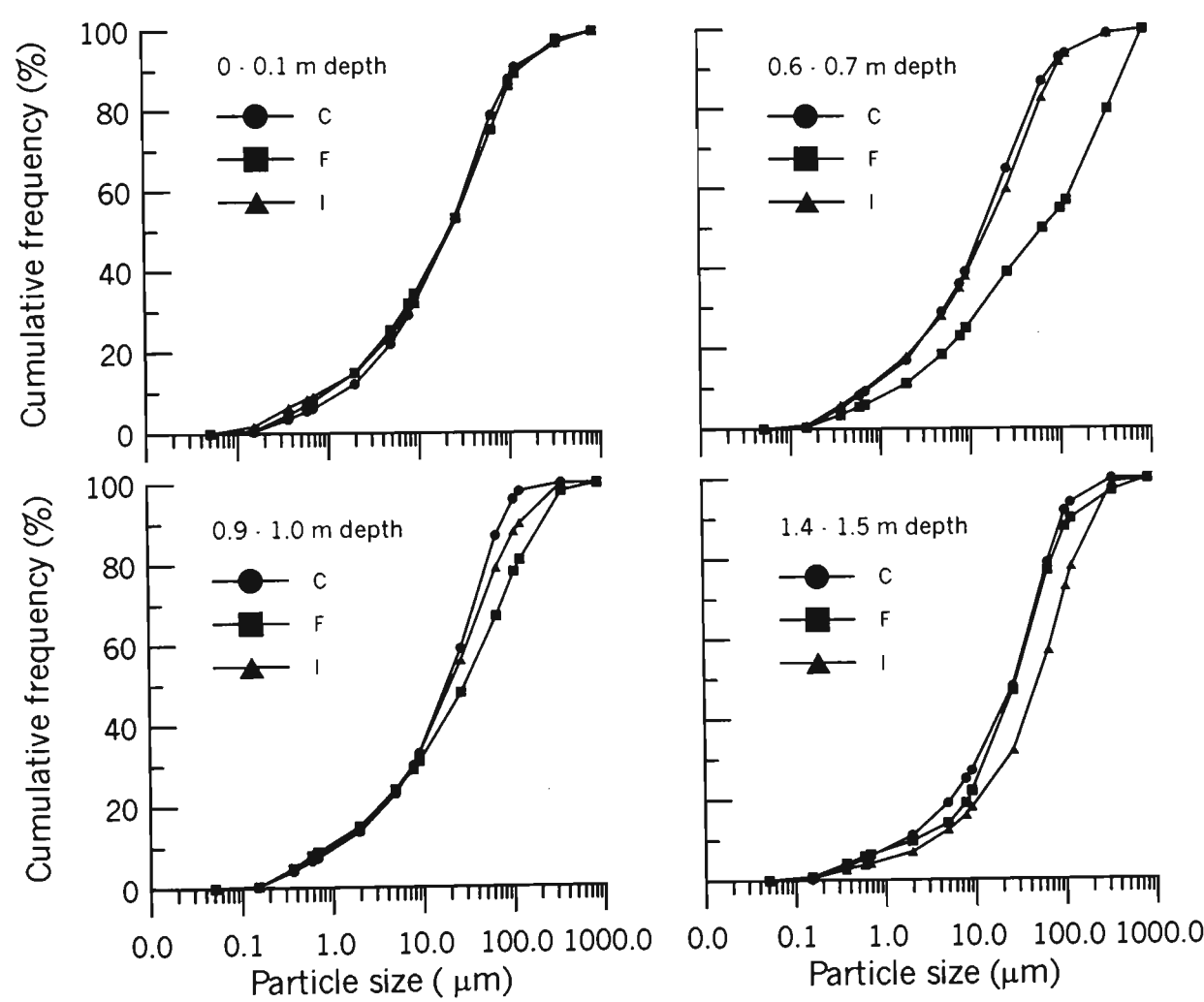


**Figure 6.15** Particle size distribution curves

The particle size distribution curves confirm the soil texturing performed in the field. At the surface (0-0.1m depth), the particle size distribution is uniform across the site suggesting that deposition of the loamy alluvial material occurred under the same conditions across the site. The percentage of larger particles increases with depth. At depths 0.6-0.7 and 0.9-1.0m, a pronounced sandy particle size distribution indicating a more energetic depositional environment occurred adjacent to F90. The difference in

sand concentrations between sites F90 and I90 may be related to the presence of the former stream channel running east-west close to Transect E. There is a general trend of the estuarine clay horizon becoming increasingly interspersed with sandy lenses as the distance from Broughton Creek decreases.

The pyritic soil sampled at 1.4-1.5 m below the surface shows a high proportion of clay and silt, indicating that they formed in a reasonably well protected environment. The percentage of clay found at these sites is significantly less than that for other locations reported on the east coast of Australia (e.g., Lin *et al.* 1995). This may be a function of the close proximity of the site to the escarpment directly to the west during the period of pyrite formation. As sediment eroded from the escarpment, courser silts and sands may have been entrapped more readily than the clay fraction in the estuarine vegetation. Prior streams that cross the site during this period may have retained sufficient power to keep clay sized particles entrained as the water carried or deposited eroded sediments across the site.

### 6.3.4.2 Bulk density and porosity

The average dry bulk density and porosity values are shown in Table 6.1

**Table 6.1:** Average dry bulk density for sites P1-5.

Depth below surface (m)	Average dry bulk density ( $\rho_d$ ) (t/m <sup>3</sup> )	Porosity	Standard deviation for $\rho_d$ (n=30)
0.3	0.80	0.70	0.14
0.6	1.11	0.58	0.26
0.9	1.05	0.60	0.27
1.2	0.95	0.64	0.27
1.5	1.03	0.61	0.23

At 0.3 m depth in the organic rich topsoil layer  $\rho_d$  was significantly lower than at any other depths. However, the pyritic soil located at 1.5 m had an unusually high  $\rho_d$  in comparison with other Australian sites where values as low as  $0.5 \text{ t/m}^3$  have been reported (e.g., White *et al.*, 1997). Often the texture of these pyritic soils is reported as unconsolidated muds or gels. The densification of the potential acid sulfate soil is thought to occur through a process called ‘ripening’ by van Breeman (1973) and Dent (1986). Water is lost through consolidation of the saturated pyritic sediment by the weight of the alluvial overburden, evaporation from the surface, and through extraction of water by plant roots. Oxidation of pyrite along preferred pathways created by old root channels produces severe acidification. The resulting increase in cation concentration in solution assists the flocculation of the unconsolidated clays. Soil aggregation increases making the profile more permeable and enhancing further oxidation of pyrite. The shrinkage of the clay by flocculation is generally irreversible. White *et al.* (1993) report that a potential sulfate soil with 80% volumetric moisture content had a shrinkage of 50% upon complete drying. The flocculated clays form stable aggregates that do not disperse following re-wetting.

#### 6.3.4.3 Saturated hydraulic conductivity

The ripening process also increases the hydraulic conductivity and air permeability. The magnitude of saturated hydraulic conductivity in the horizontal and vertical orientation is shown in Figure 6.16.

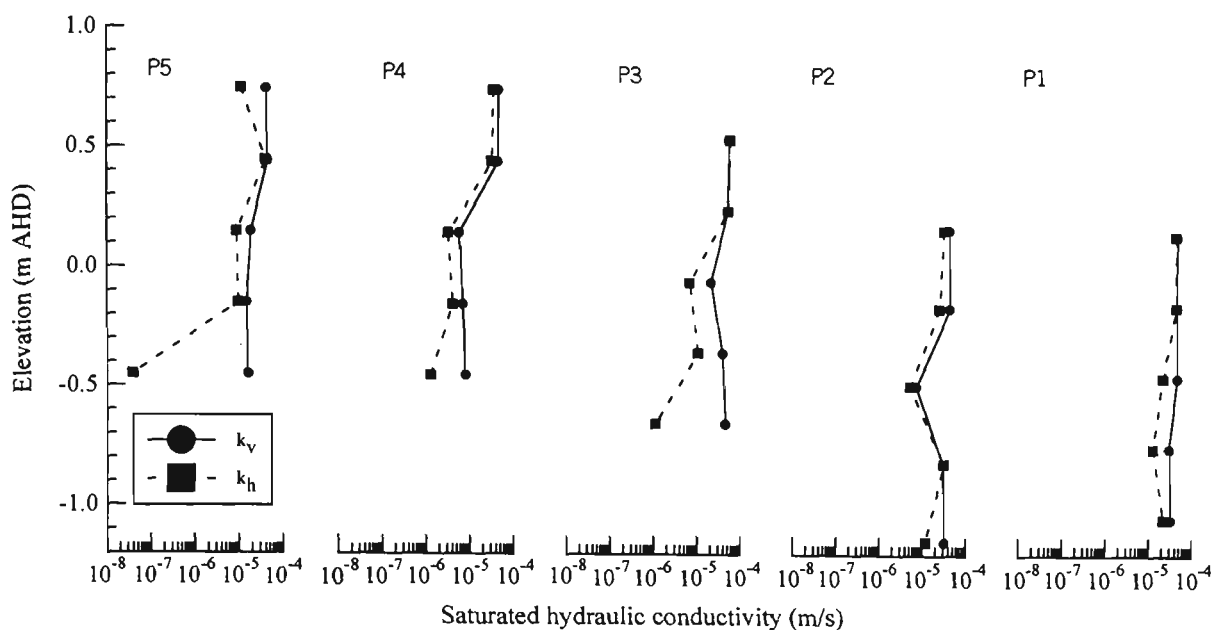


**Figure 6.16** Saturated hydraulic conductivity in the vertical and horizontal orientation

There is very little variation in saturated hydraulic conductivity ( $k_v$ ) across the site, either down the profile or between sampling locations.  $k_v$  is approximately  $10^{-4}$  to  $10^{-5}$  m/s for all samples. The uniformly high  $k_v$  ( $10^{-4}$ - $10^{-5}$  m/s) can be attributed to continuous, large diameter, vertically orientated macropores that are distributed throughout the profile to a depth of 1.5 m. Macropores as large as 13 mm diameter were observed during profile description. These may represent relic root channels of riparian or estuarine plants that were present on the site prior to clearing. On the other hand,  $k_h$  was considerably more variable both down the profile and across the site. Close to the surface,  $k_h$  was not significantly different ( $P<0.05$ ) than  $k_v$ . This can be attributed to the highly aggregated soil structure generated by vigorous biological activity. At sampling locations P3-5,  $k_h$  decreased at 0.9 and 1.2 m below the surface. In the pyritic soil layer,  $k_h$  decreased much further, from  $10^{-6}$  to  $10^{-8}$  m/s for soil samples collected at P3-5. The pyritic soil is structureless and has a tightly packed clay matrix with vertically orientated macropores. At the more sandy P1-2 locations,  $k_h$  was higher than at P3-5. The sandy nature of the pyritic soil at P1-2 contributes to the higher  $k_h$ , compared to the more clayey pyritic soils further away from Broughton Creek.

Limited data are available for comparison of the saturated hydraulic conductivity measured at this site with other sites in Australia. White *et al.* (1993) showed that saturated hydraulic conductivity measured using the auger hole method was  $3 \times 10^{-7}$  m/s for partially oxidised blue estuarine clay located near Tweed Heads, Northern NSW. As the elevation increased through the acid sulfate soil transition and jarositic zones, White *et al.* (1993) showed that saturated hydraulic conductivity increased by more than one order of magnitude. The  $K_{\text{sat}}$  data described by White *et al.* (1993) are of similar magnitude to the saturated hydraulic conductivity measured in the horizontal plane at the Berry field site. However, the auger hole technique is not able to quantify  $K_{\text{sat}}$  in the vertical plane. Given the low  $K_h$  that is apparent in the pyritic soil at Berry and Tweed Heads, groundwater table fluctuation and the transport of oxygen to the pyritic sediments, will be controlled by the vertical permeability of the soil.

#### 6.3.4.3 Moisture characteristic curves

The flow of water and air through the unsaturated part of the soil profile is extremely important in acid sulfate soils. In particular, when structural pores in the soil drain, they are able to transport oxygen. If a drained profile extends to the pyritic layer, then oxygen can be transported to the sulfidic zone where pyrite oxidation can occur. The degree of saturation or volumetric moisture content of a soil is determined by the matrix potential with which water is held in the soil pores. As such, a relationship between the soil moisture content and the distance (i.e., head difference) to the free groundwater table, called a moisture characteristic curve, can be determined. The moisture characteristic curves for 5 depths at sites P2 and P5 are shown in Figure 6.17.

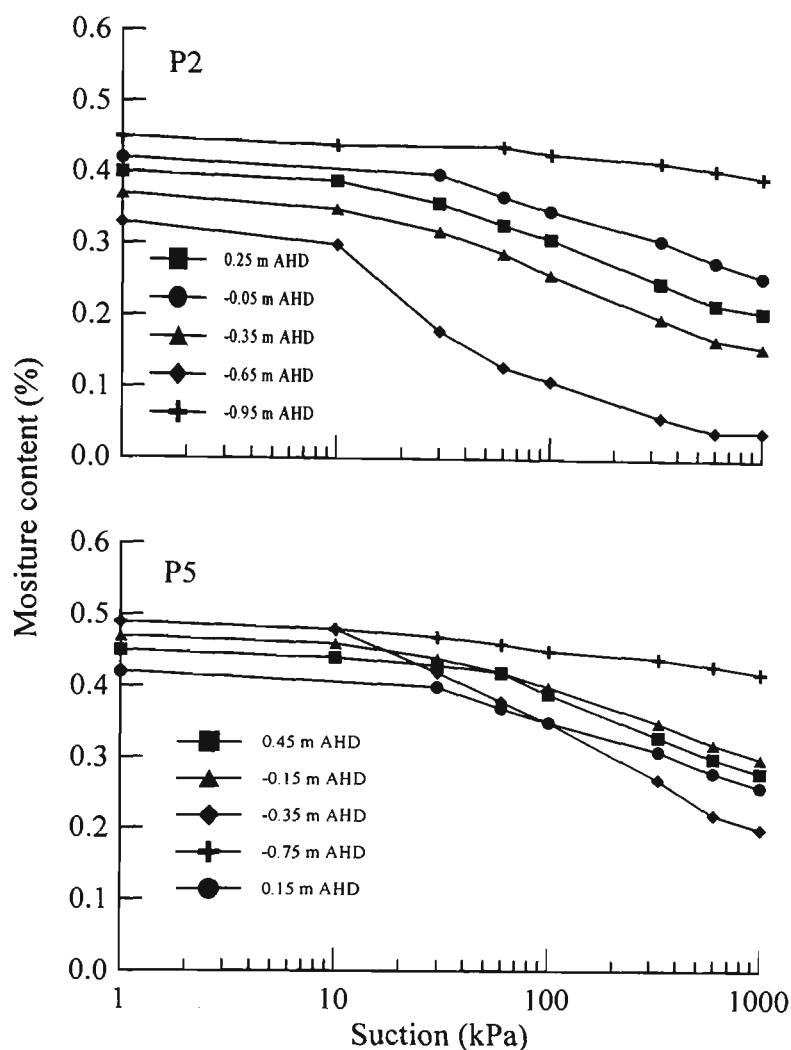


**Figure 6.17** Moisture characteristic curves

The moisture characteristic curves down the profile at P5 are similar, reflecting the clayey nature of the profile. The moisture content of all soil layers at P5 varied between 0.45-0.49 at saturation, and samples collected at 0.75 and 0.15 m AHD (or 0.3 and 0.9 m below the surface), had a moisture content of 0.31 at 1000 kPa suction. The soil at these depths had an air-entry value of 30-40 kPa, indicating that the soil was well structured and free draining. At -0.15 m AHD the soil moisture characteristics demonstrated that this layer is slightly more sandy and better drained than the overlying soil layers. By contrast, below -0.45 m AHD, the clayey, impermeable pyritic soil drained very slowly with a loss of only  $0.04 \text{ m}^3/\text{m}^3$  water by the application of 1000 kPa suction. The moisture characteristic curves for site P2 are similar to those at P5, except for the sandy material at -0.65m AHD. Here the soil had a saturated moisture content of



0.33, a very low moisture content of 0.05 at 1000 kPa, and a low air-entry value of about 10 kPa.

The moisture characteristic curves revealed low air-entry values for all soil layers overlying the pyritic soil. Low air-entry values indicate that air-filled pore space becomes available soon after the watertable falls, enabling gas to diffuse rapidly through the unsaturated part of the profile. The large cylindrical pores (diameters up to 12 mm) present in the soil profile assist the rapid diffusion of oxygen to the potential acid sulfate soil layer. The moisture characteristic data indicates that oxidation of pyrite will commence very soon after the groundwater level falls below the elevation of the pyritic soil.

Another application of the moisture characteristic curve is for the estimation of unsaturated hydraulic conductivity. Numerical models that simulate water flow and redistribution in unsaturated soil require a measure of unsaturated hydraulic conductivity at a range of suctions. Experimental determination of the unsaturated hydraulic conductivity function is difficult, expensive and tedious. An alternative to the direct measurement of the unsaturated hydraulic conductivity function is to use theoretical methods which predict the unsaturated conductivity from more easily measured soil moisture characteristic data. Closed-form analytical equations developed by van Genuchten (1980), Fredlund *et al.* (1994) and Leong and Rahardjo (1997) that adopt this approach were discussed in Chapter 2.

The RETC code for quantifying the hydraulic functions of unsaturated soils (van Genuchten *et al.*, 1991) was used to determine unsaturated hydraulic conductivity curves, using  $k_v$  and moisture characteristic data from samples taken at the site. Calculated unsaturated hydraulic curves for samples from P2 are shown in Figure 6.18.

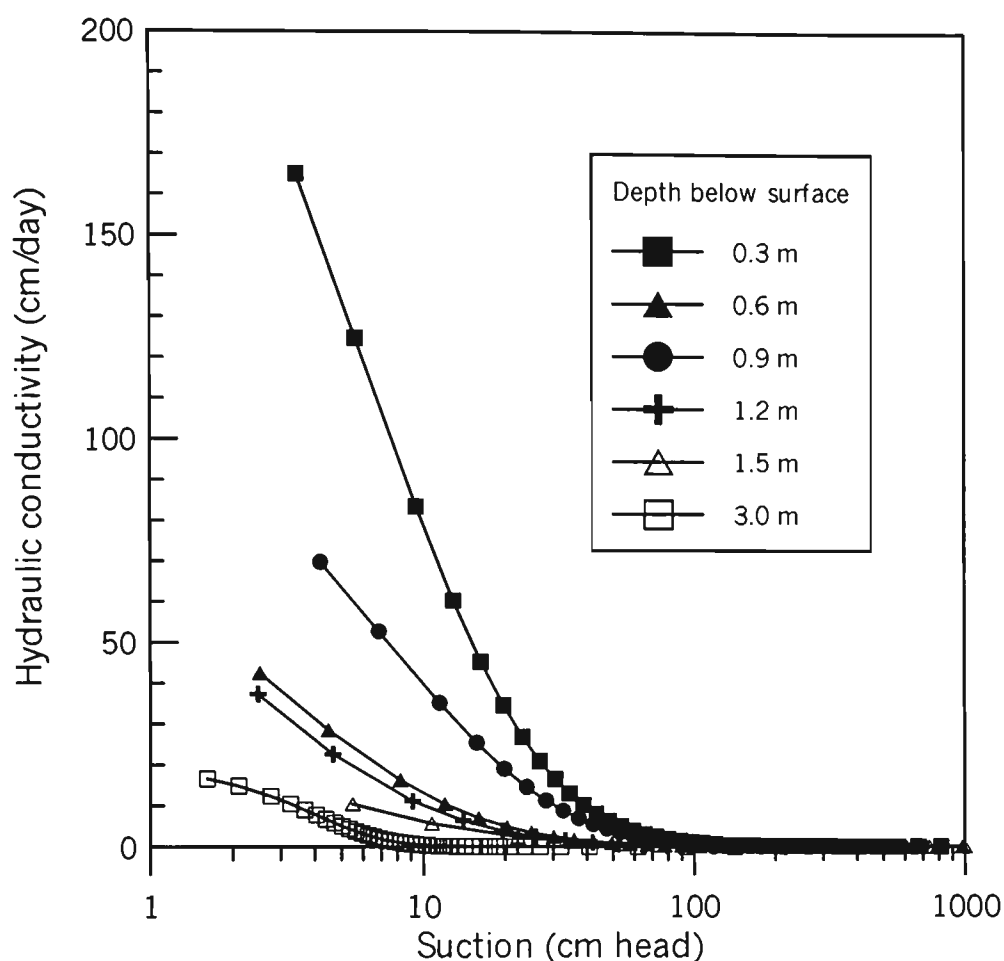


**Figure 6.18** RETC calculated unsaturated hydraulic conductivity curves.

As expected, the unsaturated hydraulic conductivity drops very quickly as the suction applied to the soil increased. The non-pyritic soil between 0-1.2 m depth remained relatively permeable up to an applied suction of about 1m. This reflects the silty/sandy clay texture of the top and estuarine soil material, as well as the well structured nature of these soils. In contrast, the clayey matrix of the pyritic soil had very low hydraulic conductivity at small matrix suctions. Visual inspection of the pyritic soil shows that the only structural features in this material are large pores (2-12 mm diameter) from old root channels. These features drain at very low suctions. Once water drains from these pores, flow has to take place in the tightly packed clay matrix. Hence, the hydraulic conductivity through the unsaturated clay matrix was very slow.

Many numerical soil water flow models use shape parameters from the van Genuchten (1980) model as input. The RETC code was used to define these shape parameters for the 6 soil layers as shown in Figure 6.18. These parameters are shown in Table 6.2.

**Table 6.2.** Soil physical properties.

Depth (m)	$\theta_r$	$\theta_s$	$\alpha$ (m <sup>-1</sup> )	n	$k_v$ (m day <sup>-1</sup> )	$k_v/k_h$
0.3	0.05	0.55	0.281	1.30	3.95	1.06
0.6	0.02	0.35	0.242	1.15	3.84	1.02
0.9	0.05	0.34	2.917	1.18	1.68	2.15
1.2	0.04	0.50	0.2247	1.29	2.08	2.36
1.5	0.06	0.49	0.4737	1.09	2.02	12.7
3.0	0.06	0.49	0.4737	1.09	0.20	1.0

notation:  $\theta_r$  and  $\theta_s$  are residual and saturated volumetric moisture contents,  $\alpha$  and n are shape parameters based on the van Genuchten (1980) equation, k is the saturated hydraulic conductivity in the vertical plane ( $k_v$ ) and in the horizontal plane ( $k_h$ ).

### 6.4 Conclusions

The consequences of inappropriate floodplain management that has led to the generation of acid from the oxidation of pyrite are clearly evident. The initial soil chemical, physical and morphological properties described in this Chapter were indicative of acid sulfate soils, and showed that substantial pyrite oxidation has occurred in the past. Other sources of acidity, namely the high Al saturation on the ECEC and the presence of various iron sulfate minerals, were described, and shown to be problematic for the

improvement of groundwater quality, irrespective of future pyrite oxidation. Evaluation of the effectiveness of installing weirs in the flood mitigation drains to maintain higher groundwater tables thereby minimising further pyrite oxidation is carried out in Chapter 8, with reference to the initial soil chemical data reported in this Chapter.

The quantification of soil physical measurements is used extensively in Chapters 9 and 11, where simulations of the groundwater regime under various drain management strategies are described. The saturated hydraulic conductivity in the vertical plane was high throughout the soil profile. In contrast,  $k_h$  is slow in the pyritic soil, indicating that the lateral movement of water and air is slow. This has implications for the manner in which the groundwater elevation is affected by rainfall, evaporation and drawdown by deep drains. These influences are described and discussed with reference to the groundwater dynamics measured at the study site in Chapter 7. The high  $k_{sat}$  in the vertical plane was shown to be caused by vertically orientated macropores. As reflected in the moisture characteristic curves, these macropores drain at small applied suctions. As the groundwater elevation falls below the pyritic soil, these macropores behave as conduits through which atmospheric oxygen is readily transported to the pyritic soil, where acid is generated.

## **Chapter 7: Groundwater dynamics**

The groundwater elevation data measured at the study site are presented in this Chapter. The data, and its interpretation, are divided in two parts, namely the pre and post weir periods. For the pre-weir period, the observed groundwater profiles and flow properties are presented. The dynamic nature of the groundwater table in the pre-weir period is further explained by exploring the processes that contribute to falling and rising groundwater tables. The contributions of evapotranspiration, drawdown from the flood mitigation drains and rainfall to the rise and fall of the groundwater table are measured and discussed. The elevation of the groundwater table is assessed relative to the height of the acid sulfate soil layer at the study site. The distribution and magnitude of acid sulfate soil exposed to oxidising conditions (that is, above the groundwater table) across the study site is determined. The implications of the magnitude and distribution of exposed acid sulfate soil for soil and water quality at the study site is discussed.

For the post-weir period, the observed groundwater profiles and flow properties are presented. A general increase in the elevation of the groundwater profile was observed, in conjunction with a substantial change in the direction of groundwater flow caused by the maintenance of higher water levels in the drain. Installation of the weirs, in conjunction with more consistent rainfall, caused the groundwater table to cover the pyritic soil layer throughout the post-weir monitoring period. However, in piezometer transects where the weirs had no influence, groundwater drawdown caused pyritic soil to be exposed to oxidising conditions. A comparison between the pre and post weir groundwater table dynamics is presented and potential improvements with respect to the adoption of adjustable weirs is also discussed.

## 7.1 Introduction

The generation of acidic products from the oxidation of pyrite is primarily determined by the oxidation/reduction status of the acid sulfate soil. The oxidation/reduction status of the soil is determined by the degree of saturation of the soil pore space. Once pore space saturation is achieved, reducing conditions prevail. As such, pyrite oxidation is controlled by the elevation of groundwater relative to the elevation of the acid sulfate soil. If the location of acid sulfate soil is below the groundwater table (and therefore in a reduced state), no oxidation of pyrite can take place, except by the reduction of  $\text{Fe}^{3+}$  (see Equation 2.5). In contrast, where the groundwater level falls below the elevation of the acid sulfate soil, air can enter drained soil pores causing oxidising conditions within the pyritic zone and the subsequent generation of acidic oxidation products. The transport of these acidic oxidation products is also determined by the position of the groundwater relative to the elevation of water in nearby drains or creeks. If the elevation of the groundwater is higher than the water level in nearby drains, then a potential difference exists, causing groundwater (and its constituent chemical components) to flow towards and discharge into the drain via the seepage face above the drain water level. If the elevation of groundwater is lower than the water level in nearby drains, then the direction of flow may be reversed, causing water to flow from the drains into the surrounding shallow aquifer.

In order to develop acid sulfate soil management strategies at a sub-catchment scale, an understanding of the factors that determine the position of groundwater relative to the height of the acid sulfate soil layer as well as the processes which control the transport of oxidation products from the soil to surface waters must be determined. White *et al.* (1997) suggest that it is essential to know:

- the dynamics of the groundwater table relative to the acid sulfate soil layer,
- the impact of climate, drain and land management on the floodplain water balance and its control of water table dynamics and export of oxidation products.

The dynamics of the groundwater table relative to the position of the acid sulfate soil layer and the factors that control both the elevation and movement of groundwater at the study site are examined in this Chapter.

**7.2 Pre-weir groundwater dynamics**

Groundwater elevations measured during the period 18 July 1997 - 13 October 1998 (the pre-weir period) show that the shallow, unconfined groundwater aquifer is highly dynamic and responsive to both climatic influences and drawdown from the flood mitigation drains. Rapid fluctuations in groundwater elevations can be seen in Figure 7.1(a,b) for piezometer transects C, D, F, H, I and K. The groundwater elevation was generally different between piezometers both within a transect and also between transects, indicating that conditions for groundwater flow are present.

The groundwater table is strongly influenced by both the drawdown action of the flood mitigation drains and climatic effects. These influences combine to control groundwater elevation, movement and direction of flow. The maximum and minimum groundwater elevations for some piezometers relative to the ground surface and the upper elevation of the potential acid sulfate soil layer measured during the pre-weir period are shown in Table 7.1.

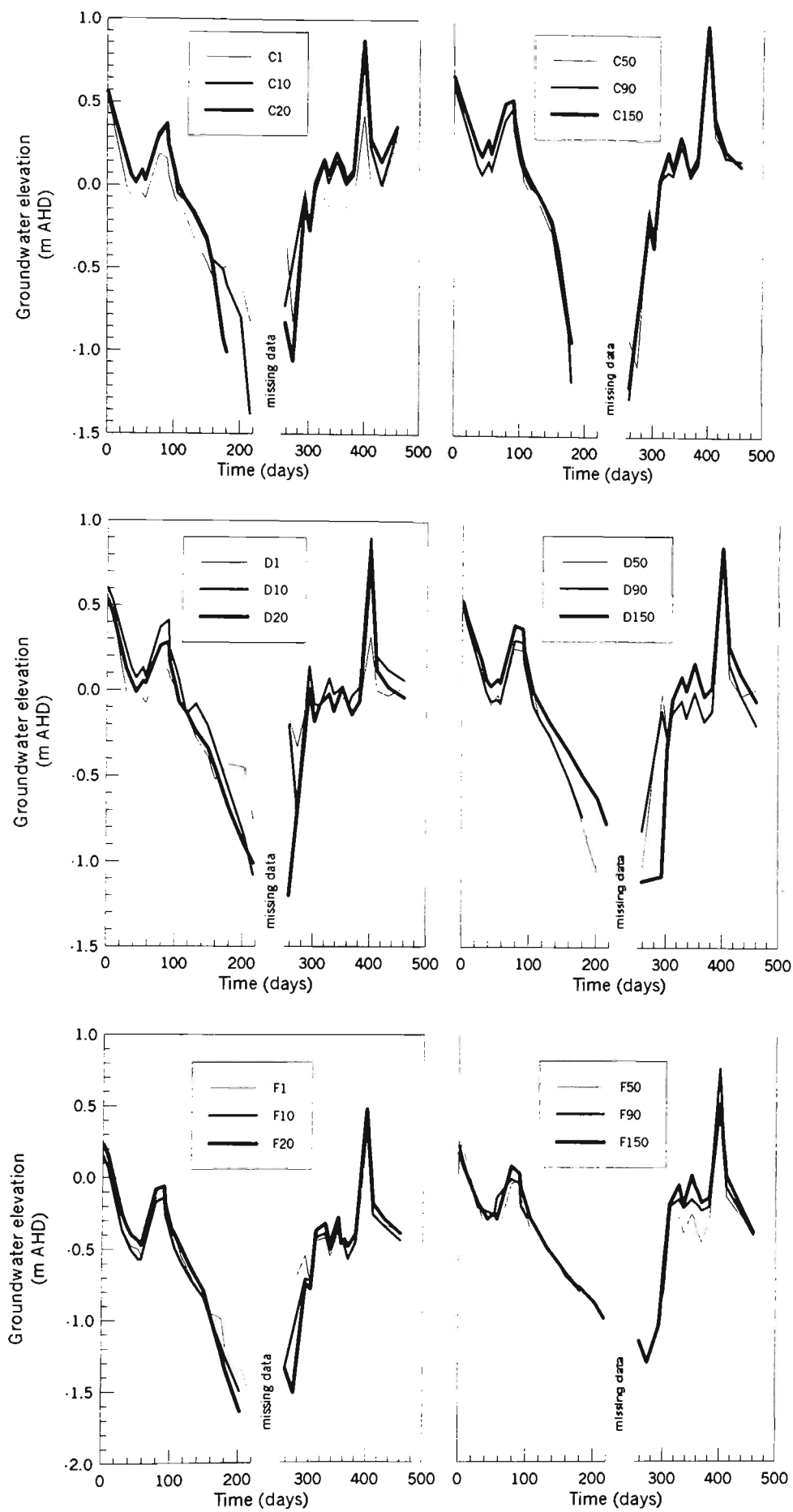


**Figure 7.1a** Pre-weir groundwater elevations at piezometer transects C,D and F.



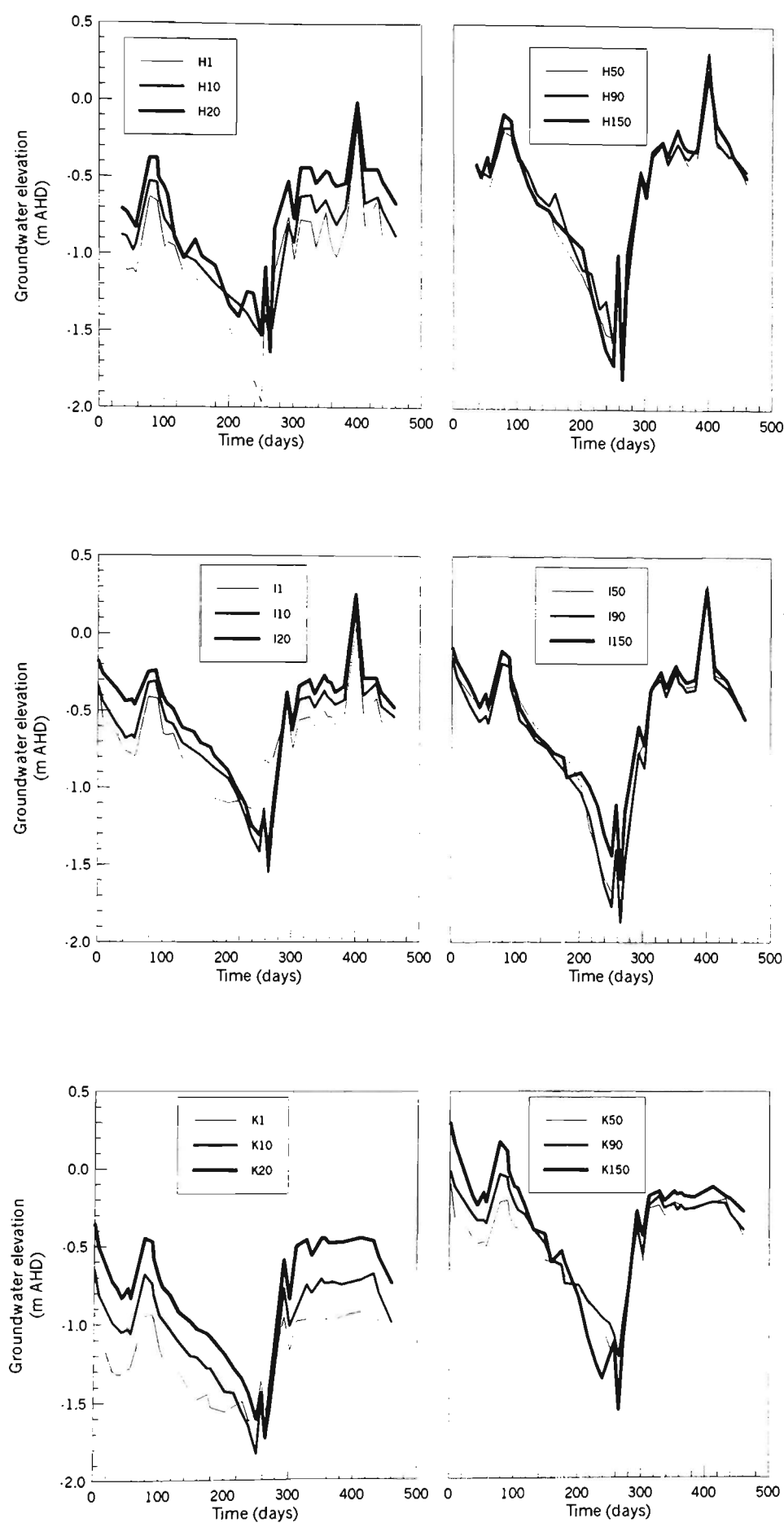


**Figure 7.1b** Pre-weir groundwater elevations at piezometer transects H, I and K.

**Table 7.1** Relations between groundwater elevations and soil topography

Piezometer	Mean GWL (m AHD)	Max GWL (m AHD)	Min GWL (m AHD)	Surface (m AHD)	ASS layer (m AHD)
C1	-0.12*	0.51	-0.83*	0.98	
C10	-0.03*	0.79	-1.38*	0.97	-0.3
C20	-0.01*	0.88	-1.06*	0.97	
C50	0.02*	0.95	-1.15*	0.97	
C90	0.06*	0.97	-1.27*	0.98	-0.3
C150	0.11*	0.99	-1.20*	1.05	
F1	-0.52*	0.28	-1.50*	0.56	
F10	-0.52*	0.41	-1.50*	0.53	-0.7
F20	-0.50*	0.48	-1.64*	0.51	
F50	-0.36*	0.54	-1.16*	0.67	
F90	-0.22*	0.77	-0.80*	0.80	-0.6
F150	-0.33*	0.52	-1.3*	0.75	
I1	-0.69	0.04	-1.14	0.49	
I10	-0.65	0.16	-1.55	0.47	-0.7
I20	-0.54	0.25	-1.44	0.45	
I50	-0.61	0.33	-1.85	0.35	
I90	-0.65	0.30	-1.87	0.33	-0.7
I150	-0.55	0.30	-1.59	0.42	
K1	-1.19	-0.86	-1.62	0.35	
K10	-1.04	-0.65	-1.83	0.42	-0.8
K20	-0.82	-0.36	-1.73	0.47	
K50	-0.50	-0.10	-1.20	0.61	
K90	-0.44	-0.02	-1.22	0.72	-0.7
K150	-0.37	0.29	-1.56	0.69	

\* mean and minimum values too low due to missing data where GW fell below depth of piezometer

The maximum height of the watertable identified in Table 7.1 is very close to the ground surface. When high intensity, short duration rainfall events occurred, flooding

of the study site was common. Four flood events caused inundation of the site for short periods of less than three days at days 69 (105 mm rain), 87 (87mm rain), 415-16 (176 mm rain) and 424-27 (324 mm rain). The maximum depth of flood water covering the site was approximately 1 m, as shown in Plate 7.1 of the flood at day 87.

Groundwater elevation measurements were taken as soon as safe entry to the study site could be obtained after the flooding event (usually 2-4 days). Table 7.1 show that maximum groundwater elevations at piezometers 1-20 meters from the drain are lower than the ground surface, indicating that rapid drawdown of groundwater close to the ground surface occurs as the water level in the drains recedes. The drawdown action of a large field drain adjacent to piezometer transect K is also evident. The piezometers at transect K are installed approximately 2 m from a field drain which has an invert of -0.6 m AHD. The maximum groundwater level at transect K is lower than other piezometers transects, particularly at distances greater than 10 m from the main flood mitigation drain, due to the operation of the field drain. The removal of shallow groundwater by large, deep drains influences the dynamics of groundwater at the site. Excess surface flood water was rapidly removed by the flood mitigation drains and the operation of the floodgate at Broughton Creek. The discharge of flood water through the floodgate during the day 87 event is shown in Plate 7.2.

The rapid removal of excess surface water during flooding or large rainfall events where runoff/ponding occurred by the flood mitigation drainage system has implications for the maximum groundwater elevations measured at the site. A simplified representation of the water balance of a coastal floodplain may be described by (White *et al.* 1997):

$$\begin{array}{ccccccc}
 P + I + L_i & = & E_t + R + L_o + D + \Delta S & & & & (7.1) \\
 \text{inputs} & & \text{outputs} & & & & \text{storage}
 \end{array}$$

where,  $P$  is precipitation,  $I$  is irrigation,  $L_i$  is the lateral inflow of water,  $E_t$  is evapotranspiration,  $R$  is surface runoff,  $D$  is drainage to the water table,  $\Delta S$  is change in soil moisture content above the water table, and  $L_o$  is the lateral outflow.

Under undrained circumstances,  $R$  and  $L_o$  are relatively small, resulting in the inundation of low lying backswamps for considerable periods of time (ie, up to 3 months). In order to use such low lying areas for agricultural purposes, extensive drainage networks have been constructed to efficiently remove surface water. One-way floodgates have been installed where drainage systems discharge into tidal systems at low tide to protect against inundation and to drain the land as quickly as possible. Drainage systems have greatly increased the rate of  $L_o$ . Where backswamps may have been inundated for say 100 days under natural hydraulic conditions, the installation of floodgated drainage systems has resulted in excess water being removed from backswamps in less than one week. Since drainage does not alter  $P$  or  $E_t$  (assuming that crop vigour approximates native vegetation water use) but greatly increases  $L_o$ , a net increase in the water discharged from the system occurs. This results in less water being available to prolong the maintenance of reducing conditions in the pyritic layers as rainfall inputs cease and processes that give rise to groundwater lowering prevail.



**Plate 7.1** Flood event caused by 87 mm rainfall at day 87.



**Plate 7.2** Discharge of flood water through floodgate at day 87.

### *7.2.1 Observed groundwater profile during pre-weir period*

Groundwater monitoring commenced on 18 July 1997 (day 1). The preceding period had been wet, with 215 mm rainfall since 1 June 1997. About 160 mm rainfall fell between 26-28 June 1997, indicating that some flooding may have occurred at the study site. As such, the groundwater elevation at day 1 was reasonably high across the whole site. Groundwater elevations shown in Figure 7.1(a,b) between days 1-58 show a constant fall in groundwater elevation across the site.

During the initial monitoring period (days 1-58), the groundwater elevation measured in the piezometers was always the lowest close to the drains, but rose to an equilibrium elevation in the piezometers further away from the drains (usually  $\approx 50$  m from the drain). The shape of the groundwater table measured along piezometer transects was relatively flat within the fields at distances greater than 20 m from the drain and increased in slope towards the drain as the piezometer location become closer to the drain. A diagrammatic representation of this groundwater regime is shown in Figure 7.2(a). The direction of the groundwater flow will be referred to as a positive gradient as the groundwater elevation falls from the centre of the study area towards the drain. The positive gradient is a necessary condition for the lateral flow of groundwater from the centre of the study area to the drain, and for subsequent discharge of groundwater into the drain water through seepage faces in the drain walls.

However, groundwater elevation data measured in piezometer transects do not always show a positive gradient towards the drain. During periods of low rainfall and high evapotranspiration, groundwater elevations in piezometers further away from the drains became lower than the elevation of water in the drains. The direction of groundwater flow will be referred to as a negative gradient as the groundwater elevation falls from the drain towards the centre of the surrounding fields. A diagrammatic representation of this groundwater regime is shown in Figure 7.2(b). The negative gradient is a

necessary condition for the lateral flow of groundwater from the drain into the surrounding field. Given the negative groundwater gradient, no discharge of groundwater into the drains is possible.

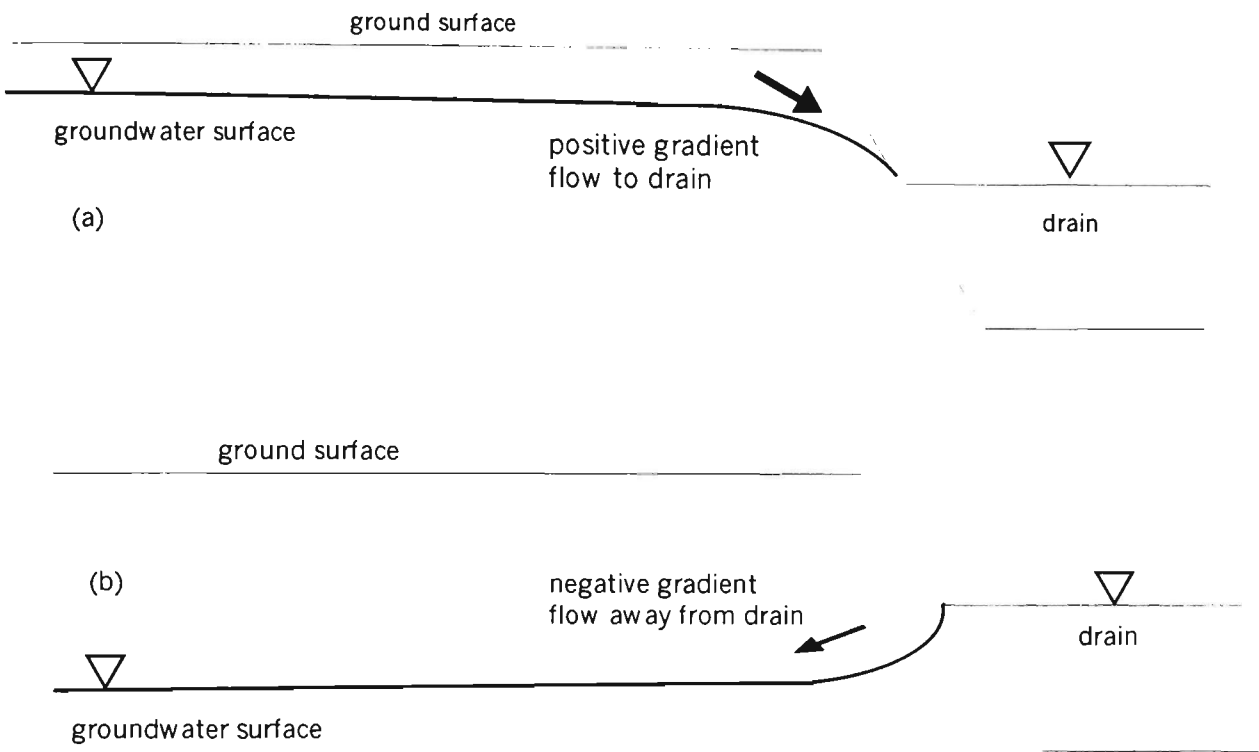


**Figure 7.2** Positive (a) and negative (b) groundwater gradients towards drains

Conditions suitable for the attainment of negative groundwater flow gradients commenced after the large rainfall event that occurred on day 83. At day 83, the groundwater elevation was at the ground surface as a result of flooding across the site. Positive gradient groundwater flow prevailed resulting in groundwater drawdown close to the drains. Piezometer data from transect I is shown in Figure 7.3 to illustrate the change between positive and negative groundwater flow gradients.

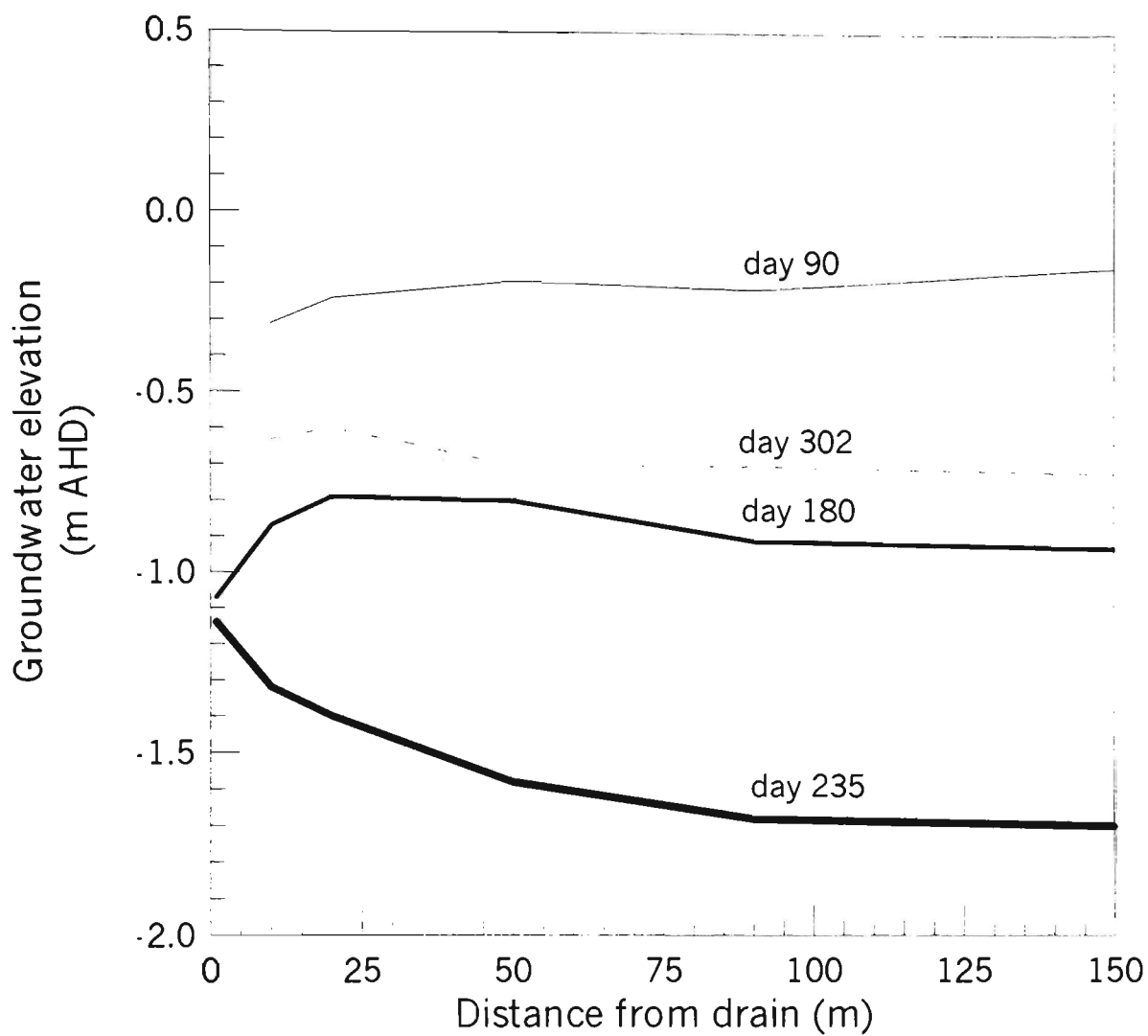


**Figure 7.3** Groundwater elevation at Transect I showing positive and negative gradients.

The two dimensional hydraulic gradients for groundwater flowing towards the East-west drain were calculated from groundwater elevation data measured at Transect I. These hydraulic gradients, and their flow directions, are shown in Table 7.2



**Table 7.2** Hydraulic gradients and flow directions for Transect I

Day	Distance (m)	Hydraulic gradient (i)	Direction of flow gradient (-/+)
90	1	0.1800	+
	10	0.0122	+
	20	0.0070	+
	50	0.0017	+
	90	0.0007	+
	150	0.0002	+
180	1	0.0300	+
	10	0.0222	+
	20	0.0080	+
	50	0.0003	-
	90	0.0027	-
	150	0.0003	-
235	1	0.0300	-
	10	0.0056	-
	20	0.0060	-
	50	0.0110	-
	90	0.0010	-
	150	0.0002	-
302	1	0.1500	+
	10	0.0133	+
	20	0.0030	+
	50	0.0033	-
	90	0.0002	-
	150	0.0002	-

The two dimensional hydraulic gradients and flow directions shown in Table 7.2 for Transect I are typical of the groundwater regime in coastal lowlands where deep flood mitigation control the magnitude of the hydraulic gradient and the flow direction. Table 7.2 shows that a larger hydraulic gradient exists close to the drain than further from the

drain. During relatively wet periods (eg, days 90 and 302), the magnitude of the hydraulic gradient immediately adjacent to the drain is three orders of magnitude greater than the hydraulic gradient at 90 m distance from the drain. Similarly, during drought conditions where the drain is supplying water to the groundwater table, the magnitude of the hydraulic gradient close to the drain is considerably greater than that further away from the drain. The hydraulic gradient data show that the rate of groundwater flow in the central part of the field site is very slow, and that the lower water level in the drain causes rapid discharge of water from the groundwater table to the drains when the hydraulic gradient is positive.

The direction of flow of groundwater may not always be in the same direction along a piezometer transect. Table 7.2 shows that during days 180 and 302, the direction of groundwater flow is positive close to the drains (i.e., 1-20 m distance from the drains) but is negative at greater distances from the drains. Positive and negative flow direction may occur during rising or falling groundwater regimes where the steady state groundwater elevation in the field (ie, at a distance from the drain) is close to the drain water level. Rapid additions or losses from the groundwater table caused by rainfall or evapotranspiration may be greater than the hydraulic conductivity of the soil, thereby facilitating higher groundwater elevations close to the drain than both the water level in the drain and the groundwater elevation at a greater distance from the drain.

The influence of the flood mitigation drains on the groundwater hydrology of the site is best carried out by examining the groundwater elevation, hydraulic gradients and flow directions in three dimensional space. A three dimensional representation of the groundwater surface at day 90 is shown in Figure 7.4.

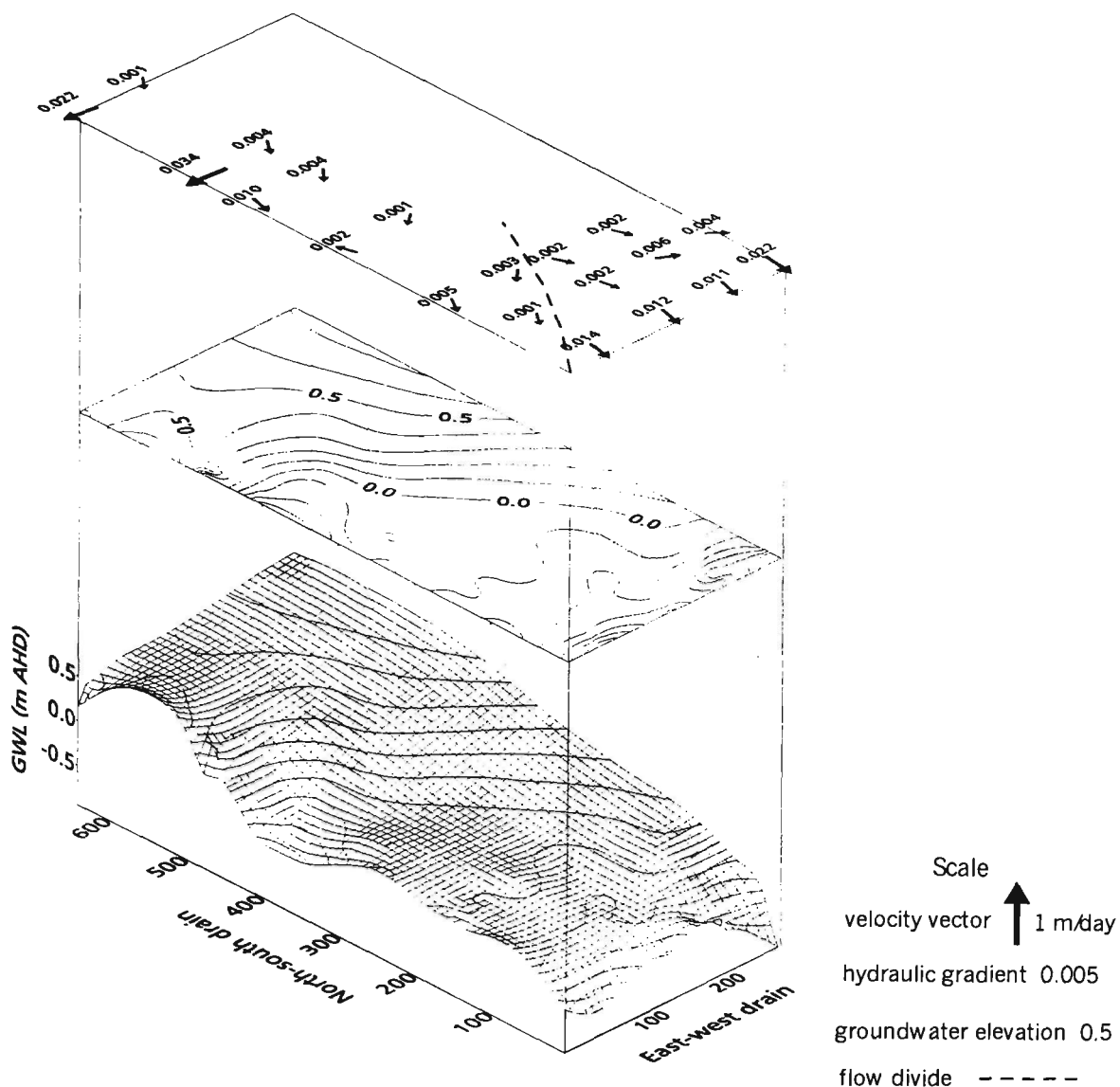


**Figure 7.4** Groundwater elevation profile - day 90.

Figure 7.4 shows that a positive gradient exists across the site, indicating that groundwater is flowing from the field and discharging into the drain via seepage faces in the drain. The primary direction of groundwater flow is in a north-south direction, towards the east-west drain. This trend in the direction of flow of groundwater generally corresponds to the direction of slope of the land surface. However, a positive gradient is also present along the entire length of the north-south drain, indicating that both drains substantially drawdown the surrounding groundwater. Two localised site drainage features are evident in Figure 7.4. Firstly, at about 400 m on the north-south drain, excessive groundwater drawdown is observed close to the drain. This local drawdown phenomena is caused by the presence of a prior stream channel that traverses

the site in an east-west direction. As demonstrated in Chapter 5, the prior stream channel exhibits properties consistent with higher energy deposition than the surrounding land. In effect, the buried stream bed behaves as an underground drain that is connected to the north-south drain. When high groundwater elevations exist nearby, the buried creek channel causes groundwater to flow into, then along the axis of the prior creek, which then discharges into the north-south drain. The second localised drainage feature is adjacent to the east-west drain at 280 m. A field drain runs parallel with the north-south drain and discharges into the east-west drain at 280 m. To ensure efficient surface drainage, the discharge point of the field drain was deepened to -1.0 m AHD, slightly higher than the average low tide level. The deepened discharge point grades back to the depth of the field drain (about 0.8m below the surface) over a distance of approximately 50 m. This deeper field drainage section was able to generate localised positive groundwater gradients when high groundwater elevations prevailed.

The drain water level quickly established itself at an elevation of -1.1 m AHD, or low tide level, after the excess surface water from the day 83 rainfall event subsided. Lower than average rainfall (102 mm) between days 90-180 did not cause any measurable runoff in the study area or rise in the drain water level. Groundwater drawdown continued through this period, lowering the groundwater elevation along the length of the piezometer transect. Prolonged seepage in the absence of groundwater recharge from either rainfall or upland groundwater movement resulted in a relatively flat groundwater profile, where the water level in the drain is in equilibrium with the surrounding groundwater level. This equilibrium was achieved around day 180. The three dimensional groundwater profile observed at the site on day 180 is shown in Figure 7.5.

Although positive gradients exist along the axes of both major drains, the slope of the groundwater surface in the centre of the study area has become flatter as a result of groundwater discharge through the seepage faces in the drains. The establishment of a negative gradient from the major north-south drain at 600 m is evident. This negative gradient has been generated through rapid groundwater drawdown and discharge through the action of the permeable prior stream bed described above. Lowering of the

groundwater by evapotranspiration also accounts for a general lowering of the groundwater surface across the site.

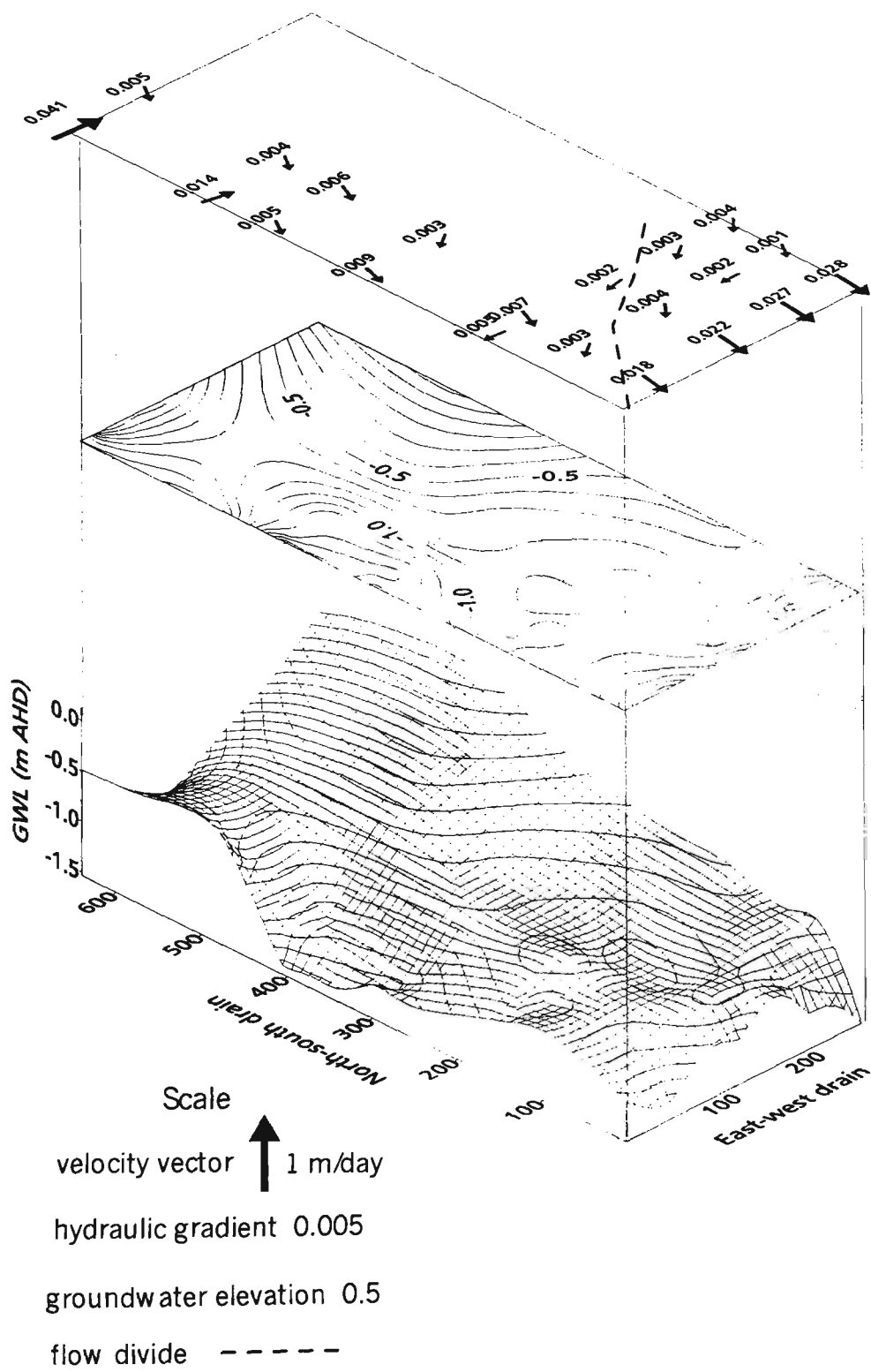


**Figure 7.5** Groundwater elevation profile - day 180.

During the period day 180-235, calculated potential evapotranspiration was approximately 233 mm with only 58 mm of rainfall being measured. Where evapotranspiration exceeds the groundwater recharge, groundwater is removed from shallow aquifers. From Figure 7.3 at day 235, it is apparent that the groundwater level falls progressively more as the distance from the drain increases. This is caused by evapotranspiration removing water from the soil profile. The groundwater levels close to the drain are maintained by the constant water level (low tide level) in the drains. Seepage has occurred through the drain walls, though the resupply rate from the drains is not sufficiently rapid to transport water laterally through the lower soil layers to influence groundwater levels further away from the drains. As described previously in Chapter 5, the saturated hydraulic conductivity of the acid sulphate soil layer is very low in the horizontal plane (about  $1 \text{ m day}^{-1}$ ), thereby limiting recharge of groundwater from the drains. A partial 3 dimensional representation of the groundwater profile at day 235 is shown in Figure 7.6. Unfortunately, the groundwater level fell below the depth of the piezometers installed in transects C, D, E and F during the drought period experienced during the summer of 1997-98. Figure 7.6 shows the groundwater elevation profile from the site close to the junction of the two major drains. Nevertheless, the groundwater elevation adjacent to the north-south drain at 200-600 m was less than -1.1 m AHD and created a negative hydraulic gradient away from the north-south drain.

Figure 7.6 shows that the elevation of the groundwater surface falls as the distance away from the drains increases. In general, the groundwater surface is flat across the site. Lowering of the groundwater surface was dominated by evapotranspiration during the hot, dry summer period in 1997-98.



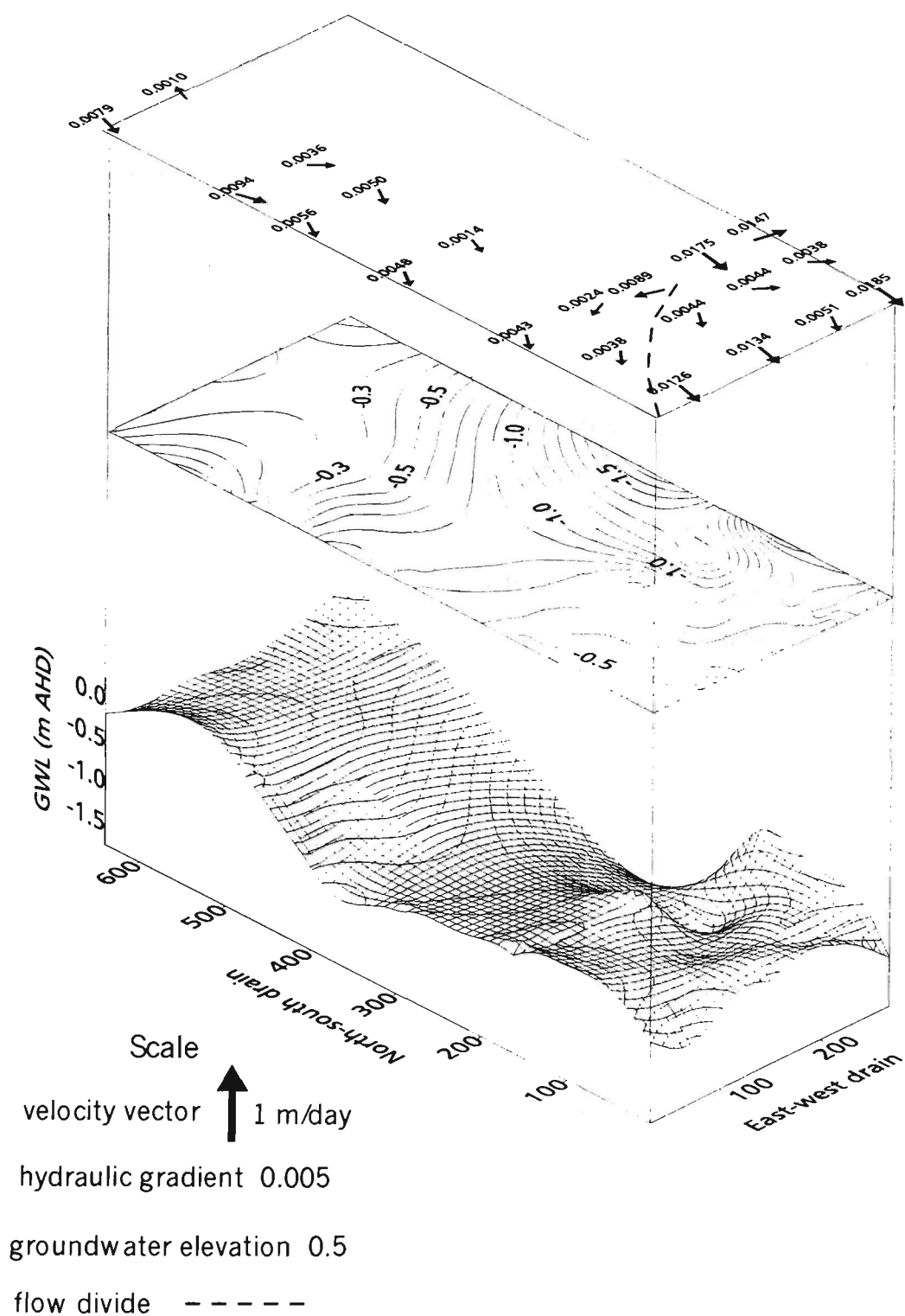


**Figure 7.7** Groundwater elevation profile - day 302

Two site features appear to have retarded the recharge of higher groundwater elevations across the site. Firstly, the prior stream channel feature appears to have re-established a positive groundwater flow gradient immediately after the groundwater elevation increased as a result of rainfall between days 290-300. Removal of the groundwater by



lateral movement to the prior creek channel resulted in a flat groundwater surface establishing at a deeper depth than may have been expected from this volume of rainfall. In addition, during the summer of 1997-98, the field drain extending parallel to the north-south drain from 280 m along the east-west drain was extended northwards and also deepened. The drawdown effect of this deep field drain at 300 m north of the drain's discharge point is clearly visible on Figure 7.7.

A significant volume of rainfall (113 mm) fell between days 290-300 causing a substantial rise in the groundwater elevation across all piezometers in Transect I (see Figure 7.3), as well as re-establishing a positive groundwater flow gradient towards the drain. A further 210 mm rainfall fell between days 302-362. This volume of rainfall was sufficient to recharge the groundwater so that positive hydraulic gradients similar to those initially observed at the start of groundwater monitoring at the site were established. The groundwater profile observed on day 362 is shown in Figure 7.8.

As shown in Figures 7.4-7.8, the elevation of the groundwater table fluctuates between the ground surface and a depth greater than -1.7 m AHD. Fluctuations in groundwater elevations are caused by the drawdown effect of deep artificial drains and climatic controls, particularly rainfall and evapotranspiration. The factors influencing the dynamics of the groundwater will now be examined in further detail.

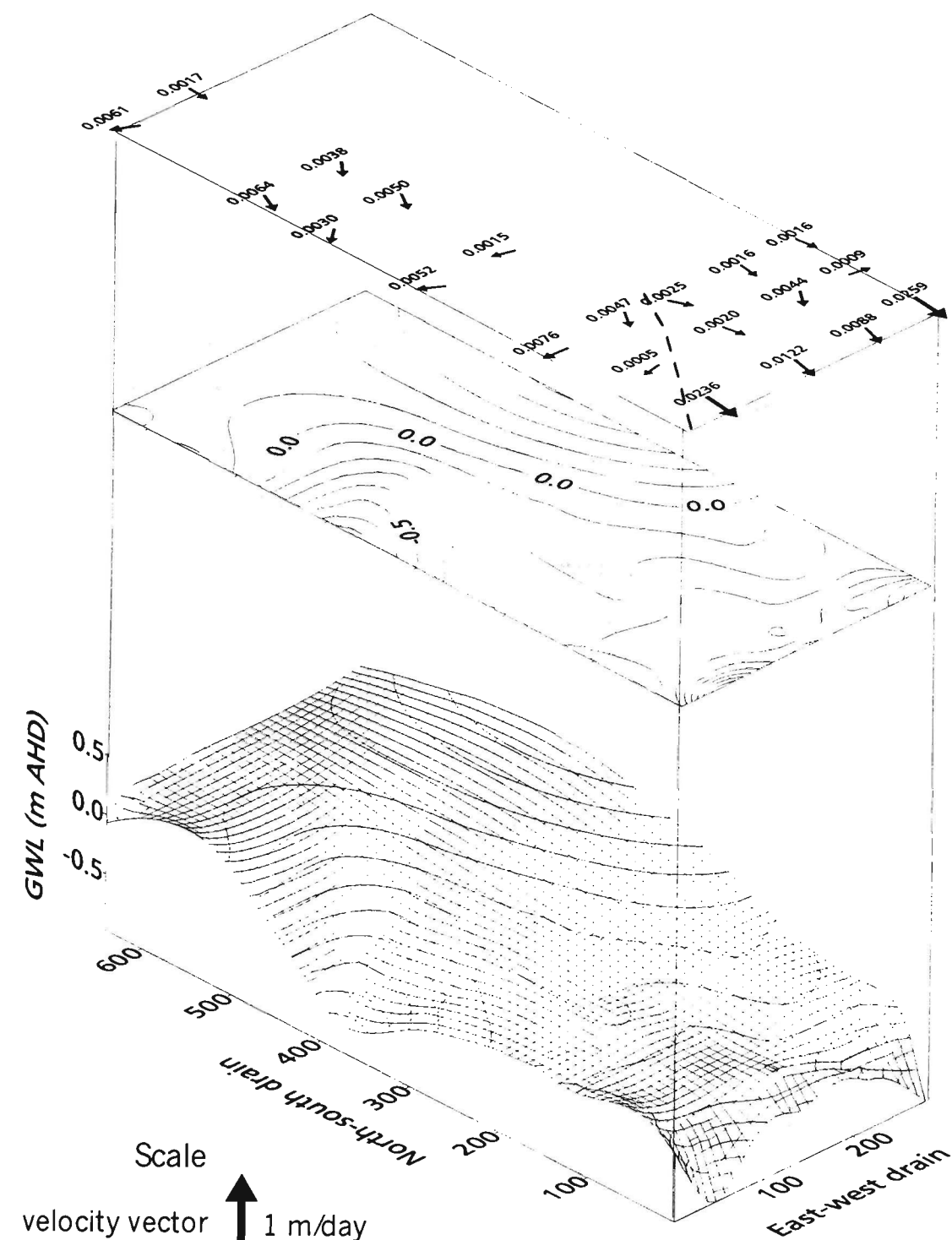


**Figure 7.8** Groundwater elevation profile - day 362

### 7.3 Groundwater dynamics - falling groundwater table

Falling, shallow, unconfined groundwater levels in low lying coastal floodplains are caused by either lateral drainage or evapotranspiration. Where considerable development or modification of the floodplain has taken place for agricultural purposes or to provide protection from flood waters, the magnitude of groundwater removal by lateral subsurface flow to artificial drains is substantially greater than that which can occur under natural conditions. Deep drainage systems that lower groundwater levels below the elevation of acid sulfate soil layers are often major contributors to the acidification of estuaries (White *et al.*, 1997; Sammut *et al.*, 1996). In the Broughton Creek catchment, the Shoalhaven City Council (1992) monitored pH in the Creek, drains and at the floodgate junctions and concluded that the drains were discharging large volumes of acidic water into Broughton Creek.

Better understanding of how lateral drainage and evapotranspiration influences groundwater dynamics is required to develop appropriate groundwater management strategies to manage acid sulfate soils. Evapotranspiration and lateral drainage are investigated in the pre-weir period at the Berry study site to determine their relative importance. An assessment of groundwater dynamics during periods of negative and positive hydraulic gradients is also carried out.

#### 7.3.1 Evapotranspiration

Lowering of groundwater by evapotranspiration is evident by comparing hourly groundwater elevation with evapotranspiration calculated using hourly meteorological data measured at the weatherstation. Figure 7.9 shows the fall in groundwater elevation at C10 during a 4 day period starting 13 March 1998. This particular period and

piezometer was chosen to assess the influence of evapotranspiration on groundwater table fall, because the water in the adjacent drain had all but dried up thereby causing a negative groundwater flow gradient to exist. Thus, daily falls in groundwater elevation can only be attributed to evapotranspiration.

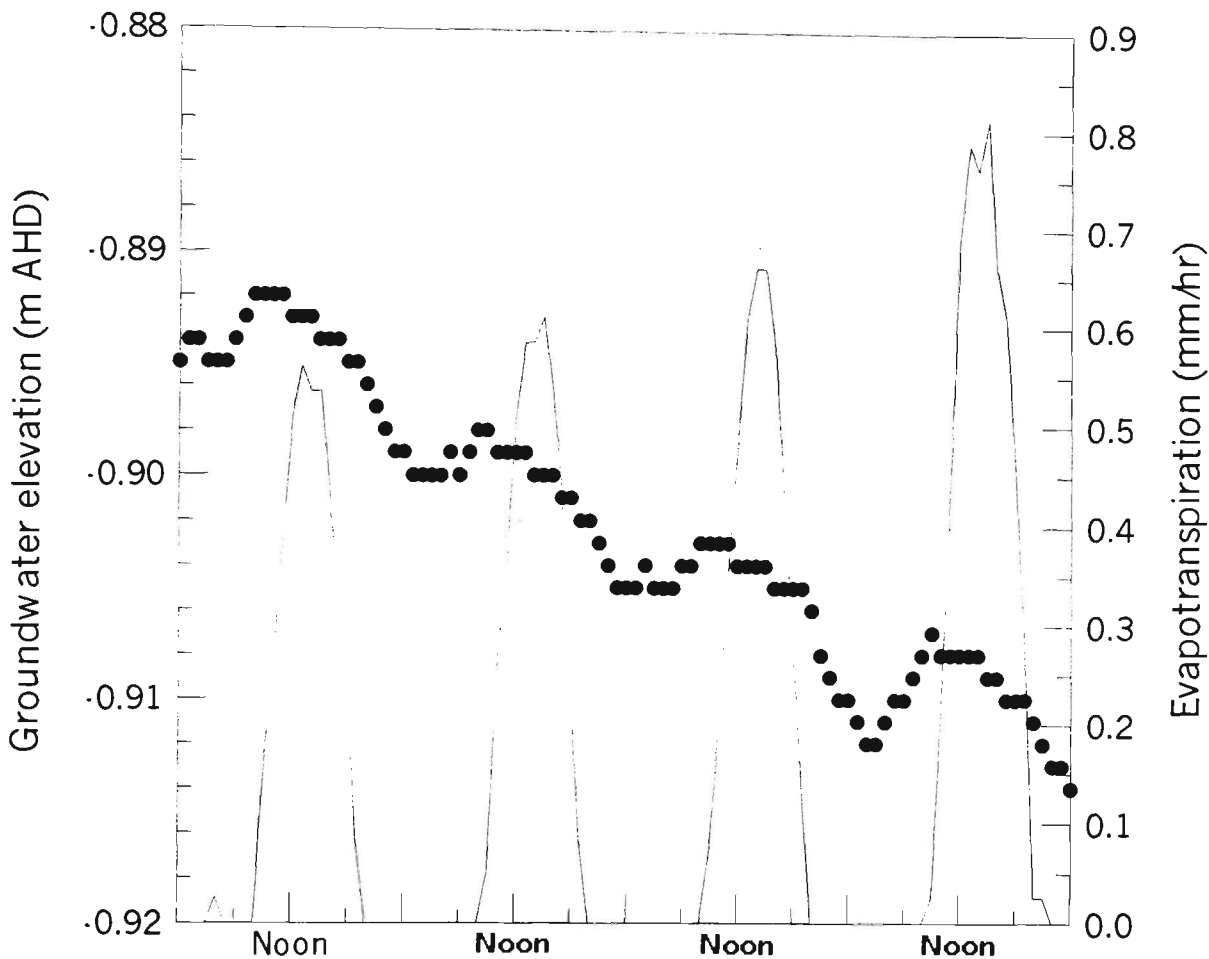


**Figure 7.9** Hourly groundwater elevation and calculated evapotranspiration

Figure 7.9 demonstrates that the fall in hourly groundwater elevation is related to the onset of positive evapotranspiration rates. Groundwater elevation starts to fall at about 8 am, once solar radiation begins to drive potential evapotranspiration. The rate of groundwater fall increases throughout the day as the rate of evapotranspiration increases. A reasonably constant rate of groundwater fall (approximately  $6 \times 10^{-4}$  m/hr) was observed in the afternoon as the rate of evapotranspiration begins to decrease. This may be as a result of water moving upwards from the groundwater into the soil to re-establish the soil moisture characteristic equilibrium from the moisture lost from the soil

earlier in the day. After midnight, an increase in the elevation of the groundwater elevation is observed. Given the close proximity of the piezometer to the drain (10 m), this groundwater recharge may be attributed to lateral flow with a negative flow gradient from the drain to the field. A negative flow gradient in Transect C was measured during this period as shown in Figure 7.1(a) and Figure 7.3. The low lateral permeability ( $< 1 \text{ m day}^{-1}$ ) of the soil at depth is not sufficient to re-supply the groundwater with enough volume of water to replace the loss of groundwater from the preceding days evapotranspiration losses.

During the period 9-25 March 1998 (days 235-252), the groundwater elevation was lower than the level of water in the nearby drains. As demonstrated above, some recharge of the groundwater occurs on a daily basis from seepage from the drains, however the losses attributed to evapotranspiration (up to  $13 \text{ mm day}^{-1}$ ) are greater than the recharge rate (up to  $4 \text{ mm day}^{-1}$  close to the drains). Groundwater elevation was recorded at hourly intervals at piezometer locations C10, F10 and K10 during this period. The water level recorder at I10 malfunctioned during this monitoring period. The hourly groundwater elevation data were averaged for each day so that a daily rate of groundwater fall could be determined. Figure 7.10(a) shows that at all three monitoring locations, a uniform daily groundwater table fall of  $6 \text{ mm day}^{-1}$  occurred. The first three groundwater elevations recorded at K10 are likely to be erroneous as the groundwater level may have taken some time (in this case a few days) to re-establish an equilibrium after placing the water level recorder into the piezometer. The sudden rise in the groundwater elevation at day 243 at F10 is unexplainable, though is likely to be associated with the water level recorder settling on its rope tether or being knocked.

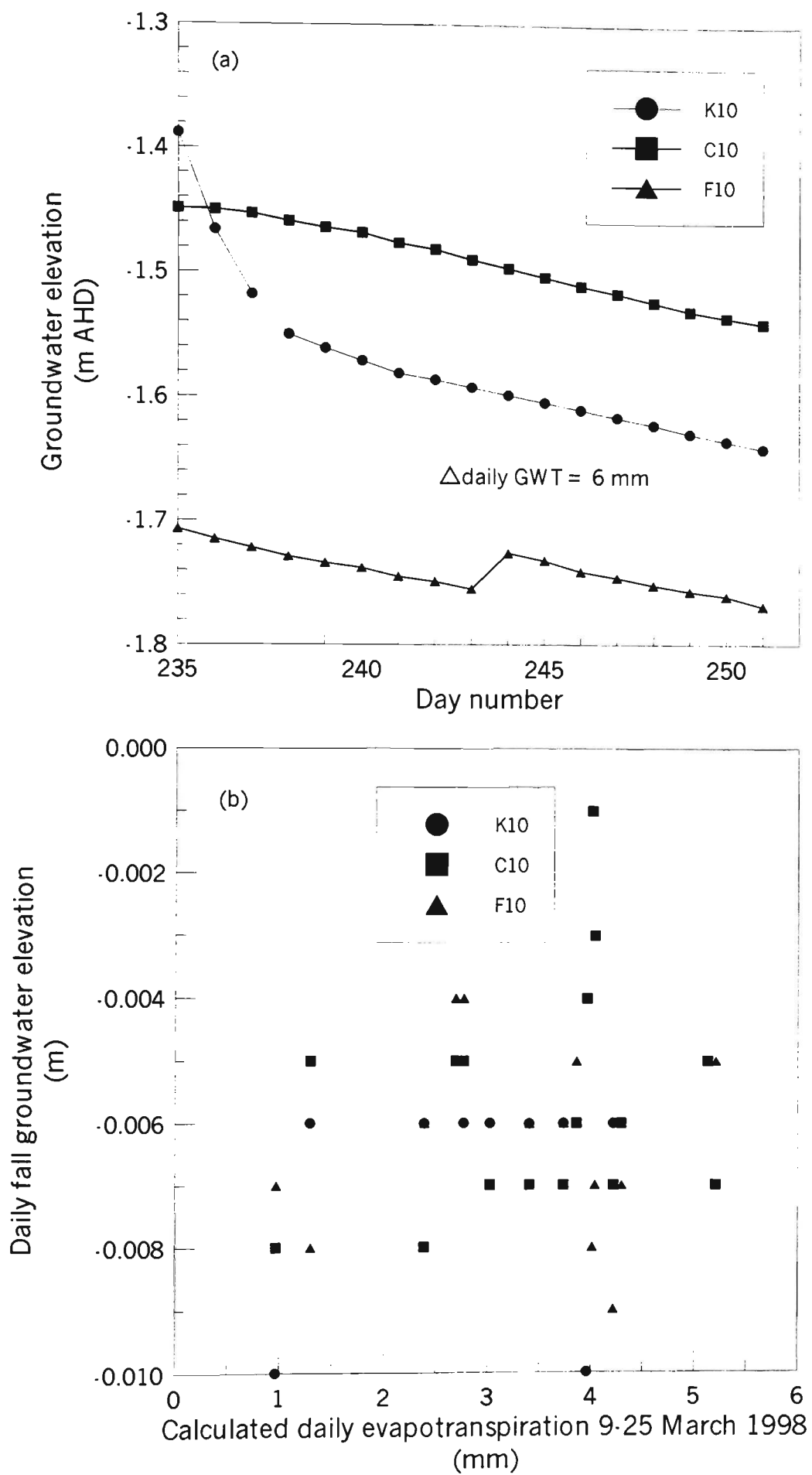


**Figure 7.10** Daily fall in groundwater elevation at C10, F10, K10.

Figure 7.10(b) shows the relationship between calculated evapotranspiration and the daily change in the groundwater level at C10, F10 and K10 during days 235-252 when a negative flow gradient from the drains was in place. Clearly there is no quantifiable relationship between the magnitude of daily evapotranspiration and the fall in groundwater elevation measured at these sites. Wilson (1995) demonstrated that a weak relationship (linear regressions with  $r^2$  between 0.52-0.62) existed between daily evapotranspiration calculated using the Penman method and daily groundwater level fall during a period of negative flow gradient for a site under sugarcane near Tweed Heads (Northern NSW). The poor relationship between daily groundwater table fall and calculated evapotranspiration can be attributed to errors associated with measuring microclimate influences for specific monitoring sites. However, Wilson (1995) found that daily water table falls averaged monthly had a stronger relationship (linear regressions with  $r^2$  between 0.77-0.83) with the monthly average of evapotranspiration. Unfortunately, the period where a negative flow gradient was present during the summer of 1997-98 corresponds with the initial installation (9 March 1998) and the subsequent failure of the water level recorders that were installed at C10, F10, I10 and K10, and drought breaking rains that occurred in April 1998 that re-established a positive flow gradient towards the drain. Negative flow gradients did not re-establish during the pre-weir period. Using the limited sample of data that was collected in March 1998, the average daily fall in groundwater elevation was  $6 \text{ mm day}^{-1}$  and the average daily potential evapotranspiration was 3.5 mm, suggesting that 1.7 mm fall in groundwater occurs for every 1 mm of potential evapotranspiration. Wilson (1995) found that evapotranspiration accounted for about 2.4 mm groundwater fall per mm evapotranspiration for acid sulfate soils under sugarcane at his Tweed Heads study site.

Because negative groundwater flow gradients were established during days 235-252, the recharge of groundwater that was observed at night (Figure 7.9) would also occur during the day, even though losses attributed to evapotranspiration were sufficient to lower the elevation of groundwater during the day and early night periods. The calculation of evaporative loss from the groundwater at the three piezometer sites with water level recorders at 10 m distance from the drains is likely to underestimate the influence of the magnitude of evapotranspiration on the groundwater table due to recharge from the

drain. In essence, this under-estimation of evaporative losses from the groundwater table becomes more apparent as the distance from the drain increases.

In order to assess the importance of distance from the drains on the rate of groundwater fall during the period where negative flow gradients prevailed, average daily groundwater falls were calculated using the manually collected groundwater elevation data from all piezometer transects. Given that the manual groundwater elevation data are not as precise as the pressure sensor data, the relationship between potential evapotranspiration and groundwater fall are indicative only.

The average daily change in groundwater elevation for piezometer transects D, E, G and I are shown in Figure 7.11(a). Figure 7.11(b) shows the average daily change in groundwater elevation for all manual piezometer data collected between 8 January and 25 March 1998 (days 175-252), where the error bars are standard deviations. A general trend was observed where the average daily fall in groundwater increased as distance from the drain increased. There is considerable variability between piezometer transects - particularly at piezometer locations furthest away from the drains where crop performance may have been variable through the dry period.

The influence of recharge from the drain is greatest at the piezometers located 1 m from the drain. At the 1 m location, groundwater fall was about  $2 \text{ mm day}^{-1}$ , and this increased to a rate of approximately  $10 \text{ mm day}^{-1}$  at 20 m distance from the drain. The rate of groundwater fall between 50-150 m distance from the drain was reasonably stable at approximately  $13 \text{ mm day}^{-1}$ . The stable nature of daily groundwater fall at piezometer locations in excess of 50 m distance from the drains suggests that any recharge of the groundwater from lateral flow from the drains is negligible. This indicates that evapotranspirative losses from the water table are in the order of  $13 \text{ mm day}^{-1}$  across the study site. This is considerably higher than the rate calculated by Wilson (1995) for acid sulfate soil under sugarcane. However, the severe drought conditions experienced at this time contribute to this very high rate of groundwater fall.



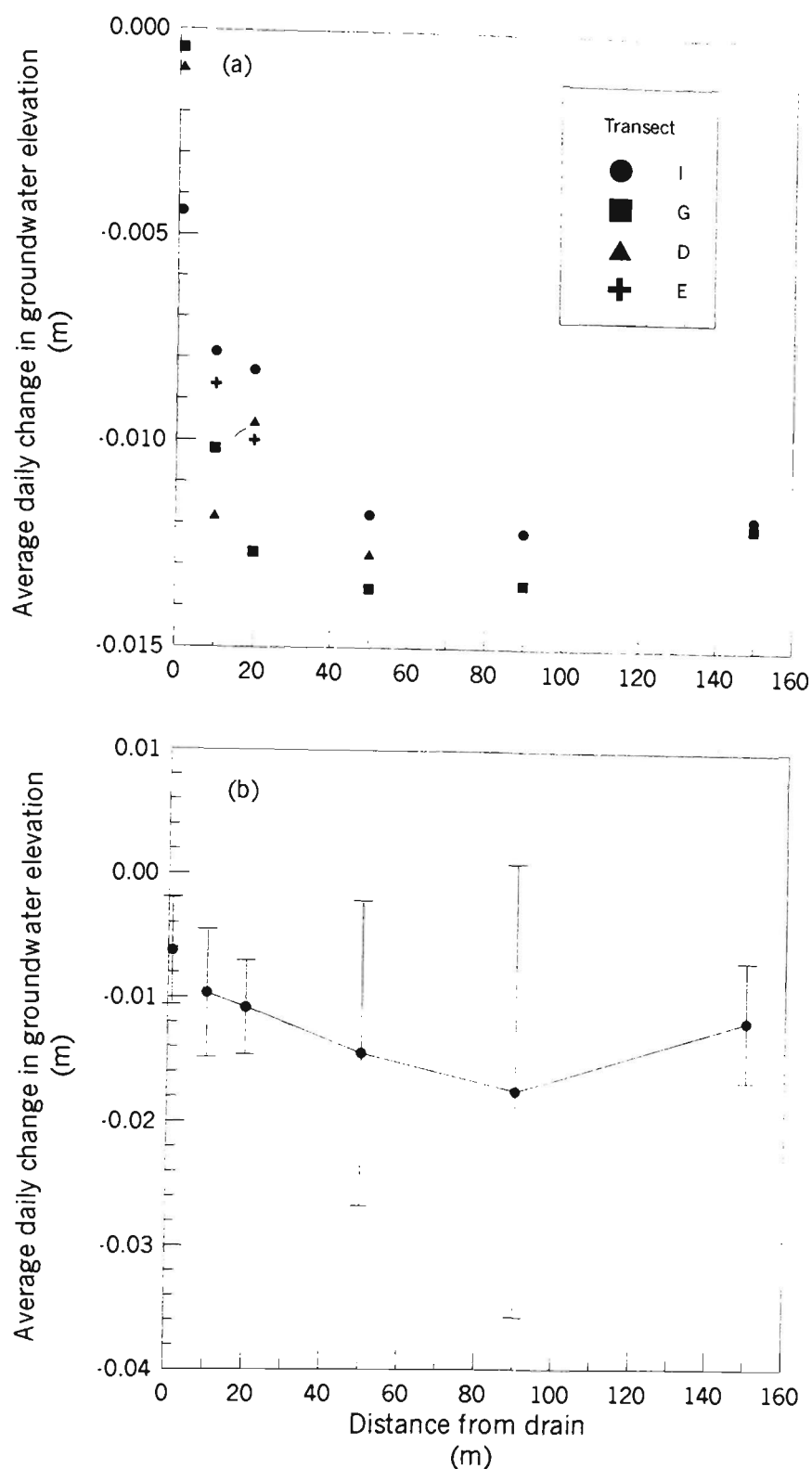


**Figure 7.11** Average daily change in groundwater elevations during negative groundwater flow gradients (i.e., flow away from the drain).

The higher rate for groundwater lowering by evapotranspiration at the Berry study site is, on first inspection, difficult to interpret. Sugarcane is a vigorous, deep rooting crop that is very successful in utilising deep reserves from water stored in the soil profile, including groundwater. The pasture on the Berry study site is considerably less vigorous

and is shallow rooting. As such, the effect of plant transpiration lowering the groundwater table should be less at Berry than for sugarcane at Tweed Heads. One important aspect of soil-atmosphere interaction not incorporated into evapotranspiration equations is the nature of soil macroporosity and its connectivity between the atmosphere and the groundwater. As described in Chapter 5, the porosity of the soil profile is very high ( $n = 0.6$ ) until the dense, Pleistocene clay horizon is encountered at about 2 m below the surface. Large, continuous macropores are also prevalent through the profile and extend well into the potential acid sulfate soil layer. These macropores may act as direct conjugates to the groundwater table, enabling direct atmospheric evaporation to lower the elevation of groundwater.

### *7.3.2 Drainage*

The groundwater dynamics shown in Figures 7.3-7.8 demonstrate that the operation of the deep floodmitigation drains have a profound effect on removing shallow groundwater from the site. The invert of the flood mitigation drains is deeper than the elevation of the low tide level in Broughton Creek. The operation of the flood gate at the discharge point of the drain and Broughton Creek ensures that the water level in the drains is maintained at low tide level. As such, the elevation of water in the drains controls the drawdown of the surrounding groundwater rather than the elevation of the base of the drain. Where the invert of the drain rises above low tide level, such as the north-south drain adjacent to piezometers transects A-D, the elevation of the drain invert may influence the magnitude of groundwater drawdown.

The low tide elevation of the drainage system is approximately -1.1 m AHD. As the low tide level controls the depth to which groundwater drawdown can occur, the control that the design and operation of the drains has on lowering the watertable is defined by the hydraulic head of water in the drain. To investigate the influence of the drains on

groundwater drawdown, the rate of daily groundwater elevation fall at an elevation greater than -1.1 m AHD (i.e. positive hydraulic gradients) was assessed.

The drawdown of groundwater at C10, F10 and I10 after the flood event that occurred on day 398-399 is shown in Figure 7.12. Figure 7.12 shows that excess surface water is removed very quickly from the site after heavy rainfall. The level of the groundwater recedes rapidly in the top soil horizon (approx 0.5 m deep). The rate of groundwater change slows as the elevation of the groundwater falls according to the soil physical properties of the underlying soil horizons and the decreasing hydraulic head between the water level in the drain and the groundwater elevation.

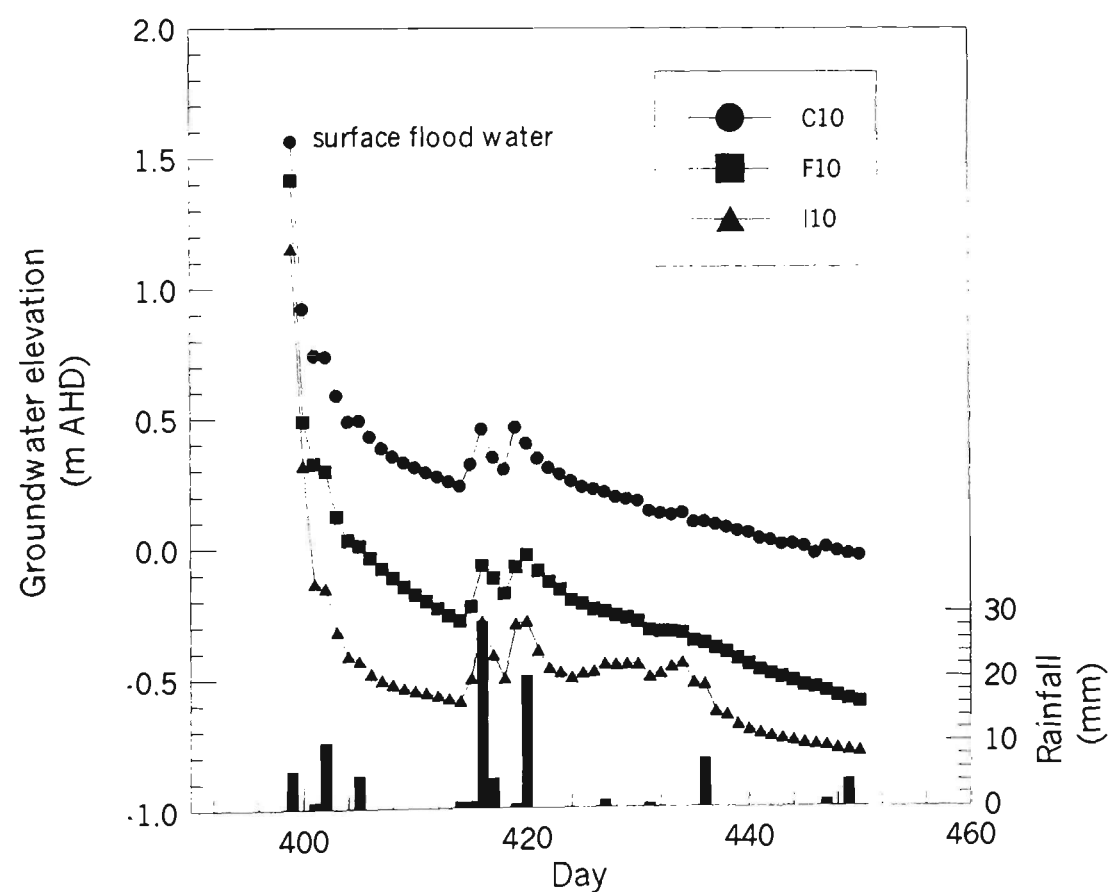


**Figure 7.12** Fall of the groundwater level after a flood event

Average daily falls in the groundwater elevation at C10, F10, I10 and K10 were calculated and plotted against the groundwater elevation in Figure 7.13

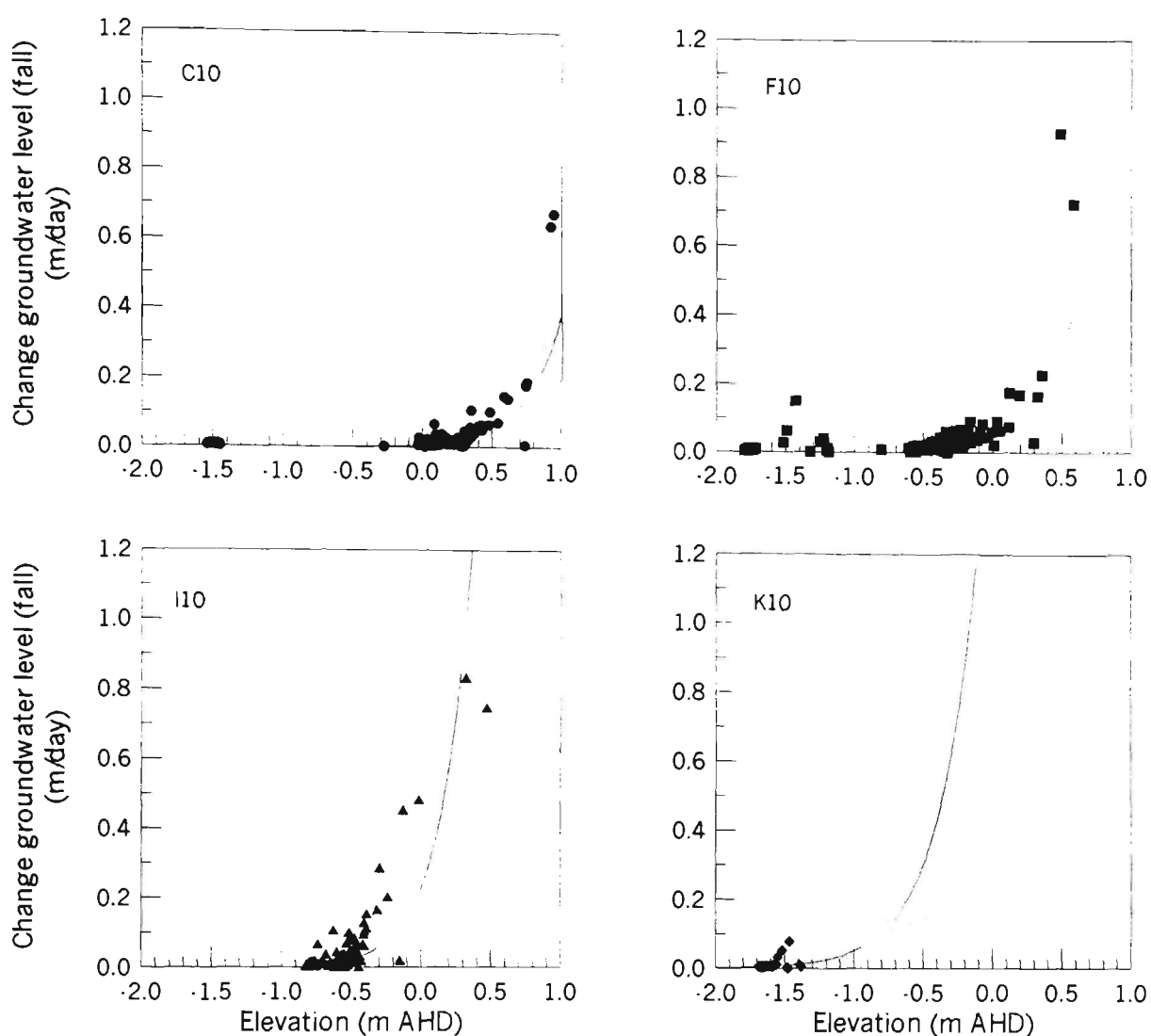


**Figure 7.13** Daily rate of groundwater fall at 10 m from the drain

Figure 7.13 shows that the rate of change in groundwater elevation is related to the initial groundwater elevation. As the elevation of the groundwater falls, the daily rate of change of the groundwater elevation also falls. Regression analysis showed that the rate of change in groundwater elevation was exponentially related to the elevation according to the equation:

$$\log(\Delta h) = ah + b \quad (7.2)$$

where;  $h$  is the groundwater elevation (m AHD),  $a$  and  $b$  are regression coefficients.

The regression coefficients describing the rate of groundwater fall during periods of positive groundwater flow gradients are shown in Table 7.3.

**Table 7.3** Regression equations: rate of groundwater fall

Piezometer	Regression coefficient (a)	Regression coefficient (b)	r <sup>2</sup>
C10	3.99	-4.94	0.53
F10	3.23	-2.80	0.52
I10	4.61	-1.47	0.47
K10	3.57	0.58	0.12

Given that the saturated hydraulic conductivity of the soil in the first metre of the soil profile is very high (approx 3-4 m day<sup>-1</sup>, see Chapter 5), the primary determinant for the rate of groundwater fall is the magnitude of the current hydraulic gradient or excess head driving the flow of groundwater towards the drain. If no additional groundwater recharge occurs, the fall in groundwater elevation will be proportional to logarithm of the potential between the groundwater surface and the elevation of the water in the drain. When the groundwater elevation approaches the drain water level, potential evapotranspiration the predominant driver of the change in groundwater elevation.

During the pre-weir period, the water level in the drain quickly achieved its equilibrium elevation of approximately -1.1 m AHD. If sufficient rainfall had fallen so that the groundwater had completely recharged and caused surface flooding, a head in the order of 1.5 m caused rapid discharge through the seepage face in the drain wall and caused the groundwater to fall by about 0.2 m day<sup>-1</sup>. This high rate of fall rapidly declined as the head became less. The horizontal hydraulic conductivity of the potential acid sulfate soil controlled the rate of groundwater fall once the groundwater approached that elevation. The combination of small heads and associated low horizontal hydraulic conductivity resulted in daily falls in groundwater elevation of less than 0.05 m day<sup>-1</sup>.

## 7.4 Groundwater dynamics - rising groundwater table

Rising groundwater tables are controlled by rainfall. Small increases in the elevation of the groundwater table are also possible due to lateral seepage from the drains or Broughton Creek when negative groundwater flow gradients exist (as demonstrated in Figure 7.9). However, lateral inflow is relatively minor in comparison to the contribution associated with groundwater recharge as a result of rainfall, and will not be discussed further. To accurately describe the rainfall - rise in groundwater elevation relationship, rainfall events were assessed against groundwater elevation data measured by the water level recorders at C10, F10 and I10. The magnitude of rainfall per event and the initial depth of the groundwater table are investigated as factors that control the rise in the groundwater elevation.

Not all rainfall events were of sufficient magnitude to produce an increase in the elevation of the groundwater table. For the elevation of the groundwater to rise, sufficient rainfall has to fall so that the unfilled storage components, such as leaf interception and soil void space are filled, and the remaining rainfall is able to be transported to the saturated zone at depth within the soil. Rainfall events which did not result in any detected rise in the elevation of the groundwater level at C10, F10 or I10 were investigated. The magnitude of the rainfall event and the initial elevation of the groundwater table at the start of the rainfall event is shown in Figure 7.14

Figure 7.14 shows that daily rainfall events of up to 12 mm may have no measurable increase in the elevation of the groundwater table. No clear cumulative rainfall threshold exists above which a confident prediction of an increase in the groundwater elevation could be made. Where the groundwater level is within approximately 0.5 m of the ground surface (ie. within the top soil layer), a cumulative rainfall threshold of about 3 mm must be exceeded before there is an increase in the groundwater level. However, the data becomes considerably more variable once the depth to the groundwater table goes deeper than the top soil layer. Numerous soil physical factors such as the wetting/drying status of the soil and associated hysteresis of the moisture retention curve

and vegetative cover are involved in defining the minimum amount of rainfall required to cause a rise in the groundwater elevation.

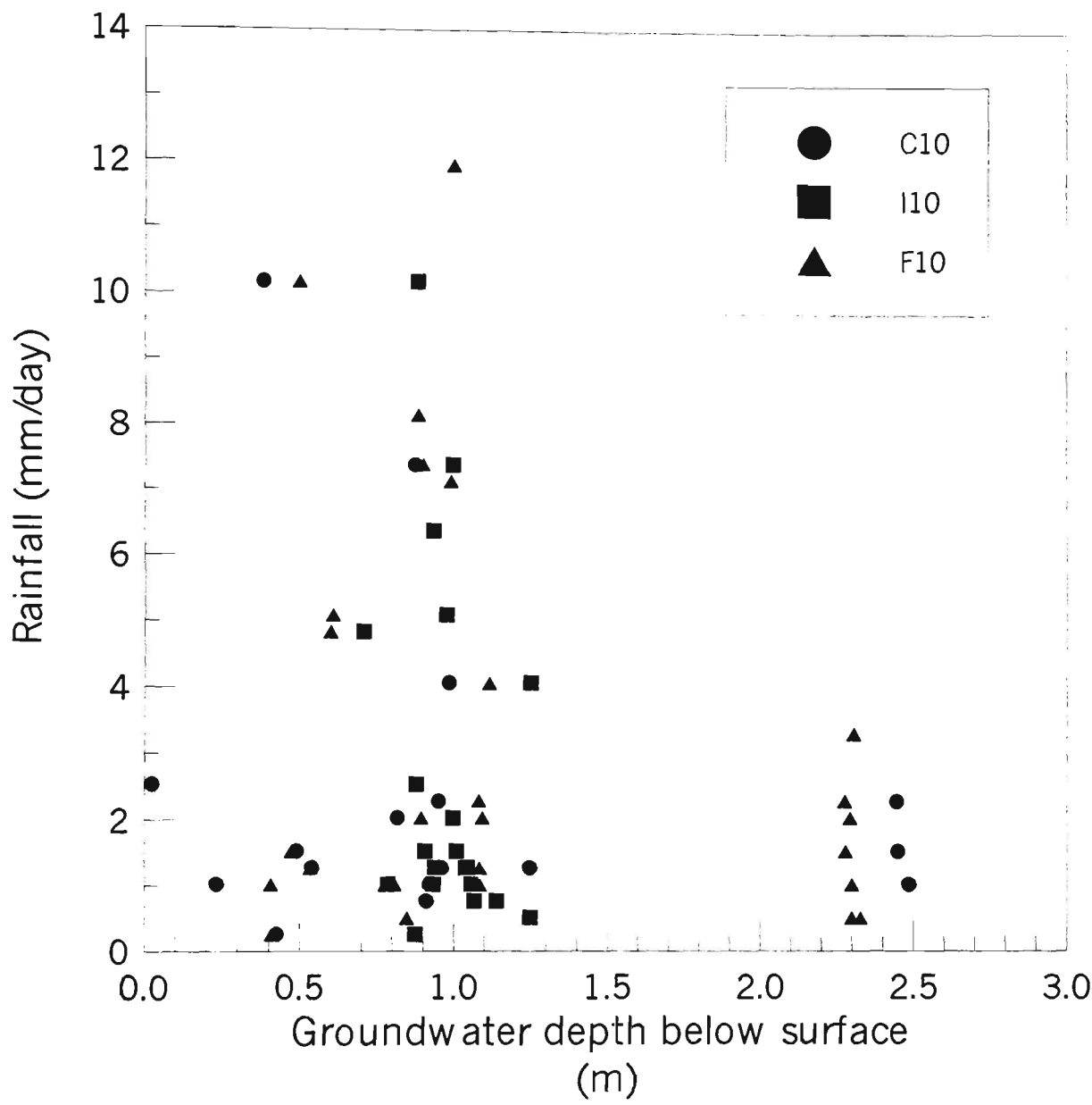


**Figure 7.14** Rainfall events that caused no increase in the groundwater elevation.

Rainfall events that resulted in an increase in the elevation of the groundwater table were analysed. Where groundwater rise occurred as a result of rainfall falling over a number of days, the sum of the rainfall recorded during that period was calculated and plotted against the total increase in groundwater elevation over that period. The cumulative increase in groundwater elevation plotted against cumulative rainfall per event is shown in Figure 7.15. Only rainfall events where the initial groundwater elevation was lower than the soil surface were analysed. Once rainfall gives rise to

surface flooding, no soil moisture storage component has to be overcome to increase the elevation of the surface water level.

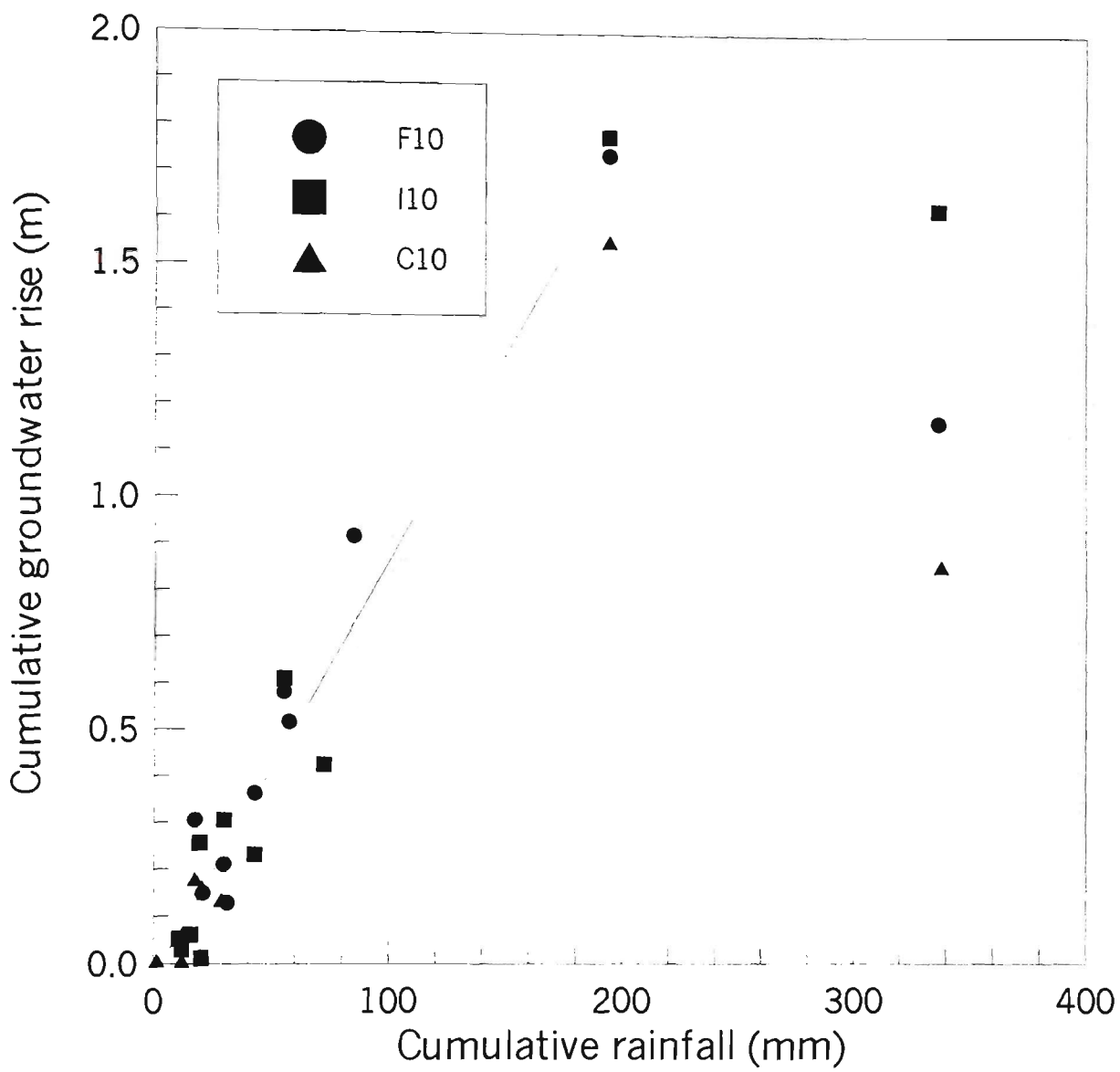


**Figure 7.15** Rise in groundwater elevation due to rainfall.

Three points did not conform to the general pattern of the linear regression equation. The cumulative rainfall for these points was in excess of 330 mm and occurred over a four day period. Although the initial groundwater level was below the ground surface at the start of this rainfall event, the magnitude and intensity of the rainfall caused surface runoff to occur, giving rise to a significantly different relationship between cumulative rainfall and cumulative rise in groundwater elevation. These data were excluded from further analysis.



A linear regression curve of cumulative rainfall against cumulative groundwater rise for all data points from C10, F10 and I10 where the groundwater level did not exceed the ground surface elevation is shown in Figure 7.15. The linear regression equation is:

$$\Delta\text{GWL} = 0.00893 \times \text{RF} - 0.0297 \qquad r^2 = 0.96 \qquad (7.2)$$

where;  $\Delta\text{GWL}$  is the cumulative rise in groundwater elevation (m) and RF is the cumulative rainfall per event (mm).

Equation (7.2) indicates that the magnitude of a rainfall event is the most significant control on the magnitude of the rise in groundwater level ( $r^2 = 0.96$ ,  $P < 0.05$ ). Equation (7.2) has a negative intercept, which indicates that at least 3.3 mm of rainfall is required to initiate a rise in the groundwater level, irrespective of the initial depth of the groundwater table. Multiple regression analysis where the initial depth of the groundwater table was also included with the cumulative rainfall did not improve the prediction given by Equation (7.2).

Analysis of the manually collected piezometer data was not able to accurately determine a precise relationship between cumulative rainfall and the rise in groundwater elevation, although a generalisation can be made suggesting that increased rainfall gives rise to greater elevation in groundwater. The rise in groundwater elevation for piezometers in Transect I is shown in Figure 7.16.

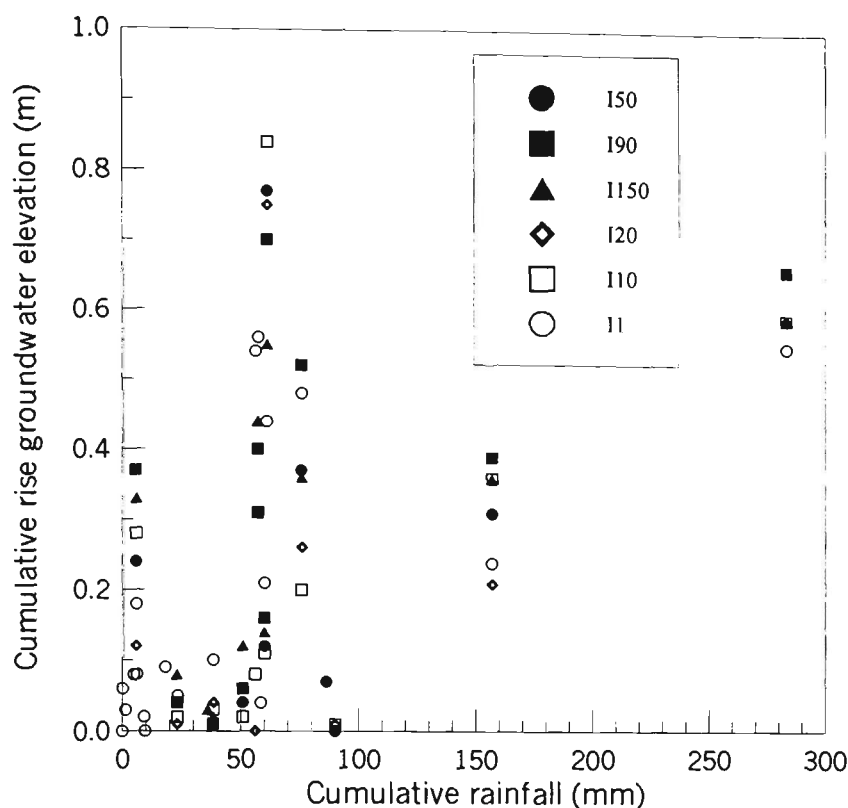


**Figure 7.16** Cumulative rise in groundwater elevation caused by rainfall (Transect I)

The major problem with the analysis for the manual data is the length of time between measurements. This is particularly evident where up to 90 mm of rainfall was recorded during a period between piezometer measurements, yet no net increase in the elevation of the groundwater level was observed. The difference in groundwater elevation between successive piezometer measurements invariably incorporated periods of rapid groundwater rise after rainfall, followed by groundwater drawdown caused by drainage and/or evapotranspiration. Shorter monitoring periods, preferably using water level data loggers that record groundwater elevation on a daily basis, are required to adequately define the relationship between rising groundwater and rainfall.

### 7.5 Oxidation of pyritic soil during the pre-weir period

Pyrite oxidation and the subsequent generation of sulfuric acid occurs when oxidising conditions exist within the potential acid sulfate soil. An assessment of the magnitude

of pyrite oxidation can be made by examining how oxidising conditions occur in the potential acid sulfate soil horizon. A simplified method of determining the magnitude of pyrite oxidation in potential acid sulfate soils is to relate the groundwater elevation to the depth of the acid sulfate soil. Given the assumption that acid generation is primarily caused by pyrite reacting with oxygen, the magnitude of pyrite oxidation can be correlated to the length of time and total volume of acid sulfate soil exposed to oxygen above the groundwater table.

The degree of saturation, and hence oxidation status, within a volume of potential acid sulfate soil is complex due to the structure of the soil. As discussed in Chapter 5, the potential acid sulfate soil comprises of a relatively massive silty clay matrix which has high air entry values, low porosity and low oxygen diffusivity. As the elevation of the groundwater falls below the upper surface of the potential acid sulfate soil layer, the silty clay matrix between macropores remains highly saturated due to capillary rise from the groundwater. The height of the saturated zone above the groundwater table depends on the air entry suction of the soil, the rate of change of the elevation of the groundwater table and whether the soil is in a drying or wetting phase (Ritzema, 1994). The potential acid sulfate soil at the study site has an air entry value of about 0.5 m, indicating that the soil will remain saturated at a height 0.5 m above the water table. However, as the rate of change in the elevation of the groundwater table is very fast (e.g. up to  $13 \text{ mm day}^{-1}$  in the drying phase), the height of the capillary fringe may be less than 0.5 m. In spite of the capacity of the potential acid sulfate soil to remain in a nearly saturated state at a higher elevation than the groundwater table (ie, where  $\psi = 0 \text{ kPa}$ ), the oxygen diffusivity in heavy clay soil has been reported to increase rapidly as reasonably small volumes (e.g.  $0.05 \text{ m}^3/\text{m}^3$ ) of the available pore space drain (Hodgeson and MacLeod, 1989).

The structure of potential acid sulfate soil at the study site is also characterised by large, continuous macropores that have a very low air entry values and high rates of oxygen transport. The macropore channels themselves drain rapidly, becoming available for the diffusion of atmospheric oxygen to the potential acid sulfate soil immediately adjacent to the macropore walls. The surface area available for pyrite oxidation within the macropores is approximately  $2.84 \text{ m}^2/\text{m}^3$  soil, given that the density of macropores was

about 300/m<sup>2</sup> and the average radius of the macropores was about 1.5 mm. This appears to be sufficient to cause the oxidation of pyrite within the immediate zone of soil around the macropore channel. The presence of jarosite and iron encrustations in and around macropore channels respectively in the potential acid sulfate soil layer is evidence of the oxygen transport and pyrite oxidisation associated with the macropore structures. The dynamic nature of the groundwater table also ensures that the macropores rapidly fill with oxygen from the atmosphere. As the groundwater elevation falls, air is sucked into the macropore space by the lower air pressure created within the macropore by the receding groundwater. The rate of oxygen transport into these macropores may be significantly greater than the rate expected by diffusion alone if oxygen is also transported by convective processes as well as by diffusion. Given the physical structure and properties of the potential acid sulfate soil, it is useful to characterise the groundwater elevation as the lowest bound of possible oxidising conditions in the soil.

The length of oxidation episodes and the volume of potential acid sulfate soil exposed above the groundwater table is shown in Figures 7.17-7.19. As previously discussed, the elevation of the potential acid sulfate soil is variable across the site. Similarly, the elevation of the groundwater table is variable, resulting in periods where the acid sulfate soil layer is either above or below the groundwater table.

In some instances, the acid sulfate soil layer may be above the groundwater table in one part of a piezometer transect but not in another. This is particularly evident where the water level in the drain is in equilibrium with the low tide level in Broughton Creek (approximately -1.1 m AHD), causing pronounced groundwater drawdown close to the drain. This is demonstrated in Figure 7.18, where the groundwater elevation at H1, I1 and K1 is lower than the potential acid sulfate soil layer during the periods of positive flow gradients. Where sufficient drawdown has occurred, a shallow, narrow band of potential acid sulfate soil can be maintained in a drained state during relatively wet periods. Figure 7.17 shows that at Transect I, a band of potential acid sulfate soil approximately 5 m wide was influenced by drainage drawdown so that the level of groundwater was below the potential acid sulfate soil layer for most of the pre-weir period. Maintenance of drained acid sulfate soil close to the drain facilitates constant

leakage of acidic leachate through the seepage faces on the drain bank whenever small increases in groundwater elevation from rainfall cause groundwater to discharge through the newly acidified zone at the top of the acid sulfate soil layer. This is demonstrated on Figure 7.17 where positive groundwater flow gradients exist through regions of drained potential acid sulfate soil adjacent to the drain.

The length of time that the necessary conditions (i.e., where the groundwater table is below the upper surface of the potential acid sulfate soil layer) for pyrite oxidation were present during the pre-weir period is shown in Figure 7.19. During the drought period experienced in summer 1997-98, the groundwater table fell below the upper surface of the potential acid sulfate soils at all locations for a considerable length of time. In most instances, the potential acid sulfate soil became exposed during November 1997 and remained in an unsaturated state until substantial rainfall fell in May 1998. The average length of exposure of the potential acid sulfate soil to oxidising condition was 205 days. This represents approximately 45% of the pre-weir trial period.

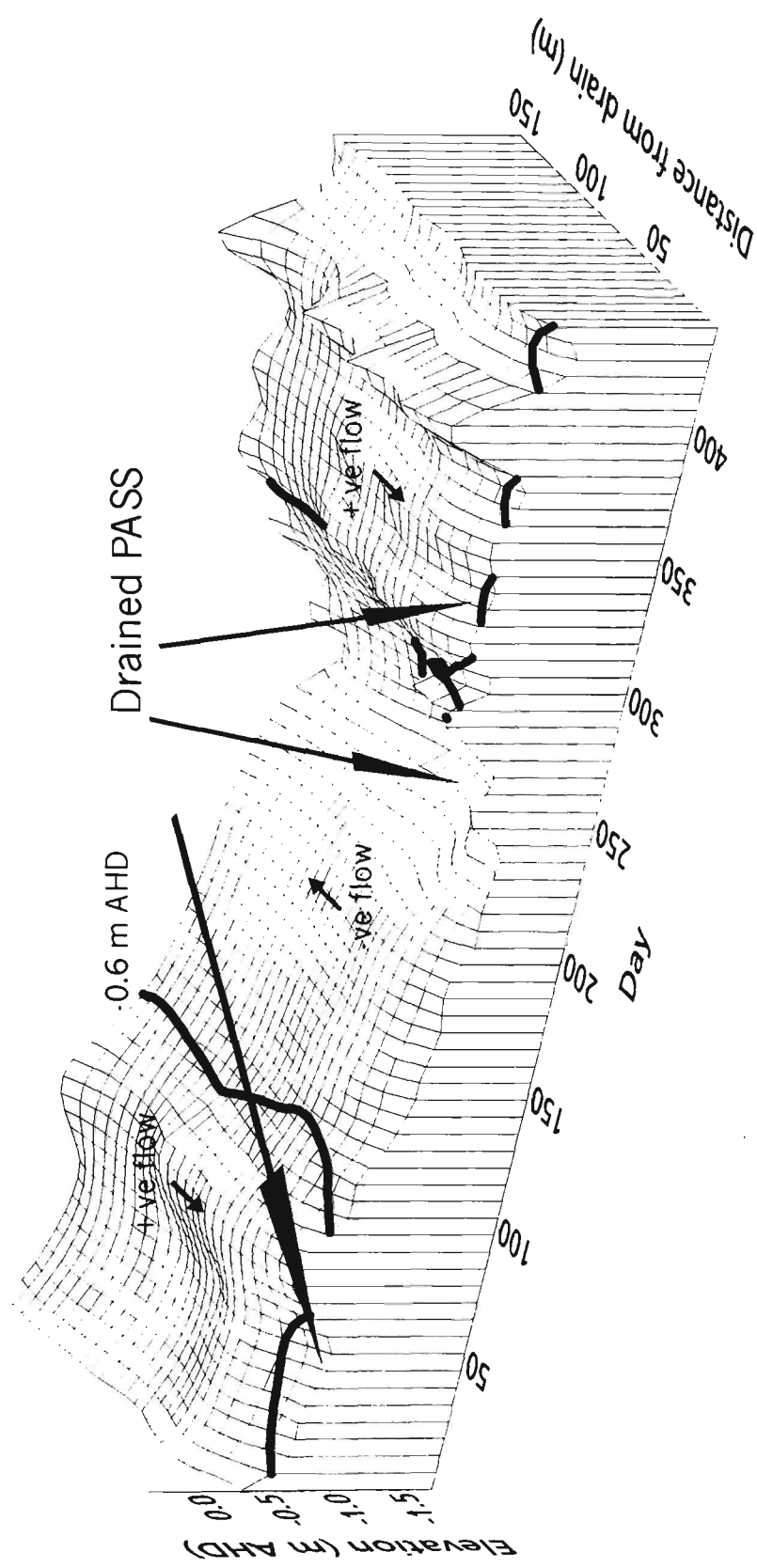


**Figure 7.17** Groundwater elevation for Transect I. Contour line is elevation of potential acid sulfate soil.

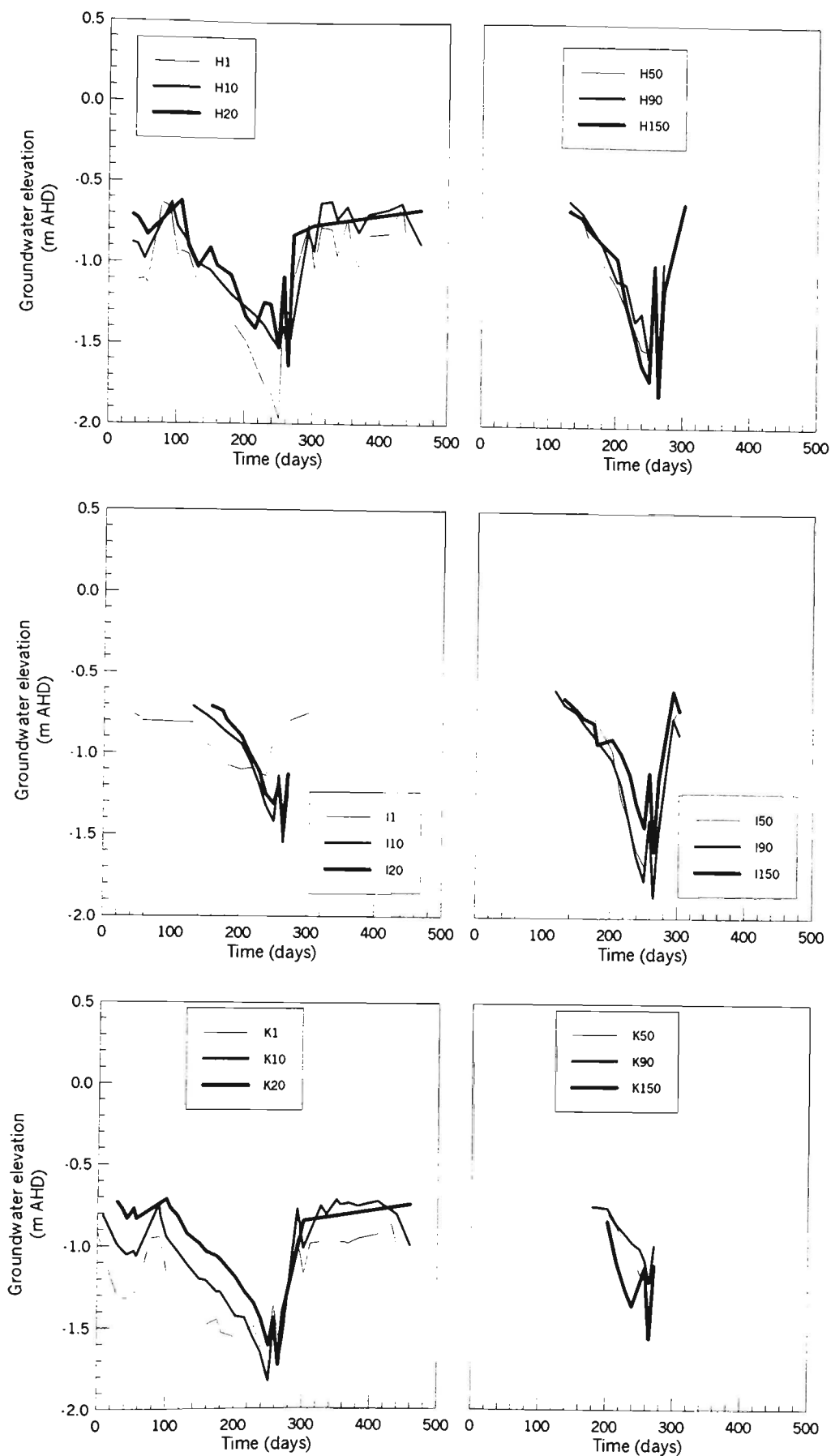


**Figure 7.18** Period where the groundwater is below the upper boundary of the potential acid sulfate soil for Transects I, J and K.

As described above, drawdown caused by the flood mitigation drains can result in aeration of potential acid sulfate soils close to the drains whilst at distances further from the drain saturated conditions prevail. This is clearly evident in the Figure 7.19, where the number of days where the groundwater is below the acid sulfate soil layer is greater for piezometer locations close to the drains (1 and 10 m) than for piezometers further away (50, 90, 150 m) from the drains. In many piezometer transects, there is a linear trend of decreasing oxidation exposure time as the distance from the drain increases, although the slope of the decreasing trend is variable depending on the soil physical properties and severity of drainage affecting each piezometer transect. Linear regression of the piezometer distance from the drain against the length of time that the potential acid sulfate soil was above the groundwater table for all the data except E1, E20, H1, H10, K1 and K10 gave:

$$T_e = -0.21 \times D + 184 \qquad r^2 = 0.3 \qquad (7.3)$$

where;  $T_e$  is exposure time (days) and  $D$  is distance from the drain (m).

Equation (7.3) confirms the trend of shorter length of time available for pyrite oxidation further away from the drain. The utility of equation (7.3) is extremely poor, given that it only predicts the length of time available for pyrite oxidation during the conditions that prevailed during the pre-weir monitoring period. Similarly, the equation is not transferable to other sites given its underlying dependence on the physical properties of both the soil and the drainage system at this site.

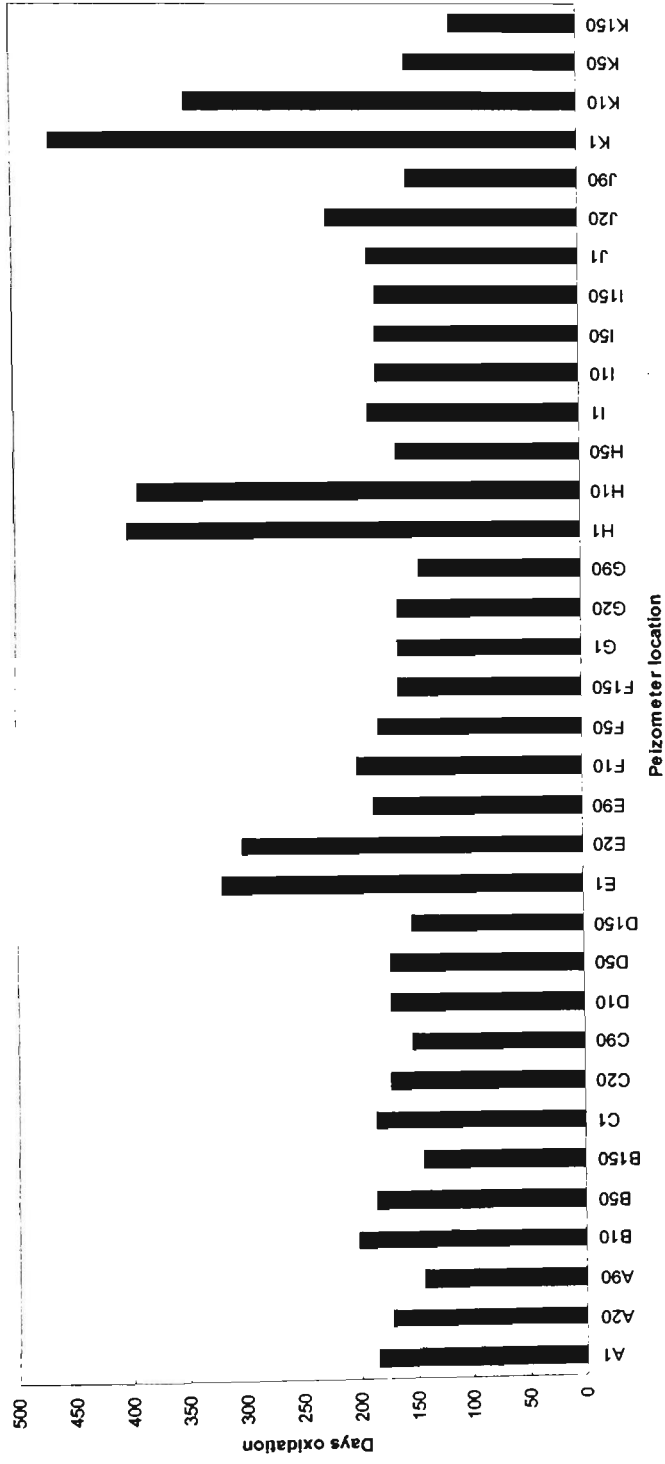
There are three locations shown in Figure 7.19 at which the length of time for pyrite oxidation in the potential acid sulfate soil is significantly longer than the average 205 days. These locations include: a) E1 - E20, b) H1 - H10, and c) K1 - K10.

As previously discussed in this Chapter and in Chapter 5, there is a preferential drainage pathway associated with a former creek channel located adjacent to Transect E. The

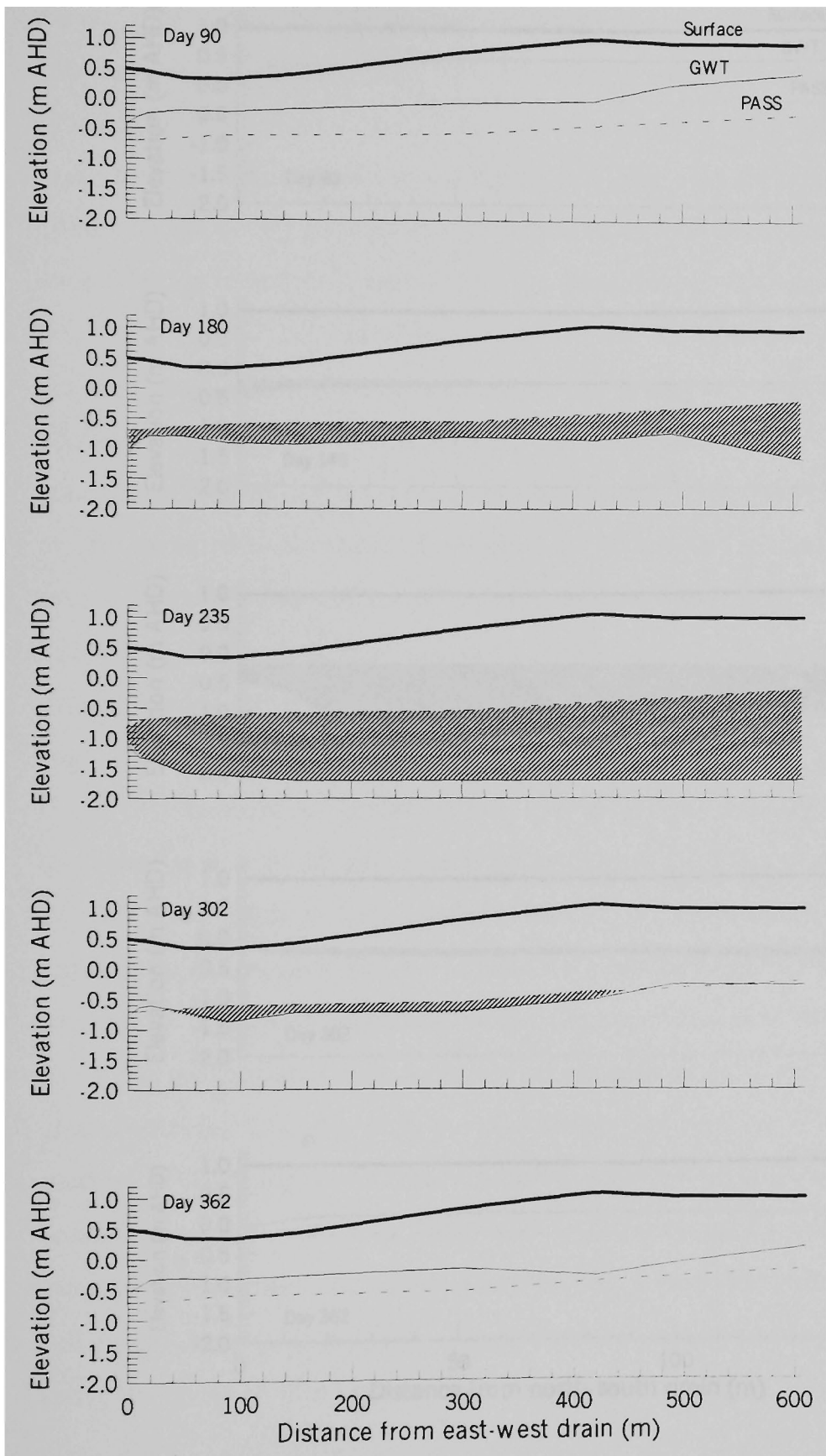


increased groundwater drawdown promoted by this former creek channel resulted in 320 days (70% of pre-weir period) and 302 days (66% of pre-weir period) of oxidation at E1 and E20 respectively. Similar rapid groundwater drawdown occurs adjacent to the piezometer Transect K, where the influence of the large field drain shown in Figure 7.4 is described. Groundwater drawdown by both the field drain and the flood mitigation drain resulted in 462 days (100%) and 347 days (75%) days where the potential acid sulfate soil was exposed to aeration. Groundwater drawdown is also accelerated close to the junction of the two flood mitigation drains as the groundwater has a greater seepage face area to discharge from. The greater capacity to remove groundwater at the junction of the two drains resulted in 401 (87%) and 392 (79%) days of oxidising condition at H1 and H10.

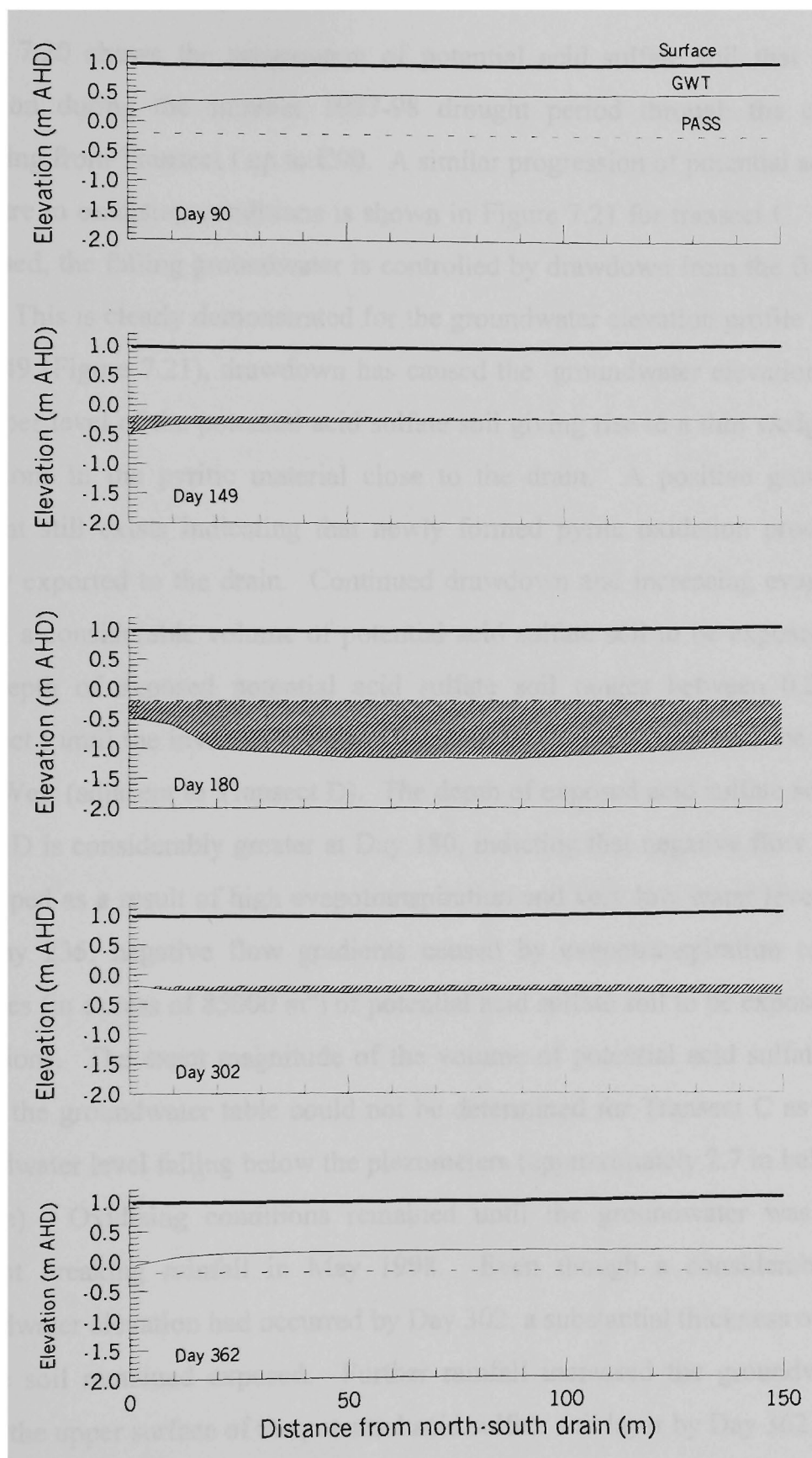
The amount of pyrite able to be oxidised during a period of low groundwater elevation is also influenced by the magnitude of groundwater fall below the upper surface of the potential acid sulfate soil layer. The volume of potential acid sulfate soil exposed by the falling groundwater table across two cross sections of the site is shown in Figures 7.20 and 7.21.



**Figure 7.19** Number of days where the groundwater is below the elevation of the upper surface of the potential acid sulfate soil layer



**Figure 7.20** Relationship between the elevation of the groundwater table and the potential acid sulfate soil. Transect I through F90, E90, D90 and C90. Hatched area is where the GWL is below the PASS, thereby creating oxidising conditions.



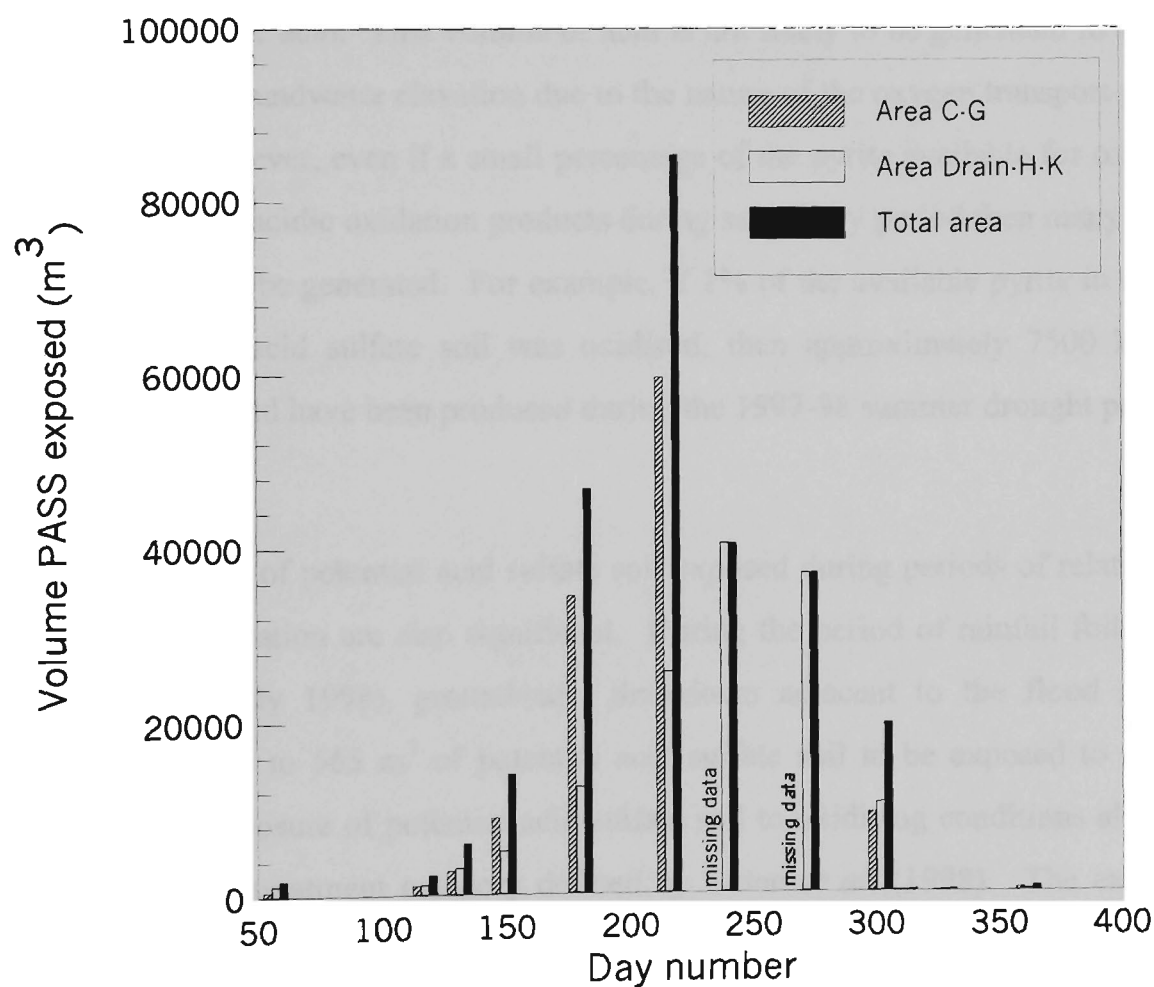
**Figure 7.21** Relationship between the elevation of the groundwater table and the potential acid sulfate soil. Transect C. Hatched area is where the GWL is below the PASS, thereby creating oxidising conditions.

Figure 7.20 shows the progression of potential acid sulfate soil that is exposed to oxidation during the summer 1997-98 drought period through the centre transect extending from Transect I up to C90. A similar progression of potential acid sulfate soil exposure to oxidising conditions is shown in Figure 7.21 for transect C. As previously discussed, the falling groundwater is controlled by drawdown from the flood mitigation drain. This is clearly demonstrated for the groundwater elevation profile at Day 90. By Day 149 (Figure 7.21), drawdown has caused the groundwater elevation to fall below the upper level of the potential acid sulfate soil giving rise to a thin wedge of oxidising conditions in the pyritic material close to the drain. A positive groundwater flow gradient still exists indicating that newly formed pyrite oxidation products could be rapidly exported to the drain. Continued drawdown and increasing evapotranspiration caused a considerable volume of potential acid sulfate soil to be exposed by Day 180. The depth of exposed potential acid sulfate soil ranges between 0.2-0.5 m along Transect I until the invert of the north-south drain begins to rise near the location of the High Weir (adjacent to Transect D). The depth of exposed acid sulfate soil in Transects C and D is considerably greater at Day 180, indicating that negative flow gradients have developed as a result of high evapotranspiration and very low water levels in the drain. By Day 235, negative flow gradients caused by evapotranspiration caused massive volumes (in excess of  $85000 \text{ m}^3$ ) of potential acid sulfate soil to be exposed to oxidising conditions. The exact magnitude of the volume of potential acid sulfate soil exposed above the groundwater table could not be determined for Transect C as a result of the groundwater level falling below the piezometers (approximately 2.7 m below the ground surface). Oxidising conditions remained until the groundwater was recharged by drought breaking rainfall in May 1998. Even though a considerable rise in the groundwater elevation had occurred by Day 302, a substantial thickness of potential acid sulfate soil remained exposed. Further rainfall increased the groundwater elevation above the upper surface of the potential acid sulfate soil layer by Day 362.

The volume of potential acid sulfate soil exposed to oxidising condition was calculated for the “L” shaped area (about 11.85 ha) incorporating piezometer transects C-K and bound by the two flood mitigation drains. This “L” shaped area was divided into two regions, the first between Transects C-G and the second between the first 150 m of the

north-south drain through Transects H-K. The volume of acid sulfate soil exposed above the water table for various dates in the pre-weir period is shown in Figure 7.22

Figure 7.22 shows that a massive volume of potential acid sulfate soil was exposed to oxidising conditions between November 1997 and May 1998 as the groundwater elevation fell. At Day 216, approximately 85330 m<sup>3</sup> of potential acid sulfate soil was exposed above the groundwater table. Further falls in the groundwater elevation may have occurred in the region bound by Transects C-G, giving rise to a larger volume of potential acid sulfate soil being exposed to oxidising conditions. This could not be determined due to missing data caused by the groundwater falling below the level of the piezometers.



**Figure 7.22** Volume of potential acid sulfate soil exposed to oxidising conditions in the area bounded by Transects C-K.

Stone *et al.* (1998) indicate that a detailed management plan would be required if in excess of 1000 m<sup>3</sup> of potential acid sulfate soil with an oxidisable sulfur content of 0.3% was disturbed during development activities. They suggest that a “very high” level of treatment would be required for this magnitude of soil disturbance in order to minimise the risk to the environment. Clearly, the volume of potential acid sulfate soil, which has an oxidisable sulfur content ~2.5-4%, exposed by low groundwater elevations caused by drainage drawdown and evapotranspiration during the pre-weir period is significantly greater than the criteria suggested by Stone *et al.* (1998).

Complete oxidation of the volume of potential acid sulfate soil exposed by the low groundwater during the drought period could theoretically generate in the order of 7.5 x10<sup>5</sup> kg of sulfuric acid. This volume of acid is not likely to be generated in any single period of low groundwater elevation due to the nature of the oxygen transport properties of the soil. However, even if a small percentage of the pyrite available for oxidation is transformed into acidic oxidation products during such a dry period then many tonnes of acid are likely to be generated. For example, if 1% of the available pyrite in the 85330 m<sup>3</sup> of potential acid sulfate soil was oxidised, then approximately 7500 kg of 1M sulfuric acid would have been produced during the 1997-98 summer drought period.

Smaller volumes of potential acid sulfate soil exposed during periods of relatively high groundwater elevation are also significant. During the period of rainfall following the drought (May-July 1998), groundwater drawdown adjacent to the flood mitigation drains caused up to 565 m<sup>3</sup> of potential acid sulfate soil to be exposed to oxidation. This level of exposure of potential acid sulfate soil to oxidising conditions also falls in the “very high” treatment category defined by Stone *et al.* (1998). The exposure of substantial volumes (100-2000 m<sup>3</sup>) of potential acid sulfate soil close to the drains by groundwater drawdown represents a serious threat to the water quality within the drain. A relatively small rainfall event will cause minor increases in the elevation of the groundwater flowing through the oxidised zone, giving rise to the frequent acidification of the groundwater that is about to be discharged into the drainage system.

## 7.6 Post-weir groundwater dynamics

The weirs were successfully commissioned on 1 October 1998 (day 440) after substantial repairs were carried out to address bank erosion that was caused by heavy rainfall events between April-August 1998. Groundwater elevation was measured until 9 October 1999 (day 813).

Installation of the weirs resulted in a substantial change in the shallow groundwater regime of the study site. In summary, the groundwater table was maintained above the pyritic layer for the entire monitoring period after the installation of the weirs, except in the area adjacent to piezometer transect K where the groundwater was controlled by the drain downstream of the low weir. Higher drain water elevations that were maintained by the weirs reduced groundwater drawdown close to the drains and established lower hydraulic gradients. In some instances, the groundwater flow direction changed so that acidic groundwater did not discharge into the drains.

### *7.6.1 Observed groundwater profile during post-weir period*

The transient groundwater elevation data measured at the site during the post-weir period for piezometer transects C, D, H, I and K are shown in Figures 7.23(a,b). For ease of comparison between the pre and post weir periods, Figure 7.23 has been plotted on the same vertical scale as Figure 7.1(a,b).



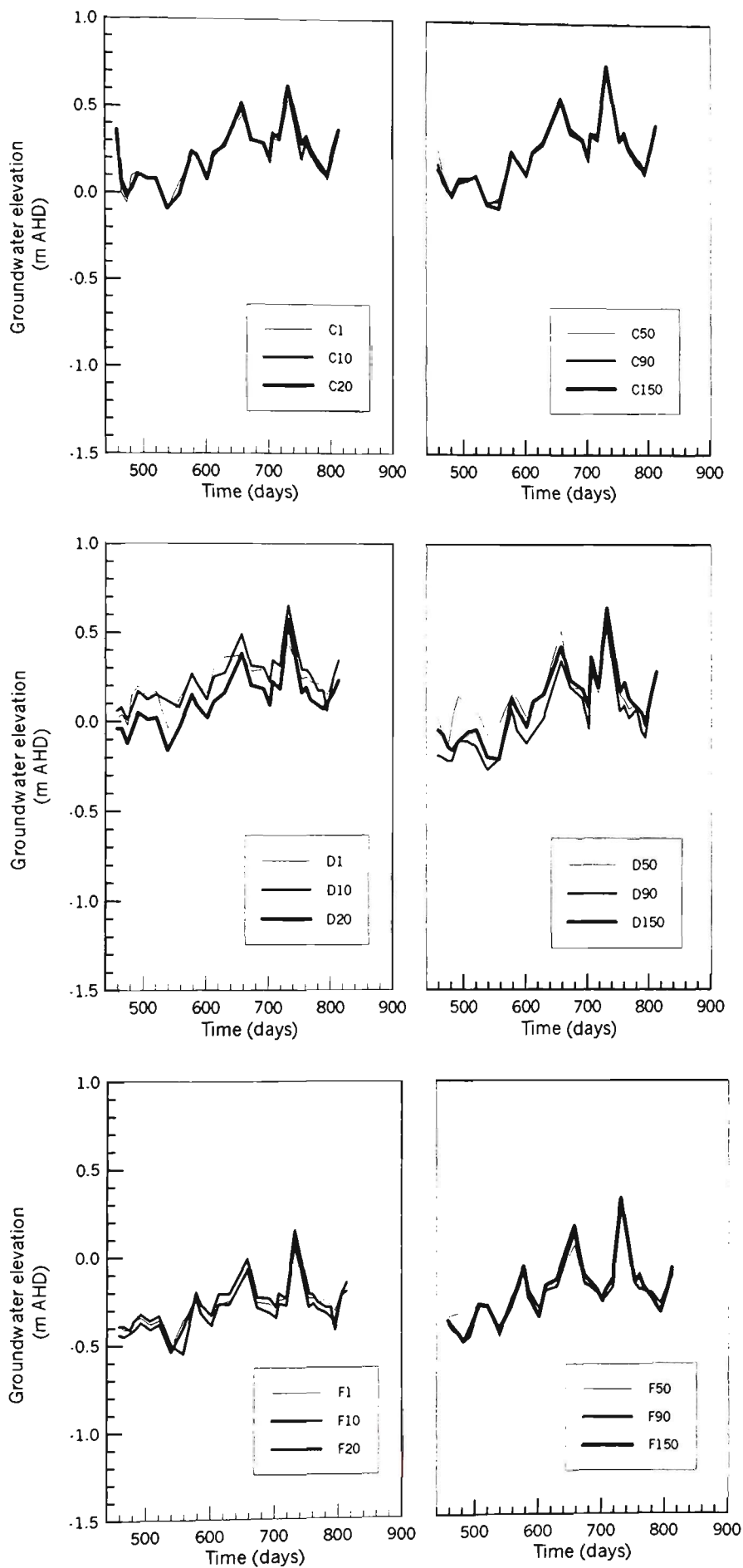


**Figure 7.23(a)** Post-weir groundwater elevations at piezometer transects C, D and F.

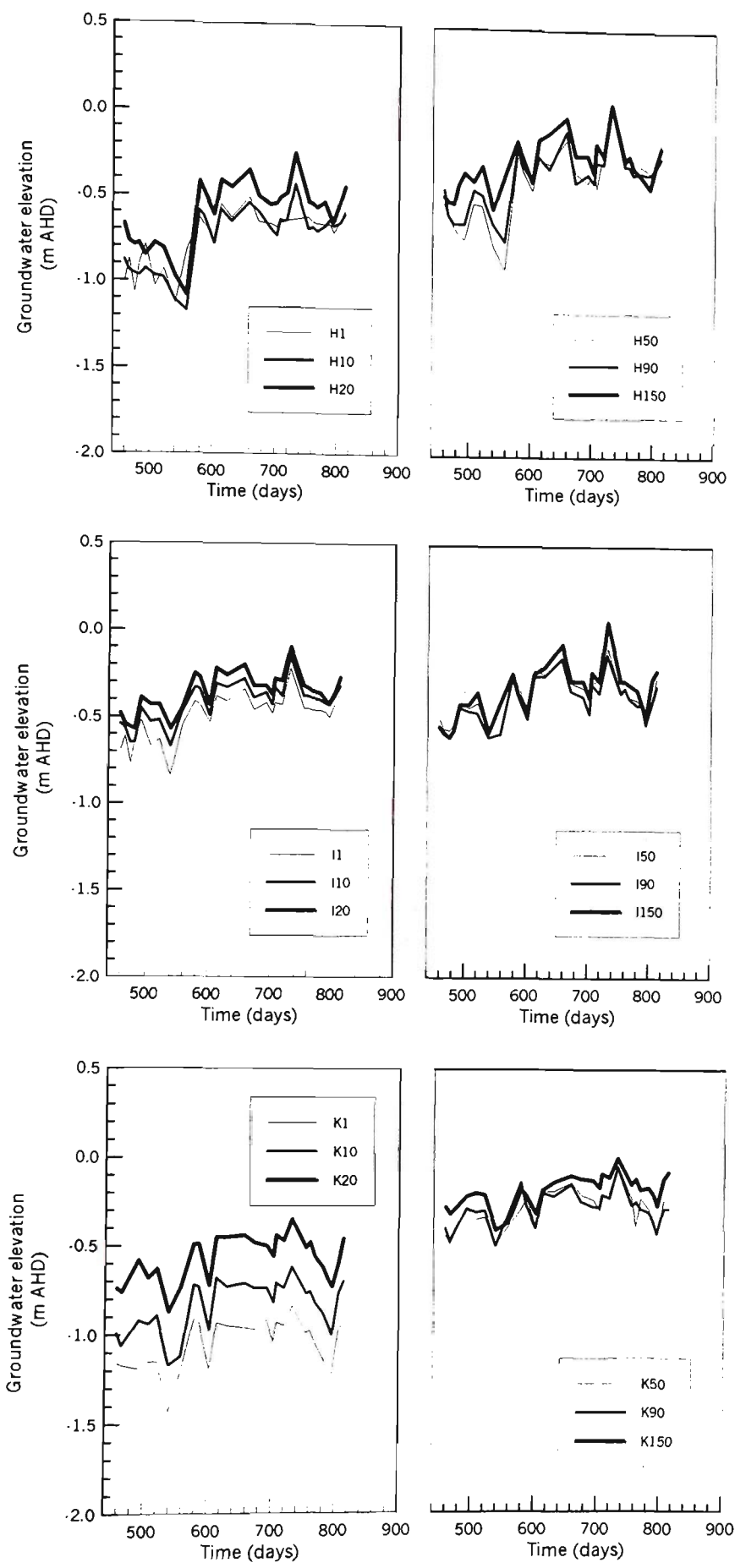


**Figure 7.23(b)** Post-weir groundwater elevations at piezometer transects H, I and K.

As shown in Figure 7.23(a), maintenance of higher water levels in the drain through the installation of the high and medium weirs substantially reduced the drawdown effect of the drains on the groundwater table in transects C, D and F. Similarly, drawdown has reduced by the installation of the low weir for groundwater elevations measured in Transects H and I (Figure 7.23b). In contrast, the groundwater drawdown caused by the unweired section of drain adjacent to transect K remains pronounced.

Maintenance of the higher drain water levels by the weirs reduced the magnitude of the hydraulic gradient for groundwater flowing towards the drains, and in some instances reversed the direction of groundwater flow away from the drains. The magnitude of the hydraulic gradients and direction of flow for transects C and I are shown in Table 7.4.

**Table 7.4** Hydraulic gradients and flow directions for Transect C and I

Distance from drain (m)	Hydraulic gradient (+ flow to drain - flow away from drain)			
	Day 539	Day 673	Day 768	Day 813
Transect C				
0	0.000	-0.001	-0.006	0.001
10	0.000	0.000	0.003	0.003
20	0.002	0.002	0.001	0.001
50	0.000	0.000	0.000	0.000
90	0.000	0.001	0.000	0.000
Transect I				
0	0.019	0.008	0.008	0.005
10	0.010	0.007	0.004	0.004
20	0.001	0.001	0.001	0.000
50	0.000	0.000	0.000	0.000
90	0.001	0.000	0.000	0.000

Table 7.4 shows that at Transect C, maintenance of the drain water level at 0.0 m AHD (or higher in high flow periods) gives rise to very small hydraulic gradients, particularly

when the direction of groundwater flow is towards the drain. In some instances (e.g. days 673 and 768) the direction of groundwater flow is reversed so that water from the drain flows into the groundwater aquifer. At transect C, the low hydraulic gradient and periodic reversal of flow direction minimise the transport of pyrite oxidation products generated during the pre-weir drought period to the drain.

At transect I, the hydraulic gradient is in excess of an order of magnitude greater than that calculated for transect C. This is due to the lower water level maintained by the low weir (-0.7 m AHD). Throughout the post-weir monitoring period the groundwater flow was in the direction of the drain, indicating that the pyrite oxidation products entrained in the groundwater would be discharged to the East-west drain above the low weir. However, installation of the low weir has reduced the hydraulic gradient by an order of magnitude in comparison to the hydraulic gradient calculated during the pre-weir period (see Table 7.2). The reduction in the magnitude of the groundwater hydraulic gradient by the installation of the weir is significant when it is considered in terms of minimising the volume of pyrite oxidation products discharged into the drains and subsequently Broughton Creek. In effect, reduction of the groundwater hydraulic gradient attenuates the groundwater discharge hydrograph which in turn reduces the amount of pyrite oxidation products discharged into the drain per time period. The reduced volume of acidic products being discharged to Broughton Creek through the floodgates during low tide periods may be within the buffering or assimilation capacity of the Creek, thereby minimising environmental degradation. The reduced daily discharge of acidic products into the drain may be particularly helpful if modified floodgates are installed in conjunction with weirs to allow for controlled saline intrusion into the drains during high tide periods to neutralise some of the acidity discharged from the groundwater. A modified floodgate concept and worked example showing the benefits of controlled salt water intrusion is described in Chapter 13.

A three dimensional representation of the groundwater hydrology at the study site is shown in Figures 7.24 and 7.25 for days 538 and 768. The influence of the weirs in maintaining elevated groundwater tables is evident. At locations of the high weir (HW) and medium weir (MW) at 150 and 450 m along the North-south drain, the groundwater

is maintained at a higher elevation on the upstream or Northern side of the weir. The groundwater hydraulic gradient vectors show the direction of flow has changed from the pre-weir direction where groundwater flowed towards the drain to a North-south orientation where little or no groundwater discharges to the North-south drain.

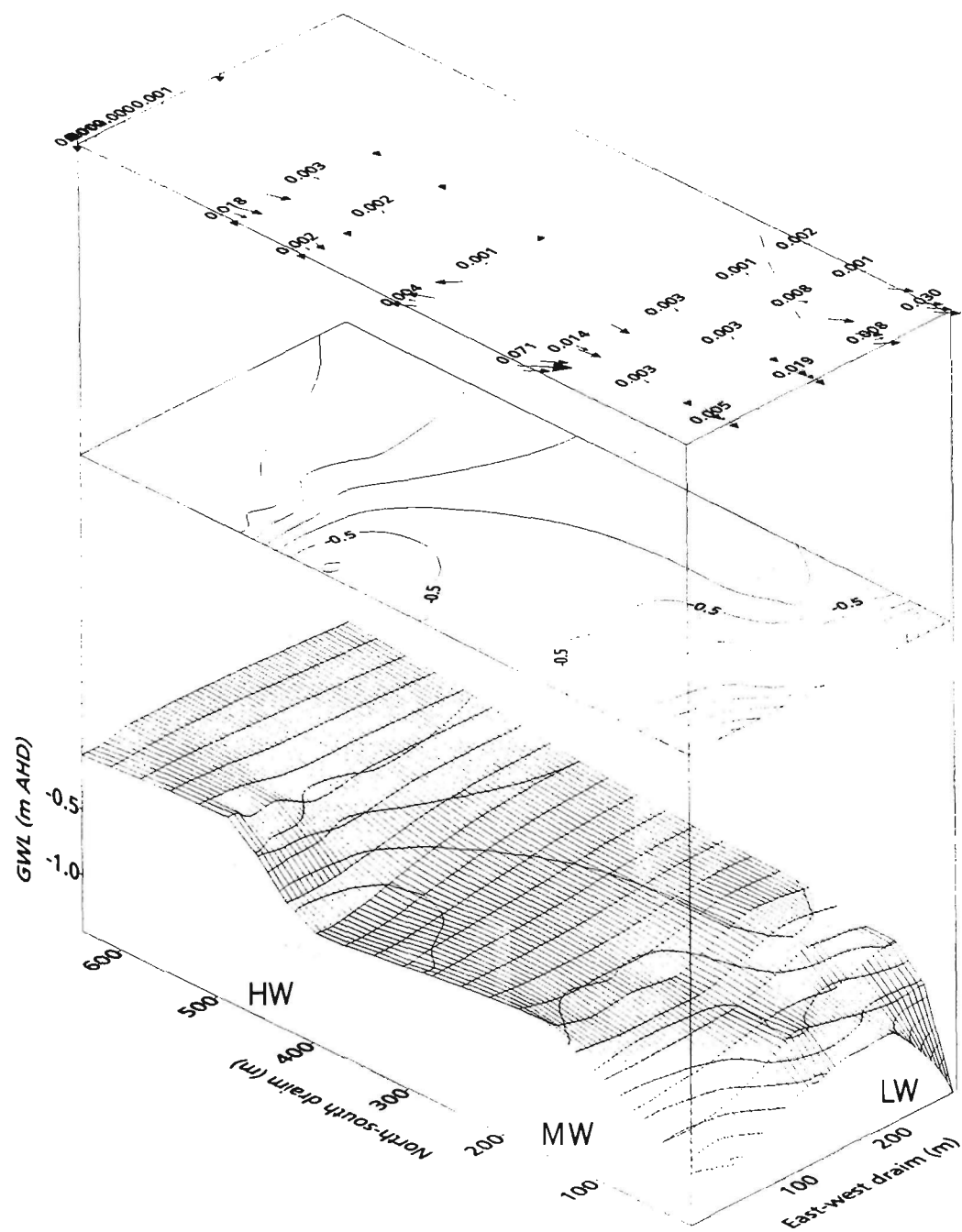


**Figure 7.24** Groundwater elevation profile at day 539

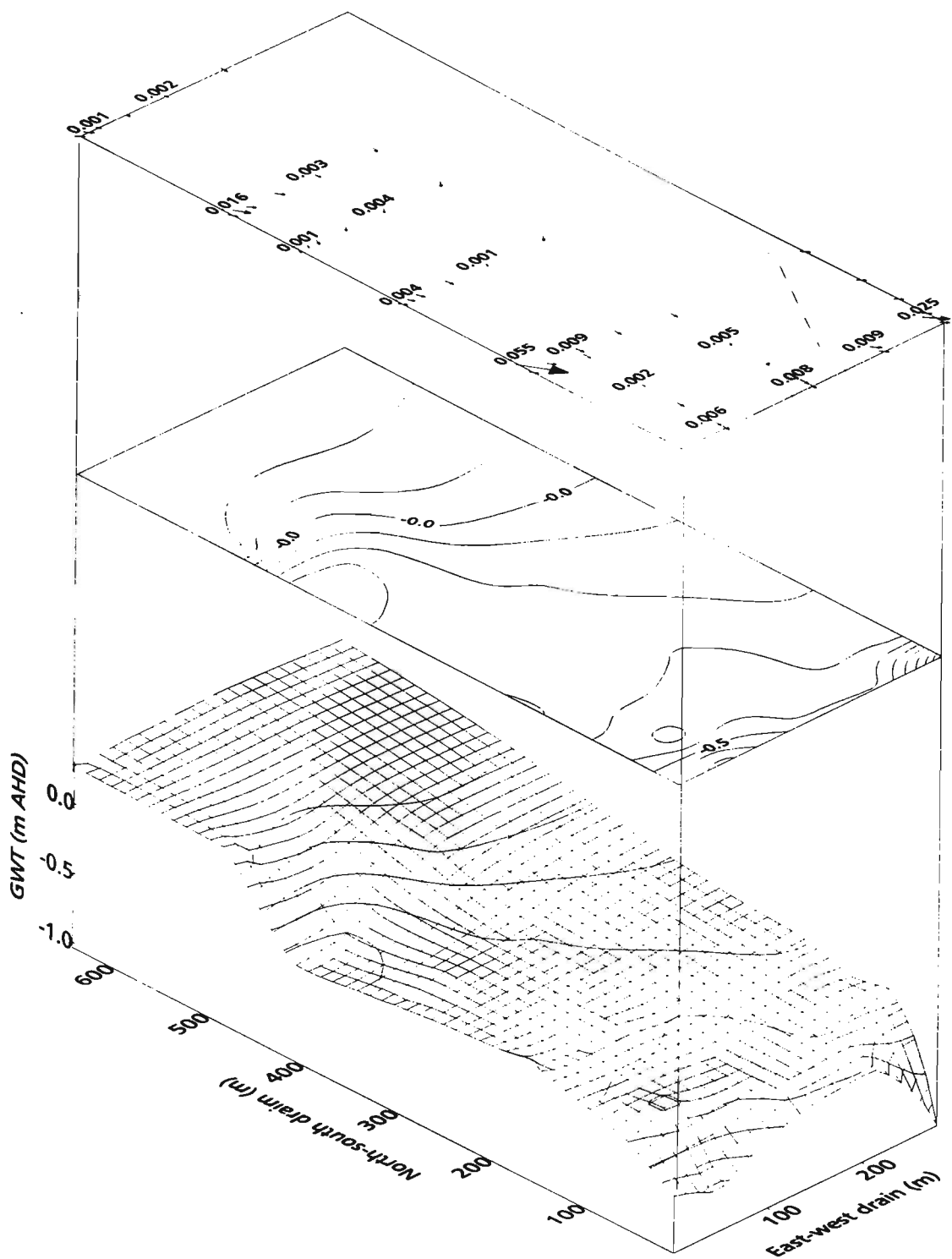


**Figure 7.25** Groundwater elevation profile at day 768

The only areas where a substantial departure to the direction of groundwater flow was observed along the North-south drain axis was adjacent to Transect E, where the prior stream channel creates a preferential flow path of groundwater discharge directly into the North-south drain. However, as shown in Figures 7.24 and 7.25, the influence of the

prior stream channel in changing the general orientation of the hydraulic gradients is limited to approximately 50 m distance from the drain.

As previously noted during the pre-weir period, at the junction of the North-south and East-west drains, groundwater elevation is lowered as a result of local drawdown from both drains. Again, this preferential local lowering of the groundwater table is facilitated by maintenance of different drain water levels either side of the medium weir.

Maintenance of the drain water level at -0.7 m AHD by the low weir in the East-west drain promoted the discharge of groundwater to the drain along this axis. As shown in Figures 7.24 and 7.25, the direction of the hydraulic gradient vectors is towards the East-west drain and the magnitude of the hydraulic gradient increases as the groundwater flows closer to the drain. However, as previously discussed, the magnitude of the hydraulic gradient is substantially lower after the installation of the low weir than under drain water levels controlled by the floodgate. This is clearly in evidence by the groundwater drawdown on the floodgate side of the low weir, adjacent to transect K. The water level in the drain below the low weir can be as much as 0.7 m lower than the water level maintained by the low weir. This created a substantial groundwater hydraulic gradient towards the East-west drain below the low weir. This is shown on Figures 7.24 and 7.25 where the groundwater flow divide has moved from the North-south/East-west drain interface for the pre-weir groundwater regime to the east of the low weir during the post-weir period. The large hydraulic gradients established by the low drain water level below the low weir gives rise to an increase in the groundwater hydraulic gradient and change in groundwater flow direction on the downstream side of the low weir. The drawdown caused by the low drain water level below the low weir caused the groundwater table to fall below the pyritic layer for much of the post-weir monitoring period.

7.7 Comparison between pre and post weir groundwater profiles

Figures 7.26 (a,b) compare the groundwater elevations at Transect C, F, I and K with respect to the elevation of the pyritic soil layer.

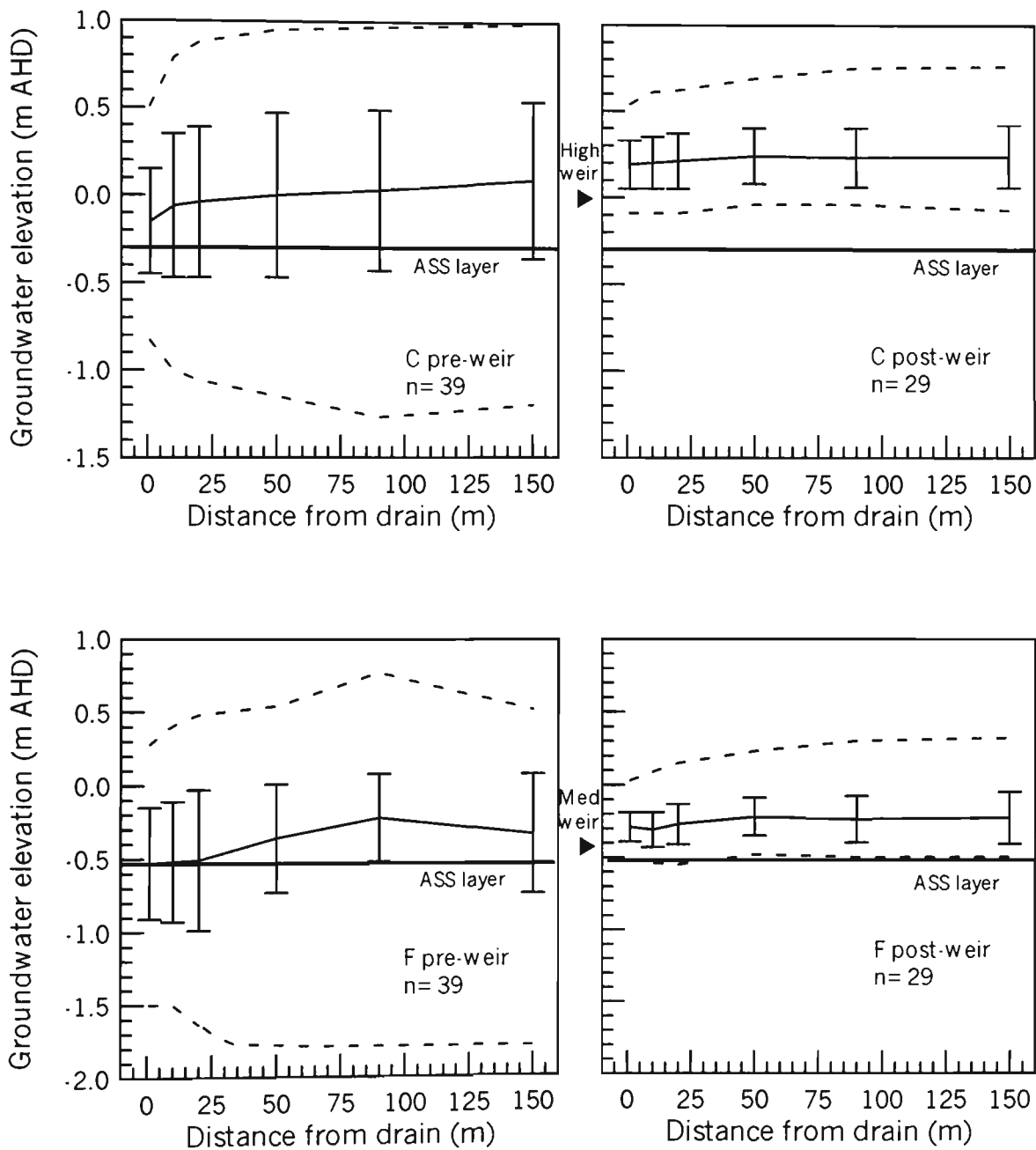


**Figure 7.26(a)** Comparison of the average groundwater elevation at transects C and F, also showing the maximum and minimum groundwater elevation and standard error bars.



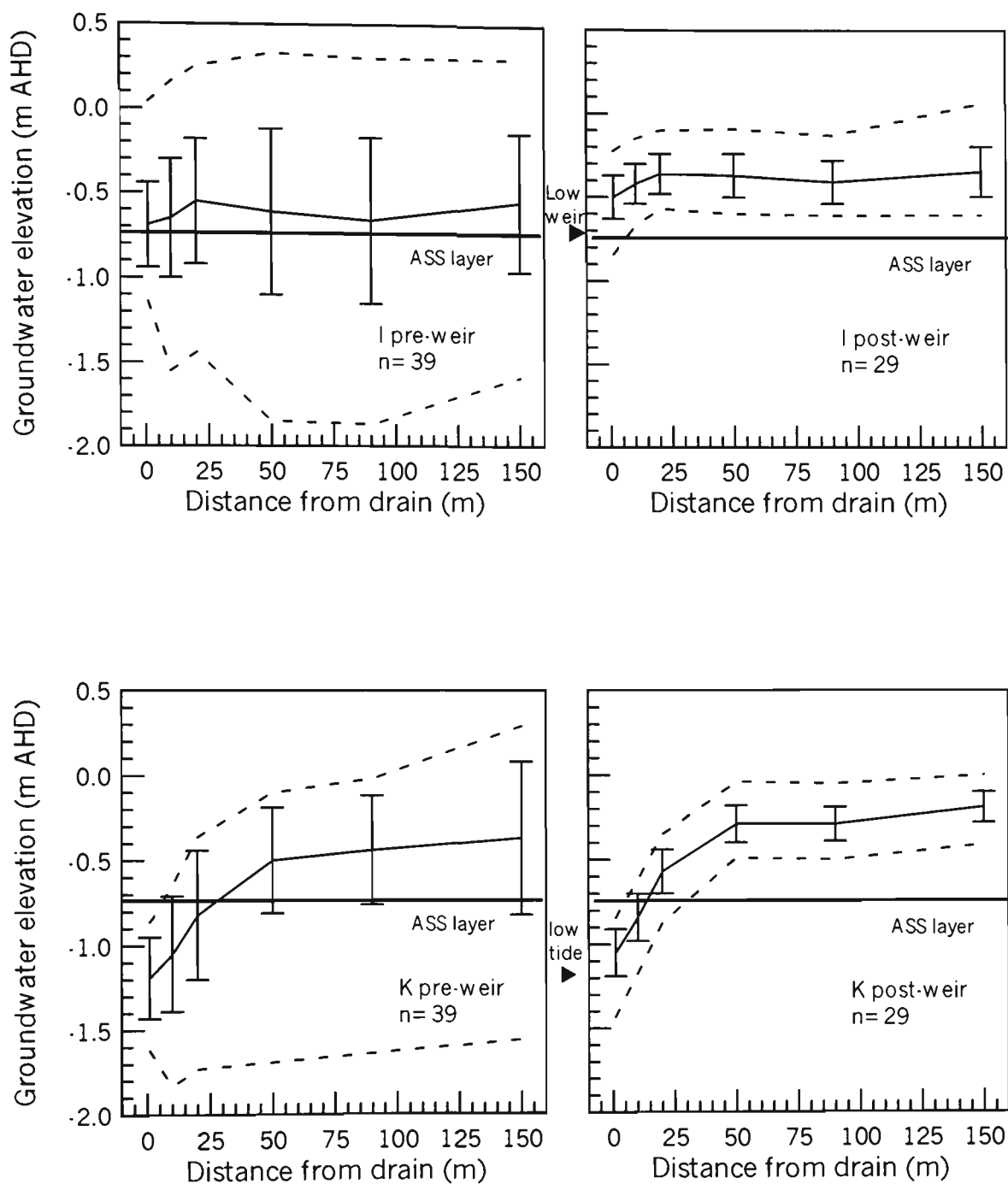


**Figure 7.26(b)** Comparison of the average groundwater elevation at transects I and K, also showing the maximum and minimum groundwater elevation and standard error bars.

The most rewarding difference in the groundwater regime as a result of the installation of the weirs is the general increase in elevation of the groundwater table. During the post-weir monitoring period the groundwater table was always at a higher elevation than

the pyritic soil in areas controlled by weirs. Table 7.5 shows that as the elevation of the water maintained behind the weirs increased, the difference in the average groundwater elevation close to the drain between the pre and post weir periods also increased. The increase in groundwater elevation was less pronounced at distanced further away from the drains. The higher groundwater elevations measured at transect K are as a results of generally wetter conditions during the post-weir period and an increase in lateral groundwater flow from surrounding areas influenced by the installation of the weirs. However, the increase in groundwater elevation at transect K close to the drain is less than for the other transects were weirs were installed.

**Table 7.5** Difference in average groundwater elevation after installation of the weirs.

	Piezometer distance from drain (m)					
Transect	1	10	20	50	90	150
C	0.32	0.24	0.24	0.23	0.18	0.14
F	0.24	0.22	0.24	0.15	-0.02	0.11
I	0.20	0.24	0.20	0.26	0.27	0.21
K	0.16	0.23	0.26	0.24	0.16	0.20

The general increase in the average elevation of the groundwater table offers substantial protection against the development of conditions conducive for pyrite oxidation in the sulfidic soil. Limiting groundwater drawdown by reducing the hydraulic gradient between the water level in the drain and the adjacent groundwater means that the primary process of lowering the groundwater table becomes evapotranspiration. The additional volume of groundwater maintained by the installation of the weirs would have to be removed by evapotranspiration in order for the groundwater table to fall into the pyritic soil. If a maximum rate of groundwater evapotranspiration of 13 mm/day is applied (see Figure 7.11), then the higher groundwater table maintained by the weirs provides up to an additional 25 days of protection against the onset of pyrite oxidising conditions, relative to that of the pre-weir drained state. Given that intervals where no rain falls with a 25 day period are relatively rare in coastal NSW, the additional volume

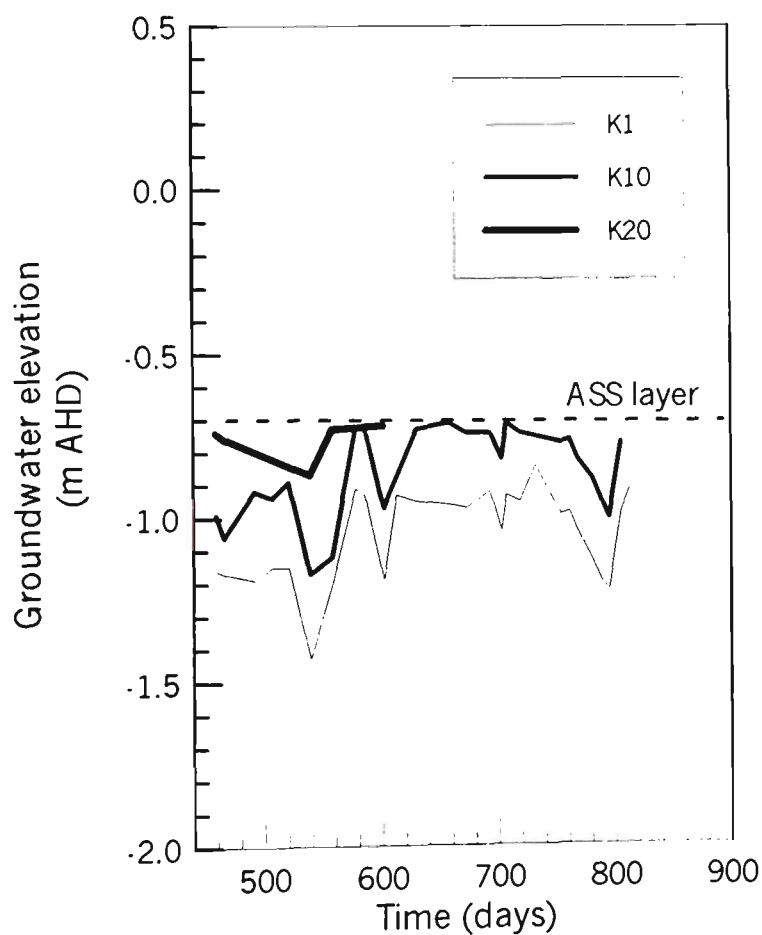
of groundwater stored in the soil profile offers substantial protection against the onset of acid generation.

The degree of groundwater elevation control offered by installation of the weirs was also encouraging. As shown in Figures 7.26 (a,b), the average groundwater elevation at 1 m distance from the drain is approximately 0.2 m higher than the elevation of the weir. Due to the small hydraulic gradients imposed by the installation of the weirs, the increase in the groundwater table elevation at greater distances from the drain was, on average, within 0.2 m of the groundwater table at 1 m distance from the drain. Importantly, for the climatic conditions that prevailed during the post-weir period (i.e. approximately the long term average monthly rainfall and evapotranspiration), the lowest recorded groundwater elevation at 1 m distance from the drain was less than 0.2 m below the elevation of the weir. Indeed, the set of observed groundwater tables within 1 standard deviation of the average groundwater elevation were always at a higher elevation than the water level maintained in the drain by the weir.

This shows that the elevation of the groundwater table could be readily manipulated by the application of adjustable weirs. For example, during periods of low rainfall the weir plate might be maintained in an elevated position so that a groundwater hydraulic gradient flowing away from the drain was maintained to ensure that the groundwater table was at its highest position. In contrast, during wet conditions the weir plate might be lowered to facilitate controlled groundwater drawdown for agronomic purposes. A related aspect of the weir-groundwater table performance was the maximum elevation of the groundwater table measured during the post-weir period. Figures 7.26 (a,b) show that the highest groundwater table elevations are lower than the maximum groundwater tables observed during the pre-weir period. Although this is related to the length of time between the groundwater observation and the recession of flood water, Figures 7.26 (a,b) demonstrate that the implementation of weirs do not reduce the ability of the surface soil to drain rapidly. Observations made in the field during flood events indicated that installation of the weirs had no effect on the rapid escape of excess surface water.

7.8 Oxidation of pyritic soil during the post-weir period

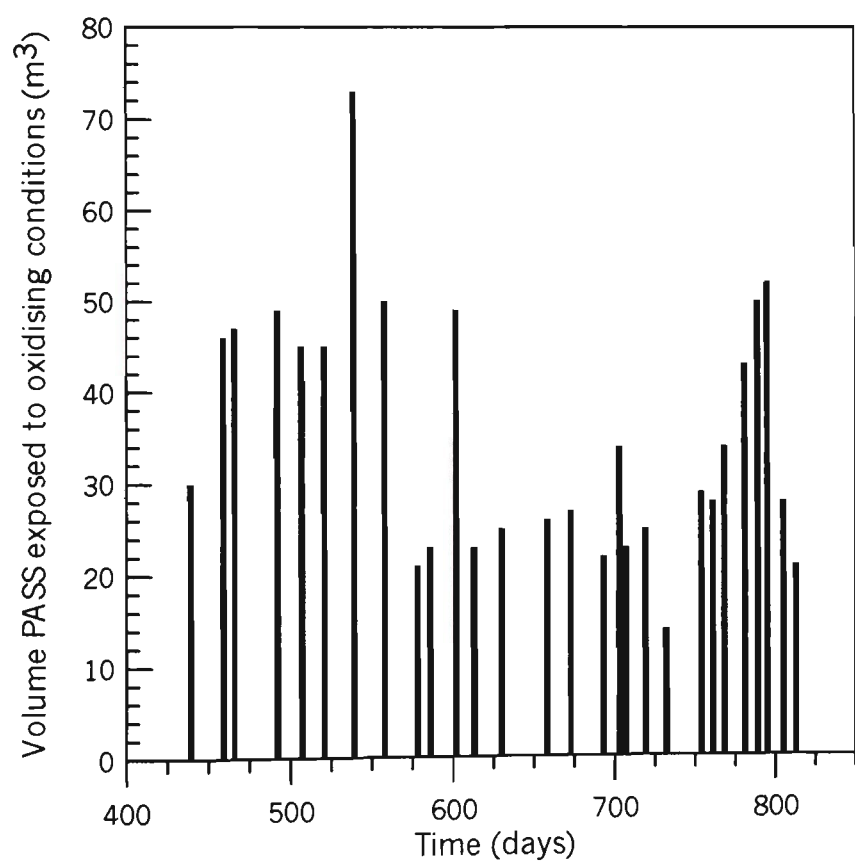
Reduction of the groundwater drawdown by the installation of the weirs, coupled with regular rainfall events, maintained the groundwater table in a position above the pyritic soil layer throughout the post-weir period for all piezometer transects located upstream of a weir. As shown in Figures 7.24 and 7.25, the only areas where substantial groundwater drawdown occurred was adjacent to Transect K, where the water level in the drain was controlled by the floodgate, rather than maintained by a weir. The length of time and the depth of the groundwater table below the pyritic soil layer (-0.7 m AHD) is shown in Figure 7.27.



**Figure 7.27** Period where the groundwater is below the upper boundary of the pyritic soil for Transect K.

Figure 7.27 shows that up to 0.7 m of pyritic soil was above the groundwater table at 1 m from the drain at Transect K during the post-weir period. As the distance from the drain increased, the effect of groundwater drawdown caused by the low water level in the drain reduced the amount of pyritic soil exposed to oxygen above the groundwater table. Figure 7.26 also shows that pyritic soil was always above the groundwater table in the first 10 m from the drain, irrespective of the volume of rainfall.

The preferential drawdown of the groundwater below the low weir caused a substantial volume of pyritic soil to be exposed to oxidising conditions. The volume of pyritic exposed during the monitoring period is shown in Figure 7.28.



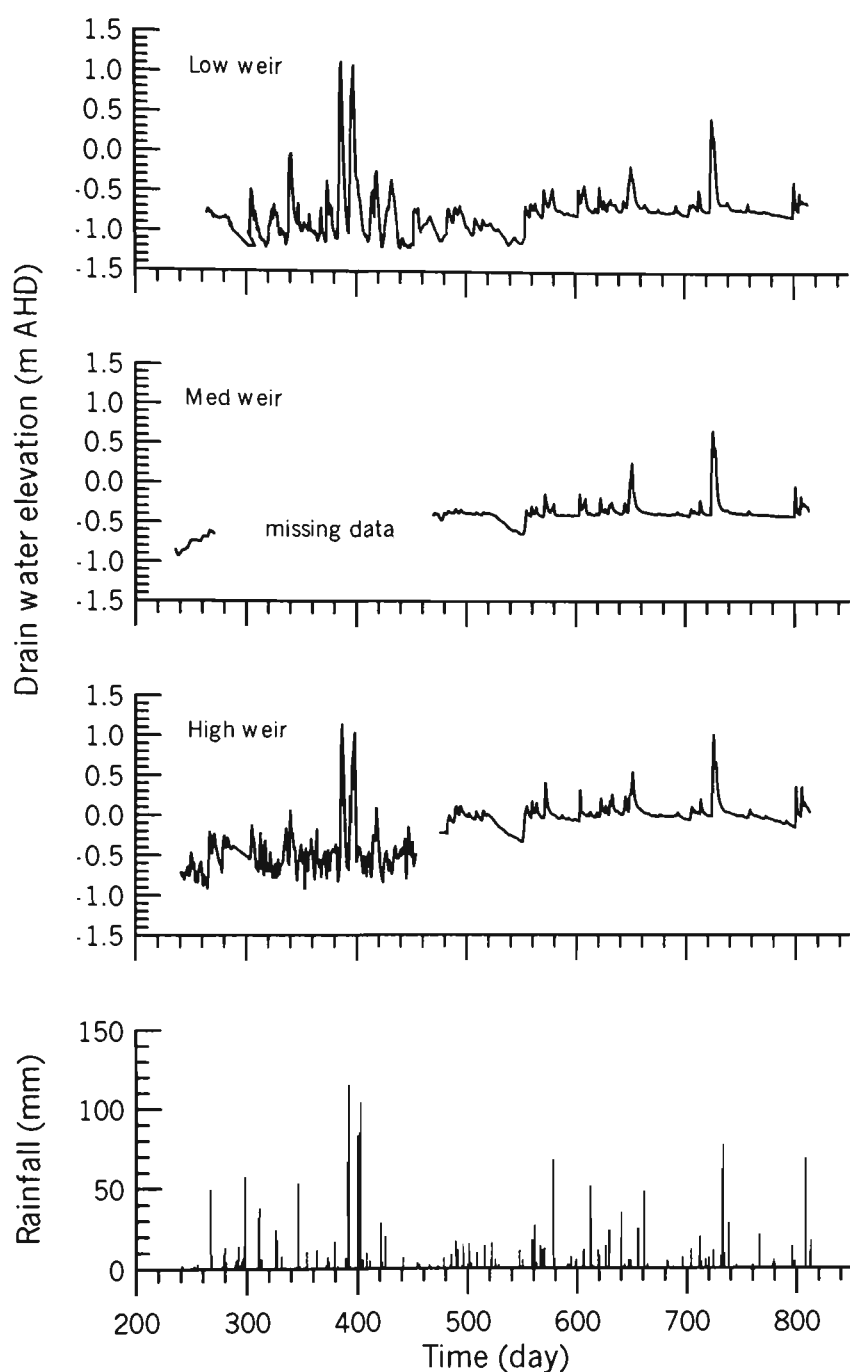
**Figure 7.28** Volume of pyritic soil exposed to oxidising conditions adjacent to Transect K during the post-weir period.

Figure 7.28 shows that between 15-74 m<sup>3</sup> of pyritic soil is exposed to oxidising conditions due to groundwater drawdown adjacent to Transect K. Although the volume of pyritic soil exposed during the post-weir period is considerably less than that exposed

during the pre-weir period (see Figure 7.22), the continual generation of acid coupled with the preferential flow of groundwater through this region may create an acidic problem in the East-west drain below the low weir. Figure 7.23(b) shows that the groundwater elevation fluctuates in accordance to the volume of rainfall. Where the groundwater elevation increases, pyrite oxidation products that have been generated in the volume of pyritic soil above the groundwater table will be entrained in the groundwater and rapidly discharged to the East-west drain.

## **7.9 Drain water level**

The water level in the drains measured by the automatic water level recorders is shown in Figure 7.29. The influence of rainfall on the drain water elevation is also shown in Figure 7.29.



**Figure 7.29** Drain water level measured at the weir locations.

The influence of the weir is illustrated after day 440 by the higher steady state elevation of the water level in the drain than that measured before the installation of the weirs. Prior to the installation of the weirs, the steady state drain water level was in excess of 0.5 m lower than after the installation of the weirs, primarily due to the operation of the floodgate at the junction of the drains and Broughton Creek. During the post-weir period, the steady state drain water levels were determined by the elevation of the weir plates, which were -0.7, -0.4 and 0.0 m AHD for the low, medium and high weirs,

respectively. The water levels were maintained at or above the elevations of the weir plates, except for the period between days 520-560 where low rainfall and high evapotranspiration lowered the drain water level by about 0.3 m below the weir elevation. The lowering of the drain water level by evapotranspiration and seepage into the surrounding groundwater aquifer during prolonged periods of low rainfall may reduce the effectiveness of the weirs in maintaining the adjacent groundwater table above the pyritic soil layer. However, the water level in the drains could be maintained through dry periods by the discharge of treated effluent into the drains or pumping brackish water from Broughton Creek. As shown in Figure 7.29, fluctuations in the water level in the drains are determined by the magnitude of rainfall events. However, the drain water level quickly receded after the cessation of intense rainfall. The installation of the weirs did not prolong the removal of excess surface water from the study site, demonstrating that the flood mitigation drain remain efficient at transporting flood waters.

Measurement of the drain water level enabled the daily discharge of water across the weirs to be calculated according to published weir discharge equations. The total volume of water discharged over the three weirs is shown in Table 7.6.

**Table 7.6** Total discharge across weirs

Weir	Volume of discharge ( x 10 <sup>6</sup> m <sup>3</sup> )
low	2.36
medium	1.19
high	0.25

The increase in the volume of water discharged over the weirs is due to the input of water from different parts of the catchment with respect to the placement of the weirs in the drainage system. The volume of water discharged over the low weir is approximately the total discharge through the floodgates. Therefore, the total volume of



acid discharged into Broughton Creek can be calculated by multiplying the daily volume of water discharged by the acidity of the water.

## **7.10 Conclusions**

The installation of weirs in flood mitigation drains was successful in terms of maintaining the groundwater table above the pyritic soil layer. Comparison of the drain water levels shows that the weirs maintain a higher steady state water level in the drains. The higher drain water level reduced the hydraulic gradients by about one order of magnitude and adjacent to the high and medium weirs changed the groundwater flow direction. Lower hydraulic gradients between the groundwater aquifer and the drain water level minimised groundwater drawdown which gave rise to the maintenance of higher groundwater tables after the installation of the weirs. Adjustment of the weir level relative to the elevation of the pyritic soil layer enables land managers to manipulate the groundwater table so that the pyritic soil is maintained under reducing conditions for as long as possible without compromising the performance of the flood mitigation drains.

Maintenance of the groundwater table above the pyritic layer is also influenced by climatic factors. As demonstrated during the pre-weir period, high daily rates of evapotranspiration and low rainfall led to very low groundwater tables that exposed large volumes of pyritic soil to oxidising conditions. Clearly, installation of weirs in flood mitigation drains cannot prevent lowering of the groundwater table by evapotranspiration. However, as further demonstrated in Chapters 8 and 10 by using numerical simulation techniques, maintenance of higher drain water levels can minimise both the length of time and the volume of pyritic soil exposed to oxidising conditions during drought events.

## **Chapter 8: Soil and water quality with respect to groundwater dynamics**

### **8.1 Introduction**

The change in soil chemistry, groundwater and drain water quality parameters that occurred with respect to the groundwater dynamics are described in this Chapter, which is divided into two parts. Firstly, the soil attributes that influence change in the soil chemistry are described. In this section, the temporal changes in soil pH and electrical conductivity are presented and discussed. These data show that the generation of acid is determined by the groundwater elevation, and that maintenance of high groundwater levels after pyrite oxidation does not substantially improve the chemical properties of the soil.

The second part of this Chapter describes changes in the groundwater and drain water chemical properties. The groundwater and drain water chemical properties that were measured at the site are described and related to the groundwater hydrology that influences the generation and transport of pyrite oxidation products. The evolution of groundwater toxicity from pyrite oxidation is explored, and an assessment technique for interpreting the general toxicity of groundwater after pyrite oxidation events is presented.

### **8.2 Change in soil chemistry**

The generation of pyrite oxidation products went through the greatest change at C90 in accordance with changes in the groundwater regime. In order to facilitate a concise

discussion, the soil pH and EC data presented in this Chapter are restricted to that measured at C90. Data from other sampling locations are presented in Appendix B.

The soil pH profiles measured during the course of the field trial are shown in Figure 8.1.

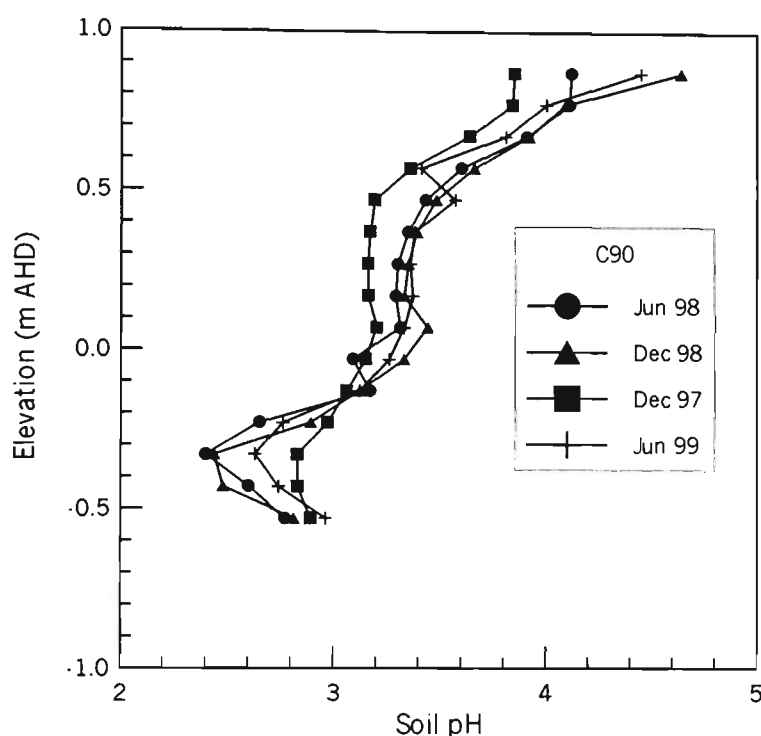


**Figure 8.1** Change in soil pH

From Figure 8.1, it is evident that there is very little change in the soil pH in the upper 1 m of the profile. In contrast, the soil pH changes considerably between -0.2 and -0.5 m AHD, according to the position of the groundwater table at the time of sampling. At the first sampling (Dec 97), the groundwater table had not yet fallen into the pyritic soil layer, and as such the soil pH was relatively high (approximately 2.8) which is indicative of pyritic soil that has undergone oxidation in the past but that has been buffered or diluted by higher groundwater tables for some time. However, as the groundwater table fell into the pyritic soil during the summer/autumn of 1998, the soil pH fell considerably. The June 1998 soil pH profile shows that acid generation had occurred in the upper 0.2 m (i.e., -0.3 to -0.4 m AHD) of the pyritic soil layer. At these depths the soil pH fell by approximately 0.5 of a pH unit from the initial measurements.

The smaller reduction in soil pH at -0.2 and -0.5 m AHD is probably due to the diffusion of acid entrained in the soil pore water rather than as a result of pyrite oxidation. The installation of the weirs and the maintenance of high groundwater tables that fully saturated the pyritic layer did not have an immediate effect on soil pH. As shown in Figure 8.1 for the December 1998 profile, the soil pH is unchanged in the pyritic soil layer, although in the highly acidic layer above the pyritic soil layer some increase in the soil pH has occurred, presumably as a result of acid transport and dilution. The soil pH below -0.0 m AHD began to increase and trend back towards the pH conditions measured at the beginning of the trial by December 1999. Although some increase in the soil pH (approximately 0.3 unit) was measured in the pyritic soil that had undergone oxidation during the drought period of low groundwater tables, the maintenance of high groundwater tables throughout the second half of 1998 and all of 1999 did not facilitate a substantial improvement in the soil pH.

As similar soil chemical evolutionary process was observed for the soil EC as for soil pH. The soil EC profiles measured during the course of the field trial are shown in Figure 8.2.

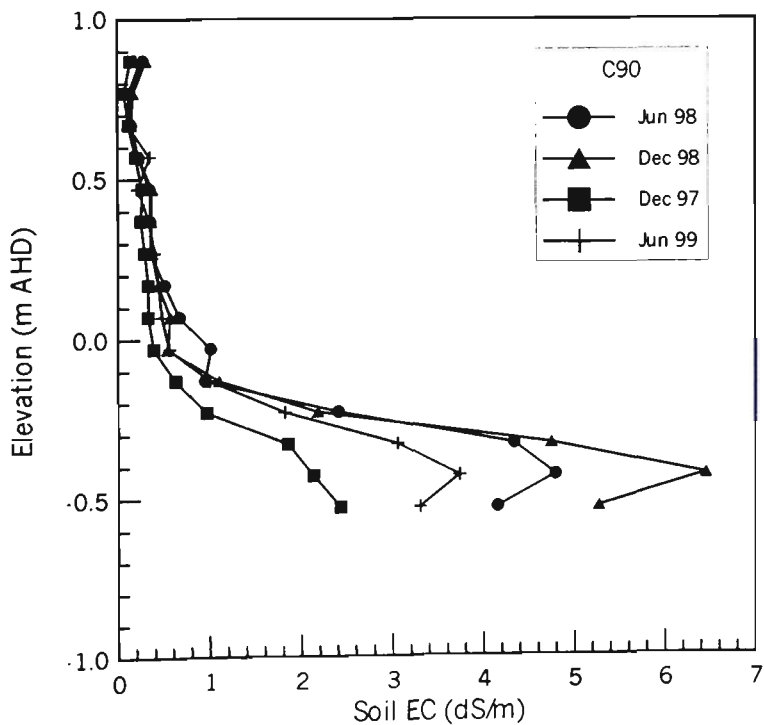


**Figure 8.2** Change in soil electrical conductivity

The soil EC is a function of the concentration of dissolved solids present in the soil water. As such, the soil EC is sensitive to the generation of pyrite oxidation products. At the initial soil sampling, an increase in the soil EC was measured from approximately 0.2 dS/m in the top soil to in excess of 2 dS/m in the highly acidic part of the soil profile in and slightly above the pyritic layer. This indicates that pyrite oxidation had occurred in the past. However, the initial soil EC data from the lower part of the soil profile also suggests that substantial transport and dilution of the pyrite oxidation products has occurred since the last pyrite oxidation event. A large increase in the soil EC was measured in June 1998 relative to that measured in December 1997. This is due to the generation of pyrite oxidation products during the period of low groundwater tables. The elevated soil EC was maintained as a result of entrainment and re-distribution of the pyrite oxidation products in the groundwater in the December 1998 measurements. However, maintenance of high groundwater tables throughout 1999 began to dilute the concentration of pyrite oxidation products in the soil, thereby lowering the soil EC. As shown later in this Chapter, measurement of EC can be a useful indicator of the concentration of pyrite oxidation products in the soil or groundwater, and can give some indication of the evolutionary stage before/during or after pyrite oxidation events.

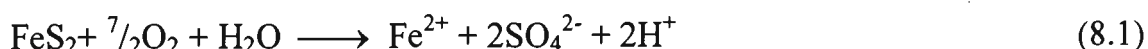
### **8.3 Change in water quality parameters associated with pyrite oxidation**

The chemical composition of groundwater in acid sulfate soil areas is largely determined by the generation of acidic products from the oxidation of pyrite during periods where the groundwater elevation has fallen below the pyritic soil layer. Other factors such as the ability of the soil to neutralise acidity, the dissolution of acidic iron and aluminium minerals that have previously formed as a consequence of severe acidification caused by pyrite oxidation, and the exchange of cations between the soil solution and the soil cation exchange sites also influence the geochemistry of the groundwater. Limiting, or at least managing, the generation of acid and other pyrite oxidation products, such as; dissolved sulfate, iron and aluminium, is the primary goal for the development of acid sulfate soil management strategies. Given this goal, the success of acid sulfate soil management techniques can be monitored by measuring the concentration of acidic

pyrite oxidation products in the groundwater. A range of dissolved aqueous ionic species were regularly monitored in groundwater and drain water samples that were collected on a monthly basis through both the pre and post-weir periods. The water quality parameters measured include: basic cations ( $\text{Ca}^{2+}$ ,  $\text{Mg}^{2+}$ ,  $\text{Na}^+$ ,  $\text{K}^+$ ), acidic cations ( $\text{Al}^{3+}$  and  $\text{Fe}^{2+}$ ), anions ( $\text{Cl}^-$  and  $\text{SO}_4^{2-}$ ), pH and electrical conductivity. In order to facilitate a concise discussion of the groundwater chemistry during the trial, the groundwater quality data presented in this Chapter are restricted to that measured at piezometer C90. Data from other piezometers are presented in Appendix B.

### 8.3.1 *Generation of pyrite oxidation products in groundwater*

The adequacy of strategies designed to prevent or minimise pyrite oxidation through works that control the elevation of the groundwater table can be assessed by analysis of the pyrite oxidation products entrained in the groundwater. The generation of pyrite oxidation products occurs according to Equation (8.1).



As such, evaluation of the concentration of  $\text{Fe}^{2+}$ ,  $\text{SO}_4^{2-}$  and  $\text{H}^+$  can provide a measure of the success of groundwater management techniques. Given the low pH of the samples, all Fe measured was assumed to be in the  $\text{Fe}^{2+}$  form. The concentrations of these analytes, as well as the groundwater pH, during the course of the field trial is shown in Figure 8.3.

As shown in Chapter 7, the groundwater regime that was monitored during the study can be divided into four distinct parts, namely;

1. an initial period of high groundwater tables and hydraulic gradients under the influence of deep flood mitigation drains,

2. a period of low groundwater tables caused by high rates of evapotranspiration and low rainfall,
3. re-establishment of (1) until the commissioning of the weirs at day 440,
4. maintenance of high groundwater tables and low hydraulic gradients in areas bound by drains with elevated water levels caused by the weirs.

Given these changes in the groundwater regime, the evolution of the concentration of pyrite oxidation products and other related chemical attributes of the groundwater can be assessed.

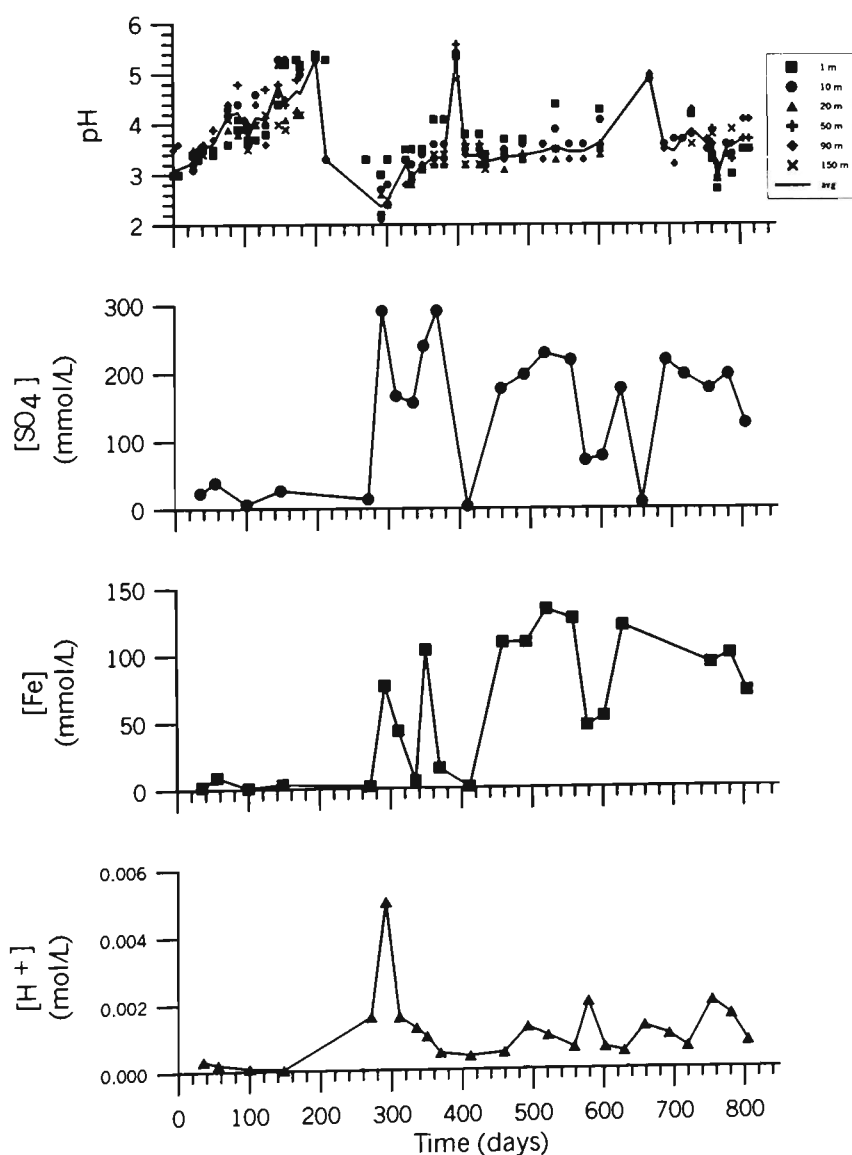


**Figure 8.3** Concentration of pyrite oxidation products at C90.

At the beginning of the monitoring period, even though the groundwater table was located above the pyritic soil, the average groundwater pH was less than 3.5 in all transects. This is indicative of acidification caused by previous pyrite oxidation, and subsequent transport and re-distribution of acidic pyrite oxidation products. However, the groundwater pH quickly began to improve. This is due to two separate phenomena. In the first 100 days of the field trial, a substantial volume of rainfall fell, including two events that caused surface flooding. The flooding transported soluble acid to the surface where it was removed from the site. After the period of heavy rainfall, the groundwater table began to recede rapidly. Between days 100-270, a severe rainfall deficit caused the groundwater table to fall well below the pyritic soil layer. During this period, the groundwater pH rose above 5, and in some instances increased to 6.5.

As described in Chapter 6, the pyritic subsoil at approximately 2 m depth below the surface has a substantial shell layer. Similarly, as the pyritic soil at this depth is unlikely to have undergone any substantial oxidation, a high concentration of basic cations is likely to be present on the cation exchange sites. Both the shell and exchangeable basic cations combine to neutralise any acidity entrained in the groundwater, thereby increasing its pH. This relatively high groundwater pH persisted until rainfall caused the groundwater table to rise through the pyritic soil that had undergone oxidation during the drought. Rising groundwater entrained the acidity generated by pyrite oxidation, causing the groundwater pH to fall rapidly. At the breaking of the drought near day 270, groundwater pH fell to 2.5-3.5 across all piezometer transects. At C90, the lowest groundwater pH of the whole monitoring period was recorded (pH 2) after these drought breaking rains. The magnitude of the pH fall was proportional to the depth of pyritic soil exposed to oxidising conditions during the drought. As described in Chapter 7, the groundwater table fell most below the pyritic layer in the north-eastern part of the site. This is reflected in the lowest values of pH 2 at transects C and D. Where the groundwater exposed a smaller volume of pyritic soil to oxidation (e.g., transects H-K), then the pH fell to approximately 3. From days 270-400, the groundwater pH increased to approximately 4. During this period, heavy rainfall transported acid from the soil to the drain via hydraulic gradients that flowed towards the drains. In addition, rainfall diluted the concentration of acid in the groundwater.



Both these processes increased the groundwater pH. On days 415 and 424, heavy rainfall caused surface flooding which once again removed acid from the groundwater thereby resulting in higher pHs. However, the receding groundwater quickly returned to approximately pH 4. The commissioning of the weirs on day 440, and the subsequent maintenance of the groundwater table above the pyritic layer did not appreciably improve the groundwater pH through to the end of the monitoring period. In the absence of heavy rainfall causing surface flooding, the groundwater pH remained stable approximately at pH 4.

As  $\text{pH} = -\log[\text{H}^+]$ , the concentration of  $\text{H}^+$  in the groundwater followed the opposite trend to that of pH. At the beginning of the monitoring period, the  $\text{H}^+$  concentration was less than 0.0005 mol/L. This increased to a maximum of approximately 0.005 mol/L at C90 at day 270 after the period of pyrite oxidation, with all other piezometers recording  $\text{H}^+$  concentration in excess of 0.001 mol/L. Although rainfall caused short periods where the acidity was either diluted or removed from the groundwater, an equilibrium  $\text{H}^+$  concentration between 0.001-0.002 mol/L remained in the groundwater through the remainder of the trial.

The concentration of dissolved  $\text{SO}_4^{2-}$  was very high throughout the trial period. At the start of the trial, the  $\text{SO}_4^{2-}$  concentration was approximately 30 mmol/L, indicating that pyrite oxidation was likely to have taken place at this site in the past. To place this  $\text{SO}_4^{2-}$  concentration in some perspective, ANZECC (1992) recommend that stock water (the least rigorous assessment criteria they publish) contain no more than 10 mmol/L of sulfate. The  $\text{SO}_4^{2-}$  concentration remained between 10-40 mmol/L through the first 270 days of the trial, even through the drought period where low groundwater tables caused pyrite oxidation to occur. This was due to the pyrite oxidation products being maintained within the soil water held under suction above the groundwater table. After rainfall, sulfate was entrained in the rising groundwater. After day 270, the highest  $\text{SO}_4^{2-}$  concentration of 300 mmol/L was recorded at C90; however, at the other piezometer locations the  $\text{SO}_4^{2-}$  concentration was less than 150 mmol/L. High rainfall events periodically lowered the  $\text{SO}_4^{2-}$  concentration in the groundwater, but the  $\text{SO}_4^{2-}$

concentration remained at the elevated levels achieved immediately after day 270 for the remainder of the trial.

During the first 270 days of the trial, the Fe concentration remained between 0.5-15 mmol/L. The high concentration of Fe in the groundwater cannot be attributed to recent pyrite oxidation as the groundwater table was higher than the pyritic soil at the start of the monitoring period. Similarly, in the period where low groundwater tables fell below the pyritic soil during the first 270 days of the trial, the Fe liberated by pyrite oxidation was held within the soil matrix under suction, which made it unavailable to the groundwater. Given these relationships to the groundwater regime during the first 270 days, the concentration of Fe in the groundwater is likely to be controlled by the precipitation or dissolution of Fe minerals. This equilibrium can be maintained by either:  $\text{Fe}(\text{OH})_3$  precipitating as the pH of high-Fe groundwater increases as a result of  $\text{H}^+$  consuming reactions (e.g., neutralisation by shelly deposits), or the dissolution of previously precipitated  $\text{Fe}(\text{OH})_3$  where the concentration of Fe is reduced through mass transport or reaction with pyrite. Dubrovsky *et al.* (1984) suggested that similar concentrations of Fe dissolved in groundwater within pyritic tailings empondments are maintained by the dissolution or precipitation of solid Fe phases.

After day 270, where the groundwater rose through the pyritic soil that had undergone oxidation between days 100-270, the concentration of Fe measured in the groundwater increased markedly. The concentration of Fe, measured at C90 at day 291, was 76 mmol/L. The Fe concentration increased to a maximum of 133 mmol/L by day 521. The increase in the Fe concentration was less pronounced at other piezometer locations, with maximum Fe concentrations of 20, 48, 44, 3, 8, 6, and 5 mmol/L measured at C10, F10, F90, I10, I90, K10 and K90, respectively. As previously discussed for groundwater pH, the magnitude of the maximum Fe concentration in the groundwater was proportional to the depth of pyritic soil exposed to oxidising conditions during the drought.

The elevated concentrations of Fe appeared to be maintained in the groundwater from day 270 onwards. This Fe may be from a number of sources, predominantly pyrite oxidation and the dissolution of previously precipitated iron sulfate or oxy-hydroxide minerals. As described in Equation (8.1),  $\text{Fe}^{2+}$  is a product of pyrite oxidation, and will be available for transport when high groundwater conditions return after pyrite oxidation events. Where the depth of pyrite exposed to oxidising conditions is reasonably deep (in this case in excess of 1 m), oxygen may be able to diffuse a considerable lateral distance from macropores into the pyritic soil. As the saturated hydraulic conductivity of the pyritic soil matrix is very low, the transport of  $\text{Fe}^{2+}$  from the soil matrix to the soil solution may be slow, depending upon the elevation of the groundwater table by rainfall. As a result,  $\text{Fe}^{2+}$  is supplied to the groundwater over a considerable length of time. The concentration of dissolved Fe in the groundwater can be assessed by the examination of the ratio of Fe to  $\text{SO}_4$ . Equation (8.1) shows that for every mole of pyrite that is oxidised, 1 mole of Fe and 2 moles of  $\text{SO}_4$  are produced, giving a Fe: $\text{SO}_4$  ratio of 0.5. Figure 8.4 shows the Fe: $\text{SO}_4$  ratio in groundwater.

Until the breaking of the drought at day 270, the Fe: $\text{SO}_4$  ratio was less than 0.5 in all piezometers. This suggests that Fe was being lost from the groundwater, relative to the concentration of dissolved  $\text{SO}_4$ , probably via precipitation to solid phase, Fe minerals. van Breeman (1985), Dubrovsky *et al.* (1984) and Drever (1997) referred to the loss of dissolved Fe by this path. In the period immediately after day 270 when the pyrite oxidation products are entrained in the groundwater, a Fe: $\text{SO}_4$  ratio close to 0.5 should be expected. However, within the 50 day period proceeding day 270, the Fe: $\text{SO}_4$  ratio was much lower than expected, in some instances falling to less than 0.01. A possible explanation for this low Fe: $\text{SO}_4$  ratio is the formation of siderite,  $\text{FeCO}_3$ . Siderite can precipitate where there is sufficient  $\text{CO}_3^{2-}$  (from shell), and where pH 6-8 and pe -5-0 (Drever, 1997). These conditions were present during the period when low groundwater tables contributed to pyrite oxidation between days 100-270, particularly within transects F-K where substantial shell deposits were observed at depth within the pyritic soil (see Chapter 6). If siderite was precipitated during the period of low groundwater tables, then Fe produced by pyrite oxidation may have been lost from the soil water, giving rise to a lower than expected Fe: $\text{SO}_4$  ratio.

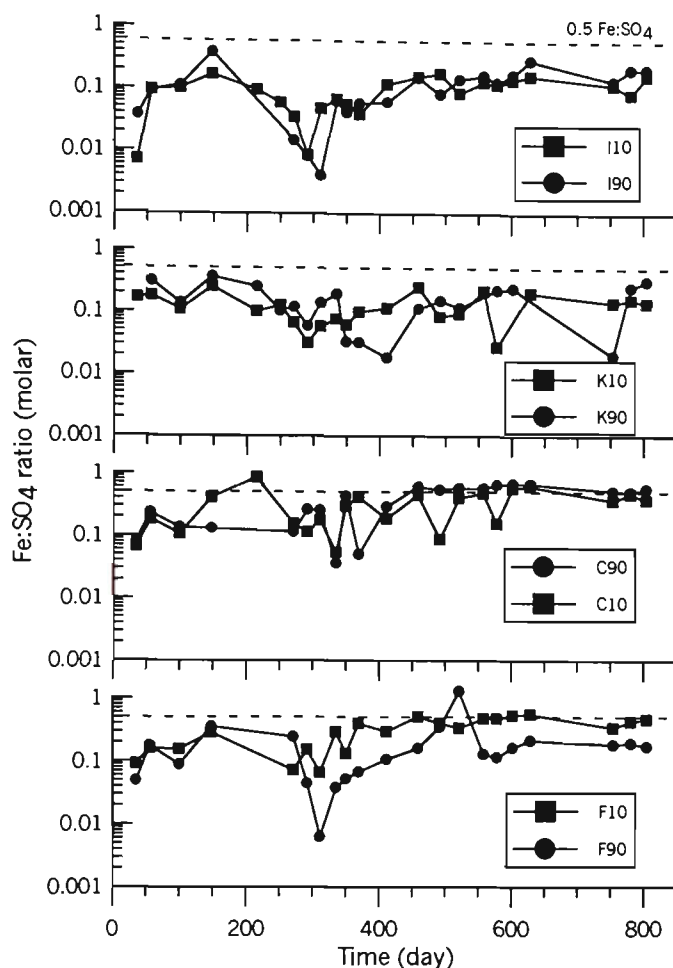


**Figure 8.4** Fe:SO<sub>4</sub> ratio in groundwater

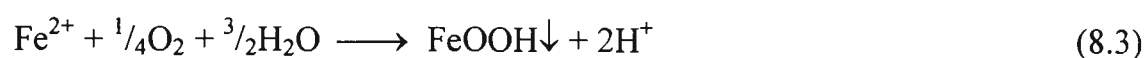
In the piezometers where very low groundwater tables led to groundwater pH < 3 from day 270 onwards (e.g., C10, C90, F10), the Fe:SO<sub>4</sub> ratio increased from the lower than expected values to an equilibrium of about 0.5 from approximately day 450. Low groundwater pH (<6) causes the dissolution of siderite according to:



which would release dissolved Fe<sup>2+</sup> into the groundwater. If the precipitation/dissolution reaction involving siderite does occur, the concentration of dissolved Fe in the groundwater would be controlled by the kinetics of these reactions. The relatively slow increase in the Fe:SO<sub>4</sub> ratio from the low experienced after day 270

to the 0.5 equilibrium at day 450 could be due to a kinetically controlled siderite dissolution reaction. An alternative source of dissolved Fe in the groundwater is from the dissolution of previously precipitated iron minerals.

In contrast, where less acidic conditions prevailed after day 270 (i.e., transects I and K), the pH-pe conditions may be more conducive to the precipitation of Fe minerals from the groundwater. When the groundwater fluctuates close to the surface through relatively porous, well aerated soil,  $\text{Fe}^{2+}$  may oxidise according to:

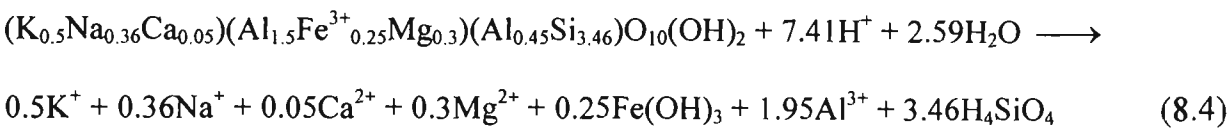


Equation (8.3) shows that as  $\text{Fe}^{2+}$  is oxidised and precipitated, the concentration of Fe dissolved in the groundwater will be reduced. Schwertmann and Fitzpatrick (1992) also suggested that organic ligands have a high affinity for dissolved Fe, causing its removal from the groundwater. As shown in Chapter 6, the organic carbon concentration in the top soil layer is high (>5-8%). When rainfall causes the groundwater table to flow through the organic rich top soil layer, Fe may form complex minerals with organic matter, removing it from solution.

### 8.3.2 *Evolution of the groundwater chemistry*

The oxidation of pyrite generates large quantities of acidic products, but the environmental toxicity of acidic groundwater is determined by the concentration of  $\text{Al}^{3+}$  and the total acidity as measured by the sum of all the acidic cations; namely  $\text{H}^+$ ,  $\text{Fe}^{2+}$  and  $\text{Al}^{3+}$ . The concentration of  $\text{Al}^{3+}$  and the sum of all the acidic cations is shown in Figure 8.5.

The supply of dissolved  $\text{Al}^{3+}$  at low groundwater pH may be regulated by two distinct mechanisms. The first mechanism is the dissolution of aluminosilicate clays as they are attacked by acid. Nriagu (1978) showed that the acid hydrolysis of the mineral illite, which is common in estuarine clays, proceeds according to:



This reaction shows that for every mole of illite that undergoes hydrolysis, 1.95 moles of  $\text{Al}^{3+}$  are made available for uptake by the groundwater. In contrast, at low pH and high sulfate activities, Nordstrom (1982) showed that the concentration of  $\text{Al}^{3+}$  in solution is controlled by the solubility of a variety of  $\text{Al-OH-SO}_4$  minerals. At  $\text{pH} < 3.3$ , Nordstrom (1982) showed that jurbanite may be the most stable Al mineral that controls the concentration of  $\text{Al}^{3+}$  in solution. A more complete review and assessment of the importance of Al minerals in controlling the concentration of  $\text{Al}^{3+}$  in solution is given in Chapter 13.

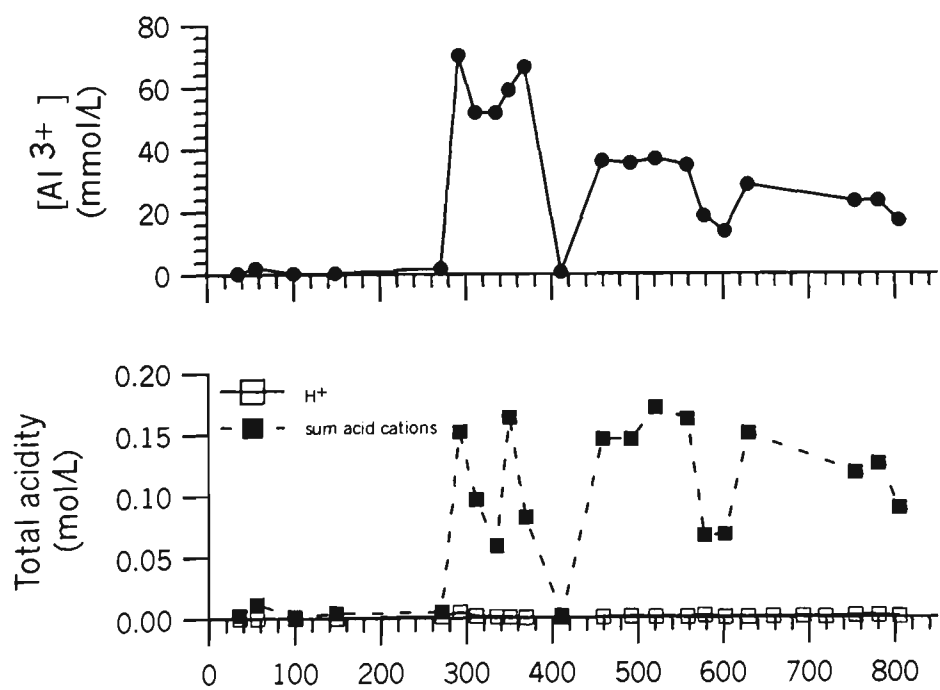


**Figure 8.5** Groundwater  $\text{Al}^{3+}$  and total acidity concentration.

During the initial 270 days, the  $\text{Al}^{3+}$  concentration in the groundwater decreased from about 5 to 0.1 mmol/L as the pH increased from 3.5 to 5. However, after day 270 when the groundwater pH fell to less than 3, the concentration of dissolved  $\text{Al}^{3+}$  rose by approximately 2 orders of magnitude. The maximum  $\text{Al}^{3+}$  concentration measured in the groundwater was 70 mmol/L at C90. ANZECC (1992) recommend that for marine waters, the concentration of dissolved  $\text{Al}^{3+}$  should not exceed 0.02 mmol/L where  $\text{pH} < 6.5$ . Clearly, the concentration of dissolved  $\text{Al}^{3+}$  in the groundwater was extremely high, and posed a particular threat to estuarine health once it is discharged into drains and rivers (Nordstrom, 1982; Sammut *et al.*, 1996).

The maintenance of high  $\text{Al}^{3+}$  concentrations measured in the groundwater from day 270 may be attributed to the dissolution of both alumino-silicate clay and  $\text{Al-OH-SO}_4$  minerals. As suggested by Equation (8.4), the hydrolysis of aluminosilicate clays at low pH gave rise to the liberation of high concentrations of  $\text{Al}^{3+}$  soon after the groundwater rose through the oxidised pyritic soil. Figure 8.5 shows that the maximum  $\text{Al}^{3+}$  was recorded between days 270-370, which correspond to the lowest groundwater pH. However, as the groundwater pH came to an equilibrium at approximately pH 4 after subsequent heavy rainfall events and maintenance of high groundwater tables, the  $\text{Al}^{3+}$  concentration did not fall to the levels previously experienced during the pre-weir period when similar groundwater pH was measured. The relatively high  $\text{Al}^{3+}$  concentration may be caused by the dissolution of previously precipitated aluminium minerals that are increasingly soluble as pH increases from about 3.3 (Nordstrom, 1982).

In many instances, pH is used to assess change in groundwater acidity. However, as explained by Hicks *et al.* (1999), pH underestimates the total acidity concentration by not considering other acidic dissolved cations such as  $\text{Fe}^{2+}$  and  $\text{Al}^{3+}$ . Given the low pH of the groundwater, all measured Fe was assumed to be in the  $\text{Fe}^{2+}$  form. The total acid concentration (i.e., sum  $\text{H}^+$ ,  $\text{Al}^{3+}$  and  $\text{Fe}^{2+}$  concentration) in the groundwater is shown in Figure 8.5. The concentration of total groundwater acidity was very high, with C90 approaching a maximum of 0.2 mol/L. The contributions of  $\text{Fe}^{2+}$  and  $\text{Al}^{3+}$  to the total

acidity concentration were significant. At these locations, the  $H^+$  concentration measured by pH represented only a small fraction of the total acidity in the groundwater. Hicks *et al.* (1999) suggested total acidity should be assessed by acid-base titration rather than relying on pH. However, given the low equilibrium pH value of the groundwater after day 270, the extra effort of using laboratory titrations rather than pH measurements could only be justified if acid neutralisation management techniques were to be employed.

As demonstrated above, the oxidation of pyrite generates acidic reaction products as well as the liberation of other toxic materials such as  $Al^{3+}$ . However, the relative contribution of these elements to the overall groundwater chemistry was not uniform throughout the monitoring period. The chemistry of the groundwater can be assessed by reviewing the relative contribution of three of the major constituents of the groundwater affected by the generation of acidic condition by pyrite oxidation, namely;  $SO_4^{2-}$ ,  $Fe^{2+}$  and  $Al^{3+}$ . The evolution of elements in the groundwater is shown in Figure 8.6.

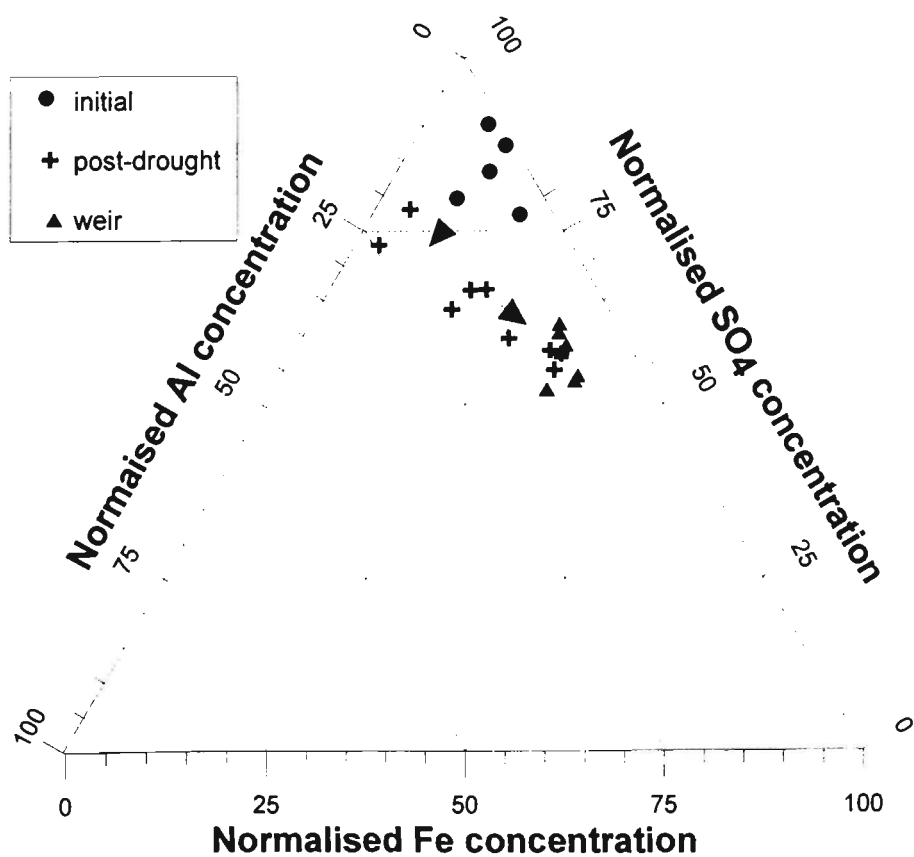


**Figure 8.6** Evolution of groundwater chemistry at C90



In the initial period up until day 270, the composition of the groundwater was dominated by residual sulfate from previous pyrite oxidation episodes. Sulfate contributed about 80-85% of the ionic composition of the groundwater during this period. In contrast, the relative contribution of both  $\text{Fe}^{2+}$  and  $\text{Al}^{3+}$  was 10-15% and  $< 5\%$ , respectively. Given the increasing pH of the groundwater, the necessary conditions for the precipitation of Fe and Al hydroxy-sulfate minerals were met, resulting in a loss of potentially toxic  $\text{Al}^{3+}$  and  $\text{Fe}^{2+}$  from the groundwater system.

The relative contribution of the groundwater ionic constituents went through an appreciable change once the pyrite oxidation products that had been generated during days 100-270 were entrained in the rising groundwater during the post-drought period. As shown in Figure 8.7, the proportion of relatively benign  $\text{SO}_4^{2-}$  fell to 65%, whereas the contribution of  $\text{Al}^{3+}$  and  $\text{Fe}^{2+}$  rose to 20% and 15%, respectively. Of particular concern was the relative abundance of  $\text{Al}^{3+}$  in the groundwater. This showed that conditions necessary for the liberation of  $\text{Al}^{3+}$  from clays and/or aluminium sulfate minerals occurred during the pyrite oxidation process. Numerous authors (e.g., Sammut *et al.*, 1995; Nordstrom, 1982) have indicated that elevated levels of  $\text{Al}^{3+}$  pose a threat to the environment, particularly for gilled organisms.

The relative composition of the groundwater chemistry evolved further with the maintenance of high groundwater tables after the installation of the weirs. The relative contribution of  $\text{Al}^{3+}$  fell from its maximum at day 270 to an equilibrium of 7% at the end of the monitoring period, indicating that  $\text{Al}^{3+}$  was being lost from the groundwater. As shown in Figure 8.5, the concentration of  $\text{Al}^{3+}$  in the groundwater underwent a gradual decrease from day 440. The loss of  $\text{Al}^{3+}$  can probably be attributed to the precipitation of Al-OH- $\text{SO}_4$  minerals. In contrast, the relative importance of  $\text{Fe}^{2+}$  in the groundwater increased to approximately 30%. The evolutionary change in the relative contribution of  $[\text{Al}^{3+}]$  to  $[\text{Fe}^{2+}]$  in the groundwater during the monitoring period is also demonstrated in Figure 8.7. The prevalence of  $\text{Fe}^{2+}$  in the groundwater posed a different threat to the environment than well documented effects of  $\text{Al}^{3+}$ . ANZECC (1992) does

not provide guideline concentrations for the concentration of Fe in marine waters, but  $\text{Fe}^{2+}$  entrained in groundwater can be transported to drains and/or waterways where it later oxidises, forming  $\text{H}^+$ . The generation of this acidity can form at a distance from its source, depending on the pH-pe conditions of the receiving water, thereby posing a pH related threat in downstream environments.

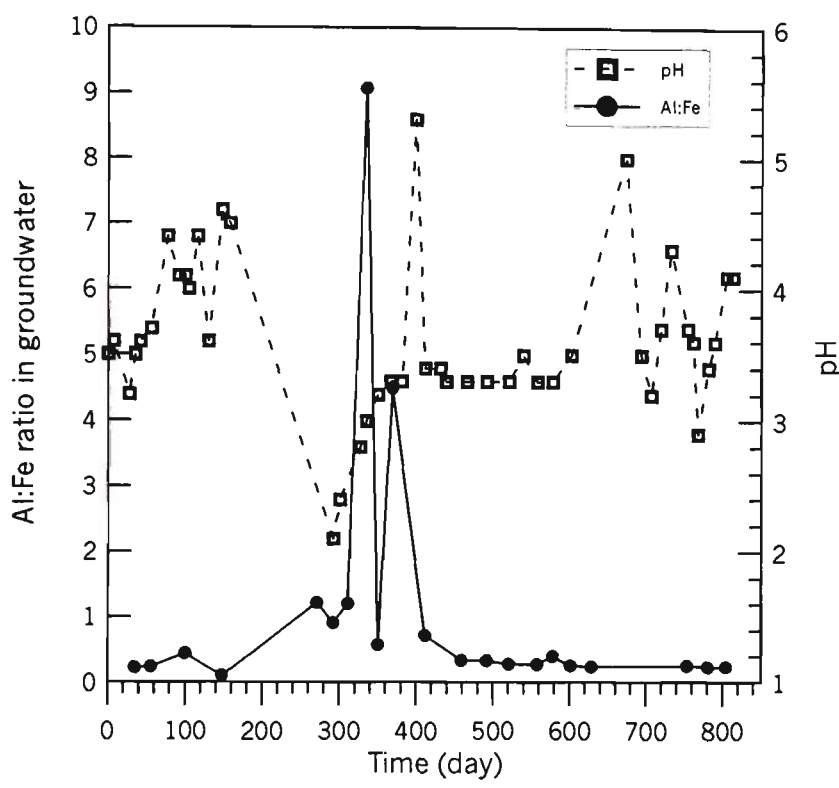


**Figure 8.7** The  $\text{Al}^{3+}:\text{Fe}^{2+}$  molar ratio in groundwater at C90.

The evolutionary change in the relative contribution of  $\text{Al}^{3+}$  and  $\text{Fe}^{2+}$  to the groundwater chemistry has significant environmental protection implications. It is generally acknowledged that  $\text{Al}^{3+}$  is the more toxic acidic cation, particularly to gilled organisms. As shown in Figure 8.7, the Al:Fe molar ratio in the groundwater only increased above 0.3 during the period immediately after pyrite oxidation, and only persisted whilst  $\text{pH} < 3.3$ . The pH dependency of the magnitude of the Al:Fe ratio suggests that the concentration of  $\text{Al}^{3+}$  was controlled by the stability of jurbanite,  $\text{Al}(\text{SO}_4)(\text{OH})$ . Nordstrom (1982) showed that in  $\text{SO}_4^{2-}$  rich water, jurbanite is metastable at  $\text{pH} < 3.3$ , but at higher pH other Al-OH-SO4 minerals such as alunite,  $\text{KAl}_3(\text{SO}_4)_2(\text{OH})_6$ , and gibbsite,  $\text{Al}(\text{OH})_3$ , tend to control the concentration of  $\text{Al}^{3+}$  in solution. Although the

theoretical geochemistry indicates that jurbanite may play a role in controlling the concentration of  $\text{Al}^{3+}$  in the groundwater, no actual measurements of jurbanite in acid sulfate soils have been reported.

The evolution of chemical constituents in the groundwater from the dissolution of clays under acidic conditions is further demonstrated in Figure 8.8 by the increase in basic cation concentration after pyrite oxidation.

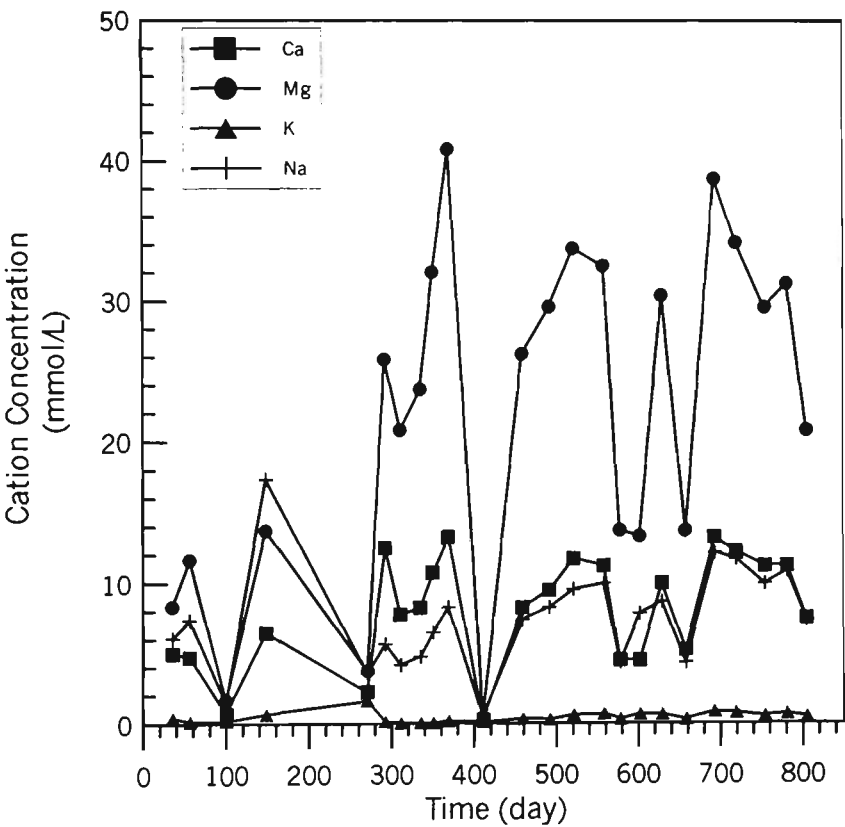


**Figure 8.8** Concentration of basic cations measured at C90.

Equation (8.4) shows that under acidic conditions, marine clays can hydrolyse, thereby liberating basic cations. Willett *et al.* (1992) also showed that other heavy metal cations can be dissolved into the groundwater in toxic and bio-available forms.

The basic cation suite is dominated by  $\text{Ca}^{2+}$ ,  $\text{Mg}^{2+}$  and  $\text{Na}^{+}$ . At locations C10, C90, F10 and F90, the concentration of basic cations was  $\text{Mg} > \text{Ca} > \text{Na} > \text{K}$ . In contrast, at I10, I90,

K10 and K90, Na replaces Mg as the dominant dissolved cation. Although the concentrations and relative composition of the basic cations were reasonably uniform throughout the monitoring period, an increase in the cation concentrations was detected after day 270 when highly acidic groundwater conditions provided a favourable environment for clay hydrolysis.

As discussed in Chapter 6, the evolutionary sequence of the soil profile at the site may have involved the deposition of the estuarine sediments at locations C and F slightly before the deposition of similar sediments closer to Broughton Creek (i.e., locations I and K). In keeping with their depositional environment, the estuarine sediments may have been predominantly Na-clays; however, with prolonged freshwater flushing, Na may have been replaced with Mg dissolved in runoff or from soil erosion from higher in the catchment. As such, the soils at C and F may have a higher concentration of Mg relative to Na than the soils at I and K. Upon acid dissolution, the release of cations would reflect the cation composition of the constituent clays.

The supply of  $\text{Ca}^{2+}$  may also be derived by the dissolution of clays, however, the concentration of  $\text{Ca}^{2+}$  attached to the cation exchange sites down all the soil profiles described in Chapter 6 was often greater by an order of magnitude than those of the other basic cations. During the dissolution of clay minerals,  $\text{Al}^{3+}$  is released into solution in much greater concentrations than other cations. The high concentration of  $\text{Al}^{3+}$  may exchange with  $\text{Ca}^{2+}$  from the cation exchange site and release  $\text{Ca}^{2+}$  into solution.

In contrast to Ca, Mg and Na, the concentration of K was very low at all times. This is somewhat unexpected given that Equation (8.4) indicates that substantial amounts of  $\text{K}^+$  should be liberated during the clay hydrolysis if the dominant mineral was illite. A possible explanation of the low  $\text{K}^+$  concentration may be the precipitation of jarosite and alunite. Both these minerals require  $\text{K}^+$  and  $\text{SO}_4^{2-}$ , in conjunction with  $\text{Fe}^{3+}$  and  $\text{Al}^{3+}$ , for the precipitation of jarosite and alunite, respectively, at low pH. As described in Chapter 6, jarosite was observed in and immediately above the pyritic soil. Willett and

Walker (1982) reported jarosite concentrations of up to 240 mmol/kg in pyritic soils that have undergone oxidation at a nearby location. The necessary conditions for the formation of these minerals are met when the basic cations are made available to the groundwater from clay dissolution. Hence, the precipitation of K-SO<sub>4</sub> minerals under acid condition may account for the low concentration of K<sup>+</sup> in the groundwater.

8.3.3 Assessment of pyrite oxidation by anion concentration

Although chloride is not a pyrite oxidation product, or an ion that is a potential threat to maintenance of environmental quality, the concentration of chloride in the groundwater offers some insight into the pyrite oxidation process. The concentration of chloride in the groundwater during the monitoring period is shown in Figure 8.9.

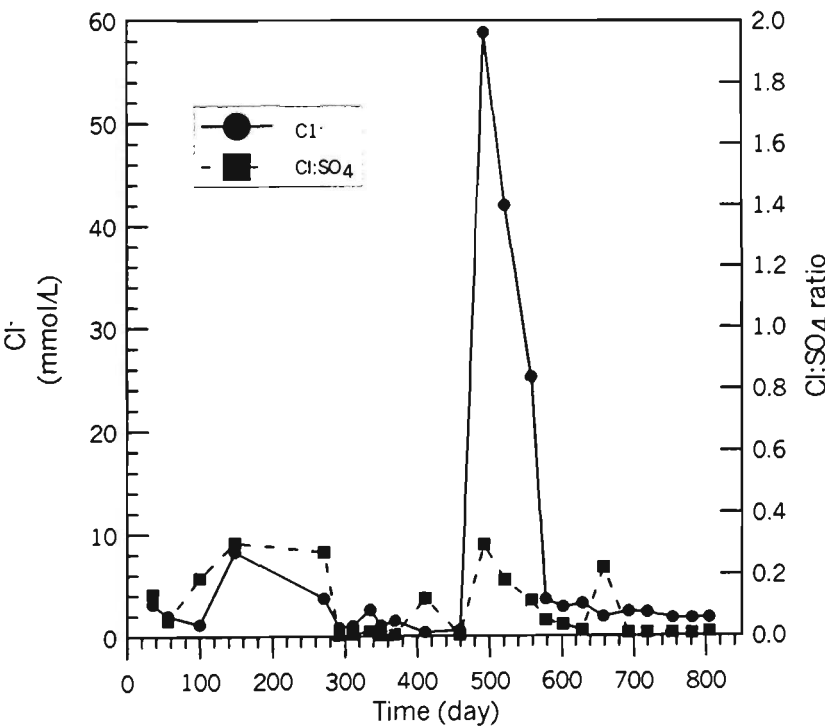


**Figure 8.9** Chloride concentration and Cl:SO<sub>4</sub> ratio at C90.

Chloride is a conservative species in groundwater. This is demonstrated in Figure 8.9, where the concentration of  $\text{Cl}^-$  in the groundwater changes very little. The concentration of  $\text{Cl}^-$  in the groundwater generally remained less than 10 mmol/L. The rapid rise and decline in  $\text{Cl}^-$  concentration between days 450-550 may have been due to  $\text{Cl}^-$  entrained in floodwater from the heavy rainfall events preceding this period. However, as shown in Figure 8.9, excess  $\text{Cl}^-$  was quickly flushed from the groundwater system.

The low chloride concentrations in the groundwater indicated that any  $\text{Cl}^-$  that would have been present during the deposition of the pyritic and other estuarine sediments have been removed by freshwater flushing. Similarly, the low  $\text{Cl}^-$  concentration confirms that there was little salt water intrusion for either Broughton Creek or the flood mitigation drains. This is expected given the low lateral saturated hydraulic conductivity of the clayey sediments at mean tide level.

Mulvey (1983) proposed that the  $\text{Cl}:\text{SO}_4$  ratio of groundwater could be used to determine whether pyrite oxidation had occurred. On a mass basis, the  $\text{Cl}:\text{SO}_4$  ratio of sea water is about 7.2. Mulvey (1983) suggested that where the  $\text{Cl}:\text{SO}_4$  ratio falls below 2, then this is indicative of landscapes affected by pyrite oxidation. Figure 8.9 shows that the  $\text{Cl}:\text{SO}_4$  ratio of the groundwater measured at the study site was always less than 1, and therefore falls within the criterion of an acid sulfate soil affected area. However, the  $\text{Cl}:\text{SO}_4$  ratio is a poor indicator of pyrite oxidation where substantial freshwater inputs occur. In freshwater bodies, the  $\text{Cl}:\text{SO}_4$  ratio is usually less than 7.2 in the absence of pyrite oxidation.

#### *8.3.4 Evaluation of the status of groundwater chemistry after pyrite oxidation*

A variety of techniques are available for the assessment of water quality (e.g., ANZECC 1992 guidelines) and for the determination of past pyrite oxidation (e.g.,  $\text{Cl}:\text{SO}_4$  ratio proposed by Mulvey, 1993). However, these assessment criteria do not provide

information with respect to where on the evolutionary pathway, from the initial entrainment of pyrite oxidation products into rising groundwater after a period of low groundwater tables, through to the attainment of groundwater with lower concentrations of toxic elements after ongoing neutralisation or dilution. As shown in Figure 8.6, the relative proportions of  $\text{Al}^{3+}$ ,  $\text{Fe}^{2+}$  and  $\text{SO}_4^{2-}$  describe an evolution of the groundwater chemistry during different groundwater phases that control pyrite oxidation. The assessment of the groundwater chemistry can be simplified from Figure 8.6 by plotting the Al:Fe ratio against the Cl:SO<sub>4</sub> ratio as shown in Figure 8.10.

Figure 8.10 shows that the classification of the groundwater chemistry can be divided into three distinct parts, each reflecting the composition of the dissolved cations that are most environmentally damaging (i.e., the Al:Fe ratio), and the anion balance of the groundwater (i.e., the Cl:SO<sub>4</sub> ratio), which can give an indication of the length of time or amount of flushing since pyrite oxidation has occurred. The most toxic groundwater composition is shown in area 1, where the Al:Fe ratio > 2 indicating that the groundwater is enriched with  $\text{Al}^{3+}$  that is likely to be in a toxic form as the pH must be less than 3.3. In addition, the Cl:SO<sub>4</sub> ratio is less than 0.15, which indicates that the groundwater is enriched with  $\text{SO}_4^{2-}$  from recent pyrite oxidation. At this stage there has not been sufficient opportunity for dilution of the groundwater by heavy rainfall events or groundwater flow away from the site of pyrite oxidation to reduce the concentration of  $\text{SO}_4^{2-}$  in the groundwater. As such, area 1 which is bound by the Al:Fe ratio > 2 and Cl:SO<sub>4</sub> ratio < 0.15 is indicative of the groundwater composition stage after a pyrite oxidation event.

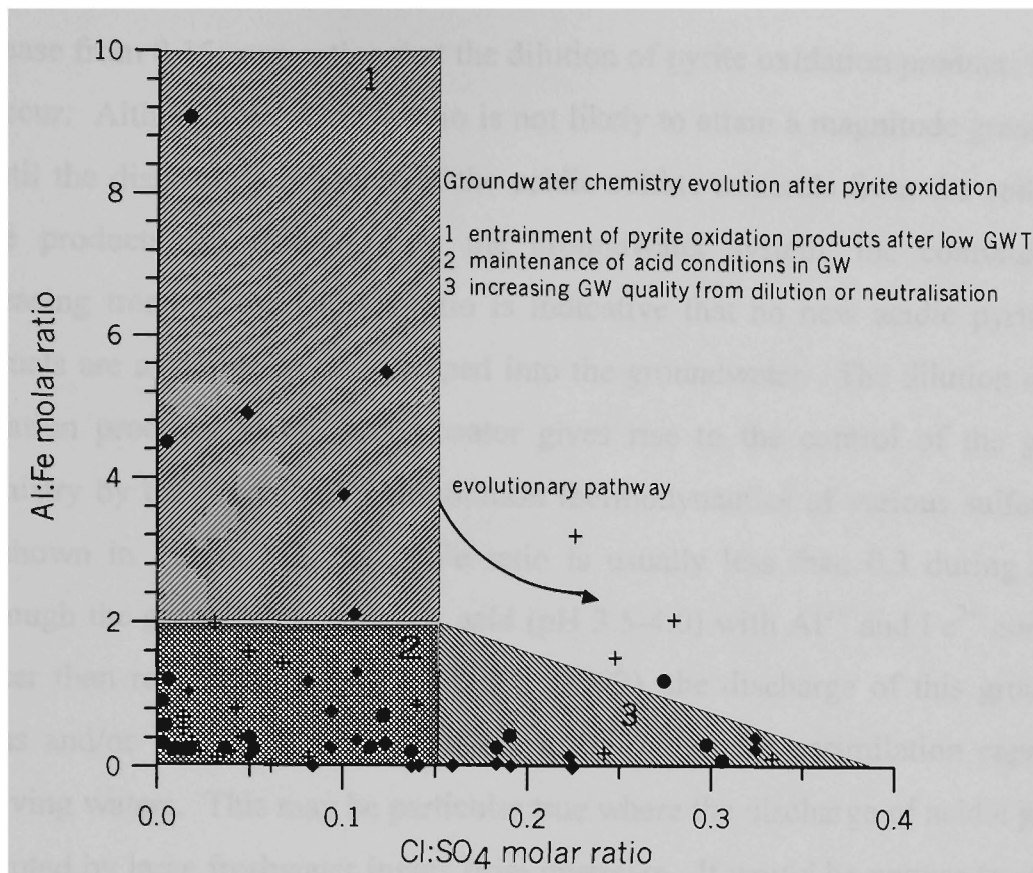


**Figure 8.10** Assessment techniques for evolutionary change in groundwater chemistry

The next stage in the evolution of the groundwater chemical regime after a pyrite oxidation event is defined by area 2. In this zone, there has been little opportunity for export of the pyrite oxidation products through groundwater flow or dilution from rainfall, as indicated by  $\text{Cl}:\text{SO}_4 < 0.15$ . However, internal buffering within the soil/groundwater continuum has resulted in the reduction of the Al:Fe ratio to less than 2. As described above, this is indicative of the increase in groundwater pH from less than 3.3, where the necessary conditions for the loss of  $\text{Al}^{3+}$  from the groundwater due to the precipitation of  $\text{Al-OH-SO}_4$  minerals takes place. Although the Al:Fe ratio is still reasonably high within area 2, the decreasing magnitude of the  $\text{Al}^{3+}$  concentration indicates that discharge of this groundwater to nearby drains and/or waterways may not pose such an environmental threat as groundwater from area 1.

The evolution of the groundwater to the conditions described within area 3 pose the least threat to the environment. Within area 3, there is a tendency for the  $\text{Cl}:\text{SO}_4$  ratio to



increase from 0.15, suggesting that the dilution of pyrite oxidation products is beginning to occur. Although the Cl:SO<sub>4</sub> ratio is not likely to attain a magnitude greater than 1 or 2 until the dissolution products of the acidic sulfate minerals from the soil occurs and these products are flushed from the groundwater system, the continuation of an increasing trend in the Cl:SO<sub>4</sub> ratio is indicative that no new acidic pyrite oxidation products are available to be entrained into the groundwater. The dilution of the pyrite oxidation products in the groundwater gives rise to the control of the groundwater chemistry by the precipitation/dissolution thermodynamics of various sulfate minerals. As shown in Figure 8.7, the Al:Fe ratio is usually less than 0.3 during this period. Although the groundwater remains acid (pH 3.5-4.0) with Al<sup>3+</sup> and Fe<sup>2+</sup> concentrations greater than recommended by ANZECC (1992), the discharge of this groundwater to drains and/or waterways is more likely to be within the assimilation capacity of the receiving waters. This may be particular true where the discharge of acidic groundwater is diluted by large freshwater inputs from upstream. It would be unwise to consider that groundwater with the characteristics defined by area 3 poses negligible threat to the environment, but rather area 3 is indicative of the groundwater conditions controlled by the dissolution of acidic minerals caused by historical pyrite oxidation, and not the generation of extremely toxic groundwater quality conditions caused by pyrite oxidation.

A simple field based interpretation of the groundwater status can also be achieved by the measurement of electrical conductivity (EC). The EC increased in accordance with the concentration of the major dissolved ions in the groundwater such as SO<sub>4</sub><sup>2-</sup>, Al<sup>3+</sup> and Fe<sup>2+</sup>. Interpretation of the EC data is aided by its relationship with the total dissolved solids (TDS) of the groundwater. The relationship between groundwater EC and TDS (i.e. the sum of all SO<sub>4</sub><sup>2-</sup>, Cl<sup>-</sup>, Al<sup>3+</sup>, Fe<sup>2+</sup>, Ca<sup>2+</sup>, Mg<sup>2+</sup>, K<sup>+</sup>, and Na<sup>+</sup> in mg/L) for all piezometers is shown in Figure 8.11.

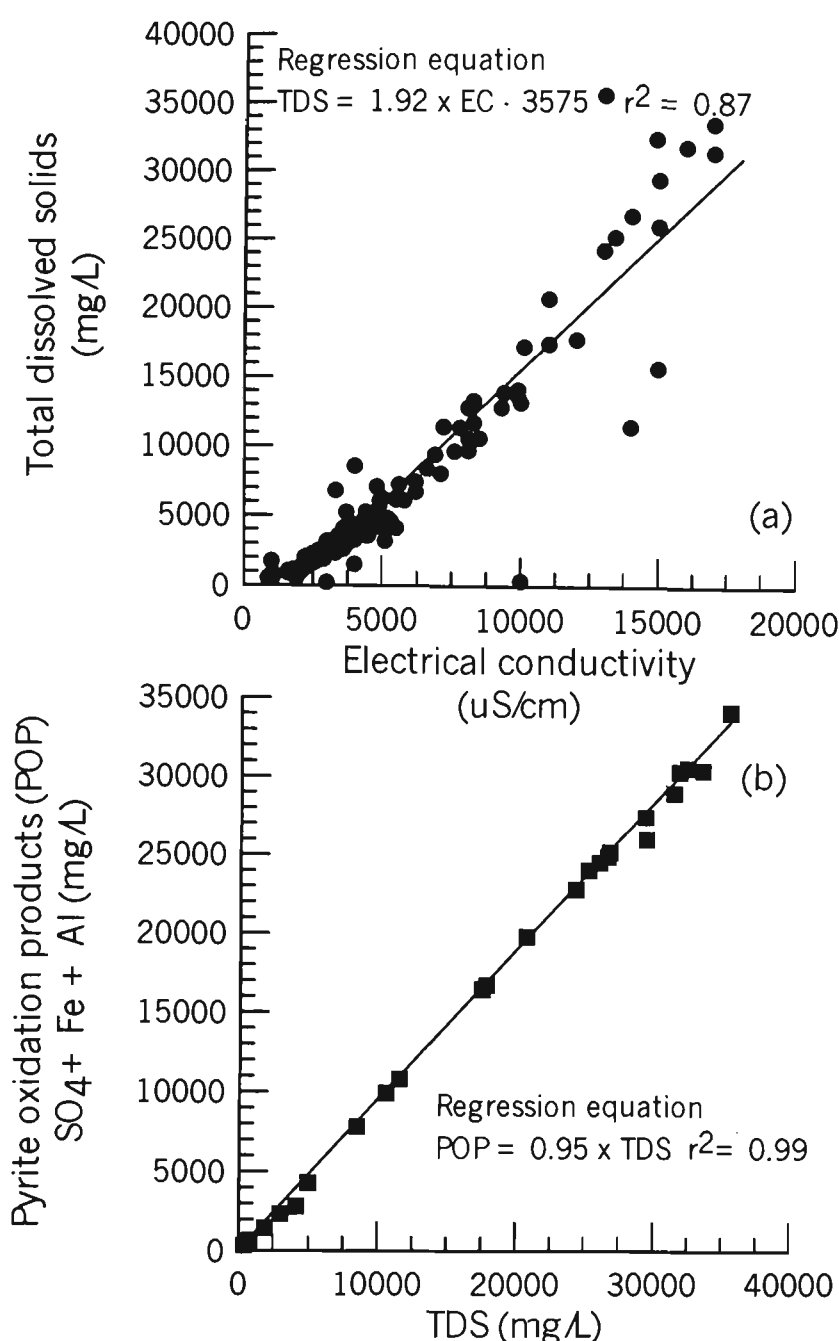


**Figure 8.11** Relationship between electrical conductivity, total dissolved solids, and the sum of the toxic pyrite oxidation products.

All EC measurements, with the exception of those measurements taken immediately after heavy rainfall events where EC is unusually low, were in excess of the ANZECC (1992) criterion of  $2800 \mu S/cm$  for long term agricultural irrigation practices. As shown in Figure 8.11 (b), the sum of the pyrite oxidation products  $SO_4^{2-}$ ,  $Al^{3+}$ , and  $Fe^{2+}$  comprised 95% of the TDS. As such, EC can be readily used to estimate the concentration of pyrite oxidation products in the groundwater. When used in conjunction with pH, the EC values can provide solid information on the evolution of

the groundwater chemistry without expensive chemical testing. At other locations, entrapped marine salts in the potential acid sulfate soil may also contribute to the magnitude of EC.

#### *8.3.5 Change in pyrite oxidation product concentration in the drain water*

As shown in Chapter 7 and Section 8.3.2, the groundwater hydrology and chemical composition are inherently linked and combine to generate extremely poor quality groundwater. This groundwater discharges into the flood mitigation drains, from which it is then subsequently discharged into Broughton Creek. The release of low pH drain water with elevated concentrations of  $\text{Fe}^{2+}$  and/or  $\text{Al}^{3+}$  has been demonstrated to cause environmental degradation in Broughton Creek (Pease *et al.*, 1997) and other NSW estuaries (e.g., Sammut *et al.*, 1996). The transient water quality profiles measured at the three weir locations showed similar trends to those of the groundwater quality, although the concentration of the pyrite oxidation products in the drain were substantially less than in the groundwater as a result of dilution. The concentrations of pyrite oxidation products in the drain are shown in Figure 8.12. Climatic factors also affected the drain water quality, particularly during the pre-weir period, where low flow condition in the drain enabled saline water from Broughton Creek to intrude into the drains.

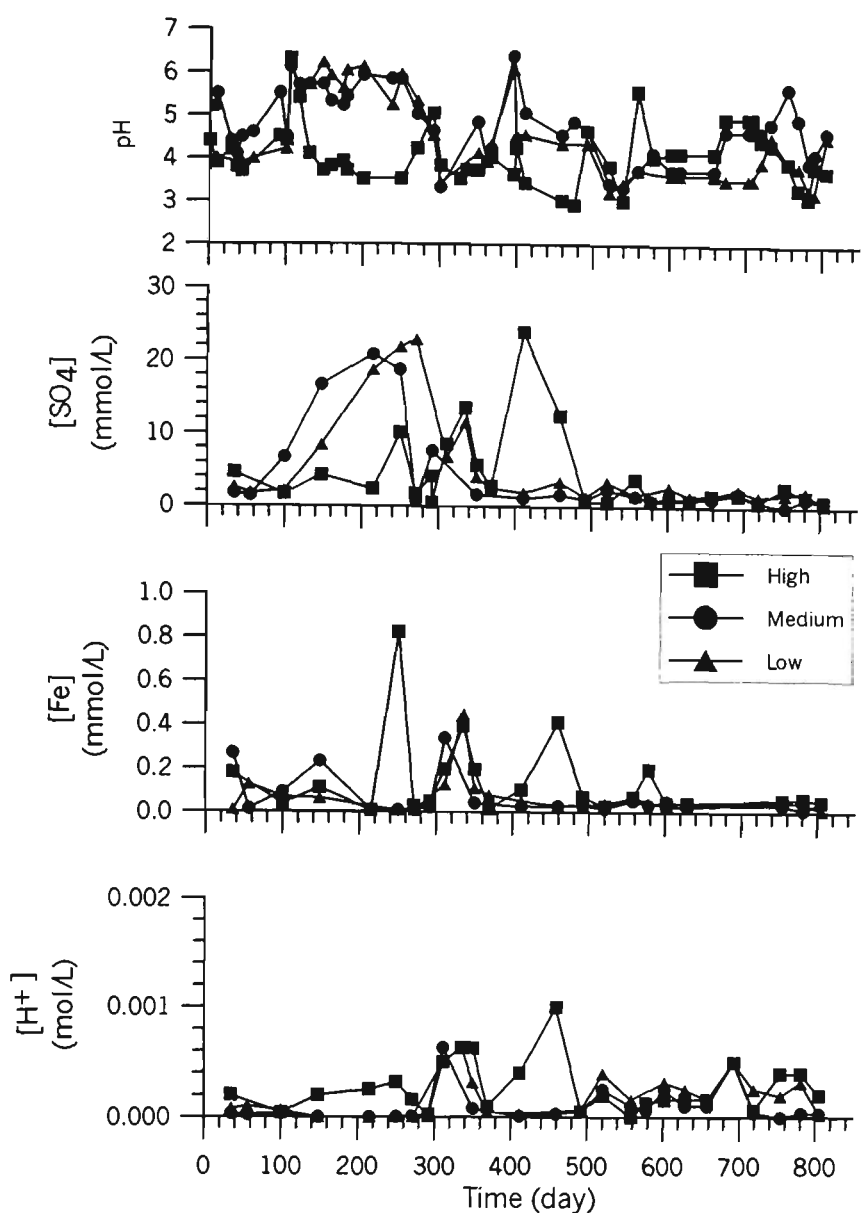


**Figure 8.12** Concentration of pyrite oxidation products in the drains.

The pH of the water in the drains ranged between 3-6 during the study. ANZECC (1992) guidelines recommend that for protection of aquatic ecosystems, the pH of freshwater should be within pH 6.5-9.0 or less than 0.2 pH unit change for marine waters. Clearly, the pH of the drain water discharged into Broughton Creek during most of the study period did not meet these criteria. Figure 8.12 shows that during the initial 100 days of the pre-weir period, the drain water pH was about 4 at both the high and low weir locations. The pH of the drain water at the medium weir varied between 4-5.5. This variation was caused by freshwater dilution from the drain transporting water from the elevated ground to the west of the site that enters the North-south drain downstream

of the high weir. The low drain water pH was indicative of the discharge of acidic groundwater containing pyrite oxidation products into the drains. As shown in Chapter 7, groundwater hydraulic gradients during this period were of a relative high magnitude and caused groundwater to flow from the field towards the drain.

The absence of substantial rainfall between days 100-270 gave rise to a significant increase in the drain water pH, particularly at the low and medium weir locations. As shown in Chapter 7, the drought period caused a reversal of the direction of the hydraulic gradients (i.e., groundwater flow away from the drains). As such, the discharge of acidic groundwater was restricted during this time. In addition, very low or no flow conditions prevailed in the drains. Similarly, there was little freshwater input into Broughton Creek, giving rise to the intrusion of saline water from the Shoalhaven River further up the Creek than usual. The floodgate at the junction of Broughton Creek and the flood mitigation drain did not exclude saline water from the Creek due to a number of factors, including: faulty seals, warped gates and obstructions jamming the gates open. Intrusion of saline water, which has an acid buffering capacity of about  $2.5 \text{ mol H}^+/\text{m}^3$ , can neutralise residual acid in the drains and result in the establishment of reasonably neutral conditions in the drains (i.e., pH 6-7). The intrusion of saline water did not extend to the high weir sampling location due to the geometry/elevation of the drain invert. During this dry period, the pH of the drain water at the high weir generally remained less than pH 5 (except for 2 measurements where pH > 5). At the high weir location, the depth of the water in the drain was very shallow (approximately 0.2 m) between days 100-270. This low water level may have exposed iron monosulfides that had previously precipitated onto the drain invert to atmospheric oxygen, resulting in the rapid generation of acid. Similarly, the pyritic soil along the side of the drain was exposed to oxidising conditions and may have acidified the drain via transport through the capillary fringe.

After day 270, when rainfall caused groundwater discharge into the drains (see Chapter 7), the drain water pH fell from pH 5.8-6.0 to pH 3.3-3.4 at the medium and low weir locations, respectively. Clearly, acid that had been generated from the oxidation of pyrite during the period of low groundwater tables had been entrained in the

groundwater and transported to the drains. Increased flow in the drains between days 270-290 may have increased the pH of the drain water from pH 3.5 to pH 5 at the high weir location, however, low pH conditions (pH 3.8) prevailed after day 290.

The magnitude of the drain water pH after day 400 was largely determined by the flow characteristics of the drain and the groundwater. As shown in Figure 8.12, at days 400 and 700, relatively high pH conditions prevailed at all weir locations. This was primarily due to large volumes of freshwater being discharged through the drains and diluting the concentration of acidity in the drain water. As the flow of water in the drains receded, a combination of the discharge of acidic groundwater into the drains and less freshwater dilution gave rise to lower drain water pH.

As shown in Chapter 7, the installation of the weirs from day 440 changed the magnitude and direction of the hydraulic gradients of the groundwater. Adjacent to the high weir, smaller hydraulic gradients reduced the rate of acid discharge into the drain. This resulted in a small increase from pH 4.0 to pH 4.3 for the average drain water pH during the pre and post weir periods. In contrast, the equilibrium pH value for drain water sampled at the low weir location did not show any improvement as a result of installing the weirs. Calculation of the direction of the hydraulic gradients in Chapter 7 showed that the predominant groundwater flow was in a north to south direction after the installation of the weirs, indicating that acid entrained in the groundwater after pyrite oxidation would be discharged primarily along the east-west drain. This is evident in the average drain water pH values during the post-weir period. The average pH values measured at the high, medium and low weirs were 4.3, 4.2 and 3.7, respectively, indicating that the installation of the weirs had altered the distribution of acid discharge into the drains, and hence, the pH of the drain water adjacent to the weir locations.

The concentrations of  $\text{SO}_4^{2-}$  in the drain water, and on the Broughton Creek side of the floodgate, are shown in Figure 8.12. During the initial 100 days of the trial, the concentration of  $\text{SO}_4^{2-}$  in the drain water was 2-5 mmol/L at all sampling locations. The intrusion of saline water between days 100-270 caused the  $\text{SO}_4^{2-}$  concentration in drain

water to increase significantly. Sea water has a  $\text{SO}_4^{2-}$  concentration of about 28.1 mmol/L. Towards the end of the drought period when saline intrusion up Broughton Creek was most pronounced, the  $\text{SO}_4^{2-}$  concentration in the drains at the floodgate, low and medium weir locations approached that of sea water. In contrast, the  $\text{SO}_4^{2-}$  concentration at the high weir was significantly lower. However, the  $\text{SO}_4^{2-}$  concentration measured at the high weir location increased during this period, possibly as a result of the oxidation of iron monosulfides. Upon breaking of the drought conditions, the  $\text{SO}_4^{2-}$  concentration fell to less than 1 mmol/L due to freshwater dilution in the drains, but then increased to 10-14 mmol/L at all the weir locations, as acidified groundwater was discharged into the drains. However, at the medium and low weir locations the  $\text{SO}_4^{2-}$  concentration quickly receded to lower levels between 1-3 mmol/L. High concentrations of  $\text{SO}_4^{2-}$  prevailed at the high weir location until the installation of the high weir.

Until the change in groundwater elevation and flow direction caused by the high weir, the very high concentrations of  $\text{SO}_4^{2-}$  measured in the groundwater adjacent to the high weir (i.e., C10 and C90) were discharged into the North-south drain upstream of the high weir. After the installation of the weirs and the associated change groundwater flow directions, the average  $\text{SO}_4^{2-}$  concentrations at the high and low weirs were 1.4 and 1.8 mmol/L, respectively. The  $\text{SO}_4^{2-}$  concentration at the medium weir was 1.1 mmol/L, having been diluted by freshwater inputs from the drain below the high weir. The increase in  $\text{SO}_4^{2-}$  concentration from the high to the low weir location was further confirmation of the change in groundwater flow regime caused by the installation of the weirs.

The concentration of Fe in the drain water was high throughout the monitoring period. ANZECC (1992) guidelines suggest that the concentration of Fe in freshwater should not exceed 0.02 mmol/L for protection of aquatic ecosystems. The temporal variability of dissolved Fe in the drain water followed that of pH and  $\text{SO}_4^{2-}$ . During the initial 200 days, Fe concentration varied between 0.1-3 mmol/L. Surprisingly, the Fe concentration remained relatively high until day 150 (i.e., 0.06-0.2 mmol/L), well into the period where salinity intrusion into the drain has resulted in the neutralisation of some drain

acidity. With further increases in drain pH, the Fe concentration in the drain water fell below ANZECC (1992) criteria until the return of drought breaking rainfall after day 270. As shown in Figure 8.12, the Fe concentration in the drain peaked at day 310, with 0.45, 0.35 and 0.40 mmol/L measured at the low, medium and high weir locations, respectively. The maximum concentrations of Fe in the drain water corresponded with the return of acidic conditions in the drain caused by the discharge of groundwater containing pyrite oxidation products. Although the maximum Fe concentration in the drain water was associated with the ‘first flush’ of the acidic groundwater after the period of pyrite oxidation, the concentration of Fe in the drain water remained in excess of ANZECC (1992) for the remainder of the trial. The high concentration of Fe in the drain water has several implications. Firstly, dissolved  $\text{Fe}^{2+}$  can readily oxidise to  $\text{Fe}^{3+}$  which generates additional acidity. White *et al.* (1997) referred to this Fe oxidation “acidity at a distance”, because it generates additional acid away from its source. Further to the oxidation of  $\text{Fe}^{2+}$ , various iron precipitates form, which can smother aquatic plants and bottom dwelling organisms. Lastly, high concentrations of  $\text{Fe}^{2+}$  and  $\text{SO}_4^{2-}$  in drain water can lead to the precipitation of iron monosulfides. Thick layers of iron monosulfides have been observed in the flood mitigation drains. These sulfidic precipitates oxidise very rapidly when exposed to oxidising conditions, and can act as a additional source of acidity when they are disturbed.

#### 8.3.6 Discharge of acidic cations to the drain water

As shown in Figure 8.13, the concentration of  $\text{Al}^{3+}$  in the drain water was high throughout the monitoring period. ANZECC (1992) guidelines suggest that the concentration of  $\text{Al}^{3+}$  in freshwater should not exceed 0.0002 mmol/L, where the  $\text{pH} < 6.5$ , for protection of aquatic ecosystems.



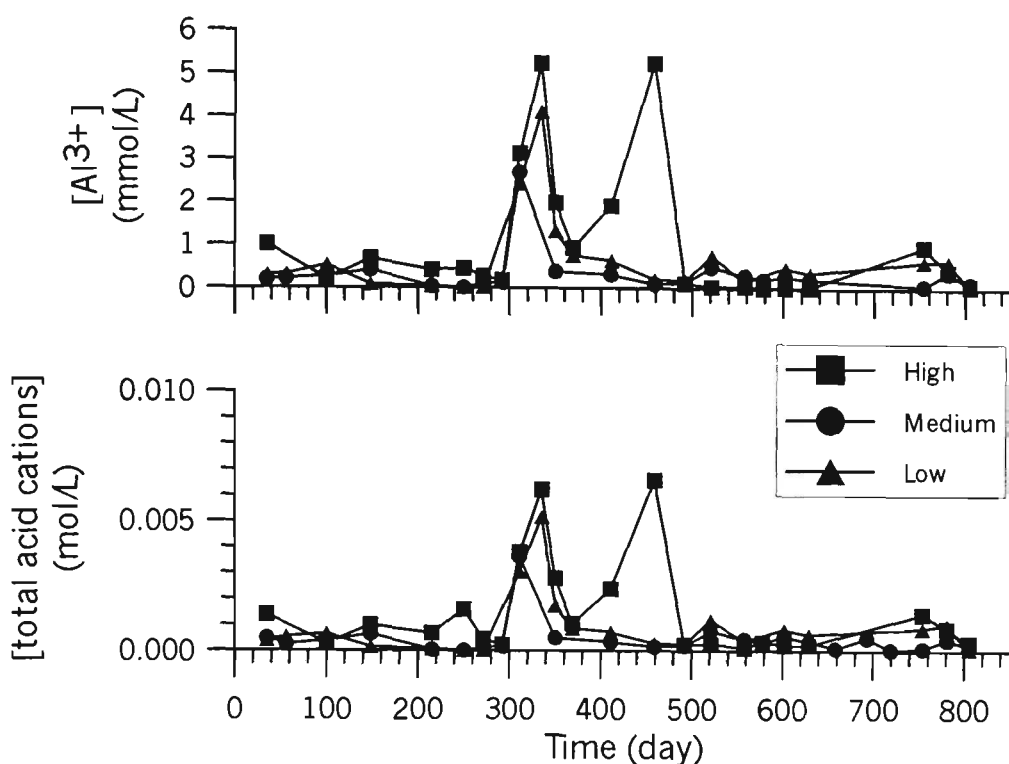


**Figure 8.13** Concentration of acidic cations in drain water

The concentration of  $\text{Al}^{3+}$  dissolved in the drain water followed the same trend as pH and Fe. In the initial 200 days,  $\text{Al}^{3+}$  concentration varied between 0.03-1.00 mmol/L. The increases in drain pH associated with saline intrusion caused the concentration of Al in the drain water to approach ANZECC (1992) criteria until the return of drought breaking rainfall after day 270. The concentration of dissolved  $\text{Al}^{3+}$  is determined by the pH, where the concentration of  $\text{Al}^{3+}$  increases exponentially with every unit decrease in pH. As such, the  $\text{Al}^{3+}$  concentration recommended by ANZECC (1992) at pH 5.5-6.6 may not necessarily pose a significant threat to estuarine health. Sammut *et al.* (1995) suggested that the form of  $\text{Al}^{3+}$  at pH > 5.5 may not contribute to fish disease and/or mortality to the same degree as the forms of  $\text{Al}^{3+}$  at pH < 5.5. Consequently, even through the concentration of  $\text{Al}^{3+}$  was greater than the ANZECC (1992) criteria between days 200-270, the relatively high pH may have altered the form of the  $\text{Al}^{3+}$ , rendering it relatively benign to aquatic organisms.

The concentration of  $\text{Al}^{3+}$  in the drain peaked at day 310, with 4.1, 2.7, 5.2 and 1.8 mmol/L at the low, medium, high weirs and floodgate, respectively. These  $\text{Al}^{3+}$

concentrations are 5 orders of magnitude greater than the recommended ANZECC (1992) criterion, and correspond with the toxic forms of  $\text{Al}^{3+}$  present at low pH. The concentration of  $\text{Al}^{3+}$  receded after the initial first flush of acidified groundwater into the drains, but it remained up to 4 orders of magnitude greater than the ANZECC (1992) criteria for the remainder of the trial. After the installation of the weirs, the concentration of  $\text{Al}^{3+}$  measured at the low weir location was between 0.1-0.3 mmol/L greater than that measured at the medium or high weir locations. Again, this confirms the altered groundwater hydrological regime imposed by the weirs, where groundwater discharge to the drains now occurred along the East-west drain.

The concentrations of the total acidic cations in the drain water are shown in Figure 8.13. In contrast to some of the more acidic groundwater, the proportion of acidity contributed by  $\text{Al}^{3+}$  and  $\text{Fe}^{2+}$  was relatively low in the drain water. This was particularly evident for total acidity measured at the medium weir. A possible explanation for the smaller contribution of these acidic cations to the total drain water acidity is that they readily form Fe and Al precipitates within the drain, which increase the  $\text{H}^+$  concentration but reduce the concentration of  $\text{Al}^{3+}$  and  $\text{Fe}^{2+}$  in dissolved forms. Rust and milky blue-white flocs were frequently observed in the drain water, which are commonly thought to be precipitates of iron and aluminium, respectively.

The concentration of acidity being discharged through the drain is high, particularly with respect to the expected near neutral status of Broughton Creek. The total amount of acidity that was discharged from the flood mitigation drain was calculated by multiplying the measured acidity of the drain water by the calculated daily volume of drain water that flowed over the low weir. During high flow periods when flushing of the drain occurred quickly, the concentration of acidity in the drain was set at zero. The amount of acid discharged between days 454-813 was estimated to be  $2.3 \times 10^6$  moles  $\text{H}^+$ , or approximately 111 tonnes  $\text{H}_2\text{SO}_4$ . This equates to an average discharge of acidity at approximately 1 mole  $\text{H}^+/\text{m}^3$ . Within the Broughton Creek floodplain there are 21 similar flood mitigation drainage structures that are within areas underlain by pyritic soils. If all these drains discharged a similar volume of acid, then Broughton Creek received in excess of 2000 tonnes of acid during 1998-1999. Other studies report

similar magnitudes of acid being discharged into estuarine rivers in NSW. Sammut *et al.* (1996) estimated that 950 tonnes  $\text{H}_2\text{SO}_4$  were discharged into the Richmond River during a single flood event from a 3000 ha catchment affected by over-drained acid sulfate soils. Wilson *et al.* (1999) reported that 1185 tonnes  $\text{H}_2\text{SO}_4$  was discharged into the Tweed River between March and August 1992 from acidified drains.

#### 8.3.7 Ingress of saline water into the drains

Water quality parameters such as the concentrations of chloride and basic cations provide additional information with respect to developing strategies that minimise the discharge of acid from the drains into Broughton Creek. . This is particular relevant where floodgates are modified to enable saline intrusion, or if existing floodgates leak. The nature of saline intrusion from Broughton Creek into the drains is shown in Figure 8.14.

The basic cation suite is dominated by  $\text{Na}^+$  from the intrusion of saline water from Broughton Creek, although during periods where freshwater discharge through the drains dominates, the cation suite was not dominated by any single cation species. Similarly, the concentration of  $\text{Cl}^-$ , shown in Figure 8.14, was related to the ingress of saline water from the Creek. From day 150-270, the concentration of  $\text{Na}^+$  and  $\text{Cl}^-$  in the drain increased rapidly, and approached the concentration of  $\text{Na}^+$  and  $\text{Cl}^-$  found in sea water, about 450 and 550 mmol/L, respectively.

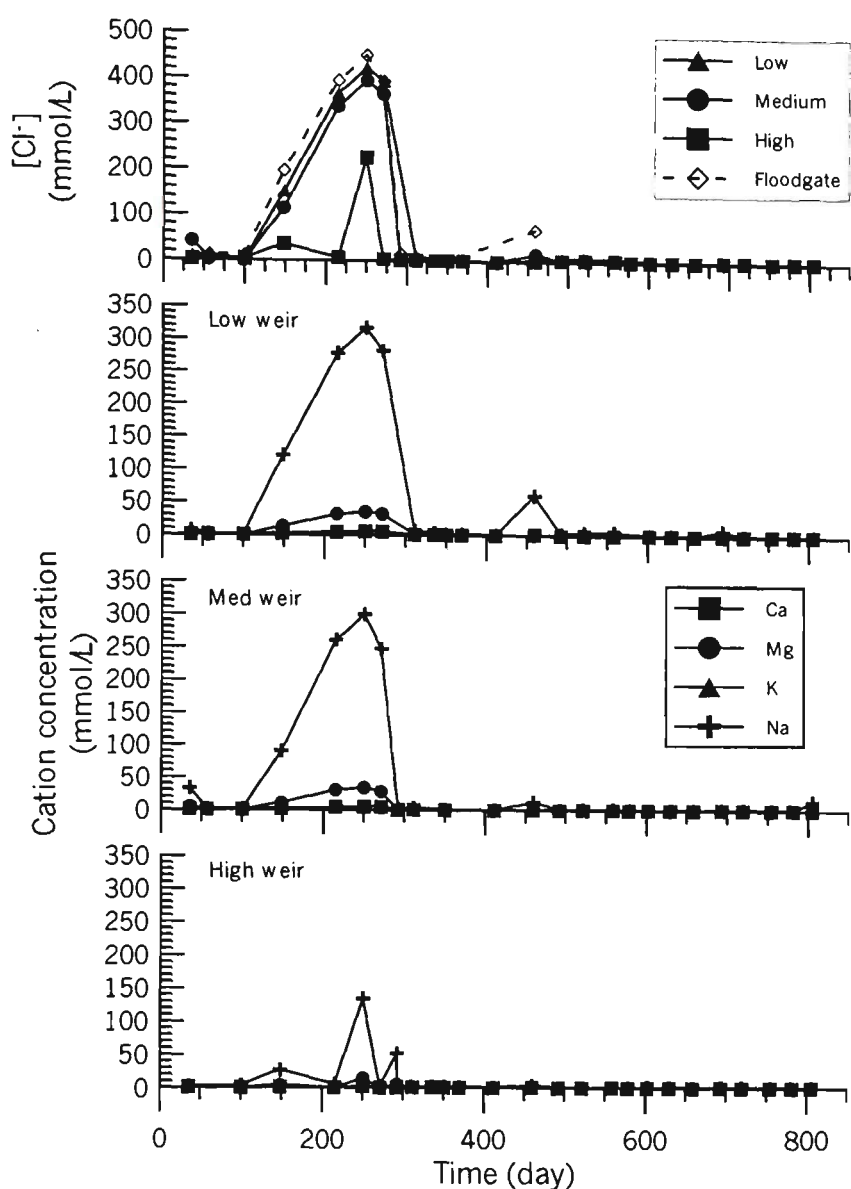


**Figure 8.14** Saline intrusion characterised by chloride and cation concentration

The ingress of saline water into the drain highlights some issues with the design and operation of the floodgate. In terms of minimising the impact of acid discharge to Broughton Creek, the ingress of saline water into the drains has a positive influence in raising the drain water pH. However, the design of the floodgate system should preclude any saline intrusion. The intrusion of saline water into the drain is due to operational problems such as floodgate warping, foreign objects jamming the gate open, poor sealing between the gate and the culvert. Clearly, these operational problems are difficult to overcome without regular maintenance and vigilance of the floodgate. Similarly, there is no control of the amount or rate of saline water ingress into the drain. Some farmers have expressed a view that any saline intrusion into these flood mitigation

drains is unwanted for reasons associated with salt damage to crops/pasture. However, the operational constraints inherent in the floodgate design mean that uncontrolled intrusion of salty water from the Creek into the drains will occur during low flow periods.

The lack of control over intrusion of saline water into the drain, coupled with the beneficial influence of increasing the drain water pH by using the natural buffering capacity inherent in saline water, suggests that a new system of allowing a controlled volume of saline water into the drain system should be investigated. A brief introduction to the potential benefit achieved by controlled saline intrusion is given in Chapter 13.

## 8.4 Conclusions

The installation of the weirs in flood mitigation drains was not successful in terms of improving the quality of groundwater or soil chemistry. The soil and groundwater quality data showed that substantial amounts of pyrite oxidation products were generated during the pre-weir period when the groundwater table fell into the pyritic layer. This produced extremely poor quality groundwater (i.e. low pH and high EC,  $\text{SO}_4^{2-}$ , Al, Fe). Maintenance of higher groundwater tables after the installation of the weirs did not give rise to substantial improvement in the groundwater quality. Although the maintenance of higher groundwater tables minimised any 'new' acid being generated from pyrite oxidation, the acid 'stored' within the soil profile in the forms of iron and aluminium sulfate minerals, acidic cations on the ECEC and dissolved sulfuric acid was sufficient to keep the groundwater at low pH. The maintenance of poor groundwater quality by mineral dissolution and acid ECEC is confirmed in Chapter 13.

Assessment of the groundwater chemistry using the normalised concentration of  $\text{SO}_4$ , Al and Fe, as well as the Al:Fe molar ratio against the Cl: $\text{SO}_4$  molar ratio showed that an

evolutionary pathway could be developed that describes the status of the groundwater with respect to its 'toxicity'. Where the groundwater table had been maintained above the pyritic layer for some time (e.g. days 1-100), the composition of the groundwater was dominated by  $\text{SO}_4$ , with relatively small concentrations of Fe and Al, indicating that the water quality is being controlled by the 'stored' acid in the soil profile. After pyrite oxidation, the relative contribution of Fe and Al increased, which indicates that the toxicity of the groundwater increased as a result of the acid generated during a period of low groundwater tables (i.e. days 100-270). The contribution of dissolved Al fell relatively quickly after maintenance of the groundwater table by installation of the weirs. In contrast, the relative contribution of dissolved Fe remained high. This indicated that although the 'toxicity' of the groundwater from dissolved Al fell, the ability of the groundwater to discharge high concentration of  $\text{Fe}^{2+}$  which can subsequently at some distance downstream was still maintained for a long time after pyrite oxidation ceased.

Water quality monitoring in the drains showed that a large volume of acid was discharged from the drains into Broughton Creek (approximately 111 tonnes  $\text{H}_2\text{SO}_4$  in 359 days). The magnitude of acid discharge from the drains is similar to that reported from the North Coast of NSW. The drain water quality was modified by the intrusion of saline water into the drains from Broughton Creek. When saline water did intrude into the drain (coupled with little discharge of acidic groundwater into the drain), the drain water pH increased to in excess of 5. This indicates that controlled opening of floodgates to neutralise acidic drain water *in situ* may prove an effective method of minimising the discharge of slugs of acid into waterways.

**MANAGEMENT OF ACID SULFATE SOILS BY  
GROUNDWATER MANIPULATION**

**Volume II**

**DOCTOR OF PHILOSOPHY**

from

**UNIVERSITY OF WOLLONGONG**

by

**BRUCE GEOFFREY BLUNDEN**  
B.Nat Res. (Hons), M.Eng.

Faculty of Engineering  
October 2000

## **Chapter 9: Evaluation of surface and groundwater management strategies for drained acid sulfate soil using existing numerical models**

### **9.1 Introduction**

This Chapter evaluates water management options that may be applicable for the management of acid sulfate soils at the Berry study site using two numerical models. In addition, the utility of the numerical models used for this purpose is also assessed. Groundwater regimes were simulated using FEMWATER, a 3D finite element flow and transport model for variably saturated media (Lin *et al.* 1997), and the oxidation of pyrite was simulated using the Simulation Model for Acid Sulfate Soils (SMASS) developed by Bronswijk and Groenenberg (1992). Soil and climate data collected during 1997-98 from the study site are used as input for the models which are described in detail in Chapters 6 and 5, respectively. The modelling period includes a wet period with groundwater being close to the surface as well as a prolonged dry period that resulted in the groundwater falling below the acid sulfate soil layer.

### **9.2 Methods and materials**

Two numerical models, FEMWATER and SMASS, were used to simulate the groundwater regime and pyrite oxidation that occurred at the study site during 1997-98. A description of both model, and the initial and boundary conditions applied for the simulation is described below.



### 9.2.1 FEMWATER

FEMWATER simulates water flow through variably saturated soils by solving a modified Richards equation for various initial and boundary conditions. The governing equations are:

$$\frac{\rho}{\rho_0} F \frac{\partial h}{\partial t} = \nabla \cdot \left[ K \cdot \left( \Delta h + \frac{\rho}{\rho_0} \Delta z \right) \right] + \frac{\rho^*}{\rho_0} q \quad (9.1)$$

$$F = \alpha' \frac{\theta}{n} + \beta' \theta + n \frac{dS}{dh} \quad (9.2)$$

where:  $F$  is a storage coefficient,  $h$  is pressure head,  $t$  is time,  $K$  is the hydraulic conductivity tensor,  $z$  is potential head,  $q$  is the source and/or sink,  $\rho$  is water density at chemical concentration  $C$ ,  $\rho_0$  is the reference water density at chemical concentration zero,  $\rho^*$  is the density of either injected fluid or withdrawn water,  $\theta$  is the moisture content,  $\alpha'$  is modified compressibility of the medium,  $\beta'$  is modified compressibility of water,  $n$  is porosity of the medium and  $S$  is the degree of saturation.

The hydraulic conductivity tensor  $K$  is given by:

$$K = \frac{\rho g}{\mu} k = \frac{\left( \frac{\rho}{\rho_0} \right) \frac{\rho_0 g}{\left( \frac{\mu}{\mu_0} \right) \mu_0}} k_s k_r = \frac{\rho / \rho_0}{\mu / \mu_0} K_{so} k_r \quad (9.3)$$

where:  $\mu$  is the dynamic viscosity of water at chemical concentration  $C$ ,  $\mu_0$  is the referenced dynamic viscosity at zero chemical concentration,  $k$  is the permeability tensor,  $k_s$  is the saturated permeability tensor,  $k_r$  is the relative permeability or relative hydraulic conductivity, and  $K_{s0}$  is the referenced hydraulic conductivity tensor.

The referenced value is usually taken at zero chemical concentration. The density and dynamic viscosity of water are functions of chemical concentration and they are assumed to take the following form:

$$\frac{\rho}{\rho_0} = a_1 + a_2C + a_3C^2 + a_4C^3 \tag{9.4}$$

and

$$\frac{\mu}{\mu_0} = a_5 + a_6C + a_7C^2 + a_8C^3 \tag{9.5}$$

where;  $a_1, a_2, \dots, a_8$  are the parameters used to define concentration dependence of the water density and viscosity and  $C$  is the chemical concentration.

The Darcy velocity is calculated by:

$$V = -K \cdot \left( \frac{\rho_0}{\rho} \Delta h + \Delta z \right) \tag{9.6}$$

The initial conditions for the flow equation are given by:

$$h=h_i(x,y,z) \text{ in } R \tag{9.7}$$

where; R is the region of interest and  $h_i$  is the prescribed initial condition, which can be obtained by either field measurements or by solving the steady state Equation 9.1

The boundary conditions for the flow equation are given by:

a) Dirichlet conditions (specified pressure head boundary):

$$h=h_d(x_b, y_b, z_b, t) \text{ on } B_d \quad (9.8)$$

b) hydraulic gradient flux conditions:

$$-n.K.\left(\frac{\rho_0}{\rho}\Delta h\right)=q_n(x_b, y_b, z_b, t) \text{ on } B_n \quad (9.9)$$

and

$$-n.K.\left(\frac{\rho_0}{\rho}\Delta h + \Delta z\right)=q_c(x_b, y_b, z_b, t) \text{ on } B_c \quad (9.10)$$

c) variable conditions during precipitation periods

$$h=h_p(x_b, y_b, z_b, t) \text{ on } B_v \quad (9.11)$$

or

$$-n.K.\left(\frac{\rho_0}{\rho}\Delta h + \Delta z\right)=q_p(x_b, y_b, z_b, t) \text{ on } B_v \quad (9.12)$$

e) variable conditions during non-precipitation periods:

$$h=h_p(x_b, y_b, z_b, t) \text{ on } B_v \quad (9.13)$$

or

$$h=h_m(x_b, y_b, z_b, t) \text{ on } B_v \quad (9.14)$$

or

$$-n.K.\left(\frac{\rho_0}{\rho}\Delta h + \Delta z\right) = q_e(x_b, y_b, z_b, t) \quad \text{on } B_v \quad (9.15)$$

where:  $(x_b, y_b, z_b)$  is the spatial coordinate on the boundary,  $n$  is the outward unit vector normal to the boundary,  $h_d$  is the Dirichlet functional value,  $q_n$  is the gradient flux value,  $q_e$  is the flux value,  $B_d$  is the Dirichlet boundary,  $B_n$  is the gradient flux boundary,  $B_e$  is the flux boundary,  $B_v$  is the variable boundary,  $h_p$  is the ponding depth,  $q_p$  is the throughfall of precipitation on the variable boundary,  $h_m$  is the minimum pressure on the variable boundary,  $q_e$  is the evaporation rate on the variable boundary.

Only one of the equations (9.11)-(9.15) is used at any point on the variable boundary at any time. A complete description of FEMWATER is given by Lin *et al.* (1997). The FEMWATER simulations were constructed using the Groundwater Modelling System 2.1 software and run on a 166 MHz Pentium PC. Solutions were calculated and saved for daily timesteps.

### 9.2.2 Element properties and numerical solution

The computational discretization used by FEMWATER is a three dimensional mesh. The elements used in the simulation are triangular prisms, each with six nodes. A schematic of a FEMWATER elements is shown in Figure 9.1.

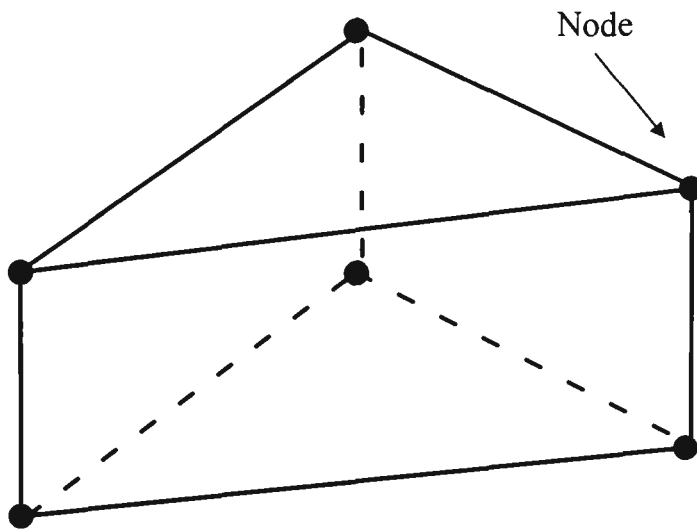


**Figure 9.1** Triangular prismatic element used by FEMWATER

At all six nodes, a non-linear flow equation is solved by the Galerkin finite element method. The flow equation is non-linear function of the pressure head. FEMWATER uses a pointwise iterative matrix solver in conjunction with a Gaussian quadrature scheme. The pointwise iterative matrix solver uses the basic successive iterative method to solve the matrix equation, including the Gauss-Seidel method, successive under-relaxation and successive over-relaxation techniques. When the matrix is diagonally dominant, the pointwise iterative solver provides a convergent solution. However, convergence may be slow. A maximum of 40 iterations were allowed for solving the non-linear flow equation, or until a steady state convergence criteria of  $10^{-3}$  for the pressure head was achieved.

### 9.2.3 *Material properties for FEMWATER*

Soil physical parameters used to define the material properties in FEMWATER were determined from saturated hydraulic conductivity and moisture characteristic data. A

complete description of these data is given in Chapter 6. A summary of the material properties used in the FEMWATER simulations is given in Table 9.1.

**Table 9.1.** Soil physical properties.

Depth (m)	$\theta_r$	$\theta_s$	$\alpha$ (m <sup>-1</sup> )	n	$k_v$ (m day <sup>-1</sup> )	$k_v/k_h$
0.3	0.05	0.55	0.281	1.30	3.95	1.06
0.6	0.02	0.35	0.242	1.15	3.84	1.02
0.9	0.05	0.34	2.917	1.18	1.68	2.15
1.2	0.04	0.50	0.2247	1.29	2.08	2.36
1.5	0.06	0.49	0.4737	1.09	2.02	12.7
3.0	0.06	0.49	0.4737	1.09	0.20	1.0

where  $\theta_r$  and  $\theta_s$  are residual and saturated volumetric moisture contents,  $\alpha$  and  $n$  are shape parameters based on the van Genuchten (1980) equation,  $k$  is the saturated hydraulic conductivity in the vertical plane ( $k_v$ ) and in the horizontal plane ( $k_h$ ).

*9.2.4 FEMWATER mesh and boundary conditions*

A variety of potential acid sulfate soil management options are feasible given the climatic and hydrological conditions at this site. Weirs have been installed in the flood mitigation drains with the intention of raising drain water levels above the acid sulfate soil layer to minimise groundwater drawdown and reduce the rate of acid discharge into the drains. Infrastructure for the application of treated sewage effluent from the nearby Berry Sewage Treatment Plant (BSTP) has recently been installed. Given the current

rate of effluent generation at the BSTP, it is feasible that irrigation could be applied at a rate of 25mm every 7 days to pasture paddocks underlain by acid sulfate soils. Current land management practice includes application of effluent to areas not underlain by acid sulfate soils, resulting in an application of 25mm to the acid sulfate soils areas every 14 days.

The abovementioned acid sulfate soil water management strategies were simulated using FEMWATER by constructing a finite element mesh 150m long (the length of a piezometer transect) and 5m deep, assigning material properties to six soil layers and applying appropriate boundary conditions. A schematic diagram of the FEMWATER mesh with symbols showing various boundary conditions and the initial groundwater elevation is shown in Figure 9.2a. The plan view of the mesh used in the groundwater simulations showing the element geometry and location of the nodes is shown in Figure 9.2b. All triangular solid elements used in the 3D finite element simulation have six nodes, one at each corner, and the complete mesh consisted of 1235 elements and 1728 nodes.

The drain water levels were defined as either a variable head (ie. drain simulation) or as a constant head (ie. weir simulation) at the elements across the drain-soil interface. A cross section of the drain and weir simulation head boundary conditions at the drain-soil interface are shown in Figure 9.3. The depth of the flood mitigation drain at the site are also shown in Figure 9.3.





**Table 9.2:** FEMWATER boundary conditions

Water management strategy	Boundary conditions	Description
Existing situation - deep drains	<ul style="list-style-type: none"><li>• transient head boundary for drain water elevations as measured at site</li><li>• transient variable flux boundary for rainfall-evapotranspiration flux at ground surface as measured at site</li></ul>	Deep flood mitigation drains that intersect the sulfidic soil layer. Transient drain water level varies between -0.6 and -1.0 m AHD depending on rainfall and leakage through floodgate.
Elevated drain water level weir at -0.5 m AHD	<ul style="list-style-type: none"><li>• constant head boundary for drain water elevation at -0.5 m AHD</li><li>• transient variable flux boundary for rainfall-evapotranspiration flux at ground surface as measured at site</li></ul>	Elevated drain water level held by temporary weir. Weir adjacent to the piezometer transect used in simulations is set at -0.5 m AHD. Assume adequate water supply to maintain drain water level.
Effluent irrigation	<ul style="list-style-type: none"><li>• transient head boundary for drain water elevations as measured at site for existing conditions</li><li>• addition of 25 mm irrigation every 7 or 14 days into SWACROP</li></ul>	Application of effluent irrigation in accordance with supply rate for whole farm (14-day cycle) or acid sulfate soil area (7-day cycle).
Elevated drain water levels with effluent irrigation	<ul style="list-style-type: none"><li>• constant head boundary for drain water elevation at -0.5 m</li><li>• addition of 25 mm irrigation every 7 or 14 days into SWACROP</li></ul>	Combination of applying elevated drain water level using weirs with effluent irrigation.

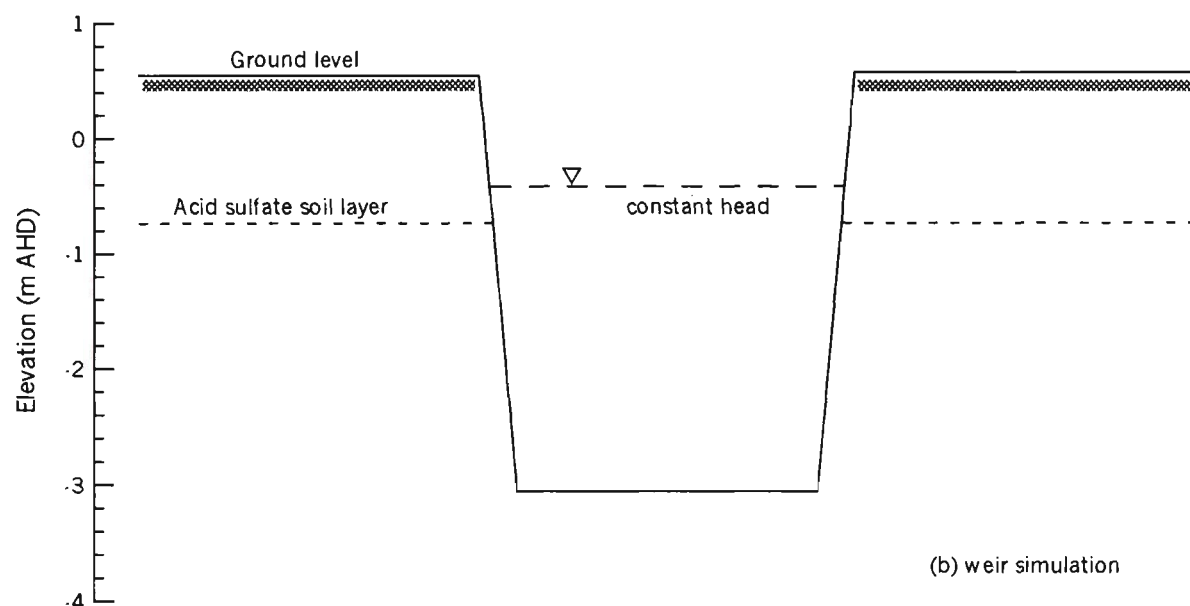
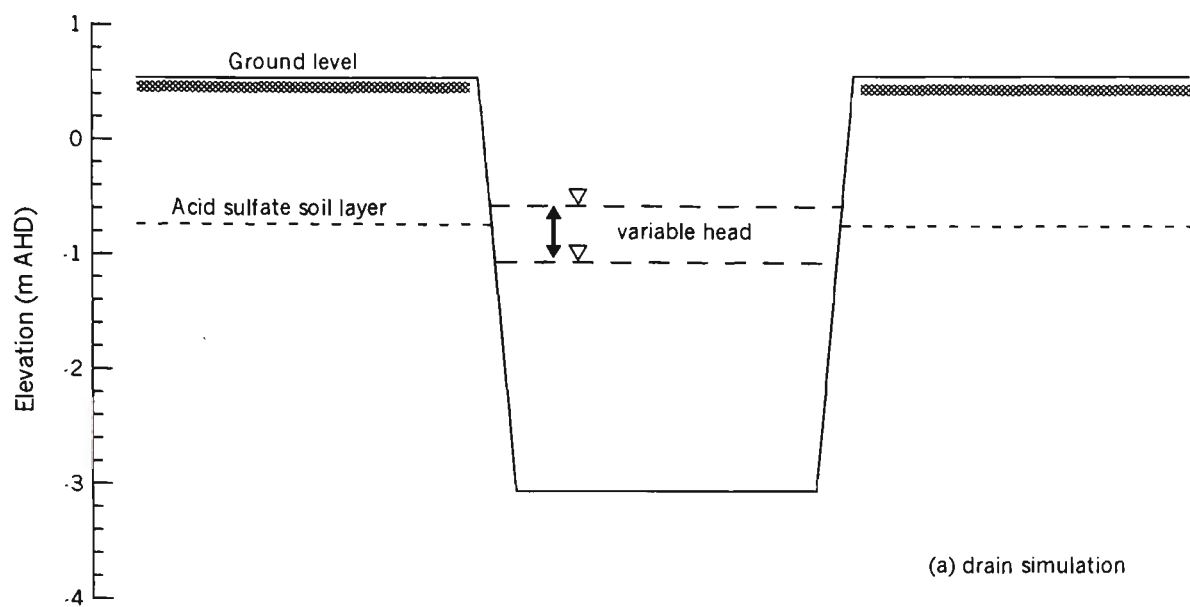


**Figure 9.3** Cross section of the drain and weir simulations, and dimension of the flood mitigation drain.

#### *9.2.5 Bottom flux boundary calibration*

Removal of water by evapotranspiration from the groundwater table, particularly water extraction by plant roots at depth, is difficult to be modelled explicitly by FEMWATER. Rather, evapotranspiration from the surface was simulated using a variable water flux boundary condition at the mesh boundary using the difference between daily rainfall and calculated evapotranspiration. This results in an underestimation of the lowering of the groundwater table by evapotranspiration. To overcome this inadequacy in FEMWATER, a variable flux boundary was used to simulate deep drainage at the bottom of the mesh (Fig. 9.2a). The flux through the bottom of the mesh was determined by matching the observed groundwater levels measured in piezometers located 10 m and 90 m from the drain with the elevation of the piezometric surface calculated by FEMWATER. The relationship between the observed and simulated groundwater elevations from Transect I at the study site at 10 m and 90 m distance from the drain are shown in Figure 9.4. The bottom flux rate varied between 0.0045 and 0.006 m/day.

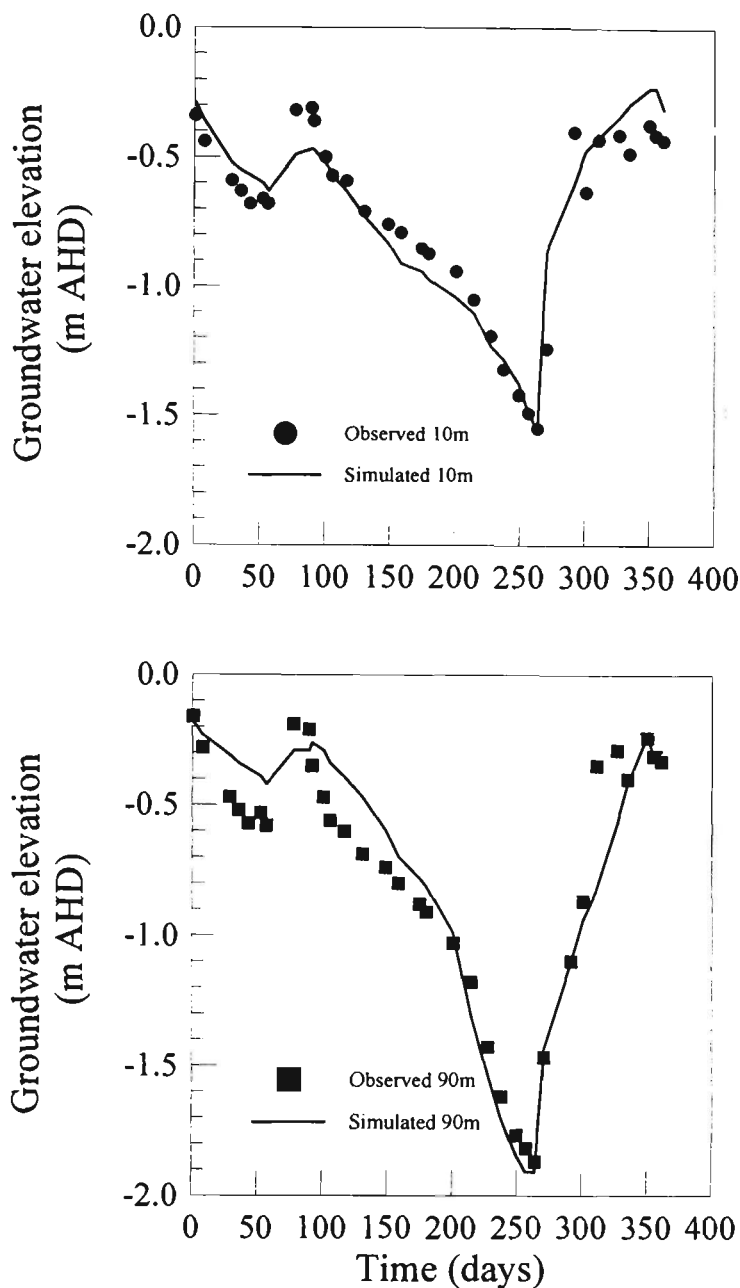


**Figure 9.4.** Observed and simulated groundwater elevations.

#### 9.2.6 Simulation Model for Acid Sulfate Soils (SMASS)

SMASS is fully described by Bronswijk and Groenenberg (1992). An overview of the model is also presented in Chapter 3. The SMASS comprises four sub-models that compute the one dimensional vertical water and solute transport, pyrite oxidation and chemical reactions in the acid sulfate soil profile. The vertical water transport in the soil profile is calculated by the water transport model SWACROP developed by Belmans *et al.* (1983). Subsequently, the air filled porosity at various depths are calculated from the

difference of the porosity and the moisture content. Next, the air content profile and oxygen diffusion coefficients are calculated in the oxygen transport and pyrite oxidation sub-model. The oxygen concentration in the profile is derived from the diffusion of oxygen into the soil from the atmosphere and the consumption of oxygen in the soil by organic matter decomposition and oxidation of pyrite. The pyrite oxidation rate at a given depth is determined by the concentration of oxygen at that depth. The model calculates the amount of  $H^+$ ,  $SO_4^{2-}$  and  $Fe^{3+}$  generated during pyrite oxidation according to a spherical reduction numerical scheme. The oxidation products are redistributed through the soil profile depending on the water fluxes within the solute transport sub-model.

Bronswijk *et al.* (1995) and Van den Bosch *et al.* (1998) use SMASS to evaluate water management strategies for sustainable land use of acid sulfate soil in coastal lowlands in South East Asia where acid sulfate soil is very close to the surface. SMASS was validated by Bronswijk *et al.* (1993), Bronswijk *et al.* (1995) and Van den Bosch *et al.* (1998) for their study site conditions and was found to be in good agreement with data measured from the field or in laboratory experiments.

#### 9.2.7 SMASS material and boundary conditions

The soil moisture content and water transport in the soil profile was determined using the SWACROP water balance model that supports SMASS. The material properties required for SWACROP are the same as those required for FEMWATER, which are shown in Table 9.1. Evapotranspiration from the soil was determined using the Penman-Monteith method with site weather data collected by the weather station and used as input data for the surface boundary. Daily groundwater elevation was either from measured piezometer data (for the existing drained simulation) or from the simulated groundwater elevation using FEMWATER (for the weir simulation). The irrigation options were simulated by the addition of 25 mm irrigation at a 7 or 14-day

cycle directly into SWACROP in conjunction with the drain or weir groundwater levels. SWACROP simulates the redistribution of water through the soil profile and calculates the elevation of the groundwater table. For the irrigation simulations, the groundwater elevation data were taken from the SWACROP output.

Laboratory and field data were used to initialise SMASS. A summary of the data requirements for SMASS is given in Table 9.3. Samples were collected at 10 and 90 m distance from the drain in 0.1 m increments to a depth of -1.5 m AHD, in July 1997. The chemical properties of the soil at the study site are fully described in Chapter 6. The chemical properties of soil from deeper in the profile was estimated using information collected during profile descriptions.

The initial pyrite concentration, organic matter content (total carbon), soil pH and cation exchange capacity used to initialise SMASS are shown in Figure 9.5. The average pyrite crystal size of 1  $\mu\text{m}$  was measured using a scanning electron microscope and was used to initialise SMASS for all sulfidic soil layers. No evidence of large framboidal pyrite clusters was found for the sulfidic soil collected at this site. The distribution of pyrite crystal size determined from a sample collected at -0.95 m AHD at 90 m from the drain is shown in Figure 6.3. SMASS was compiled and run using UNIX F77. Input files were developed using a PC text editor.

**Table 9.3: SMASS input data**

<b>SMASS input data</b>	<b>Method</b>
Dry bulk density	Gravimetric determination using cores
Average aggregate radius	Soil profile description
Pyrite concentration	Peroxide Oxidation Combined Acidity and Sulfate (Ahern <i>et al</i> , 1998)
Organic matter content	Leco C, N, S (total carbon)
Mean pyrite diameter	Scanning electron microscope
Soil pH	pH probe
Cation Exchange Capacity	unbuffered BaCl <sub>2</sub> method
<u>Constants</u>	
soil temperature	measured groundwater temperature
oxygen diffusion coefficient (sat aggregate)	literature (Bronswijk <i>et al.</i> , 1993)
Henrys constant	literature (Bronswijk <i>et al.</i> , 1993)
oxygen diffusion coefficient (air)	literature (Bronswijk <i>et al.</i> , 1993)
oxygen concentration in air	literature (Bronswijk <i>et al.</i> , 1993)

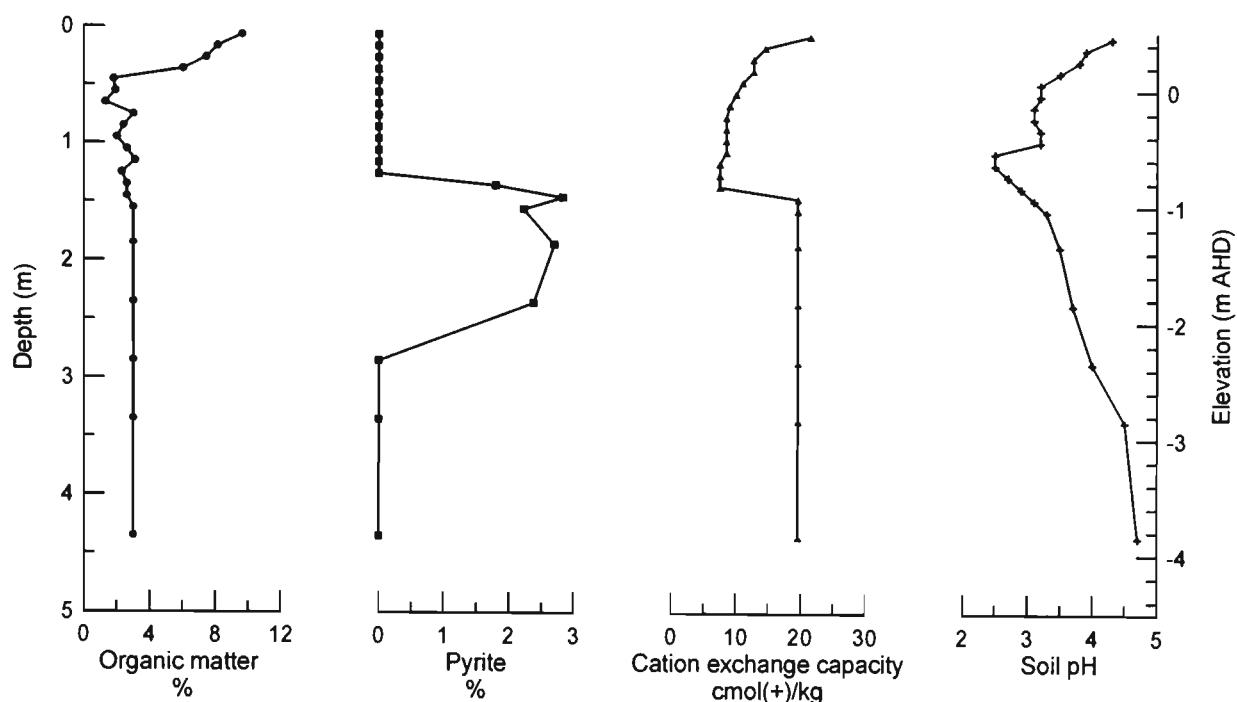


**Figure 9.5.** Initial soil chemical properties for SMASS.

### 9.3 Results and discussion

The results of the four surface and groundwater management options simulated using FEMWATER and SMASS are presented in this section. This includes; a comparison between the observed and simulated groundwater profiles for existing drained situation, the simulated groundwater profiles for weir and irrigation management options, and the simulated moisture content profiles that resulted for the different water management options. The amount of sulfate generated by the oxidation of pyrite for each water management strategy is determined and used to assess the effectiveness of the strategies. For ease of presentation, two dimensional figures have been presented.

#### 9.3.1 Observed groundwater profiles for existing drained situation

Groundwater levels varied considerably during the study period and have largely been controlled by groundwater drawdown from the drains, rainfall and evapotranspiration.



A series of two dimensional groundwater profiles shown in Figure 9.7 illustrate the influence of these factors for the 365 day period starting 18 July, 1997 for the existing deep drainage situation. The profile at day 28 shows a typical drainage profile where the level of water in the drain is below the groundwater level in the surrounding catchment. The hydraulic gradient causes groundwater to flow towards the drain and discharge to the drain through seepage faces in the drain walls. Seepage from the field into the drain continues whilst the hydraulic gradient is in that direction. Prolonged seepage in the absence of groundwater recharge from either rainfall or upland groundwater movement results in a relatively flat groundwater profile where the water level in the drain is in equilibrium with the surrounding groundwater level. This equilibrium was achieved around day 179.

From Figure 9.6 at day 238, it is apparent that the groundwater level falls progressively more as the distance from the drain increases. This is caused by evapotranspiration and deep drainage removing water from the soil profile. The influence of evapotranspiration and deep drainage on the groundwater elevation at piezometers 10 and 90 m from the drain are shown in Figure 9.7. Figure 9.7 demonstrates that evapotranspiration and deep drainage has had a more substantial impact on the groundwater level at 90 m than 10 m. The groundwater level at 10 m has been maintained by the constant water level (low tide level) in the drains. Seepage has occurred through the drain walls, though the resupply rate from the drains is not sufficiently rapid to transport water laterally through the lower soil layers to influence groundwater levels further away from the drains.

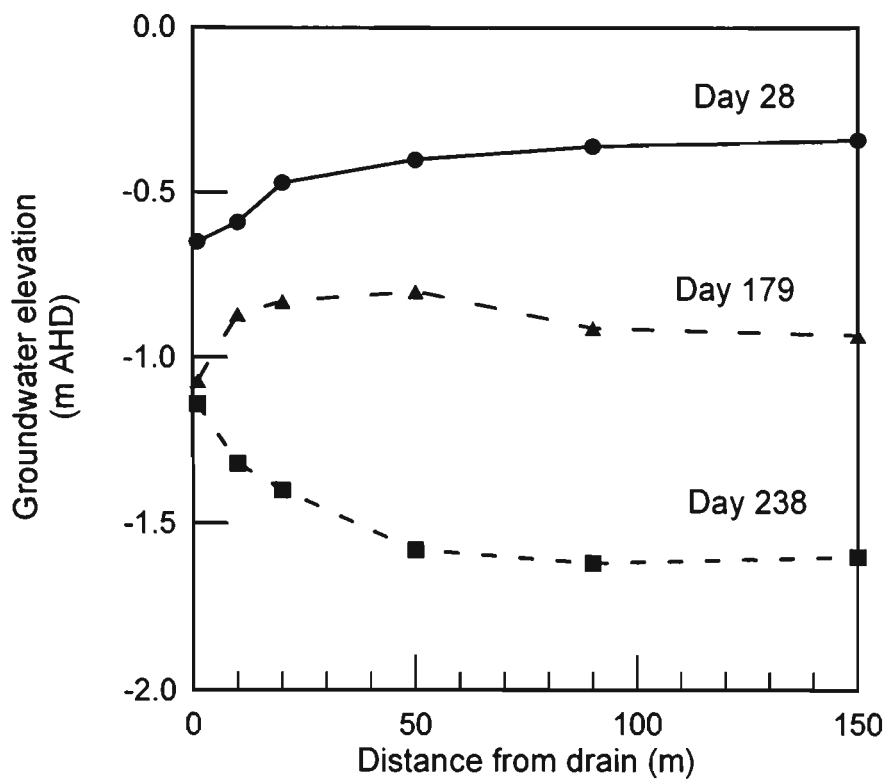


**Figure 9.6.** Groundwater profiles from deep drains.

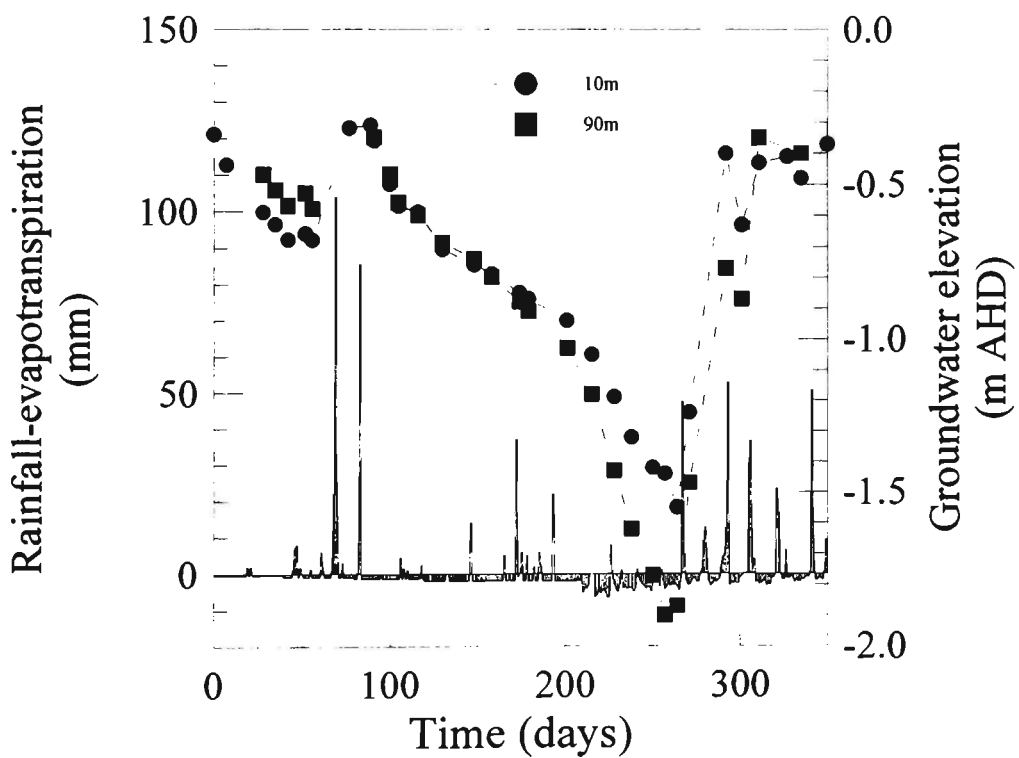


**Figure 9.7** Groundwater elevation at 10 and 90m from drain with rainfall - evapotranspiration.

### *9.3.2 Simulated groundwater profiles for water management options*

The relationship between the observed and simulated groundwater elevations at 10 m and 90 m distance from the drain for the existing drained situation is shown in Figure 9.8. The FEMWATER simulation for the existing drained situation is in good agreement with the observed groundwater elevation data. This indicates that FEMWATER is able to adequately simulate the groundwater hydrology of the study site. One inadequacy of the simulation was that the elevation of the simulated groundwater table was underestimated immediately after heavy periods of rainfall (eg. Day 69 and 83) that led to flooding on the study site. This is attributed to an underestimation of the volume of water available for infiltration on the surface rainfall-evapotranspiration boundary in the simulation. Also, at the study site a large component of surface flood water is run-on water that originates on adjacent upland areas. The resulting unsteady surface flows were not incorporated in the numerical analysis based on FEMWATER.

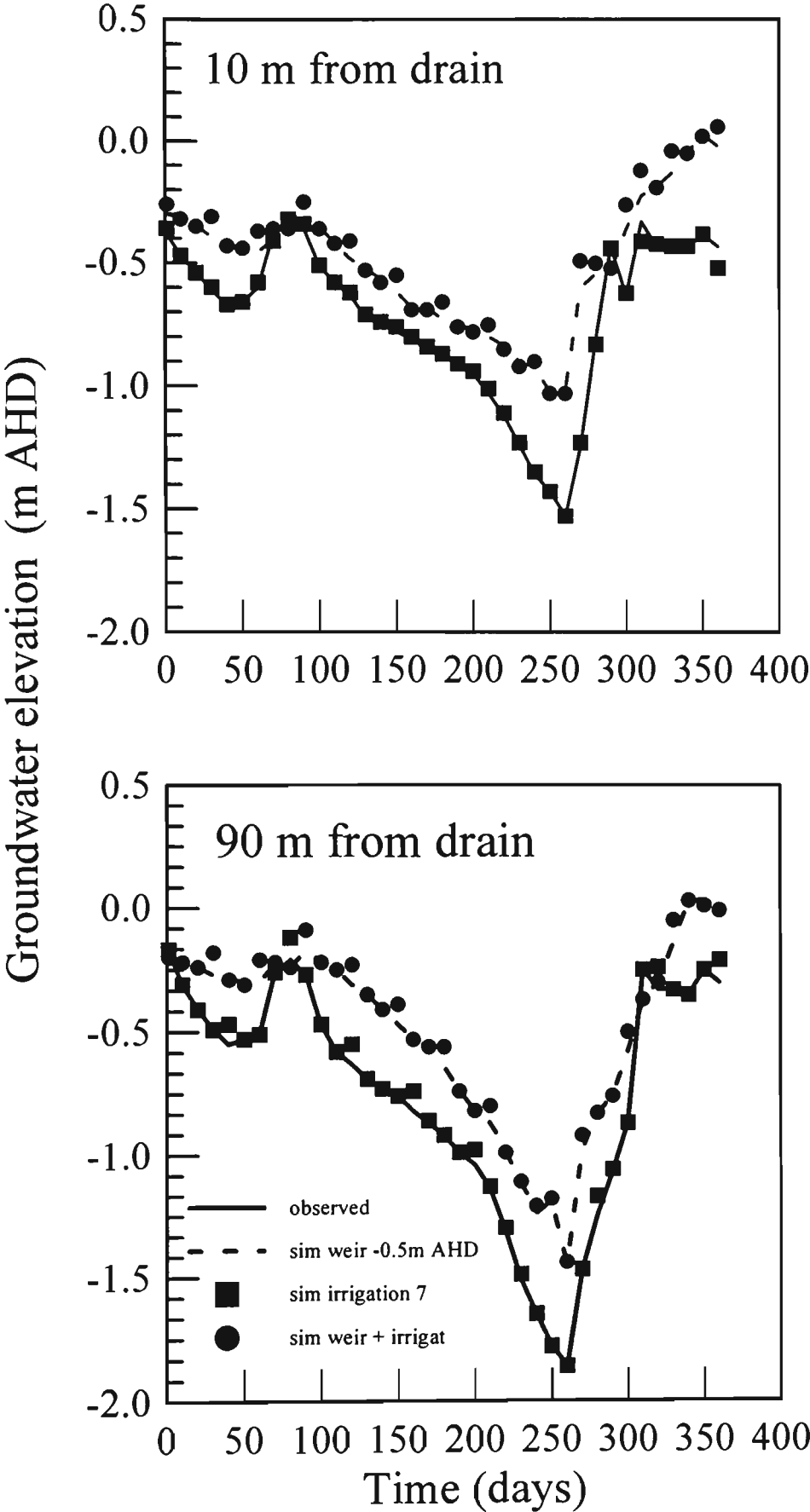


**Figure 9.8.** Observed and simulated groundwater elevations for water management options.

A substantial increase in the elevation of groundwater level at 10 m and 90 m distance from the drain was achieved by maintaining the water level of the drain at -0.5 m AHD by a weir. During the worst part of the drought period where groundwater levels fell well below the elevation of the acid sulfate soil layer, maintenance of the drain water level at -0.5 m AHD resulted in the groundwater at 10 and 90m from the drain being 0.5 m and 0.4 m higher than under the existing drained conditions.

Irrigation on a 14 day cycle in conjunction with installation of the weir did not appreciably increase the groundwater level above that achieved by the elevated drain water levels from the weir alone. Small transient peaks about 5 mm high occurred in the elevation of the groundwater surface on a 14 day cycle that was consistent with the timing of the application of the effluent in the weir and irrigation simulation. Application of irrigation alone at either the 7 or 14 day rate did not influence the elevation of the groundwater level.

### *9.3.3 Measured and simulated pyrite concentration for the existing drained situation*

The pyrite concentration of the sulfidic soil at elevations of -0.7, -0.8 and -0.9 m AHD was determined from samples collected at 90 m distance from the drain in July 1998 (ie. the end of the simulation period). The measured pyrite concentrations at these depths at both the start and end of the simulation period, as well as the pyrite concentrations calculated by SMASS at the end of the simulation, are shown in Figure 9.9.

The computed pyrite concentration in the soil profile at 90 m from the drain after 365-days for the drain simulation correspond well with the measured pyrite concentration. The amount of pyrite consumed during oxidation was overestimated by SMASS at -0.7 m AHD by 0.2 %FeS<sub>2</sub> compared to the measured pyrite concentration. At both -0.8 and -0.9 m AHD, SMASS underestimated pyrite consumption by 0.1 % FeS<sub>2</sub> compared to

the measured pyrite concentration. Given the likely variability in the pyrite concentration of the sulfidic soil, the calculation of pyrite concentration by SMASS is in good agreement with field data. Bronswijk *et al.* (1993) also showed close agreement between the pyrite concentration computed by SMASS and measured data from column experiments, and experience similar or greater differences between measured and computed pyrite concentrations.

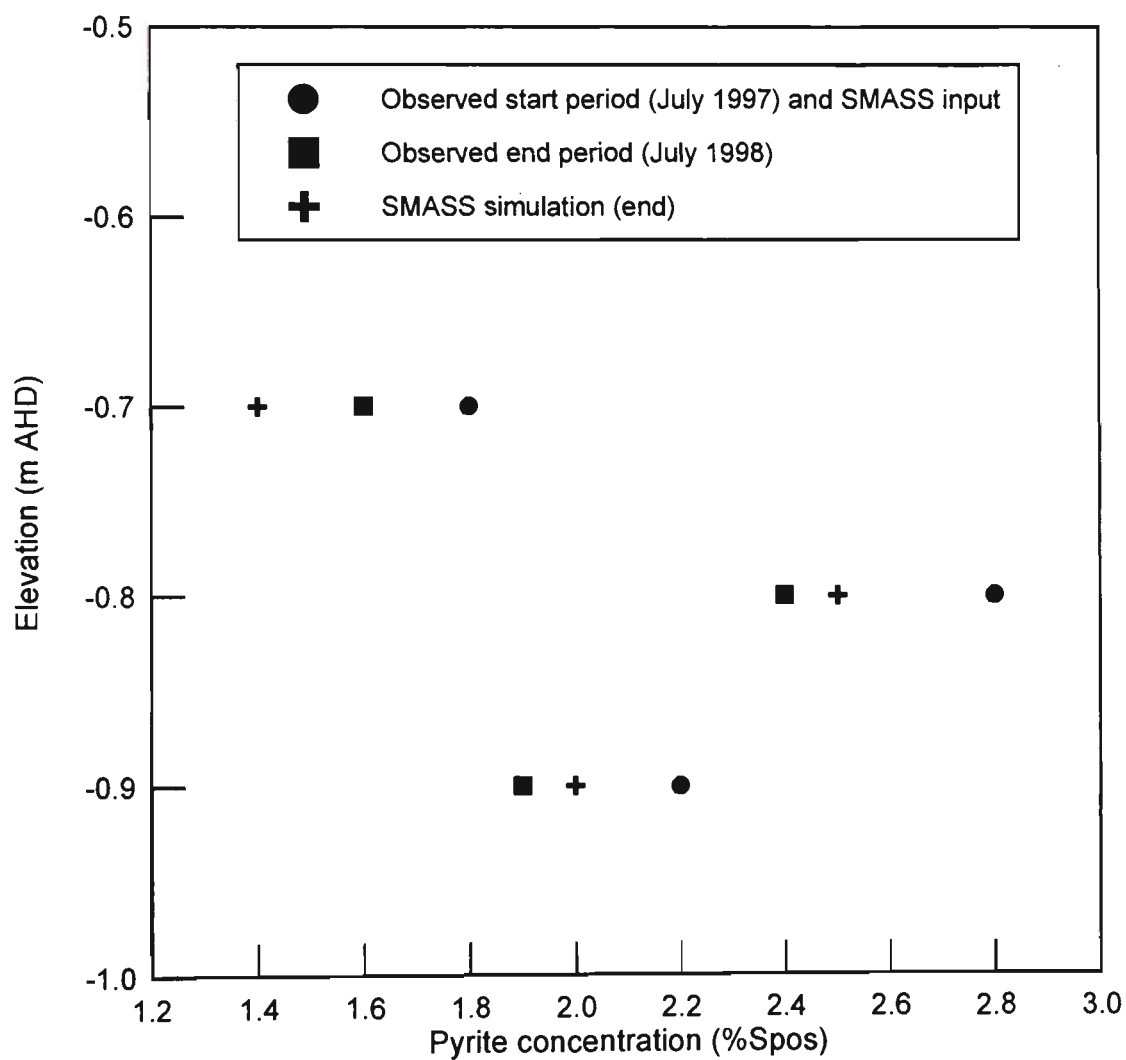


**Figure 9.9** Measured and simulated pyrite concentrations with depth.

#### 9.3.4 *Simulated sulfate production and pyrite consumption for water management options.*

The generation of sulfate by the consumption of pyrite at 10 m and 90 m from the drains for the water management options is shown in Figure 9.10. The onset of sulfate production occurs when the groundwater elevation falls below the level of the sulfidic soil at an elevation of -0.7 m AHD. This enables oxygen to diffuse to the sulfidic soil layer and cause pyrite oxidation in accordance with Equation 2.7.

The generation of sulfate and the consumption by pyrite by oxidation was greatest in the existing drained state. For the period simulated, the existing conditions produced 14.3 mol sulfate/m<sup>2</sup> from the oxidation of 0.86 kg pyrite/m<sup>2</sup> at 10 m distance from the drain and 15.4 mol sulfate/m<sup>2</sup> from the oxidation of 0.92 kg pyrite/m<sup>2</sup> at 90 m from the drain. Pyrite oxidation commenced at day 190 at 10 m distance from the drain and at day 200 at 90 m distance from the drain and ceased at days 280 and 290, respectively.

Application of 25mm of irrigation on a 7-day cycle reduced the time of sulfate production by 20 days with oxidation of pyrite ceasing at day 260. The application of 25mm of irrigation on a 7-day cycle was shown to be the most effective water management strategy in reducing the amount of sulfate generated or pyrite oxidised. The amount of sulfate produced under the 7-day irrigation option was 2.7 mol/m<sup>2</sup> from the oxidation of 0.16 kg pyrite/m<sup>2</sup> at 10 m distance from the drain and 3.3 mol sulfate/m<sup>2</sup> from the oxidation of 0.20 kg pyrite/m<sup>2</sup> at 90 m from the drain.

Irrigation on a 14-day cycle did not influence the length of sulfate production period relative to the existing situation and was the worst of the simulated water management options. The 14-day irrigation option produced 10.9 mol sulfate/m<sup>2</sup> from the oxidation of 0.66 kg pyrite/m<sup>2</sup> at 10 m distance from the drain and 12.1 mol sulfate/m<sup>2</sup> from the oxidation of 0.72 kg pyrite/m<sup>2</sup> at 90 m from the drain.

Installation of the weir in the drains to maintain a drain water level of -0.5 m AHD was successful in minimising the time of oxidation and the generation of sulfate. Oxidation of pyrite occurred between days 230 and 270 at both 10 and 90 m distance from the drains for the weir water management option. The weir options resulted in a significant reduction in the amount of pyrite oxidised and sulfate generated, though these options were not as successful as the application of 25 mm irrigation on a 7-day cycle. The elevated drain water level - weir option produced 3.6 mol sulfate/m<sup>2</sup> from the oxidation of 0.22 kg pyrite/m<sup>2</sup> at 10 m distance from the drain, and 6.7 mol sulfate/m<sup>2</sup> from the oxidation of 0.40 kg pyrite/m<sup>2</sup> at 90 m from the drain. Application of irrigation on a 14-day cycle in addition to implementation of the weir resulted in a small additional reduction in the time of pyrite oxidation and generation of sulfate.

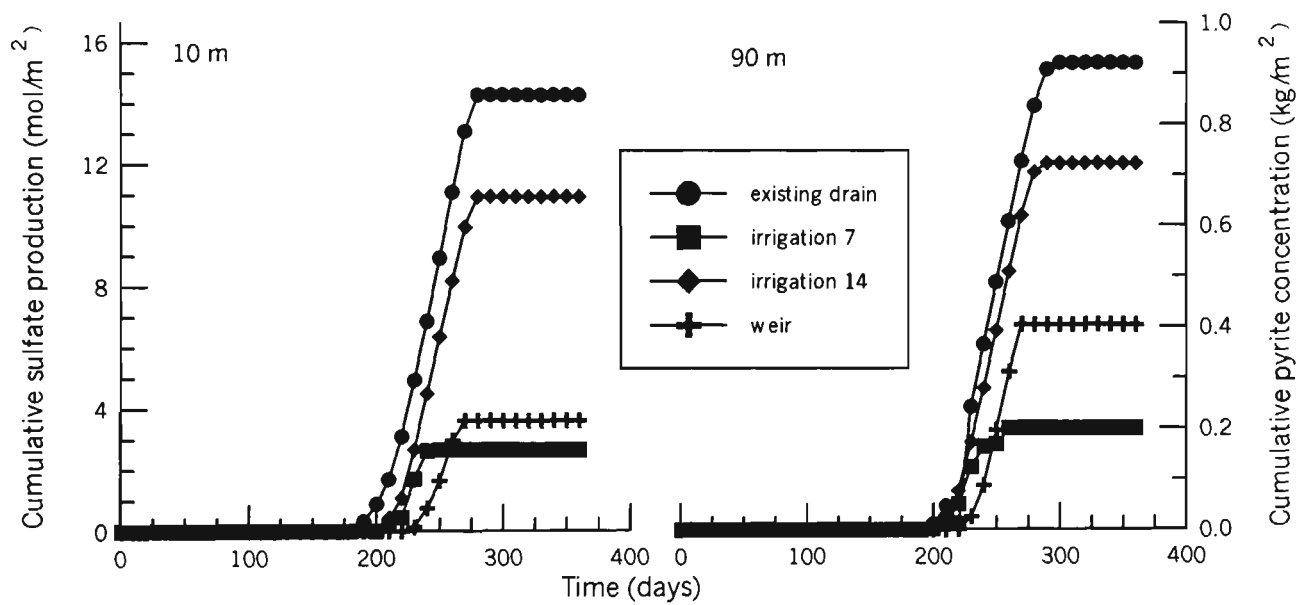


**Figure 9.10.** Cumulative sulfate production and pyrite consumption from water management options

Figure 9.11 shows the amount of pyrite that has oxidised at each depth as a percentage of the pyrite present at the start of the simulations. The 7 day irrigation and both the weir strategies limited the consumption of pyrite to about 10% in the upper acid sulfate soil layer, with decreasing amounts of pyrite being consumed down to a depth of 1.65 m below the surface at 10m distance from the drain (Figure 9.11). In contrast, the existing



situation and 14 day irrigation treatment consumed relatively large amounts of the initial pyrite concentration to a depth of 1.85 m below the surface.

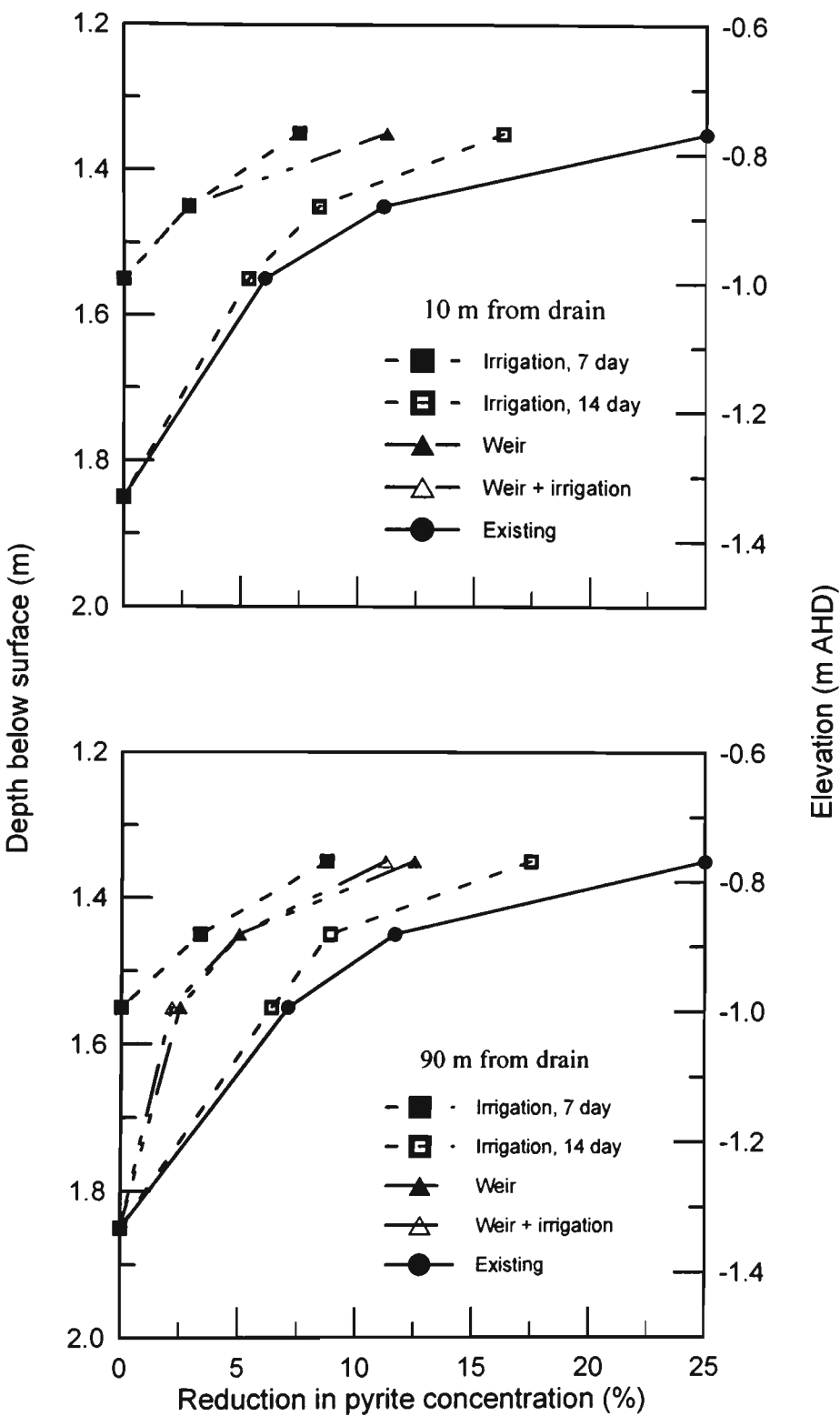


**Figure 9.11.** Amount of pyrite oxidised during simulation period.

The magnitude of the reduction in the amount of pyrite present in the soil experienced during the simulation period (which included a severe drought) for the existing over-drained situation emphasises the need for better water management to minimise the generation of acidity from the oxidation of pyrite. Bronswijk *et al.* (1995) suggested the promotion of pyrite oxidation in the upper part of the acid sulfate soil layer and flushing of the acidic oxidation products from the soil as a suitable technique for agriculture in Indonesia where acid sulfate soils are close to the surface. Bronswijk *et al.* (1995) showed that complete oxidation of acid sulfate soils that were prone to oxidation could be achieved in as little as 3-4 years for the Indonesian site. The strategy of promoting pyrite oxidation and leaching of the acidic oxidation products is unlikely to be successful at this site. Under existing conditions for this site it would take in excess of four similarly severe drought periods to completely oxidise the remaining pyrite from the first 0.1m of the acid sulfate soil layer. Deeper deposits of acid sulfate soils would remain and pose acid generation problems in subsequent drought periods. The soil and leachate transported to the drains would remain at a low pH until all the pyrite in the oxidised acid sulfate soils was consumed and internal buffering within the soil neutralised the store of acidity present in the soil. Given the large quantity of acidity already existing in the soil profile, this neutralising process would take many decades. Poor agricultural productivity and environmental degradation would persist during this period.

#### 9.3.5 *Simulated moisture content profiles for water management options*

The concentration of oxygen at a specific place in the soil profile is determined by both the consumption of oxygen in the soil and the rate of diffusion of oxygen into the soil pore space. SMASS determines the oxygen diffusivity in soil pore space ( $D_s$ ) according to Equation (9.16):

$$D_s = F[1 - (1 - \epsilon_a)^{2/3}]D_o \quad (9.16)$$

where;  $F$  is tortuosity,  $\epsilon_a$  is air filled porosity and  $D_o$  is oxygen diffusivity in air.

The magnitude of  $D_s$  defined in Equation (9.16) can be reduced where high water saturation in the soil results in small values of  $\epsilon_a$ . The simulated volumetric moisture content profiles for the existing over-drained state, irrigation of 25mm on a 7 day cycle and the implementation of the weir at 10 m and 90 m distance respectively, from the drain are shown for day 250 in Figure 9.12. Day 250 represents the situation where groundwater elevations are lowest resulting in high pyrite oxidation and sulfate generation.

Figure 9.12 shows that the reduction in sulfate production from pyrite oxidation can be attributed to high water saturation in different parts of the profile for the irrigation and weir water management options. For the irrigation strategy, the upper 0.3 m of the soil profile is at a nearly saturated state with volumetric moisture content of about 50%. The high moisture status of the surface soil reduces  $\epsilon_a$  to about 5% which results in a very low oxygen diffusivity in the soil pore space near the surface. The nearly saturated layer acts as an oxygen barrier which reduces the amount of oxygen that can be transported to the deeper pyritic sediments. The very high soil moisture content at the surface shown in Figure 9.12 is only for the day when the irrigation was applied. In subsequent days, the simulation redistributes the irrigation water down the soil profile, resulting in increased oxygen transport down the soil profile.

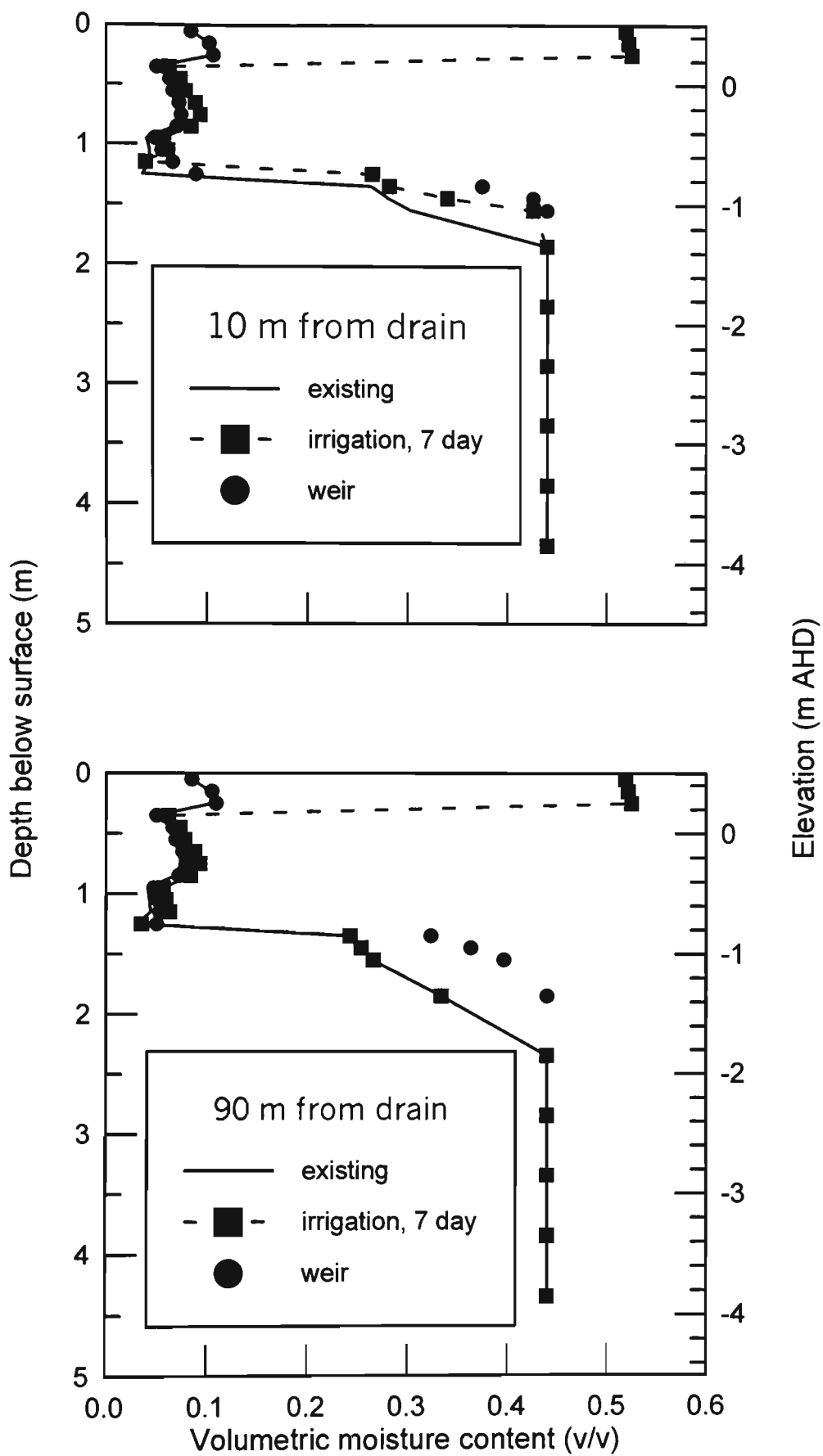


**Figure 9.12.** Volumetric moisture content distribution at day 250.

The weir strategy relies upon maintenance of highly saturated soil layers at depth. At 1.35 m (i.e., the depth of the acid sulfate soil layer) the air-filled porosity for the weir option is 6.5% and 11.6% at 10 m and 90 m distance respectively, from the drains, whereas the air-filled porosity for the 7 day irrigation is 15.8% and 19.7% at 10 and 90m respectively. According to Equation (9.16), the diffusivity of oxygen in the acid sulfate soil will be less for the weir option than the irrigation alternative. Reduction of  $D_s$  in the acid sulfate soil layer may restrict the amount of pyrite oxidation and the depth that oxidation of pyrite can occur. Figure 9.12 shows that air-filled pore space is available to transport oxygen to a depth of 2.35 m for the irrigation option at 90 m distance from the drain whereas saturation occurs at a depth of 1.85 m for the weir alternative. In addition, the moisture content of the soil is higher between 1.35 m and 1.55 m depth for the weir options than the irrigation option, thereby reducing the diffusivity of oxygen according to Equation (9.16).

### 9.3.6 *Assessment of water management options*

All the water management options simulated using FEMWATER and SMASS were effective in reducing the oxidation of pyrite in the sulfidic soil relative to the existing over drained situation. The relative effectiveness of the water management strategies in comparison to the existing situation is shown in Figure 9.13.

Application of 25 mm irrigation on a 7-day cycle reduced sulfate production to 11% and 6% of the existing situation at 10 m and 90 m from the drain respectively. However, irrigation on a 14-day cycle reduced sulfate production to only 76% and 78%. Maintenance of an oxygen barrier of nearly saturated soil is the key for reducing the oxidation of pyrite in the underlying sulfidic soil. Application of irrigation as a strategy to minimise pyrite oxidation requires careful consideration. Due to the unreliable rainfall patterns in Eastern Australia, the ability to secure sufficient volumes of water for irrigation during dry summer periods is difficult. If irrigation rates are relaxed or

insufficient then rapid pyrite oxidation may occur when groundwater levels fall below the elevation of the sulfidic soil layer. However, where secure sources of irrigation exist, such as effluent from sewage treatment plants, then significant reductions in the oxidation of pyrite may be achieved.

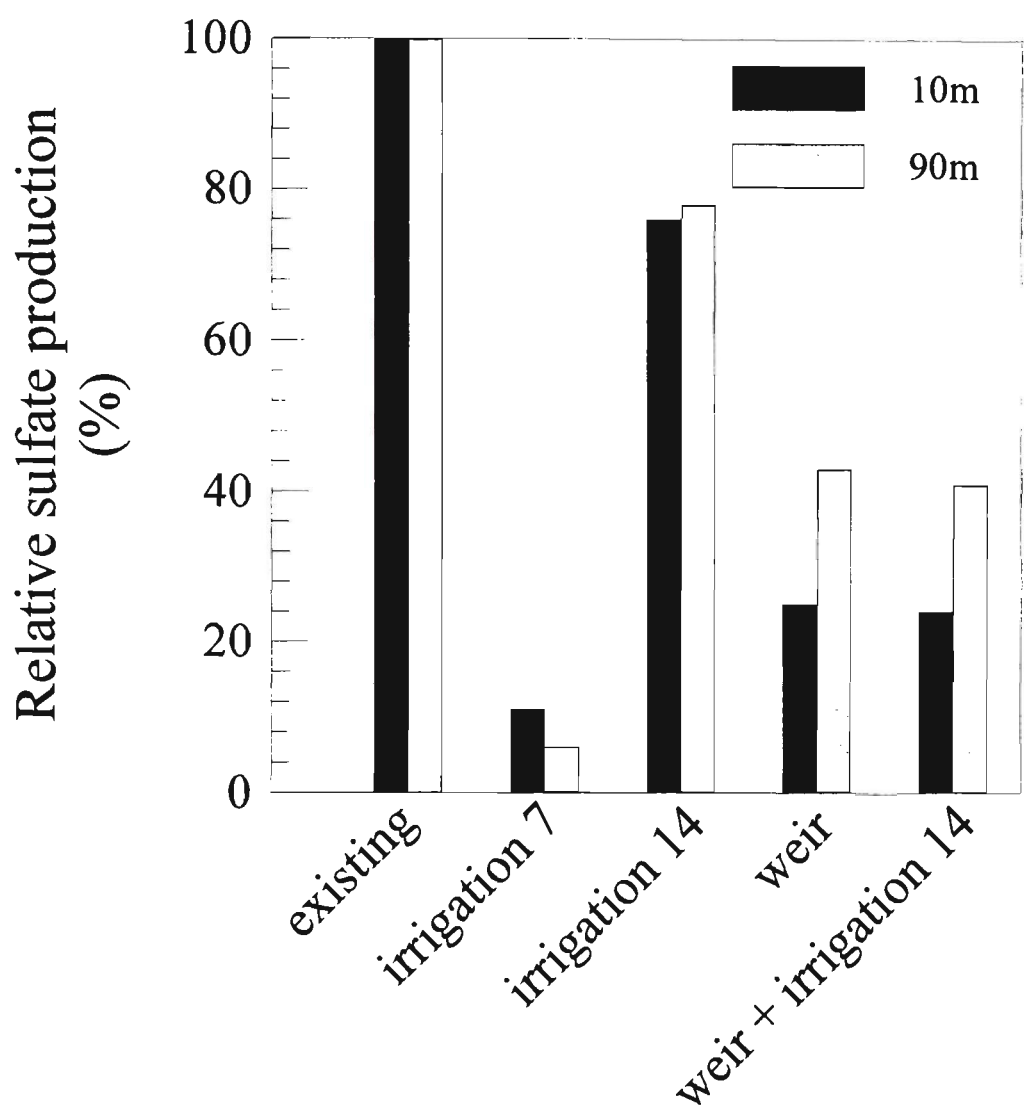


**Figure 9.13.** Relative sulfate production for water management options.

Simulation of the groundwater regime caused by the installation of a weir in the drain to maintain a drain water level of -0.5 m AHD resulted in a reduction to 25% and 43% of the existing situation at 10 m and 90 m from the drain, respectively. The addition of irrigation on a 14-day rotation to the weir option reduced sulfate production only by another 1-2%. Sulfate production occurred between days 230-260 which corresponds

with the worst part of the drought period. The onset of sulfate production occurred at day 190 for the irrigation options. This suggests that implementation of the weir strategy delays the onset of oxidising conditions in the sulfidic soil. Under 'normal' climatic conditions, it is envisaged that elevated drain water levels will maintain groundwater levels above the sulfidic soil horizon. Where a rainfall deficit occurs, evaporation from the open drain water surface may result in a reduction of the water level in the drain. Strategies to minimise evaporation from the drain or to 'top up' drain water levels should be considered during dry periods. The addition of brackish water into drains from nearby waterways may be an appropriate source of water for maintenance of drain water height. Given the very low saturated hydraulic of the sulfidic soil in the horizontal plane, intrusion of saline water into the groundwater would not be significant. Figure 9.6 demonstrates that recharge from the drain into the surrounding groundwater occurs extremely slowly.

Implementation of elevated drain water levels using weirs may also prove to be effective in reducing the acid discharge rate into the drains because the hydraulic gradient from the groundwater to the drain will be reduced. The smaller hydraulic gradient retards the discharge rate of the existing acidity in the soil to the drain. The slower acid discharge rate may enable the natural buffering capacity of the receiving waters to neutralise the slow leakage of acidity.

Determination of the titratable acidity using the total actual acidity method (Ahern *et al.*, 1998) for the upper 1.5 m of the soil profile showed that approximately  $88 \text{ mol H}^+/\text{m}^2$  (which corresponds to the equivalent of 43 tonnes  $\text{H}_2\text{SO}_4/\text{ha}$ ) existed at the start of the study period. The oxidation of  $0.92 \text{ kg FeS}_2/\text{m}^2$  during the study period under the existing drained conditions caused the equivalent of an additional 15 tonnes  $\text{H}_2\text{SO}_4/\text{ha}$  to be generated and made available for export. The pyrite oxidised during the period of low groundwater elevation represents about 35% of the acid originally stored within the soil profile. This suggests that high rates of evapotranspiration experienced during droughts, coupled with inappropriate drainage practices, play a significant part in the generation of acid. In addition, these acidifying events cause basic cations on the cation exchange sites to be replaced with acidic actions such as aluminium and hydrogen

(Ritsema et al., 1992). The acidified soil causes the groundwater to become acidic, irrespective of groundwater elevation, as the groundwater achieves chemical equilibrium with the soil. Groundwater pH measured at the study site is usually within the range 3.2-4, even when the groundwater elevation is higher than the sulfidic soil layer. However, immediately after pyrite oxidation, the groundwater pH falls to less than 3.

### 9.3.7 Other acid sulfate soil management strategies

The simulation data presented in this paper indicates that water table management is the key to the sustainable use of land affected by acid sulfate soils. The re-design of drainage systems that influence groundwater drawdown may ultimately be the most effective acid sulfate soil management technique, though it is expensive and physically demanding. White *et al.* (1997) suggest that broad shallow drains may improve the removal of excess surface water from agricultural land thereby reducing the instance of waterlogging without causing drawdown of the groundwater table typical of deep narrow drains. Lawrie and Murphy (1996) report that replacing deep drains with shallow spoon drains, laser levelling to promote efficient overland flow, effluent irrigation and surface liming have had a positive effect on acid sulfate soil affected land near Bomaderry (NSW). These works are associated with the disposal of high strength effluent from an adjacent industrial activity making the adoption of acid sulfate soil and/or agricultural management practices of secondary importance. The capital expenditure required for drain filling/reshaping and laser levelling would be difficult to justify for agricultural activities involving grazing.

Liming has been the traditional response to managing acid soil. In excess of 40 tonnes of  $\text{H}_2\text{SO}_4$ /ha are stored within the upper 1.5 m of the soil profile. This would require a similar tonnage of lime to be thoroughly incorporated into this soil in order to neutralise the existing acid. Acidity generated in the future by pyrite oxidation would require



similar treatment. Adoption of large scale liming treatment on broad acre agricultural land is prohibitively expensive given its productivity.

## 9.4 Conclusions

Appropriate surface and groundwater management is the key to the sustainable management of acid sulfate soils. Observed groundwater elevation data showed that the groundwater fell below the acid sulfate soil layer for a period of about 70 days for the existing drained situation during the summer of 1997-98. This caused the oxidation of pyrite in the acid sulfate soil and the subsequent generation of a considerable volume of sulfuric acid.

Simulation of water management strategies that reduce the diffusivity of oxygen into the pyritic material were shown to be effective in reducing the amount of pyrite oxidation in comparison to the existing drained situation. Application of 25 mm of irrigation on a 7 day cycle was demonstrated to be the most effective strategy to reduce pyrite oxidation. Irrigation on a 14 day cycle was shown to be the least effective. This indicated that the volume and amount of irrigation applied must be carefully managed so that a permanent oxygen barrier is maintained near the soil surface to minimise the transport of oxygen to underlying acid sulfate soil layers. Securing an adequate supply of irrigation water may pose a significant challenge in El Niño influenced eastern Australia.

Installation of weirs in the existing drains was also found to be effective. Maintenance of drain water levels at -0.5m AHD increased the groundwater levels by 0.5m and 0.4m at 10m and 90 m, respectively, from the drains during the most severe part of the 1997-98 summer drought period. Simulations indicate that the amount of pyrite oxidised was reduced by 75% and 57% at 10 m and 90 m with respect to the existing situation for the weir option. Additional irrigation in conjunction with the weir option further reduced the amount of pyrite oxidised by 1-2%. Maintenance of drain water levels during

prolonged dry periods could be achieved by pumping readily available sources of brackish estuarine water into the drains. Saline intrusion is not expected due to the very low permeability of the acid sulfate soils in the horizontal plane. The cost of installing weirs to maintain drain water levels or irrigation systems are reasonably low and may have direct benefits for pasture productivity. Other alternatives such as liming or redesign of drainage systems are considerably more expensive.

The numerical analysis of the various water management options investigated above demonstrates that it is important to understand the groundwater regime and its subsequent impact on the oxidation of pyrite in two or three dimensions. SMASS is a one dimensional model, and as such, is of limited use in assessing the implications of water management strategies on a farm or sub-catchment scale, particularly where drawdown from large drains or evapotranspiration from crops is expected to result in variable groundwater elevation across a site. To overcome this shortcoming, a pyrite oxidation model for acid sulfate has been developed for application with the output of 3D FEMWATER simulations. This model is presented in Chapter 10.

## **Chapter 10: A pyrite oxidation model for assessing groundwater management in acid sulfate soils**

### **10.1 Introduction**

A model that simulates the magnitude and distribution of pyrite oxidation in acid sulfate soil in a three dimensional landscape is described in this Chapter. In the first part of the Chapter, the relevant equations which describe the transport of oxygen through soil macropores and into the soil matrix where aerobic conditions exist are derived using a similar approach to that used by Bronswijk *et al.* (1993). The theoretical approach shows that the generation of acidic oxidation products is dependent on the concentration of oxygen in the aerobic part of the soil matrix. Where anaerobic conditions exist, no pyrite oxidation occurs. The transport of oxygen down the soil macropores is assumed to be a one-dimensional (1D) process, ignoring the component of lateral migration into the surrounding soil matrix.

The second part of this Chapter shows how these equations are solved numerically. The numerical scheme for 1D pyrite oxidation is described, and the Fortran 77 code for the simulation model based on these equations is presented in Appendix C. A description of how the 1D pyrite oxidation numerical scheme is linked to the 3D soil moisture content distribution produced from the simulation of saturated/unsaturated conditions using FEMWATER is also given. A comparison of the analytical and numerical solutions for the oxygen consumption terms derived in the pyrite oxidation model gives very good agreement, indicating that the numerical approach adopted in the ASS3D Fortran code accurately calculates that amount of pyrite oxidised in the soil matrix.

## 10.2 Theoretical formulations for the pyrite oxidation model.

A number of fundamental processes must be simulated in order to model the transport of oxygen, and its consumption by pyrite, in structured acid sulfate soils. In this model, equations that describe the; oxygen transport down macropores, pyrite oxidation in the aerobic soil matrix, oxygen transport in the soil matrix, and oxygen diffusion and consumption in the macropores are presented using a similar approach to that developed by Bronswijk *et al.* (1993). However, some substantial differences including; the partitioning of the concentration of oxygen in water into the fraction consumed by pyrite and other factors and the relationship between air-filled porosity and oxygen diffusivity are incorporated into this model. In addition, a more elegant solution to the linear approximation of the steady state oxygen diffusion into the aerobic part of the soil matrix is also derived. The formulation of these equations is shown below.

### 10.2.1 Oxygen transport down macropores

The oxidation of pyrite in acid sulfate soils is largely determined by the concentration of oxygen. Other factors of secondary nature such as the oxidation of pyrite by reducing  $\text{Fe}^{3+}$  have been neglected. The concentration of oxygen at a particular depth in the soil determines the rate of pyrite oxidation at that depth (Dent, 1986). The oxygen consumption at any depth is dependent on: a) the diffusion of oxygen into the soil, and b) the consumption of oxygen in the soil. Christensen *et al.* (1986) and Elberling *et al.* (1994) describe this relationship between oxygen concentration, supply and consumption as:

$$\epsilon_g \frac{\partial C_a(x)}{\partial t} = \frac{\partial}{\partial x} \left( D_s(\epsilon_g) \frac{\partial C_a(x)}{\partial x} \right) - \alpha_v \quad (10.1)$$

where;  $C_a(x)$  is the concentration of oxygen in air-filled pores ( $\text{m}^3$  per unit volume of soil),  $D_s$  is the diffusion coefficient of oxygen in air-filled pores ( $\text{m}^2 \text{d}^{-1}$ ),  $t$  is time (d),  $x$  is distance (m),  $\epsilon_g$  is air-filled porosity ( $\text{m}^3 \text{m}^{-3}$ ), and  $\alpha_v$  is the volumetric consumption rate ( $\text{m}^3 \text{m}^{-3} \text{d}^{-1}$ ).

Equation (10.1) is difficult to solve analytically due to the heterogeneity of porosity down a soil profile, the dependence of  $D_s$  on the air-filled pore space and the influence of the oxygen consumption rate. However, Equation (10.1) can be simplified by assuming that the steady state oxygen concentration profile forms quickly, say within minutes or hours. Therefore, where that oxygen concentration profile in the soil is calculated on a daily time step (i.e. at a steady state) then Equation (10.1) simplifies to:

$$\frac{\partial}{\partial x} \left( D_s(\epsilon_g) \frac{\partial C_a(x)}{\partial x} \right) = \alpha_v \quad (10.2)$$

The physical structure of the acid sulfate and the overlying soil layers largely determines  $D_s$ . For the acid sulfate soils encountered at the Berry site and elsewhere in Australia (e.g., Wilson, 1995), the most outstanding structural feature of the soil is the presence of large (2-10 mm diameter), continuous and straight macropores created by previous plant root activity. Roots of growing plants are confined to the upper 0.5 m top soil horizon of the soil profile where acidity and dissolved aluminium do not restrict root exploration. The older macropore channels within the clayey matrix at deeper depths do not have organic matter remnants. These macropores are surrounded by a tightly packed clayey matrix with massive structure. Thin section analysis of a similarly structured acid sulfate soil from Indonesia by Bronswijk *et al.* (1993) showed that the acid sulfate soil immediately adjacent to macropores have experienced pyrite oxidation, whereas the pyrite contained in the soil matrix further away from the structural features of the soil had not been oxidized. This has also been observed during profile description in Australia (Wilson, 1995; Blunden and Indraratna, 2000). A photograph of the structural features of the potential acid sulfate soil at 1.5 m depth from the Berry trial site is shown in Plate 10.1.



**Plate 10.1** Structural features of the potential acid sulfate soil at 1.5 m depth.

Thin section analysis of a similarly structured acid sulfate soil from Indonesia by Bronswijk *et al.* (1993) shows that the acid sulfate soil immediately adjacent to macropores has experienced pyrite oxidation, whereas the pyrite contained in the soil matrix further away from the structural features of the soil had not been oxidised. Roots of growing plants are confined to the upper 0.5 m top soil horizon of the profile where acidity and dissolved aluminium do not restrict root exploration. The older macropore channels within the clayey matrix at deeper depths do not have organic matter remnants.

The nature of the soil structure applied in this pyrite oxidation model and by Bronswijk *et al.* (1993) is shown in Figure 10.1. The schematic representation of the soil structure shows that oxygen diffuses vertically from the atmosphere into the soil through the air-filled macropores. The oxygen in the macropores is dissolved into the soil solution at

the macropore walls where it can diffuse into the soil matrix. The dissolved oxygen is then consumed by pyrite oxidation.

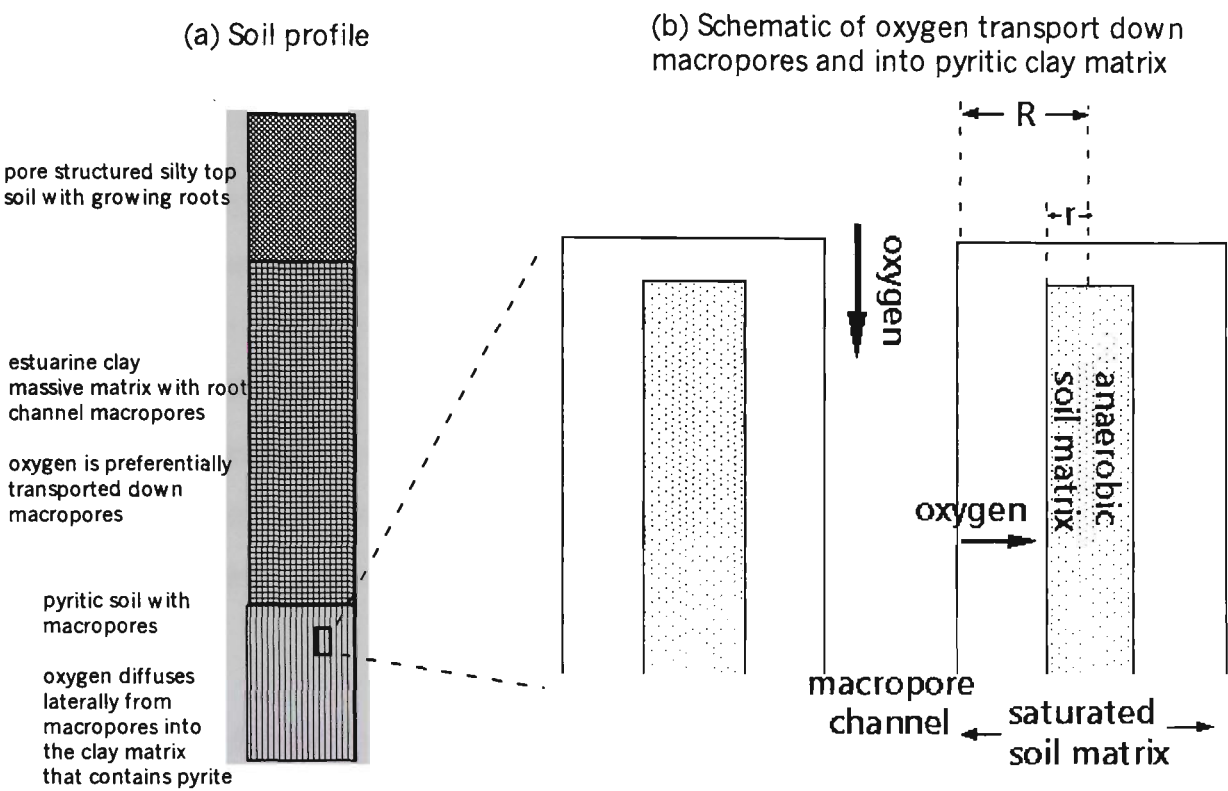


**Figure 10.1** Schematic of the soil structure and oxygen transport in the pyrite oxidation model.  $R$  is the radius of the soil aggregates,  $r$  is the radius of the anaerobic zone.

The clayey nature of these estuarine sediments and their macropore dominated structure control the transport of both air and water in the vertical and horizontal plane. As shown in Chapter 6, the saturated hydraulic conductivity ( $K_{sat}$ ) in the vertical orientation was substantially greater than  $K_{sat}$  in the horizontal plane, particularly in the clayey soil horizons. The analysis of oxygen transport and subsequent pyrite oxidation described in this Chapter is limited to structured soil where air and water transport is dominant in the vertical orientation. The analysis may not be applicable for granular or well packed materials such as sands, gravels or for granular pyritic rock wastes.

### 10.2.2 pyrite oxidation in the aerobic soil matrix

The oxidation of pyrite is simulated in this model as the consumption of oxygen within the soil matrix. The amount of oxygen consumed during pyrite oxidation is dependent on the local oxygen concentration in the soil solution (Dent, 1986). Bronswikj *et al.* (1993) show that the relative importance of oxygen consumption by organic matter is very small in comparison to the oxygen consumed by pyrite. White *et al.* (1997) suggest that the concentration of organic matter in Australian acid sulfate soil is very low and insufficient to reduce dissolved sulfate back to sulfide. Therefore, the consumption of oxygen by organic matter is not explicitly modelled but is assumed to a constant small value where aerated conditions exist.

The oxidation of pyrite is based on the “spherical reduction” concept first described by Davis and Ritchie (1986) and adopted by most processed based numerical models of pyrite oxidation subsequently. This concept has two assumptions:

- a) the rate of mass loss from the pyrite crystals as a result of oxidation is proportional to the surface area of the crystals; and
- b) the crystals are spheres of equal diameter.

The first assumption has been confirmed by Moses and Herrmann (1991) who showed that pyrite oxidation is a first order rate reaction with respect to the surface/volume ratio of pyrite crystals. The second assumption is not valid for the distribution of pyrite in acid sulfate soils (see Chapter 6). However, the addition of a stochastic numerical scheme to account for a distribution of pyrite crystal diameters is expensive and adds little with respect to the assessment of various acid sulfate soil management practices in a 3D landscape.



Given these assumptions, the rate of pyrite dissolution by the consumption of oxygen is given by:

$$\frac{\partial m}{\partial t} = -KA \quad (10.3)$$

where:  $A$  is the surface area of pyrite crystals ( $\text{m}^2$ ),  $K$  is the rate constant ( $\text{kg m}^{-2} \text{d}^{-1}$ ),  $m$  is the mass of pyrite ( $\text{kg}$ ), and  $t$  is time ( $\text{d}$ ).

In a unit volume ( $\text{m}^3$ ) of acid sulfate soil:

$$A = N\pi d^2 \quad (10.4)$$

where  $N$  is the number of pyrite crystals per  $1 \text{ m}^3$  of acid sulfate soil, and  $d$  is the diameter of the pyrite crystals ( $\text{m}$ ).

$N$  is equal to the volume of pyrite in  $1 \text{ m}^3$  soil divided by the volume of one pyrite crystal. The volume of pyrite in  $1 \text{ m}^3$  of soil is equal to  $C_{\text{FeS}_2}/\rho$ , where  $C_{\text{FeS}_2}$  is the pyrite content ( $\text{kg m}^{-3}$ ), and  $\rho$  is the density of pyrite ( $\text{kg m}^{-3}$ ). The magnitude of  $N$  is represented by:

$$N = \frac{C_{\text{FeS}_2} / \rho}{\frac{1}{6}\pi d^3} \quad (10.5)$$

Using the Davis and Ritchie (1986) spherical diameter reduction concept, substituting equation (10.5) into equation (10.4), the resulting expression from equation (10.3) gives:

$$\frac{\partial m}{\partial t} = -K \frac{6C_{\text{FeS}_2}}{\rho d} \quad (10.6)$$

Equation (10.6) shows that the rate of pyrite oxidation is dependent on a few easily determined parameters (that is,  $C_{\text{FeS}_2}$  using wet chemical methods,  $d$  from thin section SEM, and  $\rho$  from literature). Obtaining the value of the rate constant,  $K$ , is more problematic. In the past, no rate constants have been evaluated specifically for pyrite oxidation in acid sulfate soils, however, a host of  $K$  values have been reported in the geochemical literature. These rate constants are usually derived from tightly controlled laboratory experiments using mixtures of pyrite crystals and water. It is not clear whether laboratory derived  $K$  values are applicable for the simulation of pyrite oxidation in the field. The oxidation of pyrite in sulfidic sediments is likely to be affected by numerous physical and chemical processes that occur in the soil. These may include; the formation of coatings on pyrite crystals that change the contact mechanism of oxygen with the pyrite, chemical buffering processes within the soil that alter the amount of acid ultimately available for transport in the groundwater, and various catalytic bacterial processes that influence the pyrite oxidation rate under different pH conditions. These conditions are not replicated in tightly controlled laboratory determinations of pyrite oxidation. As a result, the experimentally derived  $K$  values are only indicative of the rate of pyrite oxidation in soils.

McKibben and Barnes (1986) experimentally derived  $K$  values in the laboratory for similar temperature and pH conditions found in acid sulfate soils. McKibben and Barnes (1986) found that:

$$K = 0.051877\sqrt{C_w} \quad (10.7)$$

where;  $C_w$  is the concentration of dissolved oxygen ( $\text{kg m}^{-3}$ ) in water.

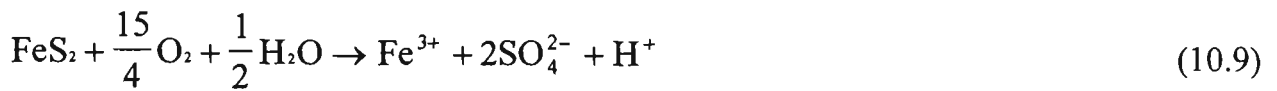
Developing Bronswijk *et al.* (1993) further,  $C_w$  can be partitioned such that  $C_w = C_p + C_{om}$ , where  $C_p$  and  $C_{om}$  are the concentrations of oxygen consumed by pyrite and other factors such as organic matter decomposition respectively in acid sulfate soil.

Substitution of equation (10.7) into equation (10.6) gives:

$$\frac{\partial m}{\partial t} = \frac{0.311262 C_{FeS_2}}{\rho d} \sqrt{C_p + C_{om}} \times \frac{0.311262 C_{FeS_2}}{2\sqrt{C_p} \rho d} \quad (10.8)$$

where  $\frac{dm}{dt}$  now represents the rate of disappearance of pyrite crystals as a result of oxidation by oxygen and by the oxidation of organic substances in the soil. The consumption of oxygen by organic matter (that is, the right hand term in Equation [10.8]) is relatively small in comparison to the consumption of oxygen by pyrite oxidation. It is therefore reasonable to neglect the right hand site of Equation (10.8) and replace it with a small constant value. Bronswijk *et al.* (1993) also use this approach. The organic matter concentration measured in the pyritic soil at the field site was less than 3% (see Chapter 6). Sensitivity analyses were conducted to determine the impact of  $C_{om}$  on  $\frac{\partial m}{\partial t}$ . The amount of oxygen consumed by 3%  $C_{om}$  when no pyrite is present in the soil was 14 kg/day. In comparison, the amount of pyrite consumed when both  $C_p$  and  $C_{om}$  are 3% was 2907 kg/day. This indicated that the contribution of organic matter to overall oxygen consumption in the pyritic soil was very small.

The reaction equation for pyrite oxidation by oxygen is:



Therefore, in aerobic conditions 1 mole of pyrite consumes 3.75 moles of oxygen during complete oxidation, which is equal to 1 kg of pyrite consuming 1 kg of oxygen. Thus, Equation (10.8) may also be expressed as the mass oxygen consumption rate,  $\alpha_m$ , by pyrite oxidation within the soil matrix, that is:

$$\alpha_m = \frac{0.311262C_{\text{FeS}_2}}{\rho d} \sqrt{C_p} + \text{OM} \quad (10.10)$$

where OM can be regarded as a small constant used to account for the consumption of oxygen by sources other than pyrite in the soil.

### 10.2.3 Oxygen transport in the soil matrix

At some distance ( $R-r$ , see Figure 10.1) from the macropore wall into the soil matrix, the consumption of oxygen by pyrite will equal the supply of oxygen through the macropore wall. The remainder of the soil matrix is assumed to remain anaerobic. As shown in Plate 10.1 and the thin section work of Bronswijk *et al.* (1993), the anaerobic fraction of the soil is relatively high. This is due to the low oxygen diffusion coefficients for the wet clayey soil matrix and the high rate of oxygen consumption in the aerobic zone immediately adjacent to the macropore as a result of pyrite oxidation. In the aerobic part of the soil matrix, the oxygen concentration decreases from the macropore wall to zero at the aerobic-anaerobic boundary.

A differential equation describing the oxygen diffusion and consumption in the soil matrix needs to be solved in order to calculate the dissolved oxygen concentration profile and aerobic volume in the matrix. The formulation of such a differential

equation and its solution depend on the geometry of the soil structure. Nethertheless, where the length of the oxygen diffusion path is small and the consumption of oxygen by pyrite is high, the diffusion of dissolved oxygen can be approximated as diffusion into a semi-infinite block. On the basis of this assumption, the steady state diffusion equation for the aerobic part of the soil matrix (Equation 10.2), where the oxygen consumption term is described by Equation (10.10), can be written as the ordinary differential equation:

$$D_w \frac{d^2 C_w(x)}{dx^2} = \frac{0.311262 C_{FeS_2}}{\rho d} \sqrt{C_p} + OM \quad (10.11)$$

where:  $D_w$  is the diffusion coefficient of oxygen in the soil aggregate ( $m^2 d^{-1}$ ). The boundary conditions for Equation (10.11) as per Figure 10.1,

$$\begin{aligned} x = r & \quad dC_w(x)/dx = 0 \\ x = R & \quad C_w(x) = C_b \end{aligned}$$

$C_b$  is the concentration of oxygen in the water at the boundary between the soil matrix and the macropores ( $kg m^{-3}$ ), and is calculated according to Henry's law:

$$[O_2]_{air} = H_k \times [O_2]_{water}, \quad (10.12)$$

where;  $H_k$  is the temperature dependant Henry's constant and  $[O_2]$  is the concentration of oxygen in air and water.

Given that changes in the pyrite concentration and the diameter of pyrite crystals are very small for small time steps (say hourly), the values for  $C_{FeS_2}$  and  $d$  in Equation (10.11) can be held constant for one model time step (1 day).

There is no analytical solution to Equation (10.11), so a linear approximation between oxygen consumption and dissolved oxygen concentration was assumed. Using such a linear approximation, the right hand side of Equation (10.11) becomes:

$$D_w \frac{d^2 C_w(x)}{dx^2} = A' C_p(x) + OM' \quad (10.13)$$

where;  $A' C_p(x)$  is the apparent mass oxygen consumption rate resulting from pyrite oxidation and  $OM'$  is the apparent mass oxygen consumption rate resulting from other oxygen consuming processes (e.g., organic matter, bacteria). Note that  $OM'$  is very small relative to the oxygen consumed by pyrite oxidation.

A more elegant form of the solution to the linear approximation than that described by Bronswijk *et al.* (1993) is described in (Equation 10.14) for the steady-state oxygen concentration in the aerobic part of the soil matrix for  $r < x < R$ .

$$C_p(x) = \left( C_b + \frac{OM'}{A'} \right) \left\{ \frac{\cosh \sqrt{\beta}(x-r)}{\cosh \sqrt{\beta}(R-r)} \right\} - \frac{OM'}{A'} \quad (10.14)$$

Hence, the radius of the anaerobic zone is:

$$r = R - \frac{\cosh^{-1} \chi}{\sqrt{\beta}} \quad (10.15)$$

where,  $\beta = \frac{A'}{D_w}$  and  $\chi = 1 + \frac{A' C_b}{OM'}$ .

For the anaerobic part of the soil matrix ( $x < r$ ),  $C_w(x)=0$ .

By calculating the radius of the anaerobic zone,  $r$  (m), and solving Equation (10.13) for  $C_p(x)$  for  $r < x < R$ , the total mass of oxygen consumed,  $\varphi_T$  ( $\text{kg m}^{-3} \text{d}^{-1}$ ) in the soil matrix can be determined by:

$$\varphi_T = \int_r^R [A' C_p(x) + OM'] dx \quad (10.16)$$

A derivation of the solution for  $\varphi_T$  is given in Appendix D. The solution to Equation (10.16) becomes:

$$\varphi_T = \left[ \frac{A' C_b + OM'}{\sqrt{\beta}} \right] \tanh \sqrt{\beta} (R - r) \quad (10.17)$$

$S_o$  is the specific surface area of the soil through which oxygen diffusion takes place in  $1 \text{ m}^3$  of soil ( $\text{m}^{-1}$ ) or a measure of the soil structure. In this model, the soil structure with in the matrix is assumed to be a plate structure hence,  $S_o = 1/R$ . Thus, Equation (10.17) becomes:

$$\varphi_T = \left( \left[ \frac{A' C_b + OM'}{\sqrt{\beta}} \right] \tanh \sqrt{\beta} (R - r) \right) \times S_o \quad (10.18)$$

The calculation of the amount of oxygen consumption by organic mater ( $\varphi_{OM}$ ) is simple because it is assumed to be at a constant rate in the aerobic fraction of the soil matrix,  $(R-r)/R$ , whereby:

$$\varphi_{OM} = \frac{OM'(R - r)}{R} \quad (10.110)$$

Thus, the steady state amount of oxygen consumed by pyrite oxidation is calculated by:

$$\varphi_{\text{FeS}_2} = \varphi_{\text{T}} - \varphi_{\text{OM}} \quad (10.20)$$

From the amount of oxygen consumed by pyrite (Equation. 10.20), the amount of pyrite oxidised is calculated, and the production of  $\text{Fe}^{3+}$ ,  $\text{H}^+$  and  $\text{SO}_4^{2-}$  is determined accordingly.

#### 10.2.4 Oxygen diffusion and consumption in the macropores

The vertical, steady state oxygen distribution in the air-filled macropores is described by Equation (10.2). The consumption term ( $\alpha_v$ ) is derived from the mass consumption of oxygen at the macropore walls ( $\varphi_{\text{T}}$ ). Application of the Boyle-Gay-Lussac Law gives:

$$D_s(\epsilon_g) \frac{\partial C_a(x)}{\partial x^2} = \alpha_v = 2.56 \times 10^{-3} \cdot T \cdot \varphi_{\text{T}} \quad (10.21)$$

where: T is the absolute temperature (Kelvin).

Numerous empirically derived analytical equations describing a relationship between the air-filled porosity and the oxygen diffusion coefficient exist in the literature. In this model, the oxygen diffusion through the macropores is described by (Troeh *et al.*, 1982):



$$D_s(\epsilon) = \left( \frac{\epsilon - 0.01}{0.99} \right)^{1.3} \times D_0 \quad (10.22)$$

The transport of oxygen down macropores and through the soil matrix in conjunction with simultaneous consumption of oxygen by pyrite oxidation is the key to this model. The oxygen concentration in the air-filled macropores is dependent on the consumption of oxygen at the macropore walls. No account of gas consumption by growing plant roots is considered. Simultaneously, the oxygen consumption inside the clay matrix is dependent on the oxygen concentration in the air-filled macropores. These calculations are solved by an iterative process in the numerical model.

### 10.3 Numerical model

The pyrite oxidation model described in this chapter was developed to work in conjunction with the output from FEMWATER simulations. A flow chart of the FEMWATER - ASS3D model process is shown in Figure 10.2.

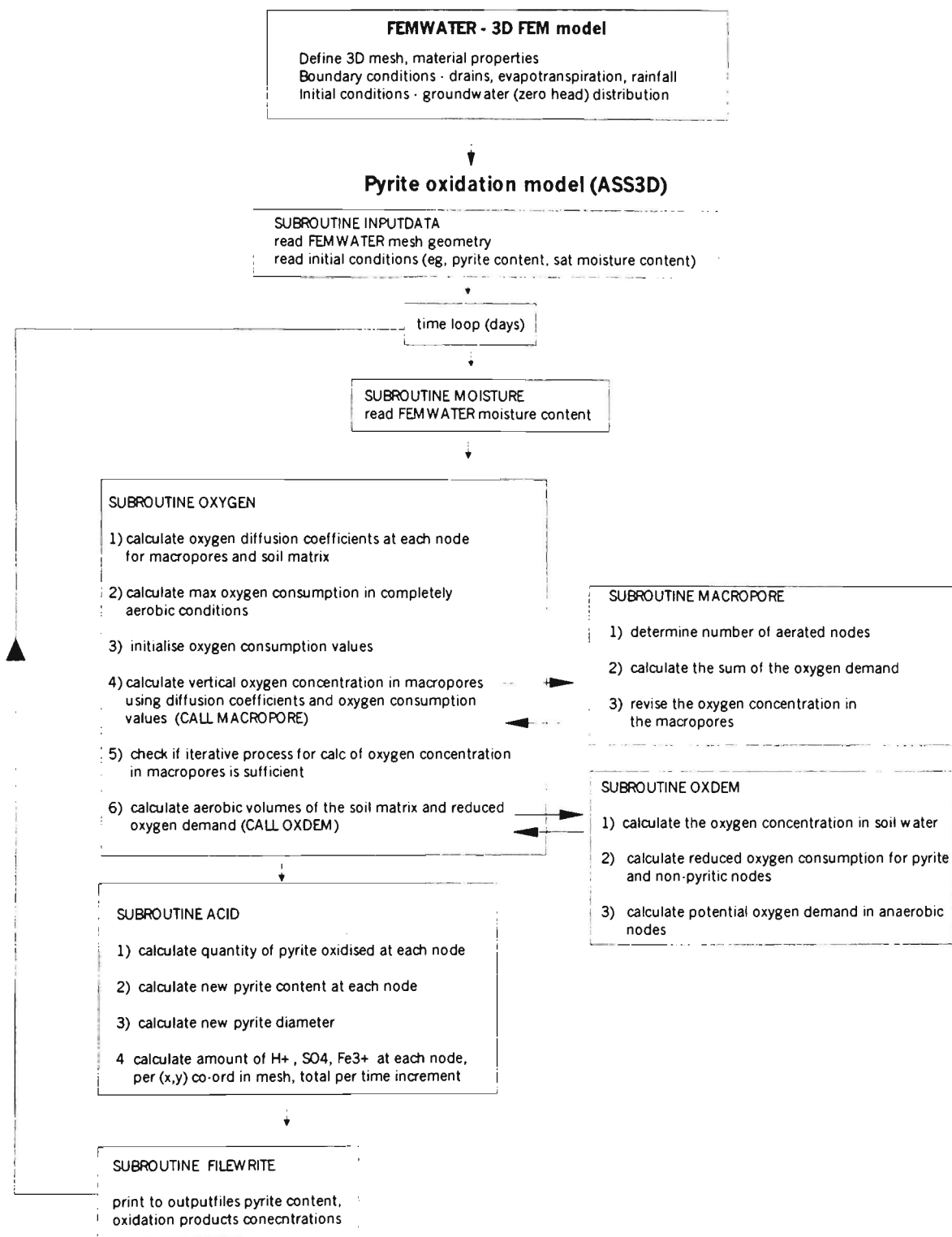


**Figure 10.2** Flow chart of FEMWATER and ASS3D models

Before running ASS3D, FEMWATER computes the moisture content distribution for a 3D finite element mesh for each day of the simulation. The mesh geometry and the moisture content data are used as input for the ASS3D model. The flowchart shows the sequence in which the physical and chemical processes are calculated in ASS3D for one time step. That is:

1. the air-filled porosity profile is determined;
2. oxygen diffusion and oxygen consumption values are calculated;
3. the oxygen concentration in the soil matrix is calculated;
4. the amount of pyrite oxidised is determined
5. the new pyrite content and diameter for the next time step is calculated
6. the amount of pyrite oxidation products generated is calculated and written to a file.

The complete listing of the ASS3D.FOR program developed for the pyrite oxidation model is shown in Appendix C. The program was written in FORTRAN 77 and compiled using Lahey F77I3, a FORTRAN compiler with extended memory capacity. The liberal use of comment statements within the code has been used so that readers can follow and understand what calculations are taking place. Similarly, care has been taken to assign names to variables in the code to make understanding easier. The main numerical part of the model is in three subroutines OXYGEN, MACROPORE and OXDEM where the oxygen transport and consumption terms are calculated.

## **10.5 Comparisons between analytical and numerical solutions**

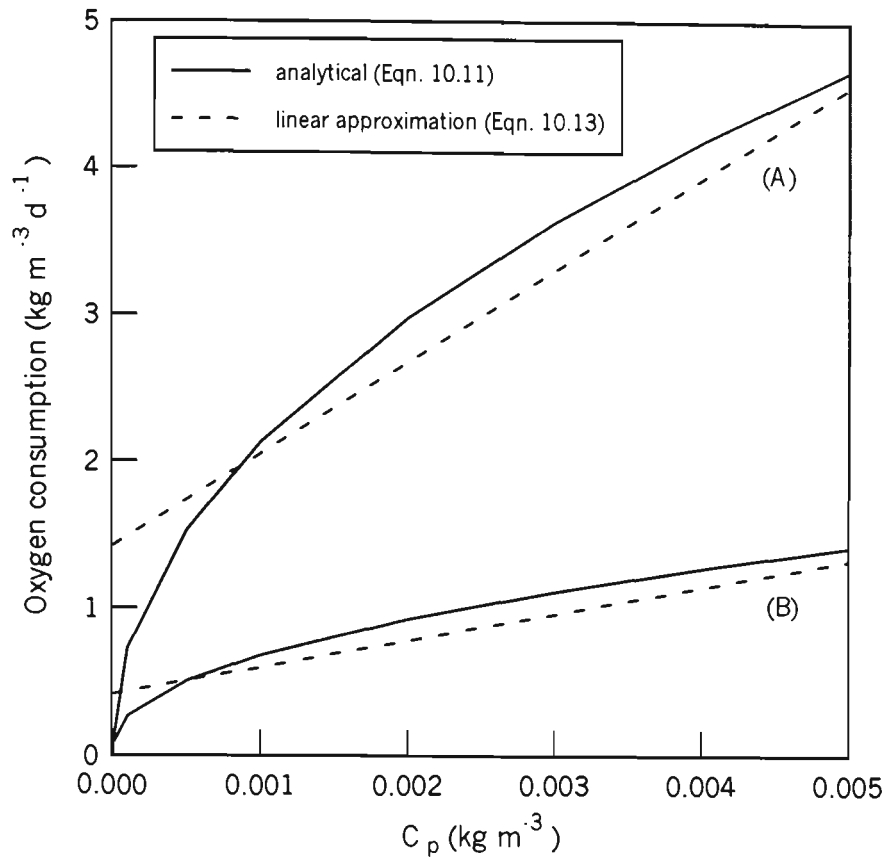
In order to assess the validity of the scheme implemented in the numerical model and the assumptions implicit in the linear approximations used to calculate the amount of

oxygen consumption, a comparison between the numerical solution of Equation (10.11) and the analytical solution of the linear approximation of Equation (10.13) was carried out. The comparison was made for two concentrations of pyrite representing the high (A: 52.2 kg m<sup>-3</sup>) and low (B: 15.2 kg m<sup>-3</sup>) bounds of pyrite concentration found at the study site. A summary of the analytical and numerical factors is shown in Table 10.1.

**Table 10.1** Variables required for of the analytical and numerical solutions  
for two pyrite concentrations.

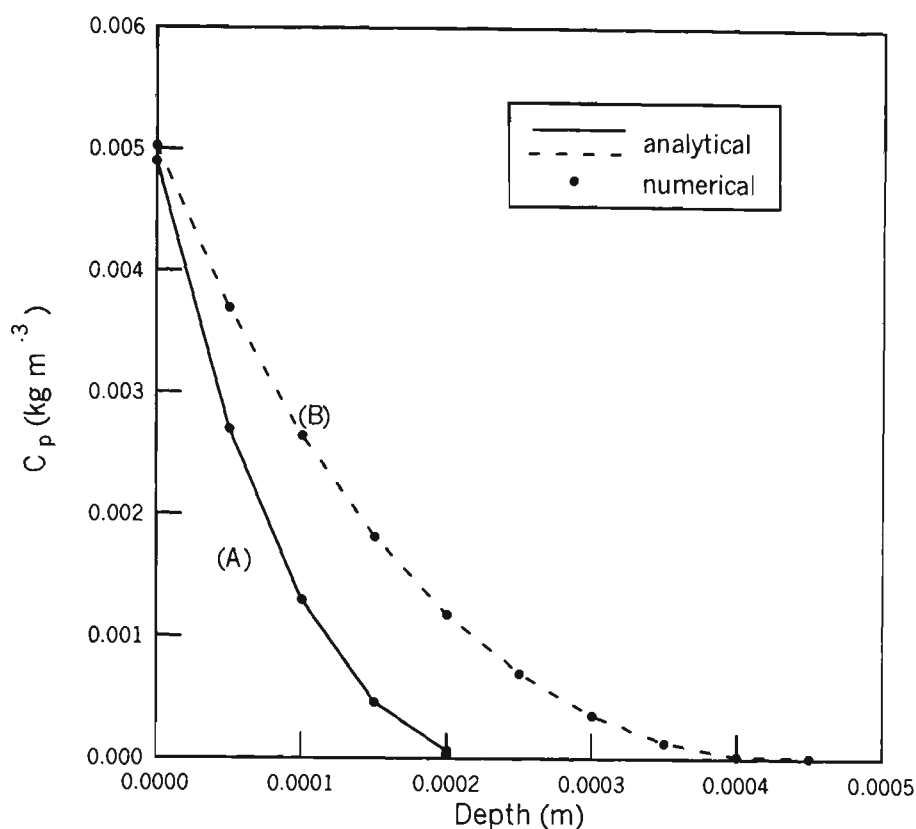
Variable	High (A: 52.2 kg m <sup>-3</sup> )	Low (B: 15.2 kg m <sup>-3</sup> )
C <sub>FeS2</sub>	52.2	15.2
A	64.98	18.90
OM	0.08	0.08
A'	627.71	182.53
OM'	1.43	0.41
C <sub>b</sub>	5.17 x 10 <sup>-3</sup>	4.93 x 10 <sup>-3</sup>
R	6.67 x 10 <sup>-3</sup>	6.67 x 10 <sup>-3</sup>
r	6.44 x 10 <sup>-3</sup>	6.24 x 10 <sup>-3</sup>

Figure 10.3 shows that there is good agreement for the calculation of oxygen consumption in dependence of the local dissolved oxygen concentration according to Equation (10.11) and its linear approximation Equation (10.13) for high and low pyrite concentrations. The solutions were calculated for 0 < C<sub>p</sub> < 0.005, which is the likely range for dissolved oxygen concentrations for the climatic conditions prevalent at the study site. However, this assumption was not tested by measuring the concentration of dissolved oxygen in the soil water at various depths or the concentration of oxygen in the soil air in the macropores.



**Figure 10.3** Solution of Equations (10.11) and (10.13) for oxygen consumption in dependence of the local dissolved oxygen concentration.

Figure 10.4 shows excellent agreement between the dissolved oxygen concentration profiles extending from the macropore wall into the soil matrix obtained with the analytical solution (Equation 10.14) and the numerical solution of Equation (10.11).



**Figure 10.4** Dissolved oxygen concentration profiles into the saturated soil matrix.

The most important parameter in the comparison of the numerical and analytical solutions is the value of the mass of oxygen consumption in the soil matrix ( $\phi_T$ ). The value of  $\phi_T$  determines the amount of pyrite oxidised in the soil matrix (Equation 10.18). The difference between the analytical and numerical solutions was very small. Values of  $\phi_T$  for the two pyrite concentrations described above are shown in Table 10.2.

**Table 10.2** Analytical and numerical values for  $\phi_T$ .

Pyrite concentrations	numerical $\phi_T$	analytical $\phi_T$	% difference
A ( $52.2 \text{ kg m}^{-3}$ )	0.085	0.084	1.1
B ( $15.2 \text{ kg m}^{-3}$ )	0.047	0.044	2.2

The small difference between the numerical and analytical solutions indicates that the model accurately simulated the oxidation of pyrite in the soil matrix, given the various assumptions implicit in the model.

## 10.6 Conclusions

A modified approach for calculating pyrite oxidation in a soil macropore/matrix system has been developed by the approach described by Bronswijk *et al.* (1993). This approach accounts for vertical oxygen transport through macropores and the subsequent lateral diffusion of oxygen into the soil matrix. As oxygen is supplied to the matrix, it is consumed by pyrite and other oxygen depleting processes. A numerical solution to the theoretical model was developed and used in the computer simulation model ASS3D, where pyrite oxidation is simulated within a 3D mesh. This allows for better assessment of acid sulfate soil management strategies at the field or sub-catchment scale. The numerical approach is based on a linear approximation between oxygen consumption and dissolved oxygen concentration. The numerical scheme is in good agreement with analytical solutions. This indicates that, given the assumptions noted for the theoretical model, the amount of oxidation products calculated in the numerical model is an accurate approximation of the pyrite oxidation process described in the theoretical model. Validation and some applications of the ASS3D model are described in Chapter 11.

## **Chapter 11: Validation and application of ASS3D**

### **11.1 Introduction**

The accuracy and application of the ASS3D model that is described in Chapter 10 is investigated in this Chapter. In the first part of this Chapter, ASS3D is validated by comparing the model output to measured field data. ASS3D output compares favourably with the change in pyrite concentration measured at the end of the period simulated. Comparison of the cumulative sulfate concentration measured in the groundwater during the period simulated is also in good agreement with the theoretical amount of sulfate produced via pyrite oxidation predicted by ASS3D. These comparisons indicate that ASS3D accurately predicted the pyrite oxidation that occurred during the simulation period.

The second part of this Chapter demonstrates the application of the ASS3D model. Four drain management alternatives are simulated, namely the existing drained state, maintenance of elevated drain water levels at -0.5 and -0.3 m AHD through the installation of weirs at these elevations, and the effect of removing the floodgates to allow tidal ingress into the drains. All of the alternative drain management options were demonstrated to be beneficial in terms of reducing the amount of acidic oxidation products generated. However, some problems associated with excessively high groundwater tables were noted for the -0.3 m AHD weir option.

### **11.2 Validation of ASS3D**

Validation of the ASS3D model was carried out by comparing the final pyrite concentration and cumulative sulfate production calculated by ASS3D, and that



measured in the field during the pre-weir period where the drain functioned in its existing state.

11.2.1 FEMWATER simulation of the existing drained state

The existing drained state at the study site was simulated using FEMWATER by constructing a finite element mesh 150 m long (the length of a piezometer transect at the study site), 5m deep and 40 m wide (the width of a field at the study site), assigning material properties to six soil layers and applying appropriate boundary conditions (Fig. 8.1). The atmospheric and drain water level boundaries were determined from field data collected between July 1997/98. The atmospheric boundary was defined as a transient variable flux at the nodes at the top of the finite element mesh. The drain water level was defined as a variable head at the elements across the drain-soil interface. The variable head boundary conditions for elevation of the water level in the drain is shown in Figure 11.1.

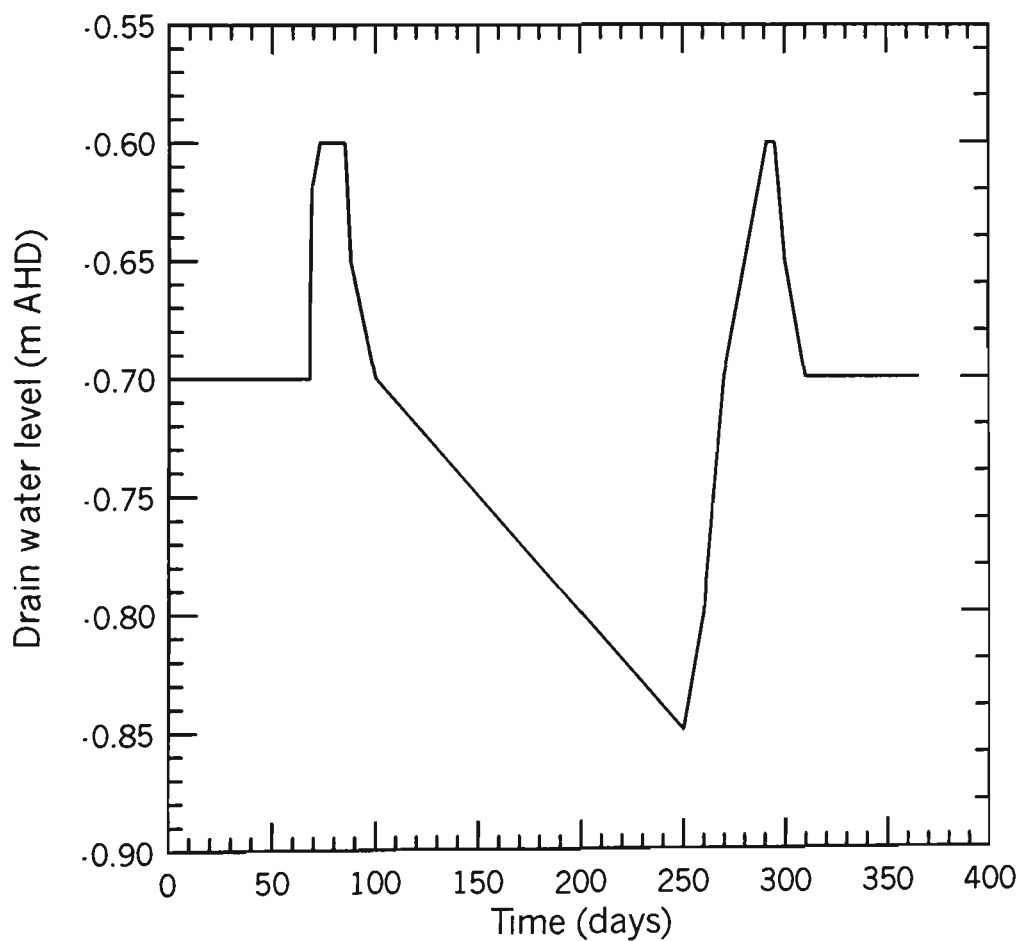


**Figure 11.1** Drain water elevation boundary condition for the existing drain simulation

The initial static water pressure was taken from piezometer data collected at the site and applied as a pressure head distribution for the saturated and unsaturated parts of the soil profile. The FEMWATER model, and a comprehensive description of the mesh, boundary and initial conditions used for this simulation was described earlier in Chapter 9.

### *11.2.2 ASS3D input data*

As shown in Figure 10.2, three input files are required for ASS3D. Two of these input files, namely the moisture content distribution data for each time step and the mesh geometry data are generated by FEMWATER. The initial pyrite concentration and pyrite crystal size data, as well as soil state information describing the oxygen diffusion coefficients, soil aggregate radius and saturated soil moisture content is given in the ASS3D input file. This data was derived from field observation, laboratory measurements and the literature.

At the start of the ASS3D simulation, the properties defined in the ASS3D data input file are assigned to the nodes in the vertical plane for the FEMWATER mesh in order from top to bottom. At time zero, it is assumed that the pyrite concentration and crystal size are uniform across the mesh for a particular depth. For example, at the fifth node down the vertical plane (depth approximately -0.7 m AHD), the initial pyrite concentration was 2.26%.

The geometry of the mesh was shown in Figure 9.1. Two dimensional cross sections of groundwater elevation at three times during the simulation are shown in Figure 11.2. A video file of the complete groundwater elevation and moisture content distribution data sets for the existing drained state is provided on the attached CD.

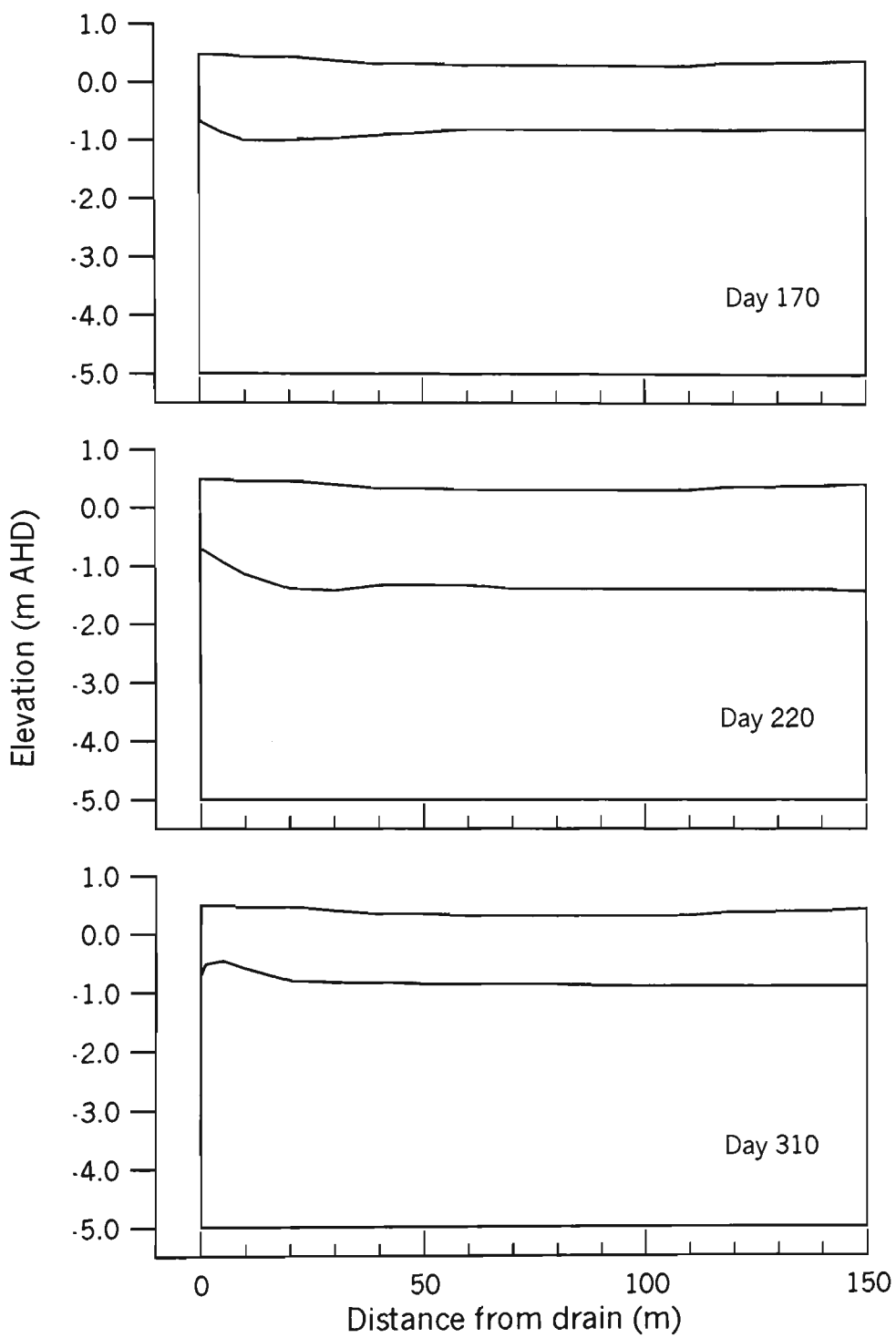


**Figure 11.2** Simulated groundwater elevation.

*11.2.3 Simulated pyrite oxidation for the existing drained state*

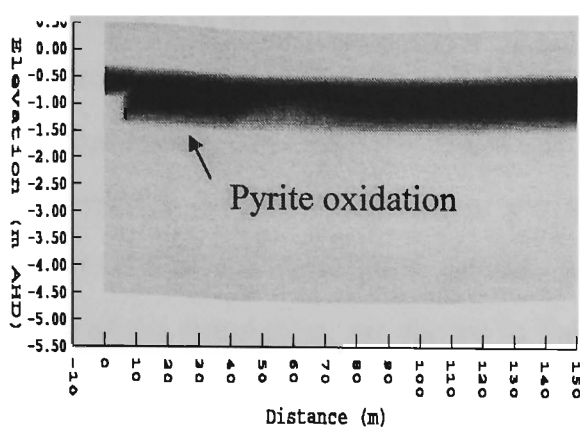
The distribution of pyrite oxidation at three times during the simulation for the existing drained state is shown in Figure 11.3. The magnitude and distribution of pyrite

oxidation across the study area vary with time, and are dependant on the elevation of the groundwater table. Video animations of the distribution and magnitude of pyrite oxidation during the simulation period for the existing drained state are available on the attached CD.

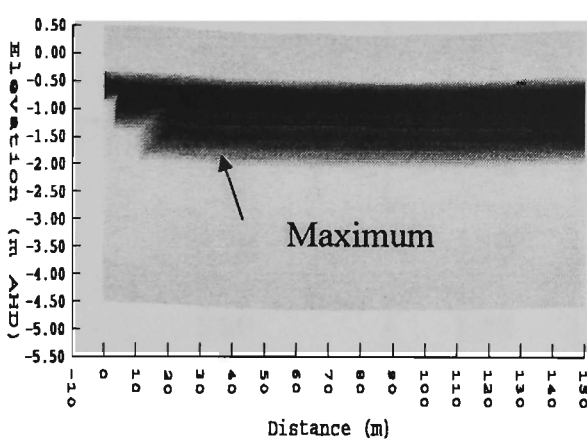
At Day 170, the groundwater table has fallen below the acid sulfate soil layer. The zone of pyrite oxidation extends across the whole simulation area for the drained situation and has progressed down approximately 0.6 m into the pyritic layer. The groundwater table fell to its maximum depth around Day 250 which caused pyrite oxidation to extended in excess of 1 m into the pyritic soil layer. The thickness of the oxidised zone is less close to the drain than further out into the field. The groundwater table is supplemented by seepage through the drain walls for the area immediately adjacent to the drain. At distances greater than 20 m from the drain, evaporative losses from the groundwater are greater than the recharge rate, thereby giving rise to lower groundwater table elevations away from the drain. This in turn enables the pyrite oxidation front to progress to deeper depths as the distance increases away from the drain.

By Day 310, the groundwater table had risen as a result of significant rainfall. A small area of pyrite oxidation still occurred adjacent to the drain. Though the volume of oxidising acid sulfate soil appears relatively small to that previously exposed to oxidising conditions, the ongoing oxidation of pyrite in the acid sulfate soil layer immediately adjacent to the drains poses a severe problem for the water quality in the drain. As acidic pyrite oxidation products are generated in this volume of soil close to the drain, small rainfall events will ensure that acid is continually discharged into the drainage system.

Day 170 drain



Day 250 drain



Day 310 drain

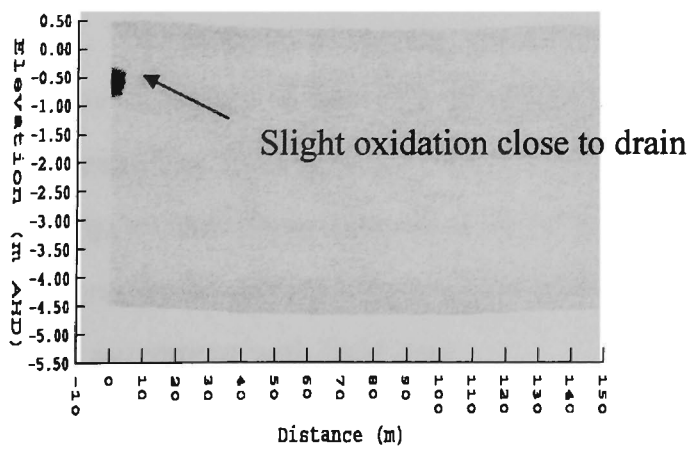


**Figure 11.3** Distribution of simulated sulfate production from pyrite oxidation for the existing drained state

11.2.4 Validation of ASS3D against measured field data

The pyrite concentration of the sulfidic soil at elevations of -0.7, -1.0 and -1.5 m AHD was determined from samples collected at 90 m distance from the drain in July 1998 (i.e., the end of the simulation period). Although these measurements are subject to sampling and laboratory errors, the measured pyrite concentrations at these depths at both the start and end of the simulation period, as well as the predictions made by ASS3D at the end of the simulation, are shown in Table 11.1

**Table 11.1** Measured and simulated pyrite concentrations

Elevation (m AHD)	Initial observed pyrite concentration (%)	Final simulated pyrite concentration (%)		Final observed pyrite concentration (%)
		10 m	90 m	90 m
-0.7	2.26	2.10	2.06	1.97
-1.0	1.60	1.48	1.49	1.50
-1.5	0.20	0.20	0.20	0.20

The computed pyrite concentration in the soil profile at 90 m from the drain after 365-days for the drain simulation correspond well with the measured pyrite concentration from the field. The amount of pyrite consumed during oxidation was slightly underestimated (by 0.09 %) at the -0.7 m AHD depth node relative to the pyrite concentration measured on field samples. At -1.0 m AHD, a very small overestimate of the amount of pyrite oxidised was calculated by ASS3D. Given the likely variability in the pyrite concentration of the sulfidic soil, the calculation of pyrite concentration by ASS3D is in good agreement with field data.

The accuracy ASS3D can also be tested by comparison of the simulated sulfate production with groundwater quality data collected from the study site. Figure 11.4 shows the sulfate generated by pyrite oxidation calculated by ASS3D for the existing drained situation for the simulation period.

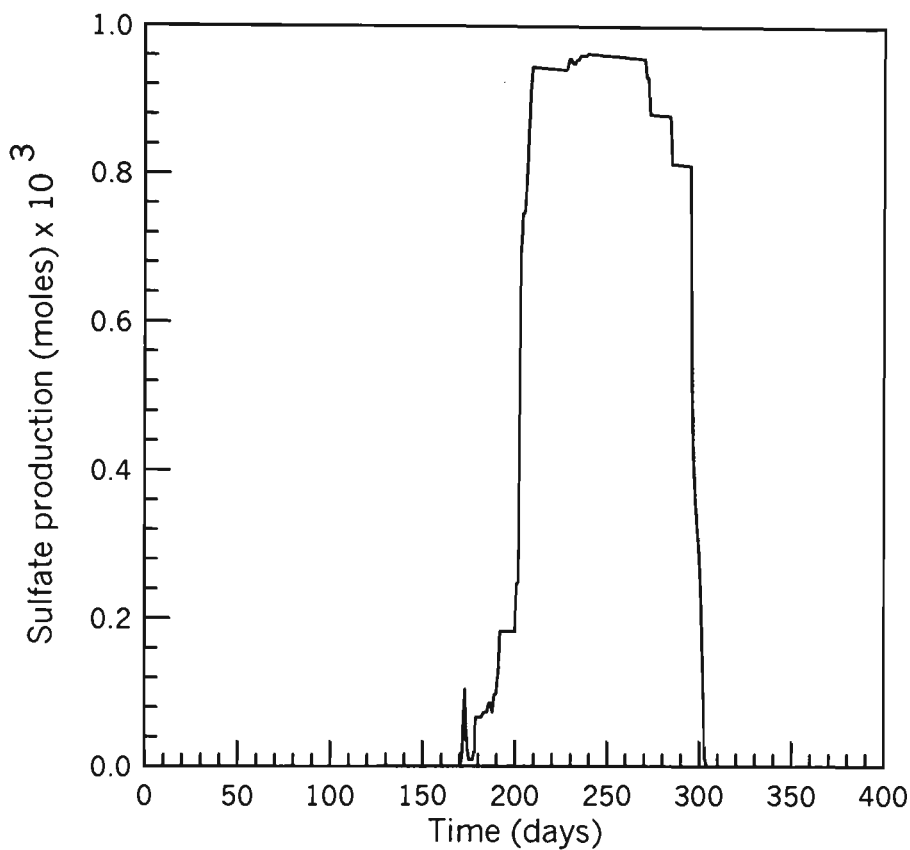


**Figure 11.4** Simulated sulfate production from pyrite oxidation for the existing drain

The cumulative amount of sulfate produced by pyrite oxidation was  $91 \times 10^3$  mol for the drain simulation. This compares well with the theoretical amount of sulfate generated by pyrite oxidation in the field. Calculation of the amount of sulfate produced by pyrite oxidation from the difference between the initial and final pyrite concentrations shown in Table 11.2 shows that approximately  $127 \times 10^3$  mol was generated in the field. The under-estimation of the amount of sulfate generated from the oxidation of pyrite by ASS3D may stem from a number of factors. Firstly, the distribution of pyrite oxidation is not even across the study area, with less pyrite being oxidised close to the drain. Hence, the approximation of  $127 \times 10^3$  mol of sulfate being generated from the theoretical calculation based on initial and final pyrite concentrations at 90 m distance from the drain may be an over-estimate of the total amount of pyrite actually oxidised.

Another important factor is the distribution of pyrite crystals within the soil structure/matrix. For computational simplicity, the ASS3D model, as well as many other pyrite oxidation models (e.g., Bronswijk *et al.*, 1993; Wunderly *et al.*, 1996), assume that pyrite is uniformly distributed throughout the soil matrix. However, Bush and Sullivan (1999) show that a considerable proportion of the pyrite occurs within and adjacent to macropores. This pyrite would be more prone to oxidation compared with pyrite distributed away from the macropores due to the preferential and rapid diffusion of oxygen down the macropores. The amount of sulfate generated by pyrite oxidation by ASS3D is approximately 72% of that determined by the difference between the initial and final pyrite concentration measured from the field. Dent (1986) suggested that many pyrite oxidation models under-estimate the actual field oxidation rate by about 30%, and Bush and Sullivan (1999) argue that the distribution of pyrite and its relationship to soil structure may be the reason for this underestimation.

The areal distribution of pyrite oxidation simulated by ASS3D is reflected in the concentration of sulfate measured in the groundwater. Close to the drain (10 m), the amount of sulfate measured is less than that further away from the drain (90 m). In the ASS3D simulation, a similar distribution of pyrite oxidation was calculated, with larger volumes of pyritic being exposed to oxidising condition at distances greater than 20 m from the drain than close to the drain. The simulated cumulative sulfate production curve (Figure 11.4) also corresponds well to the cumulative sulfate concentration measured in the groundwater (Figure 11.5).



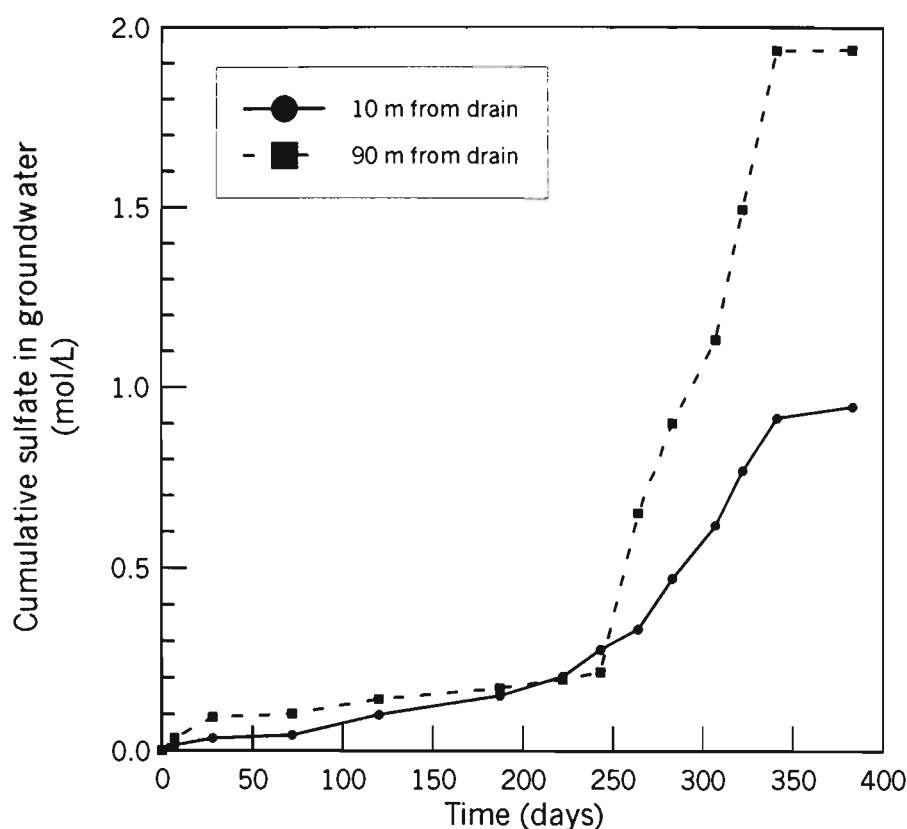


**Figure 11.5** Cumulative sulfate measured in groundwater at 10 m and 90 m from the drain.

In Figure 11.4, sulfate production commences at approximately Day 170 for the drain simulation and stops at approximately Day 310. At 10 m from the drain, the cumulative sulfate measured in groundwater begins to increase at the same time. The sulfate concentration in the groundwater at 10 m continues to rise after Day 300 as the sulfate generated further from the drain is transported towards the drain, and as the sulfate generated by pyrite oxidation between Days 170-300 re-equilibrates in the vertical groundwater profile by diffusion according to its concentration gradient. The marked increase in sulfate concentration measured at 90 m from the drain does not commence until approximately Day 250, which corresponds to the period of drought breaking rainfall and rising groundwater tables. This indicates that the sulfate generated by pyrite oxidation during the period where the groundwater table was lower than the acid sulfate soil layer was held in the vadose zone under suction in the soil matrix and was not available for re-distribution until the groundwater table rose.

Given the assumptions within the ASS3D model and field variability, the simulated and measured data are in close agreement, and they demonstrate that ASS3D accurately calculates the amount of pyrite oxidised. The exact magnitude of the amount of pyrite oxidised, and the corresponding amounts of acidic oxidation products generated, can be considered of secondary importance, particularly where the objective of the ASS3D model is to determine the relative merits of potential drain management schemes that may reduce the generation of acidic pyrite oxidation products. Groundwater drawdown or recharge by seepage from the drain into the soil is not uniform across the study site. As such, the study of drain management alternatives relative to their influence on the soil moisture content distribution across a site and hence the amount of pyrite oxidised under any particular drain management scheme can be successfully investigated using the FEMWATER-ASS3D modelling system.

### **11.3 Application of ASS3D to assess drain management options**

A variety of drain management options are available for the manipulation of the surrounding groundwater table. Many of these management schemes may be advantageous with respect to minimising the amount of acidic products generated by oxidised pyrite. A series of three FEMWATER-ASS3D simulations were carried out to assess the performance of; the installation of weirs at -0.5 and -0.3 m AHD, and the opening of floodgates to allow the ingress of water from Broughton Creek. The simulated generation of pyrite oxidation products was compared to the simulation of the existing drained state.

#### *11.3.1 Drain boundary conditions for FEMWATER simulation*

Individual drain-soil interface boundary conditions were developed for each of the drain management options that were simulated. These boundary conditions were either

constant head (for the weir simulations) or variable head (for the tide and existing drain simulations). The magnitude of the head boundary representing the water level in the drain for the various options is shown in Figure 11.6.

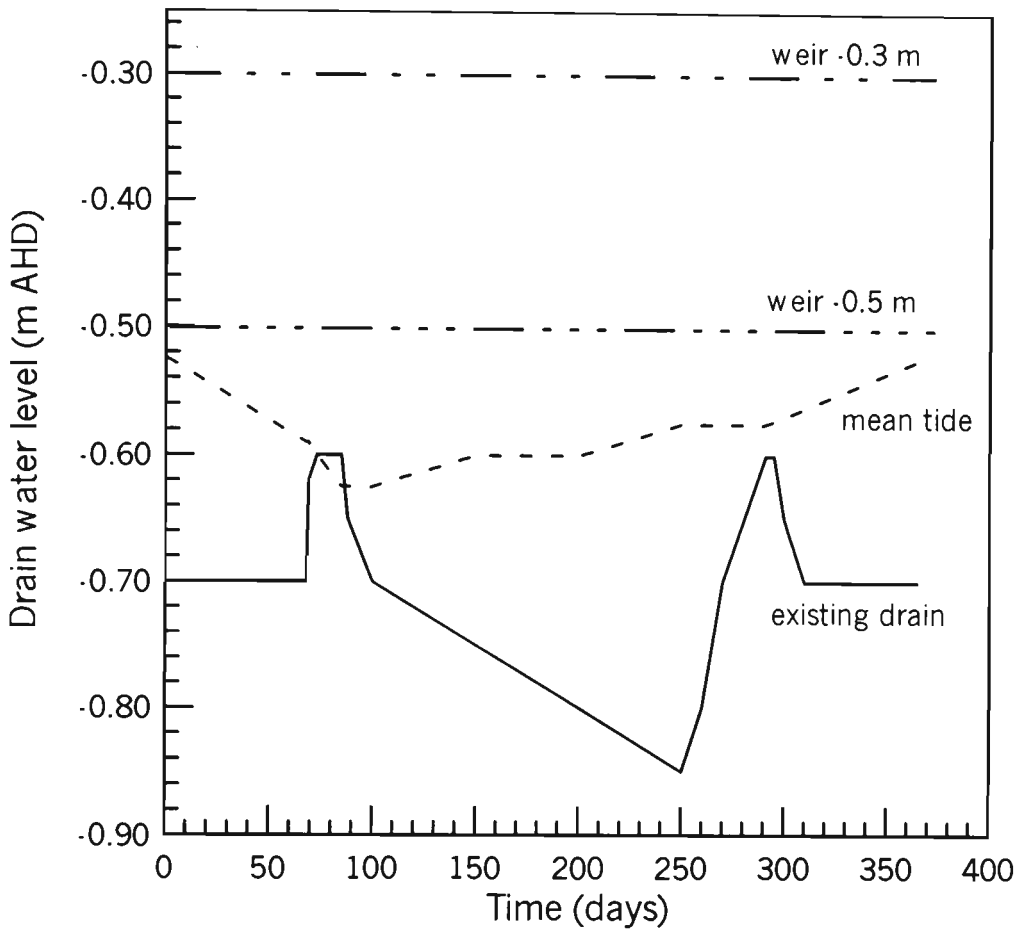


**Figure 11.6** FEMWATER head boundary conditions used to simulate the drain water level for the various drain management options

The variable head boundary condition for the tidal ingress simulation was a calculated mean tide level taken from published maximum and minimum tide elevation data for the Shoalhaven River (Australian National Tide Tables, 1997). Clearly, the high and low tide elevations vary during the course of a day by as much as 1 m in Broughton Creek adjacent to the study site. In order to assess the applicability of using the daily mean tide level at a daily time step for the FEMWATER simulation of the tidal ingress management option, a comparison between applying a variable head boundary for the expected tidal fluctuation at hourly time steps and the mean tidal drain water levels at

daily time steps was performed. The FEMWATER simulation of the variable head tidal boundary was carried out for the conditions between Days 134-142, a period where no rainfall occurred. The variable tidal water level in the drain (i.e. the transient head boundary at hourly time steps) is shown in Figure 11.7.

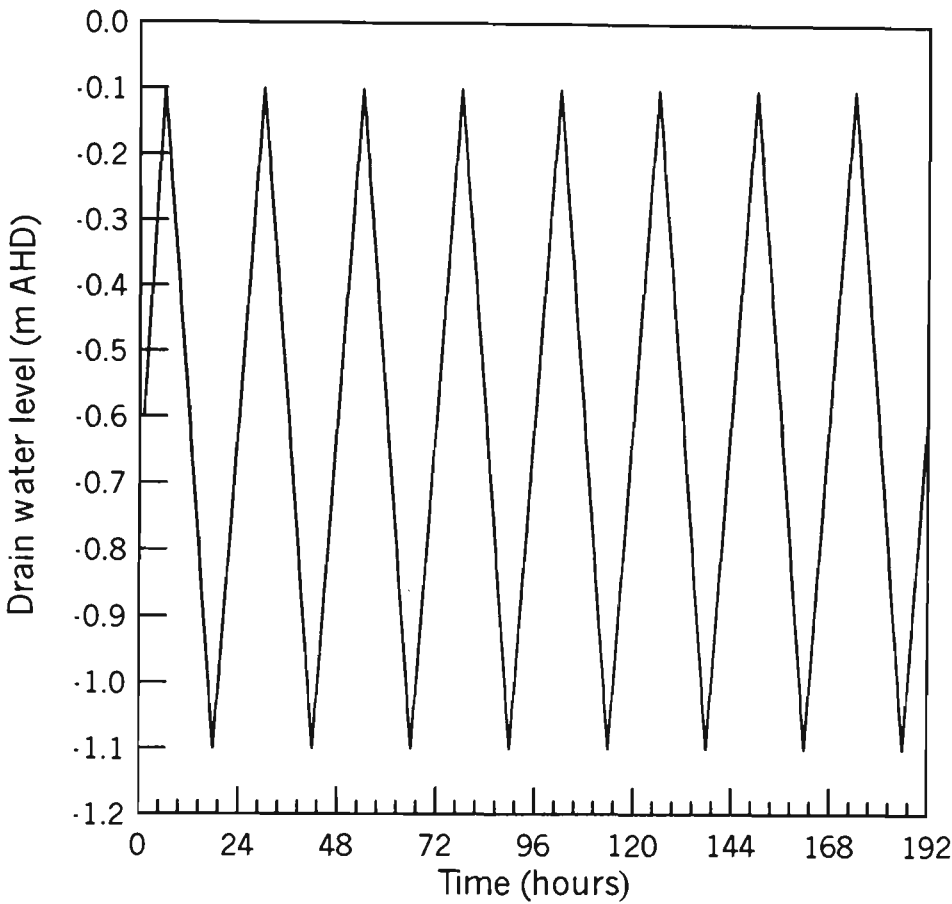


**Figure 11.7** Drain water level under tidal influence.

The groundwater elevations at 1 m, 5m, 10 m and 50 m distance from the drain for the transient tidal drain water level is shown in Figure 11.8. The groundwater elevation data for the transient drain water level simulation was compared to the groundwater elevation where the drain water level was maintained at -0.6 m AHD (i.e. the mean tidal drain water level during Days 134-142 also at a hourly time step). The groundwater elevation data for the FEMWATER simulation performed for the mean tidal level on a daily time step is also shown in Figures 11.9 and 11.10.

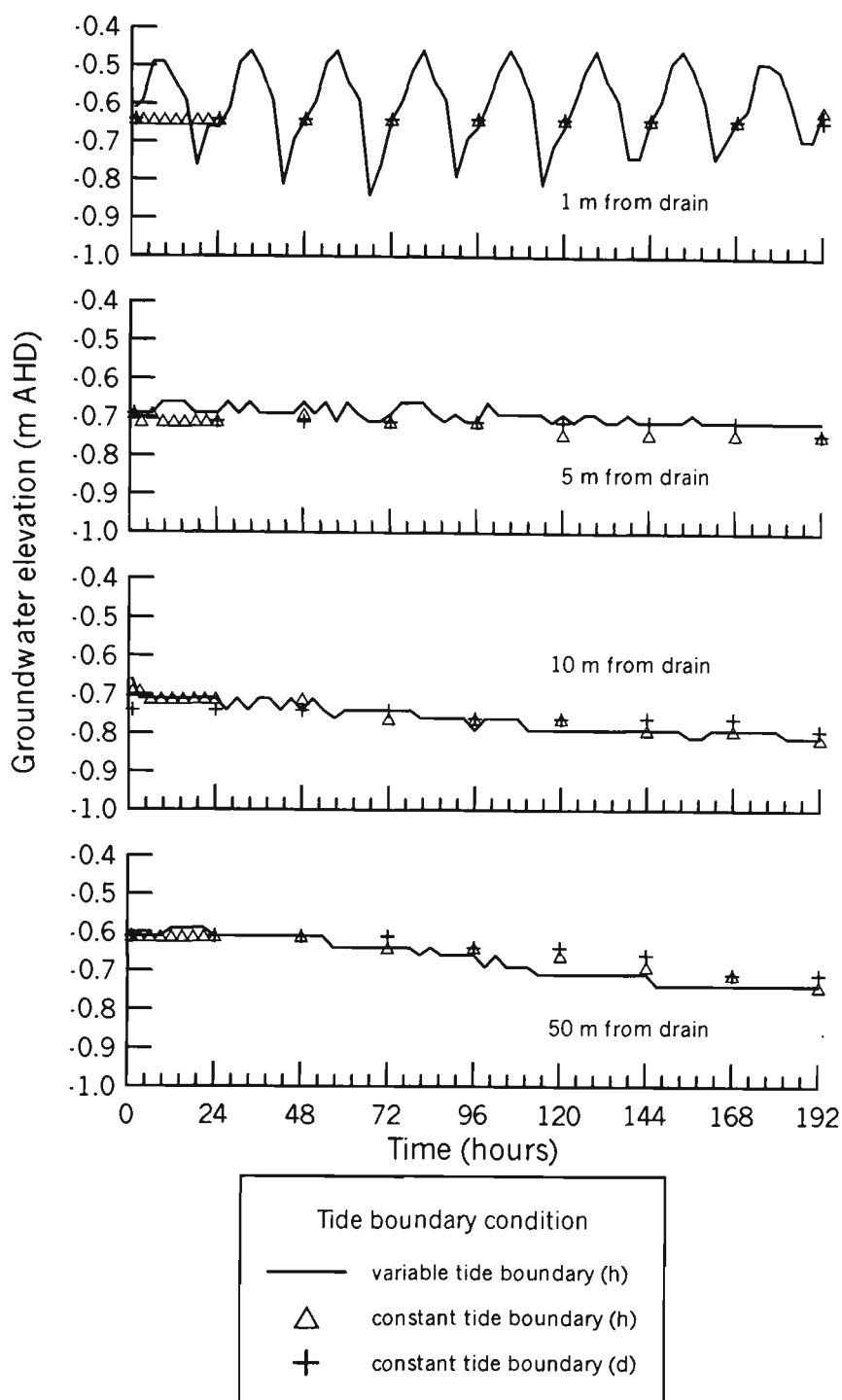


**Figure 11.8** Groundwater elevation for drain water levels simulated by variable tidal range on an hourly time step, constant drain level on an hourly time step and constant drain level on an daily time step.

Figure 11.8 demonstrates that the transient water level caused by tidal fluctuations in the drain for the hourly time step simulation only influences groundwater elevation very close to the drain. At 1 m distance from the drain, the amplitude of the daily fluctuation in the groundwater elevation is as much as 0.17 m. However, as the distance from the drain increases to 5 m, the amplitude of the daily fluctuation is restricted to 0.03 m. As

the distance away from the drain increases to 10 m and 50 m, no fluctuation in the groundwater elevation was observed. The influence of the transient tidal fluctuations on the adjacent groundwater elevation are small due to the low horizontal saturated hydraulic conductivity of the soil. Clearly, for the short period during a day where high drain water levels persist, insufficient water is able to seep from the drain into the surrounding soil to substantially raise the groundwater table. As shown in Figure 10.8, groundwater drawdown also occurs close to the drain during the low tide period.

At 5 m, 10m and 50 m distance from the drain, the groundwater elevations calculated by the variable tidal level boundary (hourly time step), constant tidal level (hourly time step) and constant mean tidal level (daily time step) are within 0.05 m. Given the close agreement between the groundwater elevations at 5 m, 10 m and 50 m distance from the drain for all the tidal drain water levels boundary conditions simulated, the application of the daily mean/daily time step in the FEMWATER simulation was considered to be appropriate for studying tidal ingress into the drainage system, and subsequent simulation of pyrite oxidation in ASS3D.

Constant head boundary conditions were used for the simulation of raised water levels using weirs. Two water levels were selected; -0.5 m and -0.3 m AHD, which ensured that the pyritic soil in the drain bank was submerged by 0.2 and 0.5 m of water in the drain, respectively. These two weir elevations encompass the range of depths that the weirs installed in the field trail submerged the adjacent pyritic soil at their respective locations.

The existing drain system with the one-way floodgate that does not allow the ingress of tidal water was simulated using a variable head boundary. The elevation of the water level in the drain uses drain water elevation data collected from the field.

11.3.2 FEMWATER simulations - groundwater elevation

Manipulation of the drain-soil boundary conditions had a large influence on the elevation on the simulated groundwater table across the mesh area. The groundwater elevation at 10 m and 90 m distance from the drain is shown in Figure 11.9 for the existing drain, weirs at -0.5 and -0.3 m AHD and the tidal ingress drain management options. Figures 11.10 (a,b,c) also show the simulated groundwater elevation for the three drain management options at Days 230, 250 and 270 (i.e. the period where low groundwater tables cause pyrite oxidation to occur).

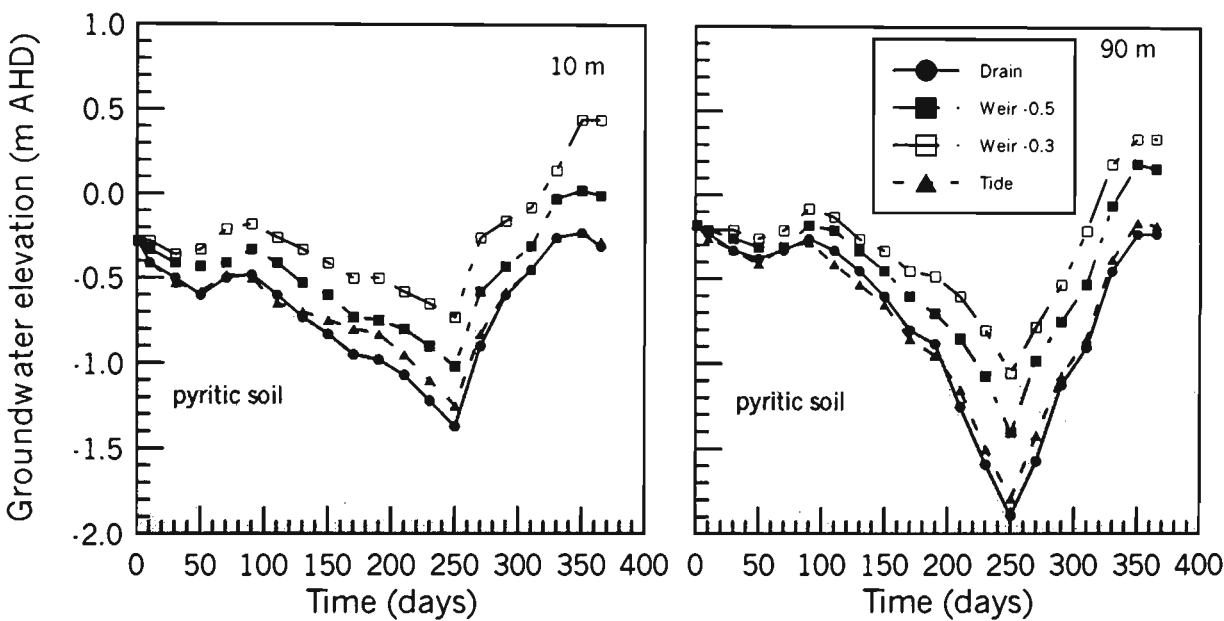


**Figure 11.9** Simulated groundwater elevations for various drain management options.

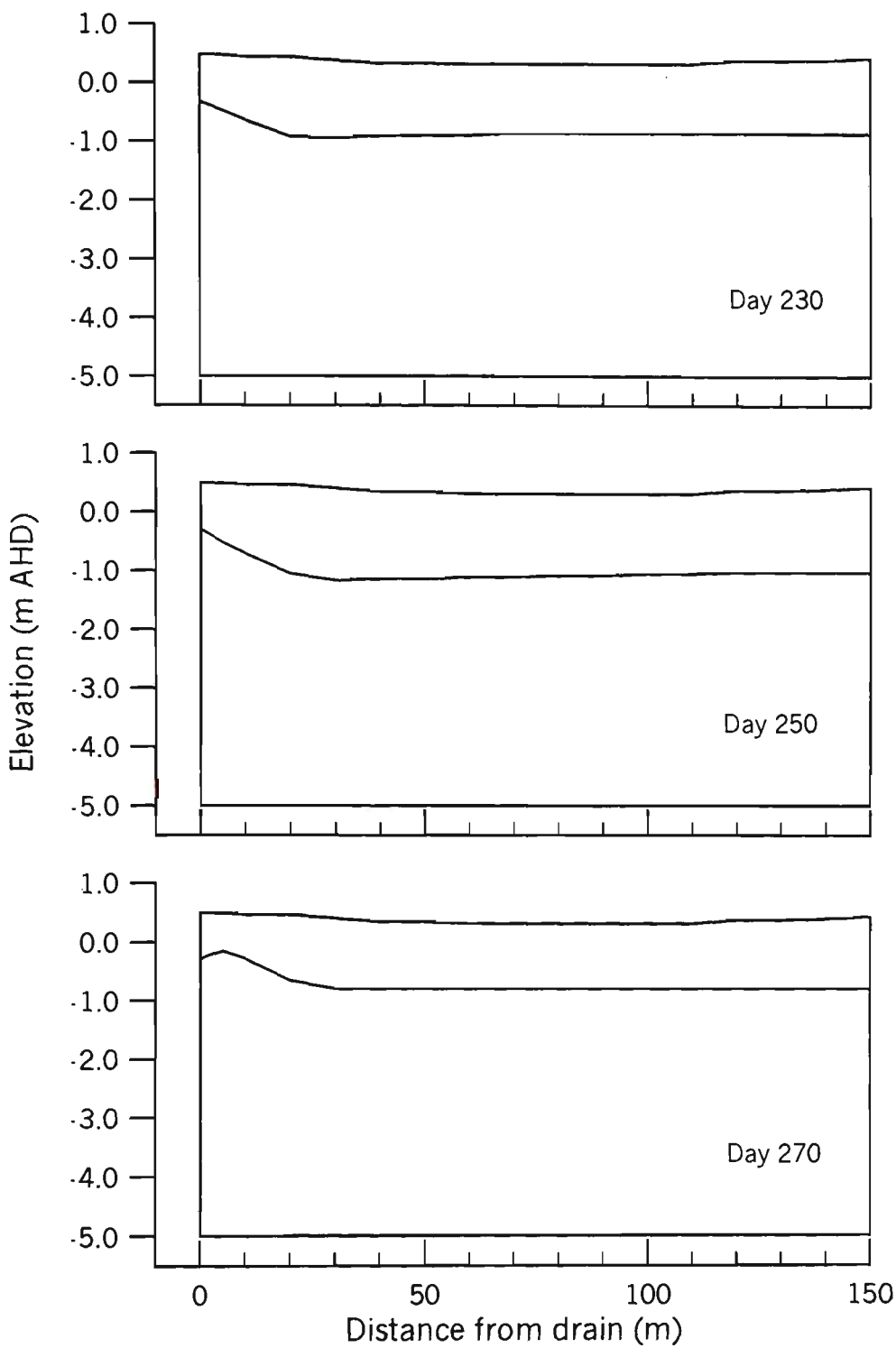


**Figure 11.10(a)** Groundwater elevation at Days 230, 250 and 270 for the Weir -0.3 m AHD drain management option.



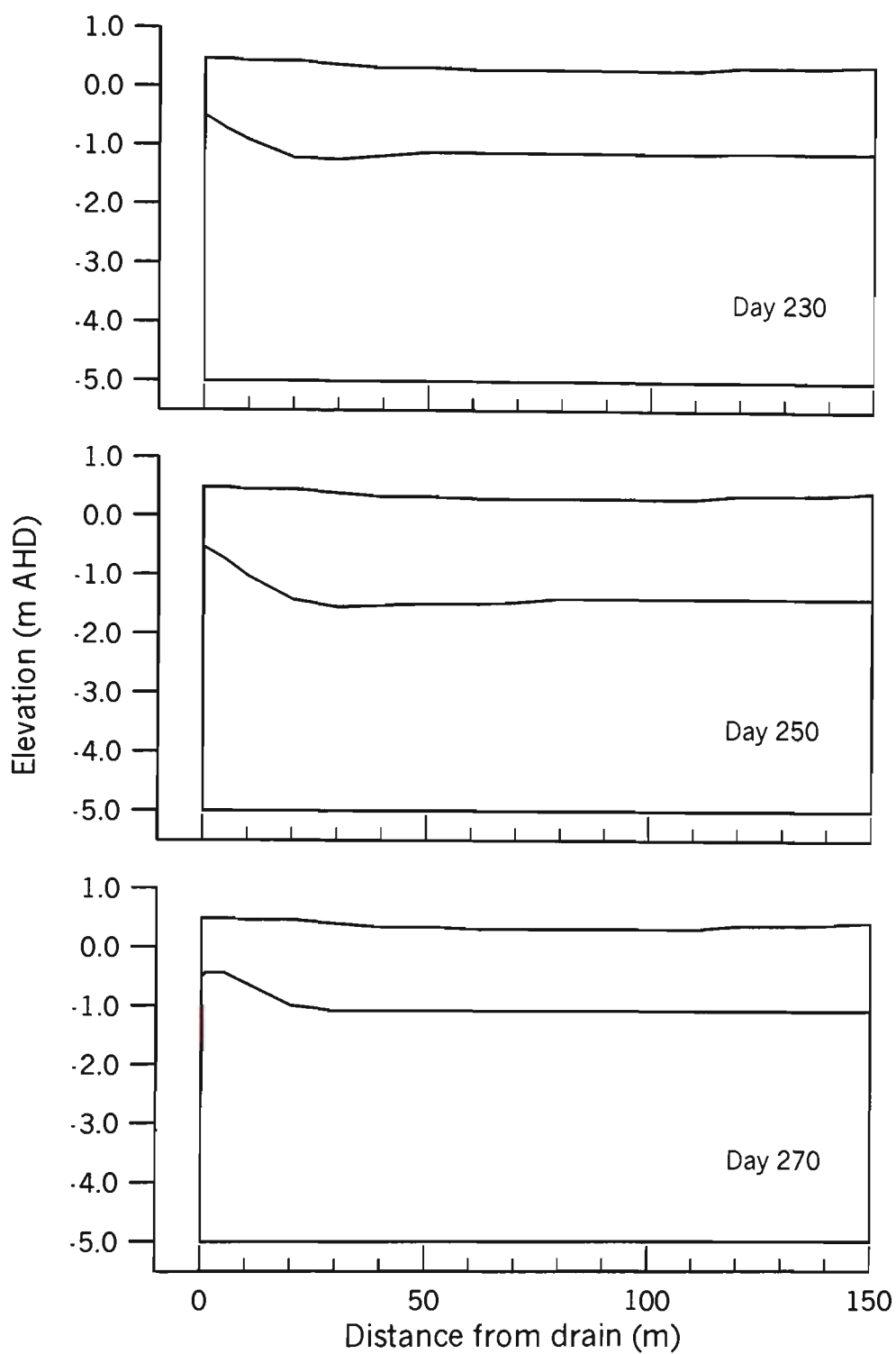


**Figure 11.10(b)** Groundwater elevation at Days 230, 250 and 270 for the Weir -0.5 m AHD drain management option.

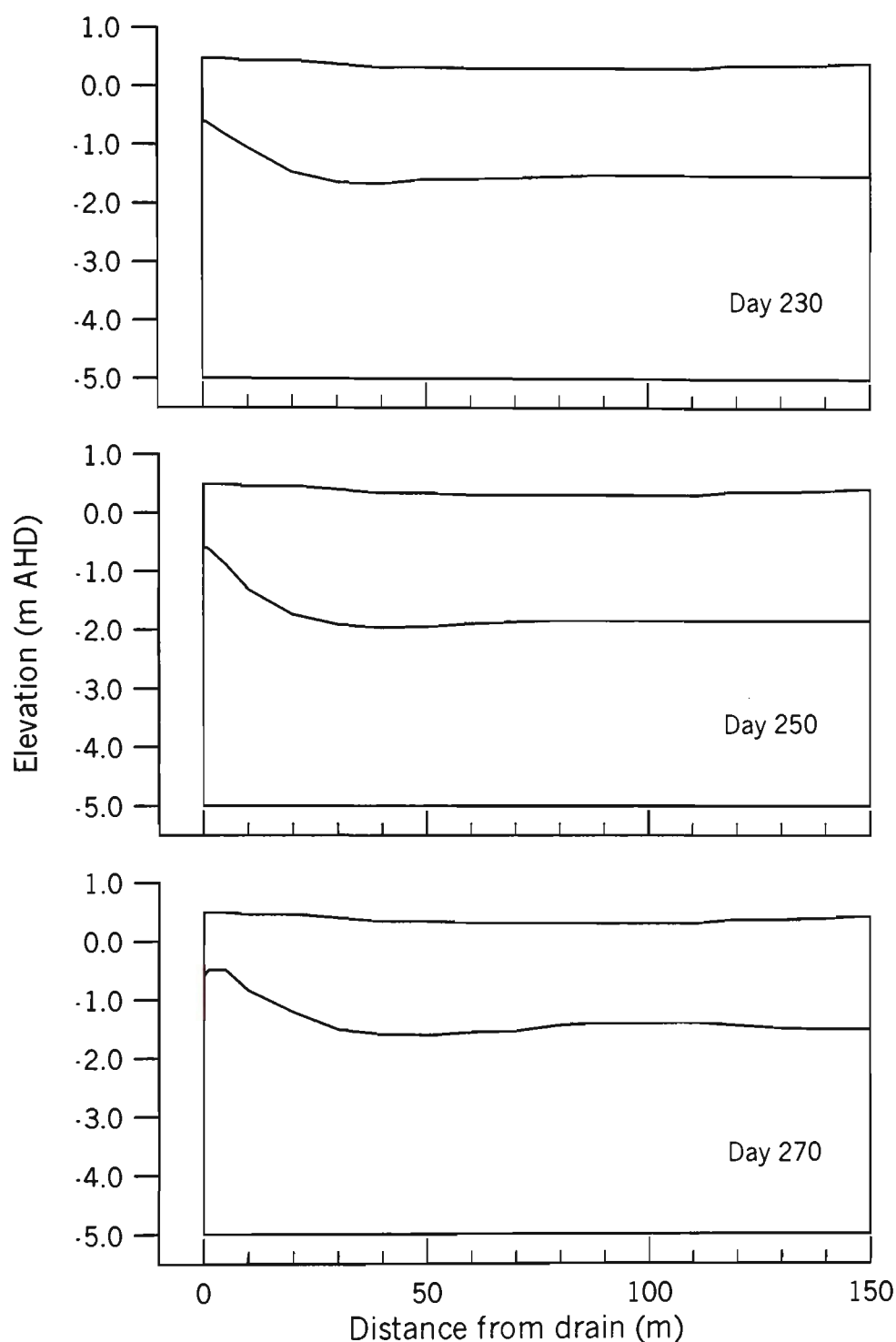


**Figure 11.10(c)** Groundwater elevation at Days 230, 250 and 270 for the tidal ingress drain management option.

A substantial increase in the elevation of groundwater level was achieved by maintaining a constant, elevated water level in the drain by a weir. During the worst part of the drought period (Day 250) where groundwater levels fell well below the elevation of the sulfidic soil layer, maintenance of the drain water level at -0.5 m AHD

resulted in the groundwater at 10 and 90 m from the drain being 0.35 m and 0.49 m higher than under the existing drained conditions, respectively. Maintenance of the water level in the drain at -0.3 m AHD resulted in the groundwater at 10 m and 90 m from the drain being 0.64 m and 0.84 m higher than under the existing conditions, respectively. Increasing the drain water level by allowing tidal ingress did not substantially improve the groundwater elevation. At day 250, the groundwater elevation increased by only 0.12 m at 10 m distance from the drain and 0.10 m at 90 m distance from the drain.

All the alternative drain management options increase the elevation of the groundwater table relative to the observed groundwater elevation measured under the existing drained situation. As such, adoption of any of these alternative drain management options may be considered as an improvement with respect to reducing the amount of pyrite oxidised during periods of low groundwater tables. On initial inspection, it appears that the application of the -0.3 m AHD weir is the most successful option in maintaining the groundwater table above the pyritic soil. However, maintenance of the drain water level at this elevation may give rise to a series of other land management problems. Figure 11.9 shows that groundwater table for the -0.3 m AHD weir simulation is at an elevation of 0.44 m AHD at 10 m distance from the drain and 0.34 m AHD at 90 m distance from the drain between Days 350-365, which corresponds to a period of high rainfall. The surface elevation at 10 m and 90 m distance from the drain is 0.47 m and 0.33 m AHD, respectively. Thus, maintenance of the drain water level at -0.3 m AHD has resulted in the groundwater table being at or very close to the surface. Surface ponding may pose numerous detrimental land management-agricultural productivity problems including, waterlogging which can degrade crop/pasture growth and reduced trafficability/access. White *et al.* (1997) indicate that if surface ponding is maintained for periods longer than 3-5 days, then substantial yield penalties may develop where non-waterlogging crops or pastures are grown. This is certainly the case at the Berry field site where the predominant pastures are rye grass dominated and where corn and sorghum are grown as fodder crops. Access and trafficability is also restricted during periods where surface ponding occurs due to the low shear strength of the soil. Surface undrained failure of soil is easily caused adversely affecting trafficability of farm machinery. Similarly,

tillage and crop planting is restricted due to poor mobility and inappropriate soil moisture conditions for the generation of a well structured seed bed.

Application of the weir at -0.5 m AHD maintains an unsaturated surface soil layer even during heavy rainfall events. At the end of the simulation period, the distance from the surface to the groundwater table was 0.46 m and 0.17 m at 10 and 90 m distance from the drain, respectively. Given the shallow rooted nature of the crops/pasture grown at the study site, maintenance of this depth of unsaturated soil is likely to be sufficient to minimise yield penalties resulting from prolonged waterlogging.

#### *11.3.3 ASS3D simulations - sulfate production*

The ASS3D model was applied to the three drain management options simulated using FEMWATER. ASS3D was compiled so that the concentration and distribution of sulfate produced during pyrite oxidation was computed. The magnitude and distribution of sulfate produced during the 365 day simulation period are shown in the video animations of the sulfate production on the attached CD. A discussion of the distribution of pyrite oxidation - sulfate production is given below.

The distribution of sulfate generated by pyrite oxidation for the existing drained state shows a number of interesting features. At Day 170, the groundwater table has fallen below the sulfidic soil layer. The zone of pyrite oxidation extends across the whole simulation area for the drained situation and has progressed down approximately 0.6 m into the pyritic layer. The groundwater table fell to its maximum depth around Day 250. In the drain simulation, pyrite oxidation extended in excess of 1 m into the acid sulfate soil layer. The thickness of the oxidised zone is much less close to the drain than further out into the field. For all the drain management simulations, the groundwater table is supplemented by seepage through the drain walls for the area immediately adjacent to the drain. At distances greater than 20 m from the drain, evaporative losses from the

groundwater are greater than the recharge rate, thereby giving rise to lower groundwater table elevations away from the drain. This in turn enables the pyrite oxidation front to progress to deeper depths as the distance increases away from the drain. By Day 310 the groundwater table had risen as a result of significant rainfall. However, a small area of pyrite oxidation still occurred for close to the drain. Though the volume of oxidising acid sulfate soil appears relatively small to that previously exposed to oxidising conditions, the ongoing oxidation of pyrite in the sulfidic soil layer immediately adjacent to the drain still poses a severe problem for the water quality in the drain. As acidic pyrite oxidation products are generated in this volume of soil close to the drain, small rainfall events will ensure that acid is continually discharged into the drainage system. This implies that lime treatment close to the drains at critical depths or on the drain seepage face is desirable and should be considered irrespective of the groundwater management strategy.

In contract, the maintenance of elevated drain water levels by the weirs has reduced the vertical and horizontal distribution of the zone of pyrite oxidation. At Day 250 where the groundwater table approaches its lowest level, the zone of pyrite oxidation extends from a distance of approximately 10 m distance from the drain and to a maximum depth of 0.6 m into the sulfidic soil for the -0.5 m AHD weir. For the -0.3 m AHD weir, the zone of pyrite oxidation is not spatially continuous across the simulated field. Zones of pyrite oxidation extend from approximately 15-70 m and 120-150 m from the drain, and to a maximum depth of 0.4 m into the sulfidic soil. At Days 230 and 270, the groundwater elevation is higher than the upper surface of the sulfidic soil layer which precludes any pyrite oxidation. The higher drain water elevation simulated for both weir options removes the small volume of oxidising pyritic soil close to the drain.

The generation of sulfate and the consumption by pyrite by oxidation was, as expected, greatest in the existing drained state. For the period simulated, the existing drained conditions produced  $91 \times 10^3$  mol sulfate from the oxidation of pyrite over the  $6000 \text{ m}^2$  mesh area (i.e, 40 m x 150 m). The three drain management options simulated using FEMWATER-ASS3D resulted in substantial improvements in the amount of sulfate

produced from the oxidation of pyrite. The amount of sulfate generated with respect to the various drain management options simulated is shown in Figure 11.11.

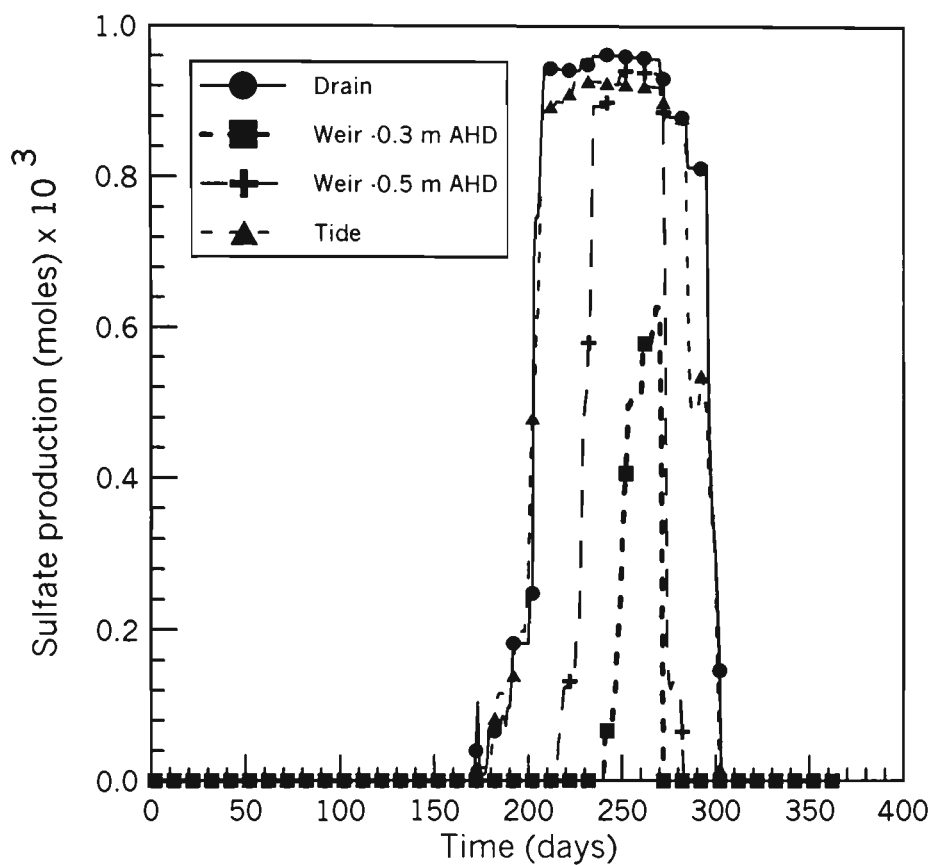


**Figure 11.11** Sulfate production for the ASS3D simulation of drain management options

Installation of the weir in the drains was the most successful drain management option in terms of reducing the amount of pyrite oxidation. Application of weir in the drains was the most successful drain management strategy. Maintenance of the drain water level at -0.3 m AHD resulted in  $12.5 \times 10^3$  mol sulfate being generated, whereas maintenance of the drain water level at -0.5 m AHD resulted in  $42 \times 10^3$  mol sulfate being generated. Allowing tidal ingress resulted in  $85 \times 10^3$  mol sulfate being produced.

11.3.4 Assessment of simulated drain management options

All the water management options simulated using FEMWATER-ASS3D were effective in reducing the oxidation of pyrite in the sulfidic soil relative to the existing over drained situation. The relative effectiveness of the water management strategies in comparison to the existing situation is shown in Figure 11.12.

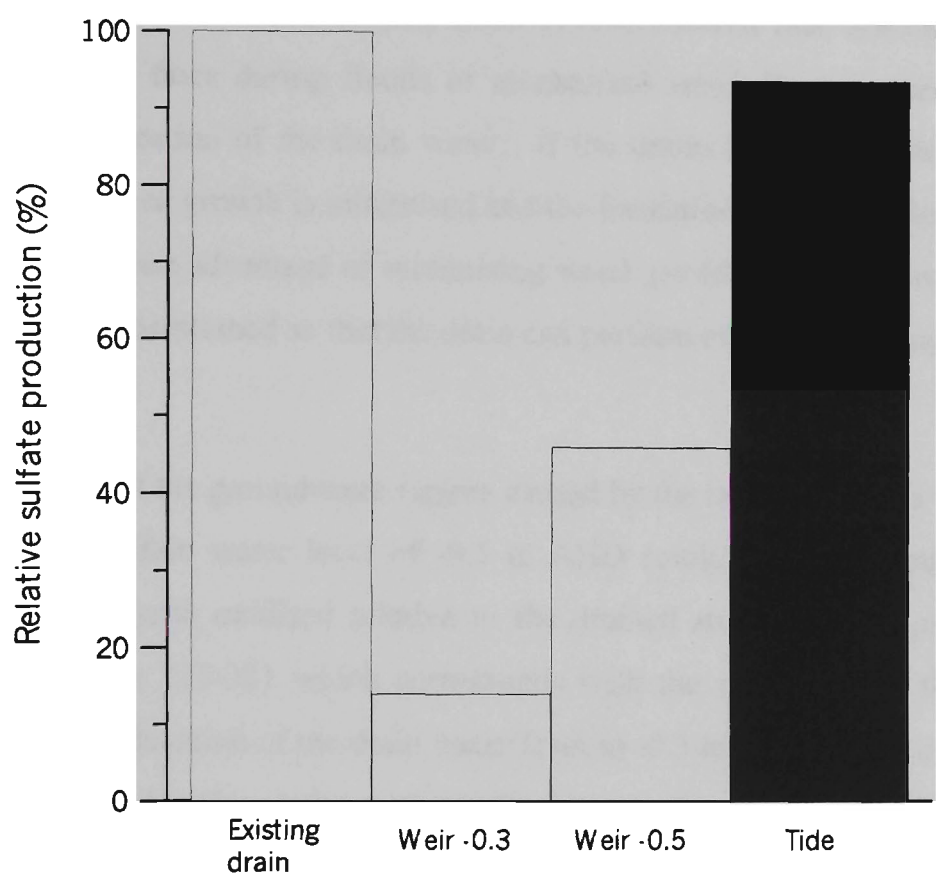


**Figure 11.12** Relative effectiveness of drain management strategies

Opening the floodgates to allow tidal ingress into the drain did not give a substantial improvement in the amount of pyrite oxidised during the simulation period. Tidal ingress resulted in an improvement of only 6% relative to the drained state. However, several advantages of allowing tidal ingress into the drain may accrue irrespective of its immediate influence on the elevation of the surrounding groundwater table. The main advantage of tidal intrusion into the drain is the exchange of brackish water from the

creek . Brackish water has an acid buffering potential (e.g, sea water has approximately  $2.5 \text{ mol H}^+/\text{m}^3$  acid neutralising capacity) which can, at least in part, neutralise acidity released into the drains from the adjacent acidic groundwater before it is transported to the creek. Saline water also acts as an effective weed control mechanism in the drain. Where the drains are predominantly fresh, as is the case when weirs are installed and/or where the floodgates do not leak, aquatic weeds establish and grow rapidly. As the drain water has a high concentration of dissolved sulfate from previously oxidised pyrite, conditions for the precipitation of iron monosulfides ( $\text{FeS}$ ) onto the drain invert are often present. Sullivan and Bush (1999) showed that disturbance of these iron monosulfide flocs during floods or mechanical weed clearing operations can lead to rapid acidification of the drain water. If the drains are exposed to regular salt water intrusion, weed growth is minimised and the formation of iron monosulfides cannot take place. Another advantage of minimising weed growth is that the hydraulic integrity of the drain is maintained so that the drain can perform efficiently during flood periods.

Simulation of the groundwater regime caused by the installation of a weir in the drain to maintain a drain water level of  $-0.5 \text{ m AHD}$  resulted in a reduction of 54% of the amount of pyrite oxidised relative to the drained state. Sulfate production occurred between days 215-281 which corresponds with the worst part of the drought period. Raising the elevation of the drain water level to  $-0.3 \text{ m AHD}$  resulted in even less pyrite being oxidised (14% relative to the drained state). For the  $-0.3 \text{ m AHD}$  weir simulation, the oxidation of pyrite was confined to the time between days 240-268. This shows that implementation of the weir strategy delays the onset of oxidising conditions in the sulfidic soil. The onset of pyrite oxidation was delayed by 35 days for the  $-0.5 \text{ m AHD}$  weir and by 70 days for the  $-0.3 \text{ m AHD}$  weir, respectively. This delay provides a higher level of security that rain will fall and 'top up' the groundwater table. The average rainfall record for Berry (see Chapter 4) shows that rainfall is relatively uniformly distributed through the year. As such, prolonged dry periods are relatively unusual. Under 'normal' climatic conditions, it is envisaged that elevated drain water levels would maintain groundwater levels above the sulfidic soil horizon all of the time.



#### 11.4 Limitations of the ASS3D model

The pyrite oxidation model ASS3D computes the magnitude and distribution of  $H^+$ ,  $SO_4^{2-}$  and  $Fe^{3+}$  generated during the oxidation of acid sulfate soils, thereby making assessment of various acid sulfate soil groundwater management strategies possible. However, there is no linkage between the amount of pyrite oxidation products generated and their concentration in groundwater. Entry of the concentration of daily pyrite oxidation products may be possible in the contaminant transport component of FEMWATER by using a source/sink boundary condition at nodes within the acid sulfate soil layer. This may enable the concentration of oxidation products in the groundwater or the amount of acid being discharged into the drains to be calculated. However, there are a number of impediments to this approach. Firstly, the source/sink boundary nodes are generally used to represent injection wells in FEMWATER contaminant transport simulations. In order to simulate the introduction of a contaminant into the FEMWATER simulation, it is necessary to prescribe the concentration of the contaminant and the volume of the fluid being injected. Clearly for acid sulfate soils, there is no injection of a fluid, rather the assimilation of a quantity of pyrite oxidation products within the groundwater. A second complication is the manner in which the acid oxidation products are generated, then stored, in the oxidising acid sulfate soil layer. As the groundwater table falls below the acid sulfate soil layer, pyrite oxidation takes place in the unsaturated part of the soil matrix. The oxidation products do not immediately mix with the groundwater, but are held in suction within the pore space. It is not until the groundwater table rises back through the zone of oxidation that the oxidation products mix with the groundwater. A final impediment is the organisation of source/sink boundary conditions nodes in the FEMWATER simulation. For every individual node within the acid sulfate soil layer, a source/sink boundary node would require the development of a separate input file with the amount of oxidation product generated on a daily basis. Although this task can be performed by the application of a purpose built, time managed subroutine, it would become increasingly arduous as the mesh size and volume of acid sulfate soil increased.

## 11.5 Advantages of the 3D pyrite oxidation model approach

In Chapter 8, the application of SMASS using groundwater elevation data derived from FEMWATER simulations showed that the amount of sulfate produced by pyrite oxidation was reduced by 75% and 57% at 10 m and 90 m from the drain respectively, in the -0.5 m AHD weir simulation relative to the drained simulation. Applying SMASS at two distinct locations, either close or further away from the drains, showed that a substantial improvement in the management of the acid sulfate soil could be achieved by the installation of a weir in the drains. However, this approach did not enable an estimation of the total reduction of the magnitude of pyrite oxidised or its distribution across an extensive area (at the field scale in this case). By combining ASS3D with the FEMWATER moisture content data directly, the magnitude of the pyrite oxidised, either at a single day or for a whole simulation period, can be determined. Application of ASS3D to the FEMWATER simulation showed that the total reduction in the amount of pyrite oxidised for the whole simulation area was 54%. In addition, areas which are likely to pose particular water quality problems on an ongoing basis, for example oxidation in the acid sulfate soil layer very close to the drain, can be readily identified using the three dimensional modelling approach. This is difficult to achieve using a number of arbitrarily chosen locations for one dimensional assessment using a model such as SMASS.

Another advantage of the ASS3D model and its connectivity with FEMWATER, is the ability to present graphical and video representations of both the groundwater regime, soil moisture content and the magnitude/distribution of pyrite oxidation. For ease of presentation, two-dimensional diagrams of the groundwater elevation and sulfate production were presented in this study. However, the simulated amounts of sulfate production were for a field of 150 x 40 m. This is a particularly powerful tool when demonstrating/explaining the importance of appropriate drain management practices to land managers.

## 11.6 Recommendations

An objective of this research was to develop a 3D model where the influence of various groundwater management practices on the oxidation of pyrite in acid sulfate soils could be assessed. Section 11.3 of this Chapter demonstrates that ASS3D can be used to achieve this purpose. However, in order to improve the ASS3D model, future model development may include:

- a procedure to ‘inject’ the pyrite oxidation product(s) into the soil water in the unsaturated part of the soil matrix where they are generated. The pyrite oxidation products can then undergo re-distribution and transport once the groundwater rises through the oxidised layer(s);
- coupling ASS3D with an existing geochemical model (for example, MINTEQA2) to solve the complex geochemistry between the groundwater and the soil, the groundwater pH, and to compute the precipitation/dissolution of sparingly soluble oxidation products such as jarosite. Modeling of the steady state groundwater quality may be achieved if such a geochemical model was coupled with ASS3D;
- incorporation of a probabilistic assessment procedure where known distributions of various parameters (for example; pyrite crystal size, pyrite concentration) can be entered into the program and run many times to assess the relative importance of various input parameters (i.e. sensitivity analysis);
- incorporation of a function describing the pyrite distribution within the soil macropore-matrix continuum. If, as Bush and Sullivan (1999) suggest, most pyrite is associated within or close to macropores, then the apparent under-estimation of the amount of pyrite oxidised by ASS3D and other pyrite oxidation models may be overcome;
- development of a soil chemical and physical property database from well studied sites so that realistic input parameters can be used to initialise the model for assessment of sites that may differ from the Berry study site.

## 11.7 Conclusions

ASS3D has been shown to accurately simulate the magnitude and distribution of pyrite oxidation in sulfidic soils during periods of low groundwater elevation. Measured and computed pyrite contents correspond well for the existing floodgated drainage system that caused groundwater to fall below the sulfidic soil layer, which subsequently generated substantial amounts of acidic pyrite oxidation products. Given the capacity of ASS3D to accurately simulate the oxidation of pyrite in sulfidic soils, ASS3D can be used to assess the effectiveness of various drain management strategies that can be used to reduce pyrite oxidation caused by low groundwater tables.

ASS3D was used to assess the effectiveness of the installation of weirs at -0.5 and -0.3 m AHD, as well as the influence of removing floodgates to allow the ingress of tidal water into the drains. The simulations showed that the oxidation of pyrite was significantly reduced by the installation of the weirs, although some issues associated with very high groundwater tables possible leading to prolonged flooding were noted for the -0.3 m AHD weir option. Opening floodgates to allow the ingress of tidal water into the drain only had a marginal influence on the adjacent groundwater elevation. The ASS3D output is able to be assessed both spatially across a study site at a specific time, as well as temporally by either calculating the total cumulative concentration of pyrite oxidation products (i.e.  $\text{SO}_4^{2-}$ ,  $\text{H}^+$ ,  $\text{Fe}^{2+}$ ) generated over the simulation period or saving the spatial view of the magnitude and distribution of pyrite oxidation products generated as a video file. Appreciation of both the magnitude and distribution of pyrite oxidation as well as the fluctuations in the groundwater table elevation using FEMWATER enables better understanding of the relationship between acid generation and the groundwater regime for various potential drain management options.

## Chapter 12: Laboratory modelling of acid generation

### 12.1 Introduction

Experiments that determine the rate of pyrite oxidation have largely been confined to complex laboratory studies (e.g., McKibben and Barnes, 1986; Sasaki, 1994; Moses *et al.*, 1987). It is not clear whether laboratory derived rates of pyrite oxidation are applicable for the oxidation of pyrite in the field. The oxidation of pyrite in sulfidic sediments is likely to be affected by numerous physical and chemical processes that occur in the soil. These may include the formation of coatings on pyrite crystals that change the contact mechanism of oxygen with the pyrite, chemical buffering processes within the soil that alter the amount of acid ultimately available for transport in the groundwater, and various catalytic bacterial processes that influence the pyrite oxidation rate under different pH conditions. These conditions are not replicated in tightly controlled laboratory determinations of pyrite oxidation, so their suitability as predictive tools in sulfidic soil is questionable.

Bronswijk *et al.* (1995) used the numerical simulation model SMASS to calculate a linear expression relating the amount of pyrite oxidation per year to the average depth of groundwater level below the pyritic layer. Although the rate of pyrite oxidation determined using this modeling approach was validated against field data, the determination of the pyrite oxidation rate is dependant on the rate term used within the model, which was adapted from laboratory based experimental work. However, the simple linear expression that was derived by Bronswijk *et al.* (1995) for the rate of pyrite oxidation is of considerable use to land management practitioners, in that the independent variable for the regression equation is the depth of the groundwater table below the pyritic soil, a convenient parameter that can be obtained by ongoing monitoring of piezometers in the field.

Ritsema *et al.* (1992) studied the transformation of a potential acid sulfate soil into actual acid sulfate soil in column experiments, where the concentration of pyrite oxidation products was monitored for a period of 800 days. During the drainage phase of their experiments, the concentration of pyrite oxidation products was shown to increase in an exponential fashion from the onset of oxidising conditions for a pyritic soil that contained no soil carbonates. The rate of acid generation in a column that had a substantial supply of soil carbonates was significantly lower. The column experiments performed by Ritsema *et al.* (1992) demonstrate the effect of low groundwater tables and carbonate concentration on the generation of acidity. However, no correlation was made between the depth of the groundwater below the pyritic soil or the length of exposure to oxidising condition with respect to the amount of acid generated.

In this Chapter, the rate of acid generation from the oxidation of pyrite is determined for field and laboratory structured pyritic soil. The magnitude of the change in acid production is linked to the height of the pyritic soil above the groundwater table and the time that the pyritic soil remains in that state. Empirical equations that describe the acid generation rate for homogenous and macropore structured soil are presented in this Chapter. Application of these equations enable land managers to determine the amount of acid produced during periods, where the groundwater table is below the pyritic soil in a semi-quantifiable fashion.

## **12.2 Experimental methods**

The rate of acid generation was determined by maintaining cores of field or laboratory structured pyritic soil at simulated heights above the groundwater table for 1, 2, 4 and 7 weeks. After the allotted period of time, the amount of acidity in the sample was measured using wet chemical methods. Multiple regression analysis was used to assess the relative importance between the time of exposure to oxidising conditions and sample height above the groundwater table with respect to the titratable acidity of the sample.

### *12.2.1 Soil sampling and preparation*

Intact field structured samples of pyritic soil was collected from a depth of approximately 1.5 m below the ground surface from the field site. A backhoe pit was excavated and a bench was prepared in order to sample the sub-surface pyritic soil layer. Sixty samples were collected in 50 mm diameter x 50 mm high PCV cores that were pushed into the pyritic soil in a vertical orientation in order to preserve the soil macroporosity caused by historical plant root activity. These intact cores were carefully excavated from the bench then wrapped in cling wrap and plastic bags to minimise pyrite oxidation in the field. The samples were kept refrigerated at 4°C until the acid generation rate experiments commenced.

A large volume of bulk pyritic soil was also collected from the backhoe pit and managed to minimise pyrite oxidation until the start of the acid generation experiments. The bulk pyritic soil was placed into a large mechanical mixer where it was thoroughly homogenised so as to destroy any macroporosity that had developed in the field and to ensure a uniform distribution of pyrite through the soil. This uniform pyritic soil was packed into the PVC cores to the same dry bulk density of the field structured soil (i.e., 1000 kg/m<sup>3</sup>). The measured initial pyrite concentration of the uniform pyritic soil was less than that of the undisturbed samples. This dilution may have been caused by taking bulk soil material from deeper depths in the field where the pyrite concentration is lower than the upper 0.1 m of the pyritic soil where the undisturbed samples were taken.

Three laboratory structures were imposed onto the cores of uniformly packed pyritic soil. These structures include:

- a) bulk uniform structure (no pores);
- b) 5 vertically orientated 'pores' made by pushing a 3 mm diameter wire through the sample (5 pores);

- c) 10 vertically orientated 'pores' made by pushing a 3 mm diameter wire through the sample (10 pores).

The importance of macropore structure and the distribution of pyrite relative to the position of the macropores could be assessed by comparison of the field structured samples with the laboratory samples. In the laboratory pyritic soil with no artificial pores, oxygen was expected to diffuse through the air-filled pore space within the soil matrix. Given that the air-filled pores space in the uniform soil matrix is not continuous, then the rate of oxygen diffusion and subsequent pyrite oxidation was expected to be relatively low. Similarly, the uniform distribution of pyrite within the soil matrix was expected to minimise the rate of acid generation.

The influence of large, continuous pores was assessed by the generation of artificial pores. As the number of artificial pores increases, so to does the surface area through which oxygen can diffuse into the pyritic soil. It was expected that the artificial pores would drain upon the application of a small suction, thereby simulating the transport of oxygen into field structured pyritic soil. However, the uniform distribution of pyrite through the soil matrix is not the same as in the field where pyrite tends to cluster inside macropores.

#### *12.2.2 Application of variable depth to groundwater table*

The field and laboratory structured samples were maintained at a specific suction that simulated the height of a sample above the groundwater table. The various samples were divided into five different 'height above the groundwater table' classes, including: 0 m (i.e., saturated), 0.5 m, 1.0 m, 2.0 m and 5.0 m, which cover the range of groundwater fall below the pyritic soil likely to be encountered in eastern Australian coastal floodplains.



Samples that were maintained at 0 m suction were placed in a plastic tray and were submerged with approximately 5 mm of distilled water. Then the tray was covered with aluminium foil to minimise evaporative losses. Water was occasionally added to the tray to keep the samples covered.

A suction table was constructed for the samples maintained at 0.5 m suction. The suction table comprised a 600 mm diameter x 200 mm high section of PVC pipe that was capped at the bottom. A 600 mm diameter rigid mesh was bonded to the PVC pipe approximately 100 mm from the bottom. A tap was installed at the sealed base, from which a plastic tube was attached so that a hanging column of water (which controlled the suction) could be applied. In order to create a suction to the base of the samples, approximately 10 mm of diatomaceous earth was poured in slurry form onto the rigid mesh. The soil samples were placed on to the slurry, then the height of water in the hanging column was adjusted so that a suction of 0.5 m was applied to the sample. A plastic lid was placed over the suction table to minimise evaporation.

The samples that were maintained at 1 m , 2m and 5 m height above the groundwater table were placed onto a 1 bar ceramic plate. Good soil-plate contact was achieved by using a thin slurry of diatomaceous earth. The samples and the ceramic plates were placed into a pressure vessel that was used to determine soil moisture characteristic properties. Pressures of 10 kPa, 20 kPa and 50 kPa were applied via a regulated source of high pressure air.

After the application of the appropriate suction for the allotted period of time, the soil samples were removed from the applied suction. The top and bottom 2 mm of the sample was sliced off to remove any acid that had been generated on the exposed top surface of the core and to remove any diatomaceous earth from the bottom of the sample. The soil samples were weighed, then oven dried at 85°C and weighed again for the determination of the soil moisture content. The samples were ground and passed through a 2 mm sieve prior to the measurement of soil acidity.

### 12.2.3 Measurement of soil acidity

The Peroxide Oxidation - Combined Acidity and Sulfate (POCAS) method described by Ahern *et al.* (1998) was used to determine the actual and potential acidity of the samples. Five grams of ground soil was made into a 1:5 suspension with 1 M KCl and shaken overnight. An aliquot was filtered and then titrated against 0.25 M NaOH until pH 5.5. 2 ml of 30% hydrogen peroxide was added to the aliquot to oxidise any dissolved iron, then the sample was adjusted to pH 5.5 by the further addition of 0.25 M NaOH. The total actual acidity of the soil was determined from the total volume of NaOH used.

Potential acid sulfate soil was oxidised by applying additions of 5 ml 30% H<sub>2</sub>O<sub>2</sub> to 10 g soil samples suspended in 2 M KCl. The suspension was placed over a water bath at 85°C and further additions of H<sub>2</sub>O<sub>2</sub> were applied until effervescence ceased, indicating that all pyrite in the potential acid sulfate soil had been oxidised. Aliquots were filtered, then titrated to pH 5.5 with 0.25 M NaOH (including the addition of 2 ml H<sub>2</sub>O<sub>2</sub> for iron oxidation) for determination of total potential acidity. An aliquot was also diluted for determination of peroxide extractable sulfate. Peroxide Oxidisable Sulfur (S<sub>pos</sub> %) and Total Sulfuric Acidity (TSA) were calculated by subtracting the KCl extract measurements from the H<sub>2</sub>O<sub>2</sub> extracts for acidity and sulfate, respectively.

## 12.3 Results and discussion

### 12.3.1 Soil moisture characteristics

The soil moisture characteristic curves were determined for both the field and laboratory structured samples to assess the volume of air-filled pore space that exists upon drainage. No difference in the moisture characteristic curves for the different macropore

structures imposed onto the laboratory samples was observed. The moisture characteristic curves for the field and laboratory structured (10 pores) soil is shown in Figure 12.1.

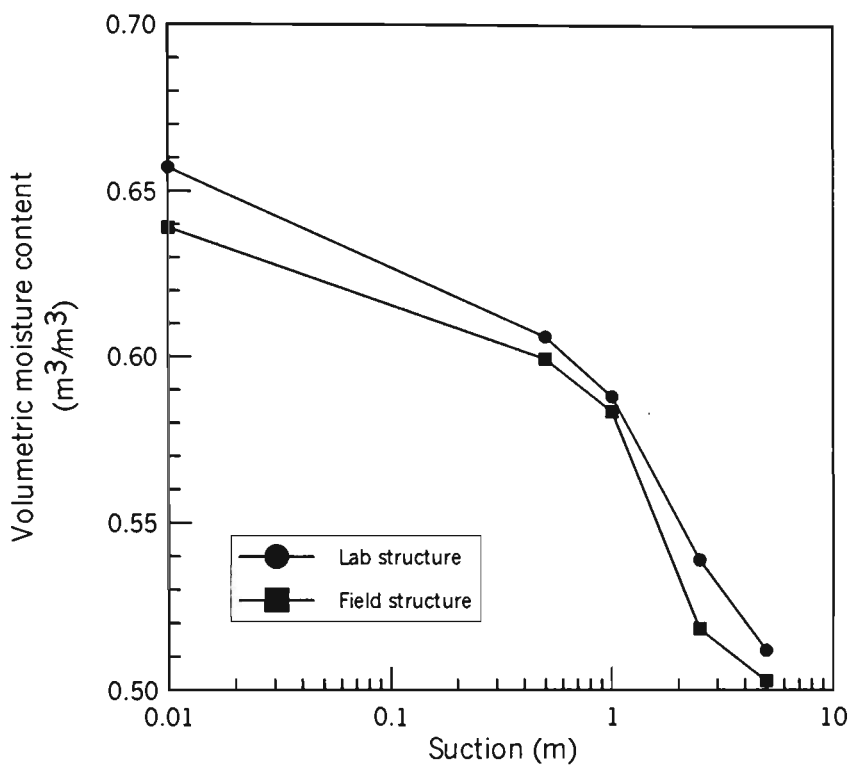


**Figure 12.1** Moisture characteristic curves for field and laboratory structures soils

The moisture characteristic curves are typical of clay soils with a uniform matrix structure and macroporosity consisting of relative large, continuous pores. From an applied suction of 0.5 m, the drainage of water from the soil pore space is consistent between the field and laboratory samples, with moisture content of both soil structural types reducing from about 0.6 (m³/m³) to 0.5 (m³/m³) at 5 m of applied suction. This is indicative of pore water drainage from a uniformly packed clay matrix. Hodgson and MacLeod (1989) suggest that oxygen diffusion through clayey soils may begin once the air-filled porosity increases to about 0.05 (m³/m³). From Figure 12.1, an air-filled porosity of 0.05 (m³/m³) is achieved in the soil matrix by the application of approximately 2 m suction. As shown in Chapter 7, the fall of the groundwater table to 2m below the pyritic soil layer is only likely to occur as a result of severe rainfall deficits and/or very high transpiration rates. Yet acid generation from the oxidation of

pyrite occurs where the groundwater table is less than 2 m below the pyritic soil layer. This indicates that oxygen is being transported to the sites of pyrite oxidation by mechanism other than matrix diffusion.

Drainage of the macropore component of the soil porosity occurs rapidly upon the application of a very small suction. As shown in Figure 12.1, approximately 0.05 ( $\text{m}^3/\text{m}^3$ ) of pore space is available for the transportation of air as a result of the application of 0.5 m suction. Based on the theoretical height of capillary rise in a continuous straight tube (Ritsema, 1994), the macropores that have been drained by the application of a 0.04 m suction are approximately 1.5 mm diameter, with pores of smaller diameter remaining saturated. For the laboratory structured samples where the macropores in the 5 and 10 pore samples were at least 3 mm diameter, an applied suction of 0.5 m was sufficient to drain these structures completely.

Given the preferential drainage of large macropores as a result of relatively small fall in the groundwater table, oxygen can be transported through these large air-filled macropores. The oxygen reacts with the pyritic soil on the macropore walls and generates acid. As such, generation of acid in pyritic soil with substantial macroporosity should occur at a faster rate than a tight clayey matrix where a relatively large suction must be applied to drain sufficient pore space to facilitate oxygen diffusion.

This is a particularly important consideration if the concentration of oxygen in pyritic soil is calculated by the application of oxygen diffusivity equations that use air-filled pore space as the independent variable (e.g. Hodgson and MacLeod, 1989; Troeh *et al.*, 1982) where the air-filled porosity is determined by numerical models that simulate water flow through homogenous porous media. In this case, the diffusion of oxygen to the pyritic soil will be under-estimated which then leads to the under-estimation of the amount of acid generated by pyrite oxidation.

12.3.2 Acid generation in field structured soil

The magnitude of titratable acidity in the field structured soil samples that was generated after different exposure times and suctions is shown in Figure 12.2.

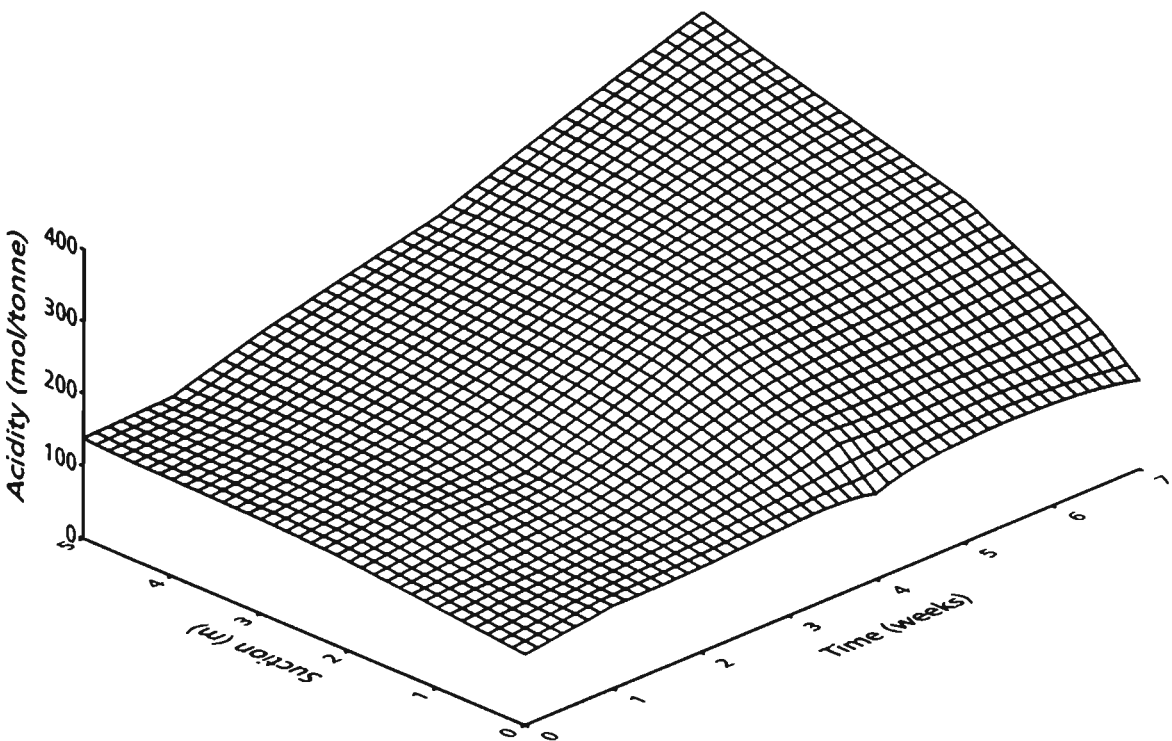


**Figure 12.2** Acid generation with respect to suction and time for field structured pyritic soil

As shown in Figure 12.2, the initial soil acidity in the field samples was 100 mol/tonne, indicating that pyrite oxidation has occurred in the past at the study site. As both the length of exposure to oxidising conditions and the magnitude of suction applied to the samples increased, the magnitude of the titratable acidity in the samples increased. Simple regression equation coefficients for the prediction of acidity using suction and time as independent variables are shown in Tables 12.1 and 12.2.

**Table 12.1** Regression equations for soil acidity against suction

$A_{\text{time}}=aS + b$			
Time (weeks)	a	b	$r^2$
1	5.8	118	0.73
2	12.3	121	1.00
4	20.5	156	0.69
7	47.7	150	0.96

**Table 12.2** Regression equations for soil acidity against time

$A_{\text{suction}}=ct + d$			
Suction (m)	c	d	$r^2$
0.5	10.1	113	0.80
1	15.5	109	0.93
2	23.2	117	0.93
5	38.3	102	0.99

where; A is acidity (mol H<sup>+</sup>/tonne), t is time (weeks) and S is suction (m).

From Figure 12.2 and the high  $r^2$  coefficients achieved by the simple regression equations, the soil acidity increases in a linear fashion with respect to both time and suction. However, the high correlations involving time and suction suggest that both these variables are important in the generation of acidity.

The generation of soil acidity by pyrite oxidation was confirmed by the decrease in the percentage of peroxide oxidisable sulfur (%S<sub>pos</sub>) with respect to both time of exposure and the magnitude of applied suction. The %S<sub>pos</sub> of the field structured samples measured initially and at times 2 and 7 weeks is shown in Table 12.3.

**Table 12.3** Change in the pyrite concentration of field structured sample

Suction (m)	%S <sub>pos</sub>		
	initial	week 2	week 7
0.0	3.94	3.58	3.50
0.5		3.53	3.27
1.0		3.50	3.22
2.0		3.44	3.14
5.0		3.39	2.83

As expected, the magnitude of %S<sub>pos</sub> measured at weeks 2 and 7, respectively, decreased with respect to the applied suction. However, as time increases, the rate of decrease in %S<sub>pos</sub> increases according the magnitude of suction applied. For instance, the difference in %S<sub>pos</sub> at week 2 between the samples at 0 and 5 m suction was only 0.19 %, whereas at week 7 it was 0.67%. The acceleration in the rate of pyrite oxidation after acidification begins may be due to the catalytic effect of acidophilic bacteria such as *T. thiooxidans* and *T. ferrooxidans* (Evangelou, 1995).

### 12.3.3 Acid generation in laboratory structured soil

The magnitude of titratable acidity in the laboratory structured soil samples that was generated after different exposure times and suctions is shown in Figure 12.3. As for the field samples, the generation of acidity in the laboratory samples is controlled by both the magnitude of the applied suction and the length of exposure to oxidising conditions. The magnitude of the titratable acidity maintains a linear relationship with respect to the length of time the sample is exposed to oxidising conditions where the degree of suction is held constant. However, the rate of increase in the magnitude of titratable acidity tends to decrease as suction increases for samples measured at the same

time. This suggests that the rate of acid generated in the soil is controlled by structure of the air-filled pore space that is able to transport oxygen to the pyrite and the distribution of the pyrite in the sample. As shown in Figure 12.1, the large structural pores in the soil drain rapidly and enable pyrite oxidation to occur within and on the surface of the macropore. However, as the applied suction increases, the rate of increase in the air-filled pore space made available for oxygen transport decreases. In addition, the air-filled pore space that becomes available under relatively high suctions is in the soil matrix, which has highly tortuous gas diffusion pathways. As such, the rate of oxygen transport into the soil matrix is relatively slow which reduces the rate of acid generation in the sample.

The distribution of pyrite with respect to the position of the macropores will also influence the rate of acid generation. Bush and Sullivan (1999) showed that a considerable proportion of the pyrite occurs within and adjacent to macropores. Given that the distribution of pyrite in the laboratory samples is uniform, the amount of pyrite available for oxidation increases at a decreasing rate with respect to increases in applied suction. This is in contrast to field structured samples where most of the pyrite would be exposed to oxidising conditions in large pores by the application of relatively small suctions.



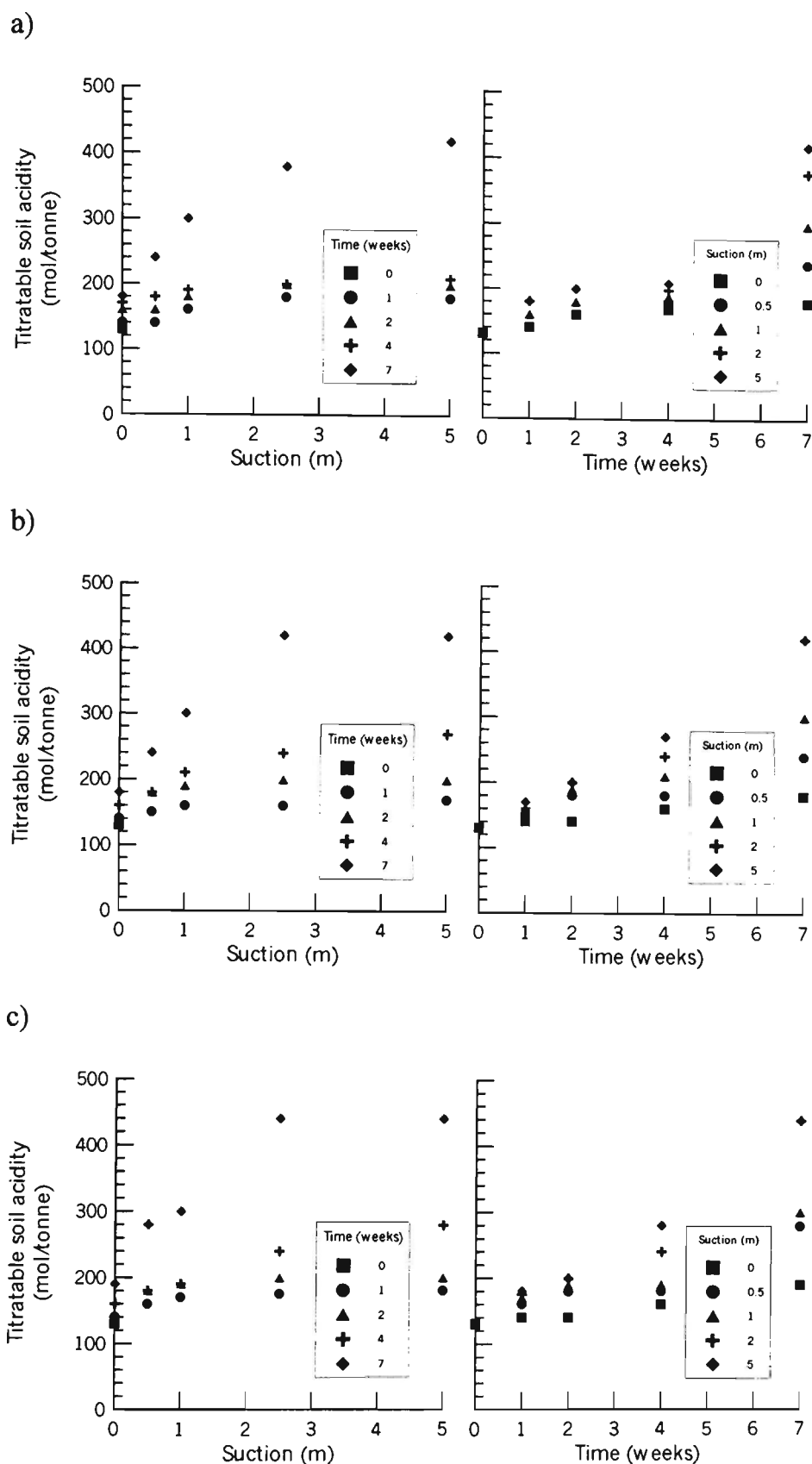


**Figure 12.3** Acid generation with respect to suction and time for laboratory structured pyritic soil with; a) no pores, b) 5 pores and c) 10 pores.

The magnitude of %S<sub>pos</sub> at week 7 for the laboratory structured samples is shown in Table 12.4.

**Table 12.4** Change in the pyrite concentration of laboratory structured samples

	%S <sub>pos</sub> at week 7				
initial %S <sub>pos</sub> = 2.73	Suction (m)				
Sample	0.0	0.5	1.0	2.5	5.0
No pores	2.63	2.12	1.92	1.54	1.35
5 pores	2.50	1.99	1.92	1.48	1.28
10 pores	2.47	1.92	1.92	1.28	1.15

The amount of pyrite remaining in the samples after 7 weeks of oxidation is related to the magnitude of the applied suction, with the most pyrite oxidation occurring at the highest suctions and relatively little pyrite oxidation occurring under near saturated conditions. A relationship also exists between the number of artificial macropores in the sample and the %S<sub>pos</sub>. As the number of artificial macropores increases, the surface area from which oxygen can diffuse into the pyritic soil also increases. At full saturation, the difference in %S<sub>pos</sub> between the differently structured samples is small due to the limited diffusivity of oxygen through water. However, as the artificial pores are drained by the application of a suction, the %S<sub>pos</sub> at a specific suction decreases due to the larger air-soil surface interface in the samples.

The acidity generated in the soil samples after the application of a known suction for a particular time was calculated by subtracting the initial soil acidity from the measured soil acidity. This enabled contour plots of acid generation to be plotted using the depth to the groundwater table (i.e, suction, m) and time as independent variables. Contour plots of acid generation are shown in Figure 12.4.

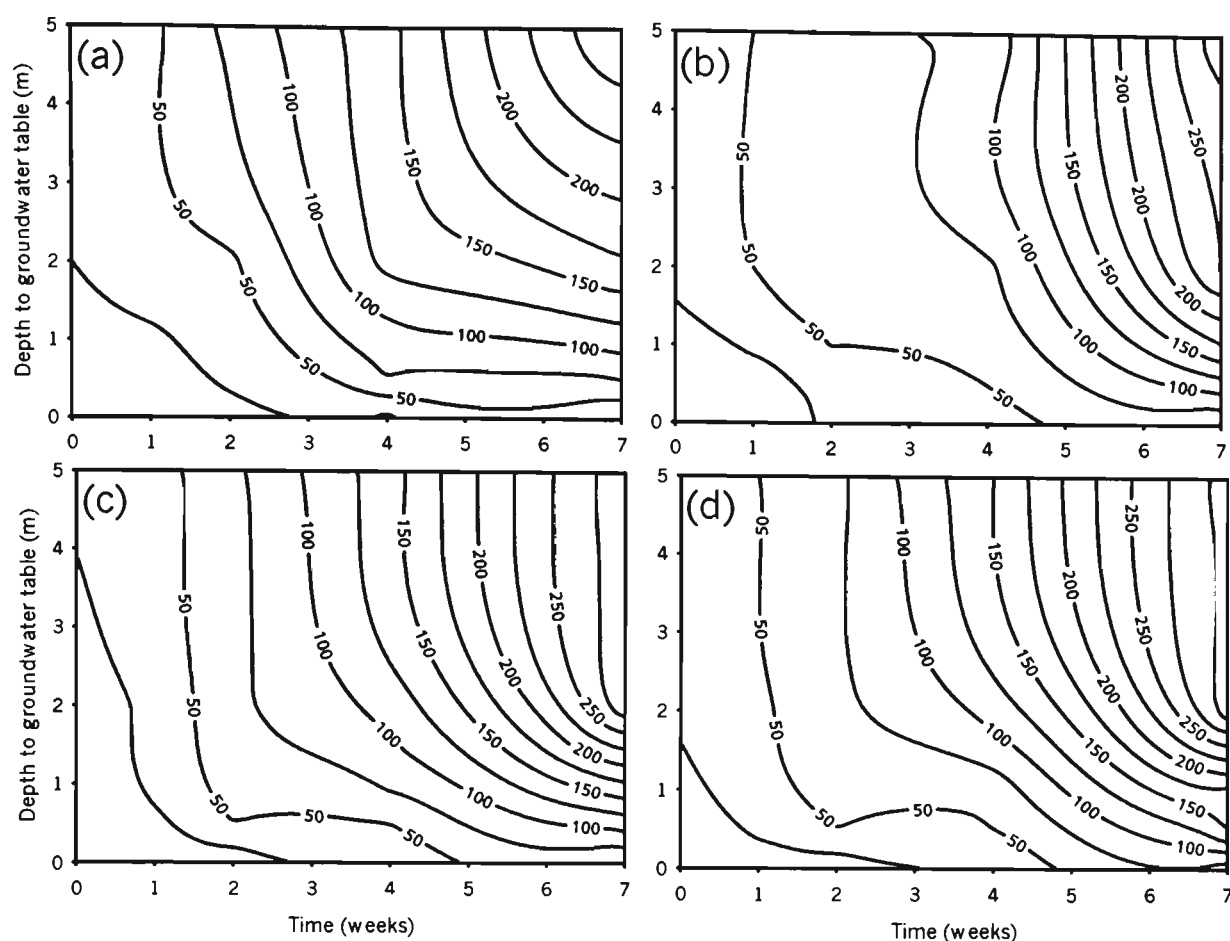


**Figure 12.4** Amount of acid generated (mol H<sup>+</sup>/tonne) for: (a) field structure and laboratory structure with (b) no pores, (c) 5 pores, (d) 10 pores.

The shape of the acid generation contours reflect the nature of the soil structure and the distribution of pyrite in the samples. Where the soil samples have macroporosity, either naturally occurring structure from the field or artificially created in the laboratory, the acid generation contours have an “L” shape. This is related to the drainage of the macropores under low suctions. As shown in Figures 12.4(a,c,d) at any specific time, acid generation increases slowly at suctions less than 1 m, due to maintenance of water films within the macropore that restrict the transport of oxygen. Pyrite oxidation in the structured samples at low suctions is limited to where oxygen can diffuse through large, partially drained macropores. The horizontal orientation of the acid generation contours that occur at low suctions in the structured samples indicate that pyrite oxidation occurs rapidly once macropore drainage occurs.

Once pyrite oxidising conditions are established in the structured samples by the application of a low suction, the rate of acid generation that occurs upon the application of a greater suction is controlled by the distribution of the pyrite in the soil. In Figure 12.4(a), the acid generation contours at suctions greater than 1 m change from a horizontal orientation for suctions less than 1 m to an orientation of approximately 60° from the horizontal for the field structured samples. This suggests that pyrite crystals are located adjacent to or within the large structural features in the soil. As the groundwater table falls and drains increasingly smaller pores, oxygen is able to diffuse to the location of the pyrite crystals to generate acid. As the magnitude of the groundwater fall below the pyritic soil increases, the rate of acid generation slows, suggesting that less pyrite is available for oxidation in the aerated part of the soil matrix away from the macropores.

In contrast, the acid generation contours for the laboratory structured samples (Figures 12.4[c,d]) at suctions greater than 1 m change from a horizontal orientation to a near vertical orientation. This indicates that even as the groundwater table continues to fall below the pyritic soil which increases the air-filled pore space within the soil matrix, the uniformly distributed pyrite within the soil matrix limits the generation of acid. In effect, slow oxygen diffusion through the air-filled fraction of the clay matrix, combined with the uniformly distributed pyrite crystal distribution, minimises the exposure of pyrite to oxidising conditions within the soil matrix.

The relatively slow rate of acid generation in pyritic soil with uniformly distributed pyrite crystals in a uniform clay matrix is confirmed in Figure 12.4(b). After sufficient air-filled pore space is created for the diffusion of oxygen by the application of 1 m suction, the orientation of the acid generation contours is nearly vertical, similar to the orientations for the 5 and 10 pore laboratory samples. This suggests, that where the pyrite crystals are uniformly distributed through a clayey matrix, that pyrite oxidation is relatively insensitive to groundwater fall.

Multiple regression of the time (t, weeks) of exposure of the pyritic soil to oxidising conditions, and the depth of the groundwater table (gwt, m) below the pyritic soil with respect to the generation of acid (A, mol H<sup>+</sup>/tonne) gave the regression coefficients that are shown in Table 12.5 using the equation:

$$A = m_t t + m_s gwt \tag{12.1}$$

**Table 12.5** Multiple regression coefficients for Equation 12.1

Soil structure	Coefficient $m_t$	Coefficient $m_s$	$r^2$
field	13.7	18.4	0.72
lab no pores	18.3	12.9	0.68
lab 5 pores	19.6	15.0	0.69
lab 10 pores	21.2	15.9	0.70

The contour plots and multiple regression equations show that the generation of acid is dependent on both the length of exposure to oxidising conditions and the depth of the groundwater table. For the field structured pyritic soil, the generation of acid is more dependant on the magnitude of the applied suction relative to time of exposure than the laboratory samples, confirming the importance of the heterogenous distribution of pyrite within large soil structural features. In contrast, the  $m_t$  coefficient for the laboratory samples is larger than  $m_s$ , suggesting that acid generation is more sensitive to the length of exposure to oxidising conditions than the applied suction.

## **12.4 Implications for better understanding of acid sulfate soil**

### *12.4.1 Assessment of acid generation in the field*

Land managers are often prepared to install piezometers to monitor groundwater elevation and pH in areas affected by acid sulfate soils. Groundwater monitoring is relatively inexpensive, easy to perform and provides good information with respect to the conditions necessary for the generation of acid from the oxidation of pyrite, i.e., the depth of groundwater relative to the pyritic soil and the length of exposure of the pyritic soil to oxidising conditions. However, the rate and magnitude of acid generation is difficult to determine using groundwater monitoring alone. To accurately monitor acid generation, expensive soil sampling and laboratory testing procedures are required. Given the expense of determining the magnitude and rate of acid generation in acid sulfate soils, few land managers are prepared to monitor acid generation over an extended period of time.

Where the height of the groundwater table relative to the elevation of the pyritic soil is known, a reasonably accurate estimation of the amount of acidity generated during a extended period of pyrite oxidation can be made using Equation (12.1) or Figure 12.4. This has the advantage of enabling land managers to quantify the amount of acid generated for periods where the groundwater table is below the pyritic soil. Quantification of the amount of acid generated has a number of benefits, including; better appreciation of the magnitude of the acidity problem which may facilitate a desire to implement/investigate better management alternatives, comparison between groundwater management and/or drainage techniques/trials and timing of drain bank liming applications.

12.4.2 Numerical modelling

As shown in Figure 12.4, the magnitude of acid generation is determined by the suction applied to the pyritic soil, the length of time the soil is maintained under oxidising conditions and the distribution of pyrite crystals with respect to the structural features of the soil. This has fundamental implications for the definition of numerical schemes for modelling pyrite oxidation in acid sulfate soils. As described in Chapters 3 and 11, numerical models that calculate the amount of acid generated in pyritic soil, including ASS3D and SMASS, assume that the pyrite is uniformly distributed through the soil matrix.

To better simulate the oxidation of pyrite in acid sulfate soils, the non-uniform distribution of pyrite crystals between macropores and the soil matrix should be implicitly modelled. A schematic diagram of such an approach is shown in Figure 12.5.

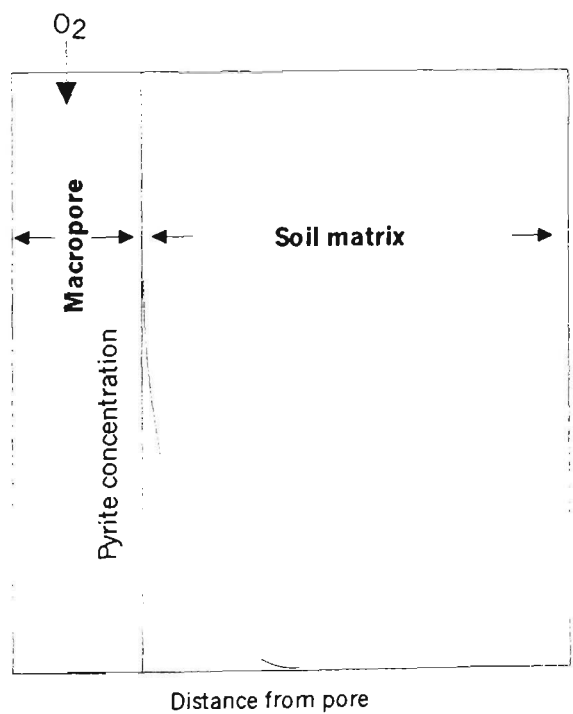


**Figure 12.5** Implicit model linking macropore oxygen diffusion and pyrite crystal distribution.

In Figure 12.5, the distribution of pyrite is heavily skewed towards the macropore, where a high concentration of pyrite is expected to be present at the macropore-soil matrix interface and very little pyrite is expected to occur within the soil matrix. The incorporation of a spatially aligned function for pyrite concentration may be expensive in terms of computing a revised pyrite concentration distribution function for every element that adjoins a macropore for every time iteration where pyrite oxidation has occurred. However, as discussed in Chapter 11, the problem of under-estimating acid generation from numerical schemes which assume uniform pyrite distribution through the soil matrix may be overcome. In addition, the application of such a numerical scheme for the simulation of pyrite oxidation in a macropore structured soil may be useful in developing surface water management strategies such as demand irrigation where oxygen diffusion from the soil surface down macropores to the pyritic soil can be minimised by maintenance of thin water films inside the macropores.

## 12.5 Conclusions

The length of time of exposure of pyritic soil to oxidising conditions and the depth of the groundwater below the pyritic soil can be used to quantify the amount of acid generated by pyrite oxidation. These independent variables can be easily and inexpensively measured in the field. This provides land managers with a simple tool with which they can estimate the amount of acid produced under various groundwater management regimes. However, this approach is clearly dependant on the nature of the soil structure, the concentration of pyrite and its distribution in the soil. Further testing of a variety of soil using this experimental technique should be performed if the multiple regression coefficients for Equation 12.1 were to be applied to pyritic soils other than those at the Berry field site.



The shape of the acid generation contour plots indicates that the distribution of pyrite in the soil requires further investigation by developers of numerical acid sulfate soil simulation models. A substantial difference between the rate of acid generation was found between the field samples with non-uniform distribution of pyrite and the laboratory samples, with or without macropores, that had uniform distribution of pyrite. As such, numerical models that assume uniform distribution of pyrite throughout the soil matrix tend to underestimate the magnitude of pyrite oxidation, particularly at suction of about 1 m.

## **Chapter 13: Application of geochemical concepts to the management of pyritic soil**

### **13.1 Introduction**

Field based monitoring and the application of numerical simulation modelling presented in previous Chapters demonstrate that the generation of acid from pyrite oxidation can be minimised through the installation of theirs in flood mitigation drains. However, as shown in Chapter 8, the groundwater and drain water quality remain poor after the establishment of high groundwater table conditions. Clearly, the application of strategies than minimise the generation of new acid from oxidised pyrite will not result in substantially improved water quality in the short term.

In this Chapter, the management of the existing acid that is present in the soil, groundwater and drains is addressed by the application of geochemical concepts. Two potential acid management strategies are investigated. Firstly, the potential benefits associated with allowing a controlled volume of saline water to intrude into the flood mitigation drains during high tide is investigated. A worked example is used to illustrate the potential improvement in water quality discharged from the drains to Broughton Creek.

The second area of investigation is associated with the iron and aluminium geochemistry of acidic minerals in the actual acid sulfate soil. Two geochemical equilibrium models are used to demonstrate that; the groundwater quality will remain poor for a substantial period of time due to the dissolution of acidic iron and aluminium minerals, and the injection of a calcium carbonate slurry into the soil will improve the groundwater quality and facilitate the rapid dissolution of these acidic minerals.

## 13.2 Controlled saline intrusion into flood mitigation drains with weirs

As shown above, saline water that intrudes into the drain can, at least in part, neutralise acidity before the drain water is discharged into the Creek. Water is discharged from the drain twice per day, when low tide in the Creek causes the floodgates to open in accordance with the hydraulic gradient. As the water level in the Creek rises with the incoming tide, the floodgates close (if not jammed open etc) and a reservoir of acidic water collects behind the floodgate awaiting discharge to the Creek upon the next change in tide. The controlled discharge of saline water from the Creek into the drain during the mid-high tide period may reduce the ‘slug’ like effect of twice daily acidic discharge into Broughton Creek. A brief justification and exploration of this system is described below.

### *13.2.1 Worked example: change in pH due to controlled saline intrusion*

Figure 4.8 shows that the low weir is approximately 250 m from the position of the floodgate. At low tide, water in the drain below the low weir is discharged into Broughton Creek. The difference in water level between the floodgate and behind the low weir is about 1.0 m, which corresponds to a volume of 2000 m<sup>3</sup>. During normal low flow conditions in the drain, about 1000 m<sup>3</sup> flows over the low weir and is discharged to Broughton Creek during the two daily low tide cycles. The average total cation acidity of the 1000 m<sup>3</sup> that flows into the 250 m section of the drain between the floodgate and the low weir is approximately 1 mole H<sup>+</sup>/m<sup>3</sup>. As such, up to 1000 moles H<sup>+</sup> (equivalent to 100 kg H<sub>2</sub>SO<sub>4</sub>) may be discharged to Broughton Creek during each low tide discharge event.

In order to neutralise some of this acidity before it is discharged into Broughton Creek during the next low tide period, a controlled volume of saline water from the Creek could be discharged into the 250 m section of the drain between the floodgate and the

low weir. This requires the installation of a control valve into the floodgate that allows for the discharge of saline water from the Creek to the drain. A variety of control valve systems are available for this purpose. A schematic diagram of this neutralisation system is shown in Figure 13.1

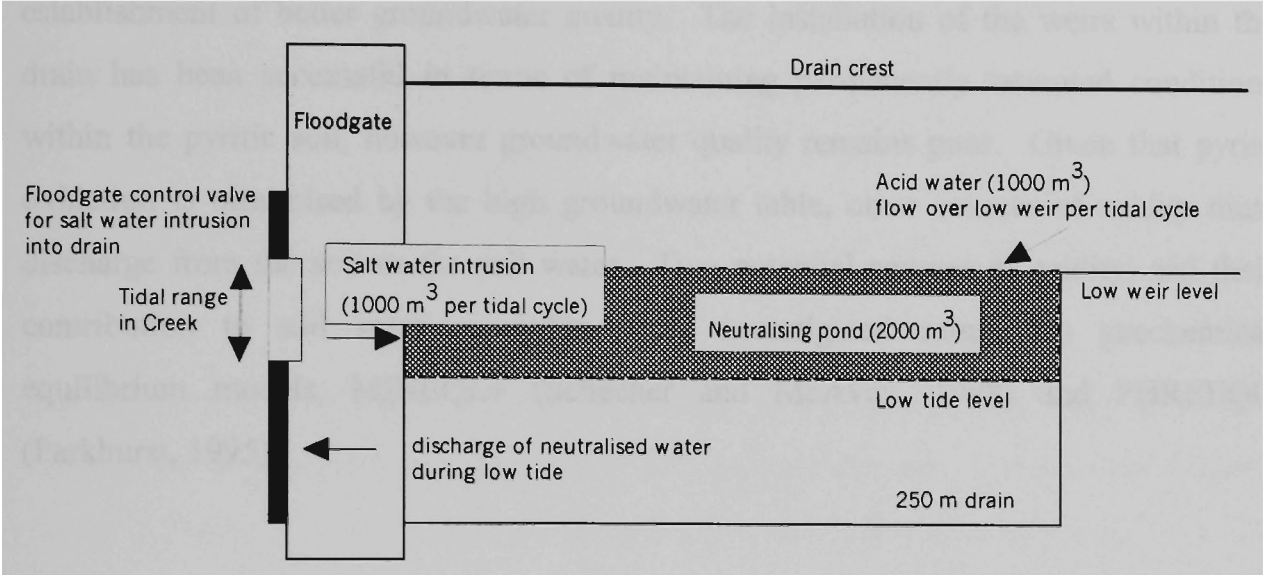


**Figure 13.1** Neutralising pond strategy for controlled salt water intrusion into drain.

In effect, this section of the drain could operate as a neutralising pond for drain water prior to its discharge. About 1000 m<sup>3</sup> of water flows over the low weir between each low tide, leaving an excess volume of 1000 m<sup>3</sup> in the neutralising pond before overtopping of the low weir occurs. If 1000 m<sup>3</sup> of water from the Creek with a neutralising capacity of 0.625 mole H<sup>+</sup>/m<sup>3</sup> (i.e ¼ neutralising capacity of sea water) was discharged into the neutralising pond between the low tide cycles, then this would neutralise 625 of the 1000 moles flowed over the low weir during this period, thereby leaving only 325 moles H<sup>+</sup> to be discharged into Broughton Creek. The neutralisation of this volume of acidity prior to discharge should increase the pH of the drain water by 1-2 units, relative to the pH of the drain water behind the low weir.

### 13.3 Geochemical modelling of groundwater in actual acid sulfate soil

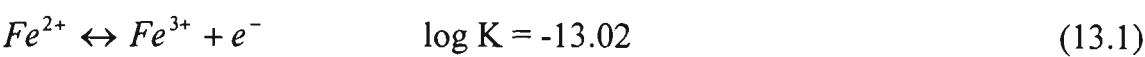
The original premises of this research was that the maintenance of a high water table that excludes oxygen from the pyritic soil would reduce pyrite oxidation and lead to the establishment of better groundwater quality. The installation of the weirs within the drain has been successful in terms of maintaining permanently saturated conditions within the pyritic soil, however groundwater quality remains poor. Given that pyrite oxidation is minimised by the high groundwater table, other sources of acidity must discharge from the soil to the soil water. Two potential sources of acidity, and their contribution to soil solution acidity, were investigated using two geochemical equilibrium models, MINEQL+ (Schecher and McAvoy, 1998) and PHREEQC (Parkhurst, 1995).

#### 13.3.1 *Application of chemical equilibrium concepts*

In order to predict the pH and concentration of dissolved cations in the groundwater that is maintained above the pyritic layer, an understanding of the geochemistry of iron and aluminium is important because the hydrolysis and precipitation/dissolution reactions involving these metals act as strong pH buffers. Although kinetic factors control the attainment of equilibrium between the solid phases and the soil solution, equilibrium concepts can be used to calculate the aqueous speciation of ions, as well as to identify the relationships between the soil solution chemistry and the soil phases present in the soil (Dubrovsky *et al*, 1985). Equilibrium calculations can indicate particular solid phases that may limit the concentration of important aqueous ions. The chemical equilibrium model MINEQL+ (Schecher and McAvoy, 1998) was used to determine the equilibrium geochemistry of the groundwater - solid phase system where the groundwater had been maintained above the pyritic layer for in excess of 12 months.

13.3.2 Iron geochemistry

The aqueous speciation of Fe is a function of pH and the availability of complexing ligands such as SO<sub>4</sub>. In addition, Fe speciation is also a function of the redox potential of water, expressed as pe (-log electron activity). The ratio of Fe<sup>2+</sup> to Fe<sup>3+</sup> can be calculated from the relationship (Drever, 1997):



The interrelations between Fe activity, pH and pe enable the speciation of Fe and various iron solid phases to be illustrated by a pe - pH diagram. The pe - pH diagram shown in Figure 13.2 was calculated using Fe, SO<sub>4</sub> and K activities of 5 x 10<sup>-3</sup>, 1 x 10<sup>-2</sup> and 5 x 10<sup>-4</sup> respectively, which are typical concentrations measured in the groundwater during the post-weir period.

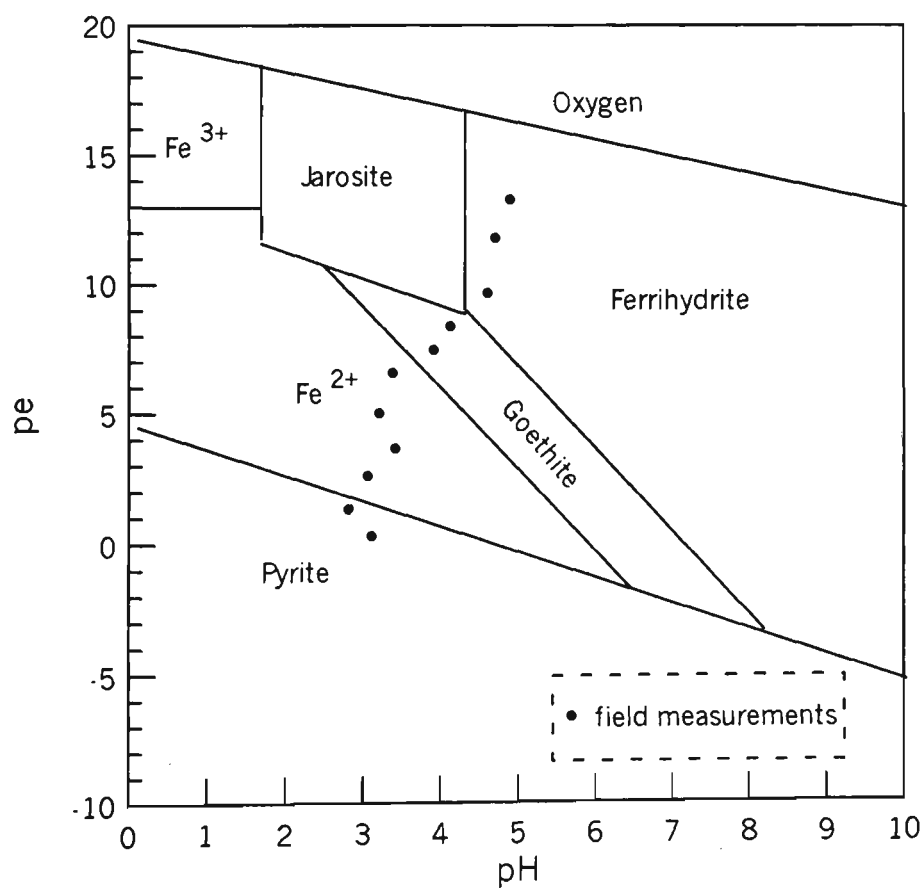


**Figure 13.2** Plot of pe - pH for Fe speciation in groundwater during post-weir period.

The phase diagram shown in Figure 13.23 was developed for a typical suite of minerals commonly found within the Fe-O-H<sub>2</sub>O-S system (van Breeman, 1985). The reactions and equilibrium constants (Drever, 1997) used to develop Figure 13.2 are:

Reaction	log K
$\text{FeS}_2_{\text{pyrite}} + 2\text{H}^+ + 2\text{e}^- = \text{Fe}^{2+} + 2\text{HS}^-$	-18.48
$\text{FeOOH}_{\text{goethite}} + 3\text{H}^+ = \text{Fe}^{3+} + 2\text{H}_2\text{O}$	-1.0
$\text{Fe}(\text{OH})_3_{\text{ferrihydrite}} + 3\text{H}^+ = \text{Fe}^{3+} + 3\text{H}_2\text{O}$	4.89
$\text{KFe}_3(\text{SO}_4)_2(\text{OH})_6_{\text{jarosite}} + 6\text{H}^+ = \text{K}^+ + 3\text{Fe}^{3+} + 2\text{SO}_4^{2-} + 6\text{H}_2\text{O}$	-14.8

The progressive change in the soil pH and pe measured when the groundwater table was 0.8 m below the ground surface during the post-weir period is also shown in Figure 13.2. The data show that with increasing depth in the soil, the soil pH is maintained between 2.9-3.5, indicating that Fe<sup>2+</sup> remains in solution, and is the dominant Fe species present. At higher elevations conditions conducive to the precipitation of ferrihydrite (α-Fe(OH)<sub>3</sub>) occur. The precipitation of ferrihydrite occurs where pe values are in excess of 9, and organic matter and/or lime present in the top soil layers increase soil pH above 4.5,. At pe between 7-10 and pH 4-5, goethite may also precipitate. Rust mottles, presumably goethite, were observed throughout the soil matrix in the top 1 m of the soil profile.

The stability field for jarosite (KFe<sub>3</sub>(SO<sub>4</sub>)<sub>2</sub>(OH)<sub>6</sub>) is also shown in Figure 13.2. The pe - pH calculations show that jarosite has a large stability field for typical K, SO<sub>4</sub> and Fe activities found in the low pH soil above the pyritic layer. Interestingly, plotting the pe - pH data measured in the soil during the post-weir period, shows that precipitation of jarosite is prevented by the low pe of the soil immediately above the pyritic layer. This is at odds with field observations where jarosite has been identified throughout the zone

of low pH soil above the pyritic layer. It is likely that jarosite can only precipitate in or close to soil macropores where higher pe values exist as a result of groundwater draining from these pores and enable oxygen to diffuse from the surface down the macropores. The distribution of jarosite in the soil appears to be closely aligned with structural features in the soil.

### 13.3.3 Saturation indices

The pe-pH phase diagram shown in Figure 13.2 is specific for one set of conditions, in this case Fe, SO<sub>4</sub> and K activities of  $5 \times 10^{-4}$ ,  $1 \times 10^{-3}$  and  $5 \times 10^{-5}$ , respectively. A change in these concentrations will alter the position of the boundaries between the stability fields. As each point plotted on Figure 13.2 represents a water sample with a specific Fe and SO<sub>4</sub> concentration, the proximity to equilibrium of the individual samples must be performed by other methods. This comparison is facilitated by the calculation of saturation indices (SI) from the ion activity products (IAP) and the solubility product ( $K_{sp}$ ) where:

$$SI = \log(IAP/K_{sp}) \quad (13.2)$$

A negative SI indicates undersaturation with respect to the particular mineral, while a positive SI indicates supersaturation or where mineral precipitation may occur. The SI calculated for various Fe and Al minerals likely to occur within the soil profile after pyrite oxidation are shown in Figure 13.3.



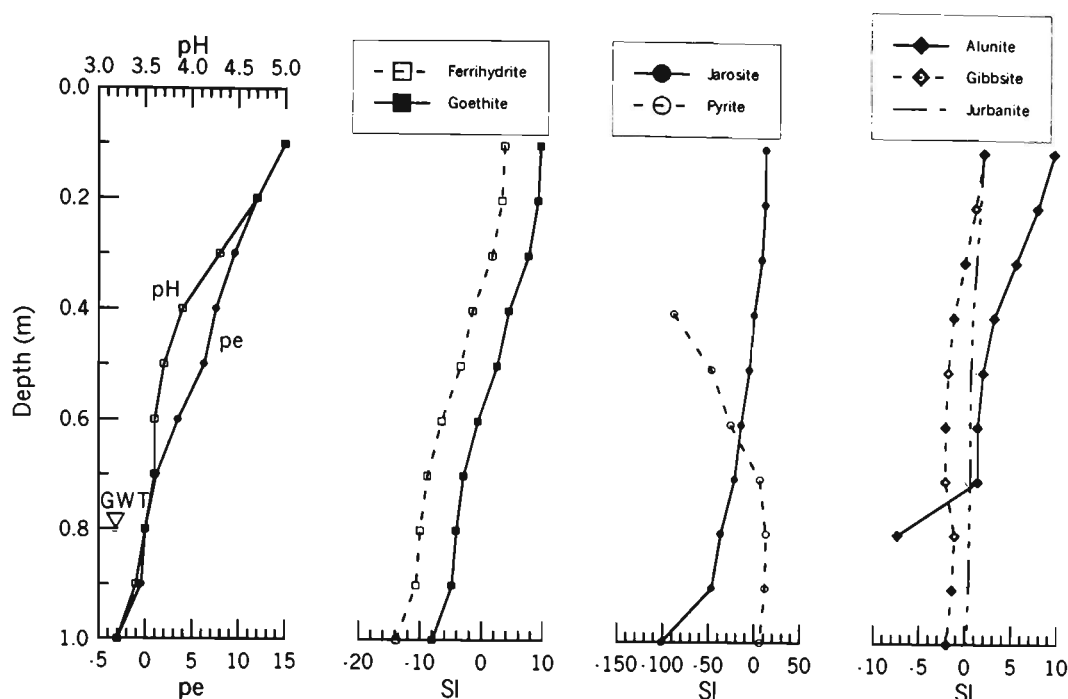


**Figure 13.3** Saturation Indices (SI) for Fe and Al minerals at measured pH-pe for Fe, Al,  $\text{SO}_4$  and K activities of  $5 \times 10^{-3}$ ,  $1 \times 10^{-3}$ ,  $5 \times 10^{-2}$  and  $5 \times 10^{-4}$ , respectively.

Figure 13.3 shows that the necessary conditions for the precipitation of  $\text{Fe}(\text{OH})_3$ ,  $\text{FeOOH}$  and  $\text{KFe}_3(\text{SO}_4)_2(\text{OH})_6$  exist within the upper 0.5 m of the soil profile. As expected from the phase diagram shown in Figure 13.2, goethite precipitates lower in the profile than ferrihydrite. Rust coloured minerals that resemble goethite and ferrihydrite have been observed in the upper 0.5 m of the soil profile at the study site. At lower depths in the soil profile, the SI for ferrihydrite and goethite are negative, indicating that these minerals are under-saturated with respect to the chemical conditions in the soil solution. Under-saturation facilitates the dissolution of these minerals. The dissolution of ferrihydrite and goethite releases  $\text{Fe}^{3+}$  into the soil solution.

Positive SI for jarosite is present in the upper 0.3 m of the soil profile. As previously discussed, jarosite is not observed in this part of the soil profile. Rather, the low pH and high pe conditions necessary for the precipitation of jarosite are present in and adjacent to macropores in the 0.5 m immediately above the pyritic layer. Figure 13.2 shows that in the part of the soil profile where jarosite mottles are observed in the field (i.e., 0.8-1.0 m depth), the SI for jarosite are negative, indicating that dissolution of jarosite is likely

to occur. The dissolution of jarosite provides a source of  $\text{SO}_4$ ,  $\text{Fe}^{3+}$  and  $\text{H}^+$  to the soil solution. Jarosite dissolution buffers the soil pH at approximately 3.7-4.0.

Figure 13.3 also shows that a positive SI exists for pyrite in the lower 0.3 m (i.e., 0.7 - 1.0 m depth) of the soil profile. Although the pyritic layer does not begin until a depth of approximately 1.3 m, the positive SI indicate that the necessary pH and pe conditions for the precipitation of pyrite exist in this part of the soil profile. The ongoing precipitation is likely to be controlled by bacterial catalysts that rely on an available source of organic matter to reduce sulfate to sulfide (Dent, 1986). However, as shown in Chapter 6, the concentration of organic matter within the pyritic layer at the site is likely to be too low to provide an appropriate environment for sulfate reducing bacteria to exist at the field site.

The aqueous chemistry of Al is similar of Fe in as much as that it occurs in the 3+ valance state. However, the solubility of aluminium solid phase minerals is not pe dependent. The concentration of Al in natural waters of near-neutral pH is limited by the solubility of amorphous or crystalline aluminium hydroxide or clay minerals (Dubrovsky *et al.*, 1985). However, van Breeman (1985) suggested that Al concentrations in acidic, high sulfate waters are controlled by the precipitation of basic aluminium sulfates.

The SI values for aluminium solid phases including alunite, gibbsite and jurbanite are shown in Figure 13.3. Based on a review of the literature on acid leachate from pyritic mine spoils, Nordstrom (1982) proposed that alunite ( $\text{KAl}_3(\text{SO}_4)_2(\text{OH})_6$ ) is likely to control the Al solubility in water at pHs between 3.3 and 5.7 containing  $10^{-2}$  M sulfate. Figure 13.3 shows that the SI for alunite is positive for the region above the groundwater table, suggesting that dissolved  $\text{Al}^{3+}$  may be lost from the soil water by precipitating alunite. However, Norstrom (1982) suggested that the precipitation of alunite may be kinetically inhibited and first precipitate as more complex Al- $\text{SO}_4$ -OH minerals such as basaluminite ( $\text{Al}_4(\text{SO}_4)(\text{OH})_{10}$ ). Similarly, jurbanite ( $\text{AlSO}_4\text{OH}\cdot 6\text{H}_2\text{O}$ ) has a positive SI for the whole soil profile. Norstrom (1982) and van Breeman (1985)

suggest that jurbanite is the Al-limiting phase in acid mine water with  $\text{pH} < 3.3$ , although jurbanite has never been directly measured in acid sulfate soils. For the typical groundwater  $\text{Al}^{3+}$ ,  $\text{SO}_4^{2-}$  and  $\text{K}^+$  concentrations of the groundwater that were used to calculate the SI values shown in Figure 13.3, the groundwater is undersaturated with respect to gibbsite. However, jurbanite is close to saturation down the whole soil profile and over-saturated where the soil  $\text{pH} > 3.6$ .

To graphically illustrate the relationship between pH and aluminium solubility, the aluminium concentration in the groundwater, and the lines describing the solution equilibrium with the solid phases of gibbsite and jurbanite, were plotted on a graph of  $\text{Al}^{3+}$  activity versus pH (Figure 13.4), where  $\text{SO}_4^{2-}$  activity was held at  $10^{-2}$ .

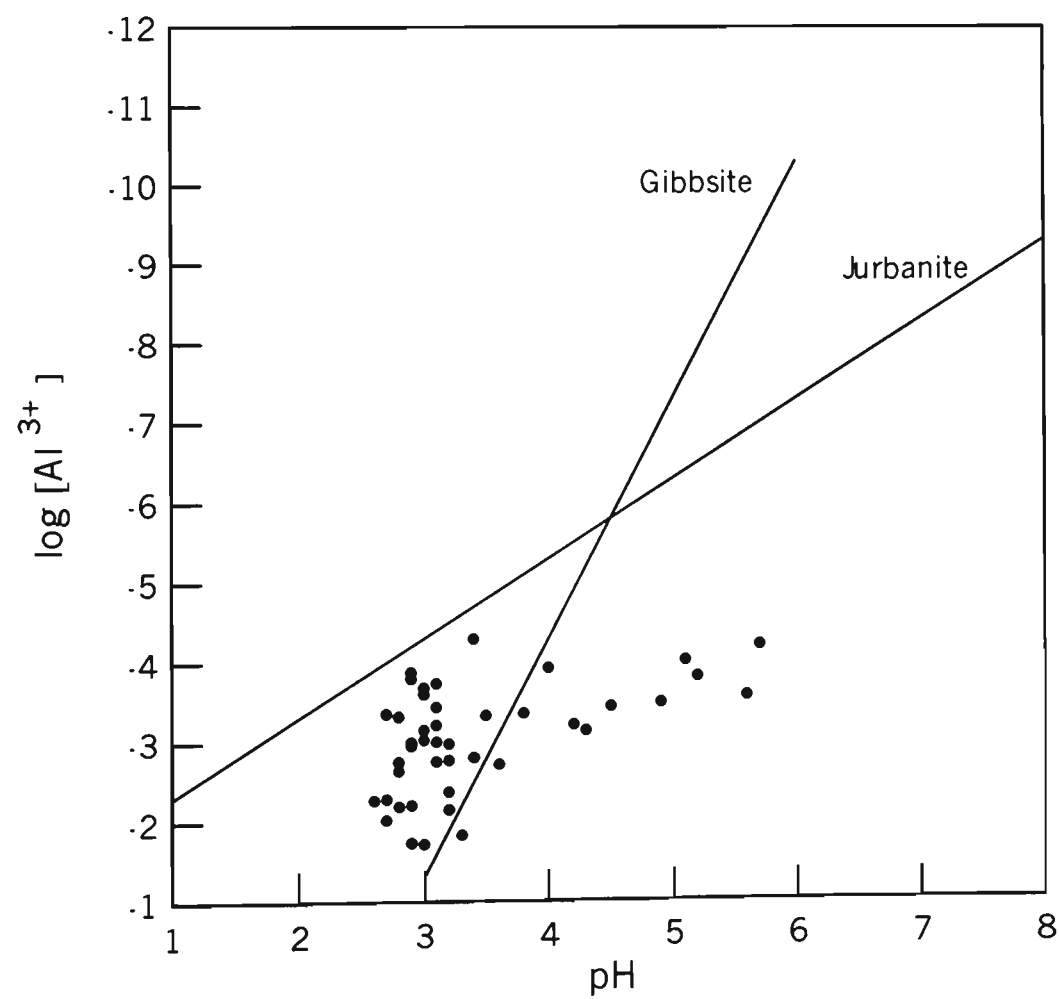


**Figure 13.4**  $\text{Al}^{3+}$  activity versus pH with lines of equilibrium with respect to aluminium solid phases gibbsite and jurbanite.

Between pH 3.3-4 the  $\text{Al}^{3+}$  activity follows the trend of the gibbsite equilibrium line. The higher than predicted  $\text{Al}^{3+}$  activity at pH >4 is likely to be associated with the maintenance of equilibrium conditions with the highly Al-saturated soil colloids, rather than the dissolution of previously precipitated acidic-Al minerals. As the pH falls below 3.3 the data suggests that gibbsite is under-saturated and that  $\text{Al}^{3+}$  is tending towards an equilibrium with jurbanite or some other Al-SO<sub>4</sub>-OH mineral.

Whilst the relationship between the  $\text{Al}^{3+}$  concentration in groundwater and aluminium solid phases can be instructive with respect to understanding the importance of various acid minerals on the equilibrium geochemistry of the groundwater during periods of high water tables when pyrite oxidation is minimised, it is likely that several equilibria occur between aqueous Al and several solid phases. In addition, Dubrovsky *et al.* (1985) suggest that disequilibrium may occur locally due to the inability of precipitation/dissolution reactions to keep up with changes in pH. This may be particularly apparent after pyrite oxidation events generate large volumes of high molarity acid which may enhance the liberation of Al from alumino-silicate clay minerals or from the preferential exchange of  $\text{H}^+$  for  $\text{Al}^{3+}$  from cation exchange sites within the soil profile.

The evaluation of the MINEQL+ simulations, in conjunction with observations of yellow and rust mottles in the soil profile at the field site, indicates that Fe and Al may be precipitating as hydroxysulfate solid phases such as jarosite and jurbanite. The presence of these solid phases has important consequences for the geochemical evolution of the groundwater in soil profiles previously subject to pyrite oxidation. As the concentration of SO<sub>4</sub> and Fe in the groundwater decrease once pyrite oxidation is minimised by permanent saturation, the hydroxysulfate minerals will dissolve, adding Fe, Al and SO<sub>4</sub> to the groundwater. The Fe and Al will then reprecipitate as hydroxides, with the release of  $\text{H}^+$ , causing a decrease in the groundwater pH. During this period, other metals associated with the hydroxysulfate solid phases would also go into solution. Thus acidic, low pH conditions will continue to be produced in the

groundwater until all of the previously precipitated hydroxysulfate minerals are dissolved. Nordstrom (1982) also applied the stability of various minerals in the  $\text{Al}_2\text{O}_3\text{-SO}_3\text{-H}_2\text{O}$  system for interpretation of groundwater quality in previously acidified soils affected by pyrite oxidation. Nordstrom (1982) proposed that under continuing acid infiltration through the unsaturated zone, basic aluminium sulfates will form as a storage sink and source of sulfate. When high intensity rainfall occurs, causing groundwater to rise and a dilution of the acid stored in the unsaturated zone giving a higher soil water pH, there will be a tendency for the basic aluminium sulfates to dissolve and revert back to aluminium hydroxides or hydrated aluminosilicate clays, thereby releasing sulfate into the soil water. The conclusion is that poor water quality is likely to persist until the basic aluminium or iron sulfate minerals dissolve and soluble sulfate, aluminium and iron is leached from the soil.

The prognosis of acidic groundwater prevailing for some time after the maintenance of groundwater management practices that minimise subsequent pyrite oxidation was confirmed by PHREEQC (Parkhurst, 1995) simulations. Two simulation were conducted using PHREEQC to investigate the contribution of the acid saturated cation exchange sites (the CEC simulation) and the combined effect of the acid saturated cation exchange sites and the dissolution of jarosite and alunite (the CEC/mineral simulation) to the maintenance of poor water quality during periods of high groundwater elevation. An additional simulation was conducted to assess the beneficial effect of injecting a lime slurry into the soil solution. The results of these simulations are shown in Appendix E.

### **13.4 Conclusions**

The existing or stored acidity in acid sulfate soil profiles must be recognised during the development of strategies for the management of pyritic soils. Given the development of acidic iron and aluminium minerals in the soil after pyrite oxidation, it is unlikely that

physical groundwater management strategies alone will result in improved groundwater and drain water quality within an acceptable time frame. Addition geochemical management strategies should be used in conjunction with the maintenance of elevated groundwater tables to manage both the existing and potential acidity. Two geochemical management strategies, namely the controlled intrusion of saline water into flood mitigation drains and the injection of calcium carbonate into the acidic soil layers, show considerable potential in being able to minimise the discharge of acid to the environment.

## Chapter 14: Summary and recommendations

### 14.1 Summary

The effectiveness of a groundwater manipulation strategy for the management of acid sulfate soils at the sub-catchment scale was validated by this research. The research included:

- The implementation and assessment of the effectiveness of manipulating groundwater levels by the installation of weirs in flood mitigation drains at a 120 ha sub-catchment located near Berry on the South Coast of NSW. Groundwater and drain water chemistry and hydrological processes were monitored throughout the field trial, including before and after the installation of the weirs. Monitoring data was used to validate improvements in the groundwater regime with respect to the necessary conditions that are required for pyrite oxidation and the change in groundwater and drain water chemistry.
- Groundwater management strategies were tested by the application of an existing acid sulfate soil simulation model (Bronswijk *et al.*, 1992) and by the development and implementation of a improved pyrite oxidation model that simulated the generation of acid over a 3D landscape.
- Laboratory testing of the rate of acid generation in field and laboratory structured pyritic soil. This experiment demonstrated the relationships between magnitude and rate of acid generation from pyrite oxidation with respect to the nature of the soil macroporosity and the distribution of pyrite within the soil.

- The ongoing acidic nature of the groundwater and soil was investigated using two geochemistry simulation model. In addition, potential acid management strategies were investigated using geochemical approaches.

This research has demonstrated that the elevation of the groundwater table can be manipulated by the installation of weirs in flood mitigation drain. Groundwater table elevations measured at the Berry field site, as well as groundwater simulation modeling outcomes, showed that significant improvements can be made in minimising the volume of pyritic soil exposed to oxidising conditions by reducing groundwater drawdown close to the drains.

During the pre-weir period, the elevation of the groundwater table was determined by groundwater drawdown caused by the water level in the drains, the magnitude of evapotranspiration and the volume of rainfall. In periods where a rainfall deficit occurred, groundwater drawdown and evapotranspiration caused the groundwater table to fall into the pyritic soil layer, thereby creating the necessary conditions for pyrite oxidation. Groundwater drawdown caused by the flood mitigation drains was primarily responsible for lowering the groundwater table to approximately the low tide level, however, evapotranspiration was then responsible for lowering the groundwater table below low tide level. The rate and magnitude of pyrite oxidation was demonstrated to be proportional to the length of time of exposure to oxidising conditions and the magnitude of the fall in the groundwater table below the pyritic soil. This was demonstrated both in the field and in tightly controlled laboratory experiments.

During the period where the groundwater table was at its lowest elevation, the drain water level was higher than the surrounding groundwater table, indicating that the hydraulic conductivity of the pyritic soil was too low to enable the recharge of the shallow groundwater aquifer by lateral flow from the drains. The groundwater hydraulic gradient flowed from the drain into the fields, thereby minimising the discharge of pyrite oxidation products into the drain. During the period where pyrite oxidation was occurring, both the groundwater and drain water quality were relatively high due to



internal acid buffering in the soil and buffering from saline water intruding into the drains from Broughton Creek, respectively.

After significant rainfall caused the groundwater table to rise through the zone where pyrite oxidation had occurred during the period of low groundwater table elevation, the pyrite oxidation products become entrained in the groundwater giving rise to extremely acidic groundwater conditions (about pH 2). Heavy rainfall also changed the groundwater hydrology so that groundwater discharged through the seepage faces in the drain, thereby acidifying the water in the drains. The hydraulic gradients measured during the latter part of the pre-weir period (i.e., after heavy rainfall) were relatively large and indicated that the rate of discharge of pyrite oxidation products from the groundwater to the drains was high.

Higher groundwater levels that arose from the installation of weirs minimised the production of 'new' acid from the oxidation of pyrite by oxygen. In addition, maintenance of higher drain water levels gave rise to lower groundwater hydraulic gradients where the groundwater flow was towards a drain. This has the advantage of reducing the rate of acid discharge to the drain. Lower hydraulic gradients may result in less slug like discharges of pyrite oxidation products into waterways during and immediately after flooding events. In this respect, the weirs offer a substantial improvement in the management of both acid generation and transport to the drains (and subsequently Broughton Creek) with respect to the existing flood mitigation drainage system.

The elevated groundwater levels did not improve long-term groundwater quality. The nature of the 'stored' acid in the soil profile previously caused by pyrite oxidation kept the groundwater pH maintained at 3.5-4.0. In addition, the concentration of dissolved aluminium and iron remained high in accordance with the dissolution of acidic minerals and equilibrium reaction with the aluminium saturated cation exchange sites. The maintenance of poor groundwater quality was simulated by employing geo-chemical modeling techniques using site specific input data. These simulations demonstrated the

relative contribution of the acidic minerals and the Al saturated CEC with respect to the maintenance of acidic groundwater. This modeling showed that the maintenance of a high groundwater table in soils that contain acidic minerals caused by previous pyrite oxidation will lead to the dissolution of these minerals, thereby maintaining acidic groundwater condition with high concentrations of Al and Fe.

The development of management solution with respect to the 'stored' component of acidity that is present on soil cation exchange sites and acid minerals that control the concentration of dissolved hydrogen, aluminium and iron in the soil water is required if the implementation of weirs is to be ultimately successful. Alternatively, systems that implicitly acknowledge the presence of low pH/high aluminium concentration in the groundwater are required. Re-construction of drainage schemes in low lying coastal floodplains that remove excess surface water but do not remove the poor quality groundwater may prove to be more successful than the retro-fitting of existing drains with weirs and better floodgates that aim to reduce the flux of acid to adjacent waterways. However, the implementation of drainage re-construction at a catchment scale will be expensive. As demonstrated in this research, combinations of groundwater manipulation techniques such as installing weirs in flood mitigation drain, in conjunction with acid buffering techniques such as controlled saline intrusion through modified floodgates to buffer acidic drain water may offer further water quality improvements relative to the existing over-drained state.

The substantial advantages of the application of coupled groundwater - pyrite oxidation simulation models was also demonstrated in this research. In the first instance, the Simulation Model for Acid Sulfate Soils (SMASS) developed by Bronswijk and Groenenberg (1992) was used to simulate the magnitude of pyrite oxidation at two distances from the drain during a period of substantial groundwater change in the pre-weir period. Although SMASS was demonstrated to accurately simulate the magnitude of pyrite oxidation that occurred during the period where the groundwater table fell into the pyritic layer, it was also shown that it was difficult to use SMASS to evaluate drain management strategies in a three dimensional landscape where the influence of groundwater drawdown induced by large drains and the effect of evapotranspiration on

the groundwater table elevation is not uniform. In order to overcome this limitation of SMASS, an improved theoretical approach was developed and applied in conjunction with a commercially available three dimensional groundwater flow model FEMWATER (Lin *et al.*, 1997) to simulate the magnitude and distribution of pyrite oxidation. The new 3D approach was called ASS3D.

The primary advantage of ASS3D lies in its ability to predict the magnitude and distribution of pyrite oxidation for a given drain and surface geometry, climatic regime and soil material properties. As demonstrated in Chapter 11, this facilitates testing of appropriate drain water levels so that optimal weir elevation can be implemented without resorting to expensive and time consuming field trials. In addition, the implications of various groundwater management practices with respect to the magnitude and distribution of pyrite oxidation can be easily appreciated by using the video animation capacity of the GMS software. This capacity enables the importance groundwater management strategies to be readily communicated to other researchers, land managers and farmers.

## **14.2 Recommendations for further research**

### ***14.2.1 Field investigations***

This research has demonstrated that the elevation of the groundwater table above the pyritic soil layer will not give rise to substantially improved groundwater or drain water quality in the short term due to: the dissolution of acidic minerals in the soil; the acid saturated cation exchange capacity of the soil; and, the large store of soluble sulfuric acid generated from previous pyrite oxidation in the soil profile. Although elevation of the groundwater table minimises the potential for the generation of new acid from the oxidation of pyrite, techniques to minimise the effect of the acid stored in the soil need to be developed for use in conjunction with better groundwater management strategies in order to reduce the impact of acidity on a short time scale. Field trials of geo-

chemical techniques that neutralise acidity or mitigate against its impact on the environment should be investigated as a matter of urgency. As suggested in this research, geo-chemical techniques worthy of further investigation include:

- Controlled intrusion of saline water from estuarine waterways into drains through the installation of a modified floodgate. This practice might best be carried out in conjunction with the operation of weirs in order to better manipulate the volume of acidic drain water requiring partial neutralisation by the saline water. Care must be taken to ensure that saline water does not overtop the drains to cause surface salinity problems that may negatively impact on crop growth. Similarly, the lateral intrusion of salt from the drain into the soil should be investigated to assess the potential for long term salinisation of soil used for agronomic purposes. If these salinity issues can be shown not to adversely affect soil quality, then the demonstration of improved floodgate design and improved drain water quality may facilitate the adoption of this relatively cost effective acid management strategy.
- Creation of sub-surface barriers by the method of ‘deep chemical mixing’ has been conducted in the past by geotechnical engineers (Miura *et al.*, 1986; Bergado *et al.*, 1996). Detailed methodology and concepts of sub-surface chemical mixing have been described by Indraratna (1983). In Australia, the effectiveness of lime stabilisation has been demonstrated recently by Indraratna (1996). Given the nature of pyrite oxidation and the subsequent distribution of acidic oxidation products, it may be worthwhile exploring the potential use of deep chemical mixing techniques to mitigate the adverse consequences of acid generation by the creation of an active lime barrier above the pyritic layer. Mathematical models incorporating hydraulic fracturing of clay, lime injection pressure and the rate of lateral diffusion of lime can be found in the geotechnical engineering literature (Hausmann, 1990). Research involving “barrier technologies” for the treatment of acidic leachate from pyritic rock spoil be carried out by the Australian Nuclear Science and Technology Organisation and the University of NSW may also be applicable.

In addition to field trials of geo-chemical acid management strategies, improvements in the design and application of weirs should also be investigated. This project employed three weirs each at a different elevation relative to the pyritic soil layer. Although the effectiveness of the weirs was established in terms of maintaining a higher groundwater table, little control of the water level was maintained behind the weir. In order to improve the control of both the groundwater table and the drain water level, a design of adjustable weirs should be completed (NB: preliminary work is currently being undertaken by the University of Wollongong and tested to assess its effectiveness).

#### *14.2.2 Laboratory investigations*

Laboratory investigations that improve the understanding of the processes that contribute to the rate and magnitude of acid generation require additional research. Two areas of investigation have been identified through this research. These include:

- Understanding of the linkages between the distribution of pyrite crystals/framboids within the pyritic soil, the size, continuity and distribution of structural features within the soil, the transport of oxygen in these structural features and the generation and transport of pyrite oxidation products. The preliminary laboratory work presented in this thesis indicated that the rate of acid generation is influenced by the structure and distribution of pyrite with respect to that structure. However, more tightly controlled experiments that quantify these properties in a more rigorous manner may provide valuable information in regard to the acid generation process in pyritic soils.
- Fundamental research with respect to the formation and dissolution of acidic iron and aluminium sulfate minerals. The maintenance of poor groundwater quality after the elevation of the groundwater table is related to the type, concentration and dissolution properties of these acidic minerals. In order to develop management

strategies to control acidity in coastal floodplains, better understanding of the geochemistry of these acidic minerals is required.

#### *14.2.3 Numerical modelling*

A number of improvements in the manner in which pyrite oxidation or acid generation is modelled have been identified in this research. These include:

- The implementation of a chemical transport component to the pyrite oxidation models so that the pyrite oxidation products can then undergo re-distribution and transport once the groundwater rises through the oxidised layers;
- Coupling ASS3D with an existing geochemical model to solve the complex geochemistry between the groundwater and the soil, the groundwater pH, and to compute the precipitation/dissolution of sparingly soluble oxidation products such as jarosite. Modelling of the steady state groundwater quality may be achieved if such a geochemical model was coupled with ASS3D;
- Incorporation of a probabilistic assessment procedure where known distributions of various parameters (e.g., pyrite crystal size, pyrite concentration) can be entered into the program and run many times to assess the relative importance of various input parameters (i.e. sensitivity analysis);
- Further study of the most appropriate type of finite elements and slope functions that are most compatible with unsaturated and saturated flow through clay and the transport of acidic contaminants.

- Incorporation of a function describing the pyrite spatial distribution within the soil macropore-matrix continuum. If, as Bush and Sullivan (1999) suggest, most pyrite is associated within or close to macropores, then the apparent under-estimation of the amount of pyrite oxidised by ASS3D and other pyrite oxidation models may be overcome;
- Development of a soil chemical and physical property database from well studied sites so that realistic input parameters can be used to initialise the model for assessment of sites that may differ from the Berry study site.

## References

ACLEP (1995) Draft Australian Soil and Land Survey Handbook Vol 5. Soil physical measurement and interpretation for land evaluation. (Eds. K. Coughlan, N. McKenzie, W. McDonald and H. Cresswell). CSIRO Canberra.

Ahern, C., McElnea, A., Baker, D. (1998) Peroxide Oxidation Combined Acidity and Sulfate (POCAS). In 'Acid Sulfate Soil Manual'. (Eds. Y Stone, C Ahern, B Blunden) NSW Government: Sydney.

ANZECC (1992) Australian Water Quality Guidelines for Fresh and Marine Waters. Australian and New Zealand Environment Conservation Council. Canberra.

Australian National Tide Tables (1997) Hydrographic Service, Royal Australian Navy. Canberra.

Australian Rainfall and Runoff (1998) A Guide to Flood Estimation. The Institution of Engineers, Australia. Barton, ACT.

Bayley (1975) Shoalhaven. History of the Shire of the Shoalhaven (2<sup>nd</sup> Edition). Soath Coast Printers. Port Kembla. Australia.

Belmans, C., Wesseling, J.G., and Feddes, R.A. (1983) Simulation model of the water balance of a cropped soil: SWATRE. *Journal of Hydrology*, **63**, 271-286.



Bergado, D., Anderson, L. and Miura, N. (1996) Soft ground improvement in lowland environments. ASCE Press, pp 427.

Blunden, B. and Naylor, S. (1995) Environmental Guidelines: Assessing and Managing Acid Sulphate Soils. Environment Protection Authority Chatswood.

Blunden B, Indraratna B, and Nethery A (1997) Effect of groundwater table on acid sulfate soil remediation. In 'Geoenvironment 97.' (Eds A Bouazza, I Kodikara B Parker) Balkema, Rotterdam. pp. 549-554.

Blunden, B., Indraratna, B. and Morrison, J. (1998). Problems of acid sulphate soils and their remediation by watertable management. 2nd International Conference on Environmental Management, University of Wollongong, Australia.

Blunden, B. and Indraratna, B. (2000) Evaluation of surface and groundwater management strategies for drained sulfidic soil using numerical simulation models. *Australian Journal of Soil Research*, 38, in press

Blunden, B. and Indraratna, B. (2000) Pyrite oxidation model for assessing groundwater management strategies in acid sulfate soils. *Journal of Geotechnical and Geoenvironmental Research* (accepted).

Bouwer, H. (1974) Developing drainage design criteria. In 'Drainage for Agriculture'. (Ed. van Schilfgaarde) American Society of Agronomy, Madison. USA.

Brinkman, R. (1982) Directions of further research on acid sulfate soils. In 'Proceedings of the Bangkok Symposium on Acid Sulfate Soils'. (Eds. Dost and van Breeman). IRRI Publication 31, Wageningen, The Netherlands.

Bronswijk, J. and Groenenberg, J. (1992) A simulation model for acid sulphate soils: I basic principles. In 'Selected papers of the Ho Chi Minh City Symposium on Acid Sulphate Soils.' (Eds Dent and van Mensvoort). ILRI Publication 53. Wageningen, The Netherlands.

Bronswijk, J., Nugroho, K., Aribawa, J., Groenberg, J. and Ritsema, C. (1993) Modeling of oxygen transport and pyrite oxidation in acid sulfate soils. *Journal of Environmental Quality*, **22**(2), 544-554.

Bronswijk J, Groenenberg J, Ritsema C, van Wijk A, Nugroho K (1995) Elavuation of water management strategies using a simulation model: A case study in Indonesia. *Agricultural Water Management*, **27**, 125-142.

Buman, M. (1995) Molluscs and Holocene evolution. Unpublished B.Sc (Hons) thesis. Department of Geosciences. University of Wollongong.

Bush, R. and Sullivan, L. (1996) Some things standard soil analyses don't reveal about potential acid sulphate soils oxidation. Proceedings 2nd National Conference on Acid Sulphate Soils. (Eds. Smith and Smith). pp. 72-75. Coffs Harbour.

Bush, R. and Sullivan, L. (1999) Pyrite morphology in three Australian Holocene sediments. *Australian Journal of Soil Research*, **37**, 637-653.

Brady, N. (1984) The Nature and Properties of Soils. Collier-Macmillan. New York.

Brutsaert, W. (1982) Evaporation into the Atmosphere. Theory, history and applications. Reidel Publishing Company, Dordrecht, The Netherlands.

Chapman, S. (1994) Development of a strategy for the management of acid sulphate soils in Berry, NSW. B.E thesis. University of Wollongong.

Christensen, T., Parker, B. and Refsgaard, J. (1986) A model for the unsaturated zone; oxygen transport and consumption. Danish Hydraulic Institute. Horsholm. Denmark.

Davis, G. and Ritchie, A. (1986) A model of oxidation in pyritic mine wastes: part 1 equations and approximate solution. *Applied Mathematical Modelling*, **10**, 314-322.

Davis, G., Doherty, G. and Ritchie, A. (1986) A model of oxidation in pyritic mine wastes: part 2 comparisons of numerical and approximate solutions. *Applied Mathematical Modelling*, **10**, 323-329.

Dent, D. and Bowman, G. (1996) Quick, quantitative assessment of the acid sulfate hazard. Proceedings 2nd National Conference on Acid Sulphate Soils. (Eds. Smith and Smith). pp. 96-98. Coffs Harbour.

Dent, D. (1986) Acid Sulphate Soils: a baseline for research and development. IRRI Publication No. 39. Wageningen. The Netherlands.

Downey, J. (1997) Shoalhaven City Council Senior Engineer. Personal Communication.

Drever, J. (1997) The Geochemistry of Natural Waters: surface and groundwater environments. Prentice Hall, Upper Saddle River, NJ, USA.

Dubrovsky, N., Cherry, J., Readon, E. and Vivyurka, A. (1985) Geochemical evolution of inactive pyritic tailings in the Elliot Lake uranium district. *Canadian Geotechnical Journal*, **22**, 110-128.

Easton, A., Clesceri, L. and Greenberg, A. (Eds) (1995) *Standard Methods for the Examination of Water and Wastewater*. American Public Health Association, Washington DC, USA.

Elberling, B. and Nicholson, R. (1996) Field determination of sulphide oxidation rates in mine tailings. *Water Resources Research*, **32**(6), 1773-1784.

Elberling, B., Nicholson, R. and Scharer, J. (1994) A combined kinetic and diffusion model for pyrite oxidation in tailings: a change in controls with time. *Journal of Hydrology*, **157**, 47-60.

Elberling, B., Nicholson, R., Readon, E. and Tibble, P. (1994) Evaluation of sulphide oxidation rates: a laboratory study comparing oxygen fluxes and rates of oxidation product release. *Canadian Geotechnical Journal*, **31**, 375-383.

Evangelou, V. (1995) *Pyrite Oxidation and its Control*. CRC Press. New York. USA.

Fredlund, D., Xing, A., and Huang, S. (1994) Predicting the permeability function for unsaturated soils using the soil-water characteristic curve. *Canadian Geotechnical Journal*, **31**, 533-546.

Ferguson, A. and Eyre, B. (1995) Local and regional impacts of acid runoff from acid sulfate soils environments in the lower Richmond River catchment. Centre for Coastal Management, Southern Cross University, Lismore.

Fanning, D. (1993) Salinity problems in acid sulfate coastal soils. In 'Towards the Rational Use of High Salinity Tolerant Plants'. (Eds., Lieth, H. and Masoom, A). Kluwer Academic Publishers. The Netherlands.

Hausmann, M. (1990) Engineering Principles of Ground Modification. McGraw-Hill. pp 632.

Hicks, W., Bowman, G. and Fitzpatrick. (1999) East Trinity Acid Sulfate Soils Part 1: Environmental Hazards. CSIRO Land and Water Technical Report 14/99. Canberra.

Hodgson, A. and MacLeod, D. (1989) Use of oxygen flux density to estimate critical air-filled porosity of a Vertisol. *Soil Science Journal of America*, **53**(2), 335-361.

Indraratna, B. (1983) Grout properties and methods of grouting under dam foundations. Unpublished MSc thesis, University of London.

Indraratna, B. (1996) Utilization of lime, slag and fly ash for improving colluvial clay soils in NSW. *International Journal of Geotechnical and Geological Engineering*, **14**, 169-191.

Indraratna, B. and Blunden, B. (1997) Remediation of acid sulphate soils by management of groundwater table. In 'Proceedings Second International Green Symposium on Geotechnics and the Environment'. (Ed. Sarsby), pp. 516-524 Thomas Telford Publishers, Krakow, Poland.

Indraratna, B. and Blunden, B. (1999) Nature and properties of acid sulphate soils in drained coastal lowlands in New South Wales. *Australian Geomechanics Journal*, **34**(1), 61-78.

Indraratna, B., Sullivan, J. and Nethery, A (1995) Effect of groundwater table on the formation of acid sulphate soils. *Minewater and the Environment*. **14**, 71-84.

Jaynes, D.B., Pionke, H.B and Rogowski, A.S. (1984b) Acid mine drainage from reclaimed coal strip mines 2. Simulation results of model. *Water Resources Research*, **20**(2), 243-250.

Jaynes, D.B., Rogowski, A.S., and Pionke, H.B. (1984) Acid mine drainage from reclaimed coal strip mines 1. Model description. *Water Resources Research*, **20**(2), 233-242.

Lawrie, R. and Murphy, A. (1996) Irrigated cropping on acid sulfate soils of NSW South Coast. In 'Proceedings 2nd National Conference on Acid Sulfate Soils.' (Eds RJ Smith, HJ Smith) 5-6 September, Coffs Harbour, NSW.

Leadbeater, D. (1993) The acid test: basic concerns of the fishing industry about coastal floodplain management in NSW. In 'Proceedings National Conference on Acid Sulfate Soils'. (Ed. R. Bush). pp 62-70. Coolangatta.

Leong, E. and Rahardjo, H. (1997) Review of soil-water characteristic curve equations. *Journal of Geotechnical and Geoenvironmental Research*, **123**, 1106-1117.

Lin, C and Melville, M. (1993) Controls on soils acidification by fluvial sedimentation in an estuarine floodplain, eastern Australia. *Sedimentary Geology*, **85**, 1-13.

Lin, C. Melville, M. White, I and Wilson, B. (1995) Human and natural controls on the accumulation, acidification and drainage of pyritic sediments: contrasts between the Pearl River delta, China and coastal NSW. *Australian Geographical Studies*, **33**, 77-88.

Lin, H., Richards, D., Talbot, C, Yeh, G., Cheng, J., Cheng, H. and Jones, N. (1997) FEMWATER: A three dimensional finite element computer model for simulating

density dependent flow and transport in variably saturated media. Technical Report CHL-97-12 US Army.

McKibben, M. and Barnes, H. (1986) Oxidation of pyrite in low temperature acidic solutions: rate laws and surface textures. *Geochimica Cosmochimica Acta.*, **50**, 1509-1520.

Miura, N., Koga, Y. and Nishida, K. (1986) Application of deep mixing method with lime for Ariake clay ground. *Journal of Soil Mechanics and Foundation Engineering*, **34**, 5-11.

Moses, C., Nordstrom, D., Herman, J and Mills, A. (1987) Aqueous pyrite oxidation by dissolved oxygen and by ferric iron. *Geochimica Cosmochimica Acta.*, **51**, 1561-1571.

Moses, C. and Herman, J. (1991) Pyrite oxidation at circumneutral pH. *Geochimica Cosmochimica Acta.*, **55**, 1509-1520.

Mualem, Y. (1976) A new model for predicting the hydraulic conductivity of unsaturated porous media. *Water Resources Research*, **12**, 593-622.

Mulvey, P. (1993) Pollution, prevention and management of sulfuric clays and sands. In 'Proceedings National Conference on Acid Sulfate Soils'. (Ed. R. Bush). 24-25 June 1993 Coolangatta.

Naylor, S., Chapman, G., Atkinson, G., Murphy, C., Tulau, M., Flewin, T., Milford, H. and Moran, D. (1995) Guidelines for the use of acid sulphate soils risk maps. Soil Conservation Service. Sydney.

- Neal, P. (1996) Acid sulfate soils - one dairy farmers experience. Proceedings 2nd National Conference on Acid Sulphate Soils. (Eds. Smith and Smith). pp. 172-174. Coffs Harbour.
- Nicholson, R., Gillham, R., Cherry, J., and Readon, E. (1989) Reduction of acid generation in mine tailings through the use of moisture-retaining cover layers as oxygen barriers. *Canadian Geotechnical Journal*, **26**, 1-8.
- Nordstrom, D. (1982) The effect of sulfate on aluminium concentrations in natural waters: some stability relations in the system  $\text{Al}_2\text{O}_3\text{-SO}_3\text{-H}_2\text{O}$  at 298 K. *Geochimica et Cosmochimica Acta*, **46**, 681-692.
- Nriagu, J. (1978) Dissolved silica in pore waters of Lake Ontario, Eire and Superior sediments. *Limnology and Oceanography*, **23**, 53-67.
- Nynguyen, T. and Wilander, A. (1995) Chemical conditions in acidic waters in the Plain of Reeds, Vietnam. *Water Resources*, **29**, 1401-1408.
- Parkhurst, D. (1995) PHREEQC - A computer program for speciation, reaction-path, advective transport, and inverse geochemical calculations. US Geological Survey. Water Resources Investigations Report 95-4227. Lakewood, Colorado, USA.
- Pease, M. (1994) Acid sulfate soils and acid drainage Lower Shoalhaven Floodplain, NSW. Unpublished Msc(Hons) thesis. University of Wollongong.
- Pease, M., Nethery, A. and Young, A. (1997) Acid sulfate soil and acid drainage, Lower Shoalhaven floodplain, New South Wales. *Wetlands (Australia)* **16**, 56-71.



Pons, L. (1973) Outline of genesis, classification and improvement of acid sulfate soils. In 'Acid Sulfate Soils: Proceedings of the International Symposium' 13-20 August. IRRI Publication 18 Wageningen, The Netherlands.

Pradhan, N. (1999) Determination of sulfate in acid sulfate waters by Inductively Coupled Plasma Atomic Emission Spectrometry (ICP-AES). Analytical Chemistry Information Sheet No. 99/003. NSW Environment Protection Authority. Chatswood.

Rayment, G. and Higginson, F. (1992) Australian Laboratory Handbook of Soil and Water Chemical Methods. Inkata Press. Melbourne.

Read, R. (1974) Broad scale soil survey of eastern flats, Nowra. BCRI, Department of Agriculture, Rydlemere, NSW.

Read, M. (1996) Tuckean Swamp economic study. Proceedings 2nd National Conference on Acid Sulphate Soils. (Eds. Smith and Smith). pp. 235-239. Coffs Harbour.

Refsgaard, J., Christensen, T., and Ammentorp, H. (1991). A model for oxygen transport and consumption in the unsaturated zone. *Journal of Hydrology*, **129**, 349-369.

Ritsema, H. (1994) Drainage Principles and Applications. ILRI Publication 16. Wageningen, The Netherlands.

Ritsema, C., Groenenberg, J. and Bisdom, E. (1992) The transformation of potential into actual acid sulphate soils studied in column experiments. *Geoderma*, **55**, 259-271.

Robertson, G. and Creighton, G. (1996) Draining land in acid sulfate soil areas. Proceedings 2nd National Conference on Acid Sulphate Soils. (Eds. Smith and Smith). pp. 135-136. Coffs Harbour.

Roy, P., Thom, B. and Wright, L. (1980) Holocene sequences on an embayed high-energy coast: an evolutionary model. *Sedimentary Geology*, **26**, 1-19.

Roy, P. (1984) New South Wales estuaries: their origin and evolution. In '*Coastal Geomorphology in Australia*.' (Ed. Thom). Academic Press Australia. Sydney.

Sasaki, K. (1994) Effect of grinding on rate of oxidation of pyrite in acid solutions. *Geochimica Cosmochimica Acta*. **58**, 4649-4655.

Sammut, J., Melville, M., Callinan, R. and Fraser, G. (1995) Estuarine acidification: impacts on aquatic biota of draining acid sulfate soils. *Australian Geographical Studies*, **33**, 89-100.

Sammut, J. White, I and Melville, M. (1996) Acidification of an estuarine tributary in eastern Australia due to drainage of acid sulphate soils. *Marine and Freshwater Research*. **47**, 669-84.

Scharer, J., Nicholson, R., Halbert, B. and Snodgrass, W. (1992) A computer program to assess acid generation in pyritic tailings. In 'Environmental Geochemistry of Sulfide Oxidation' (Eds: Alpers and Blowes). pp23-28. American Chemical Society. Washington, D.C.

Schecher, W. and McAvoy, D. (1998) MINEQL+ Chemical equilibrium modelling system. Version 4 for Windows. Environmental Research Software, Hallowell, ME, USA.

Schwertmann, U. and Fitzpatrick, R. (1992) Iron minerals in surface environments. In 'Biominalisation Processes of Iron and Manganese: Modern and Ancient Environments'. (Eds Skinner, H. and Fitzpatrick, R.). Catena Supplement 21. Germany.

Smith, R. and Yerbury, R. (1996) Seven Oaks ASS management demonstration sites. Proceedings 2nd National Conference on Acid Sulphate Soils. (Eds. Smith and Smith). pp. 170-172. Coffs Harbour.

Stone, Y., Ahern, C. and Blunden, B. (1998) NSW Acid Sulfate Soil Manual. NSW Government. Sydney.

Troeh, F., Jabro, J. and Kirkham, D. (1982) Gaseous diffusion equations for porous materials. *Geoderma*, **27**, 239-253.

van Breemen, N. (1973) Soil forming processes in acid sulphate soils. In 'Acid Sulphate Soils: Proceeding of the International Symposium on Acid Sulphate'. (Ed. H. Dost) pp 66-129. ILRI, Wageningen, The Netherlands.

van Breeman, N. (1985) Redox processes of iron and sulfur involved in the formation of acid sulfate soils. In 'Iron in Soils and Clay Minerals'. (Eds, Stucki, J., Goodman, B. and Schwertmann, U.) D. Reidel Publishing Company, Boston, USA. pp 825-841.

van Breeman, N. (1992) Environmental aspects of acid sulfate soils. In 'Selected Papers of the Ho Chi Minh City Symposium on Acid Sulphate Soils.' (Eds Dent and van Mensvoort). pp391-402. ILRI Publication 53. Wageningen.

van den Bosch H, Ho Long Phi, Michaelsen J, Nugroho K (1998) Evaluation of water management strategies for sustainable land use of acid sulphate soil in coastal lowlands

in the tropic. Report No. 157. Winand Staring Centre for Integrated Land, Soil and Water Research. Wageningen. The Netherlands.

van Genuchten, M. (1980) A closed form equation for predicting the hydraulic conductivity of unsaturated soils. *Soil Science Society America Journal*, **44**, 892-898.

van Genuchten, M. Th., Leij, F.J. and Yates, S.R. (1991) The RETC code for qualifying the hydraulic functions of unsaturated soils. U.S. Environmental Protection Agency. Washington, D.C.

Wada, H. and Seisuwani, B. (1988) The process of pyrite formation in mangrove soils. In 'Selected papers of the Dakar symposium on acid sulfate soils'. (Ed. H. Dost). pp 24-37. ILRI Publication 44. Wageningen, The Netherlands.

Walker, P. (1972) Seasonal and stratigraphic controls in coastal floodplain soils. *Australian Journal of Soil Research*, **10**, 127-142.

White, I. and Melville, M. (1993) Treatment and Containment of Acid Sulfate Soils. Technical Report 53, Centre for Environmental Mechanics, CSIRO, Canberra.

White, I., Wilson, B., Melville, M., Sammut, J. and Lin, C. (1996) Hydrology and drainage of acid sulfate soils. Proceedings 2nd National Conference on Acid Sulphate Soils. (Eds. Smith and Smith). pp. 103-108. Coffs Harbour.

White, I. Melville, M., Sammut, J. and Wilson, B. (1997) Reducing acidic discharges from coastal wetlands in eastern Australia. *Wetlands Ecology and Management*, **5**, 55-72.

Willett, I. And Walker, P. (1982) Soil morphology and distribution of iron and sulfur fractions in a coastal plain toposequence. *Australian Journal of Soil Research*, **20**, 283-294.

Willett, I., Crockford, R., and Milnes, A. (1992) Transformation of iron, manganese and aluminium during oxidation of a sulfidic material from an acid sulfate soil. In 'Biomineralisation Processes of Iron and Manganese - Modern and Ancient Environments' (Eds. Skinner, H. and Fitzpatrick, R.) pp 287-301. Germany, Catena Verlag.

Wilson, B. (1995) Soil and hydrological relations to drainage from sugarcane on acid sulfate soils. Unpublished PhD thesis, University of New South Wales, Sydney.

Wilson, B., White, I. and Melville, M. (1999) Floodplain hydrology, acid discharge and water quality change associated with drained acid sulfate soil. *Marine and Freshwater Research* **50**, 149-57.

Wunderly, M.D., Blowes, D.W., Frind, E.O., and Ptacek, C.J. (1996) Sulfide mineral oxidation and subsequent reactive transport of oxidation products in mine tailings impoundments: A numerical model. *Water Resources Research*, **32**(10), 3173-3187.

Young, R., Bryant, E., Price, D., Wirth, L. and Pease, M. (1993) Theoretical constraints and chronological evidence of Holocene coastal development in central and southern New South Wales, Australia. *Geomorphology*, **7**, 317-329.

**Appendix A: Climatic variables**

**A.1 Temperature**

The daily maximum, minimum and average temperatures are shown in Figure A.1(a.b).

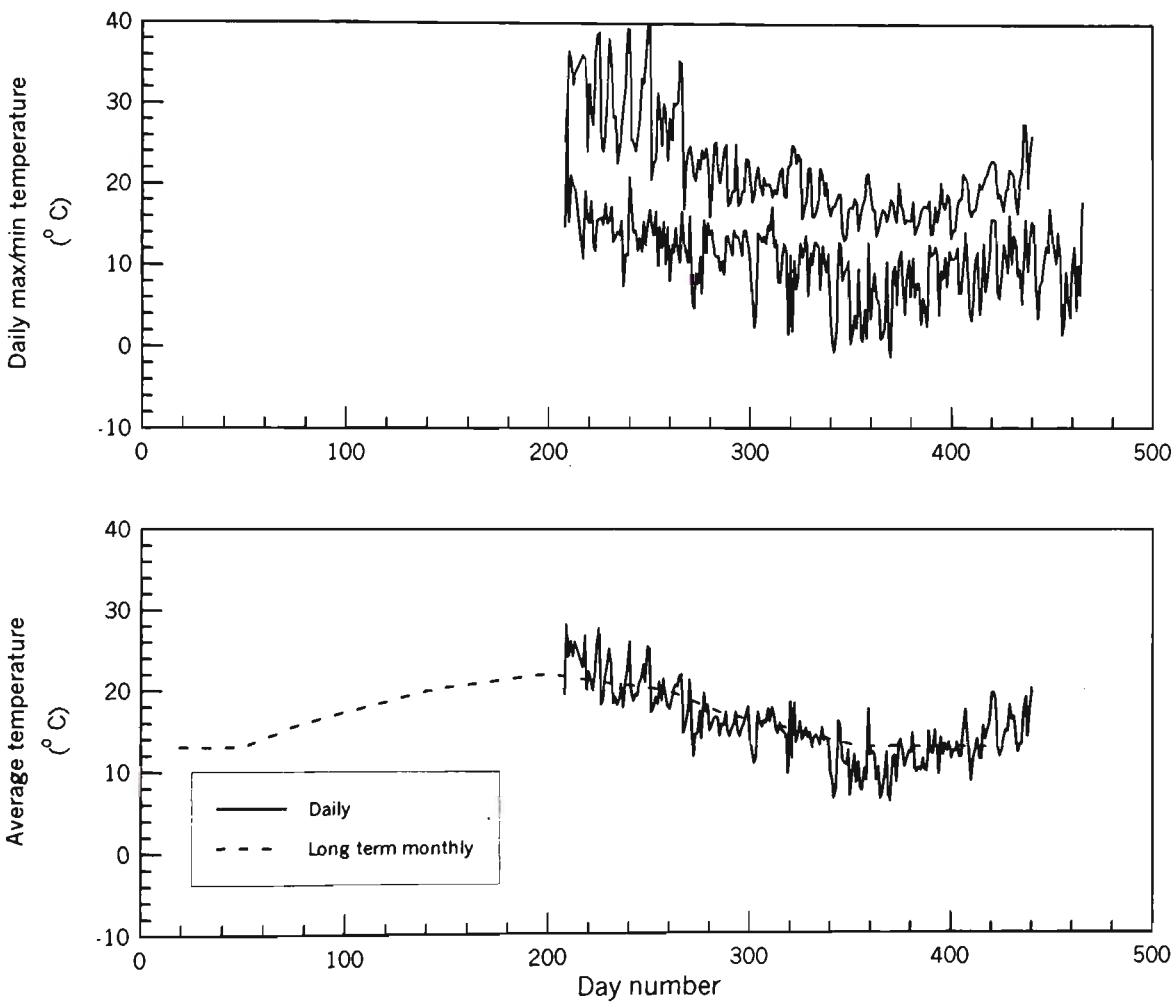


**Figure A.1a** Pre-weir temperature record.

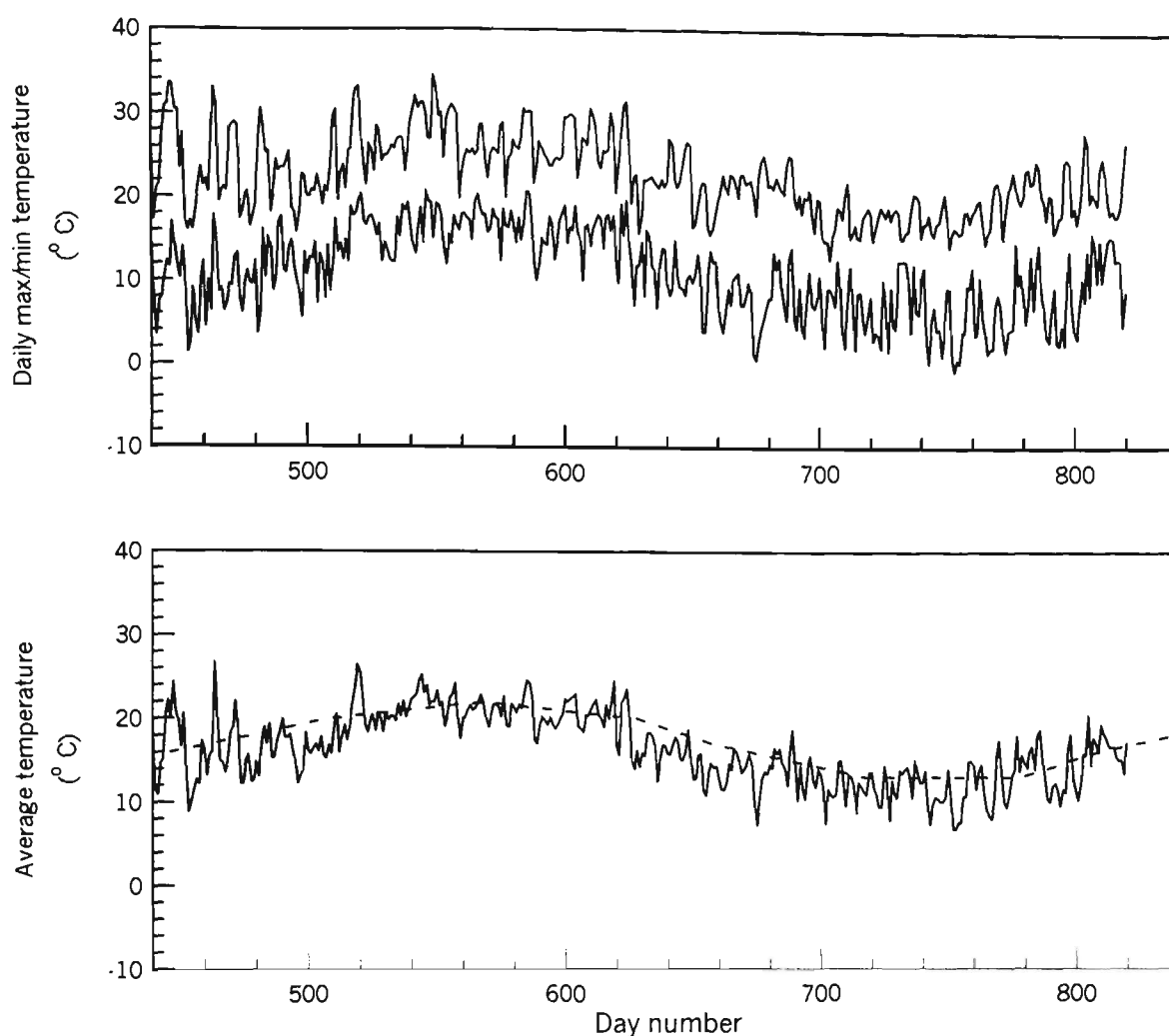


**Figure A.1b** Post-weir temperature record.

The temperature record observed at the site shows typical trends for south-eastern Australia with hot summers and mild winters. Hot temperatures in excess of 30°C were experienced for a prolonged period during the 1997-98 summer and beyond to Day 265 (April 1998). The daily average temperature between Days 208-265 is substantially hotter than the long term monthly average temperature data previously collected at the Berry Sewerage Treatment Plant (Pease, 1994). Cool to cold conditions prevailed during the winter of 1998 (Days 324-416). Daily minimum temperatures often approached or fell slightly below freezing during this period, causing mild frosts. These cold daily minimum temperatures are caused by cold-air falling from the adjacent

highlands-escarpment landscape and draining into the coastal lowland valleys. The winter season was colder than average with daily average temperatures being up to 8°C lower than the long term average. Short periods of hot temperatures were experienced during September 1998 (Day 430-440) where maximum temperatures of 30°C were recorded.

The spring of 1998 was characterised by variable temperature condition with daily maximums between 17-33°C. Between Days 460-540 the average temperature was approximately 6°C below the long term average. The 1998-99 summer (Days 540-620) recorded close to average conditions, with very few days exceeding 30°C. Figure A.1b shows that average daily temperatures varied by only  $\pm 4^{\circ}\text{C}$  relative to the long term temperature average. The autumn and winter months of 1999 (Days 620-780) were cooler than average, with daily average temperatures being approximately 6°C below average. Although this period recorded colder than average conditions, no minimum temperatures below freezing were recorded. Late winter and early spring 1999 (Days 780-813) recorded variable conditions that are characteristic of the transition between winter and summer. During this period daily average temperatures fluctuated between 12-23°C.

## **A.2 Wind speed**

Daily maximum and average wind speeds for the study site are shown in Fig A.2(a,b).



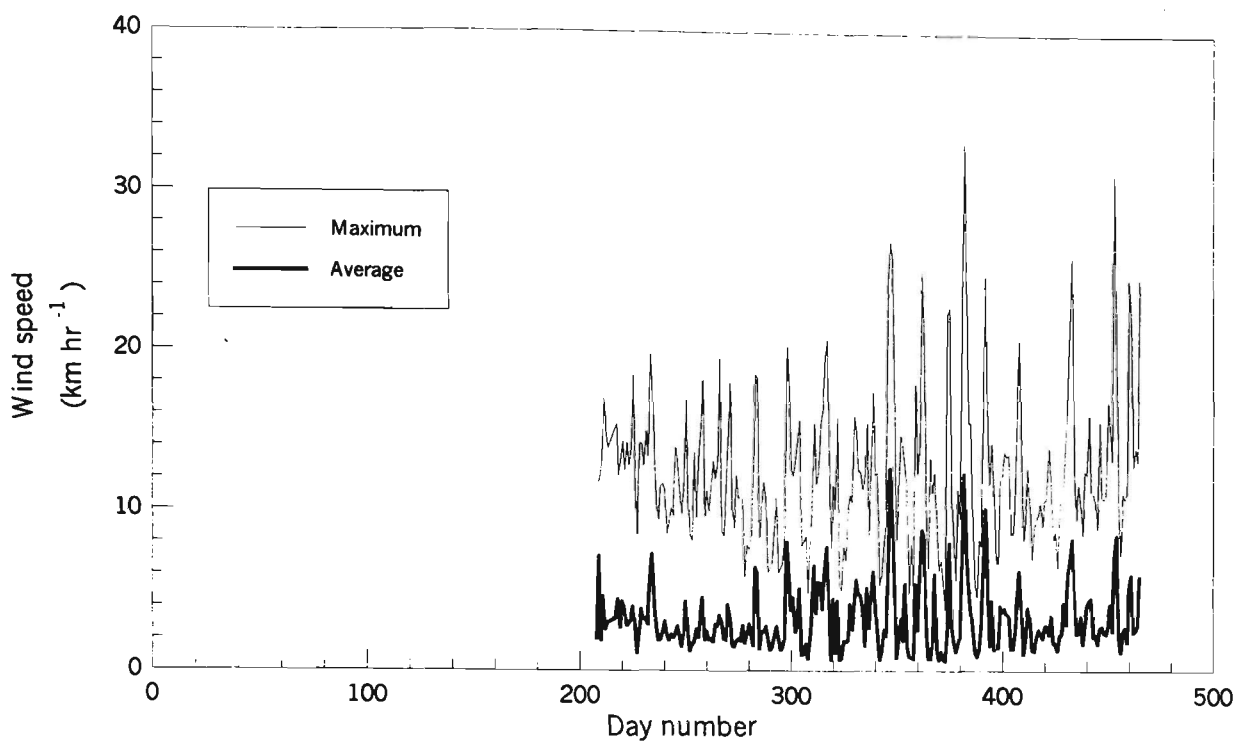


**Figure A.2a** Maximum and average wind speeds for the pre-weir period.

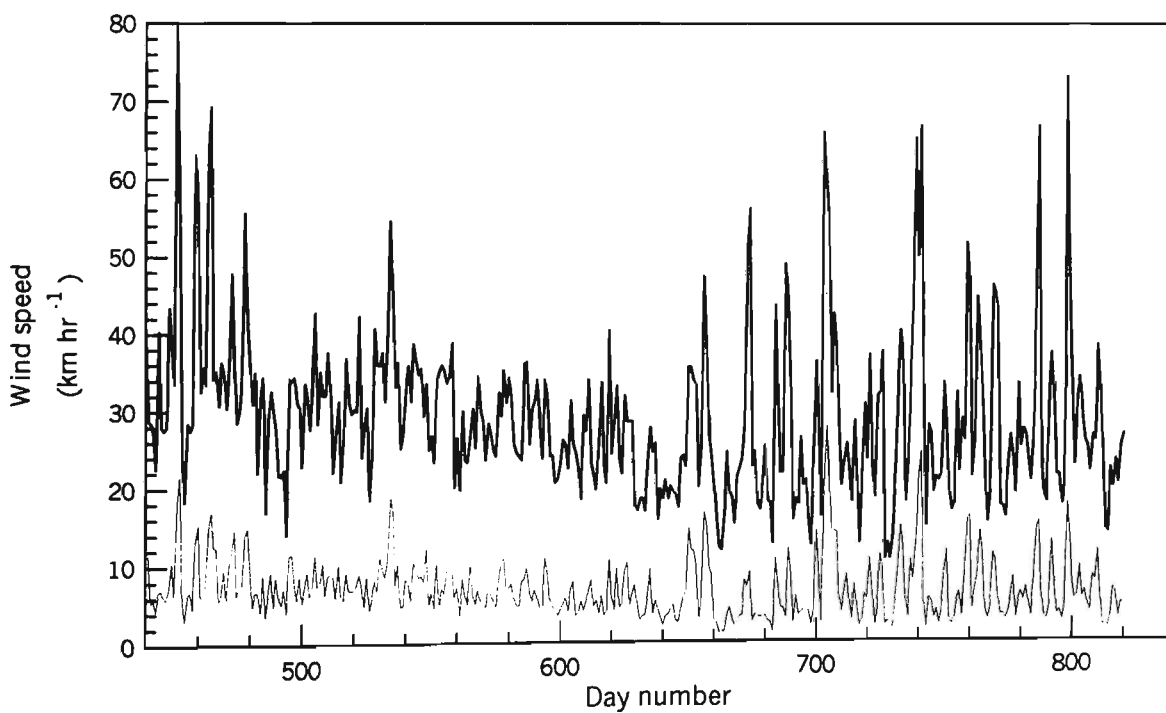


**Figure A.2b** Maximum and average wind speeds for the post-weir period.

Recorded wind speeds show a diurnal pattern with winds increasing velocity during the day and falling at night, particularly during the summer months when maritime north-easterly winds dominate. Stronger and more persistent winds from the South prevail during the winter. Strong winds in excess of  $20 \text{ km hr}^{-1}$  were recorded on numerous occasions during the winters of 1998 and 1999.

**A.3 Solar radiation**

Solar radiation is necessary for plant photosynthesis and subsequent evapotranspiration. The daily average incoming solar radiation measured at the site is shown in Figure A.3(a,b).

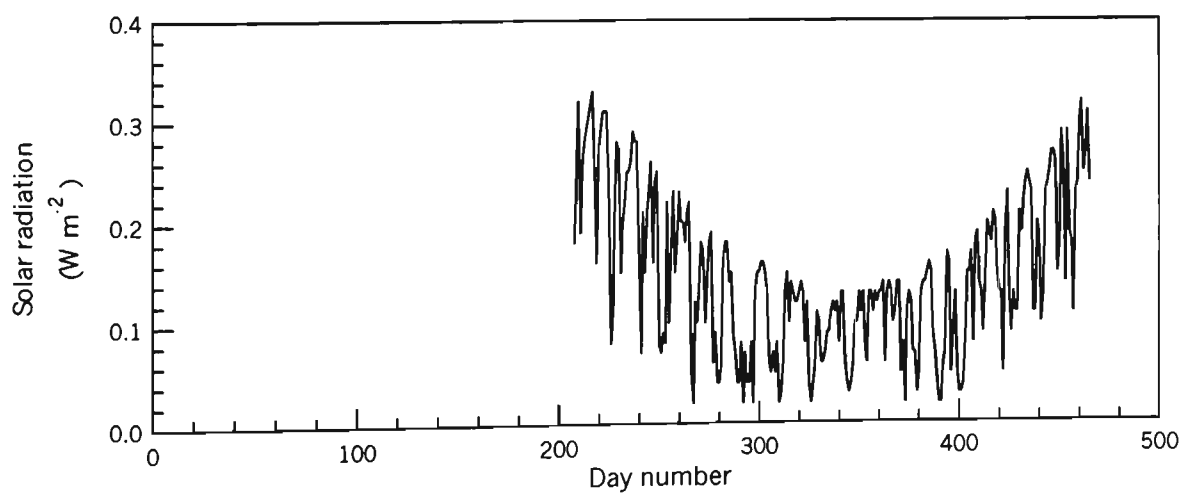


**Figure. A.3a** Incoming solar radiation for the pre-weir period.

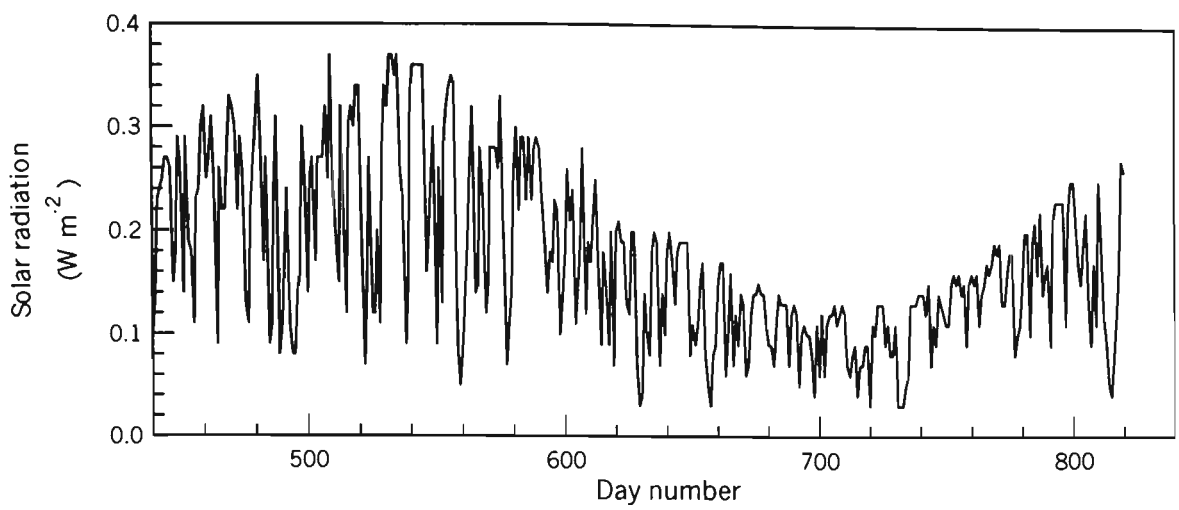


**Figure A.3b** Incoming solar radiation for the post-weir period.

As expected, solar radiation is greatest during the summer months when day lengths are longest and cloud is less persistent.

Appendix B: Groundwater quality data from all piezometer locations

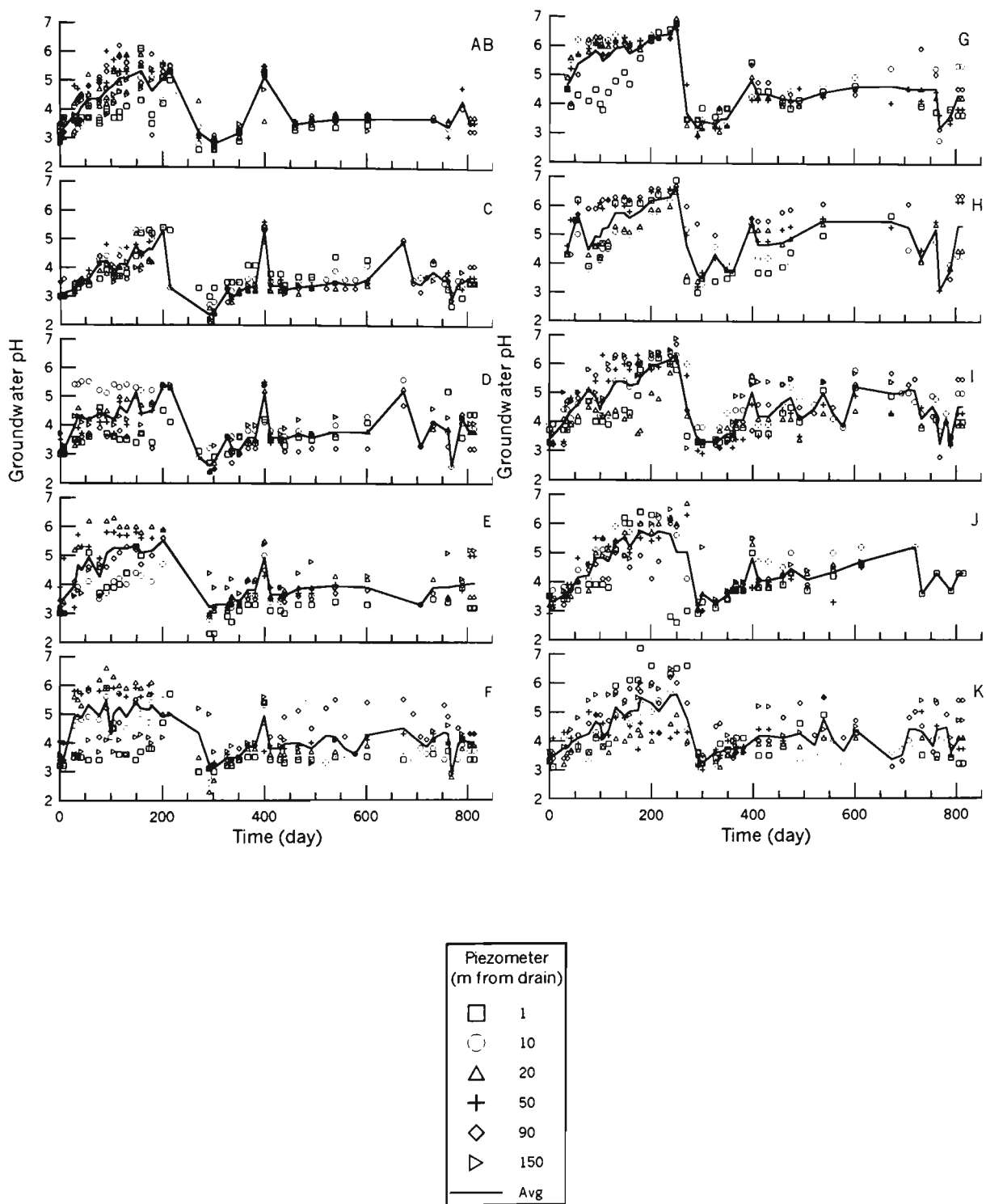
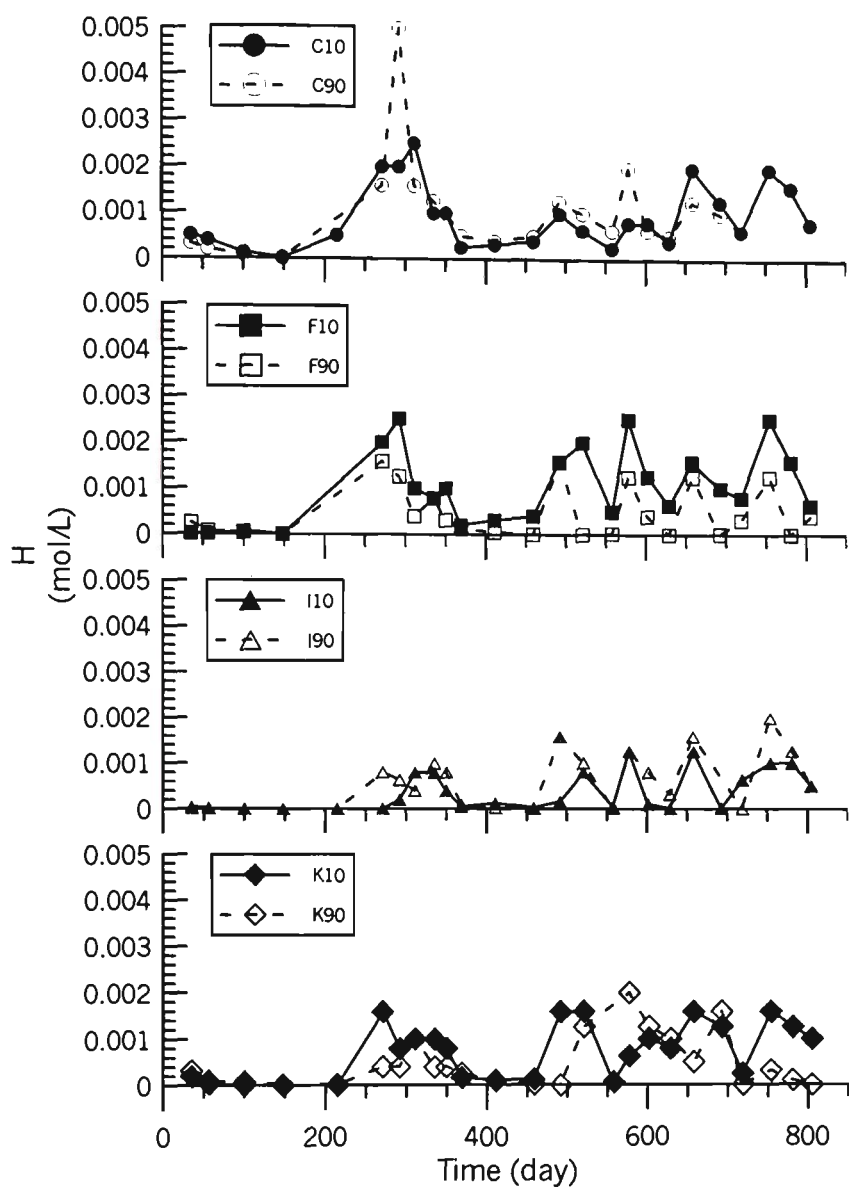
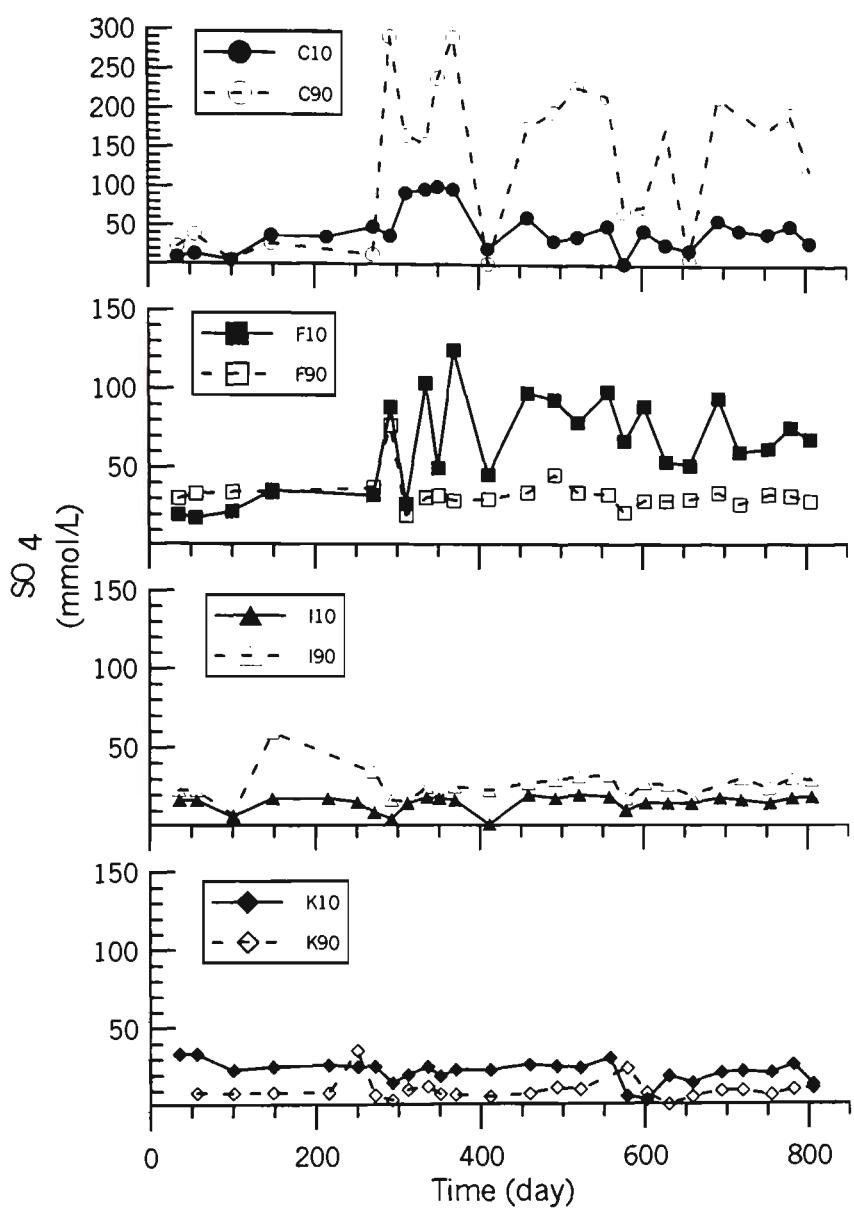


Figure B.1 Groundwater pH measured in piezometer Transects A-K.



**Figure B.2** Groundwater  $H^+$  concentration measured in piezometer Transects A-K.



**Figure B.3** Groundwater  $\text{SO}_4^{2-}$  concentration measured in piezometer Transects A-K.

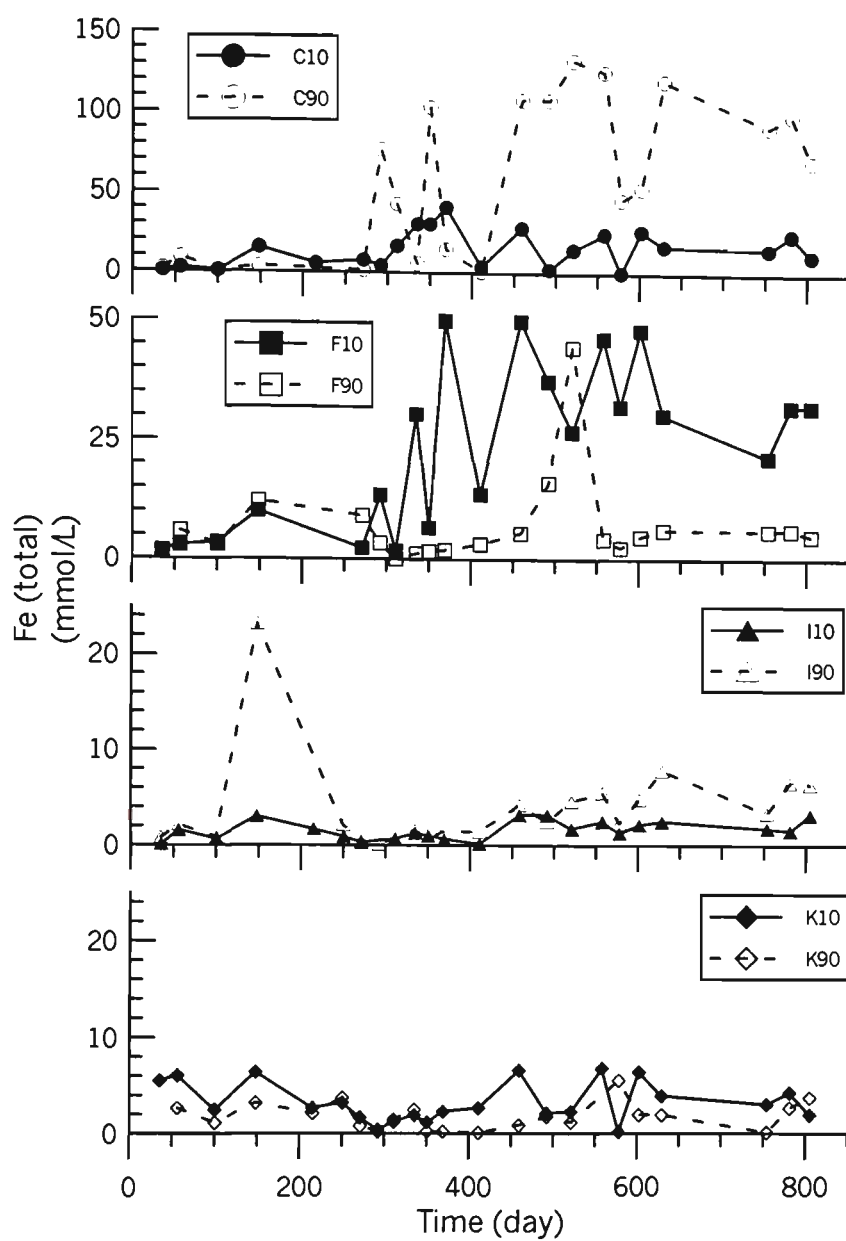


**Figure B.4** Groundwater Fe concentration measured in piezometer Transects A-K.

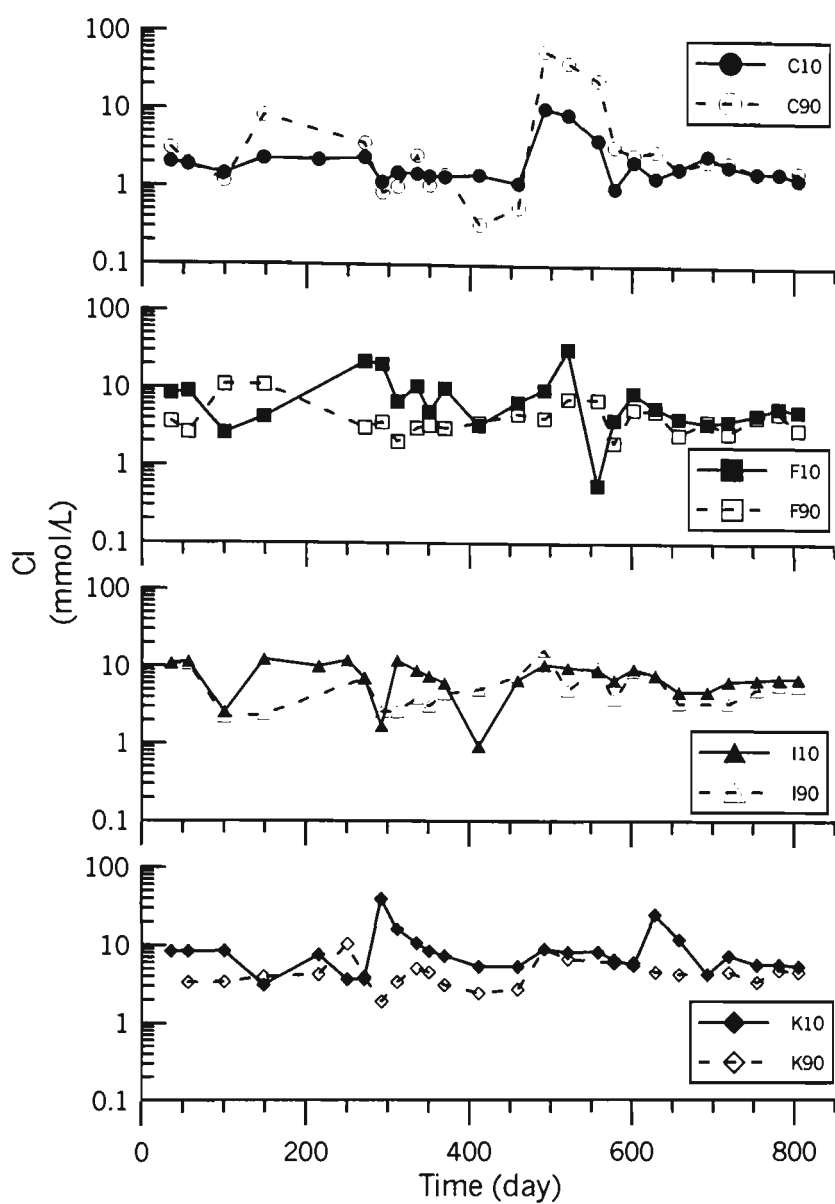


**Figure B.5** Chloride concentration in groundwater



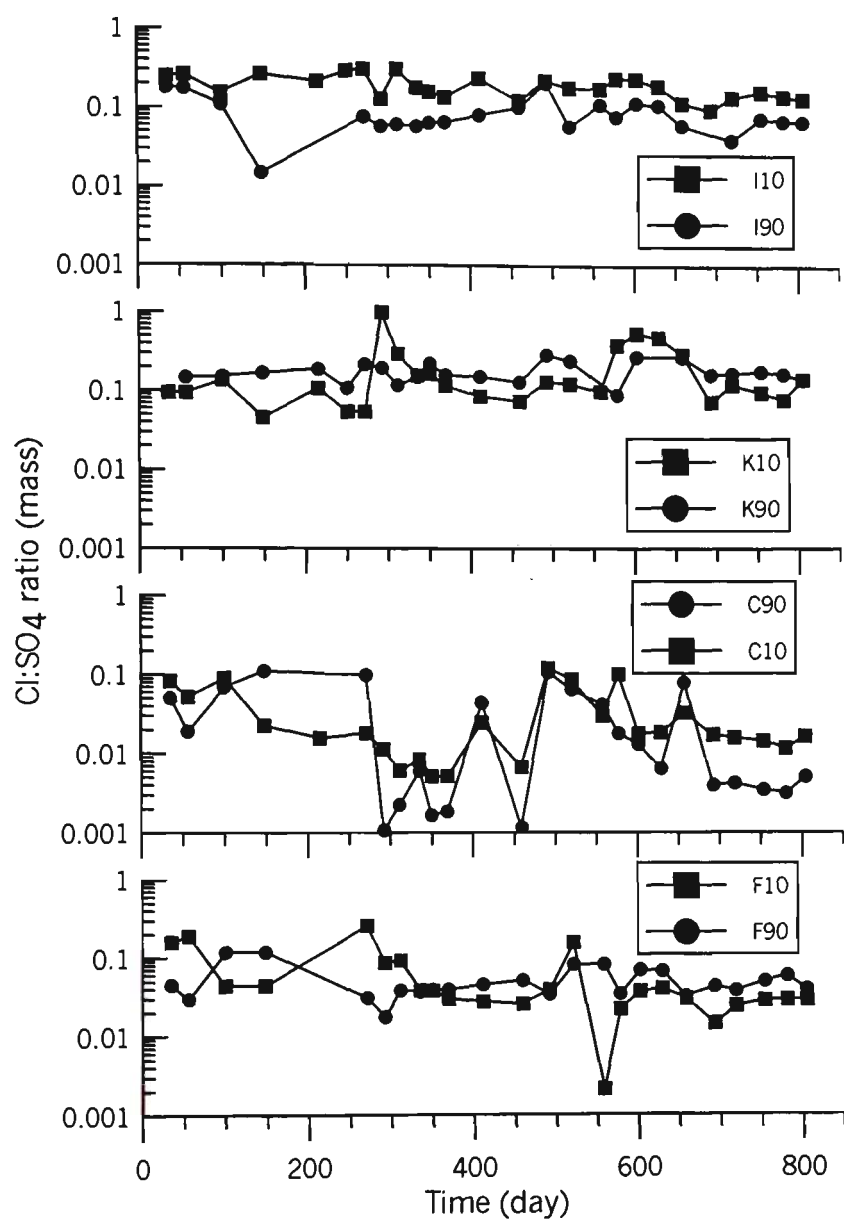


**Figure B.6** Chloride: sulfate ratio in groundwater

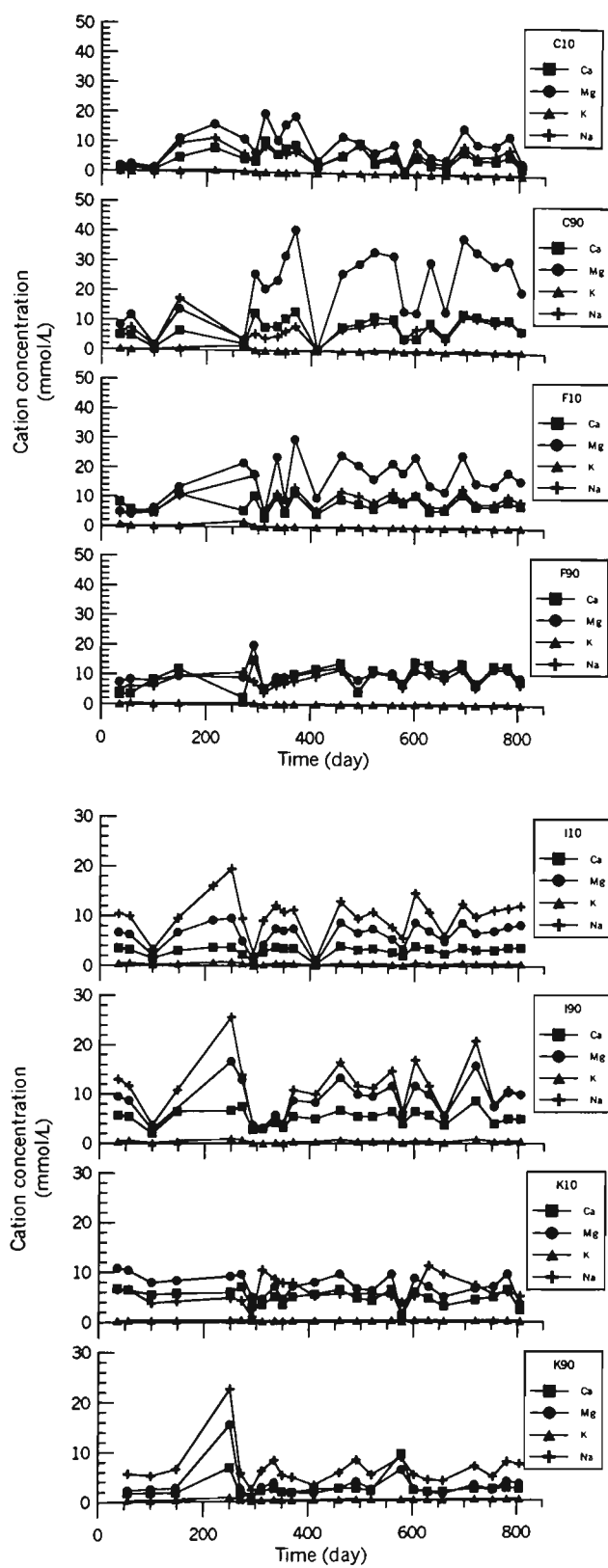


**Figure B.7** Basic cation concentration in groundwater

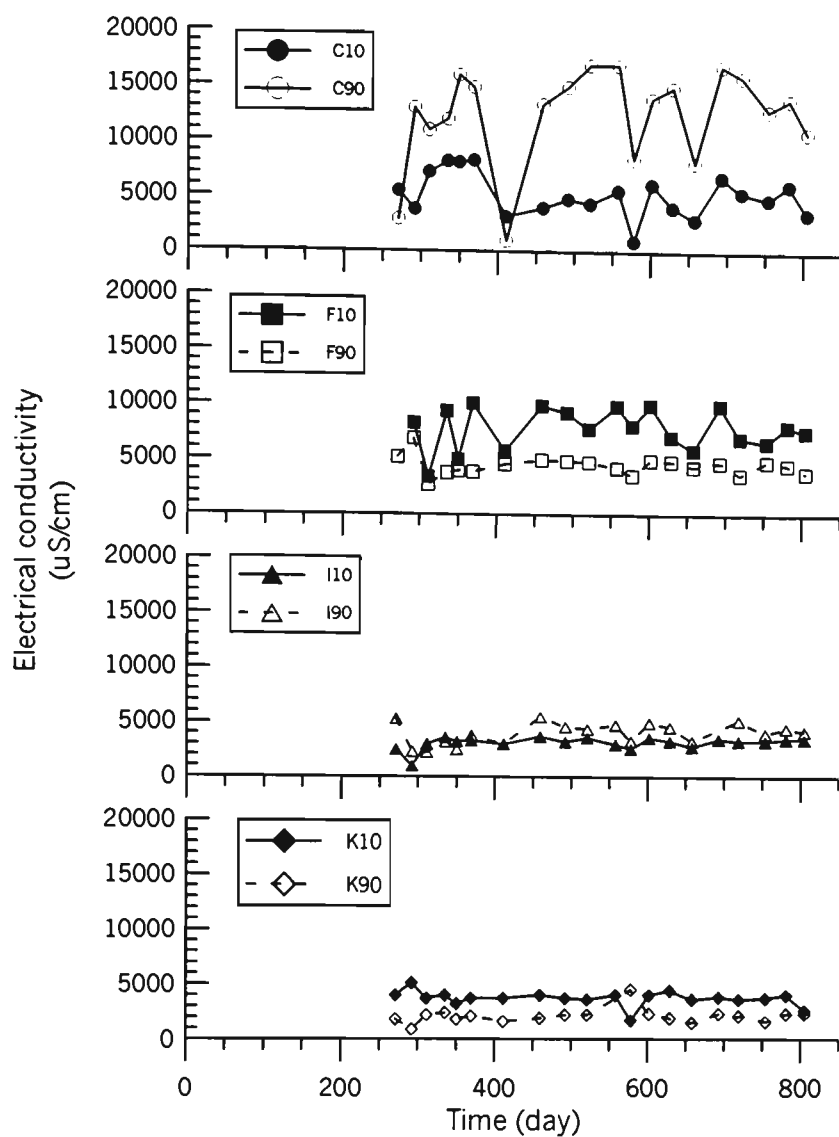


**Figure B.8** Electrical conductivity of groundwater

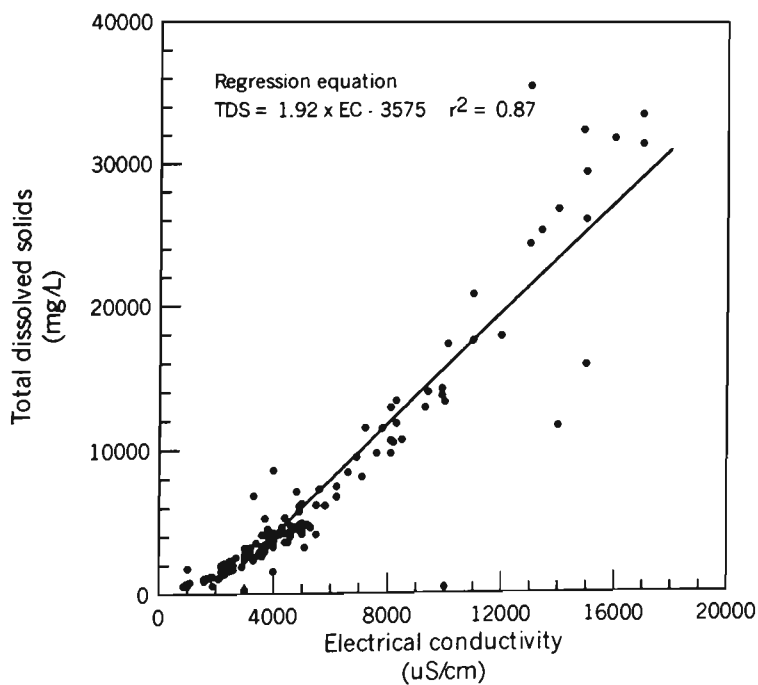


**Figure B.9** Relationship between electrical conductivity and total dissolved solids.

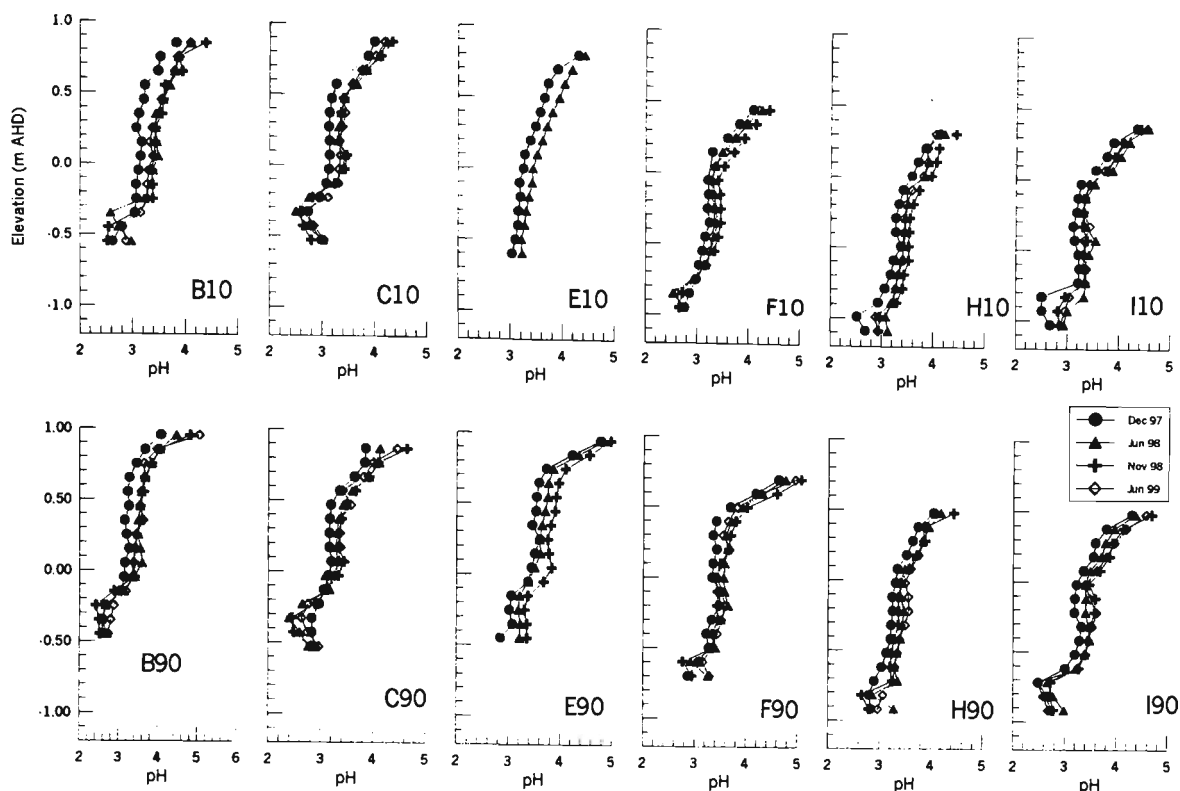


**Figure B.10** Change in soil pH.

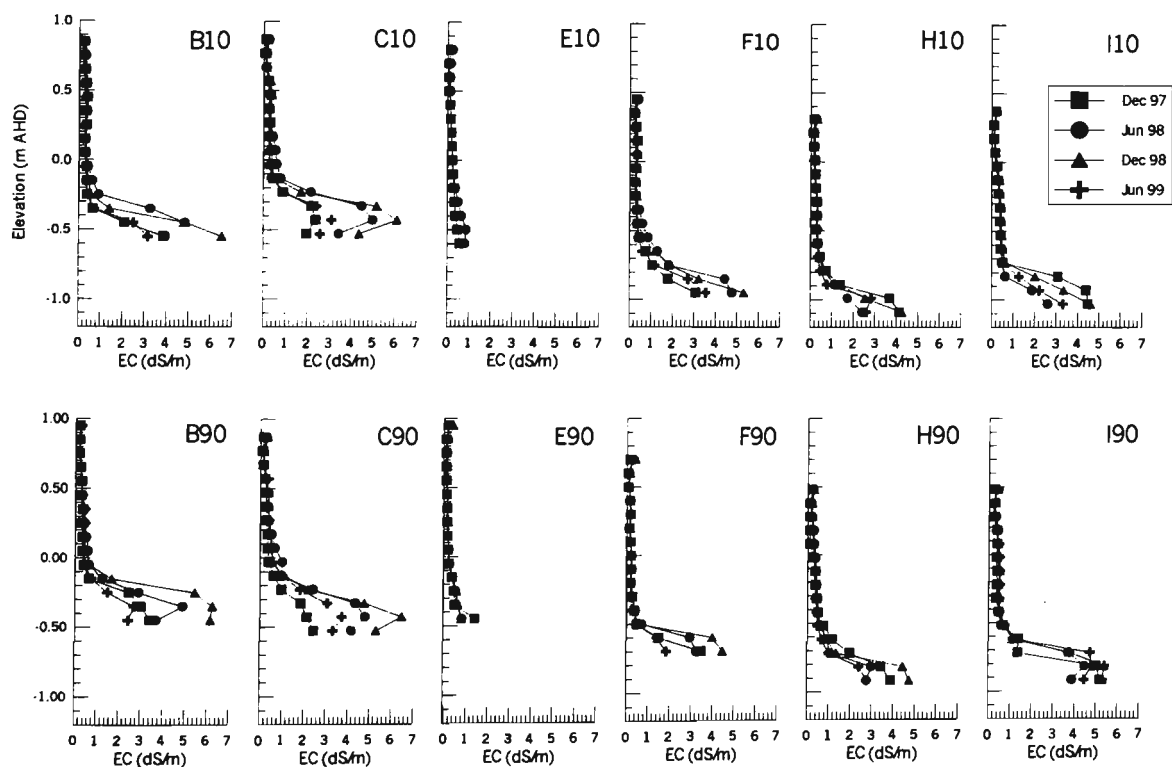


**Figure B.11** Change in soil EC.

## Appendix C: Source code for the ASS3D program.

```
c
c Program for oxidation of pyrite in acid sulfate soils developed for use with
c FEMWATER
c
program ass3d
c
c -----
c   define all variables that are swapped between subroutines
c   in the common.for file
c   local variables are defined in individual subroutines
c   -----
c
include "c:\f7713\ass\common.for"
c
c
print *, 'Input max. day number of FEMWATER simulation'
read *, numday
print *, 'maxday', numday
print *, 'running ASS3D program'
c   import various data from FEMWATER files and ASS3D data file
call inputdata
c
c   start time loop for (time) number of days
do 17 time=0,numday
```

```

    print *, 'day', time

c
c   import the node moisture content data for day time from *.mcn file
    call moisture

c
c   calculate the oxygen profile, conc, diffusion coeff etc for the profile
c   at each xx,yy co-ord
    call oxygen

c
c   calculate the amount of pyrite oxidised, H+, SO4, Fe3+ generated
c   calculate the remaining pyrite conc, size
    call acid

c
c   write various output components to a file
    call filewrite

c
17   continue

c
    print *, 'end of run'

stop

end

c*****

c
c-----

c routine to read in mesh co-ordinate data
c from GMS 2.1 - FEMWATER *.mcn file

```

```

c-----

c

subroutine inputdata

include "c:\f7713\ass\common.for"

c

c    local variables

integer i, maxx,maxy,maxz,j

real x(2000), y(2000), z(2000), node(2000),xcoord(2000),
/   ycoord(2000), nodeht(20,20,16)

character ge*5

c

c

c *****

c read in number node/element data from GMS 2.1 *.mcn file

c *****

c

open(unit=16,file='d:\ajsr\tide166\t_16610.mcn',status='old')

read(16,*)

read(16,*)

read(16,*)

read(16,*) ge, numnode

read(16,*) ge, numele

cprint *, 'Number of nodes is', numnode

cprint *, 'Number of elements is', numele

read(16,*)

cprint*, 'Hit return to continue'

```

```

c read(*,*)

c
c *****

c read in node co-ord data from GMS 2.1 *.dm3 file

c *****

c

c ge for the node tag used in *.dm3 file

c x is the x co-ordinate

c y is the y co-ordinate

c z is the z co-ordinate

c node is the node number

c

open(unit=15,file='d:\ajsr\tide166\t_16610.3dm',status='old')

c

read(15,*)

read(15,*)

read(15,*)

read(15,*)

do 500 i=1,numele
  read(15,*)
500 continue

do 501 i=1,numnode
  read(15,*) ge,node(i),x(i),y(i),z(i)
501 continue

read(15,*)

c *****

```



c calculate maximum x and y node co-ordinate

c \*\*\*\*\*

maxx=x(i)

maxy=y(i)

do 509 i=1,numnode

if(maxx.lt.x(i+1))then

maxx=x(i+1)

endif

if(maxy.lt.y(i+1))then

maxy=y(i+1)

endif

509 continue

c \*\*\*\*\*

c maxx is the maximum x co-ordinate

c maxy is the maximum y co-ordinate

c numzcoor is the number of soil layers in the z plane

c \*\*\*\*\*

c calculate the number of soil layers (z)

c \*\*\*\*\*

c print \*, 'Maximum x co-ordinate is:', maxx

c print \*, 'Maximum y co-ordinate is:', maxy

c print \*, 'Hit return to continue'

c read(\*,\*)

c

c \*\*\*\*\*

c x coordinates

```

c      *****

c      numxcoor is the number of x co-ordinates

c      numycoor is the number of y co-ordinates

c      xcoord(n) is the value of the n'th x co-ord

c      ycoord(n) is the value of the n'th y co-ord

c      *****

      xcoord(1)=x(1)

      numxcoor=1

c      print *, 'Number x coord  ', 'x co-ord', 'i'

c      print *, numxcoor, xcoord(numxcoor)

      do 526 i=2,numnode
      if(x(i).lt.x(i-1))then
          xcoord(i)=x(i)
          numxcoor=numxcoor+1
          if(xcoord(i).eq.0)then
              goto 527
          endif
      endif

      526  continue

      527  continue

c

c      *****

c      y coordinates

c      *****

      ycoord(1)=y(1)

      numycoor=1

```

```

c      print *, 'Number y coord  ', 'y co-ord', 'i'
c      print *, numycoor, ycoord(numycoor)

      do 525 i=2,numnode
      if(y(i).gt.y(i-1))then
          ycoord(i)=y(i)
          numycoor=numycoor+1

          if(ycoord(i).eq.maxy)then
              goto 523
          endif

      endif

525    continue
523    continue

c
c
c      print *, 'yy, y(yy), i, ypoint(i)'

      do 168 yy=1,numycoor

      i=yy-1

      ypoint(i)=y(yy)

c      print *, yy, y(yy), i, ypoint(i)

168    continue

c      read(*,*)

      i=1

c      print *, 'xx, x(xx), i, xpoint(xx)'

      do 171 xx=0,numxcoor-1

      xpoint(xx)=x(i)

c      print *, xx, x(i), i, xpoint(xx)

```

```

        i=i+numycoor
171  continue

c    read(*,*)

        do 183 xx=0,numxcoor-2

            xside(xx)=xpoint(xx)-xpoint(xx+1)

183  continue

c

        do 189 yy=0,numycoor-2

            yside(yy)=ypoint(yy+1)-ypoint(yy)

189  continue

c

        do 95 xx=0,numxcoor-2

            do 96 yy=0,numycoor-2

                area(xx,yy)=xside(xx)*yside(yy)

96  continue

95  continue

c

c

c    *****

c    number of z coordinates

c    *****

c

        numzcoor=numnode/(numxcoor*numycoor)

        maxz=numzcoor

c    *****

c    calculate element height (eleht)

```

```

c      *****

j=0

do 672 zz=0,numzcoor-1

    do 673 xx=0,numxcoor-1

        do 674 yy=0,numycoor-1

            j=j+1

            nodeht(xx,yy,zz)=z(j)

674          continue

673        continue

672      continue

do 195 xx=0,numxcoor-1

    do 196 yy=0,numycoor-1

        do 197 zz=1,numzcoor-1

            eleht(xx,yy,zz)=nodeht(xx,yy,zz-1)-

/            nodeht(xx,yy,zz)

197          continue

            eleht(xx,yy,0)=0

196        continue

195      continue

c

c

c

c-----

c      readng of inputdata for calculation of oxygen/pyrite concentrations

c-----

c

```

double precision vmineral

double precision gmineral

c

c

open(unit=18,file='c:\f7713\ass\test1.inp',status='old')

c

read(18,\*)

read(18,\*)

read(18,\*) (rclod(zz),zz=0,numzcoor-1)

read(18,\*)

read(18,\*) temso, dfcfcld, henry, air, dfcfoxatm

read(18,\*)

read(18,\*) (pyrperc(zz),zz=0,numzcoor-1)

read(18,\*)

read(18,\*) (pyrdia(zz),zz=0,numzcoor-1)

read(18,\*)

read(18,\*) (satmc(zz),zz=0,numzcoor-1)

c

close(unit=18)

c

c

do 10 zz=0,numzcoor-1

c

\*\*\*\*\*

c

calculation of pyrite content in kg.m-3 soil

c

\*\*\*\*\*

rest=100-pyrperc(zz)

```
vsolid=(pyrperc(zz)/5000)+(rest/2650)
```

```
vtot=vsolid/(1-satmc(zz))
```

```
pyrcont(zz)=pyrperc(zz)/vtot
```

```
vmineral=1-satmc(zz)-(pyrcont(zz)/5000)
```

```
c
```

```
c *****
```

```
c specific area of soil matrix in m2.m-3 (aggregate structure):
```

```
c *****
```

```
c
```

```
sparea(zz)=3/rclod(zz)
```

```
c
```

```
c *****
```

```
c conversion into plate structure:
```

```
c *****
```

```
c
```

```
rplate(zz)=rclod(zz)/3
```

```
c
```

```
10 continue
```

```
c
```

```
c *****
```

```
c assume that initial pyrite conc. is uniform
```

```
c in xx and yy across the FEMWATER mesh (a good way for
```

```
c determining where pyrite oxidation is a problem at the site).
```

```
c *****
```

```
c
```

```
do 11 xx=0,numxcoor-1
```

```

do 12 yy=0,numycoor-1
    do 13 zz=0,numzcoor-1
        pyrcont3(xx,yy,zz)=pyrcont(zz)
        pyrperc3(xx,yy,zz)=pyrperc(zz)
        pyrdia3(xx,yy,zz)=pyrdia(zz)
13    continue
12  continue
11  continue
c
do 22 xx=0,numxcoor-1
do 21 yy=0,numycoor-1
do 20 zz=0,numzcoor-1
    if(pyrcont3(xx,yy,zz).lt.0.00001)then
        pyroxco3(xx,yy,zz)=0
        pyrdia3(xx,yy,zz)=0
    else
c *****
c  number of pyrite crystals in a m2 within the element:
c *****
        anpyr3(xx,yy,zz)=6*pyrcont3(xx,yy,zz)/(5000*
/      3.141592654*(pyrdia3(xx,yy,zz)**3))
    endif
c *****
c  to overcome small values for anpyr3 from roundoff
c *****

```



```

        if(anpyr3(xx,yy,zz).lt.5000)then
            anpyr3(xx,yy,zz)=0
        endif
c
20    continue
21    continue
22    continue
c
c    *****
c    initialize iteration criterium
c    *****
c
    ito=0
c
c
c
close(unit=15)
return
end
c
c    -----
c
subroutine moisture
c    -----
c
include "c:\f7713\ass\common.for"
c    *****
c    read in data from GMS 2.1 *.mcn file

```

```

c      ****
c
integer j
real mcf
dimension mcf(6400)

c
read(16,*)

c
do 571 j=1,numnode
  read(16,*) mcf(j)
571  continue

c
c
****

c  assign mcf(i) to a mesh coordinate system, mesh starts
c  at (0,0,0) at top, right, front corner. Progresses along y-axis
c  until numycoor (ie x=0,z=0), then moves to x=1 and goes along
c  y-axis. Format FEMWATER mesh by selecting the surface then renumber
c
****

c
j=0
do 572 zz=0,numzcoor-1
  do 573 xx=0,numxcoor-1
    do 574 yy=0,numycoor-1
      j=j+1

```

```

                                amc(xx,yy,zz)=mcf(j)
574                                continue
573                                continue
572    continue
c
c
do 346 xx=0,numxcoor-1
    do 347 yy=0,numycoor-1
        do 348 zz=0,numzcoor-1
c            print *, 'amc', xx,yy,zz,amc(xx,yy,zz)
348            continue
c            read(*,*)
347        continue
346    continue
c
c
    return
    end
c
c-----
c    Subroutine oxygen: Calculation of steady state oxygen profiles
c-----
    subroutine oxygen
        include "c:\f77l3\ass\common.for"
c    print *, 'sub oxygen'
c    read(*,*)

```

```

c
c
real susqdi, A2, a1
,
c
c
c
c
c *****
c calculate various parameters that are constant for a
c certain water content profile:
c
c 1) diffusion coefficients for oxygen per node in macropores
c and in soil water
c *****
c
c fortran problem with constants
c manually insert constants here
satmc(0)=0.43
henry=52
c
do 12 xx=0,numxcoor-1
do 11 yy=0,numycoor-1
do 10 zz=0,numzcoor-1
c
if((satmc(zz)-amc(xx,yy,zz)).gt.0.01)then
c
c *****
c

```

```

c      layer not water-saturated
c
c      *****
c
c
c      e=satmc(zz)-amc(xx,yy,zz)
c
c
c      *****
c
c      Diff coeff of O2 in air in m2.d-1, at ambient temperature
c
c      Bakker et al, (p6):
c
c      *****
c
c
c
c
c      dfcfoxai(xx,yy,zz)=(((e-0.01)/0.99)**1.3)*1.85
c
c
c      *****
c
c      Diff coeff. of O2 in saturated aggregate in m2.day-1:
c
c      *****
c
c
c      dfcfoxso(xx,yy,zz)=1e-5
c
c      else
c
c
c      *****
c
c      layer water-saturated
c
c      *****
c
c
c
c      dfcfoxai(xx,yy,zz)=0
c
c      dfcfoxso(xx,yy,zz)=0

```

```

endif

c
c
10    continue
c    print *, 'end part 1 oxygen'
c
c
c
*****
**
c    2) maximum oxygen consumption per soil layer in complete aerobic
c    conditions
c
c
*****
**
c
do 111 zz=0,numzcoor-1

    if(pyrcont3(xx,yy,zz).lt.0.00001)then

        pyroxco3(xx,yy,zz)=0
        anafact3(xx,yy,zz)=0

c
c
c    *****
c
c    factor determing method of O2 consumption calc.
c
c    *****
c
c
else
c

```

```

c
*****
***
c      calculation of max. o2 cons of pyrite in kg pyrite/kg pyrite.day
c      at 20oC, max O2 concentration in air is 1.25 kg.m-3 (Bakker et al)
c
*****
***
c
      pyroxc3(xx,yy,zz)=0.311262*sqrt(0.21*air/henry)/
/      (pyrdia3(xx,yy,zz)*5000)
      anafact3(xx,yy,zz)=1
endif
c
c
*****
****
c      max. o2 cons of soil (fes2) in kg O2.m-3.d-1,
c      and calculation of slope (afactor) and intercept (qfactor) of
c      linear relationship between ox consumption and oxygen conc in water (oxcowa)
c
*****
****
c
      if(anafact3(xx,yy,zz).eq.0)then
c

```

```

c
*****
*****

c      no pyrite present in node (depth z), oxygen consumption is constant
c      make qfactor small +ve number to account for O2 cons. other than pyrite
c
*****
*****

c

      afactor3(xx,yy,zz)=0
      qfactor3(xx,yy,zz)=0.0000001
      else
      oxddram3(xx,yy,zz)=pyroxco3(xx,yy,zz)*pyrcont3(xx,yy,zz)
      A2=0.311262*sqrt(0.001)*pyrcont3(xx,yy,zz)/
/      (pyrdia3(xx,yy,zz)*5000)
      afactor3(xx,yy,zz)=(oxddram3(xx,yy,zz)-A2)/
/      ((0.21*air/henry)-0.001)
      qfactor3(xx,yy,zz)=oxddram3(xx,yy,zz)-
/      (afactor3(xx,yy,zz)*0.21*air/henry)

      endif

c
c
c      *****
c      max ox. cons of soil in m3.m-3.d-1:
c      *****
c
c
oxddrav3(xx,yy,zz)=2.56e-3*(temso+273)*oxddram3(xx,yy,zz)

```



```

c
111  continue
c  print *, 'end part 2 oxygen'
c
c
c  *****
c
c  3) Initialisation of ox. consumption values
c  *****
c
c
c  do 30 zz=0,numzcoor-1
c
c    if(ito.le.2.or.ito.ge.99)then
c
c      *****
c
c      iteration criterium not reached in previous oxygen
c      profile calculation. Start with new initial values:
c      *****
c
c
c      oxco23(xx,yy,zz)=0.21-zz*0.02
c
c      if(oxco23(xx,yy,zz).lt.0)then
c
c        oxco23(xx,yy,zz)=0
c
c      endif
c
c      oxco13(xx,yy,zz)=oxco23(xx,yy,zz)
c
c      oxcowa3(xx,yy,zz)=air*oxco23(xx,yy,zz)/henry
c

```

```

c
*****
****
c      at ambient temperature, Bakker et al, p 8, oxcowa in kg O2/.m3 water
c
*****
****
c
      endif
c
c      *****
c      else: start with last calculated oxygen profile
c      *****
c
      if(anafact3(xx,yy,zz).eq.1)then
c
c      *****
c      pyrite present, ox. consumpt. depending on ox. concentration
c      calculation of ox. consumption in kg O2.m-3 soil.day-1
c      *****
c
      rdodddram3(xx,yy,zz)=(sqrt(afactor3(xx,yy,zz))*
/      dfcfoxso(xx,yy,zz))*oxcowa3(xx,yy,zz)+qfactor3(xx,yy,zz)*
/      sqrt(dfcfoxso(xx,yy,zz)/afactor3(xx,yy,zz)))*sparea(zz)
      else
c
c      *****

```

```

c      no pyrite, Oxygen consumption is constant
c      calculation of ox. consumption in kg O2.m-3 soil.day-1
c      ****
c
      rdoxddram3(xx,yy,zz)=sqrt(2*qfactor3(xx,yy,zz)*
/      oxcowa3(xx,yy,zz)*dfcfoxso(xx,yy,zz))*sparea(zz)
      endif
c
c      ****
c      adjust value when aggregate is completely aerobic:
c      ****
c
      if(rdoxddram3(xx,yy,zz).gt.oxddram3(xx,yy,zz))then
      rdoxddram3(xx,yy,zz)=oxddram3(xx,yy,zz)
      endif
      rdoxddrav3(xx,yy,zz)=2.56e-3*(temso+273)*
/      rdoxddram3(xx,yy,zz)
      suoxddrav3(xx,yy,zz)=0
30    continue
c      print *, 'end part 3 oxygen'
c
      ito=1
c
1000  continue
c
c

```

```

c *****
c calculate vertical oxygen concentrations in macropores, using
c values of diffusion coefficients and oxygen consumption
c *****
c
c call macropore
c
c
c *****
c check wether iteration is sufficient
c *****
c
c
c susqdi=0
c do 110 zz=0,anuae3(xx,yy)-1
c   if(zz.eq.0)then
c     susqdi=susqdi+(0.21-oxco23(xx,yy,zz))**2
c   else
c     susqdi=susqdi+((oxco13(xx,yy,zz)-oxco23(xx,yy,zz))**2)
c   endif
110 continue
c
c if(anuae3(xx,yy).lt.5)then
c   crit=1e-4
c else
c   crit=(anuae3(xx,yy)-3)*1e-4
c endif

```

**c**

```
if(susqdi.lt.crit)goto 5000
```

C

C \*\*\*\*\*

c calculate aerobic volume of soil matrix and reduced oxygen

c consumption values

\*\*\*\*\*

**C**

call oxdem

**C**

\*\*\*\*\*

c no more than 100 iterations to determine oxygen profiles

\*\*\*\*\*

**C**

```
if(ito.ge.100)goto 5000
```

**C**

\*\*\*\*\*

c Calculation of new oxygen profile

c using new ox. consumption values

\*\*\*\*\*

**C**

```
ito=ito+1
```

**C**

```
goto 1000
```

**C**

**C**

5000 continue

c

c

c

\*\*\*\*\*

\*

c total oxygen consumption of soil profile in kg o<sub>2</sub>.m<sup>-2</sup> soil.day<sup>-1</sup>:

c

\*\*\*\*\*

\*

c

suoxddram3(xx,yy)=suoxddrav3(xx,yy,0)/(2.56e-3\*(temso+273))

c

c

\*\*\*\*\*

c various calculations for anaerobic part of profile:

c

\*\*\*\*\*

c

do 200 zz=anuae3(xx,yy),numzcoor-1

rian3(xx,yy,zz)=rplate(zz)

aevo3(xx,yy,zz)=0

oxco23(xx,yy,zz)=0

rdoxddrav3(xx,yy,zz)=0

rdoxddram3(xx,yy,zz)=0

pyroxco3(xx,yy,zz)=0

oxcowa3(xx,yy,zz)=0

200 continue

c

```

c *****

c Calculation of anaerobic radius and aerobic volumes

c *****

c

do zz=0,anuae3(xx,yy)-1

  if(anafact3(xx,yy,zz).eq.1)then

c

c *****

c pyrite present, ox. cons. depending on ox. concentration

c eq. 15, Bronswijk and Nugroho

c *****

c

  a1=afactor3(xx,yy,zz)*oxcowa3(xx,yy,zz)/

/    qfactor3(xx,yy,zz)+1

  rian3(xx,yy,zz)=rplate(zz)-alog(a1+sqrt(a1**2-1))/

/    sqrt(afactor3(xx,yy,zz)/dfcfoxso(xx,yy,zz))

c

  else

c

c *****

c no pyrite present, oxygen consumption constant

c *****

c

  rian3(xx,yy,zz)=rplate(zz)-sqrt(2*oxcowa3(xx,yy,zz)*

/    dfcfoxso(xx,yy,zz)/qfactor3(xx,yy,zz))

c

```

```

c      *****
c
c      adjust value if rian < 0
c
c      *****
c
c
c      if(rian3(xx,yy,zz).lt.0)then
c
c          rian3(xx,yy,zz)=0
c
c      endif
c
c      endif
c
c
c      *****
c
c      calculation of aerated volume of soil matrix:
c
c      *****
c
c
c
c      aevo3(xx,yy,zz)=1-(rian3(xx,yy,zz)/rplate(zz))
c
c      enddo
c
c
11  continue
12  continue
c
c
c
c      return
c
c      end
c
c
c
c-----
c
c      Subroutine oxconc: calculates vertical oxygen concentration in

```



```

c          macropore-air using values of diffusion coefficient
c          and oxygen consumption
c-----
c
c          subroutine macropore
c
c          include "c:\f7713\ass\common.for"
c
c          integer nuae, ln
c
c
c
c          print *, 'sub oxconc'
c
c
c          do 10 zz=0,numzcoor-1
c
c              oxco13(xx,yy,zz)=oxco23(xx,yy,zz)
c
c              suoxddrav3(xx,yy,zz)=0
c
10      continue
c
c
c          *****
c
c          determine number of aerated layers (nuae)
c
c          *****
c
c
c          do 20 nuae=0,numzcoor-1
c
c              if(dfcofaxi(xx,yy,nuae).le.0.00000000001)goto 30
c
c
c          *****
c
c          calculate sum of ox.demand layer zz and layers below zz

```

```

c      *****
c
      suoxddrav3(xx,yy,nuae)=rdoxddrav3(xx,yy,nuae)*
/      eleht(xx,yy,nuae)
      if(nuae.gt.0)then
        do 40 zz=nuae-1,0,-1
          suoxddrav3(xx,yy,zz)=suoxddrav3(xx,yy,zz+1)+
/      rdoxddrav3(xx,yy,zz)*eleht(xx,yy,zz)
40      continue
      endif
c
      oxco23(xx,yy,0)=0.21
c      +rdoxddrav3(xx,yy,0)/
c /      (2*dfcfoxai(xx,yy,0))*(eleht(xx,yy,0))**2-eleht(xx,yy,0)/
c /      dfcfoxai(xx,yy,0)*suoxddrav3(xx,yy,0)
      if(nuae.gt.0)then
        do 50 zz=1,nuae
          oxco23(xx,yy,zz)=oxco23(xx,yy,zz-1)+rdoxddrav3(xx,yy,zz)/
/      (2*dfcfoxai(xx,yy,zz))*eleht(xx,yy,zz)**2-
/      eleht(xx,yy,zz)/dfcfoxai(xx,yy,zz)*suoxddrav3(xx,yy,zz)
50      continue
      endif
c
      if(oxco23(xx,yy,nuae).lt.0)goto 30
c
20      continue

```

```

c
30    nuae=nuae-1
c
    suoxddrav3(xx,yy,nuae)=rdoxddrav3(xx,yy,nuae)*eleht(xx,yy,nuae)
c
    if(nuae.gt.1)then
        do 80 ln=nuae-1,0,-1
            suoxddrav3(xx,yy,ln)=suoxddrav3(xx,yy,ln+1)+
/            rdoxddrav3(xx,yy,ln)*eleht(xx,yy,ln)
80    continue
    endif
c
    if(nuae.eq.0)then
        oxco23(xx,yy,0)=0.21
        goto 95
    else
        oxco23(xx,yy,0)=0.21+rdoxddrav3(xx,yy,0)/
/        (2*dfcfoxai(xx,yy,0))*eleht(xx,yy,0)**2-eleht(xx,yy,0)/
/        dfcfoxai(xx,yy,0)*suoxddrav3(xx,yy,0)
        if(nuae.gt.0)then
            do 90 zz=1,nuae
                oxco23(xx,yy,zz)=oxco23(xx,yy,zz-1)+
/                rdoxddrav3(xx,yy,zz)/(2*dfcfoxai(xx,yy,zz))*
/                eleht(xx,yy,zz)**2-eleht(xx,yy,zz)/
/                dfcfoxai(xx,yy,zz)*suoxddrav3(xx,yy,zz)
90    continue

```

```

        endif

        endif
95    continue

c

        do 775 zz=0,numzcoor-1
775    continue

c

c

        anuae3(xx,yy)=nuae

c

c

        return

        end

c

c

c-----

c    subroutine anaerobic: Calculates anaerobic volume of soil matrix
c
c        and reduced oxygen consumption values
c-----

        subroutine oxdem

        include "c:\f77l3\ass\common.for"

c

c

        do 10 zz=0,anuae3(xx,yy)

            oxcowa3(xx,yy,zz)=air*oxco23(xx,yy,zz)/henry

c

```



```

        rdodddram3(xx,yy,zz)=sqrt(2*qfactor3(xx,yy,zz)*
/      oxcowa3(xx,yy,zz)*dfcfoxso(xx,yy,zz))*sparea(zz)
c
c      *****
c      adjust value when aggregate is completely aerobic:
c      *****
c
        if(rdodddram3(xx,yy,zz).gt.oxddram3(xx,yy,zz))then
          rdodddram3(xx,yy,zz)=oxddram3(xx,yy,zz)
        endif
        rdodddrav3(xx,yy,zz)=2.56e-3*(temso+273)*
/      rdodddram3(xx,yy,zz)
      endif
10    continue
c
c      *****
c      estimation of potential oxygen demand in anaerobic layers:
c      *****
c
      do 30 zz=anuae3(xx,yy)+1,numzcoor-1
        rdodddrav3(xx,yy,zz)=rdodddrav3(xx,yy,anuae3(xx,yy))
        rdodddram3(xx,yy,zz)=rdodddram3(xx,yy,anuae3(xx,yy))
        oxco23(xx,yy,zz)=oxco23(xx,yy,anuae3(xx,yy))
30    continue
c
c

```

```

return
end

c
c
c
*****
***
c    subroutine pyrite: Calculates amount of pyrite oxidized, remaining
c          pyrite and produced H+,Fe3+,SO42-
c
*****
***
c
c    subroutine acid
c
c    include "c:\f7713\ass\common.for"
c
c
c    double precision vmineral
c    double precision gmineral
c
c
c
c
c    do 12 xx=0,numxcoor-1
c
c    do 11 yy=0,numycoor-1
c
c
c    Feprodtot(xx,yy)=0
c    Hprodtot(xx,yy)=0
c    SO4prodtot(xx,yy)=0
c    pyroxtot(xx,yy)=0

```

c

```
do 10 zz=0,numzcoor-1
  if(pyrcont3(xx,yy,zz).lt.0.00001)then
    pyrcont3(xx,yy,zz)=0
    pyrox3(xx,yy,zz)=0
    pyrdia3(xx,yy,zz)=0
    pyrperc3(xx,yy,zz)=0
    feprod3(xx,yy,zz)=0
    so4prod3(xx,yy,zz)=0
    hprod3(xx,yy,zz)=0
  else
```

c

c \*\*\*\*\*

c quantity of FeS2 oxidized in kg FeS2/m3 soil.(1 kg FeS2=1 kg O2)

c \*\*\*\*\*

c

```
pyrox3(xx,yy,zz)=(rdoxddram3(xx,yy,zz)-qfactor3(xx,yy,zz)
/  *aevo3(xx,yy,zz))
```

c if(pyrox3(xx,yy,zz).gt.0)then

c print \*, xx,yy,zz,pyrox3(xx,yy,zz),'time', time

c read(\*,\*)

c endif

c

if(pyrox3(xx,yy,zz).lt.0)then

pyrox3(xx,yy,zz)=0

endif



```

c
c
    if(pyrox3(xx,yy,zz).ge.pyrcont3(xx,yy,zz))then
c
c      *****
c      all pyrite oxidized at depth zz
c      *****
c
c      pyrox3(xx,yy,zz)=pyrcont3(xx,yy,zz)
c      pyrcont3(xx,yy,zz)=0
c      pyrdia3(xx,yy,zz)=0
c      pyrperc3(xx,yy,zz)=0
c      else
c
c      *****
c      new pyrite content per layer in kg fes2. m-3 soil:
c      *****
c
c      pyrcont3(xx,yy,zz)=pyrcont3(xx,yy,zz)-pyrox3(xx,yy,zz)
c
c      endif
c
c      *****
c      new diameter pyrite crystals in m:
c      *****
c
c      pyrdia3(xx,yy,zz)=(6*pyrcont3(xx,yy,zz)/

```

```

/      (5000*3.141592654*anpyr3(xx,yy,zz))*0.33333333
c
c      *****
c      new weight percentage pyrite:
c      *****
c
      vmineral=1-satmc(zz)-pyrcont3(xx,yy,zz)
/      /5000
      gmineral=vmineral*2670
      pyrperc3(xx,yy,zz)=100*pyrcont3(xx,yy,zz)/
/      (pyrcont(zz)+gmineral)
c
c      *****
c      produced fe3+ in mol.l-1 soil:
c      *****
c
      feprod3(xx,yy,zz)=8.33*pyrox3(xx,yy,zz)
c
c      *****
c      produced so42- in mol.l-1 soil:
c      *****
c
      so4prod3(xx,yy,zz)=16.67*pyrox3(xx,yy,zz)
c
c      *****
c      produced h+ in mol.l-1 soil:

```

```

c      *****

c

      hprod3(xx,yy,zz)=8.33*pyrox3(xx,yy,zz)

c

c

      endif

c

c      *****

c      totals for whole profile (m2) during last timestep:

c      Fe in mol.m-2 (check that the *0.001 is required

c      *****

c

      Feprodtot(xx,yy)=Feprodtot(xx,yy)+Feprod3(xx,yy,zz)

/      *eleht(xx,yy,zz)*1

c

c      *****

c      H+ in mol.m-2

c      *****

c

      Hprodtot(xx,yy)=Hprodtot(xx,yy)+Hprod3(xx,yy,zz)

/      *eleht(xx,yy,zz)*1

c

c      *****

c      SO4 in mol.m-2

c      *****

c

```

```

so4prodtot(xx,yy)=so4prodtot(xx,yy)+so4prod3(xx,yy,zz)
/  *eleht(xx,yy,zz)*1
c
c *****
c pyrite oxidation in kg.m-2
c *****
c
c
Pyroxtot(xx,yy)=pyroxtot(xx,yy)+pyrox3(xx,yy,zz)
/  *eleht(xx,yy,zz)*1
c
c print *, xx,yy,zz,so4prod3(xx,yy,zz)
10  continue
c print *, xx, yy, so4prodtot(xx,yy)
c read(*,*)
c
c *****
c totals for whole period (Fe,H,SO4 in mol.m-2, Pyrite in kg.m-2)
c *****
c
c
Feprodsum=Feprodsum+Feprodtot(xx,yy)
Hprodsum=Hprodsum+Feprodtot(xx,yy)
SO4prodsum=SO4prodsum+Feprodtot(xx,yy)
pyroxcum=pyroxcum+pyroxtot(xx,yy)
c
11  continue
12  continue

```

```

c
c *****
c
c  calculatate the amount of ox products for element areas
c  (Fe,H,SO4 in mol/area (m2), Pyrite in kgarea (m2)
c  *****
c
c
c  do 990 xx=0,numxcoor-2
c
c  do 991 yy=0,numycoor-2
c
c    Fetotarea(xx,yy)=((Feprodtot(xx,yy)+feprodtot(xx,yy+1)+
c  /    feprodtot(xx+1,yy)+feprodtot(xx+1,yy+1))/4)*area(xx,yy)
c
c    Htotarea(xx,yy)=((hprodtot(xx,yy)+hprodtot(xx,yy+1)+
c  /    hprodtot(xx+1,yy)+hprodtot(xx+1,yy+1))/4)*area(xx,yy)
c
c    SO4totarea(xx,yy)=((so4prodtot(xx,yy)+so4prodtot(xx,yy+1)+
c  /    so4prodtot(xx+1,yy)+so4prodtot(xx+1,yy+1))/4)*area(xx,yy)
c
c    pyroxtotarea(xx,yy)=((pyroxtot(xx,yy)+pyroxtot(xx,yy+1)+
c  /    pyroxtot(xx+1,yy)+pyroxtot(xx+1,yy+1))/4)*area(xx,yy)
c
c
c  cumulative sum of area concentrations
c
c
c    Harea=Harea+htotarea(xx,yy)
c
c    Fearea=fetotarea(xx,yy)+fearea
c
c    so4area=so4area+so4totarea(xx,yy)
c
c    pyroxarea=pyroxarea+pyroxtotarea(xx,yy)

```

```

c
c      print *, xx,yy,area(xx,yy), htotarea(xx,yy)
c      print *, hprodtot(xx,yy),hprodtot(xx,yy+1)
c      print *, hprodtot(xx+1,yy), hprodtot(xx+1,yy+1)
c      read(*,*)
991    continue
990    continue

c

c

      return

      end

c      -----
c      subroutine filewrite: write output data to various files
c
c              for input into FEMWATER
c      -----
c
c
c      subroutine filewrite
c
c      include "c:\f77l3\ass\common.for"
c
c      open(unit=30,file="d:\ajsr\tide166\te_out1.dat")
c      open(unit=31,file="d:\ajsr\tide166\te_prod1.dat")
c      open(unit=32,file="d:\ajsr\tide166\tearea1.dat")
c
c      if(time.eq.0)then
10          format(A7)
11          format(A14)
12          format(A6)

```

```

13      format(A2,I8)
14      format(A12)
15      format(A5)

      write(30,10) 'DATASET'

      write(30,11) 'OBJTYPE mesh3d'

      write(30,12) 'BEGSCL'

      write(30,13) 'ND',numnode

      write(30,13) 'NC',numele

      write(30,14) 'NAME so4_out'

      endif

5      format(1X, F10.4)
6      format(1X, F10.2)
7      format(A6,E16.8)

      write(30,7) 'TS  0',time

      do 572 zz=0,numzcoor-1

          do 573 xx=0,numxcoor-1

              do 574 yy=0,numycoor-1

                  write(30,5) so4prod3(xx,yy,zz)

574                      continue

573          continue

572      continue

      if(time.eq.166)then

          print *, 'endds', numday

          write(30,15) 'ENDDS'

          close(30)

      endif

```

c

```
do 988 yy=0,numycoor-1
```

```
    do 989 xx=0,numxcoor-1
```

```
        write(31,5) so4prodtot(xx,yy)
```

```
989    continue
```

```
988 continue
```

c

```
write(32,6) SO4area
```

```
return
```

```
end
```



## Appendix D: Derivation of the solution for $\varphi_T$

Derivation of  $\varphi_T$  (Equation 9.16)

$$\begin{aligned}
 \varphi_T &= \int_r^R [A' C_w(x) + OM'] dx \quad (9.15) \\
 &= \int_r^R \left[ (A' C_b + OM') \left[ \frac{\cosh \sqrt{\beta}(x-r)}{\cosh \sqrt{\beta}(R-r)} \right] - OM' + OM' \right] dx \\
 &= \int_r^R (A' C_b + OM') \left[ \frac{\cosh \sqrt{\beta}(x-r)}{\cosh \sqrt{\beta}(R-r)} \right] dx \\
 &= \left( \frac{A' C_b + OM'}{\cosh \sqrt{\beta}(R-r)} \right) \int_r^R [\cosh \sqrt{\beta}(x-r)] dx \\
 &= \left( \frac{A' C_b + OM'}{\cosh \sqrt{\beta}(R-r)} \right) \left( \frac{1}{\sqrt{\beta}} \right) [\sinh \sqrt{\beta}(x-r)]_r^R \\
 &= \left( \frac{A' C_b + OM'}{\sqrt{\beta} \cosh \sqrt{\beta}(R-r)} \right) [\sinh \sqrt{\beta}(R-r) - \sinh(0)] \\
 \varphi_T &= \left[ \frac{A' C_b + OM'}{\sqrt{\beta}} \right] \tanh \sqrt{\beta}(R-r) \quad (9.16)
 \end{aligned}$$

**Appendix E: PHREEQC simulations**

All PHREEQC simulation were initialised with groundwater quality data typical of that measured at the field site. The CEC and mineral composition of the soil was defined, and the model was run to simulate the infiltration of 100 pore water volumes through the solid phase. The initial soil water quality and the influent water quality, approximating rainfall, used for the simulation is described in Table E.1.

**Table E.1** Initial and influent water quality for PHREEQC simulations

Analyte (mol/L)	Initial	Influent
pH	3.5	5.5
Al <sup>3+</sup>	0.0207	0.0001
Ca <sup>2+</sup>	0.008	0.0001
Cl <sup>-</sup>	0.0014	0.0001
Fe <sup>2+</sup>	0.015	0.0001
Fe <sup>3+</sup>	0.015	0.0001
K <sup>+</sup>	0.0001	0.0001
Mg <sup>2+</sup>	0.0163	0.0001
Na <sup>+</sup>	0.0061	0.0001
SO <sub>4</sub> <sup>2-</sup>	0.0099	0.0001

**E.1 Influence of acid saturated cation exchange complex on soil solution water quality**

The high level of acidic cation saturation on the cation exchange sites is a contributing factor to the maintenance of poor water quality conditions after the cessation of pyrite oxidation. As shown in Chapter 6, the effective cation capacity of the soil between 0.5 and 1.3 m below the ground surface (ie. the soil between the organic rich top soil and the pyritic layer) is about 70 %  $\text{Al}^{3+}$  and 19 %  $\text{H}^{+}$  saturated. The composition of the cation exchange complex used in the CEC simulation is shown in Table E.2.

**Table E.2.** CEC composition used in PHREEQC simulations

Exchangeable cation	Concentration (mol/kg)
AlX3	0.0723
HX	0.02
CaX2	0.0031
NaX	0.0023
KX	0.0014
MgX2	0.004

The solution pH and cation concentration calculated using PHREEQC for the CEC simulation is shown in Figures E.1-E.2.

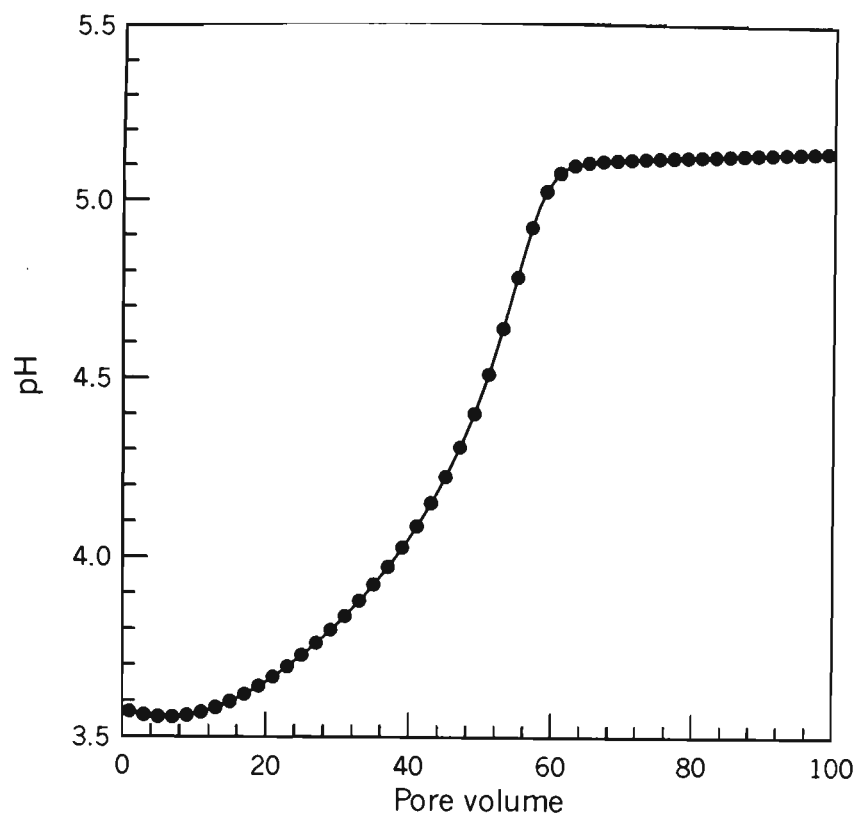


**Figure E.1** Equilibrium pH for 100 pore volume flushing for CEC simulation

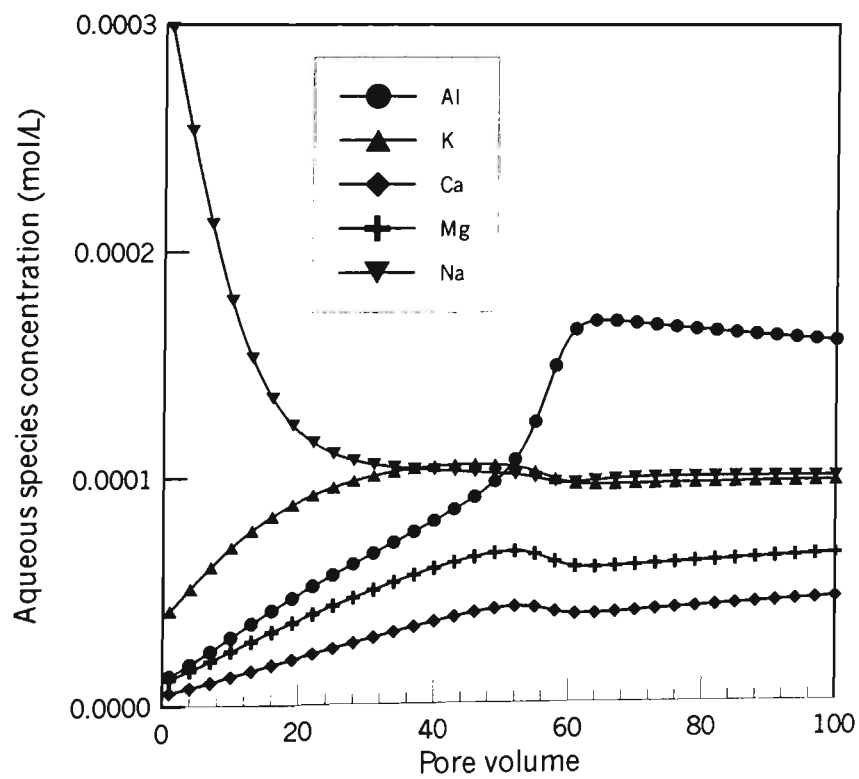


**Figure E.2** Cation concentration for 100 pore volume flushing for CEC simulation

Figure E.1 shows that the soil solution tends to an equilibrium pH of 5.2 after 60 pore water exchanges. During the initial 10 pore water exchanges, the solution pH is maintained at approximately 3.6. The next 50 pore water volume flushings show that the solution pH increases exponentially. Even after 100 pore volume flushings, the solution pH remains at 5.2, approximately 0.3 pH units less than the pH of the influent water.

The cation concentrations described in Figure E.2 shows that the monovalent cations come into equilibrium with the influent water after about 50 pore volumes. In contrast, the divalent cations are well below their concentration in the influent water, indicating they are being removed from the soil solution by the cation exchange sites. This is further supported by the concentration of  $\text{Al}^{3+}$  in the soil solution.  $\text{Al}^{3+}$  reaches its maximum concentration, about double the  $\text{Al}^{3+}$  of the influent water, after approximately 60 pore volume flushings. Clearly,  $\text{Al}^{3+}$  is being supplied to the soil solution from the cation exchange sites as  $\text{Al}^{3+}$  is being replaced by  $\text{Ca}^{2+}$  and  $\text{Mg}^{2+}$ . The  $\text{Al}^{3+}$  concentration will remain higher than the influent solution concentration until the  $\text{Al}^{3+}$  is replaced by divalent cations on the exchange sites and is subsequently flushed from the soil.

The CEC simulation indicates that poor water quality is likely to remain in excess of 60 pore water volume exchanges as a result of the liberation of  $\text{H}^+$  and  $\text{Al}^{3+}$  from the cation exchange sites. Even after 100 pore volume exchanges,  $\text{Al}^{3+}$  liberated from the exchange sites is likely to be present in the soil solution, although the relatively high pH (5.2-5.5) may facilitate the formation of less toxic forms of Al in the soil solution or the precipitation of aluminium hydroxides, thereby reducing the potential for environmental degradation from exposure to dissolved Al.

**E.2 Influence of acid saturated cation exchange complex and acidic minerals on soil solution water quality**

The soil solution water quality for a simplified soil system comprising an acid saturated CEC (as described above), as well as two common acidic minerals, jarosite ( $\text{KFe}_3(\text{SO}_4)_2(\text{OH})_6$ ) and alunite ( $\text{KAl}_3(\text{SO}_4)_2(\text{OH})_6$ ) was simulated. Both jarosite and alunite were assigned saturation indices of -2 (see Figure E.3) and initial concentrations of 1 mol/kg. Willett and Walker (1982) measured 0.25 mol/kg jarosite in acid sulfate soils sampled during 1978 from an area in the Shoalhaven floodplain. Given the potential for further generation of acidic minerals from 1978 to the present, the higher jarosite and alunite concentration used in this study is not unrealistic. The solution pH and ion concentrations calculated using PHREEQC for the CEC/mineral simulation are shown in Figures E.3-E.4.

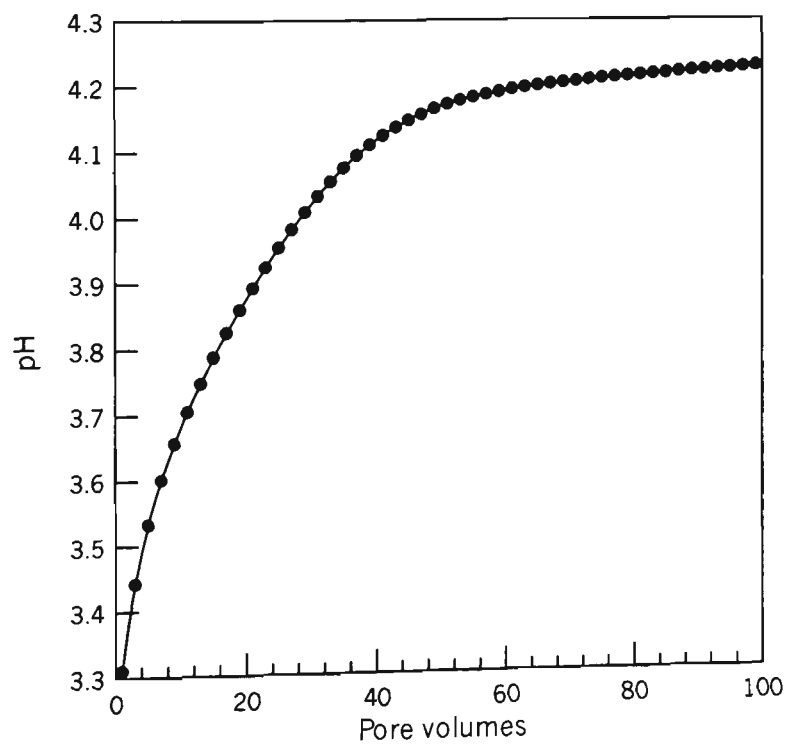


**Figure E.3** Equilibrium pH for 100 pore volume flushing for soil with measured CEC/phase composition

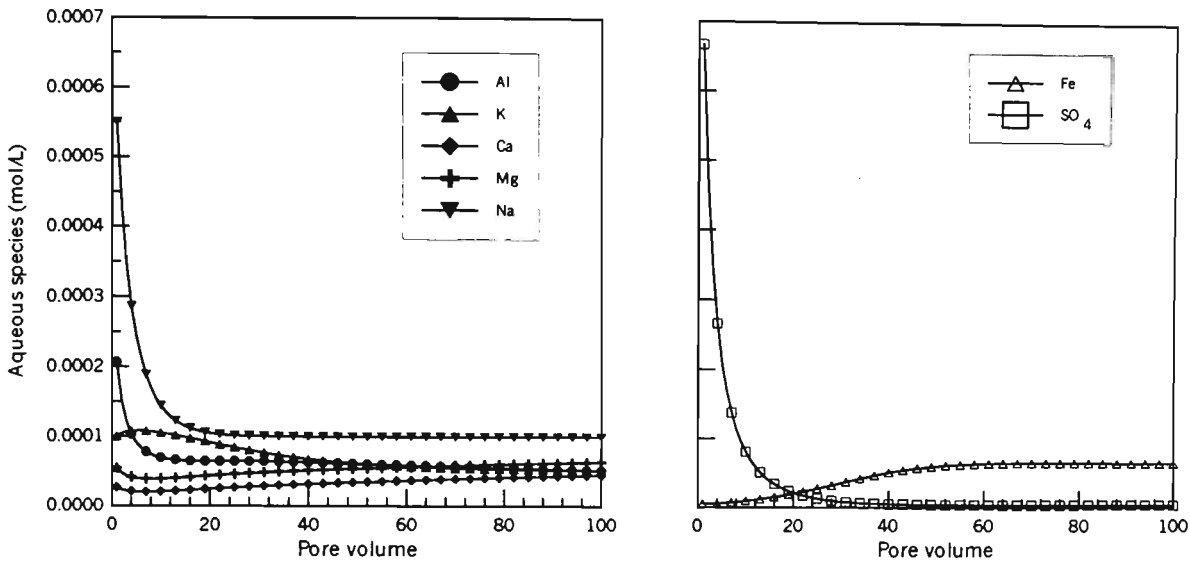


**Figure E.4** Aqueous species equilibrium for 100 pore volume flushing for soil with measured CEC/phase composition

Figure E.3 shows that the dissolution of jarosite and alunite, in conjunction with cation exchange processes, causes the soil solution pH to remain less 4.3, even after the exchange of 100 pore water volumes. After approximately 60 pore volume exchanges, the soil solution comes to an equilibrium of approximately pH 4.2. This is similar to the equilibrium groundwater pH measured at the field site during the post-weir period where the groundwater table had been maintained above the pyritic layer for a considerable period.

For every mole of jarosite that is dissolved, three moles of acidity is released into the soil solution according to Equation (E.1).



The dissolution of jarosite and alunite is evident within the first 30 pore water exchanges with increased concentrations of K and Fe present in the soil solution. Relatively high concentrations of  $\text{SO}_4$  during this period also indicate that a source of  $\text{SO}_4$  is available for transport within the pore water. During first 30 pore volume exchanges, the concentration of  $\text{SO}_4$ , Ca and Mg in the soil solution decrease from their initial concentrations (Fig. E.4). Given the abundance of  $\text{SO}_4$  in the initial soil solution, the precipitation of basic sulfate minerals such as  $\text{CaSO}_4 \cdot 2\text{H}_2\text{O}$  (gypsum) and  $\text{MgSO}_4$  may account for the loss of these ions from the soil solution. Similarly, the loss of Al from the soil solution may be indicative of the precipitation of amorphous  $\text{Al}(\text{OH})_3$ . The concentration of iron remains relatively high in the soil solution after 50 pore volume exchanges. According to the Fe-OH- $\text{SO}_4$  phase diagram described in Figure 13.2,  $\text{Fe}^{2+}$  may remain in solution at pH 4.2 when the pe is less than 7. In the saturated part of the soil profile, pe is unlikely to be largely positive (say > 3). Therefore, the removal of  $\text{Fe}^{2+}$  from the soil solution by the precipitation of  $\text{FeOOH}$  is unlikely until aeration occurs. When  $\text{Fe}^{2+}$  is oxidised to  $\text{Fe}^{3+}$  during the formation of  $\text{FeOOH}$ , an additional mole of  $\text{H}^+$  is generated, thereby buffering the soil solution pH at approximately 4-4.5.

The aqueous chemistry of acid sulfate soil solutions is very complex (Nordstrom, 1982) and beyond the scope of this research. However, useful indications of the expected groundwater quality can be made by performing simulations of the aqueous chemistry for simplified soil systems with chemical characteristics typical of soils previously exposed to pyrite oxidation and pyrite oxidation products. The contribution of the dissolution of acidic iron and aluminium sulfate minerals to soil solution acidity is relatively high compared to that released by the replacement of acidic cations on the exchange complex by basic cations. This suggests that improved groundwater quality can only be expected after the dissolution and subsequent flushing of the acidic mineral products from the soil and/or their re-precipitation to more stable amorphous hydroxides. Given the importance



of the release of acidic cations and generation of acidity from the cation exchange complexes and various minerals, reliance on groundwater manipulation strategies that minimise the oxidation of pyrite will not give rise to markedly improved groundwater quality within an acceptable time frame.

### **E.3. Controlling soil solution acidity by injecting calcium carbonate solution**

Groundwater acidity can be neutralised, and acidic minerals can be encouraged to dissolve and re-precipitate as amorphous hydroxides, by applying caustic neutralising agents such as lime to the soil. However, the application of lime to the soil is only effective when the neutralising agent is incorporated (Stone *et al.*, 1998). An alternative method of delivering neutralising agents to acidic soil is to inject either a slurry or dissolved aqueous alkaline solution into the acidic soil. Agricultural lime becomes insoluble at  $\text{pH} > 8.2$ , so the effect of injecting a solution containing 0.01 mol/L of dissolved calcium carbonate at pH 8.2 into an acidic soil with an acid CEC/minerals present was simulated using PHREEQC.

The solution pH and ion concentrations calculated using PHREEQC for the dissolved lime injection simulation is shown in Figures E.5-E.6.

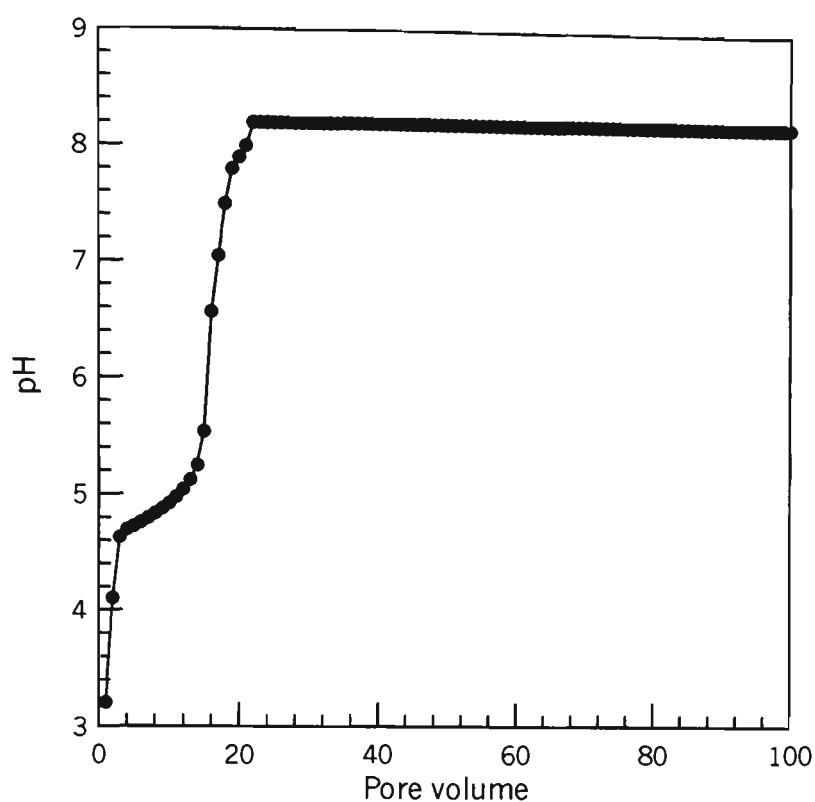


**Figure E.5** Equilibrium pH for 100 pore volume flushing for soil with measured CEC/phase composition with injection of 0.01 M  $\text{CaCO}_3$ .

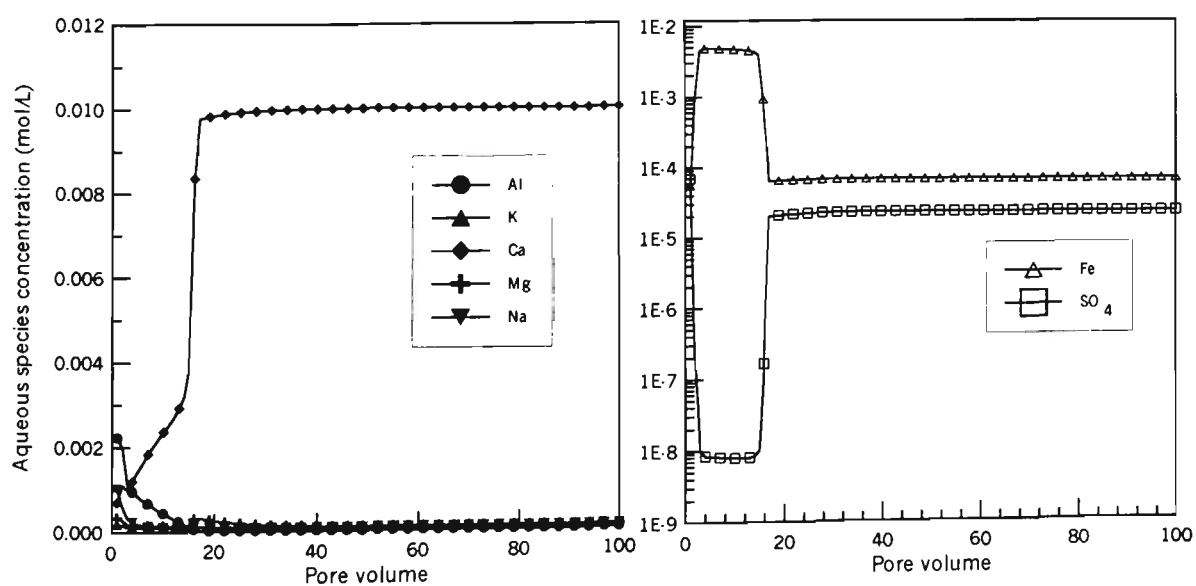


**Figure E.6** Equilibrium ion concentration for 100 pore volume flushing for soil with measured CEC/phase composition with injection of 0.01 M  $\text{CaCO}_3$ .

Figure E.5 shows that an immediate increase in soil solution pH from 3.2 to 4.6 occurred in the first 3 pore volume exchanges. The rate of pH increase was slower during the subsequent 12 pore volume exchanges. After 23 pore volume exchanges, the soil solution pH to an equilibrium of pH 8.2. The slower rate of soil solution increase calculated between pore volume exchanges 3-15 may be as a result of the dissolution of jarosite once the solution pH increased above pH 4. The iron phase diagram (Figure 13.2) shows that at pH 4, jarosite transforms to ferrihydrite or goethite. At low  $p_e$ , Drever (1997) produced a phase diagram for the Fe-O-H<sub>2</sub>O-S-CO<sub>2</sub> system that shows that siderite can precipitate at pH > 7.5. However, it is unlikely that jarosite can transform directly to more stable iron minerals via a solid-solid reaction. If jarosite dissolves and then re-precipitates as more stable minerals then the concentration of dissolved Fe in the soil water would be expected to increase as jarosite dissolves, at least in the short term. This process is simulated in Figure E.6. Similarly, SO<sub>4</sub> would be liberated by the dissolution of jarosite. However, the concentration of SO<sub>4</sub> in the soil solution is shown to decrease in Figure E.6. This may be due to the rapid precipitation of gypsum. Clearly, the SI for gypsum is positive with high concentrations of both Ca and SO<sub>4</sub> present providing saturated conditions that favour the rapid formation of gypsum. At the same time, the increasing soil solution pH may also favour the formation of amorphous Al hydroxides, thereby removing Al from the soil solution. After 20 pore volume exchanges, a steady state equilibrium is maintained, with pH and Ca concentration equal to the influent concentration. The concentration of other cations and SO<sub>4</sub> stabilise at low concentrations. Based on the geochemical simulation presented above, it appears that the injection of a dissolved lime slurry is beneficial with respect to increasing soil solution pH and promoting the dissolution of acid forming minerals.